

植物における 生態進化発生学研究拠点の形成

— 統合オミックス解析による展開 —

平成27年度～平成31年度 私立大学戦略的研究基盤形成支援事業

研 究 成 果 報 告 書



令和2年5月

学校法人名 京都産業大学

大学名 京都産業大学

研究組織名 生態進化発生学研究センター

研究代表者 木村 成介

(京都産業大学・生命科学部・教授)

平成 27 年度～平成 31 年度私立大学戦略的研究基盤形成支援事業
研究成果報告書

「植物における生態進化発生学研究拠点の形成－統合オミックス解析による展開－」

令和 2 年 5 月

学校法人名 京都産業大学

大 学 名 京都産業大学

研究組織名 生態進化発生学研究センター

研究代表者 木村 成介

(京都産業大学・生命科学部・教授)

〔 目 次 〕

◇成果報告書をまとめるにあたって・・・・・・・・・・・・・・・・・・ 1

◇研究成果報告書概要（様式2）・・・・・・・・・・・・・・・・・・ 2

◇研究成果の詳細・・・・・・・・・・・・・・・・・・ 39

成果報告書をまとめるにあたって

京都産業大学
生態進化発生学研究センター長
木村成介(生命科学部)

本報告書は、文部科学省・私立大学戦略的研究基盤形成支援事業に採択され、平成27年から令和元年度までの5年間に渡り支援を受けた研究課題である「植物における生態進化発生学研究拠点の形成－統合オミックス解析による展開－」の研究成果についてまとめたものです。

「生態進化発生学(エコ-エボ-デボ)」とは、生物の形の多様性が生じる仕組みを「発生」、「進化」、「環境」という3つの異なる観点から明らかにしようとする近年飛躍的に発展してきた学問領域です。本研究課題では、植物における生態進化発生学研究を推進すべく、京都産業大学総合学術研究所に「生態進化発生学研究センター」を設置し、総合生命科学部に所属する4名の教員が中心メンバーとなって研究を進めてきました。センターには次世代シーケンサーと解析サーバが導入され、ゲノム解析やトランスクリプトーム解析などの最新の技術を駆使した研究を展開することができました。教員だけでなく、研究員や研究補助員、また、大学院生や学部生が一丸となって共同研究を推進することで、国内外で唯一、生態進化発生学を標榜する研究センターとして、多くの重要な研究成果をあげることができたと自負しています。

さて、本研究課題の研究期間は終了しましたが、本センターは発展的に解消され、令和2年度より京都産業大学先端科学技術研究所に「植物科学研究センター」が設置されました。新研究センターでは、植物の多様性に着目し、植物が持つ多彩な能力をゲノム解析、生化学的解析、分子生物学的解析などを通じて解明することで、学術の進歩発展に寄与するとともに、その成果を社会に還元することを目的として研究をすすめています。今後も引き続き、京都産業大学の強みである植物科学研究を更に発展させ、私立大学における植物科学研究の一大拠点とすべく邁進していく所存です。

法人番号	261003
プロジェクト番号	S1511023

**平成 27 年度～平成 31 年度「私立大学戦略的研究基盤形成支援事業」
研究成果報告書概要**

- 1 学校法人名 京都産業大学 2 大学名 京都産業大学
- 3 研究組織名 生態進化発生学研究センター
- 4 プロジェクト所在地 京都市北区上賀茂本山
- 5 研究プロジェクト名 植物における生態進化発生学研究拠点の形成—統合オミックス解析による展開—
- 6 研究観点 研究拠点を形成する研究

7 研究代表者

研究代表者名	所属部局名	職名
木村 成介	生命科学部	教授

- 8 プロジェクト参加研究者数
- 7
- 名

- 9 該当審査区分
- 理工・情報
- 生物・医歯
- 人文・社会

10 研究プロジェクトに参加する主な研究者

研究者名	所属・職名	プロジェクトでの研究課題	プロジェクトでの役割
木村 成介	生命科学部・教授	葉の形態の表現型可塑性の分子機構の解明	研究の統括およびトランスクリプトーム解析など
金子 貴一	生命科学部・教授	<i>R. aquatica</i> のゲノム解析	ゲノム配列の解明およびバイオインフォマティクス解析の支援
本橋 健	生命科学部・教授	<i>R. aquatica</i> のエピゲノム解析および進化解析	エピゲノム解析、イヌガラス属植物の分子系統解析および進化解析
河邊 昭	生命科学部・准教授	<i>R. aquatica</i> のプロテオーム解析および生理学的解析	プロテオームおよび生理学的解析、生理生態的特性の解析
(共同研究機関等) 塚谷 裕一	東京大学大学院理学研究科・教授	葉形変化の進化発生学的解析	進化発生学的解析、葉形と環境の関係の発生学的解析
Neelima Sinha	University of California, Davis Professor	進化発生トランスクリプトーム解析	トランスクリプトーム情報に基づく進化発生学的解析
矢野 健太郎	明治大学農学部・准教授	バイオインフォマティクス解析	植物のバイオインフォマティクス解析の支援

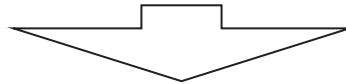
法人番号	261003
プロジェクト番号	S1511023

<研究者の変更状況(研究代表者を含む)>

旧

プロジェクトでの研究課題	所属・職名	研究者氏名	プロジェクトでの役割
R. aquatica のエピゲノム解析および進化解析	総合生命科学部・准教授	本橋 健	エピゲノム解析、イヌガラス属植物の分子系統解析および進化解析

(変更の時期:平成 27 年 4 月 1 日)



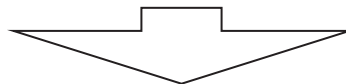
新

変更前の所属・職名	変更(就任)後の所属・職名	研究者氏名	プロジェクトでの役割
総合生命科学部・准教授	総合生命科学部・教授	本橋 健	エピゲノム解析、イヌガラス属植物の分子系統解析および進化解析

旧

プロジェクトでの研究課題	所属・職名	研究者氏名	プロジェクトでの役割
葉の形態の表現型可塑性の分子機構の解明	総合生命科学部・准教授	木村 成介	研究の統括およびトランスクリプトーム解析など

(変更の時期:平成 28 年 4 月 1 日)



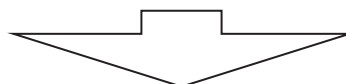
新

変更前の所属・職名	変更(就任)後の所属・職名	研究者氏名	プロジェクトでの役割
総合生命科学部・准教授	総合生命科学部・教授	木村 成介	研究の統括およびトランスクリプトーム解析など

旧

プロジェクトでの研究課題	所属・職名	研究者氏名	プロジェクトでの役割
葉の形態の表現型可塑性の分子機構の解明	総合生命科学部・教授	木村 成介	研究の統括およびトランスクリプトーム解析など
R. aquatica のゲノム解析	総合生命科学部・教授	金子 貴一	ゲノム配列の解明およびバイオインフォマティクス解析の支援
R. aquatica のエピゲノム解析および進化解析	総合生命科学部・教授	本橋 健	エピゲノム解析、イヌガラス属植物の分子系統解析および進化解析
R. aquatica のプロテオーム解析および生理学的解析	総合生命科学部・准教授	河邊 昭	プロテオームおよび生理学的解析、生理生態的特性の解析

(変更の時期:平成 31 年 4 月 1 日)



法人番号	261003
プロジェクト番号	S1511023

新

変更前の所属・職名	変更(就任)後の所属・職名	研究者氏名	プロジェクトでの役割
総合生命科学部・教授	生命科学部・教授	木村 成介	研究の統括およびトランスクリプトーム解析など
総合生命科学部・教授	生命科学部・教授	金子 貴一	ゲノム配列の解明およびバイオインフォマティクス解析の支援
総合生命科学部・教授	生命科学部・教授	本橋 健	エピゲノム解析、イヌガラス属植物の分子系統解析および進化解析
総合生命科学部・准教授	生命科学部・准教授	河邊 昭	プロテオームおよび生理学的解析、生理生態的特性の解析

11 研究の概要(※ 項目全体を10枚以内で作成)

(1) 研究プロジェクトの目的・意義及び計画の概要

地球上の多彩な生物が見せる驚くべき「形の多様性」は、古くから多くの人々を惹きつけてきた。個体の形は、「発生」の過程を経て形成され、種間に見られる形の多様性は、「進化」の過程で発生のプログラムが変化することで生じる。また、生物をとりまく「環境」は一定でなく、多くの生物は生育環境に合わせてその形を変化させる。つまり、生物の「形の多様性」が生じる仕組みを明らかにするためには、「発生」、「進化」、「環境」という3つの異なる観点から理解しなければならない。「生態進化発生学(エコ-エボ-デボ)」は、この3つの観点から生物の形の多様性を総合的に解き明かそうとするものであり、近年花開きつつある新しい研究領域である。

生物の形などの形質は、ゲノムに書き込まれた情報が、階層的かつ複合的に制御されることで発現する。したがって、生物の形の多様性が生じる仕組みを理解するためには、ゲノム、エピゲノム、トランスクリプトーム、プロテオームなど各階層のオミックス情報を統合的に解析する必要がある(「統合オミックス解析」)。一方、生態進化発生学の対象は変わった特徴をもつ非モデル生物になりがちで、これまで、ゲノム配列や転写産物の解読などのオミックス研究は技術的に困難であった。しかしながら、次世代シーケンサーの登場による技術革新により、最近になって、非モデル生物でもオミックス研究が実施できるようになってきている。

そこで本研究プロジェクトでは、京都産業大学総合学術研究所に生態進化発生学研究センターを設置し、オミックス研究において十分な実績を持つ国内外の教員が連携することで、これまで困難であった生態進化発生学研究を展開する体制を構築することを目的とした。生態進化発生学を標榜した研究拠点は国内外に見当たらず、世界に先駆けて拠点を形成することで、我が国を代表する研究拠点の形成を目指したものである。

本研究プロジェクトでは、植物の多様性に着目し、特に植物の形と環境の関係に着目して研究を進めることとした。生物が周囲の環境に応じて、その形などの表現型を変化させることを「表現型可塑性」という。この現象は発生と環境の関係を理解するために重要であり、植物の生態進化発生学研究を展開する上で最良のモデルとなりうる。本研究プロジェクトでは、表現型可塑性のメカニズムを解明し、その意義や進化過程を明らかにすることを目的とした。加えて、自然界の植物の多様な形態や形質に着

法人番号	261003
プロジェクト番号	S1511023

目し、統合オミックス解析を駆使した研究を展開していくこととした。さらには、本研究の成果を応用することで、環境ストレス耐性植物の作出など応用的な成果に結びつけることを目指した。

(2) 研究組織

本研究プロジェクトは、京都産業大学総合学術研究所生態進化発生学研究センターが中心となって推進した。本センターには、京都産業大学総合生命科学部に所属する4名の教員が主要メンバーとして参加し、木村(研究代表者)がセンター長を務めた。

木村成介(教授) : 生態進化発生学、トランスクリプトーム解析

金子貴一(教授) : ゲノム科学、ゲノム解析およびバイオインフォマティクス解析

本橋健(教授) : 植物生理学、プロテオーム解析

河邊昭(准教授) : 集団遺伝学 エピゲノム解析および進化解析

また、学外から以下の3名の研究者が参加した。

塚谷裕一(東京大学大学院理学研究科教授)

Neelima Sinha (カリフォルニア大学デービス校教授)

矢野健太郎(明治大学農学部生命科学科准教授)

本研究プロジェクトには、若手研究者として、京都産業大学総合生命科学部の4名の研究員(研究助教)に加え、PD研究員と技術補佐員も参加した。

センター長の木村が研究組織全体を統括しながら、各研究者が有機的に連携し、強力に研究をすすめていく体制を整えられた。また、国内外を含む多くの大学や研究所、企業と共同研究を推進することができた。

(3) 研究施設・設備等

本センターが目指す統合オミックス研究は、次世代シーケンサーによる大量かつ並列的な DNA の塩基配列決定技術を基礎としている。本センターの設置にあたり、次世代シーケンサー用のライブラリ作成からランの実施、データの解析まで一貫して実施できる体制を整えることとし、次世代シーケンサーとしては、illumina 社の NextSeq500 システム、また、データの解析サーバとして TAKERU for Sequencer V を導入した。これらの研究装置や設備は、他の関連機器とともに京都産業大学第一実験室棟 B1 実験研究室(35.96 m²)に設置され、生態進化発生学研究センターの拠点となった。また、プロジェクトに参加している教員の実験室や温室、クリーンルームなどを利用してプロジェクトを推進した。

(4) 研究成果の概要 ※下記、13及び14に対応する成果には下線及び*を付すこと。

本研究は、2015年度にスタートし、2020年度で5年間の研究期間を終了した。本研究プロジェクトの目的は、生態進化発生学を標榜する研究拠点(生態進化発生学研究センター)を世界で始めて設置し、統合オミックス解析を基盤として当該分野の研究を牽引することであった。センターの研究設備や装置として、イルミナ社の最新次世代シーケンサーNextSeq500 や、バイオインフォマティクス用データ解析サーバを設置するなど、統合オミックス解析を推進する体制は整備された。また、人材面でも、統合オミックス解析に実績のある教員が結集し、さらに外部の専門家が加わることで、幅広い研究を展開できる組織とした。また、若手研究員として PD 研究員、大学院生、学部生が活発に研究を推進できる体制とすることができた。5年間の研究期間で、目的とする研究基盤は形成できたと評価できる。

法人番号	261003
プロジェクト番号	S1511023

研究面でも大きな成果を上げることができた。「13 研究発表の状況」にもあるように、82報の研究論文(英語70報、日本語12報)、12報の総説・解説論文(英語3報、日本語9報)、25件の招待講演、202件の学会発表を行うなど多くの研究成果を上げることができた(以上の業績は、本学所属の研究メンバーのみ)。また、本センターにおける研究成果のほとんどは未発表であり、今後も続けて研究成果が学術論文や学会発表の形で発表される。さらに、本センターでは、学内の共同研究にとどまらず、国内外の多くの研究機関と共同研究を進めることもできた。国内で唯一、生態進化発生学を標榜する研究センターとして、当該分野を切り開くことができたと評価できるだろう。

本研究で特に着目している北米に分布する水陸両生植物 *Rorippa aquatica* の水環境への適応形質(葉の形態の表現型可塑性や栄養繁殖能)についての研究も着実に成果を上げることができた。まず、センターの基盤を利用して、*R. aquatica* のゲノム解読を終了することができた(学会 6,8,11,22,109)。また、葉の形態の表現型可塑性について、水没や温度変化に応答した遺伝子発現の変動について、トランスクリプトーム解析により明らかにすることができた(論文 4,10,13,14,21,23,40,41,56,68,78,79,80)(学会 3,8,9,13,21,39,51,56,57,59,64,67,101,113,128,133,135,145,146,148,151,154,178,179,181,182,185)。 *R. aquatica* の栄養繁殖(再生能力)についても、トランスクリプトーム解析により、そのメカニズムの一端を明らかにすることができた(論文 7,11,57)(学会 1,4,7,9,12,14,15,16,17,18,20,23,24,30,35,37,54,55,56,62,70,74,78,93,94,96,99,102,104,108,113,127,129,131,133,136,137,140,153,177,186,191)。また、*R. aquatica* の根の微生物菌叢が葉の形態に影響を与えることを発見するなど、予測していなかった成果も得られた(学会 39,81,88,114,154)。

上述の研究以外にも、センターの基盤を駆使して、植物と環境の関係に着目した研究を幅広く展開することができた。さらに、国内外の研究機関と数十件の共同研究をすすめることができた。

以上、当初の目的を期待以上に達成できたと総括できる。以下、<優れた成果が上がった点>として、代表的な研究成果について詳細を説明する。

<優れた成果が上がった点>

1. *R. aquatica* の葉の形態の表現型可塑性の研究

(1) *R. aquatica* のゲノム解析(学会 6,8,9,11,22,58,65,95,109)

R. aquatica のゲノム DNA をイルミナ社の NextSeq500 および MiSeq でシーケンスし、100Gbp 程度の配列情報を得た(約 200x カバレッジ)。また長鎖リードを得るために、PacBio でもシーケンスをおこない、12Gbp 程度の配列情報を得た(20-30x カバレッジ)。得られた Illumina リードおよび PacBio リードを用いて MaSuRCA ver3.2.1 によるハイブリッドアセンブリを行った。その結果、1,797 本の配列からなるゲノムサイズ 440Mbp のドラフトゲノムが得られた。ドラフトゲノムの N₅₀ は 1,355,881bp、最長配列は 8,916,255bp であった。k-mer 頻度分析から推定されるゲノムサイズは 450Mb 前後であり、BUSCO 解析の結果からも、今後の解析に十分なゲノム配列情報が得られたと判断できた。

R. aquatica の染色体数は 2n=30 で、近縁の *Cardamine hirsuta* の染色体数は 2n=16 である。これまでの研究で、*R. aquatica* では全染色体倍数化の後、染色体同士が融合することで現在の染色体数になったことが示唆されていた。今年度は、Hi-C 法により各染色体の連続性の情報を取得することで、断

法人番号	261003
プロジェクト番号	S1511023

片化しているコンティグから染色体スケールのスキファールド作成を試みた。3D de novo assembly pipelineを用いた自動クラスタリングと手動での修正により、15本の染色体配列(総塩基長414.3 Mbp)と、染色体にクラスタリングされなかった2043本のスキファールド(総塩基長37.9 Mbp)を得ることができた。BUSCO解析の結果、15本の染色体配列から植物全体で保存されている遺伝子の大部分が見つかった。また、*C. hirsuta*との相同性比較解析の結果からも、全染色体倍数化と染色体同士の融合の過程を経ていることが支持された。

R. aquatica には、表現型可塑性の程度が著しく異なる2つの地域系統(A株およびJ株)が存在する。両者についてシーケンスすることで一塩基多型や挿入欠失変異を同定することができた。これにより、地域系統間の比較解析が可能となった。

(2) 温度に対する応答機構の解析 (論文 14,21,23) (学会 8,9,56,59,67,78,79)

R. aquatica は生育温度に応じて発生する葉の形を変化させ、低温(20℃)では葉が複葉化してギザギザになり、高温(30℃)では葉が単葉化することがわかっている。また、生育途中で生育温度を変化させると、4日後には新しい環境に応答した葉の形になることもわかっている。そこで、生育途中で温度を変化(20℃→30℃、または、30℃→20℃)させたあと、経時的(1日、2日、4日)にRNAを単離し、トランスクリプトーム解析をおこなうことで、温度変化に応答した遺伝子発現の変動を追跡した。その結果、*KNOX1* 遺伝子などの葉の形態制御に関わる遺伝子群の発現が、温度移行後1日目には変動していることが明らかとなった。また、移行後にオーキシン関係の遺伝子群の発現が変動していた。*KNOX1* 遺伝子はオーキシンにより発現制御を受けることから、温度変化によるオーキシン量の変動が葉形を決定している可能性が示唆された。

(3) 水没に対する応答機構の研究 (論文 4,10,13) (学会 3,8,9,13,21,56,57,64)

R. aquatica は、水没すると葉の形態を大きく変化させる。そこで、水没をどのように感知して葉形を変化させているのかを分子レベルで明らかにするため、水没応答のトランスクリプトーム解析を進めた。その結果、水没に応答して嫌気呼吸に関する遺伝子の発現が変動していたことがわかった。また、エチレン関係の遺伝子群の発現が大きく変動しており、実際、植物の茎頂にエチレンを添加すると、葉の形態が水中葉に近くなることから、エチレンが水没応答に関わっているものと考えられた。水没に応答する遺伝子群の中に、フィトクロム関連の遺伝子があったことから、光質が葉の形態に与える影響を調査したところ、気中であっても赤色光の照射により葉の形態が水没葉に近くなることがわかった。この結果は、光環境が水没の感知に関わっていると示唆しており興味深い。

(4) 異形葉性のメカニズムの解析 (論文4,10,13,14,21,23,40,41,56,68,80) (学会8,9,39,51,101,113,128,133,135,145,146,148,151,154,178,179,181,182,185)

これまでの研究により、*R. aquatica*は、低温もしくは強光条件下では葉が複葉になり、高温もしくは弱光条件下では葉が単葉になることがわかっていた。また、北米大陸の南部由来の地域集団のS株は、北部由来のN株と比較して葉形変化の程度が著しく低い。そこで、まず、さまざまな温度および光強度でN株とS株を生育させ、発生初期の葉原基を含む茎頂をサンプリングしてトランスクリプトーム解析を

法人番号	261003
プロジェクト番号	S1511023

行った。*R. aquatica*の葉形は環境変化に応答して連続的に変化するので、葉の形態変化と相関して発現が変動する遺伝子群を相関分析(ピアソンの相関分析)により同定した。その結果、これまでに葉の発生に関わることが知られている遺伝子や、転写因子、植物ホルモン関係の遺伝子などが同定された。興味深いことに、植物の光受容体であるフィトクロムに相互作用する因子(フィトクロム相互作用因子)の発現が、葉の形態変化に強く相関して変動していることを見出した。最近、フィトクロム相互作用因子が、植物の光応答だけでなく、温度の応答にも関わっていることが明らかとなっており、フィトクロム相互作用因子が表現型可塑性の発現に重要な役割を果たしている可能性が明らかとなった。

(5) 水没による気孔形成の抑制機構の解析 (論文4,10,13) (学会3,8,9,13,21,56,57,64)

*R. aquatica*は、水没すると葉の形態を大きく変化させるとともに、気孔の形成が抑制される。4週間生育した*R. aquatica*を水没させると、展開中である5mm 程度の若い葉において水没後4日目には顕著な気孔形成の抑制が観察された。

また、水没後の遺伝子発現変動を経時的なトランスクリプトーム解析により解析したところ、気孔形成に重要な転写因子である*SPCH*の発現抑制が水没後1時間という早い時期に起こっていることがわかった。このような気孔形成の抑制や気孔関連遺伝子の発現抑制は、シロイヌナズナを水没させても観察されなかった。水没により、*R. aquatica*で特異的に転写量が4倍以上増加していた遺伝子は180 あり、その中で転写因子は9つあった。これらの遺伝子が水没応答に関わっている可能性がある。

また、水没時の光条件などを検討したところ、暗所では水没させても気孔形成は抑制されず、また、青色光のみを当てた場合も気孔形成は抑制されなかった。また、気中条件であっても赤色光を当てると気孔の形成が抑制された。*SPCH* の発現も気孔形成と相関していた。以上の結果から、光質などの光条件が水没の感知に重要であることが示唆された。*SPCH* の発現制御機構に着目することで、水没による気孔形成の抑制機構が明らかにできると期待できる。

2. *R. aquatica*の栄養繁殖のメカニズムの研究 (論文7,11,57)(学会1,4,7,9,12,14,15,16,17,18,20,23,24,30,35,37,54,55,56,62,70,74,78,93,94,96,99,102,104,108,113,127,129,131,133,136,137,140,153,177,186,191)

R. aquatica は、自然界において、水の流れなどの影響でちぎれた葉の断面から新しい個体を再生することで栄養繁殖をしている。この際、葉の断片の基部側の断面からのみ再生し、先端部側からは再生しない。再生のメカニズムを分子レベルで明らかにするために経時的なトランスクリプトーム解析を行なった。基部側と先端部側で比較トランスクリプトーム解析をおこなったところ、基部側でのみ再生に関わる遺伝子群の発現が誘導されていることがわかった。また、切断後初期の段階ではオーキシン応答性の遺伝子の発現が顕著に上昇していた。オーキシンやオーキシン極性輸送阻害剤の添加実験から、オーキシン極性輸送が基部側からのみの再生に関わっていることが示唆された。オーキシンの内生量を測定したところ、*R. aquatica* では、葉の切断後に基部側で IAA-Asp などの蓄積がみられた。シロイヌナズナでは同様の蓄積は観察されなかった。これらの結果から、*R. aquatica* では、葉の切断後に極性輸送で基部側にオーキシンが輸送されて蓄積することが再生のトリガーになっていると考えられ

法人番号	261003
プロジェクト番号	S1511023

た。また、再生における植物ホルモンの役割を解析し、オーキシンが根の再生、サイトカイニンがシュートの再生に関わっていることを明らかにしていた。さらに、ジベレリンが根の成長に必要であることを明らかにした。

R. aquatica がなぜ葉の断面から再生できるのかを明らかにするため、シロイヌナズナの葉を用いた比較トランスクリプトーム解析を行った。*R. aquatica* では、葉の切断直後にオーキシン応答性の遺伝子の発現が変動するが、シロイヌナズナでは同様の遺伝子発現変動は観察されなかった。葉の内部構造の形態観察の結果、*R. aquatica* ではシロイヌナズナと比較して細胞が密であることがわかった。また、*R. aquatica* は、シロイヌナズナよりも、切断後の葉の光合成活性が低下しにくく、これらのことが再生のしやすさにつながっていると考えられた。

3. 虫こぶ形成機構の解明 (論文 2,3,9、学会 2,25,31,53,79,82,106,110,111)

虫こぶは、アブラムシなどの虫こぶ形成昆虫が、植物の葉や茎などの分化した器官に寄生して作る特異な形状の器官である。虫こぶ形成昆虫は、分化全能性をもつ幹細胞を利用して植物の発生プログラムをハイジャックしていると考えられるが、そのメカニズムはわかっていない。虫こぶ形成の実験モデルとして、タマホソガとカンコノキ、ヒサカキホソガとヒサカキ、ヌルデシロアブラムシとヌルデなどの系に着目し、虫こぶのトランスクリプトーム解析をおこなった。その結果、虫こぶでは、花や果実で発現している遺伝子が強発現するなど、通常の植物組織とは全く異なる発現プロファイルを持つことがわかった。虫こぶ形成過程の遺伝子発現変動パターンについてはほとんど知見が得られていないことから、本研究の発展により新たな知見が得られると期待できる。

4. 人工オーキシンと人工受容体の創出 (論文 24)

植物ホルモンのオーキシンの生理作用を自在に操作することを可能にする人工オーキシンと人工受容体の創出に成功した。この技術を用いて、進化論で有名なチャールズ・ダーウィンが 130 年以上前にオーキシンの存在を予言するきっかけとなった植物の伸長現象(酸成長)のメカニズムの一端を明らかにすることができた。今回創出した人工オーキシンと人工受容体を利用すれば、特定のオーキシン作用だけを自在に制御することができるため、オーキシンの作用メカニズムの解明に役に立つ成果である。

5. 植物の DNA 傷害応答のマスターレギュレーターSOG1 の機能解析 (論文 1,22,39,62,63,64)(学会 36,61, 97,107,112,143,144,149,180)

モデル植物のシロイヌナズナを用いて、植物のゲノム DNA に二重鎖切断(DNA 損傷)が生じた際に、SOG1 転写因子のリン酸化部位が増えると、DNA 複製の停止、DNA 修復、プログラム細胞死、細胞分化などの DNA 損傷応答反応が徐々に強くなり、その結果、植物が DNA 損傷に対して耐性を示すことを明らかにした。また、SOG1 の強発現により、植物に DNA 損傷に対する耐性を与えることができるだ

法人番号	261003
プロジェクト番号	S1511023

けでなく、病原菌に対しての抵抗性も強くできることを発見した。

<課題となった点>

本研究プロジェクトでは、統合オミックス解析を基盤としており、高度なバイオインフォマティクス解析技術やノウハウが必要となる。最近のオミックス解析技術の発展はすざましいものがあり、いかにして最新の技術やノウハウをセンターに取り入れるかが大きな課題であった。センターの構成員が一丸となって、学会での情報収集や共同研究などを積極的に推進することで、対応することができた。

研究業績については、100 報近い研究論文を発表するなど大きな成果を上げることができた。一方、本センターでは、研究基盤を整えることからスタートし、当該分野の新規の研究に積極的に取り組んできたため、5 年間の研究期間では多くの成果が論文発表までに至らず未発表となっている。今後も、継続して研究を進めて、成果発表につなげていく必要があることが課題である。

<自己評価の実施結果と対応状況>

生態進化発生学研究センターは、京都産業大学研究機構の総合学術研究所の一組織である。自己評価として、総合学術研究所の所報(総合学術研究所所報)に活動報告を毎年度発表した。また、センターに所属する教員が定期的に集まり、研究成果の報告や研究計画の審議を行い、課題を洗い出しながら本センターを運営してきた。「13 研究発表の状況」にあるように多くの研究成果を上げることができたことから、自己評価としては、順調に研究拠点を立ち上げられたと考えている。

<外部(第三者)評価の実施結果と対応状況>

生態進化発生学研究センターの研究成果等については、京都産業大学の研究機構運営委員会(委員長:学長)及び研究機構評価委員会に毎年報告を行い、両委員会からのコメントなどに対応する形でセンターを運営してきた。また、毎年、センターが主催・共催するシンポジウムを開催し、研究成果を広く発信することで、研究成果について科学的かつ客観的な評価を受けるように努めてきた。

<研究期間終了後の展望>

本センターは、国内外で唯一、生態進化発生学を標榜する研究センターとして、多くの成果をあげてきた。5 年間の研究期間は終了したが、本センターを発展的に解消し、令和 2 年度から京都産業大学研究機構の先端科学技術研究所に「植物科学研究センター」を設置した。植物科学研究センターは、植物の多様性に着目し、植物が持つ多彩な能力をゲノム解析、生化学的解析、分子生物学的解析などを通じて解明することで、学術の進歩発展に寄与するとともに、その成果を社会に還元することを目的としている。植物科学研究センターには、京都産業大学生命科学部の植物科学を専門とする教員が 8 名参加する。今後は、これまで培ってきた植物科学に関する研究をさらに発展させ、私立大学における植物科学研究の一大拠点としたい。

法人番号	261003
プロジェクト番号	S1511023

<研究成果の副次的効果>

本センターの研究基盤を活かして、大学内(学部内)だけでなく、国内外の多くの研究機関(国内 22 研究機関、海外 15 研究機関)と共同研究をすすめることができた。また、企業との共同研究もおこなった。これらの共同研究の成果が 1 件特許申請され、また、もう 1 件が申請準備中である。

12 キーワード(当該研究内容をよく表していると思われるものを8項目以内で記載してください。)

- (1) 生態進化発生学 (2) 表現型可塑性 (3) 植物
 (4) オミックス解析 (5) 次世代シーケンサ (6) 形態の多様性
 (7) _____ (8) _____

13 研究発表の状況(研究論文等公表状況。印刷中も含む。)

上記、11(4)に記載した研究成果に対応するものには*を付すこと。

<雑誌論文>

学内研究者の業績のみ掲載

- *1. Kaoru Okamoto Yoshiyama, Naoki Aoshima, Naoki Takahashi, Tomoaki Sakamoto, Kei Hiruma, Yusuke Saijo, Jun Hidema, Masaaki Umeda, Seisuke Kimura: SUPPRESSOR OF GAMMA RESPONSE1 acts as a regulator coordinating crosstalk between DNA damage response and immune response. *Plant Molecular Biology* (2020) in press
- *2. Tomoko Hirano, Seisuke Kimura, Tomoaki Sakamoto, Ayaka Okamoto, Takumi Nakayama, Yoshihito Suzuki, Issei Ohshima, Masa H. Sato, Reprograming of the developmental program of *Rhus javanica* during initial stage of gall induction by *Schlechtendalia chinensis*. *Frontiers in Plant Science* (2020) in press
- *3. Takashi Ishida, Reira Suzuki, Satoru Nakagami, Takeshi Kuroha, Shingo Sakamoto, Miyuki T. Nakata, Ryusuke Yokoyama, Seisuke Kimura, Nobutaka Mitsuda, Kazuhiko Nishitani, Shinichiro Sawa, Root-knot nematodes modulate cell walls during root-knot formation in Arabidopsis roots. *Journal of Plant Research* (2020) in press
- *4. Gaojie Li, Shiqi Hu, Jingjing Yang, Xuyao Zhao, Seisuke Kimura, Elizabeth A. Schultz, Hongwei Hou: Establishment of an Agrobacterium mediated transformation protocol for the detection of cytokinin in the heterophyllous plant *Hygrophila difformis* (Acanthaceae). *Plant Cell Reports* (2020) published on line
5. Masaya Yamamoto, Shuhei Uji, Tomoyuki Sugiyama, Tomoaki Sakamoto, Seisuke Kimura, Toshiya Endo and Shuh-ichi Nishikawa: ERdj3B-mediated quality control maintains anther development at high temperatures. *Plant Physiology* (2020) published on line
6. Shigeru Hanamata, Jumpei Sawada, Seijiro Ono, Kazunori Ogawa, Togo Fukunaga, Ken-Ichi Nonomura, Seisuke Kimura, Takamitsu Kurusu, Kazuyuki Kuchitsu: Impact of autophagy on gene expression and tapetal programmed cell death during pollen development in rice. *Frontiers in Plant Science* 11: 172-1-19 (2020)
- *7. Rumi Amano, Hokuto Nakayama, Risa Momoi, Emi Omata, Shizuka Gunji, Yumiko Takebayashi, Mikiko Kojima, Shuka Ikematsu, Momoko Ikeuchi, Akira Iwase, Tomoaki Sakamoto, Hiroyuki Kasahara, Hitoshi Sakakibara, Ali Ferjani and Seisuke Kimura: Molecular Basis for Natural Vegetative Propagation via Regeneration in North American Lake Cress, *Rorippa aquatica* (Brassicaceae). *Plant and Cell Physiology* 61: 353-369 (2020)

法人番号	261003
プロジェクト番号	S1511023

8. Gholamreza Gohari, Asghar Mohammadi, Ali Akbari, Sima Panahirad, Mohammad Reza Dadpour, Vasileios Fotopoulos and Seisuke Kimura: Titanium dioxide nanoparticles (TiO₂ NPs) promote growth and ameliorate salinity stress effects on essential oil profile and biochemical attributes of *Dracocephalum moldavica*. **Scientific Reports** 10: 912-1-14 (2020)
- *9. Seiji Takeda, Makiko Yoza, Taisuke Amano, Issei Ohshima, Tomoko Hirano, Masa H. Sato, Tomoaki Sakamoto, Seisuke Kimura: Comparative transcriptome analysis of galls from four different host plants suggests the molecular mechanism of gall development. **PLOS ONE** 14: e0223686-1-19 (2019)
- *10. Gaojie Li, Shiqi Hu, Hongwei Hou and Seisuke Kimura: Heterophylly: Phenotypic Plasticity of Leaf Shape in Aquatic and Amphibious Plants. **Plants** 8: 420-1-13 (2019)
- *11. 郡司玄、天野瑠美、金子真也、Ferjani Ali、木村成介: アブラナ科植物 *Rorippa aquatica* の再生能力に注目した栄養生殖の教材化と授業実践. **生物教育** 60: 137-147 (2019)
12. Mai Tsujimura, Takakazu Kaneko, Tomoaki Sakamoto, Seisuke Kimura, Masayoshi Shigyo, Hiroshi Yamagishi, Toru Terachi: Multichromosomal structure of the onion mitochondrial genome and a transcript analysis. **Mitochondrion** 46: 179-186 (2019)
- *13. Saori Miyoshi, Seisuke Kimura, Ryo Ootsuki, Takumi Higaki, Akiko Nakamasu: Developmental analyses of divarications in leaves of an aquatic fern *Microsorium pteropus* and its varieties. **PLOS ONE** 14: e0210141-1-14 (2019)
- *14. 池松朱夏、木村成介: 葉の形から迫る植物の温度感知メカニズム(解説) **アグリバイオ 研究者の広場** 3: 48-51 (2019)
15. Ken Motohashi*: Development of highly sensitive and low-cost DNA agarose gel electrophoresis detection systems, and evaluation of non-mutagenic and loading dye-type DNA-staining reagents. **PLOS ONE** 14, e0222209 (2019)
16. Ken Motohashi*: A novel series of high-efficiency vectors for TA cloning and blunt-end cloning of PCR products. **Sci. Rep.** 9, 6417 (2019)
17. 本橋健*: PCR クローニングのための高効率ベクターとその利用法 **実験医学** 37, 3141-3149 (2019)
18. Okazaki S, Kaneko T, Gressent F, Nouwen N, Arrighi JF, Koebnik R, Mergaert P, Deslandes L, Teulet A, Busset N, Fardoux J, Gully D, Chaintreuil C, Cartieaux F, Jauneau A, Comorge V, Giraud E. The rhizobial type III effector ErnA confers the ability to form nodules in legumes. **Proc Natl Acad Sci USA** 116, 21758-21768 (2019)
19. Yoshida, T., Furihata, H.Y., To, T.K., Kakutani, T., Kawabe, A.: Genome defense against integrated organellar DNA fragments from plastids into plant nuclear genomes through DNA methylation. **Scientific Reports** 9, 2060 (2019)
20. Kawabe, A., Furihata, H.Y., Tsujino, Y., Kawanabe, T., Fujii, S., Yoshida, T.: Divergence of RNA editing among Arabidopsis species. **Plant Science** 280, 241-247 (2019)
- *21. Tomoaki Sakamoto, Seisuke Kimura: Plant Temperature Sensors. (Review) **sensors** 18 (2018)
- *22. Kaoru Okamoto Yoshiyama, Seisuke Kimura: Ser-Gln sites of SOG1 are rapidly hyperphosphorylated in response to DNA double-strand breaks. **Plant Signaling and Behavior** 13: e1477904 (2018)
- *23. Hokuto Nakayama, Tomoaki Sakamoto, Yuki Okegawa, Kaori Kaminoyama, Manabu Fujie, Yasunori Ichihashi, Tetsuya Kurata, Ken Motohashi, Ihsan Al-Shehbaz, Neelima Sinha, Seisuke Kimura: Comparative transcriptomics with self-organizing map reveals cryptic photosynthetic differences between two accessions in North American Lake cress. **Scientific Reports** 8: 3302 (2018)
- *24. Naoyuki Uchida, Koji Takahashi, Rie Iwasaki, Ryotaro Yamada, Masahiko Yoshimura, Takaho A. Endo, Seisuke Kimura, Hua Zhang, Mika Nomoto, Yasuomi Tada, Toshinori Kinoshita, Kenichiro Itami, Shinya Hagihara, Keiko U. Tori: Chemical hijacking of auxin signaling with an engineered auxin-TIR1 pair. **Nature Chemical Biology** 14: 299-305 (2018)
25. T Ikeda, W Tanaka, T Toriba, C Suzuki, A Maeno, K Tsuda, T Shiroishi, T Kurata, T Sakamoto, M Murai, H Matsusaka, T Kumamaru and HY Hirano. *BELLI*-like homeobox genes regulate inflorescence architecture and meristem maintenance in rice. **Plant J** , 2019, 10.1111/tbj.14230.

法人番号	261003
プロジェクト番号	S1511023

- *26. N Ogita, Y Okushima, M Tokizawa, YY Yamamoto, M Tanaka, M Seki, Y Makita, M Matsui, K Okamoto-Yoshiyama, T Sakamoto, T Kurata, K Hiruma, Y Saijo, N Takahashi and M Umeda. Identifying the target genes of SUPPRESSOR OF GAMMA RESPONSE 1, a master transcription factor controlling DNA damage response in *Arabidopsis*. **Plant J** 94: 439-453, 2018, 10.1111/tpj.13866.
27. S Tanabashi, K Shoda, C Saito, T Sakamoto, T Kurata, T Uemura and A Nakano. A Missense Mutation in the *NSF* Gene Causes Abnormal Golgi Morphology in *Arabidopsis thaliana*. **Cell Struct Funct** 43: 41-51, 2018, 10.1247/csf.17026.
28. 桶川友季, 本橋健: チオレドキシシンシステムによる光合成の調節機構 ～変動する光環境で植物はどのようにに効率良く光合成を行っているのか?～, **化学と生物** 56, 452-453 (2018)
29. 本橋健: シームレスクローニング法 ～古典的な制限酵素と DNA リガーゼを用いないクローニング～ **生物工学** 96, 20-24 (2018)
30. Kawabe A, Nukii H, Furihata H (2018) "Exploring the history of chloroplast capture in arabis using whole chloroplast genome sequencing." **International Journal of Molecular Sciences** 19: 602.
31. Masuta Y, Kawabe A, Nozawa K, Naito K, Kato A, Ito H (2018) "Characterization of a heat-activated retrotransposon in *Vigna angularis*." **Breeding Science** 68: 168-176.
32. Kawanabe T, Nukii H, Furihata H, Yoshida T, Kawabe A (2018) "The complete chloroplast genome of *Sisymbrium irio*." **Mitochondrial DNA part B** 3:488-489.
33. Yoshida T, Kawanabe T, Bo Y, Fujimoto R, Kawabe A (2018) "Genome-wide analysis of parent-of-origin allelic expression in endosperms of Brassicaceae species, *Brassica rapa*." **Plant Cell and Physiology** 59: 2590-2601.
34. Yoshida T, Tarutani Y, Kakutani T, Kawabe A (2018) "DNA Methylation Diversification at the Integrated Organellar DNA-Like Sequence." **Genes** 9: E602.
35. Kawabe A, Furihata H, Tsujino Y, Kawanabe T, Fujii S, Yoshida T (2019) "Divergence of RNA editing among *Arabidopsis* species." **Plant Science** 280: 241-247.
36. Yoshida T, Furihata H, To KT, Kakutani T, Kawabe A (2019) "Genome defense against integrated organellar DNA fragments from plastids into plant nuclear genomes through DNA methylation." **Scientific Reports** 9: 2060.
37. M. Tsujimura, T. Kaneko, T. Sakamoto, S. Kimura, M. Shigyo, H. Yamagishi, T. Terachi, Multichromosomal structure of the onion mitochondrial genome and a transcript analysis., **Mitochondrion**. 2018. S1567-7249(18)30091-6.
38. H. Yamaya-Ito, Y. Shimoda, T. Hakoyama, S. Sato, T. Kaneko, M. S. Hossain, S. Shibata, M. Kawaguchi, M. Hayashi, H. Kouchi, Y. Umehara, Loss-of-function of ASPARTIC PEPTIDASE NODULE-INDUCED 1 (APN1) in *Lotus japonicus* restricts efficient nitrogen-fixing symbiosis with specific *Mesorhizobium loti* strains., **Plant J**. 2018. 93, 5-16.
- *39. Kaoru Okamoto Yoshiyama, Kaori Kaminoyama, Tomoaki Sakamoto, Seisuke Kimura: Increased phosphorylation of Ser-Gln sites on SUPPRESSOR OF GAMMA RESPONSE1 strengthens the DNA damage response in *Arabidopsis thaliana*. **The Plant Cell** 29: 3255-3268 (2017)
- *40. Akiko Nakamasu, Nobuhiko J. Suematsu, Seisuke Kimura: Asymmetries in leaf branch are associated with differential speeds along growth axes: A theoretical prediction. **Developmental Dynamics** 246: 981-991 (2017)
- *41. Hokuto Nakayama, Neelima Sinha, Seisuke Kimura: How Do Plants and Phytohormones Accomplish Heterophylly, Leaf Phenotypic Plasticity, in Response to Environmental Cues. **Frontiers in Plant Science** 8: 1717 (2017)
42. Yaichi Kawakatsu, Hokuto Nakayama, Kaori Kaminoyama, Kaori Igarashi, Masaki Yasugi, Hiroshi Kudoh, Atsushi J. Nagano, Kentaro Yano, Nakao Kubo, Seisuke Kimura: A *GLABRA1* ortholog on LG A9 controls trichome number in the Japanese leafy vegetables Mizuna and Mibuna (*Brassica rapa* subsp. *Nipposinica* L. H. Bailey): evidence from QTL analysis. **Journal of Plant Research** 130: 539-550 (2017)

法人番号	261003
プロジェクト番号	S1511023

43. Tokizawa M, Kusunoki K, Koyama H, Kurotani A, Sakurai T, Suzuki Y, Sakamoto T, Kurata T, Yamamoto YY. Identification of Arabidopsis genic and non-genic promoters by paired-end sequencing of TSS tags. *Plant J.* **90**: 587-605 (2017)
44. Toshiaki Tameshige, Shuka Ikematsu, Keiko U. Torii and Naoyuki Uchida : Stem development through vascular tissues: EPFL-ERECTA family signaling that bounces in and out of phloem. *Journal of Experimental Botany* **68**: 45-53 (2017)
45. Shuka Ikematsu, Masao Tasaka, Keiko U. Torii and Naoyuki Uchida : *ERECTA*-family receptor kinase genes redundantly prevent premature progression of secondary growth in the *Arabidopsis* hypocotyl. *New Phytologist* **213**: 1697-1709 (2017)
46. M. Sugawara, T. Tsukui, T. Kaneko, Y. Ohtsubo, S. Sato, Y. Nagata, M. Tsuda, H. Mitsui, K. Minamisawa, Complete genome sequence of *Bradyrhizobium diazoefficiens* USDA 122, a nitrogen-fixing soybean symbiont., *Genome Announc.* **5**, e01743-16 (2017)
47. Y. Saeki, M. Nakamura, M. L. T. Mason, T. Yano, S. Shiro, R. Sameshima-Saito, M. Itakura, K. Minamisawa, A. Yamamoto. Effect of flooding and the *nosZ* gene in bradyrhizobia on bradyrhizobial community structure in the soil., *Microbes Environ.* **32**, 154-163 (2017)
48. Masayuki Sugawara, Takahiro Tsukui, Takakazu Kaneko, Yoshiyuki Ohtsubo, Shusei Sato, Yuji Nagata, Masataka Tsuda, Hisayuki Mitsui and Kiwamu Minamisawa: Complete Genome Sequence of *Bradyrhizobium diazoefficiens* USDA 122, a Nitrogen-Fixing Soybean Symbiont. *Genome Announc.* **5**: e01743-16 (2017)
49. Ken Motohashi: Evaluation of the efficiency and utility of recombinant enzyme-free seamless DNA cloning methods. *Biochem. Biophys. Rep.* **9**, 310-315 (2017)
50. Ken Motohashi: Seamless ligation cloning extract (SLiCE) method using cell lysates from laboratory *Escherichia coli* strains and its application to SLiP site-directed mutagenesis. *Methods Mol. Biol.* **1498**, 349-357 (2017)
51. Yoshida T, Furihata H, Kawabe: Analysis of nuclear mitochondrial DNAs and the factors affecting patterns of integration in plant species. *Genes and Genetic Systems* **92**: 27-32 (2017)
52. Nozawa K, Kawagishi Y, Kawabe A, Sato M, Masuta Y, Kato A, Ito H: Epigenetic Regulation of Heat-Activated Retrotransposon in Cruciferous Vegetables. *Epigenomes* **1**: 7 (2017)
53. Hosaka A, Saito R, Takashima K, Sasaki T, Fu Y, Kawabe A, Ito T, Toyoda A, Fujiyama A, Tarutani Y, Kakutani T: Evolution of sequence-specific anti-silencing systems in Arabidopsis. *Nature Communications* **8**: 2161 (2017)
54. Kawamura K, Shimizu M, Kawanabe T, Pu Z, Kodama T, Kaji M, Osabe K, Fujimoto R, Okazaki K: Assessment of DNA markers for seed contamination testing and selection of disease resistance in cabbage. *Euphytica* **213**: 28 (2017)
55. S. Masuda, K. Nozawa, W. Matsunaga, Y. Masuda, A. Kawabe, A. Kato, H. Ito: Characterization of a heat-activated retrotransposon in natural accessions of Arabidopsis thaliana. *Genes Genet. Syst.*, **91**, 293-299 (2017)
- *56. 坂本智昭、木村成介、*Rorippa aquatica* 遺伝子情報データベースの構築、*京都産業大学総合学術研究所報* **11**: 105-113 (2016).
- *57. 天野瑠美、中山北斗、木村成介、アブラナ科植物 *Rorippa aquatica* にみられる葉断面からの栄養繁殖条件の検討、*京都産業大学総合学術研究所報* **11**: 115-121 (2016).
58. 木村成介、川勝弥一、水菜と壬生菜の来歴について -文献と遺伝子から探る葉形変化の歴史-、*京都産業大学論集人文科学系列* **49**: 161-181 (2016).
59. Qingqing Cai, Hiroko Fukushima, Mai Yamamoto, Nami Ishii, Tomoaki Sakamoto, Tetsuya Kurata, Hiroyasu Motose and Taku Takahashi: The SAC51 Family Plays a Central Role in Thermospermine Responses in *Arabidopsis*. *Plant Cell Physiol* **57**: 1583-1592 (2016).
60. Shota Yamauchi, Atsushi Takemiya, Tomoaki Sakamoto, Tetsuya Kurata, Toshifumi Tsutsumi, Toshinori Kinoshita and Ken-ichiro Shimazaki: The Plasma Membrane H⁺-ATPase AHA1 Plays a Major Role in Stomatal Opening in Response to Blue Light. *Plant Physiol* **171**: 2731-2743 (2016).
61. Asuka Higo, Masaki Niwa, Katsuyuki T Yamato, Lixy Yamada, Hitoshi Sawada, Tomoaki

法人番号	261003
プロジェクト番号	S1511023

- Sakamoto, Tetsuya Kurata, Makoto Shirakawa, Motomu Endo, Shuji Shigenobu, Katsushi Yamaguchi, Kimitsune Ishizaki, Ryuichi Nishihama, Takayuki Kohchi and Takashi Araki: Transcriptional Framework of Male Gametogenesis in the Liverwort *Marchantia polymorpha* L. *Plant Cell Physiol* **57**: 325-338 (2016).
- *62. K. O. Yoshiyama, SOG1: a master regulator of the DNA damage response in plants. *Genes & Genetic Systems* **90**: 209-216 (2016) (総説)
- *63. K. O. Yoshiyama, Recent progress in research on DNA damage responses in animals and plants. *Genes & Genetic Systems* **90**: 185-186 (2016) (総説)
- *64. Alma Balestrazzi, Mohan M. Achary, Anca Macovei, Kaoru O. Yoshiyama, Ayako Sakamoto, Maintenance of genome integrity: DNA damage sensing, signaling, repair and replication in plants, *Frontiers in physiology* (2016) (著書)
65. Sachiko Masuda, Masaki Saito, Chiaki Sugawara, Manabu Itakura, Shima Eda, and Kiwamu Minamisawa: Identification of the hydrogen uptake gene cluster for chemolithoautotrophic growth and symbiosis hydrogen uptake in *Bradyrhizobium diazoefficiens*. *Microbes Environ.* **31**: 76-78 (2016)
66. Tomoyuki Minami, Misue Anda, Hisayuki Mitsui, Masayuki Sugawara, Takakazu Kaneko, Shusei Sato, Seishi Ikeda, Takashi Okubo, Hirohito Tsurumaru, Kiwamu Minamisawa: Metagenomic Analysis Revealed Methylamine and Ureide Utilization of Soybean-Associated Methylobacterium. *Microbes Environ.* **31**: 268-278 (2016)
67. 本橋健: 精製酵素をいっさい使わない"超低コスト"シームレスクローニング 実験医学 **34**, 2349-2354 (2016)
68. Y. Okegawa, K. Motohashi: Expression of spinach ferredoxin-thioredoxin reductase using tandem T7 promoters and application of the purified protein for *in vitro* light-dependent thioredoxin-reduction system. *Protein Expr. Purif.* **121**, 46-51(2016)
69. Y. Okegawa¹, M. Koshino¹, T. Okushima, K. Motohashi: Application of preparative disk gel electrophoresis for antigen purification from inclusion bodies. *Protein Expr. Purif.* **118**, 77-82 (2016) ¹These authors contributed equally to this work.
70. A. Kosugi, C. Nishizawa, A. Kawabe, E. Harada: Zinc accumulation and vegetation ecology in the allotetraploid, *Arabidopsis kamchatica* ssp. *kawasakiana*. *Plant Biotechnology* **33**, 33-37 (2016)
71. HY. Furihata, K. Suenaga, T. Kawanabe, T. Yoshida, A. Kawabe: Gene duplication, silencing and expression alteration govern the molecular evolution of PRC2 genes in plants. *Genes Genet. Syst.* **91**, 85-95 (2016)
72. T. Kawanabe, K. Osabe, E. Itabashi, K. Okazaki, ES. Dennis, R. Fujimoto: Development of primer sets that can verify the enrichment of histone modifications, and their application to examining vernalization-mediated chromatin changes in *Brassica rapa* L. *Genes Genet. Syst.* **91**,1-10 (2016)
73. K. Tonosaki, K. Osabe, T. Kawanabe, R. Fujimoto: The importance of reproductive barriers and the effect of allopolyploidization on crop breeding. *Breed Sci.* **66**, 333-349 (2016)
74. T. Kawanabe, S. Ishikura, N. Miyaji, T. Sasaki, LM. Wu, E. Itabashi, S. Takada, M. Shimizu, T. Takasaki-Yasuda, K. Osabe, WJ. Peacock, ES. Dennis, R. Fujimoto: Role of DNA methylation in hybrid vigor in *Arabidopsis thaliana*. *Proc Natl Acad Sci U S A.* **113**, E6704-E6711 (2016)
75. N. Saeki, T. Kawanabe, H. Ying, M. Shimizu, M. Kojima, H. Abe, K. Okazaki, M. Kaji, JM. Taylor, H. Sakakibara, WJ. Peacock, ES. Dennis, R. Fujimoto: Molecular and cellular characteristics of hybrid vigour in a commercial hybrid of Chinese cabbage. *BMC Plant Biol.* **16**, 45 (2016)
76. Kawamura K†, Kawanabe T†, Shimizu M, Nagano AJ, Natsumi Saeki N, Okazaki K, Kaji M, S. Dennis ES, Osabe K, Fujimoto R.: Genetic distance of inbred lines of Chinese cabbage and its relationship to heterosis. *Plant Gene* 2016 5:1-7. doi:10.1016/j.plgene.2015.10.003. († Contributed equally) †
77. 小杉亜希・高倉耕一・野間直彦・河邊昭・原田英美子「絶滅危惧種タチスズシロソウ (*Arabidopsis*

法人番号	261003
プロジェクト番号	S1511023

- kamchatica* ssp. *kawasakiana*) 個体群の個体数推定」*地域自然史と保全* 38: 51-59 (2016).
- *78. Hokuto Nakayama and Seisuke Kimura: Leaves may function as temperature sensors in the heterophylly of *Rorippa aquatica* (Brassicaceae). *Plant Signaling and Behavior* 10: e1091909 (2015)
- *79. Rumi Amano, Hokuto Nakayama, Yurika Morohoshi, Yaichi Kawakatsu, Ali Ferjani, and Seisuke Kimura: A Decrease in ambient temperature induces post-mitotic enlargement of palisade cells in North American Lake-Cress. *PLOS ONE* 10: e0141247 (2015)
- *80. Hokuto Nakayama, Kensuke Kawade, Hirokazu Tsukaya, and Seisuke Kimura: Detection of the cell proliferation zone in leaves by using EdU. *Bio-protocol* 5: e1600 (2015)
81. José Antonio Aguilar-Martinez, Naoyuki Uchida, Brad Townsley, Donnelly Ann West, Andrea Yanez, Nafeesa Lynn, Seisuke Kimura, Neelima Sinha: Transcriptional, post-transcriptional and post-translational regulation of *SHOOT MERISTEMLESS* gene expression in Arabidopsis determines gene function in shoot apex. *Plant Physiology* 167: 424-442 (2015)
82. Daisuke Ikeue, Christian Schudoma, Wenna Zhang, Yoshiyuki Ogata, Tomoaki Sakamoto, Tetsuya Kurata, Takeshi Furuhashi, Friedrich Kragler and Koh Aoki: A bioinformatics approach to distinguish plant parasite and host transcriptomes in interface tissue by classifying RNA-Seq reads. *Plant Methods* 11:34,(2015)
83. Mitsutomo Abe, Hidetak Kaya, Ayako Watanabe-Taneda, Mio Shibuta, Ayako Yamaguchi, Tomoaki Sakamoto, Tetsuya Kurata, Israel Ausin, Takashi Araki and Carlos Alonso-Blanco: FE, a phloem-specific Myb-related protein, promotes flowering through transcriptional activation of *FLOWERING LOCUS T* and *FLOWERING LOCUS T INTERACTING PROTEIN 1*. *Plant J* 83:1059-1068,(2015)
84. Kim L Johnson, Sascha Ramm, Christian Kappel, Sally Ward, Leyser Leyser, Tomoaki Sakamoto, Tetsuya Kurata, Michael W Bevan and Michael Lenhard: The *Tinkerbelle* (*Tink*) Mutation Identifies the Dual-Specificity MAPK Phosphatase *INDOLE-3-BUTYRIC ACID-RESPONSE5* (*IBR5*) as a Novel Regulator of Organ Size in Arabidopsis. *PLoS One* 10:e0131103,(2015)
85. Kaoru Kawafune, Yuichi Hongoh, Takashi Hamaji, Tomoaki Sakamoto, Tetsuya Kurata, Shunsuke Hirooka, Shin-ya Miyagishima and Hisayoshi Nozaki: Two Different Rickettsial Bacteria Invading *Volvox carteri*. *PLoS One* 10:e0116192,(2015)
86. Shojiro Tamaki, Hiroyuki Tsuji, Ayana Matsumoto, Akiko Fujita, Zenpei Shimatani, Rie Terada, Tomoaki Sakamoto, Tetsuya Kurata and Ko Shimamoto: FT-like proteins induce transposon silencing in the shoot apex during floral induction in rice. *Proc Natl Acad Sci U S A* 112(8):E901-10, (2015)
87. Y.Hirose, K.Suda, Y.-G.Liu, S.Sato, Y.Nakamura, K.Yokoyama, N.Yamamoto, S.Hanano, E.Takita, N.Sakurai, H.Suzuki, Y.Nakamura, T.Kaneko, K.Yano, S.Tabata, D.Shibata: The Arabidopsis TAC Position Viewer: A high-resolution map of transformation-competent artificial chromosome (TAC) clones aligned with the *Arabidopsis thaliana* Columbia-0 genome. *Plant Journal*, 83: 1114-1122 (2015)
88. O.M.Faruque, H.Miwa, M.Yasuda, Y.Fujii, T.Kaneko, S.Sato, S.Okazaki: Identification of *Bradyrhizobium elkanii* genes involved in incompatibility with soybean plants carrying the *Rj4* allele. *Applied and Environmental Microbiology*, 81: 6710-6717 (2015)
89. Y. Okegawa, K. Motohashi: Chloroplastic thioredoxin m functions as a major regulator of Calvin cycle enzymes during photosynthesis *in vivo*. *Plant J*, 84, 900-913 (2015)
90. Y. Okegawa, K. Motohashi: A simple and ultra-low cost homemade seamless ligation cloning extract (SLiCE) as an alternative to a commercially available seamless DNA cloning kit. *Biochem. Biophys. Rep.* 4, 148-151 (2015)
91. Y. Okegawa, K. Motohashi: Evaluation of seamless ligation cloning extract (SLiCE) preparation methods from an *Escherichia coli* laboratory strain. *Anal. Biochem.* 486, 51-53 (2015)
92. K. Motohashi: A simple and efficient seamless DNA cloning method using SLiCE from *Escherichia coli* laboratory strains and its application to SLiP site-directed mutagenesis. *BMC*

法人番号	261003
プロジェクト番号	S1511023

Biotechnol. 15, 47 (2015)

93. Kosugi A, Tamaru J, Gotou K, Furihata H, Shimizu A, Kawabe A, Harada E. Metal accumulation by *Arabidopsis halleri* subsp. *gemmaifera* at a limestone mining site. *Aust. J. Botany* 63: 134-140 (2015).
94. Genetic characterization of inbred lines of Chinese cabbage by DNA markers; towards the application of DNA markers to breeding of F₁ hybrid cultivars. Kawamura K†, Kawanabe T†, Shimizu M, Okazaki K, Kaji M, Dennis ES, Osabe K, Fujimoto R. *Data Brief*. 2015 11(6):229-237. doi: 10.1016/j.dib.2015.11.058. (†Contributed equally)

<図書>

該当なし)

<学会発表>

学内研究者の業績のみ掲載

- *1. アブラナ科 *Rorippa aquatica* にみられる傷害誘導性の再生メカニズムの解析、天野瑠美、桃井理沙、小俣恵美、中原大河、池松朱夏、坂本智昭、木村成介、第 61 回日本植物生理学会年会、大阪大学吹田キャンパス(大阪府吹田市)、2020 年 3 月 19 日-3 月 21 日(口頭)
- *2. Ab-GALFA 法を用いたヌルデの虫こぶ形成機構の解明、中山拓己、斉藤悠馬、大島一正、鈴木義人、木村成介、松浦恭和、池田陽子、武田征士、平野朋子、佐藤雅彦、第 61 回日本植物生理学会年会、大阪大学吹田キャンパス(大阪府吹田市)、2020 年 3 月 19 日-3 月 21 日(口頭)
- *3. 水陸両生アブラナ科植物 *Rorippa aquatica* の水没に応答した迅速な気孔形成抑制のメカニズム、池松朱夏、馬瀬樹志、野口楓子、坂本智昭、木村成介、第 61 回日本植物生理学会年会、大阪大学吹田キャンパス(大阪府吹田市)、2020 年 3 月 19 日-3 月 21 日(口頭)
- *4. *Rorippa aquatica* の栄養繁殖におけるシュート再生機構の解析、小俣恵美、天野瑠美、池松朱夏、桃井理沙、坂本智昭、木村成介、第 61 回日本植物生理学会年会、大阪大学吹田キャンパス(大阪府吹田市)、2020 年 3 月 19 日-3 月 21 日(ポスター)
5. シロイヌナズナのトマト斑葉細菌病菌に対する耐病性を亢進する、及びジャスモン酸の蓄積を更新する新規植物免疫活性化剤候補化合物群の作用機構の解析、中野正貴、安江啓人、舟橋汰樹、山崎逸平、斉藤優歩、北畑信隆、石賀貴子、石賀康博、安部洋、木村成介、諸橋賢吾、浅見忠男、朽津和幸、第 61 回日本植物生理学会年会、大阪大学吹田キャンパス(大阪府吹田市)、2020 年 3 月 19 日-3 月 21 日(ポスター)
- *6. *Rorippa aquatica* 染色体レベルゲノムアセンブリと比較解析、坂本智昭、坂本卓也、松永幸大、木村成介、第 61 回日本植物生理学会年会、大阪大学吹田キャンパス(大阪府吹田市)、2020 年 3 月 19 日-3 月 21 日(ポスター)
- *7. *Rorippa aquatica* の再生の研究、木村成介、新学術研究領域植物多能性幹細胞グループミーティング(柿本班、岩瀬班、吉田班、木村班)、大阪大学豊中キャンパス、2019 年 12 月 17 日(口頭)
- *8. (招待講演) 環境に応じて変身する植物:*Rorippa aquatica* の異形葉性の研究、木村成介、第 57 回植物バイテクシンポジウム「変身する生き物、変身させる生き物」、京都産業大学(京都府)、2019 年 12 月 13 日(口頭)
- *9. (招待講演) 水中への適応形質としての異形葉性と栄養繁殖:非モデル植物のオミクス解析、木村成介、バイオインフォマティクス教育セミナー2019、東京理科大学野田キャンパス(千葉県)、2019 年 12 月 9 日(口頭)
10. 細胞脱落における細胞接着の動態の解析、梶田春奈、服部和泉、中井彩香、村田真智子、木村成介、川根公樹、第 42 回日本分子生物学会年会、福岡国際会議場(福岡県)、2019 年 12 月 3 日~6 日(ポスター)
- *11. Chromosome level genome assembly of palaeopolyploid plant *Rorippa aquatica*, Tomoaki Sakamoto, Takuya Sakamoto, Sachihiro Matsunaga, Seisuke Kimura, *Frontiers in plant environmental response research: local signaling, long-distance communication and memory for developmental plasticity*, Noyori Conference Hall, Nagoya University, Nagoya-shi, Aichi, Nov. 18-19, 2019 (Poster)
- *12. Developmental analysis of the origin of cauline leaf propagules for vegetative reproduction of *Rorippa aquatica*, Shuka Ikematsu, Ami Sasaki, Rumi Amano, Tomoaki Sakamoto, Seisuke Kimura, *Frontiers in plant*

法人番号	261003
プロジェクト番号	S1511023

- environmental response research: local signaling, long-distance communication and memory for developmental plasticity, Noyori Conference Hall, Nagoya University, Nagoya-shi, Aichi, Nov. 18-19, 2019 (Poster)
- *13. The suppression mechanism of stomatal development under submerged condition in *Rorippa aquatica*, Tatsushi Umase, Fuko Noguchi, Shuka Ikematsu, Tomoaki Sakamoto, Seisuke Kimura, Frontiers in plant environmental response research: local signaling, long-distance communication and memory for developmental plasticity, Noyori Conference Hall, Nagoya University, Nagoya-shi, Aichi, Nov. 18-19, 2019 (Poster)
- *14. Developmental and molecular studies on wound-induced regeneration of *Rorippa aquatica*, Rumi Amano, Hokuto Nakayama, Risa Momoi, Shizuka Gunji, Yumiko Takebayashi, Shuka Ikematsu, Tomoaki Sakamoto, Hiroyuki Kasahara, Ali Ferjani, Seisuke Kimura, Frontiers in plant environmental response research: local signaling, long-distance communication and memory for developmental plasticity, Noyori Conference Hall, Nagoya University, Nagoya-shi, Aichi, Nov. 18-19, 2019 (Poster)
- *15. Discovery of a novel meristematic organ on the cauline leaf for natural vegetative reproduction of *Rorippa aquatica*, Shuka Ikematsu, Ami Sasaki, Rumi Amano, Tomoaki Sakamoto, Seisuke Kimura, 新学術領域研究「植物多能性幹細胞」第3回若手の会、熱海ニューフジヤホテル(静岡県熱海市)2019年10月28日～30日(口頭)(英語)
- *16. Effect of environmental condition on the efficiency of vegetative propagation of *Rorippa aquatica*, 天野瑠美、小俣恵美、中原大河、池松朱夏、坂本智昭、木村成介、新学術領域研究「環境記憶統合」第5回若手の会、御殿場高原ホテル(静岡県御殿場市)2019年9月25日～27日(ポスター)(優秀発表賞)
- *17. Discovery of a novel meristematic organ on the cauline leaf for natural vegetative reproduction of *Rorippa aquatica*, Shuka Ikematsu, Ami Sasaki, Rumi Amano, Tomoaki Sakamoto, Seisuke Kimura, 新学術領域研究「環境記憶統合」第5回若手の会、御殿場高原ホテル(静岡県御殿場市)2019年9月25日～27日(ポスター)
- *18. アブラナ科植物 *Rorippa aquatica* の茎生葉上の新奇分裂組織を用いた栄養繁殖、池松朱夏、佐々木亜美、坂本智昭、木村成介、日本植物学会第83回大会、東北大学川内北キャンパス(宮城県仙台市)、2019年9月15日～17日(口頭)
19. 京野菜であるミズナとミズナノ葉の形の解析および育種の歴史の解明、川勝弥一、坂本智昭、中山北斗、上ノ山華織、矢野健太郎、久保中央、木村成介、日本植物学会第83回大会、東北大学川内北キャンパス(宮城県仙台市)、2019年9月15日～17日(口頭)
- *20. アブラナ科 *Rorippa aquatica* にみられる傷害誘導性の再生機構の解析、天野瑠美、中山北斗、桃井理沙、小俣恵美、池松朱夏、坂本智昭、木村成介、日本植物学会第83回大会、東北大学川内北キャンパス(宮城県仙台市)、2019年9月15日～17日(口頭)
- *21. 水陸両生植物 *Rorippa aquatica* における水没に応答した気孔形成抑制メカニズムの解析、馬瀬樹志、野口楓子、池松朱夏、坂本智昭、木村成介、日本植物学会第83回大会、東北大学川内北キャンパス(宮城県仙台市)、2019年9月15日～17日(ポスター)
- *22. 古倍数性アブラナ科植物 *Rorippa aquatica* の染色体レベルゲノムアセンブリ、坂本智昭、坂本卓也、松永幸大、木村成介、日本植物学会第83回大会、東北大学川内北キャンパス(宮城県仙台市)、2019年9月15日～17日(ポスター)
- *23. *Rorippa aquatica* の栄養繁殖に見られるサイトカイニン応答、小俣恵美、天野瑠美、桃井理沙、池松朱夏、榊原均、木村成介、日本植物学会第83回大会、東北大学川内北キャンパス(宮城県仙台市)、2019年9月15日～17日(ポスター)
- *24. アブラナ科 *Rorippa aquatica* の栄養繁殖に影響を及ぼす要因、天野瑠美、小俣恵美、中原大河、池松朱夏、坂本智昭、木村成介、日本植物形態学会第31回大会、東北大学川内北キャンパス(宮城県仙台市)、2019年9月14日(ポスター)
- *25. Comprehensive transcriptome analyses of galls from four different host plants suggest common process for gall development, Seiji Takeda, Makiko Yoza, Taisuke Amano, Issei Oshima, Tomoko Hirano, Masa H. Sato, Tomoaki Sakamoto, Seisuke Kimura, The 5th Joint Symposium on “Basic and Applied Studies of Plant Natural Products for Agriculture and Human Health”, Thaksin University, Songkhla, Thailand, Sep 12, 2019 (oral)
26. Molecular mechanism of corolla elongation in Japanese morning glory, A. Shimoki, K. Ohasi, M. Toda, T. Sakamoto, S. Kimura, T. Seiji, The 5th Joint Symposium on “Basic and Applied Studies of Plant Natural

法人番号	261003
プロジェクト番号	S1511023

- Products for Agriculture and Human Health“, Thaksin University, Songkhla, Thailand, Sep 12, 2019 (oral)
27. Classification of Southeast Asian mints based on DNA markers and search for genes involved in biosynthesis of aromatic compounds, Y. Fukui, M. Saito, N. Nakamura, S. Okamoto, S. Sato, T. Sakamoto, S. Kimura, Y. Nakamura, N. Kubo, The 5 th Joint Symposium on “Basic and Applied Studies of Plant Natural Products for Agriculture and Human Health“, Thaksin University, Songkhla, Thailand, Sep 12, 2019 (oral)
28. 東南アジアのミントの SSR マーカーによる系統解析と機能性香気成分ピペリテノンオキサイドの生合成に関わる遺伝子の探索、福井友梨、齊藤萌子、中村夏野、岡本繁久、佐藤修一、坂本智昭、木村成介、中村考志、久保中央、第 37 回日本植物細胞分子生物学会、京都府立大学(京都府京都市)、2019 年 9 月 7 日～8 日(ポスター)
29. Defining codon-mediated mRNA decay and No-go decay in zebrafish embryos, Yuichiro Mishima, Seisuke Kimura, Shintaro Iwasaki, EMBO WORKSHOP: Protein Synthesis and Translational Control, EMBL Heidelberg (Heidelberg, Germany), Sep 4-7, 2019 (poster)
- *30. (招待講演) アブラナ科植物 *Rorippa aquatica* の水中適応に伴う、茎生葉上の新奇分裂組織を用いた栄養繁殖、池松朱夏、佐々木亜美、坂本智昭、木村成介、日本育種学会第 136 回講演会ワークショップ「植物の生殖と環境・ストレス」、近畿大学奈良キャンパス(奈良県奈良市)、2019 年 9 月 6 日(口頭)
- *31. RNA-seq を用いたゴール形成種-非形成種間での転写産物の比較、天野泰輔、Antoine Guiguet、濱谷昭寿、坂本 智昭、木村成介、大島一正、日本進化学会第 21 回大会、北海道大学(北海道札幌市)、2019 年 8 月 7 日～10 日(ポスター)(学生ポスター賞優秀賞)
32. (招待講演) 遺伝子と文献から探る水菜と壬生菜の歴史、川勝弥一、坂本智昭、木村成介、東京理科大学研究推進機構総合研究院アグリ・バイオ工学研究部門公開シンポジウム、東京理科大学葛飾キャンパス(東京都葛飾区)、2019 年 7 月 25 日(口頭)
33. ROS 生成・耐病性・トランスクリプトーム解析に基づく新規植物免疫活性化化合物の作用機構の解析、中野正貴、北畑信隆、安江啓人、石賀貴子、石賀康博、木村成介、諸橋賢吾、浅見忠雄、朽津和幸、東京理科大学研究推進機構総合研究院アグリ・バイオ工学研究部門公開シンポジウム、東京理科大学葛飾キャンパス(東京都葛飾区)、2019 年 7 月 25 日(ポスター)
34. Differential gene expression analysis of *Arabidopsis* seedlings reveals potential involvement of 2-phnylacetic acid in hormone crosstalk, Sam Cook, Seisuke Kimura, Hiroyuki Kasahara, The 23rd International Conference on Plant Growth Substances, University Paris-Descartes (Paris, France) June 25-29, 2019 (poster)
- *35. Discovery of a novel meristematic organ on the cauline leaf for natural vegetative reproduction of *Rorippa aquatica*, Shuka Ikematsu, Ami Sasaki, Rumi Amano, Tomoaki Sakamoto, Seisuke Kimura, International Symposium: Principles of pluripotent stem cells underlying plant vitality, Katahira Campus, Tohoku University (Sendai, Japan), May 11-14, 2019 (poster)
- *36. Effect of SOG1 overexpression on DNA damage response in meristematic tissue, Kaoru Okamoto Yoshiyama, Naoki Aoshima, Naoki Takahashi, Tomoaki Sakamoto, Masaaki Umeda, Seisuke Kimura, International Symposium: Principles of pluripotent stem cells underlying plant vitality, Katahira Campus, Tohoku University (Sendai, Japan), May 11-14, 2019 (poster)
- *37. The relationship between phytohormone and plant regeneration in nature in North American lake cress (*Rorippa aquatica*), Rumi Amano, Hokuto Nakayama, Risa Momoi, Emi Omata, Shizuka Gunji, Yumiko Takebayashi, Tomoaki Sakamoto, Hiroyuki Kasahara, Ali Ferjani, Seisuke Kimura, International Symposium: Principles of pluripotent stem cells underlying plant vitality, Katahira Campus, Tohoku University (Sendai, Japan), May 11-14, 2019 (poster)
38. Manabu Itakura, Kosuke Mitsuya, Takakazu Kaneko, Kiwamu Minamisawa: Investigation of genomic diversity and nitrogen fixation capability in indigenous *Bradyrhizobium diazoefficiens* strains, 5th Asian Conference on Plant-Microbe Symbiosis & Nitrogen Fixation, Tohoku University, Sendai, 2019.5.15-5.17
- *39. 板倉学、石塚裕樹、木村成介、上ノ山華織、金子貴一: *Rorippa aquatica* における異形葉性誘導に伴う共生細菌叢の変動、植物微生物研究会第 29 回研究交流会、サンポートホール高松、高松市、2019.9.18-9.20
40. 蒲生雄大、板倉学、榊原渉平、大谷真由、瀧井悠斗、匡紹敏、南澤究、金子貴一: *Bradyrhizobium elkanii* 系統で保存されたゲノミックアイランド: GI02 の比較解析、植物微生物研究会第 29 回研究交流会、サンポートホール高松、高松市、2018.9.19-9.20
41. 板倉学、金子貴一、三屋公佑、南澤究: *Bradyrhizobium diazoefficiens* USDA110 系統におけるゲノム構造変化と共生窒素固定能力、第 14 回日本ゲノム微生物学会年会、ウイングあいち、名古屋市、

法人番号	261003
プロジェクト番号	S1511023

2020.3.6-3.8

42. NAD-ME 型 C4 植物シコクビエの維管束鞘葉緑体における Rubisco とデンブンの対極的な偏在: 千田啓貴、大井崇生、本橋健、桶川友季、厚沢季美江、金子康子、谷口光隆、日本作物学会 第 249 回講演会、農林水産技術会議事務局筑波産学連携支援センター本館、2020 年 3 月 26 日～27日(口頭発表)
43. シロイヌナズナのチオレドキシシン m4(Trx m4)は PGR5/PGRL1 依存の光化学系 I サイクリック電子伝達を制御する: 桶川友季、本橋健、第 61 回日本植物生理学会年会、大阪大学吹田キャンパス、2020 年 3 月 19 日～21 日 (口頭発表)
44. 葉緑体 ATP 合成酵素の還元機構の解明: 関口 敬俊、吉田 啓亮、桶川友季、本橋健、若林 憲一、久堀 徹、第 61 回日本植物生理学会年会、大阪大学吹田キャンパス、2020 年 3 月 19 日～21 日 (口頭発表)
45. (招待講演) Regulation of PSI cyclic electron transport by the m-type thioredoxin: Yuki Okegawa, RIIS International Symposium, Photosynthesis Research for the Future, Okayama University, 2019.11.19-20 (Okayama, Japan)
46. The m-type thioredoxin regulates PSI cyclic electron transport: Yuki Okegawa, Ken Motohashi, 日米二国間セミナー、京都・京都市国際交流会館、2019 年 10 月 1 日～3 日 (ポスター発表)
47. 効率の高い PCR クローニング用ベクターの開発とその応用: 本橋健、第 90 回日本生化学会大会、パシフィコ横浜、2019 年 9 月 18 日～20 日 (口頭発表&ポスター発表)
48. PCR クローニング用の効率の良い新規ベクターの開発: 本橋健、第 10 回日本光合成学会年会およびシンポジウム(京都: 京都産業大学むすびわざ館)、2019 年 5 月 25 日～26 日 (ポスター発表)
49. m 型 Trx は PGR5/PGRL1 依存の PSI サイクリック電子伝達経路を制御する: 桶川友季、本橋健、第 10 回日本光合成学会年会およびシンポジウム(京都: 京都産業大学むすびわざ館)、2019 年 5 月 25 日～26 日 (ポスター発表)
50. m 型チオレドキシシンは光化学系 I サイクリック電子伝達を負に制御する: 桶川友季、本橋健、第 60 回日本植物生理学会年会、名古屋大学、2019 年 3 月 13 日～15 日 (口頭発表)
- *51. 水草に見られる水中適応形質の進化、木村成介、植物科学若手研究会 2018、阿蘇草原保全活動センター(熊本県阿蘇市)、2018 年 11 月 18 日～20 日(口頭)
52. Morphological and genetic analysis for revealing petal development of *Habenaria radiata*. Yuhki Nishikawa, Tsutomu Tachibana, Tomoaki Sakamoto, Seisuke Kimura, and Seiji Takeda, The 4 th Joint Symposium on “Basic and Applied Studies of Plant Natural Products for Agriculture and Human Health“, Kagoshima University (Kagoshima, Japan), Nov.8-9, 2018 (oral)
- *53. Molecular mechanism of insect-induced gall development in plants, Seiji Takeda, Makiko Yoza, Gaku Yamazaki, Tomoaki Sakamoto, Seisuke Kimura, and Issei Ohshima, The 4 th Joint Symposium on “Basic and Applied Studies of Plant Natural Products for Agriculture and Human Health“, Kagoshima University (Kagoshima, Japan), Nov.8-9, 2018 (oral)
- *54. *Rorippa aquatica* は茎生葉上の新奇分裂組織を栄養繁殖に用いる、池松朱夏、木村成介、新学術領域研究「植物多能性幹細胞」第 2 回若手ワークショップ、小豆島ふるさと村(香川県、小豆郡)、2018 年 10 月 4 日～6 日(口頭)
- *55. *Rorippa aquatica* を用いた葉の断面からの栄養繁殖機構の解析、天野瑠美、木村成介、新学術領域研究「植物多能性幹細胞」第 2 回若手ワークショップ、小豆島ふるさと村(香川県、小豆郡)、2018 年 10 月 4 日～6 日(口頭)
- *56. Adaptation of plants to aquatic environments: Studies on heterophylly and vegetative propagation in semi-aquatic plant, *Rorippa aquatica*, Seisuke Kimura, Ikematsu Shuka, Tomoaki Sakamoto, Rumi Amano, The 46th Naito Conference on “Mechanisms of Evolution and Biodiversity”, CHÂTERAISÉ Gateaux Kingdom SAPPORO, Japan, Oct.2-5, 2018 (poster)
- *57. 水陸両生植物 *Rorippa aquatica* における水没に応答した気孔形成抑制メカニズムの解析、馬瀬樹志、木村成介、新学術領域研究環境記憶統合第 4 回若手の会、中京大学青木湖セミナーハウスレイクビュー白馬(長野県・大町市)、2018 年 9 月 27 日～29 日(ポスター)
- *58. 異形葉植物 *Rorippa aquatica* の比較ゲノム解析、坂本智昭、木村成介、新学術領域研究環境記憶統合第 4 回若手の会、中京大学青木湖セミナーハウスレイクビュー白馬(長野県・大町市)、2018 年 9 月 27 日～29 日(ポスター)

法人番号	261003
プロジェクト番号	S1511023

- *59. *Rorippa aquatica* の温度に応答した異形葉性の制御メカニズム、池松朱夏、木村成介、新学術領域研究環境記憶統合第 4 回若手の会、中京大学青木湖セミナーハウスレイクビュー白馬(長野県・大町市)、2018 年 9 月 27 日～29 日(口頭)
60. 表現型が異なる *Aegilops mutica* 細胞質置換コムギ 2 系統の葉緑体ゲノムの比較解析、山下健太、辻村真衣、上ノ山華織、木村成介、寺地徹、日本育種学会第 134 回講演会、岡山大学(岡山県岡山市)、2018 年 9 月 22 日～23 日(口頭)
- *61. 植物 DNA 損傷応答のマスターレギュレーター-SOG1 が果たす役割、愿山(岡本)郁、坂本智昭、上ノ山華織、木村成介、日本遺伝学会第 90 回大会、奈良先端科学技術大学院大学(奈良県・生駒市)、2018 年 9 月 19 日～22 日(口頭)
- *62. *Rorippa aquatica* を用いた葉断面からの栄養繁殖機構の解析、天野瑠美、中山北斗、桃井理沙、郡司玄、竹林裕美子、坂本智昭、笠原博幸、Ali Ferjani、木村成介、日本植物学会第 82 回大会、広島国際会議場(広島県広島市)、2018 年 9 月 14 日～16 日(ポスター)
63. サギソウの花形態形成に関する遺伝子発現解析、西川友貴、立花耕、坂本智昭、木村成介、武田征士、日本植物学会第 82 回大会、広島国際会議場(広島県広島市)、2018 年 9 月 14 日～16 日(ポスター)
- *64. 水陸両生植物 *Rorippa aquatica* における水没に応答した気孔形成抑制メカニズムの解析、馬瀬樹志、野口楓子、池松朱夏、坂本智昭、木村成介、日本植物学会第 82 回大会、広島国際会議場(広島県広島市)、2018 年 9 月 14 日～16 日(ポスター)
- *65. 異形葉性植物 *Rorippa aquatica* の比較ゲノム解析、坂本智昭、木村成介、日本植物学会第 82 回大会、広島国際会議場(広島県広島市)、2018 年 9 月 14 日～16 日(ポスター)
66. シロイヌナズナを用いた新規耐病性検定法・トランスクリプトーム解析による、植物免疫活性化化合物の評価、中野正貴、北畑信隆、安江啓人、吉田祐祐実、末次真悠、佐藤静香、来須孝光、石賀貴子、石賀康博、木村成介、諸橋賢吾、浅見忠雄、朽津和幸、日本植物学会第 82 回大会、広島国際会議場(広島県広島市)、2018 年 9 月 14 日～16 日(口頭)
- *67. *Rorippa aquatica* の温度移行に応答した葉形決定メカニズムの解析、池松朱夏、北野つくし、坂本智昭、笠原博幸、木村成介、日本植物学会第 82 回大会、広島国際会議場(広島県広島市)、2018 年 9 月 14 日～16 日(口頭)
68. シロイヌナズナ小胞体品質管理変異株が高温ストレス下で示す花粉成熟異常の解析、西川周一、宇治周平、坂本智昭、山本雅也、杉山智之、木村成介、遠藤斗志也、日本植物学会第 82 回大会、広島国際会議場(広島県広島市)、2018 年 9 月 14 日～16 日(口頭)
69. イネの蒴タペト細胞のプログラム細胞死制御における転写制御ネットワーク・オートファジー・ROS 生成酵素の役割と花粉成熟における意義、澤田隼平、福永任吾、花俣繁、小野聖二郎、木村成介、野々村賢一、来須孝光、朽津和幸、日本植物学会第 82 回大会、広島国際会議場(広島県広島市)、2018 年 9 月 14 日～16 日(口頭)
- *70. *Rorippa aquatica* を用いた葉断面からの栄養繁殖機構の解析、天野瑠美、中山北斗、桃井理沙、郡司玄、竹林裕美子、坂本智昭、笠原博幸、Ali Ferjani、木村成介、日本植物形態学会第 30 回大会、広島県情報プラザ(広島県広島市)、2018 年 9 月 13 日(ポスター)
71. サギソウの複雑な花卉形態を作り上げるメカニズム解明、西川友貴、立花耕、坂本智昭、木村成介、武田征士、第 1 回植物インフォマティクス研究会、明治大学生田キャンパス(神奈川県川崎市)、2018 年 9 月 10 日(ポスター)
72. モデル植物シロイヌナズナを用いた虫こぶ形成機構の分子生物学的解析、佐藤雅彦、岡本彩花、木村成介、斉藤悠馬、田中玲帆、大島一正、平野朋子、第 36 回日本植物細胞分子生物学会、金沢商工会議所会館・石川県文教会館(石川県金沢市)、2018 年 8 月 26 日～28 日(口頭)
- 73.(招待講演) Development Ab-GALFA method, a novel assay method for analyzing molecular mechanisms underlying the gall formation process using a model plant, *Arabidopsis thaliana*, Masa H. Sato, Ayaka Okamoto, Issei Ohshima, Seisuke Kimura, Tomoko Hirano, 第 59 回日本植物生理学会年会シンポジウム「Amazing Development -Revealing Unusual Developmental Phenomena in Plants 植物が見せるユニークな発生および成長様式を読み解く」、札幌コンベンションセンター(北海道札幌市)、2018 年 3 月 28 日(口頭、英語)

法人番号	261003
プロジェクト番号	S1511023

- *74.(招待講演) Adaptation of plants to aquatic environments: Studies on vegetative propagation in semi-aquatic plant, *Rorippa aquatica*, Seisuke Kimura, 第 59 回日本植物生理学会年会シンポジウム「Amazing Development -Revealing Unusual Developmental Phenomena in Plants 植物が見せるユニークな発生および成長様式を読み解く」、札幌コンベンションセンター(北海道札幌市)、2018 年 3 月 28 日(口頭、英語)
- 75.アブラナ科植物 *Rorippa aquatica* の水中生活適応に伴う花成抑制機構の解析、池松朱夏、坂本智昭、中山北斗、木村成介、第 59 回日本植物生理学会年会、札幌コンベンションセンター(北海道札幌市)、2018 年 3 月 28 日-3 月 30 日(口頭)
- 76.A leading compound that regulate stomatal development, Hitoshi Endo, Seisuke Kimura, Naoyuki Uchida, Keiko Torii, 第 59 回日本植物生理学会年会、札幌コンベンションセンター(北海道札幌市)、2018 年 3 月 28 日-3 月 30 日(ポスター)
- 77.ミズナとミブナ(*Brassica rapa*)に見られる葉形変異の遺伝学的背景と育種の歴史の解明、川勝弥一、坂本智昭、中山北斗、上ノ山華織、五十嵐香理、矢野健太郎、久保中央、木村成介、第 59 回日本植物生理学会年会、札幌コンベンションセンター(北海道札幌市)、2018 年 3 月 28 日-3 月 30 日(ポスター)
- *78.*Rorippa aquatica* の栄養繁殖を制御する遺伝子群の探索、天野瑠美、中山北斗、桃井理沙、郡司玄、竹林裕美子、桶川友季、本橋健、笠原博幸、Ali Ferjani、木村成介、第 59 回日本植物生理学会年会、札幌コンベンションセンター(北海道札幌市)、2018 年 3 月 28 日-3 月 30 日(ポスター)
- *79.ヌルデアブラムシの虫液処理によるシロイヌナズナの形態変化および遺伝子発現変化、岡本彩花、斎藤悠馬、田中玲帆、大島一正、木村成介、平野朋子、佐藤雅彦、第 59 回日本植物生理学会年会、札幌コンベンションセンター(北海道札幌市)、2018 年 3 月 28 日-3 月 30 日(ポスター)
- 80.ROS 生成・トランスクリプトーム解析・耐病性検定に基づく、新規植物免疫活性化化合物の解析、中野正貴、北畑信隆、吉田亜祐美、斎藤優歩、佐藤静香、安江啓人、来栖孝光、石賀貴子、石賀康博、木村成介、諸橋賢吾、浅見忠男、朽津和幸、第 59 回日本植物生理学会年会、札幌コンベンションセンター(北海道札幌市)、2018 年 3 月 28 日-3 月 30 日(ポスター)
- *81.アブラナ科半水生植物 *Rorippa aquatica* における異形葉性と共生微生物の群集構造、板倉学、木村成介、上ノ山華織、金子貴一、第 12 回日本ゲノム微生物学会年会、京都大学桂キャンパス、2018 年 3 月 5 日~7 日(ポスター)
- *82. Insights into mechanisms of gall morphogenesis and the origin of gall induction, Antoine Guiguet, Issei Ohshima, Seisuke Kimura, Seiji Takeda, Françoise Laurans, Véronique Lainé-Prade, Carlos Lopez-Vaamonde, David Giron, 7th International Symposium on Cecidology –Ecology and Evolution of Gall-Inducing Arthropods, Huisun Experimental Forest Station, Taiwan, Mar. 3-8, 2018 (Oral)
83. Regulation of cyclic electron transport around Photosystem I by thioredoxin, Yuki Okegawa, Ken Motohashi, International Symposium on Photosynthesis and Chloroplast Biogenesis 2018, 7-10 November 2018, Kurashiki, JAPAN (Poster)
84. Roles of thioredoxin-dependent redox regulation in photosynthesis, Yuki Okegawa, Ken Motohashi, Japan-Finland Seminar 2018, 23-28 September 2018, Kobe, JAPAN (Poster)
85. チオレドキシニンによる光化学系 I サイクリック電子伝達制御機構の解析: 桶川友季、本橋健、第 59 回日本植物生理学会年会、札幌コンベンションセンター、2018 年 3 月 27 日~30 日(口頭発表)
86. *Brassica rapa* にみられるインプリント遺伝子とその分子進化、吉田貴徳、川邊隆大、河邊昭、日本遺伝学会 90 回大会
87. 板倉学、原新太郎、渡辺剛、三屋公佑、金子貴一、南澤究、土着 USDA110 系統ダイズ根粒菌のゲノム多様性と共生窒素固定能、日本微生物生態学会第 32 回大会、沖縄コンベンションセンター(宜野湾市)、2018.7.12-7.13
- *88. 板倉学、木村成介、上ノ山華織、金子貴一、アブラナ科半水生植物 *Rorippa aquatica* における異形葉性の誘導と共生細菌叢の変化、植物微生物研究会第 28 回研究交流会、鳥取大学(鳥取市)、2018.9.19-9.21
89. 蒲生雄大、板倉学、南澤究、金子貴一、根粒菌 *Bradyrhizobium elkanii* 系統のゲノミックアイランド多様性、植物微生物研究会第 28 回研究交流会、鳥取大学(鳥取市)、2018.9.19-9.21
90. 日下部翔平、金子貴一、安田美智子、三輪大樹、岡崎伸、佐伯和彦、佐藤修正、*Bradyrhizobium elkanii* USDA61 株の 3 型分泌エフェクターはミヤコグサに複数の防御反応を誘導する、植物微生物研究会第 28 回研究交流会、鳥取大学(鳥取市)、2018.9.19-9.21

法人番号	261003
プロジェクト番号	S1511023

- *91. Loss of flowering in semiaquatic plant *Rorippa aquatica*, Shuka Ikematsu, Tomoaki Sakamoto, Hokuto Nakayama, Seisuke Kimura, Taiwan-Japan Plant Biology 2017, Academia Sinica, Taipei, Taiwan, Nov. 3-6, 2017 (ポスター)
92. Analysis of leaf shape variation for Japanese traditional leafy vegetables Mizuna and Mibuna (cultivar of *Brassica rapa* subsp. *nipposinica*) by genetic analysis and survey of historical literature, Yaichi Kawakatsu, Hokuto Nakayama, Kaori Kamonoyama, Kaori Igarashi, Kentaro Yano, Seisuke Kimura, Taiwan-Japan Plant Biology 2017, Academia Sinica, Taipei, Taiwan, Nov. 3-6, 2017 (口頭、ポスター)
- *93. Exploration of genes regulating vegetative propagation in *Rorippa aquatica*, Rumi Amano, Hokuto Nakayama, Risa Momoi, Shizuka Gunji, Yumiko Takebayashi, Yuki Okegawa, Ken Motohashi, Hiroyuki Kasahara, Ali Ferjani, Seisuke Kimura, Taiwan-Japan Plant Biology 2017, Academia Sinica, Taipei, Taiwan, Nov. 3-6, 2017 (ポスター)
- *94. Loss of flowering due to successful vegetative reproduction in *Rorippa aquatica*、池松朱夏、木村成介、新学術領域研究環境記憶統合第3回若手の会、ホテルマホロバ・マインズ三浦(神奈川県・三浦市)、2017年10月17日～19日(ポスター)
- *95. Structural analysis of de novo assembled genome of *Rorippa aquatica*、坂本智昭、木村成介、新学術領域研究環境記憶統合第3回若手の会、ホテルマホロバ・マインズ三浦(神奈川県・三浦市)、2017年10月17日～19日(ポスター)
- *96. Exploring genes regulating vegetative propagation in *Rorippa aquatica*、天野瑠美、木村成介、新学術領域研究環境記憶統合第3回若手の会、ホテルマホロバ・マインズ三浦(神奈川県・三浦市)、2017年10月17日～19日(ポスター)
- *97. シロイヌナズナ転写因子 SOG1 を介した DNA 損傷応答の制御機構、愿山(岡本)郁、坂本智昭、上ノ山香織、木村成介、日本遺伝学会第89回大会、岡山大学(岡山県・岡山市)、2017年9月13-15日(口頭)
98. キク属モデル系統キクタクニギクにおける頭状花序形態形成機構の解析、小塚俊明、白岩一平、中野道治、坂本智昭、木村成介、谷口研至、草場信、日本植物学会第81回大会、東京理科大学(千葉県・野田市)、2017年9月8-10日(ポスター)
- *99. *Rorippa aquatica* の栄養繁殖を制御する遺伝子群の探索、天野瑠美、中山北斗、桃井理沙、郡司玄、竹林裕美子、笠原博幸、Ali Ferjani、木村成介、日本植物学会第81回大会、東京理科大学(千葉県・野田市)、2017年9月8-10日(口頭)
100. ミズナとミブナ(*Brassica rapa*)に見られる葉形変異の遺伝学的背景と育種の歴史の解明、川勝弥一、中山北斗、上ノ山華織、五十嵐香理、矢野健太郎、久保中央、木村成介、日本植物学会第81回大会、東京理科大学(千葉県・野田市)、2017年9月8-10日(口頭)
- *101. *Rorippa aquatica* の異形葉性における PHYTOCHROME INTERACTING FACTORS の機能解析、山口修二、中山北斗、坂本智昭、市橋泰範、倉田哲也、木村成介、日本植物学会第81回大会、東京理科大学(千葉県・野田市)、2017年9月8-10日(ポスター)
- *102. *Rorippa aquatica* における栄養繁殖とオーキシンの関係の解析、桃井理沙、天野瑠美、中山北斗、小島美紀子、竹林裕美子、榊原均、木村成介、日本植物学会第81回大会、東京理科大学(千葉県・野田市)、2017年9月8-10日(ポスター)
103. アブラナ科植物 *Rorippa aquatica* の水中適応に伴う花成の抑制機構の解析、池松朱夏、中山北斗、坂本智昭、木村成介、日本植物学会第81回大会、東京理科大学(千葉県・野田市)、2017年9月8-10日(ポスター)
- *104. *Rorippa aquatica* の栄養繁殖を制御する遺伝子群の探索、天野瑠美、中山北斗、桃井理沙、郡司玄、竹林裕美子、桶川友季、本橋健、笠原博幸、Ali Ferjani、木村成介、日本植物形態学会第29回大会、東京理科大学(千葉県・野田市)、2017年9月7日(ポスター)
105. ミズナとミブナ(*Brassica rapa*)に見られる葉形変異の遺伝学的背景と育種の歴史の解明、川勝弥一、中山北斗、上ノ山華織、五十嵐香理、矢野健太郎、久保中央、木村成介、日本植物形態学会第29回大会、東京理科大学(千葉県・野田市)、2017年9月7日(ポスター)
- *106. (招待講演) Ab-GALFA 法 ～モデル植物シロイヌナズナを用いた虫こぶ形成メカニズムの解明～、佐藤雅彦、岡本彩花、大島一正、木村成介、平野朋子、第35回日本植物細胞分子生物学会シンポジウム、大宮ソニックシティ(埼玉県・大宮市)、2017年8月29日～31日

法人番号	261003
プロジェクト番号	S1511023

- *107. 転写因子 SOG1 による DNA 損傷応答の統括メカニズム、愿山(岡本)郁、上ノ山香織、坂本智昭、木村成介、第 58 回日本植物生理学会年会、鹿児島大学郡元キャンパス(鹿児島県・鹿児島市)、2017 年 3 月 16 日～18 日(口頭)
- *108. 非モデル植物 *Rorippa aquatica* にみられる栄養繁殖機構の解析、天野瑠美、中山北斗、坂本智昭、桃井理沙、郡司玄、Ali Ferjani、木村成介、第 58 回日本植物生理学会年会、鹿児島大学郡元キャンパス(鹿児島県・鹿児島市)、2017 年 3 月 16 日～18 日(口頭)
- *109. *Rorippa aquatica* のドラフトゲノム解析、坂本智昭、木村成介、第 58 回日本植物生理学会年会、鹿児島大学郡元キャンパス(鹿児島県・鹿児島市)、2017 年 3 月 16 日～18 日(ポスター)
- *110. 「虫こぶ」プロジェクト:植物の形態や代謝を制御する新たな技術開発にむけて、大坪憲弘、武田征士、木村成介、佐藤雅彦、大島一成、第 58 回日本植物生理学会年会、鹿児島大学郡元キャンパス(鹿児島県・鹿児島市)、2017 年 3 月 16 日～18 日(ポスター)
- *111. Ab-GALFA: Development of a novel bioassay for dissecting of gall formation mechanism using *Arabidopsis thaliana*, Ayaka Okamoto, Tomoko Hirano, Akihisa Hamatani, Issei Ohshima, Seisuke Kimura, Masa H. Sato, 第 58 回日本植物生理学会年会、鹿児島大学郡元キャンパス(鹿児島県・鹿児島市)、2017 年 3 月 16 日～18 日(ポスター)
- *112. 植物が独自に獲得した DNA 損傷応答因子 SOG1 の機能解析、岡本郁、木村成介、平成 28 年度京都産業大学総合生命科学部シンポジウム「見ればわかる。魅せる最新の生命科学」、京都産業大学むすびわざ館(京都府・京都市)、2017 年 3 月 3 日(ポスター)
- *113. (招待講演) Adaptation of plants to aquatic environments: Studies on heterophylly and vegetative propagation in semi-aquatic plant, *Rorippa aquatica*, Seisuke Kimura, CSRS seminar, RIKEN Center for Sustainable Resource Science, Yokohama, Japan, Jan. 24, 2017(英語)
- *114. 板倉学、木村成介、上ノ山華織、金子貴一、植物-微生物相互作用によるアブラナ科半水生植物 *Rorippa aquatica* における異形葉性の誘導、植物微生物研究会第 27 回研究交流会、京都大学(宇治市)、2017.9.20-9.22
115. 西田裕貴、芳村紗奈恵、芦田建都、板倉学、岡崎伸、佐藤修正、金子貴一、根粒菌 *Bradyrhizobium elkanii* USDA94 のミヤコグサ共生に関連する T3SS エフェクターの研究、植物微生物研究会第 27 回研究交流会、京都大学(宇治市)、2017.9.20-9.22
116. 蒲生雄大、板倉学、南澤究、金子貴一、ダイズ根粒菌 Bradyrhizobium elkanii 系統の共生アイランド多様性、植物微生物研究会第 27 回研究交流会、京都大学(宇治市)、2017.9.20-9.22
117. 日下部翔平、金子貴一、安田美智子、三輪大樹、岡崎伸、佐藤修正、ミヤコグサに根粒菌の侵入阻害を誘導する *Bradyrhizobium elkanii* USDA61 株の 3 型分泌エフェクター及び宿主側因子の解析、植物微生物研究会第 27 回研究交流会、京都大学(宇治市)、2017.9.20-9.22
118. 板倉学、三屋公佑、金原一真、原新太郎、渡辺剛、菅原雅之、金子貴一、南澤究、ダイズ根粒菌 USDA110 系統のゲノム多様性と吸収型ヒドロゲナーゼゲノミックアイランド構造変化、環境微生物系学会合同大会 2017、東北大学(仙台市)、2017.8.29-8.31
119. 渡辺剛、原新太郎、新井沙和、高橋智子、三屋公佑、菅原雅之、板倉学、金子貴一、南澤究、根粒菌 *hupSL1* 変異によるダイズ根圏の H₂ 代謝と細菌群集構造の変動、環境微生物系学会合同大会 2017、東北大学(仙台市)、2017.8.29-8.31
120. ミヤコグサにエフェクター誘導性免疫反応を誘導する *Bradyrhizobium elkanii* USDA 61 株の 3 型分泌エフェクターの同定、日下部翔平、金子貴一、安田美智子、三輪大樹、岡崎伸、佐藤修正、第 58 回植物生理学会年会、鹿児島大学、2017 年 3 月 16 日～18 日
121. 板倉学、三屋公佑、金原一真、原新太郎、渡辺剛、菅原雅之、金子貴一、南澤究、土着ダイズ根粒菌 USDA110 系統株におけるゲノム多様性とゲノミックアイランド構造の変化、第 11 回日本ゲノム微生物学会年会、慶應義塾大学(藤沢市)、2017.3.2-3.4
122. SLiCE をはじめとする精製酵素を用いないシームレス DNA クローニング法の評価: 本橋健、第 90 回日本生化学会大会、神戸ポートアイランド、2017 年 12 月 6 日～9 日
123. (招待講演)シロイヌナズナの葉緑体におけるチオレドキシソ依存のレドックス制御システム: 桶川友季、第 47 回植物バイテクシンポジウム 京都府立大学稲盛記念会館 2017 年 9 月 25 日

法人番号	261003
プロジェクト番号	S1511023

124. Analysis of overexpressor of chloroplastic thioredoxins in *Arabidopsis thaliana*: 桶川友季、本橋健、第 58 回日本植物生理学会年会、鹿児島大学、2017 年 3 月 16 日～18 日
125. Evaluation of the efficiency and utility of recombinant enzyme-free seamless DNA cloning methods: 本橋健、第 58 回日本植物生理学会年会、鹿児島大学、2017 年 3 月 16 日～18 日
126. *Brassica rapa* におけるゲノムインプリント候補遺伝子の探索、川邊隆大、田中翔、吉田貴徳、河邊昭、日本育種学会 131 回講演会、名古屋大学、2017 年 3 月 29 日～30 日
- *127. Rumi Amano, Hokuto Nakayama, Risa Momoi, Shizuka Gunji, Ali Ferjani, Seisuke Kimura, Developmental and molecular studies on the mechanism of vegetative propagation in *Rorippa aquatica*, Latest Advances in Plant Development & Environmental Response, 2016 Cold Spring Harbor Asia Conference, Awaji, Japan, 2016.11.29-12.2
- *128. Hokuto Nakayama, Tomoaki Sakamoto, Yasunori Ichihashi, Manabu Fujie, Tetsuya Kurata, Seisuke Kimura, Impact of Environment on Leaf Development: Studies on Heterophylly in *Rorippa aquatica*, Latest Advances in Plant Development & Environmental Response, 2016 Cold Spring Harbor Asia Conference, Awaji, Japan, 2016.11.29-12.2
- *129. (招待講演) Rumi Amano, Risa Momoi, Seisuke Kimura, Vegetative propagation in *Rorippa aquatica*: Understanding plant regeneration using non-model species, The 45th Plant Biotechnology Symposium “International Plant Meeting in Kyoto 2016– Plant Development and Environment-“, Kyoto Sangyo University, Kyoto, 2016.11.25
130. (招待講演) 京野菜であるミズナとミズナの葉形変異と育種の歴史の解析、川勝弥一、(木村成介)、第 2 回農学中手の会、雄琴温泉湯の宿木こもれび、2016 年 11 月 10 日～11 日
- *131. 木村成介、水中への適応形質としての異形葉性と栄養繁殖の進化、植物科学若手研究会 2016、木江ふれあい郷土資料館、2016.9.29-10.1
132. 辻村真衣、出雲谷遙、執行正義、上ノ山華織、坂本智昭、木村成介、寺地徹、雄性不稔タマネギのミトコンドリア転写産物の解析、日本育種学会第 130 回講演会、鳥取大学、2016.9.24-26
- *133. (招待講演) 木村成介、水中への適応戦略としての異形葉性と栄養繁殖、日本植物学会第 80 回大会シンポジウム「Induced Development: 環境要因に誘発される発生の多様性と共通性」、沖縄コンベンションセンター、2016.9.16
134. 川勝弥一、中山北斗、上ノ山華織、五十嵐香理、八杉公基、工藤洋、永野惇、矢野健太郎、久保中央、木村成介、京野菜であるミズナとミズナに見られる葉形変異の QTL 解析、日本植物学会第 80 回大会、琉球大学、沖縄コンベンションセンター、2016.9.16-19
- *135. 山口修二、中山北斗、坂本智昭、市橋泰範、倉田哲也、木村成介、*Rorippa aquatica* の異形葉性における *PHYTOCHROME INTERACTING FACTORS* の機能解析、日本植物学会第 80 回大会、琉球大学、沖縄コンベンションセンター、2016.9.16-19
- *136. 桃井理沙、天野瑠美、中山北斗、木村成介、*Rorippa aquatica* の栄養繁殖とオーキシンの関係の解析、日本植物学会第 80 回大会、琉球大学、沖縄コンベンションセンター、2016.9.16-19
- *137. 天野瑠美、中山北斗、郡司玄、Ali Ferjani、木村成介、アブラナ科 *Rorippa aquatica* を用いた葉断面からの栄養繁殖機構の解析、日本植物学会第 80 回大会、琉球大学、沖縄コンベンションセンター、2016.9.16-19
138. 三好彩央里、中益朗子、木村成介、水生シダ *Microsorium pteropus* とその変種の葉の形態に関わる分岐構造の多様性について、日本植物学会第 80 回大会、琉球大学、沖縄コンベンションセンター、2016.9.16-19
139. 小塚俊明、中野道治、坂本智昭、木村成介、有賀悠貴、谷口研至、草場信、キクタニギク自家不和合性系統を用いたキク属モデル植物の開発、日本植物学会第 80 回大会、琉球大学、沖縄コンベンションセンター、2016.9.16-19
- *140. 天野瑠美、中山北斗、郡司玄、Ali Ferjani、木村成介、アブラナ科 *Rorippa aquatica* を用いた葉断面からの栄養繁殖機構の解析、日本植物形態学会第 28 回大会、琉球大学、2016.9.15
141. 三好彩央里、中益朗子、木村成介、水生シダ *Microsorium pteropus* とその変種の葉の形態に関わる分岐構造の多様性について、日本植物形態学会第 28 回大会、琉球大学、2016.9.15
142. 川勝弥一、中山北斗、上ノ山華織、五十嵐香理、八杉公基、工藤洋、永野惇、矢野健太郎、久保中央、木村成介、京野菜であるミズナとミズナに見られる葉形変異の QTL 解析、日本植物形態学会第 28 回大会、琉球大学、2016.9.15

法人番号	261003
プロジェクト番号	S1511023

- *143. 愿山(岡本)郁、上ノ山華織、坂本智昭、木村成介、植物における多様な DNA 損傷応答の選択機構、日本遺伝学会第 88 回大会、日本大学(三島)、2016.9.15
- *144. Kaoru (Okamoto) Yoashiyama, Kaori Kaminoyama, Tomoaki Sakamoto, Seisuke Kimura, The regulatory mechanism of DNA damage responses through SOG1 phosphorylation, Plant Genome Stability and Change 2016, Shonan Village Center, Hayama, Japan, 2016.7.7-10
- *145. (招待講演) Seisuke Kimura, Impact of Environment on Leaf Development: Studies on Heterophylly in *Rorippa aquatica*, Seminar at Institute of Molecular Plant Sciences, University of Edinburgh, Edinburgh, UK, 2016.4.7
- *146. (招待講演) Seisuke Kimura, Impact of Environment on Leaf Development: Studies on Heterophylly in *Rorippa aquatica*, Sainsbury Laboratory Symposium “Induced Plant Development”, The Sainsbury Laboratory, University of Cambridge, Cambridge, UK, 2016.4.4-6
147. 川勝弥一、中山北斗、上ノ山華織、五十嵐香理、八杉公基、工藤洋、永野惇、矢野健太郎、久保中央、木村成介、京野菜であるミズナとミブナに見られる葉形変異の QTL 解析、第 57 回日本植物生理学会年会、岩手大学、2016.3.18-20
- *148. 中山北斗、坂本智昭、市橋泰範、藤江学、倉田哲也、Neelima Sinha、木村成介、異形葉性を示す *Rorippa aquatica* の二つの地域系統を用いたトランスクリプトーム解析、第 57 回日本植物生理学会年会、岩手大学、2016.3.18-20
- *149. 岡本郁、木村成介、シロイヌナズナにおける DNA 損傷応答と SOG1 のリン酸化の関係、第 57 回日本植物生理学会年会、岩手大学、2016.3.18-20
150. 三好彩央里、中益朗子、木村成介、水生シダ *Microsorium pteropus* とその変種の葉の形態に関わる分岐構造の多様性について、第 57 回日本植物生理学会年会、岩手大学、2016.3.18-20
- *151. (招待講演) 木村成介、環境に応じて葉の形態を変化させる植物 *Rorippa aquatica* を用いた表現型可塑性の研究、東京理科大学応用生物科学科セミナー、東京理科大学、2016.3.7
152. (招待講演) 木村成介、葉っぱの形の遺伝と進化 –メンデル遺伝学で解き明かす多様な葉の形ができるしくみ–、京都産業大学リエゾンオフィス主催シンポジウム「遺伝と進化の不思議～ダーウィンとメンデルから学んだこと～」、京都産業大学むすびわざ館、2016.3.5
- *153. (招待講演) 天野瑠美、(木村成介)、切っても切っても生えてくる! 葉断面からの栄養繁殖、第 41 回植物バイテクシンポジウム「これからの植物科学」、京都産業大学、2016.1.22
- *154. 微生物群集がアブラナ科水生植物ニューベキア (*Rorippa aquatica*) における葉の形態形成に及ぼす影響、板倉学、木村成介、上ノ山華織、金子貴一、植物微生物研究会 第 26 回研究交流会、東北大学、2016 年 9 月 7 日～9 日
155. ゲノムマッピングによるダイズ根粒菌の種判定および土着ダイズ根粒菌群と接種菌群の識別、金原一真、板倉学、星野裕子、秋山博子、早津雅仁、王勇、鶴丸博人、南澤究、植物微生物研究会 第 26 回研究交流会、東北大学、2016 年 9 月 7 日～9 日
156. *Bradyrhizobium elkanii* 系統共生アイランドの塩基配列比較、西田裕貴、板倉学、佐藤修正、金子貴一、植物微生物研究会 第 26 回研究交流会、東北大学、2016 年 9 月 7 日～9 日
157. ダイズ根粒菌 *Bradyrhizobium diazoefficiens* USDA110 型菌株における吸収型ヒドロゲナーゼの多様性、渡辺剛、板倉学、三屋公佑、原新太郎、金原一真、菅原雅之、按田瑞恵、篠田亮、金子貴一、南澤究、植物微生物研究会 第 26 回研究交流会、東北大学、2016 年 9 月 7 日～9 日
158. ミヤコグサのとの相互作用に関与する *Bradyrhizobium elkanii* USDA 61 株の 3 型分泌エフェクターの解析、日下部翔平、金子貴一、安田美智子、三輪大樹、岡崎伸、佐藤修正、植物微生物研究会 第 26 回研究交流会、東北大学、2016 年 9 月 7 日～9 日
159. 根粒菌のエフェクターによるミヤコグサ根粒形成の制御、三輪大樹、安田美智子、増田幸子、金子貴一、佐藤修正、岡崎伸、植物微生物研究会 第 26 回研究交流会、東北大学、2016 年 9 月 7 日～9 日 34.
160. 有用ダイズ根粒菌 *Bradyrhizobium diazoefficiens* USDA110 型菌株におけるゲノム構造の多様性、板倉学、三屋公佑、金原一真、菅原雅之、金子貴一、南澤究、日本土壤微生物学会 2016 年度大会、岐阜大学、2016 年 6 月 11 日～12 日
161. 日下部翔平、金子貴一、安田美智子、三輪大樹、岡崎伸、佐藤修正: ミヤコグサにエフェクター誘導免疫

法人番号	261003
プロジェクト番号	S1511023

- 反応を誘導する *Bradyrhizobium elkanii* USDA61 株の III 型分泌エフェクターの解析. 日本植物生理学会 第 57 回年会、盛岡市、2016.3.18-20
162. 三屋公佑、金原一真、菅原雅之、南澤究、金子貴一、板倉学: 根粒菌 *Bradyrhizobium diazoefficiens* の種内比較ゲノム解析. 第 10 回日本ゲノム微生物学会年会、目黒区、2016.3.4-5
163. 南智之、按田瑞恵、池田成志、菅原雅之、金子貴一、佐藤修正、田畑哲之、三井久幸、南澤究: 植物共生細菌 *Methylobacterium* 属内のメタゲノム解析. 第 10 回日本ゲノム微生物学会年会、目黒区、2016.3.4-5
164. 金原一真、板倉学、鶴丸博人、星野裕子、秋山博子、早津雅仁、南澤究: ゲノムマッピングによるダイズ根粒菌の種の判定と接種菌群の追跡. 第 10 回日本ゲノム微生物学会年会、目黒区、2016.3.4-5
165. (招待講演)レドックス制御～光に応答して植物の代謝を制御する仕組み: 本橋健、関西学院大学セミナー、関西学院大学理工学部、2016 年 11 月 18 日
166. (招待講演) Thioredoxin-dependent redox regulatory system in chloroplasts, Ken Motohashi, The 17th International Congress on Photosynthesis Research, MECC Maastricht, Maastricht, Netherland, 2016.8.7-12
167. *Arabidopsis m*-type thioredoxin regulates the Calvin cycle enzymes *in vivo*.: Yuki Okegawa, Ken Motohashi, The 17th International Congress on Photosynthesis Research (国際光合成会議)(オランダ; マーストリヒト)、2016 年 8 月 7 日～12 日
168. 桶川友季、本橋健: Chloroplastic *m*-type thioredoxins as major regulators of Calvin cycle during photosynthesis. 第 57 回日本植物生理学会年会、盛岡市、2016.3.18-20
169. 本橋健、桶川友季: A simple and efficient seamless DNA cloning method using cell lysates from laboratory *Escherichia coli* strains and its application to SLiP site-directed mutagenesis. 第 57 回日本植物生理学会年会、盛岡市、2016.3.18-20
170. 琵琶湖湖岸における絶滅危惧種タチスズシロソウの金属集積性および耐性、小杉亜希、西澤千晶、河邊昭、原田英美子、第 7 回日本水環境学会関西支部研究発表会、大阪工業大学うめきたナレッジセンター、2016 年 12 月 2 日
171. 絶滅危惧種タチスズシロソウ (*Arabidopsis kamchatica* ssp. *kawasakiana*) の重金属集積性と植生調査、原田英美子、小杉亜希、西澤千晶、高倉耕一、野間直彦、河邊昭、日本植物学会第 80 回大会、琉球大学、沖縄コンベンションセンター、2016.9.16-19
172. アブラナ科植物ハタザオのゲノム解析、吉田貴徳、河邊昭、日本遺伝学会第 88 回大会、日本大学国際関係学部三島駅北口校舎、2016 年 9 月 7 日～10 日
173. アブラナ科植物 *Brassica rapa* におけるゲノムインプリンティング、吉田貴徳、薄伊納、河邊昭、日本進化学会第 18 回大会、東京工業大学大岡山キャンパス、2016 年 8 月 25 日～28 日
174. *Brassica rapa* におけるゲノムインプリント候補遺伝子の探索、川邊隆大、田中翔、吉田貴徳、河邊昭、日本育種学会第 131 回講演会、名古屋大学東山キャンパス、2017 年 3 月 29 日～30 日
175. 川邊隆大、宮路直美、高田紗都子、板橋悦子、安田剛志、藤本龍、シロイヌナズナの雑種強勢の分子機構の解明に向けた RIL の整備、日本育種学会第 129 回講演会、横浜市立大学、2016.3.21-22
176. (招待講演) 京野菜であるミズナとミブナの葉形変異と育種の歴史の解析、川勝弥一(木村研究室)、農手中手の会、小田原、2015.12.12.
- *177. アブラナ科植物 *Rorippa aquatica* にみられる葉断面からの栄養繁殖機構の解析、天野瑠美、中山北斗、桃井理沙、郡司玄、Ali Ferjani、木村成介、第 38 回日本分子生物学会年会、神戸ポートピアアイランド、2015.12.1-4
- *178. 環境に応じて葉の形態を変化させる植物 *Rorippa aquatica* を用いた表現型可塑性の研究、中山北斗、坂本智昭、市橋泰範、藤江学、倉田哲也、木村成介、第 38 回日本分子生物学会年会、神戸ポートピアアイランド、2015.12.1-4.
- *179. (招待講演) 環境に応じて葉の形態を変化させる植物 *Rorippa aquatica* を用いた表現型可塑性の研究、木村成介、第 59 回細胞のかたちと機能プロジェクト研究センターセミナー、広島大学、2015.10.19.
- *180. 植物における DNA 損傷応答の統括因子 SOG1 の制御メカニズム、愿山(岡本)郁、木村成介、日本遺伝学会第 87 回大会、東北大学川内北キャンパス、2015.9.24-26.
- *181. (招待講演) Impact on Environment on Leaf Development: Studies on Heterophylly of *Rorippa aquatica*, Seisuke Kimura, IHB seminar, Institute of Hydrobiology, Chinese Academy of Science, Wuhan, China,

法人番号	261003
プロジェクト番号	S1511023

- 2015.9.17.
- *182. (招待講演) Diversity of leaf shape and its relation to environment, Seisuke Kimura, Institute of Hydrobiology, Chinese Academy of Science, Wuhan, China, 2015.9.15.
183. 京野菜であるミズナとミブナに見られる葉形変異の QTL 解析^[SEP], 川勝弥一、上ノ山華織、五十嵐香理、中山北斗、八杉公基、工藤洋、永野敦、矢野健太郎、久保中央、木村 成介、日本植物学会第 79 回大会、朱鷺メッセ(新潟県)、2015.9.6-8.
184. 水生シダ *Microsorium pteropus* とその変種の葉の形態に関わる枝分かれ構造の多様性について、三好彩央里、中益朗子、木村成介、日本植物学会第 79 回大会、朱鷺メッセ(新潟県)、2015.9.6-8.
- *185. *Rorippa aquatica* の葉形制御機構の RNA-seq による網羅的解析、坂本智昭、中山北斗、市橋泰範、藤江学、倉田哲也、木村成介、日本植物学会第 79 回大会、朱鷺メッセ(新潟県)、2015.9.6-8.
- *186 アブラナ科植物 *Rorippa aquatica* にみられる葉断面からの栄養繁殖の発生学的解析、天野瑠美、中山北斗、桃井理沙、郡司玄、Ferjani Ali、木村成介、日本植物学会第 79 回大会、朱鷺メッセ(新潟県)、2015.9.6-8.
187. ダイコンの品種間に見られる葉形の変異に寄与する遺伝子の同定^[SEP]、久保俊彰、上ノ山華織、川勝弥一、五十嵐香理、矢野健太郎、木村 成介、日本植物学会第 79 回大会、朱鷺メッセ(新潟県)、2015.9.6-8.
188. 葉の枝分かれに見られる非対称性について、中益朗子、末松 J 信彦、木村成介、第 79 回形の科学シンポジウム、千葉工業大学、2015.6.12-14.
189. Theoretical analysis of asymmetric branched structures in dissected leaves, Akiko Nakamasu, Nobuhiko J. Suematsu, Seisuke Kimura, 48th Annual Meeting of the Japanese Society of Developmental Biologists, Tsukuba International Congress Center, 2015.6.2-5
190. 京野菜であるミズナとミブナに見られる葉形変異の QTL 解析、川勝弥一、上ノ山華織、五十嵐香理、中山北斗、八杉公基、工藤洋、永野惇、矢野健太郎、久保中央、木村成介、日本育種学会第 127 回講演会(平成 27 年度春季大会)、玉川大学、2015.3.21-22.
- *191. Developmental and molecular studies on the mechanism of vegetative propagation in *Rorippa aquatica*, Rumi Amano, Hokuto Nakayama, Shizuka Gunji, Ali Ferjani, Seisuke Kimura, 第 56 回日本植物生理学会年会、東京農業大学、2015.3.16-18.
192. QTL analysis of leaf morphological traits in Japanese traditional leafy vegetables, Mizuna and Mibuna, Yaichi Kawakatsu, Kaori Kaminoyama, Kaori Igarashi, Hokuto Nakayama, Masaki Yasugi, Hiroshi Kudoh, Atsushi J. Nagano, Kentaro Yano, Nakao Kubo, Seisuke Kimura, 第 56 回日本植物生理学会年会、東京農業大学、2015.3.16-18.
193. Genetic analysis for natural variation in leaf shape of Daikon radish (*Raphanus sativus* var. longipinnatus), Toshiaki Kubo, Kaori Kaminoyama, Yaichi Kawakatsu, Kaori Igarashi, Hokuto Nakayama, Kentaro Yano, Seisuke Kimura, 第 56 回日本植物生理学会年会、東京農業大学、2015.3.16-18.
194. Molecular mechanism of SOG1 activation in response to DNA damage, Kaoru Yoshiyama (Okamoto), Seisuke Kimura, 第 56 回日本植物生理学会年会、東京農業大学、2015.3.16-18.
195. (招待講演) QTL analysis of leaf morphological traits in Japanese traditional leafy vegetables, Mizuna and Mibuna, Yaichi Kawakatsu, Kaori Kaminoyama, Kaori Igarashi, Hokuto Nakayama, Masaki Yasugi, Hiroshi Kudoh, Atsushi J. Nagano, Kentaro Yano, Nakao Kubo, Seisuke Kimura, The 35th Plant Biotechnology Symposium “International Plant Meeting in Kyoto – Messages from young scientists II-“, Kyoto Sangyo University, Kyoto, 2015.1.16.
196. 三輪大樹、Faruque Omar、増田幸子、安田美智子、金子貴一、佐藤修正、岡崎伸: 根粒菌 3 型分泌系による根粒形成の制御機構. 植物微生物研究会 第 25 回研究交流会、つくば市、2015.9.14-16
197. Faruque Omar、三輪大樹、安田美智子、増田幸子、藤井義晴、金子貴一、佐藤修正、岡崎伸: *Rj4* 遺伝子型サイズに根粒形成する *Bradyrhizobium elkanii* トランスポゾン変異体の解析. 植物微生物研究会 第 25 回研究交流会、つくば市、2015.9.14-16
198. 日下部翔平、金子貴一、安田美智子、三輪大樹、岡崎伸、佐藤修正: ミヤコグサを用いた *Bradyrhizobium elkanii* USDA61 株との相互作用に関与する宿主側因子の解析. 植物微生物研究会 第 25 回研究交流会、つくば市、2015.9.14-16
199. 辻村真衣、金子貴一、執行正義、出雲谷遥、寺地徹: 雄性不稔タマネギのミトコンドリアゲノムの解読. 日本育種学会 第 128 回講演会、新潟市、2015.9.11-12

法人番号	261003
プロジェクト番号	S1511023

200. 桶川友季、本橋健:シロイヌナズナ *m* 型チオレドキシンはカルビンサイクル酵素の主たるレドックス制御因子として機能する. 第 38 回日本分子生物学会年会および第 88 回日本生化学会大会 合同大会, 神戸市, 2015.12.1-4
201. 本橋健、桶川友季:大腸菌粗抽出液を用いた簡便かつ高効率な Seamless DNA cloning 法. 第 38 回日本分子生物学会年会および第 88 回日本生化学会大会 合同大会, 神戸市, 2015.12.1-4
202. 桶川友季、本橋健:シロイヌナズナの *m* 型チオレドキシンの欠損はカルビンサイクルの酵素の活性化に影響を与える. 第 6 回日本光合成学会年会, 岡山市, 2015.5.22-23
203. 本橋健: 大腸菌抽出液を用いた簡便かつ高効率な Seamless DNA cloning 法. 第 6 回日本光合成学会年会, 岡山市, 2015.5.22-23
204. 河邊昭、野生植物集団の遺伝的多様度と変異の維持機構、日本遺伝学会第 87 回大会、仙台、2015 年 9 月 24 日
205. 薄伊納、吉田貴徳、河邊昭、*Brassica rapa* におけるゲノムインプリンティング候補遺伝子の探索、日本遺伝学会第 87 回大会、仙台、2015 年 9 月 25 日
206. 河邊昭、降旗初佳、吉田貴徳、シロイヌナズナ属における葉緑体の RNA エディティングの種間変異、日本遺伝学会第 87 回大会、仙台、2015 年 9 月 26 日
207. Aki Kosugi, Chiaki Nishizawa, Akira Kawabe, Emiko Harada, Heavy metal accumulation and vegetation ecology in allotetraploid *Arabidopsis kamchatica* subsp. *kawasakiana*, The Vth International Symposium on Metallomics, Beijing, China, September 9-12, 2015

<研究成果の公開状況> (上記以外)

シンポジウム・学会等の実施状況、インターネットでの公開状況等 <既に実施しているもの>

シンポジウム・研究会の開催

- (1) 第57回植物バイテクシンポジウム「変身する生き物、変身させる生き物」、京都産業大学(京都市北区)、2019年12月13日
- (2) 京都産業大学総合生命科学部生命科学セミナー「Heirloom tomatoを用いた葉の形態多様性に関する研究(中山北斗助教・東京大学大学院理学研究科)」、京都産業大学(京都市北区)、2020年1月28日
- (3) 第53回植物バイテクシンポジウム「再生と改変 ～植物の再分化能力の秘密に迫る～」、京都産業大学(京都市北区)、2018年11月30日
- (4) 第59回日本植物生理学会年会シンポジウム「Amazing Development -Revealing Unusual Developmental Phenomena in Plants - 植物が見せるユニークな発生および成長様式を読み解く-」、札幌コンベンションセンター(北海道札幌市)、2018年3月28日、(英語)
- (5) 第48回植物バイテクシンポジウム「植物研究者のフィロソフィー ～研究に何を感じ、何を想うか～」、京都産業大学(京都市北区)、2017年12月15日
- (6) 京都産業大学総合生命科学部生命科学セミナー「ゲノム研究による植物防疫への挑戦(吉田健太郎准教授・神戸大学)」、京都産業大学(京都市北区)、2017年12月7日
- (7) 京都産業大学総合生命科学部生命科学セミナー「ヒトのゲノム配列を解析する -大量データの解析で分かってきたこと、これからの課題-(藤本明洋特定准教授・京都大学)」、京都産業大学(京都市北区)、2016年12月15日

法人番号	261003
プロジェクト番号	S1511023

(8) 第41回植物バイテクシンポジウム「これからの植物科学」、京都産業大学(京都市北区)、2016年11月25日

(9) 第35回植物バイテクシンポジウム「International Plant Meeting in Kyoto 2016 -Plant Development and Environment」、京都産業大学(京都市北区)、2015年11月25日、(英語)

インターネットでの公開状況

<https://www.seisukekimura.com> (研究代表者のホームページ)
http://www.kyoto-su.ac.jp/news/20191122_345_release_it01.html
<http://www.tsukuba-sci.com/?column02=ちぎれた葉から、どのようにクローン個体が再生>
<http://tenbou.nies.go.jp/news/jnews/detail.php?i=28308>
<https://www.jiji.com/jc/article?k=2019112200319&g=soc>
http://www.kyoto-su.ac.jp/news/20191028_400a_news.html
http://www.kyoto-su.ac.jp/news/20191213_400a_57thbio_sympo.html
<https://topics.shidaiaren.or.jp/10636/>
<https://www.u-presscenter.jp/2019/12/post-42886.html>
<https://yab.yomiuri.co.jp/adv/local/release/00039911.html>
<https://www.sankeibiz.jp/business/news/191217/pr1912171513132-n1.htm>
<https://www.afpbb.com/articles/-/3259942>
<https://www.hokkaido-np.co.jp/article/375545/>
<https://opi-rina.chunichi.co.jp/release/36650release.html>
<https://www.kahoku.co.jp/release/36650.html>
<https://www.niigata-nippo.co.jp/release/?id=36650>
<https://www.niigata-nippo.co.jp/release/detail.php?id=36650>
<https://www.agara.co.jp/article/38687/>
<https://www.okinawatimes.co.jp/articles/-/511833>
<https://www.oricon.co.jp/digitalpr/36650/>
https://news.infoseek.co.jp/article/digitalprplatform_36650
https://news.biglobe.ne.jp/economy/1217/prp_191217_3338029680.html
https://www.excite.co.jp/news/article/Dprp_36650/
https://business.nifty.com/cs/catalog/business_release/catalog_prp36650_1.htm
<https://beauty.oricon.co.jp/digitalpr/36650/>
<https://japan.cnet.com/release/30414965/?ref=rss>
<https://japan.zdnet.com/release/30414965/?ref=rss>
<https://news.toremaga.com/economy/bussiness/1449648.html>
<https://www.zaikei.co.jp/releases/921113/>
<https://www.mapion.co.jp/news/release/dgpr36650/>
http://www.kyoto-su.ac.jp/news/20180124_400n_news.html
http://www.kyoto-su.ac.jp/news/20171207_345_release_ka01.html
http://www.kyoto-su.ac.jp/news/20171215_400n_sympohouoku.html
http://www.kyoto-su.ac.jp/news/20171108_400n_news.html
http://www.kyoto-su.ac.jp/news/20161125_400n_sympohouokoku.html

法人番号	261003
プロジェクト番号	S1511023

http://www.kyoto-su.ac.jp/news/20151116_news.html
http://www.kyoto-su.ac.jp/news/20151016_news.html
http://www.kyoto-su.ac.jp/news/20150926_news.html
https://www.kyoto-su.ac.jp/news/20190913_400a_news.html
https://www.kyoto-su.ac.jp/news/20190424_400a_news.html
https://www.kyoto-su.ac.jp/department/nls/news/20151016_news.html

〈これから実施する予定のもの〉

該当なし

14 その他の研究成果等

受賞など

- (1) 天野瑠美、優秀発表賞、新学術領域研究「環境記憶統合」第5回若手の会 (2019)
- (2) 天野秦輔、学生ポスター賞優秀賞、第21回日本進化学会年大会 (2019)
- (3) 池松朱夏、Outstanding Poster Award, Taiwan-Japan Plant Biology 2017, Taiwan (2017)
- (4) Best paper award, Aki Kosugi, Chiaki Nishizawa, Akira Kawabe, Emiko Harada,
The Vth International Symposium on Metallomics, Beijing, China, September 9-12 (2015)
- (5) 河邊昭、日本遺伝学会奨励賞受賞 (2015)

企業との連携

- (1) 化学系メーカー企業 1 社と共同

法人番号	261003
プロジェクト番号	S1511023

15 「選定時」及び「中間評価時」に付された留意事項及び対応

<「選定時」に付された留意事項>

該当なし

<「選定時」に付された留意事項への対応>

該当なし

<「中間評価時」に付された留意事項>

該当なし

<「中間評価時」に付された留意事項への対応>

該当なし

法人番号	261003
プロジェクト番号	S1511023

16

(千円)

年度・区分	支出額	内 訳						備考
		法人負担	私学助成	共同研究機関負担	受託研究等	寄付金	その他()	
平成27年度	施設	0						
	装置	52,497	26,249	26,248				
	設備	23,761	7,921	15,840				
	研究費	29,864	17,097	12,767				
平成28年度	施設	0						
	装置	0						
	設備	0						
	研究費	44,812	30,603	14,209				
平成29年度	施設	0						
	装置	0						
	設備	0						
	研究費	44,997	32,258	12,739				
平成30年度	施設	0						
	装置	0						
	設備	0						
	研究費	42,800	27,916	14,884				
平成31年度	施設	0						
	装置	0						
	設備	0						
	研究費	40,746	25,728	15,018				
総額	施設	0	0	0	0	0	0	0
	装置	52,497	26,249	26,248	0	0	0	0
	設備	23,761	7,921	15,840	0	0	0	0
	研究費	203,219	133,602	69,617	0	0	0	0
総計	279,477	167,772	111,705	0	0	0	0	

17

《施設》(私学助成を受けていないものも含め、使用している施設をすべて記載してください。)(千円)

施設の名 称	整備年度	研究施設面積	研究室等数	使用者数	事業経費	補助金額	補助主体
第1実験室棟(第21 実験研究室、第22実 験研究室)	S61	110.82㎡		40			
第1実験室棟(分子 生化学工学共同実 験研究室1)	S61	18.48㎡		25			
温室	H1	100㎡		40			
第1実験室棟(クリ ンルーム3、共同実 験室)	S61	203.63㎡		100			
9号館(931講義室)	H4	59.64㎡		300			
第1実験室棟(B1実 験研究室)	S61	35.96㎡		20			

※ 私学助成による補助事業として行った新增築により、整備前と比較して増加した面積

0 m²

《装置・設備》(私学助成を受けていないものは、主なもののみを記載してください。)(千円)

装置・設備の名称	整備年度	型 番	台 数	稼働時間数	事業経費	補助金額	補助主体
(研究装置) 次世代シーケンスシ ステム(NextSeq500シ ステム)	H27		1台	3,744 h	52,497	26,248	私学助成
(研究設備) 次世代シーケンス データ解析システム	H27		1台	21,024 h	23,761	15,840	私学助成
(情報処理関係設備)							

法人番号

261003

18 研究費の支出状況

(千円)

年 度	平成 27 年度		
小 科 目	支 出 額	積 算 内 訳	
		主 な 使 途	金 額
教 育 研 究 経 費 支 出			
消 耗 品 費	17,535	消耗品費	17,535
光 熱 水 費	0		0
通 信 運 搬 費	44	通信料	44
印 刷 製 本 費	0		0
旅 費 交 通 費	818	国内旅費, 国外旅費	818
報 酬・委 託 料	5,481	謝金, 業務委託費	5,481
(諸会費・支払手数料)	58	学会参加費, 支払手数料	58
(公租公課・その他の保険料)	5	空港税ほか	5
(論文投稿掲載料)	200		200
計	24,141		24,141
ア ル バ イ ト 関 係 支 出			
人件費支出 (兼務職員)	0		0
教育研究経費支出	0		0
計	0		0
設 備 関 係 支 出(1個又は1組の価格が500万円未満のもの)			
教育研究用機器備品	3,860	ゲノム解析	3,860
図 書	0		0
計	3,860		3,860
研 究 ス タ ッ フ 関 係 支 出			
リサーチ・アシスタント	0		0
ポスト・ドクター	1,863	ゲノム解析	1,863
研究支援推進経費	0		0
計	1,863		1,863
ア ル バ イ ト 関 係 支 出			
人件費支出 (兼務職員)	5,295	研究補助	5,295
教育研究経費支出	0		0
計	5,295		5,295
設 備 関 係 支 出(1個又は1組の価格が500万円未満のもの)			
教育研究用機器備品	5,065	ゲノム解析等	5,065
図 書	0		0
計	5,065		5,065
研 究 ス タ ッ フ 関 係 支 出			
リサーチ・アシスタント	1,199	ゲノム解析等	1,199
ポスト・ドクター	9,721	ゲノム解析等	9,721
研究支援推進経費	0		0
計	10,920		10,920

年 度	平成 28 年度		
小 科 目	支 出 額	積 算 内 訳	
		主 な 使 途	金 額
教 育 研 究 経 費 支 出			
消 耗 品 費	19,576	消耗品費	19,576
光 熱 水 費	0		0
通 信 運 搬 費	0		0
印 刷 製 本 費	0		0
旅 費 交 通 費	1,231	国内旅費, 国外旅費	1,231
報 酬・委 託 料	2,557	謝金, 業務委託費	2,557
(学会参加費)	161	学会参加費	161
(公租公課)	6	空港税ほか	6
(保険料)	1	保険料	1
計	23,532		23,532
ア ル バ イ ト 関 係 支 出			
人件費支出 (兼務職員)	5,295	研究補助	5,295
教育研究経費支出	0		0
計	5,295		5,295
設 備 関 係 支 出(1個又は1組の価格が500万円未満のもの)			
教育研究用機器備品	5,065	ゲノム解析等	5,065
図 書	0		0
計	5,065		5,065
研 究 ス タ ッ フ 関 係 支 出			
リサーチ・アシスタント	1,199	ゲノム解析等	1,199
ポスト・ドクター	9,721	ゲノム解析等	9,721
研究支援推進経費	0		0
計	10,920		10,920

法人番号

261003

年 度	平成 29 年度		
小 科 目	支 出 額	積 算 内 訳	
		主 な 使 途	金 額
教 育 研 究 経 費 支 出			
消 耗 品 費	25,607	消耗品費	25,607
光 熱 水 費	0		
通 信 運 搬 費	0		
印 刷 製 本 費	0		
旅 費 交 通 費	901	国内旅費, 国外旅費	901
報 酬・委 託 料	1,021	謝金, 業務委託費	1,021
(諸 会 費)	48	学会参加費	48
(論 文 掲 載 料)	650	論文投稿掲載料	650
(公 租 公 課)	4	空港税ほか	4
(支 払 手 数 料)	7	支払手数料	7
計	28,238		28,238
ア ル バ イ ト 関 係 支 出			
人 件 費 支 出 (兼 務 職 員)	5,186	研究補助	5,186
教育研究経費支出	0		0
計	5,186		5,186
設 備 関 係 支 出 (1個又は1組の価格が500万円未満のもの)			
教育研究用機器備品	316	ゲノム解析等	316
図 書	0		0
計	316		316
研 究 ス タ ッ プ 関 係 支 出			
リサーチ・アシスタント	0		0
ポスト・ドクター	11,257	ゲノム解析等	11,257
研究支援推進経費	0		0
計	11,257		11,257
ア ル バ イ ト 関 係 支 出			
人 件 費 支 出 (兼 務 職 員)	8,564	研究補助	8,564
教育研究経費支出	0		0
計	8,564		8,564
設 備 関 係 支 出 (1個又は1組の価格が500万円未満のもの)			
教育研究用機器備品	0		0
図 書	0		0
計	0		0
研 究 ス タ ッ プ 関 係 支 出			
リサーチ・アシスタント	0		0
ポスト・ドクター	10,617	ゲノム解析等	10,617
研究支援推進経費	0		0
計	10,617		10,617

年 度	平成 30 年度		
小 科 目	支 出 額	積 算 内 訳	
		主 な 使 途	金 額
教 育 研 究 経 費 支 出			
消 耗 品 費	19,473	消耗品費	19,473
光 熱 水 費	0		
通 信 運 搬 費	0		
印 刷 製 本 費	0		
旅 費 交 通 費	1,150	国内旅費, 国外旅費	1,150
報 酬・委 託 料	1,873	謝金, 業務委託費	1,873
(諸 会 費)	32	学会参加費	32
(論 文 掲 載 料)	756	論文投稿掲載料	756
(支 払 手 数 料)	11	支払手数料	11
(修 繕 費)	324	修繕費	324
計	23,619		23,619
ア ル バ イ ト 関 係 支 出			
人 件 費 支 出 (兼 務 職 員)	8,564	研究補助	8,564
教育研究経費支出	0		0
計	8,564		8,564
設 備 関 係 支 出 (1個又は1組の価格が500万円未満のもの)			
教育研究用機器備品	0		0
図 書	0		0
計	0		0
研 究 ス タ ッ プ 関 係 支 出			
リサーチ・アシスタント	0		0
ポスト・ドクター	10,617	ゲノム解析等	10,617
研究支援推進経費	0		0
計	10,617		10,617

法人番号

261003

年 度	平成 31 年度		
小 科 目	支 出 額	積 算 内 訳	
		主 な 使 途	金 額
教 育 研 究 経 費 支 出			
消 耗 品 費	12,549	消耗品費	12,549
光 熱 水 費	0		0
通 信 運 搬 費	0		0
印 刷 製 本 費	0		0
旅 費 交 通 費	761	国内旅費	761
報 酬 ・ 委 託 料	1,670	謝金, 業務委託費	1,670
(諸 会 費)	62	学会参加費	62
(支 払 手 数 料)	11	支払手数料	11
(論 文 掲 載 料)	422	論文投稿掲載料	422
(保 守 費)	3,097	保守費用	3,097
(修 繕 費)	55	修繕費	55
計	18,627		18,627
ア ル バ イ ト 関 係 支 出			
人 件 費 支 出 (兼 務 職 員)	8,625	研究補助	8,625
教 育 研 究 経 費 支 出	0		0
計	8,625		8,625
設 備 関 係 支 出 (1 個 又 は 1 組 の 価 格 が 500 万 円 未 満 の も の)			
教 育 研 究 用 機 器 備 品	3,432	ゲノム解析等	3,432
図 書	0		0
計	3,432		0
研 究 ス タ ッ フ 関 係 支 出			
リサーチ・アシスタント	1,038	ゲノム解析等	1,038
ポスト・ドクター	9,024	ゲノム解析等	9,024
研究支援推進経費	0		0
計	10,062		10,062

研究成果の詳細

Review

Heterophylly: Phenotypic Plasticity of Leaf Shape in Aquatic and Amphibious Plants

Gaojie Li ^{1,†}, Shiqi Hu ^{1,†}, Hongwei Hou ¹ and Seisuke Kimura ^{2,3,*} 

¹ The State Key Laboratory of Freshwater Ecology and Biotechnology, The Key Laboratory of Aquatic Biodiversity and Conservation of Chinese Academy of Sciences, Institute of Hydrobiology, Chinese Academy of Sciences, University of Chinese Academy of Sciences, Wuhan 430072, Hubei, China; ligaojie@ihb.ac.cn (G.L.); hushiqi@ihb.ac.cn (S.H.); houhw@ihb.ac.cn (H.H.)

² Faculty of Life Sciences, Kyoto Sangyo University, Kamigamo-motoyama, Kita-ku, Kyoto-shi, Kyoto 603-8555, Japan

³ Center for Ecological Evolutionary Developmental Biology, Kyoto Sangyo University, Kamigamo-motoyama, Kita-ku, Kyoto-shi, Kyoto 603-8555, Japan

* Correspondence: seisuke@cc.kyoto-su.ac.jp; Tel.: +81-75-705-3113

† These authors contributed equally to this work.

Received: 21 August 2019; Accepted: 14 October 2019; Published: 16 October 2019



Abstract: Leaves show great diversity in shape, size, and color in nature. Interestingly, many plant species have the ability to alter their leaf shape in response to their surrounding environment. This phenomenon is termed heterophylly, and is thought to be an adaptive feature to environmental heterogeneity in many cases. Heterophylly is widespread among land plants, and is especially dominant in aquatic and amphibious plants. Revealing the mechanisms underlying heterophylly would provide valuable insight into the interaction between environmental conditions and plant development. Here, we review the history and recent progress of research on heterophylly in aquatic and amphibious plants.

Keywords: heterophylly; submergence; environment; adaptation; molecular mechanisms

1. What is Heterophylly?

Plants display amazing morphological diversity of leaves. The leaves of some plant species can undergo considerable form alteration in response to environmental conditions via a process called heterophylly (Figure 1) [1]. Heterophylly is a type of phenotypic plasticity that is widespread among plants.

Heterophyllous plants produce dramatic, often abrupt changes in leaf morphology in response to environmental factors [1]. Interestingly, most known examples of heterophylly are found in aquatic and amphibious plants, in which submerged leaves are often dissected compared with simple terrestrial leaves [2] (Table 1). Because these plants are sometimes submerged during flooding, they have evolved to thrive and grow both under water and terrestrial conditions. Such plants often display heterophylly, which is generally regarded as a morphological process allowing adaptation to a capricious environment [2,3]. Leaf shapes are related to their function, as submerged leaves are thin, narrow, and lack cuticles and stomata, whereas terrestrial leaves are thicker, expanded, and cutinized with stomata [2,3]. An example is the narrow leaves of amphibious plants located along riverbanks where flooding always occurs. Narrow leaves are less efficient at absorbing sunlight than those that have wider blades; however, they can withstand the destructive force of water flow. Narrow or deeply serrated/lobed leaves are also present in aquatic plants, and may provide for similar interactions with the surrounding environment, including factors beyond the submerged conditions for mineral

nutrient and CO₂ uptake. These narrow or dissected leaf blade formations are likely an adaptation to underwater conditions.

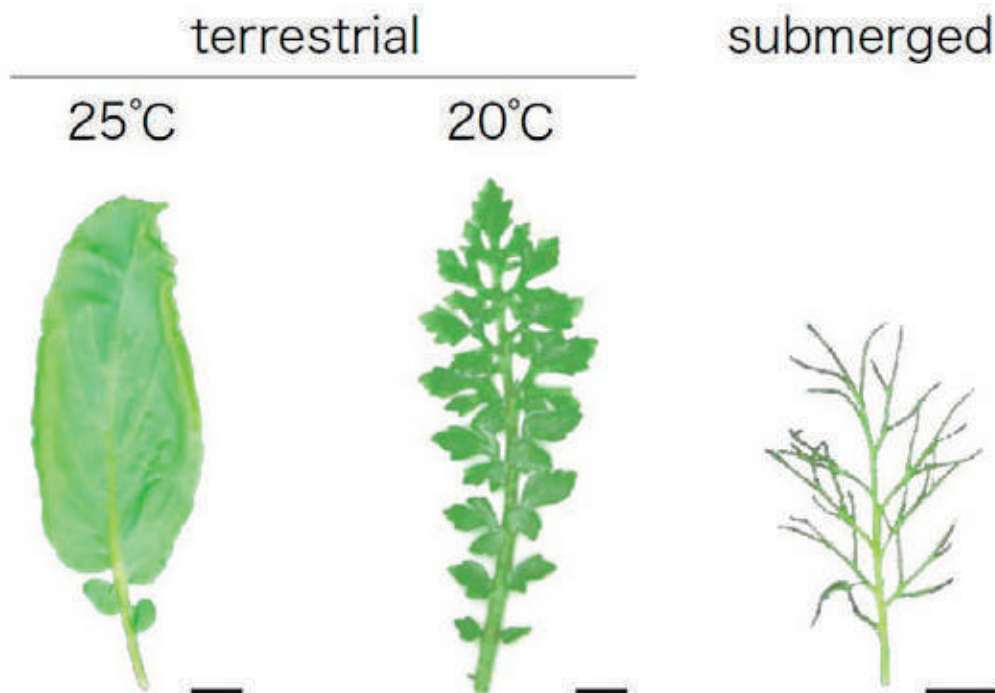


Figure 1. Heterophylly of amphibious plant, North American lake cress, *Rorippa aquatica* (Brassicaceae). North American lake cress shows distinct heterophylly between submerged and terrestrial conditions. Leaf shape alternation is also induced by changes in ambient temperature. Bars, 1cm.

The original definition of heterophylly was not strictly linked to the environment, and lacked a clear distinction from other similar processes [1]. However, heterophylly was recently defined as leaf form alteration in response to environmental conditions, unlike heteroblasty and anisophylly [1,4–6]. Heteroblasty was described as changes in leaf shape during growth development, but does not include morphological changes induced by environmental factors [1,5]. Similarly, anisophylly is usually coupled with asymmetry and phyllotaxis of leaves and stems, and also does not include morphological changes induced by environmental factors [7].

Considering the distinct differences in leaf shape between aerial and submerged conditions, elucidating the mechanisms underlying heterophylly in aquatic and amphibious plants would provide valuable insight into the interaction between the environment and plant development.

2. History of Research on Heterophylly

Heterophylly is observed in many evolutionary diverse aquatic and amphibious plant species including those belonging to the Nymphaeales, Ranunculales, Saxifragales, Myrtales, Brassicales, Lamiales, and many other orders [8–16] (Table 1). There are remarkable morphological differences in these heterophyllous plants between submerged and terrestrial environments. Leaves under submerged conditions tend to have a thin, filamentous, or linear shape, degraded vascular structure, and the leaves usually lack stomata cells, which means plants must directly absorb nutrients and exchange gas from water [2,3,17,18]. Here, we review the existing knowledge of heterophylly in different species, with a particular focus on the role of phytohormones and environmental factors in regulating heterophylly, to gain valuable insight into this phenomenon.

Table 1. Representative heterophyllous plants and treatments that can induce heterophylly.

Species	Family	Common Name	Treatments	References
<i>Alisma graminifolium</i>	Alismataceae	-	light	[19]
<i>Callitriche heterophylla</i>	Callitrichaceae	two-headed water-starwort	ABA, GA, temperature, osmotic stress	[11,20,21]
<i>Callitriche intermedia</i>	Callitrichaceae	narrowleaf water-starwort	osmotic stress, temperature	[22,23]
<i>Callitriche stagnalis</i>	Callitrichaceae	pond water starwort	GA	[20,21]
<i>Hippuris vulgaris</i>	Hippuridaceae	common mare's tail	ABA, temperature, light intensity, R/FR ratio, osmotic stress	[5,9,24,25]
<i>Hygrophila difformis</i>	Acanthaceae	Water-Wisteria	ABA, ethylene, GA, humidity, temperature	[26,27]
<i>Ilex aquifolium</i>	Aquifoliaceae	Common holly	mammalian browsing	[28]
<i>Ludwigia arcuata</i>	Onagraceae	primrose-willow	ABA, ethylene, temperature	[6,14,29,30]
<i>Marsilea quadrifolia</i>	Marsileaceae	European water clover	ABA, blue light, CO ₂	[12,13]
<i>Marsilea vestita</i>	Marsileaceae	hairy water clover	CO ₂ , light intensity, light quality	[31,32]
<i>Myriophyllum brasiliense</i>	Haloragaceae	red stemmed parrot feather	CO ₂	[33]
<i>Nuphar variegata</i>	Nymphaeaceae	yellow water lily	CO ₂ , sediment type and water depth	[34]
<i>Nuphar lutea</i>	Nymphaeaceae	yellow pond-lily	water depth	[16]
<i>Potamogeton nodosus</i>	Potamogetonaceae	longleaf pondweed	ABA	[4]
<i>Potamogeton alpinus</i>	Potamogetonaceae	-	water flow	[35]
<i>Potamogeton octandrus</i>	Potamogetonaceae	-	submerged or floating condition, development	[36]
<i>Proserpinaca palustris</i>	Haloragidaceae	marsh mermaid-weed	ABA, GA, light intensity, humidity, osmotic stress, photoperiod	[17,37,38]
<i>Proserpinaca intermedia</i>	Haloragidaceae	intermediate mermaid-weed	photoperiod	[39]
<i>Ranunculus aquatilis</i>	Ranunculaceae	water crowfoot	photoperiod	[40]
<i>Ranunculus flabellaris</i>	Ranunculaceae	yellow water buttercup	ABA, temperature, CO ₂	[33,41,42]
<i>Ranunculus trichophyllus</i>	Ranunculaceae	threadleaf crowfoot	ABA, ethylene, temperature, hypoxia	[43]
<i>Rorippa aquatica</i>	Brassicaceae	North American lake cress	GA, ethylene, temperature, light intensity	[15,44,45]
<i>Rotala hippuris</i>	Lythraceae	-	R/FR ratio, blue light intensity	[46]
<i>Sagittaria sagittifolia</i>	Alismataceae	arrowhead	light intensity	[19]

Multiple phytohormones are involved in the regulation of heterophylly. For example, gibberellic acid (GA) can induce floating plants to develop aquatic leaves in the two-headed water starwort, *Callitriche heterophylla* (Callitrichaceae), and pond water starwort, *Callitriche stagnalis*, while abscisic acid (ABA) can induce submerged plants to grow floating leaves in the two-headed water starwort [11,20,21]. Kane and Albert (1987b) [17] also found that ABA can induce the aerial leaf morphology and vasculature in submerged common mare's tails, *Hippuris vulgaris* (Hippuridaceae). Kane and Albert (1989) [10] later studied nine plant species in the genera *Myriophyllum* or *Proserpinaca* (Haloragaceae), and found that ABA plays a common role in the regulation of leaf development, induction of stomata development, increased cuticularization, and reduced leaf and epidermal cell length in these heterophyllous plants. In 1990, ABA was also observed to induce the terrestrial leaf phenotype in the yellow water buttercup, *Ranunculus flabellaris* (Ranunculaceae). Later, Lin and Yang (1999) [12] studied European water clover, *Marsilea quadrifolia* (Marsileaceae), and found that ABA could induce its terrestrial phenotype under submerged conditions.

In addition to ABA, other phytohormones regulate this process. Kane and Albert (1987a) [9] studied the functions of two phytohormones, GA and ABA, and found that both regulate the heterophylly of marsh mermaid-weed, and these two phytohormones were regulated by environmental stimuli, including photoperiod and water stress. In Piedmont primrose-willow, *Ludwigia arcuata* (Onagraceae), ABA and ethylene have antagonistic effects on the regulation of heterophylly. Ethylene induced submerged-type leaves in terrestrial conditions, while ABA induced aerial phenotypes under submerged conditions [14,29]. Furthermore, ethylene affects the frequency and direction of cell division, and low temperature also enhances the effects of ethylene in Piedmont primrose-willow [6,30]. Recent studies

on threadleaf crowfoot, *Ranunculus trichophyllus* (Ranunculaceae), showed that ABA and ethylene signaling are the key regulatory pathways for heterophylly in this species. Aquatic leaves have higher levels of ethylene and lower levels of ABA than terrestrial leaves [43].

Research on the regulation of heterophylly by environmental factors was first carried out in 1902 by McCallum (1902); the author found that marsh mermaid-weed, *Proserpinaca palustris* (Haloragidaceae), has a broad, serrated leaf shape, and well-developed vascular system when leaves are not submerged, but has a dissected, thread leaf shape, lacks a xylem, and has a weak phloem under submerged conditions. McCallum (1902) [37] tested the effects of environmental factors, such as light, nutrition, temperature, humidity, salinity, and the concentration of CO₂ and O₂, and found that humidity can significantly change the leaf shape of common mermaid-weed.

In the past several decades, a large amount of experimental work has been published on the effects of environmental conditions on the leaf shapes of heterophyllous plants [20–22,24,34,41]. For example, 30% artificial sea water (which results in high osmotic stress) resulted in the formation of aerial leaves in narrowleaf water starwort, *Callitriche intermedia*, grown under submerged conditions [22]. Furthermore, high temperature, mannitol, or artificial sea water can induce submerged plants to grow floating leaves in the two-headed water starwort [11,20,21].

The leaf form of common mare's tail is affected by light levels and the osmotic pressures in the environment in which it grows, as high light intensity or high concentrations of artificial sea water result in leaves resembling aerial ones in this plant [25]. In addition, Bodkin et al. (1980) [24] also found that a lower red light (wave length 660 nm)/far red light (wave length 730 nm) ratio (R/FR ratios) led to the growth of terrestrial leaves in common mare's tail.

Johnson (1967) [42] found that yellow water buttercups grown under different conditions have two typical heterophyllic leaves, deep lobed aquatic leaves and shallow lobed terrestrial leaves. According to Johnson [42], low temperature can induce deep lobed leaves in terrestrial plants, as there is a limited exchange of gases in low temperature or aquatic environments, and therefore the increase in this specific surface area is intended to accommodate the diffusion of gases. Later, Bristow (1969) analyzed the effect of CO₂ on yellow water buttercups, and found that 5% CO₂ induced the formation of aquatic leaves in terrestrial plants [33]. Furthermore, Cook (1969) [40] found that the divided leaf shape of white water crowfoot, *Ranunculus aquatilis*, can be induced by short photoperiods under terrestrial or submerged conditions, but this leaf shape developed only under submerged conditions with long photoperiods.

Bristow and Looi (1968) [31] tested the effects of CO₂ in the regulation of heterophylly, and found that higher CO₂ concentrations can induce aquatic phenotypes in hairy water clover, *Marsilea vestita*. Lin and Yang (1999) [12] studied European water clover and found that blue light could induce a terrestrial phenotype under submerged conditions [12]. A study on yellow water lily, *Nuphar variegata* (Nymphaeaceae), also demonstrated that concentrations of CO₂, sediment type, and water depth can all affect the leaf morphogenesis of this species [34]. In addition, a recent study showed that cold conditions and hypoxia can induce aquatic leaf shape formation in threadleaf crowfoot [43].

These studies indicate that environmental factors such as light, nutrition, temperature, humidity, salinity, concentrations of CO₂ and O₂, and phytohormones including GA, ABA, and ethylene all are involved in the heterophyllic process. Furthermore, these factors trigger multiple intracellular mechanisms that control heterophylly.

3. Environmental Factors that Induce Heterophylly

Multiple factors such as CO₂ concentration, light intensity and quality, temperature, osmotic potential, and mechanical forces are involved in the submergence response. Here we review how these environmental factors affect heterophylly.

3.1. CO₂

The CO₂ concentration of water is much higher than that of the air, but the rate of diffusion of CO₂ in water is much slower. Plants may require CO₂ at a higher rate than is available given the slow rate of diffusion under aquatic conditions. In a study on marsh mermaid-weed, plants were grown under water in vessels containing different CO₂ concentrations. A submerged leaf shape was produced in every case, indicating that, at least in the absence of CO₂, the water form of marsh mermaid-weed could not be produced [37]. In 1968, a study of an amphibious plant, hairy water clover, was published [31]. When supplied with increased concentrations of CO₂ in air, this plant exhibited many leaf characteristics of the water form, such as the orientation of leaf laminae and the shape of epidermal cells [31]. A year later, another two heterophyllous amphibious species, yellow water buttercup and red stemmed parrot feather, *Myriophyllum brasiliense* (Haloragaceae), were found to develop aquatic leaf morphology when grown on solid substrate with 5% CO₂ in air, while terrestrial plants grown with 0.03% CO₂ in air still developed terrestrial leaf morphology, and submerged plants developed an intermediate leaf morphology [33]. These results were similar to those obtained with hairy water clover. In addition, high CO₂ concentrations favored the development of submerged leaf traits over floating leaves in yellow water lily [34]. Thus, these results suggest that, during plant development, CO₂ sensing pathways are critical for the acquisition of heterophylly, although it may be HCO₃⁻ (produced by CO₂ reacting with water) that is the key factor that induces heterophylly [47].

3.2. Light Intensity

McCallum (1902) [37] used many aquatic plants to conduct experiments under different light conditions. The results uniformly indicated that light had no effect on the characteristics of developing shoots [37]. However, studies on plants in the genus *Hippuris* demonstrated that leaf shape was in some way affected by light. Broad and round aerial-type leaves developed under a light intensity of 194 μmol photons m⁻² s⁻¹, while aquatic leaves were produced at 97 μmol photons m⁻² s⁻¹ illumination [25]. Experiments on arrowhead, *Sagittaria sagittifolia* (Alismataceae), and *Alisma graminifolium* (Alismataceae) also indicated that absence of light inhibited the formation of aerial leaves, but this effect may not be directly due to the darkness and may be due to a state of inadequate nutrition instead [19].

With the rise of sequencing technology, transcriptome analysis has indicated that light intensity affects leaf form alterations in North American lake cress, *Rorippa aquatica* (Brassicaceae) [44,45]. In North American lake cress, dissected leaves with deep biserrated leaflets developed under higher light intensity (90 μmol photons m⁻² s⁻¹) whereas dissected leaves with a relatively smooth margin developed when exposed to lower light intensity (15 μmol photons m⁻² s⁻¹).

3.3. Light Quality

Light quality can also be effective in inducing heterophylly. Lin and Yang (1999) [12] reported that blue light can independently induce the transition from submerged type leaves (divided, oblanceolate leaflets, expanded in the plane of the petiole) to aerial type leaves (resembling a four-leaf clover, with quadrifid lamina expanded at an angle to the petiole) in European water clover [12]. Continuous far-red light can cause the fern hairy water clover to develop as its land form (short rhizome and long petioles) instead of the water form (long rhizome and short petioles) [32]. A study on common mare's tail indicated that when R/FR ratios exceeded a critical range, aerial leaf formation (thick cuticle, irregular rounded cells, and numerous stomata) was inhibited, and only submerged-type leaves (thin cuticle, long thin cells, and no stomata) were formed [24].

3.4. Light Photoperiod

The photoperiod controls many developmental responses in plants. The response to the photoperiod enables developmental events to be scheduled to meet with particular environmental conditions [48]. Much progress has been made towards understanding the molecular mechanisms

involved in the plant response to photoperiod, including those that govern the changes in leaf morphology. It has been shown that short days tend to promote the formation of submerged leaves (highly dissected), and long days promote the formation of aerial-type leaves (less dissected or simply trilobed) in marsh mermaid-weed [38] and intermediate mermaid-weed, *Proserpinaca intermedia* [39]. In addition, another species in the genus *Ranunculus*, white water crowfoot, also developed submerged divided-type leaves (which are composed of long, cylindrical, capillary segments) under short photoperiods, whether under terrestrial or submerged conditions [40]. However, research on variegated pond lilies suggests that the photoperiod only has a mild impact on this leaf morphology alteration [38]. In this case, alternative regulatory mechanisms may exist, such as those involving variation of energy or photosynthetically active radiation.

3.5. Temperature

In the past few decades, the effects of temperature on the determination of leaf form have been studied in many heterophyllous species. As described, low temperature induces the formation of submerged-type leaves on terrestrial shoots of yellow water buttercup [42], threadleaf crowfoot [43], marsh mermaid-weed [38], and intermediate mermaid-weed [39]. However, Cook (1968) [40] found that temperatures (between 6 and 20 °C) had almost no effect on the determination of leaf shape formation in white water crowfoot. Temperature only altered some morphological features of the divided leaves, such as the number of dichotomous branches and length of the petiole [40]. Moreover, high temperatures have been reported to induce aerial-type leaves on submerged shoots in aquatic plants, including in the two-headed starwort [11,21], narrowleaf water starwort [23], and common mare's tail [24]. A study on model plant Piedmont primrose-willow identified temperature as the most crucial factor for forming extremely elongated submerged leaves and elongated epidermal cells [30]. In 2014, researchers proposed North American lake cress as a model plant for the study of heterophylly, since it was found to have a temperature-dependent development of heterophylly. Pinnately dissected leaves developed at lower temperatures under both terrestrial and submerged conditions, indicating a common molecular mechanism of leaf morphogenesis under both of these conditions [45].

3.6. Osmotic Stress

Osmotic stress is caused by drought, salinity, or cold stress; all of these factors have had a great impact on plant evolution [49]. Osmotic stress affects both the growth and development of plants, and in particular reduces the productivity of crop plants and affects leaf size and internode length [50,51]. It also involves ABA, ethylene, and GA signaling pathways [52–54]. Several heterophyllous aquatic or amphibious plants undergo morphological changes in solutions of various osmotic pressures, including *Marsilea* species, and narrowleaf water starwort [22,23,25]. Leaves of these plants resemble aerial-type leaves when grown in solutions of high osmotic concentration. In common mare's tail, osmotic stress triggered aerial leaf development, supporting the hypothesis that osmotic stress causes submerged shoots to produce endogenous ABA, which in turn induces the formation of aerial-type leaves [5]. In a study of narrowleaf water starwort, it was suggested that increases in osmotic pressure might directly affect the primordial leaf form through turgor changes that activate an intracellular signaling cascade. A more likely hypothesis is that leaf form alteration was mediated through an auxin-dependent mechanism that responds to fluctuations in the turgor pressure of leaf cells [23].

3.7. Water Depth

For aquatic plants, water depth is a complex but key factor involved in heterophylly [55]. Many factors change with water depth, including light, pressure, temperature, and CO₂. It has been demonstrated that light availability decreases with increasing depth. For instance, areas with a water depth of 1 m in the River Rhine have a light transmission below 1% [56]. Thus, heterophylly in aquatic plants is thought to correlate with changes in water depth. A study on *Hippuris* plants implied that in deeper water of the Great Whale River, typical long and flaccid aquatic leaves developed

on stems. However, in the shallower permanent pools with depths of 12–18 inches, leaves more commonly displayed the characteristics of aerial-type leaves (thick outer walls, more lateral veins, and mesophyll) [25]. This is consistent with the results in variegated pond lilies, which indicate that shallower depths stimulate the development of floating leaves [34]. The ideas of the classic pattern of zonation also indicate that plants with floating leaves are typically dominant in shallower water, whereas submerged macrophytes are typically dominant in deeper water [55,57].

3.8. Water Flow

Aquatic plants grown in streams have various constraints linked to the water flow and adopt strategies to prevent damage due to water pressure and other hydrodynamic forces [58]. As an example, the architecture traits of the modules of *Potamogeton alpinus* (Potamogetonaceae) from slow- and fast-flowing streams have been studied [59]. It was found that in fast-flowing waters, the presence of floating leaves stabilized the vertical position of stem and caused elongation of submerged leaves; together with a reduction in shoot diameter, this reduced the pressure of the water. In addition, plants grown in fast-flowing conditions are more resistant to stretching than others grown in standing waters, which means that stems from fast-flowing conditions are more elastic and therefore less prone to damage by stretching forces [59,60].

As described above, submersion is not the only factor that regulates heterophylly, and other environmental factors also play a role [35,61,62]. The relationship between these factors and the molecular mechanism of leaf phenotype regulation needs to be further examined.

4. Molecular Basis for Heterophylly

Heterophylly is an eye-catching phenomenon that has attracted many researchers, and has been studied for a long time. Although much is known about the physiological and cytological aspects of heterophylly, the underlying mechanism regulating the process is largely unknown at the gene level. This is due to the difficulties in performing genetic, genomic, and transcriptomic analyses, because most plants that show significant heterophylly are non-model plant species, and DNA sequence information on these species is limited. However, the recent advent of next-generation sequencing technology has facilitated the analysis of genomes and transcriptomes in non-model plant species. Heterophylly is not dependent on changes in the genome sequence, but is induced by changes in the expression levels and patterns of genes involved in leaf development and environmental responses [63]. Thus, transcriptome analysis is a useful method to elucidate the mechanism of heterophylly at the gene level. In fact, several transcriptome studies have been conducted on multiple heterophyllous plant species. In this section, we summarize the recent progress regarding our understanding of the molecular basis for heterophylly.

4.1. North American Lake Cress

North American lake cress is a perennial amphibious plant whose habitat includes the bays of lakes, ponds, and streams in North America. In nature, the cress shows distinct heterophylly between submerged and terrestrial conditions (Figure 1). The plant develops pinnately dissected leaves with needle-like leaf blades under submerged conditions, while it forms simplified leaves with serrated margins under terrestrial conditions. Interestingly leaf shape alternation is induced by changes in ambient temperature [44,45]. Lower temperatures result in more dissected leaves, which resemble submerged leaves, and higher temperatures simplify the leaf shape. In this cress, the expression levels of *KNOTTED1-LIKE HOMEBOX (KNOX1)* orthologs, which are involved in leaf shape determination in many plant species, changed in response to change of ambient temperature. Furthermore, the accumulation of GA, which is regulated by KNOX1, changed in the leaf primordia. Thus, the regulation of GA levels via KNOX1 is involved in regulating heterophylly in North American lake cress [44,45]. Nakayama et al. (2014b) [45] performed RNA-seq analysis to understand global transcriptional alterations associated with heterophylly induced by temperature change. Interestingly,

the genes upregulated in the dissected leaf condition (i.e., those formed under high temperature conditions) also overlapped with those that respond to changes in high light intensity, suggesting that light intensity affects the leaf morphology of this plant. Indeed, under higher light conditions intensity ($90 \mu\text{mol photons m}^{-2} \text{s}^{-1}$), dissected leaves with deeply serrated leaflets developed, whereas under lower light conditions intensity ($15 \mu\text{mol photons m}^{-2} \text{s}^{-1}$), dissected leaves with a relatively smooth margin developed. Therefore, temperature and light intensity may affect leaf form through a common developmental mechanism. Indeed, plant photoreceptors such as phytochromes are involved in temperature sensing [64–66], leading to the hypothesis that light sensing mechanisms might be involved in regulating heterophylly in North American lake cress.

4.2. Threadleaf Crowfoot

Threadleaf crowfoot is also an amphibious plant that shows heterophylly. This plant develops radialized leaves under submerged conditions, but produces flattened broad leaves under aerial conditions. Kim et al (2018) [43] analyzed this plant to understand the molecular basis behind heterophylly. Transcriptome analysis demonstrated that two phytohormones, ethylene and ABA, are involved in regulating heterophylly. Indeed, aquatic leaves produced higher levels of ethylene and lower levels of ABA compared with terrestrial leaves. In submerged leaves, accumulation of ethylene increased the expression of *EIN3* (*ETHYLENE INSENSITIVE3*), an ethylene signaling transducer. The *EIN3*-mediated pathway induced the overproduction of abaxial genes, *KANADI* orthologs, which are implicated in the generation of radialized leaves. The overproduction of *KANADI* orthologs suppressed the expression of *STOMAGEN* and *VASCULAR-RELATED NAC-DOMAIN7* (*VND7*), resulting in lack of stomata and reduced vessel development in submerged leaves. In contrast, ABA activated the expression of adaxial genes, *HD-ZIPIII* orthologs, which increased *STOMAGEN* and *VND7* under terrestrial conditions. Such responses were not observed in the closely related species cursed buttercup, *Ranunculus sceleratus*, which does not show heterophylly. These results clearly indicate that acquisition of this ABA/ethylene signaling cascade is a key step for evolutionary adaptation to aquatic environments.

4.3. *Potamogeton octandrus*

P. octandrus is a perennial aquatic heterophyllous herb found in slow moving fresh water [36]. The floating leaves of this plant are ovate and flat, and submerged leaves are narrow and long. The leaf shape is not only affected by environmental conditions, but also by the developmental stage. In the early stage of development, only submerged type leaves are formed. When the tops of stems reach the water surface, they start producing both floating and submerged leaves. To investigate the molecular basis for this heterophylly, transcriptome analyses of submerged and floating leaves at different developmental points were performed [36]. In total, 6822 differentially expressed genes (DEGs) were identified in 81,103 unigenes. KEGG pathway enrichment analysis demonstrated that many of the DEGs could be classified in the “plant hormone signal transduction” category. Indeed, endogenous levels of hormones such as ABA, cytokinin, GA, and auxin changed between conditions, suggesting that phytohormones play important roles in regulating heterophylly [36,67]. In many heterophyllous plants, stomata and cuticle development are suppressed in submerged leaves. In *P. octandrus*, there are many genes related to stomata and cuticle development in DEGs. Elucidating their precise roles in heterophylly will provide more information on the mechanisms regulating this important process [36].

4.4. *Water-Wisteria, Hygrophila Difformis* (Acanthaceae)

Water-Wisteria is an amphibious plant belonging to the *Hygrophila* genus which contains almost 90 species. It is a fast-growing plant that has either simple leaves or highly lobed leaves, depending on the environment. Their leaf shape responds to phytohormones (such as ABA, ethylene, and GA) and environmental factors (such as humidity and temperature). Furthermore, it is easily vegetatively propagated, and can be easily transformed by *Agrobacterium tumefaciens*. Analysis of *KNOX1* of

Water-Wisteria (HdSTM and HdBP) has revealed that the expression of *KNOX1* orthologs are higher under submerged conditions than under terrestrial conditions. This result is consistent with the pattern of *KNOX1* expression in North American Lake Cress [15,45]. These characteristics suggest that Water-Wisteria is also a good model plant to study heterophylly [26]. Recently, Horiguchi et al. (2019) have analyzed the photosynthetic ability of aerial and submerged leaves of Water-Wisteria and found that this plant acclimates to a submerged environment by developing submerged leaves, and that ethylene is important for this acclimation [27].

5. Future Perspectives for Studies on Heterophylly

The mechanisms underlying heterophylly remain largely unknown. On the basis of this review, we would like to suggest some of the topics that should be included in future research in this field.

5.1. Sensing Mechanisms for Submergence

Heterophylly of aquatic and amphibious plants is induced by submergence, but it is still unknown how plants perceive submergence. In deepwater rice, *Oryza sativa* (Gramineae), accumulation of ethylene in the tissues during submergence has been shown to induce the elongation of internodes [68]. Piedmont primrose-willow is a well-studied aquatic plant that shows heterophylly and ethylene is involved in leaf shape determination in this plant [7,14,29,30]. Thus, ethylene accumulation is thought to act as a signal for submergence. ABA is known as a stress hormone, and is upregulated under drought conditions, where it functions as a central regulator and integrator of the changes in stomatal behavior, including sensitivity, elicited by external signals [69]. ABA treatment induces the formation of aerial leaves in Piedmont primrose-willow and longleaf pondweed, *Potamogeton nodosus*, which exhibit distinct heterophylly between floating and submerged leaves [4]. Both ethylene and ABA are likely used as signals in the submergence response.

North American lake cress is another plant that can change its leaf shape in response to submergence and changes in temperature and light intensity [15,44,45]. Furthermore, heterophylly in common mare's tail and *Rotala hippuris* (Lythraceae) is controlled by the ratio of red to far-red light intensity (R/FR) [46]. These results imply direct phytochrome control of the reversible transitions between different types of leaves, because water (and especially deep water) specifically absorbs longer wavelengths light, such as far-red (FR) light [70]. Recently, it was shown that phytochrome is also involved in temperature sensing in plants [64–66], which also coincides with the fact that some heterophyllous plants, such as North American lake cress, change leaf shape in response to temperature change. In conclusion, it appears that phytochrome responsiveness is important for the induction of heterophylly in aquatic plants adapted to deep water.

5.2. Epigenetic Regulation of Heterophylly

Heterophylly is induced by changes in gene expression in response to environmental conditions. Therefore, it is critical to understand how gene expression is regulated during the process. Phenotypic plasticity in traits such as flowering is controlled by epigenetic regulation in response to environmental conditions. The ability of plants to respond to environmental changes by epigenetic modifications may play an important role in regulating gene expression in heterophylly [71]. Common holly, *Ilex aquifolium* (Aquifoliaceae), is a heterophyllous tree species that shows two types of leaves, prickly and nonprickly [28]. Interestingly, the production of prickly leaves is induced by mammalian browsing, most likely as a protective response to prevent herbivory [28]. A methylation-sensitive amplified polymorphism (MSAP) analysis demonstrated that DNA methylation profiles are different between prickly and nonprickly leaves, suggesting a correlation between epigenetic status and leaf shapes [28]. It would be interesting to evaluate whether epigenetic regulation is also involved in regulating heterophylly in other species, including aquatic and amphibious plants.

5.3. Adaptive Significance of Heterophylly

In addition to the plasticity of leaves in response to different environments, the relationship between leaf shape and leaf function remains unclear. Leaves are the main photosynthetic organs of plants and have developed numerous physiological, biomechanical, and cellular adaptations to fulfill this function. Thus, one hypothesis is that leaf dissection can increase photosynthesis under particular conditions. Baker-Brosch and Peet (1997) demonstrated that lobed leaves of temperate trees are critical for early season photosynthesis, because this type of leaf can incorporate more CO₂ [72]. Recently, studies of tomato and cotton revealed that the expression level of specific genes was higher during the development of more complex leaves, which is a possible explanation for the increase in photosynthesis efficiency and fruit sugar content [73–75]. Another explanation is that leaf dissection could modulate leaf temperature. One study found that sun leaves (near the top and on the southern sides of trees) of large oaks tend to be more dissected than shade leaves, as leaf dissection could regulate thermal exchanges between leaves and the surrounding environment [76,77]. However, few studies regarding the links between leaf morphology and functions have focused on aquatic plants [36,67]. In addition, the adaptive significance of heterophylly in response to environmental heterogeneity remains unclear. Further studies will be required to address these questions.

5.4. Evolution of Heterophylly

Environmental conditions surrounding organisms are not constant, and can vary even from one minute to the next. Phenotypic plasticity, including heterophylly, may play an important role in the adaptation to such fluctuating environments. Acquiring the ability to respond to environmental changes is thought to be especially important for plants, because of their sessile lifestyle. Heterophylly is likely an adaptive feature for aquatic and water's edge environments. The process has evolved multiple times during plant evolution, and it is perceived to be an adaptive mechanism that allows plants to respond to the changeable environment [3,26–29,36,46,62–79]. Thus, heterophylly is a good example of convergent evolution. Recent progress in research on the molecular basis underlying heterophylly has highlighted the need for a comparative genomics and transcriptome approach to study this important process between plant species. Such comparative approaches will shed light on the evolutionary background of heterophylly in the near future.

Author Contributions: G.L., S.H., H.H., S.K.; writing—original draft preparation, S.K.; writing—review and editing.

Funding: This work was supported by JSPS KAKENHI (16H01472, 16K07408, 18H04787 and 18H04844 to S.K.) and by the MEXT Supported Program for the Strategic Research Foundation at Private Universities from the Ministry of Education, Culture, Sports, Science and Technology of Japan, Grant Number S1511023 to S.K. This work was also supported by grants from National Key R & D Program of China (2017YFE0128800, 2018YFD0900801) and General Project of Natural Science Foundation of China (31870384) to H.H.

Conflicts of Interest: The authors declare no conflict of interest.

References

1. Zotz, G.; Wilhelm, K.; Becker, A. Heteroblasty—A review. *Bot. Rev.* **2011**, *77*, 109–151. [[CrossRef](#)]
2. Wells, C.L.; Pigliucci, M. Adaptive phenotypic plasticity: The case of heterophylly in aquatic plants. *Perspect. Plant Ecol. Evol. Syst.* **2000**, *3*, 1–18. [[CrossRef](#)]
3. Wanke, D. The ABA-mediated switch between submersed and emersed life-styles in aquatic macrophytes. *J. Plant Res.* **2011**, *124*, 467–475. [[CrossRef](#)] [[PubMed](#)]
4. Anderson, L.W. Abscisic Acid Induces Formation of Floating Leaves in the Heterophyllous Aquatic Angiosperm *Potamogeton nodosus*. *Science* **1978**, *201*, 1135–1138. [[CrossRef](#)]
5. Goliber, T.E.; Feldman, L.J. Developmental analysis of leaf plasticity in the heterophyllous aquatic plant *Hippuris vulgaris*. *Am. J. Bot.* **1990**, *77*, 399–412. [[CrossRef](#)]
6. Kuwabara, A.; Nagata, T. Cellular basis of developmental plasticity observed in heterophyllous leaf formation of *Ludwigia arcuata* (Onagraceae). *Planta* **2006**, *224*, 761–770. [[CrossRef](#)]
7. Dengler, N.G. Anisophylly and dorsiventral shoot symmetry. *Int. J. Plant Sci.* **1999**, *160*, S67–S80. [[CrossRef](#)]

8. Davis, G.J. Proserpinaca: Photoperiodic and chemical differentiation of leaf development and flowering. *Plant Physiol.* **1967**, *42*, 667–668. [[CrossRef](#)]
9. Kane, M.E.; Albert, L.S. Integrative regulation of leaf morphogenesis by gibberellic and abscisic acids in the aquatic angiosperm *Proserpinaca palustris* L. *Aquat. Bot.* **1987**, *28*, 89–96. [[CrossRef](#)]
10. Kane, M.E.; Albert, L.S. Abscisic acid induction of aerial leaf development in Myriophyllum and Proserpinaca species cultured in vitro. *J. Aquat. Plant Manag.* **1989**, *27*, 102–111.
11. Deschamp, P.A.; Cooke, T.J. Causal mechanisms of leaf dimorphism in the aquatic angiosperm *Callitriche heterophylla*. *Am. J. Bot.* **1984**, *71*, 319–329. [[CrossRef](#)]
12. Lin, B.; Yang, W. Blue light and abscisic acid independently induce heterophyllous switch in *Marsilea quadrifolia*. *Plant Physiol.* **1999**, *119*, 429–434. [[CrossRef](#)]
13. Hsu, T.; Liu, H.; Wang, J.; Chen, R.; Wang, Y.; Lin, B. Early genes responsive to abscisic acid during heterophyllous induction in *Marsilea quadrifolia*. *Plant Mol. Biol.* **2001**, *47*, 703–715. [[CrossRef](#)]
14. Kuwabara, A.; Tsukaya, H.; Nagata, T. Identification of factors that cause heterophylly in *Ludwigia arcuata* Walt. (Onagraceae). *Plant Biol.* **2001**, *3*, 98–105. [[CrossRef](#)]
15. Nakayama, H.; Nakayama, N.; Nakamasu, A.; Sinha, N.; Kimura, S. Toward elucidating the mechanisms that regulate heterophylly. *Plant Morphol.* **2012**, *24*, 57–63. [[CrossRef](#)]
16. Klimenko, E.N. Structural and functional aspects of the *Nuphar lutea* (L.) Smith heterophylly: Ultrastructure and photosynthesis. *Cytol. Genet.* **2012**, *46*, 272–279. [[CrossRef](#)]
17. Kane, M.E.; Albert, L.S. Abscisic acid induces aerial leaf morphology and vasculature in submerged *Hippuris vulgaris* L. *Aquat. Bot.* **1987**, *28*, 81–88. [[CrossRef](#)]
18. Tsukaya, H. Comparative leaf development in angiosperms. *Curr. Opin. Plant Biol.* **2014**, *17*, 103–109. [[CrossRef](#)]
19. Arber, A. On Heterophylly in Water Plants. *Am. Nat.* **1919**, *53*, 272–278. [[CrossRef](#)]
20. McComb, A.J. The control of elongation in *Callitriche* shoots by environment and gibberellic acid. *Ann. Bot.* **1965**, *29*, 445–458. [[CrossRef](#)]
21. Deschamp, P.A.; Cooke, T.J. Leaf dimorphism in aquatic angiosperms: Significance of turgor pressure and cell expansion. *Science* **1983**, *219*, 505–507. [[CrossRef](#)]
22. Jones, H. Variation in Leaf Form in *Callitriche intermedia*. *Nature* **1952**, *170*, 848–849. [[CrossRef](#)]
23. Jones, H. Heterophylly in some Species of *Callitriche*, with especial reference to *Callitriche intermedia*. *Ann. Bot.* **1955**, *19*, 226–245. [[CrossRef](#)]
24. Bodkin, B.C.; Spence, D. Photoreversible control of heterophylly in *Hippuris vulgaris* L. *New Phytol.* **1980**, *84*, 533–542. [[CrossRef](#)]
25. McCully, M.E.; Dale, H.M. Heterophylly in *Hippuris*, a problem in identification. *Botany* **1961**, *39*, 1099–1116. [[CrossRef](#)]
26. Li, G.; Hu, S.; Yang, J.; Schultz, E.A.; Clarke, K.; Hou, H. Water-Wisteria as an ideal plant to study heterophylly in higher aquatic plants. *Plant Cell Rep.* **2017**, *36*, 1225–1236. [[CrossRef](#)]
27. Horiguchi, G.; Nemoto, K.; Yokoyama, T.; Hirotsu, N. Photosynthetic acclimation of terrestrial and submerged leaves in the amphibious plant *Hygrophila difformis*. *AoB Plants* **2019**, *11*, plz009. [[CrossRef](#)]
28. Herrera, C.M.; Bazaga, P. Epigenetic correlates of plant phenotypic plasticity: DNA methylation differs between prickly and nonprickly leaves in heterophyllous *Ilex aquifolium* (Aquifoliaceae) trees. *Bot. J. Linn. Soc.* **2013**, *171*, 441–452. [[CrossRef](#)]
29. Kuwabara, A.; Ikegami, K.; Koshihara, T.; Nagata, T. Effects of ethylene and abscisic acid upon heterophylly in *Ludwigia arcuata* (Onagraceae). *Planta* **2003**, *217*, 880–887. [[CrossRef](#)]
30. Sato, M.; Tsutsumi, M.; Ohtsubo, A.; Nishii, K.; Kuwabara, A.; Nagata, T. Temperature-dependent changes of cell shape during heterophyllous leaf formation in *Ludwigia arcuata* (Onagraceae). *Planta* **2008**, *228*, 27–36. [[CrossRef](#)]
31. Bristow, J.M.; Looi, A. Effects of Carbon Dioxide on the Growth and Morphogenesis of *Marsilea*. *Am. J. Bot.* **1968**, *55*, 884–889. [[CrossRef](#)]
32. Gaudet, J. *Marsilea vestita*: Conversion of the Water Form to the Land Form by Darkness and by Far-Red Light. *Science* **1963**, *140*, 975–976. [[CrossRef](#)]
33. Bristow, J.M. The effects of carbon dioxide on the growth and development of amphibious plants. *Botany* **1969**, *47*, 1803–1807. [[CrossRef](#)]

34. Titus, J.E.; Sullivan, P.G. Heterophylly in the yellow waterlily, *Nuphar variegata* (Nymphaeaceae): Effects of CO₂, natural sediment type, and water depth. *Am. J. Bot.* **2001**, *88*, 1469–1478. [[CrossRef](#)]
35. Chitwood, D.H.; Sinha, N.R. Evolutionary and environmental forces sculpting leaf development. *Curr. Biol.* **2016**, *26*, R297–R306. [[CrossRef](#)]
36. He, D.; Guo, P.; Guggler, P.F.; Guo, Y.; Liu, X.; Chen, J. Investigating the molecular basis for heterophylly in the aquatic plant *Potamogeton octandrus* (Potamogetonaceae) with comparative transcriptomics. *PeerJ* **2018**, *6*, e4448. [[CrossRef](#)]
37. McCallum, W.B. On the nature of the stimulus causing the change of form and structure in *Proserpinaca palustris*. *Bot. Gaz.* **1902**, *34*, 93–108. [[CrossRef](#)]
38. Wallenstein, A.; Albert, L. Plant Morphology: Its control in proserpinaca by photoperiod, temperature, and gibberellic acid. *Science* **1963**, *140*, 998–1000. [[CrossRef](#)]
39. Kane, M.E.; Albert, L.S. Environmental and growth regulator effects on heterophylly and growth of *Proserpinaca intermedia* (Haloragaceae). *Aquat. Bot.* **1982**, *13*, 73–85. [[CrossRef](#)]
40. Cook, C.D. On the determination of leaf form in *Ranunculus aquatilis*. *New Phytol.* **1969**, *68*, 469–480. [[CrossRef](#)]
41. Young, J.P.; Dengler, N.G.; Donnelly, P.M.; Dickinson, T.A. Heterophylly in *Ranunculus flabellaris*: The effect of abscisic acid on leaf ultrastructure. *Ann. Bot.* **1990**, *65*, 603–615. [[CrossRef](#)]
42. Johnson, M.P. Temperature Dependent Leaf Morphogenesis in *Ranunculus flabellaris*. *Nature* **1967**, *214*, 1354–1355. [[CrossRef](#)]
43. Kim, J.; Joo, Y.; Kyung, J.; Jeon, M.; Park, J.Y.; Lee, H.G.; Chung, D.S.; Lee, E.; Lee, I. A molecular basis behind heterophylly in an amphibious plant, *Ranunculus trichophyllus*. *PLoS Genet.* **2018**, *14*, e1007208. [[CrossRef](#)]
44. Nakayama, H.; Fukushima, K.; Fukuda, T.; Yokoyama, J.; Kimura, S. Molecular Phylogeny Determined Using Chloroplast DNA Inferred a New Phylogenetic Relationship of *Rorippa aquatica* (Eaton) E.J. Palmer & Steyermark (Brassicaceae)—Lake Cress. *Am. J. Plant Sci.* **2014**, *5*, 48–54.
45. Nakayama, H.; Nakayama, N.; Seiki, S.; Kojima, M.; Sakakibara, H.; Sinha, N.; Kimura, S. Regulation of the KNOX-GA gene module induces heterophyllic alteration in North American Lake Cress. *Plant Cell* **2014**, *26*, 4733–4748. [[CrossRef](#)]
46. Momokawa, N.; Kadono, Y.; Kudoh, H. Effects of light quality on leaf morphogenesis of a heterophyllous amphibious plant, *Rotala hippuris*. *Ann. Bot.* **2011**, *108*, 1299–1306. [[CrossRef](#)]
47. Raven, J.A.; Beardall, J. The ins and outs of CO₂. *J. Exp. Bot.* **2015**, *67*, 1–13.
48. Jackson, S.D. Plant responses to photoperiod. *New Phytol.* **2009**, *181*, 517–531. [[CrossRef](#)]
49. Upadhyaya, H.; Sahoo, L.; Panda, S. *Molecular Stress Physiology of Plants*; Springer: Berlin/Heidelberg, Germany, 2012.
50. Al-Karaki, G.N. Growth, water use efficiency, and sodium and potassium acquisition by tomato cultivars grown under salt stress. *J. Plant Nutr.* **2000**, *23*, 1–8. [[CrossRef](#)]
51. Najla, S.; Vercambre, G.; Pagès, L. Tomato plant architecture as affected by salinity: Descriptive analysis and integration in a 3-D simulation model. *Botany* **2009**, *87*, 893–904. [[CrossRef](#)]
52. Hu, X.; Li, N.; Wu, L. Quantitative iTRAQ-based proteomic analysis of phosphoproteins and ABA-regulated phosphoproteins in maize leaves under osmotic stress. *Sci. Rep.* **2015**, *5*, 15626. [[CrossRef](#)] [[PubMed](#)]
53. Skirycz, A.; Claeys, H.; De Bodt, S. Pause-and-Stop: The Effects of Osmotic Stress on Cell Proliferation during Early Leaf Development in Arabidopsis and a Role for Ethylene Signaling in Cell Cycle Arrest. *Plant Cell* **2011**, *23*, 1876–1888. [[CrossRef](#)] [[PubMed](#)]
54. Zhang, S.; Yang, R.; Huo, Y. Expression of cotton PLATZ1 in transgenic *Arabidopsis* reduces sensitivity to osmotic and salt stress for germination and seedling establishment associated with modification of the abscisic acid, gibberellin, and ethylene signalling pathways. *BMC Plant Biol.* **2018**, *18*, 218. [[CrossRef](#)] [[PubMed](#)]
55. Spence, D.H.N. The Zonation of Plants in Freshwater Lakes. *Adv. Ecol. Res.* **1982**, *12*, 37–125.
56. Vervuren, P.; Blom, C.; Kroon, H. Extreme flooding events on the Rhine and the survival and distribution of riparian plant species. *J. Ecol.* **2003**, *91*, 135–146. [[CrossRef](#)]
57. Richards, P.; Sculthorpe, C. The Biology of Aquatic Vascular Plants Edward Arnold. *J. Ecol.* **1968**, *56*, 915. [[CrossRef](#)]
58. Paterson, D.M.; Black, K.S. Water flow, sediment dynamics and benthic biology. *Adv. Ecol. Res.* **1999**, *29*, 155–193.

59. Robioneck, A.; Banas, K.; Chmara, R.; Szymeja, J. The avoidance strategy of environmental constraints by an aquatic plant *Potamogeton alpinus* in running waters. *Ecol. Evol.* **2015**, *5*, 3327–3337. [[CrossRef](#)]
60. Bociag, K.; Galka, A.; Lazarewicz, T.; Szymeja, J. Mechanical strength of stems in aquatic macrophytes. *Acta Soc. Bot. Pol.* **2011**, *78*, 181–187. [[CrossRef](#)]
61. Minorsky, P.V. The hot and the classic. *Plant Physiol.* **2003**, *133*, 1671–1672. [[CrossRef](#)]
62. Nakayama, H.; Sinha, N.R.; Kimura, S. How do plants and phytohormones accomplish heterophylly, leaf phenotypic plasticity, in response to environmental cues. *Front. Plant Sci.* **2017**, *8*, 1717. [[CrossRef](#)] [[PubMed](#)]
63. Schlichting, C.D.; Wund, M.A. Phenotypic plasticity and epigenetic marking: An assessment of evidence for genetic accommodation. *Evolution* **2014**, *68*, 656–672. [[CrossRef](#)] [[PubMed](#)]
64. Legris, M.; Klose, C.; Burgie, E.S.; Rojas, C.C.R.; Neme, M.; Hiltbrunner, A.; Wigge, P.A.; Schafer, E.; Vierstra, R.D.; Casal, J.J. Phytochrome B integrates light and temperature signals in *Arabidopsis*. *Science* **2016**, *354*, 897–900. [[CrossRef](#)] [[PubMed](#)]
65. Jung, J.; Domijan, M.; Klose, C.; Biswas, S.; Ezer, D.; Gao, M.; Khattak, A.K.; Box, M.; Charoensawan, V.; Cortijo, S.; et al. Phytochromes function as thermosensors in *Arabidopsis*. *Science* **2016**, *354*, 886–889. [[CrossRef](#)] [[PubMed](#)]
66. Sakamoto, T.; Kimura, S. Plant temperature sensors. *Sensors* **2018**, *18*, 4365. [[CrossRef](#)]
67. Li, X.; He, D.; Guo, Y. Morphological structure and physiological research of heterophylly in *Potamogeton octandrus*. *Plant Syst. Evol.* **2019**, *305*, 223–232. [[CrossRef](#)]
68. Hattori, Y.; Nagai, K.; Furukawa, S.; Song, X.J.; Kawano, R.; Sakakibara, H.; Wu, J.; Matsumoto, T.; Yoshimura, A.; Kitano, H.; et al. The ethylene response factors SNORKEL1 and SNORKEL2 allow rice to adapt to deep water. *Nature* **2009**, *460*, 1026–1030. [[CrossRef](#)]
69. Dittrich, M.; Mueller, H.M.; Bauer, H.; Peirats-Llobet, M.; Rodriguez, P.L.; Geilfus, C.-M.; Carpentier, S.C.; Rasheid, K.S.; Kollist, H.; Merilo, E.; et al. The role of *Arabidopsis* ABA receptors from the PYR/PYL/RCAR family in stomatal acclimation and closure signal integration. *Nat. Plants* **2019**. [[CrossRef](#)]
70. Holmes, M.G.; Klein, W.H. The Light and Temperature Environments. In *Plant life in aquatic and amphibious habitats*; Blackwell Scientific Publisher: Oxford, UK, 1987; pp. 3–22.
71. Liu, X.; Luo, M.; Yang, S. Role of epigenetic modifications in plant responses to environmental stresses. Setting the Stage for the Next Generation: Epigenetic Reprogramming During Sexual Plant Reproduction. In *Nuclear Functions in Plant Transcription, Signaling and Development*; Springer: Berlin/Heidelberg, Germany, 2015.
72. Baker-Brosch, K.F.; Peet, R.K. The ecological significance of lobed and toothed leaves in temperate forest trees. *Ecology* **1997**, *78*, 1250–1255. [[CrossRef](#)]
73. Chitwood, D.H.; Kumar, R.; Headland, L.R. A quantitative genetic basis for leaf morphology in a set of precisely defined tomato introgression lines. *Plant Cell* **2013**, *25*, 2465–2481. [[CrossRef](#)]
74. Andres, R.J.; Coneva, V.; Frank, M.H. Modifications to a *LATE MERISTEM IDENTITY1* gene are responsible for the major leaf shapes of Upland cotton (*Gossypium hirsutum* L.). *Proc. Natl. Acad. Sci. USA* **2016**, *114*, E57. [[CrossRef](#)] [[PubMed](#)]
75. Vuolo, F.; Mentink, R.A.; Hajheidari, M. Coupled enhancer and coding sequence evolution of a homeobox gene shaped leaf diversity. *Genes Dev.* **2016**, *30*, 2370–2375. [[CrossRef](#)] [[PubMed](#)]
76. Helliker, B.R.; Richter, S.L. Subtropical to boreal convergence of tree-leaf temperatures. *Nature* **2008**, *454*, 511–514. [[CrossRef](#)] [[PubMed](#)]
77. Vogel, S. Leaves in the lowest and highest winds: Temperature, force and shape. *New Phytol.* **2009**, *183*, 13–26. [[CrossRef](#)] [[PubMed](#)]
78. Palacio-lopez, K.; Beckage, B.; Scheiner, S.M.; Molofsky, J. The ubiquity of phenotypic plasticity in plants: A synthesis. *Ecol. Evol.* **2015**, *5*, 3389–3400. [[CrossRef](#)] [[PubMed](#)]
79. Iida, S.; Ikeda, M.; Amano, M.; Sakayama, H.; Kadono, Y.; Kosuge, K. Loss of heterophylly in aquatic plants: Not ABA-mediated stress but exogenous ABA treatment induces stomatal leaves in *Potamogeton perfoliatus*. *J. Plant Res.* **2016**, *129*, 853–862. [[CrossRef](#)]



© 2019 by the authors. Licensee MDPI, Basel, Switzerland. This article is an open access article distributed under the terms and conditions of the Creative Commons Attribution (CC BY) license (<http://creativecommons.org/licenses/by/4.0/>).

RESEARCH ARTICLE

Comparative transcriptome analysis of galls from four different host plants suggests the molecular mechanism of gall development

Seiji Takeda^{1,2*}, Makiko Yoza¹, Taisuke Amano¹, Issei Ohshima¹, Tomoko Hirano¹, Masa H. Sato¹, Tomoaki Sakamoto³, Seisuke Kimura^{3,4,5*}

1 Graduate School of Life and Environmental Sciences, Kyoto Prefectural University, Kyoto, Japan, **2** Biotechnology Research Department, Kyoto Prefectural Agriculture Forestry and Fisheries Technology Center, Seika, Kyoto, Japan, **3** Department of Bioresource and Environmental Sciences, Faculty of Life Sciences, Kyoto Sangyo University, Kyoto, Japan, **4** Department of Industrial Life Sciences, Faculty of Life Sciences, Kyoto Sangyo University, Kyoto, Japan, **5** Center for Ecological Evolutionary Developmental Biology, Kyoto Sangyo University, Kyoto, Japan

* seijitakeda@kpu.ac.jp (ST); seisuke@cc.kyoto-su.ac.jp (SK)

OPEN ACCESS

Citation: Takeda S, Yoza M, Amano T, Ohshima I, Hirano T, Sato MH, et al. (2019) Comparative transcriptome analysis of galls from four different host plants suggests the molecular mechanism of gall development. PLoS ONE 14(10): e0223686. <https://doi.org/10.1371/journal.pone.0223686>

Editor: Haitao Shi, Hainan University, CHINA

Received: June 13, 2019

Accepted: September 25, 2019

Published: October 24, 2019

Copyright: © 2019 Takeda et al. This is an open access article distributed under the terms of the [Creative Commons Attribution License](https://creativecommons.org/licenses/by/4.0/), which permits unrestricted use, distribution, and reproduction in any medium, provided the original author and source are credited.

Data Availability Statement: Accession numbers for the RNA-seq data are as follows: DRA008530 (A. montana), DRA008531 (E. japonica), and DRA008532 (G. obovatum).

Funding: This work was supported by JSPS KAKENHI Grant Number 17H06260 and the strategic prioritized research in KPU to IO, ST and MHS, JSPS KAKENHI 16H05068 to MHS, JSPS KAKENHI 18K6366 to ST, JSPS KAKENHI 16H01472, 16K07408, 18H04787, and 18H04844 to SK, and MEXT Supported Program for the Strategic Research Foundation at Private

Abstract

Galls are plant structures generated by gall-inducing organisms including insects, nematodes, fungi, bacteria and viruses. Those made by insects generally consist of inner callus-like cells surrounded by lignified hard cells, supplying both nutrients and protection to the gall insects living inside. This indicates that gall insects hijack developmental processes in host plants to generate tissues for their own use. Although galls are morphologically diverse, the molecular mechanism for their development remains poorly understood. To identify genes involved in gall development, we performed RNA-sequencing based transcriptome analysis for leaf galls. We examined the young and mature galls of *Glochidion obovatum* (Phyllanthaceae), induced by the micromoth *Caloptilia cecidophora* (Lepidoptera: Gracillariidae), the leaf gall from *Eurya japonica* (Pentaphylacaceae) induced by *Borboryctis euryae* (Lepidoptera: Gracillariidae), and the strawberry-shaped leaf gall from *Artemisia montana* (Asteraceae) induced by gall midge *Rhopalomyia yomogicola* (Oligotrophini: Cecidomyiidae). Gene ontology (GO) analyses suggested that genes related to developmental processes are up-regulated, whereas ones related to photosynthesis are down-regulated in these three galls. Comparison of transcripts in these three galls together with the gall on leaves of *Rhus javanica* (Anacardiaceae), induced by the aphid *Schlechtendalia chinensis* (Hemiptera: Aphidoidea), suggested 38 genes commonly up-regulated in galls from different plant species. GO analysis showed that peptide biosynthesis and metabolism are commonly involved in the four different galls. Our results suggest that gall development involves common processes across gall inducers and plant taxa, providing an initial step towards understanding how they manipulate host plant developmental systems.

Universities (Grant Number S1511023) to SK. The funders had no role in study design, data collection and analysis, decision to publish, or preparation of the manuscript.

Competing interests: The authors have declared that no competing interests exist.

Introduction

Plants are not only food sources but also living microenvironments for other organisms. Plant galls are generated by insects, nematodes, fungi, bacteria, and viruses, among which, galls created by insects vary widely in terms of their shapes and colors. The estimated number of gall insect species ranges from 21,000 to 211,000 [1–2], and the structure of these galls is generally different from those of plant organs that develop normally, indicating that gall insects manipulate the plant developmental system and build a convenient structure for themselves [1].

Insect galls are induced by a wide range of species including flies, beetles, Hemiptera, wasps, midges, micromoths, and aphids. There is empirical evidence that effectors from insects, including phytohormones (auxin, cytokinin, and abscisic acids) and proteins are involved in gall generation [3–6]. Studies of green-island symptoms suggest that cytokinin supplied by insects to plants is synthesized by symbiont bacteria [7–8]. In some galls, initiation is stimulated by female oviposition [9]. This suggests that secretion from insects stimulate plant cell differentiation to generate the gall structure, although the molecular mechanism for gall initiation and development still remains unclear.

Gall development can be divided into the following processes: (1) secretion of signaling molecules from insects, (2) perception of the signals by plants, (3) plant cell regeneration and differentiation, and (4) organization of gall tissue. During these processes, insects need to suppress the plant's defense responses [6]. Although many studies have described the gall structure and features, galls development seems to be a complex pathway, such that the molecular mechanism of gall development still remains unclear, due to wide variation in gall and host plant species. Recent progress in next generation sequencing (NGS) has allowed us to outline the biological processes in many organisms. Transcriptome analyses in several galls have been reported recently. For example, the gall transcriptome of *Metrosideros polymorpha*, induced by psyllid (Hemiptera), suggested the involvement of auxin response in the gall [10]. The horned galls of *Rhus chinensis* and *Rhus javanica* accumulate high amounts of tannins that make up to 60–70% of its total dry weight, protecting them from herbivory. Transcriptomes of both host plants and gall aphids have helped elucidate the molecular mechanisms of tannin biosynthesis and aphid reproduction, respectively [11–12]. Another example is the gall of wild grapevine (*Vitis riparia*) generated by phylloxera (*Daktulosphaira vitifoliae*), suggesting that pathways of floral organ development and procambium differentiation are involved in gall development [13]. These reports propose the molecular mechanism of interaction between gall insects and host plants, although, the gall structure varies widely making it difficult to identify the fundamental processes of gall development.

To understand the molecular mechanism of gall development, we performed RNA-sequencing-based transcriptome analyses for leaf galls from four different plant species. The leaf gall of *Glochidion obovatum* (Phyllanthaceae) (kankonoki-ha-fukure-fushi in Japanese, meaning swollen leaf gall of *G. obovatum*) is induced by the micromoth *Caloptilia cecidophora* (Lepidoptera: Gracillariidae), and develops into swollen and hard structures (Fig 1A–1C). The larva of this micromoth is the leaf miner up to the second instar, taking nutrients from leaf epidermal cells. After the third instar, it moves inside the leaves and generates a gall within leaf tissue [14]. Leaf gall of *Eurya japonica* (Pentaphylacaceae) (called hisakaki-ha-fukure-fushi in Japanese, meaning swollen leaf gall of *E. japonica*) is generated by another micromoth *Borboryctis euryae* (Lepidoptera: Gracillariidae), with a structure thinner than that of the gall of *G. obovatum* (Fig 1D–1H). This larva is also the leaf miner at an early stage, and later transforms to galling larva [15].

Together with these micromoth-induced galls, we selected the strawberry-shaped gall on leaves of *Artemisia montana* (Asteraceae), called yomogi-ha-eboshi-fushi (meaning *A. montana* hat-shaped gall on leaf, in Japanese), which is generated by a gall midge *Rhopalomyia yomogicola* (Oligotrophini: Cecidomyiidae) (Fig 1I–1K) [4]. Gene ontology (GO) analyses for

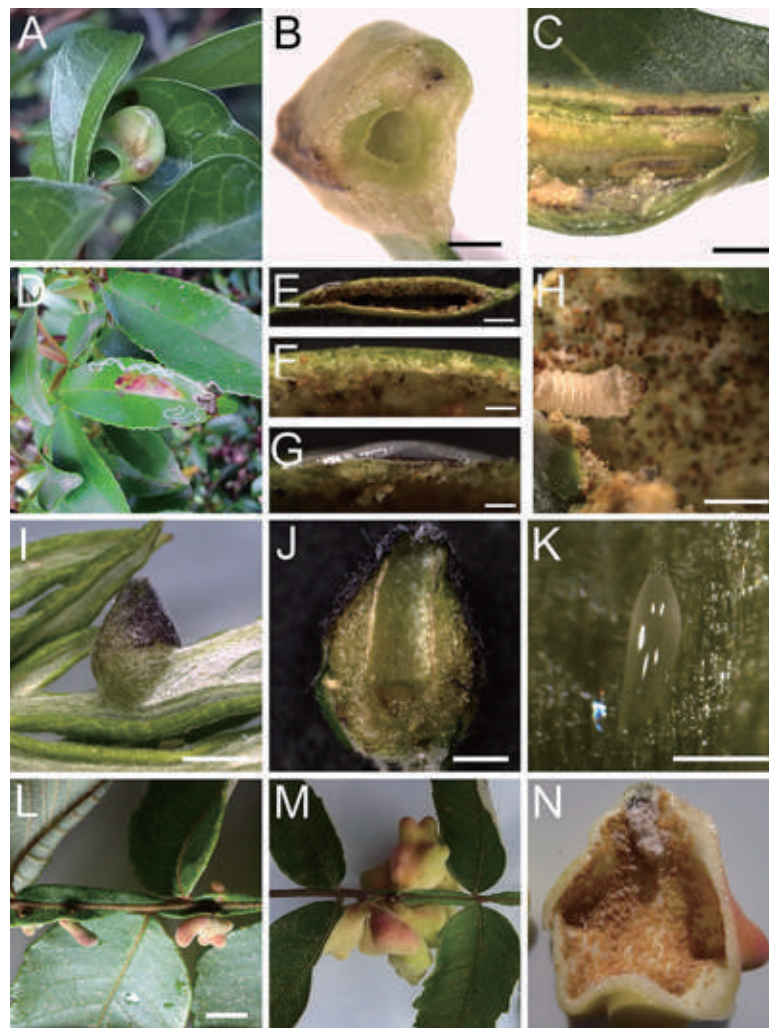


Fig 1. Galls used in this study. (A–C) The gall of *G. obovatum*. (A) The gall generated on a leaf. (B) Transverse section of the gall. (C) Longitudinal section of the gall, showing larva inside. (D–H) Gall of *E. japonica*. (D) Leaf showing the trace of leaf miner (white line) and the gall in the middle of the leaf. (E) Cross sections of the gall. Notably, this gall has rather thin layers compared to the other galls. (F) Upper part of the gall section of (E), showing thin layer of cells. (G) Cross section of trace of leaf miner in (E), showing the detached cuticle layer. (H) The larva inside the gall. (I–K) Galls of *A. montana*. (I) Intact gall on the leaf. (J) Longitudinal section of the gall. (K) Egg inside the gall. (L–N) Galls of *R. javanica*. (L) Early stage galls developing on the winged rachides. (M) Later stage galls. (N) Transverse section of the gall, showing many aphids living inside. Scale bars: B, E, H, J, 1 mm; C and I, 2 mm; F, G, K, 0.2 mm; L, 10 mm.

<https://doi.org/10.1371/journal.pone.0223686.g001>

transcripts in these three plant species suggested that development-related genes are upregulated in galls, whereas photosynthesis-related genes are downregulated. Comparison of transcripts in galls of these three species and another leaf gall on *Rhus javanica* (Fig 1L–1N), induced by the aphid *Schlechtendalia chinensis* (Hemiptera: Aphidoidea), suggested that 38 genes are commonly up-regulated in leaf galls from different plant species.

Materials and methods

Sample collection and microscopy

Galls on leaves of *G. obovatum* and *E. japonica* were originally collected from Tomogashima Island (Kada, Wakayama, Japan) and Kibogaoka Cultural Park (Yasu, Shiga, Japan),

respectively, and both have been successfully reared in the laboratory [14,15]. For *G. obovatum*, the galls with the third instar larva were collected as young galls, and those with the fourth to fifth larva as mature galls. In both cases, the collected galls were cut in half and the larva removed. The intact leaves from the same tree were collected as control samples. For *E. japonica*, the gall with the fourth instar inside was collected, cut, and larva removed. Intact leaves from the same tree were collected as control samples. Galls and leaves of *A. montana* were collected from Kyoto Prefectural University, Seika campus (Seika, Kyoto, Japan). Gall and larva RNA were extracted to avoid physical stress by dissection, since the size of the gall was small. Collection, RNA extraction and RNA-sequencing of galls and leaves from *R. javanica* were performed by collaborators (Hirano and Sato, in preparation). All samples were frozen in liquid nitrogen and kept at -80°C until required for RNA extraction. Photos were taken with an S8AP0 stereomicroscope mounted with an EC3 digital camera (Leica, Germany).

RNA extraction and RNA-sequencing

In each plant species, three independent samples were used for RNA extraction. Total RNA was extracted from approximately 0.05 g of galls or leaves by two different methods. The RNA from *G. obovatum* young and mature leaves, and *E. japonica* leaves and galls were extracted using the Nucleospin RNA Plant and Fungi kit (Macherey-Nagel, Germany) following the manufacturer's instruction. All other RNA extractions were performed using a modified protocol with the RNeasy Plant Mini Kit (QIAGEN, Germany) [16]. For RNA-seq analysis, 0.5 μg of the total RNA samples was used for library preparation after RNA integrity was confirmed by running samples on an Agilent RNA 6000 Nano Chip (Agilent Technologies, U. S. A). All libraries were prepared using Illumina TruSeq Stranded mRNA LT Sample kit according to the manufacturer's instructions (Illumina, U. S. A). The pooled libraries were sequenced on an Illumina NextSeq500 sequencing platform, and single-end reads of 76 bp length were obtained. The reads from each species were assembled *de novo* into contigs using Trinity [17] with quality trimming of reads and strand specific assembly. The obtained reads were mapped to the *de novo* assembled RNA contigs using BWA (<http://bio-bwa.sourceforge.net>) [18]. The count data were subjected to a trimmed mean of M-value (TMM) normalization in EdgeR [19]. The transcript expression and digital gene expressions (DGEs) were defined using the EdgeR GLM approach [19], and genes with false discovery rates (FDRs) < 0.01 , sum (total number of mapped reads) > 1 , and $\log_2\text{FC} > 1$ (up-regulated) or $\log_2\text{FC} < -1$ (down-regulated) were classified as differentially expressed genes (DEGs), which were used for functional prediction by a BLASTX search against the Arabidopsis protein database (TAIR10). The gene number was estimated after the overlapped the Arabidopsis Gnome Initiative (AGI) number was eliminated. For GO analysis, we used PANTHER classification system through the TAIR database [20]. Accession numbers for the RNA-seq data are as follows: DRA008532 (*G. obovatum*), DRA008531 (*E. japonica*), and DRA008530 (*A. montana*), and one for *R. javanica* is described in another manuscript (Hirano and Sato, in preparation).

Results and discussion

Transcriptomes of galls from different plant species

To elucidate the molecular mechanism of gall development, we isolated RNA from galls and leaves, followed by library construction and RNA-sequencing by NGS (S1 Table). For *G. obovatum* galls, we analyzed both young (inside larva at third instar) and mature galls (fourth to fifth instar). In both cases, genes related to developmental processes were up-regulated and photosynthesis-related genes were down-regulated in galls compared to those in leaves (Fig 2 and S1 Fig). The transcriptome of another micromoth-induced leaf gall on *E. japonica*

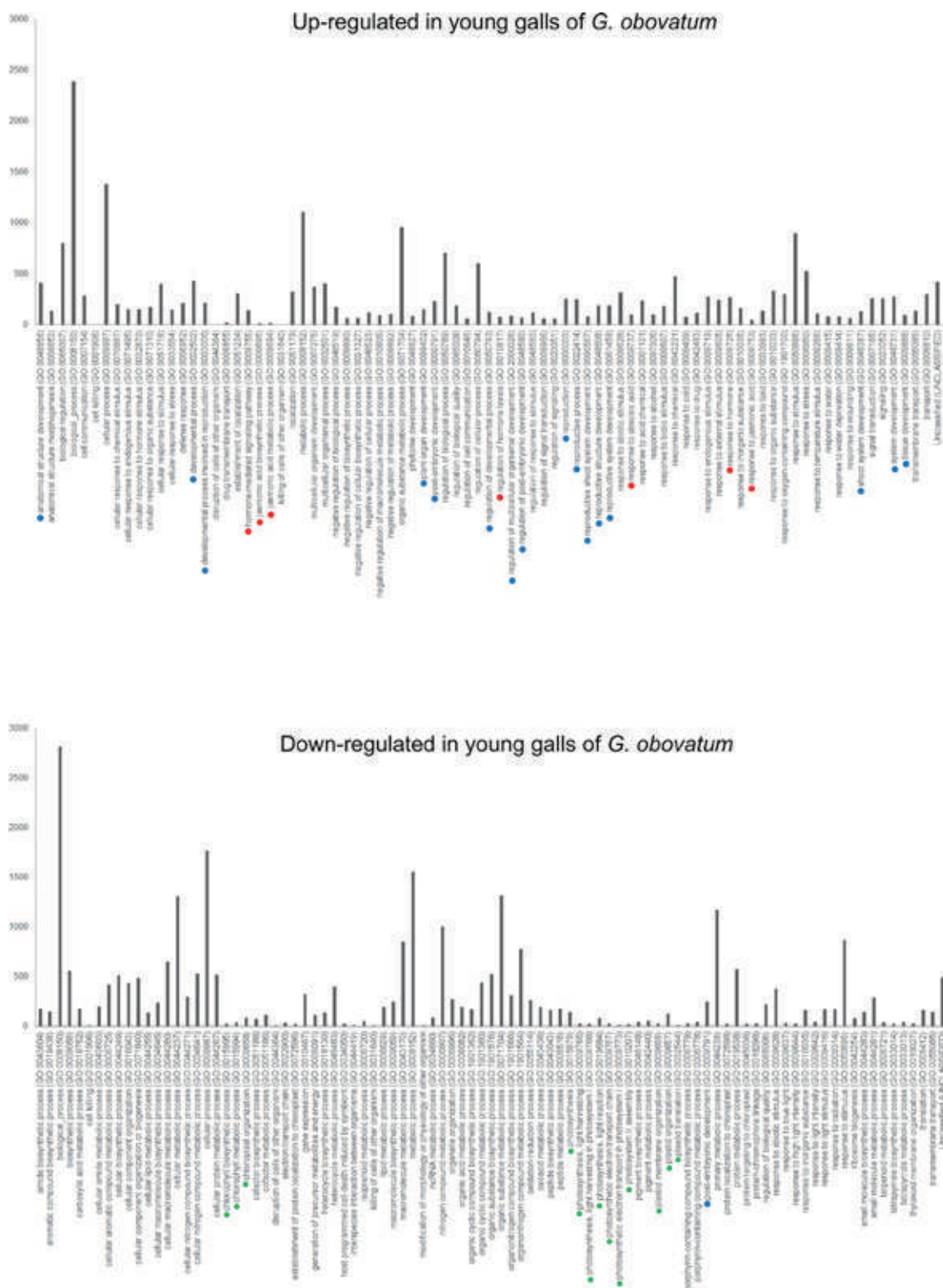


Fig 2. Gene ontology (GO) analysis (biological process) of young gall and leaf from *G. obovatum*. Colored dots indicate similar biological GO: blue, developmental process; red, phytohormone; and green, photosynthesis.

<https://doi.org/10.1371/journal.pone.0223686.g002>

suggested that genes related to development as well as cell cycle were up-regulated in galls (Fig 3). In leaf galls induced by the gall midge on *A. montana*, the genes related to developmental processes and cell wall organization were up-regulated (Fig 4). In these three galls, photosynthesis-related genes were down-regulated (Figs 2–4). These results suggest that leaf galls from different plant species commonly down-regulate the photosynthesis activity and express genes related to developmental process for gall morphogenesis. Notably, the three galls express different sets of genes, i.e., phytohormone-related genes in *G. obovatum*, cell cycle-related genes in *E. japonica*, and cell wall biosynthesis-related genes in *A. montana*. This difference may be one of the explanations for the unique shape of galls among different plant species.

Four different galls expressed 38 common genes

The data from RNA-sequencing of *R. javanica* were added to our analysis (Hirano and Sato et al., in preparation). We selected gall-rich genes (genes expressed in galls more than twice that in leaves (see [Materials and Methods](#)), whose molecular functions were predicted by a homology search with BLASTX to the *Arabidopsis thaliana* protein database (TAIR10). For *G. obovatum*, data from young and mature galls and leaves were combined, and gall-rich genes compared to those in leaves were extracted. The AGI code corresponding to each gene sequence was compared among the four plant species. The gene number that was expressed more than twice in galls compared to that in leaves was as follows: *A. montana*, 5,720; *E. japonica*, 1,384; *G. obovatum*, 5,092; and *R. javanica*, 4,682 (Fig 5). With comparison among these datasets, we found that 38 genes are commonly expressed in four different galls (Fig 5 and Table 1). These 38 genes may include the master regulators for gall development in different plant species.

Next, we categorize these candidate regulators based on their predicted biological and molecular functions, and discuss their contribution for gall development.

(1) Cell division and cytokinesis. In the gall, active cell division occurs to generate nutrient and shelter cells for insects, suggesting cell cycle regulation in the host tissue. We found several genes, involved in cell division and cytokinesis, that were up-regulated in four galls. The AtBRCA1 (At4g21070) is a direct transcriptional target of SUPPRESSOR OF GAMMA RESPONSE 1 (SOG1), and involved in DNA repair and cell cycle regulation [21–23]. FUSED Kinase (At1g50240) is involved in cytokinesis by interacting with kinesin protein in the phragmoplast [24–25]. Ethylene response factor 115 (ERF115/At5g07310) regulates the cell cycle of the quiescent center (QC) and surrounding stem cells in roots through direct transcriptional activation of *PHYTOSULFOKINE PRECURSOR 5* (*PSK5*) gene, which raises a sulfonated pentapeptide hormone molecule [26]. DOMINO1 (At5g62240) is a plant-specific gene family protein that is located in the nucleus and nucleolus, and is suggested to regulate nuclear size and cell division during embryogenesis [27]. Knockdown of dUTPase DUT1 (At3g46940) by RNAi causes DNA fragmentation and enhanced somatic homologous recombination [28], suggesting a DNA protection mechanism in galls. These up-regulated genes are likely to regulate cell proliferation in galls.

(2) Lignification and reactive oxygen species (ROS) generation. Lignification occurs in the cell layers surrounding the nutrient-rich cells, generating a shelter protecting larvae inside of the gall. AtTLP2 (At2g18280) is a transcription factor and regulates transcription of cell wall-related genes leading to homogalacturonan biosynthesis [29], suggesting that it is involved in biogenesis of cell wall components in the gall. AtPrx25 is a putative cationic cell-wall-bound peroxidase and is involved in lignin biosynthesis through oxidation of phenolic compounds and/or ROS generation [30–31]. These ROS are involved in many cellular processes including cell wall modification. Interestingly, ROOT HAIR DEFECTIVE 2 (RHD2,

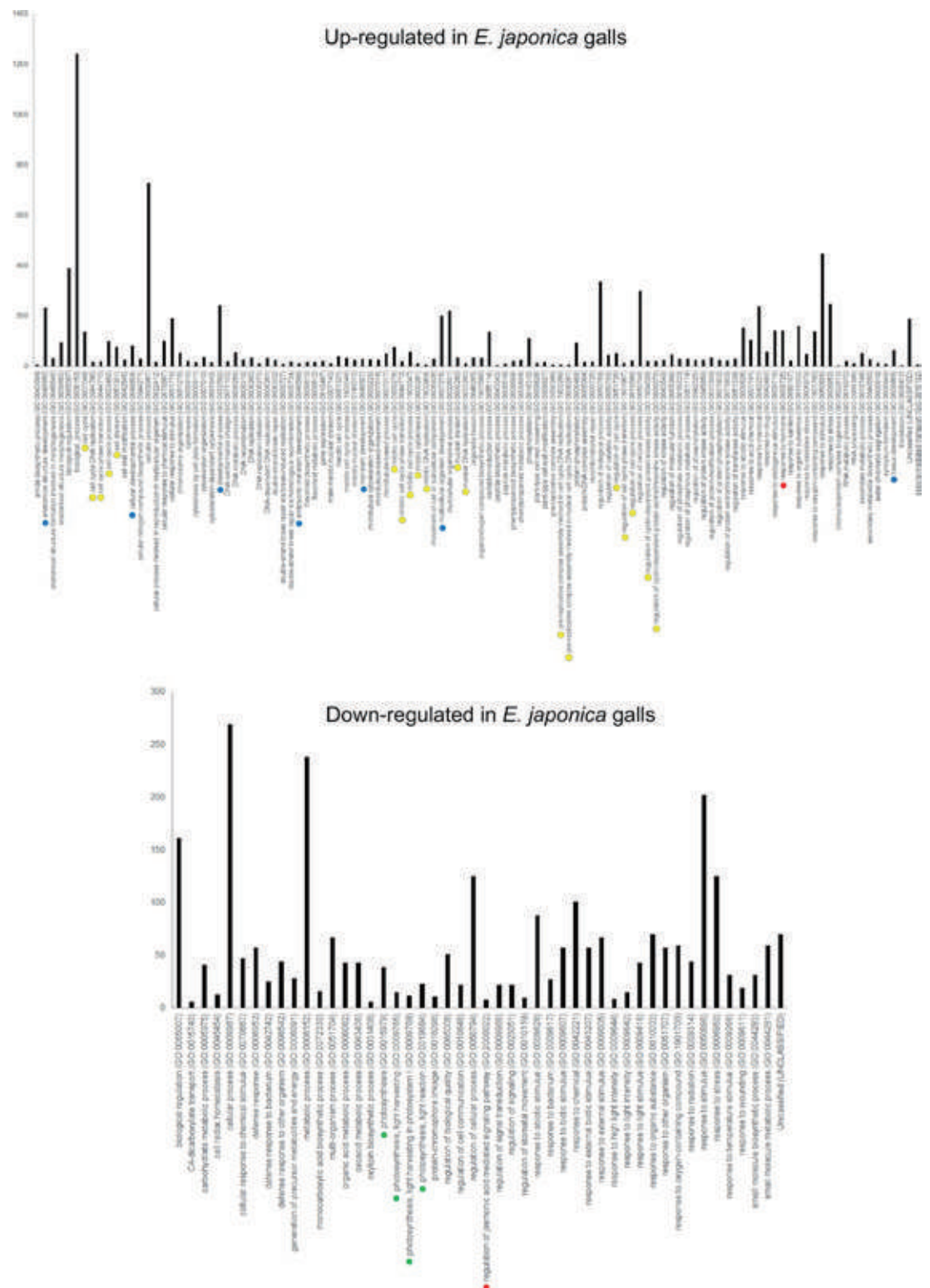


Fig 3. Gene ontology (GO) analysis (biological process) of gall and leaf from *E. japonica*. Colored dots indicate similar biological GO: blue, developmental process; red, phytohormone; yellow, cell cycle; and green, photosynthesis.

<https://doi.org/10.1371/journal.pone.0223686.g003>

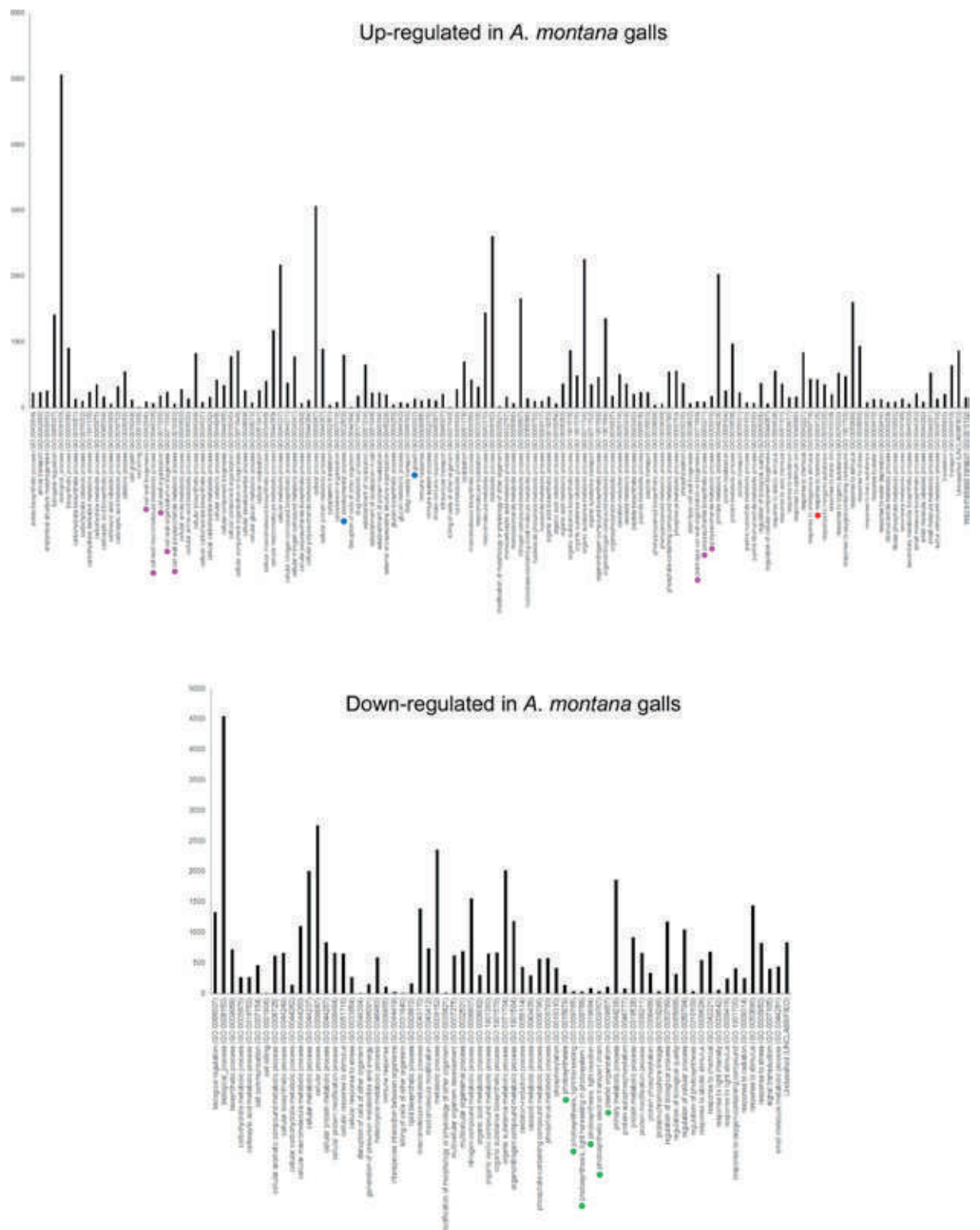


Fig 4. Gene ontology (GO) analysis (biological process) of gall and leaf from *A. montana*. Colored dots indicate similar biological GO: blue, developmental process; red, phytohormone; magenta, cell wall organization; and green, photosynthesis.

<https://doi.org/10.1371/journal.pone.0223686.g004>

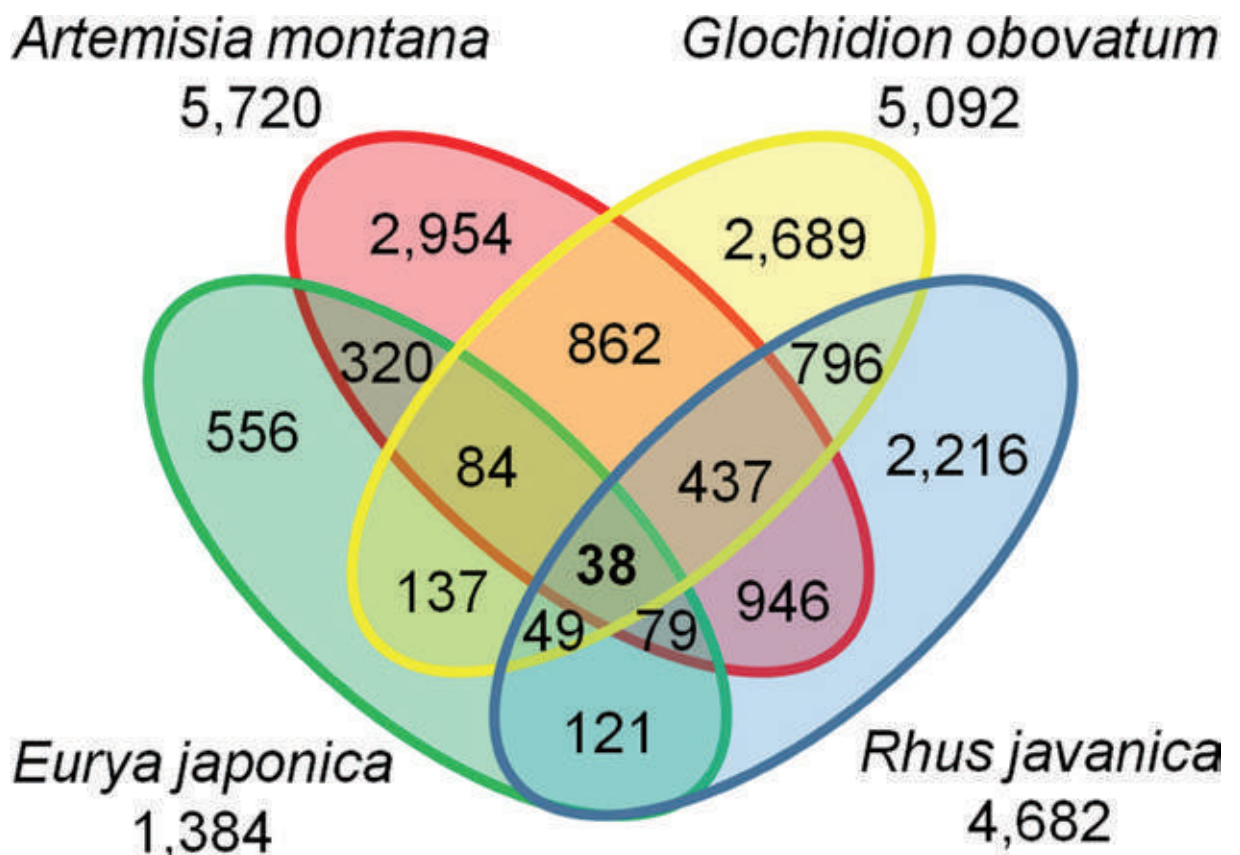


Fig 5. Venn diagram of transcriptome results for the 4 different galls. The number of genes that are upregulated more than twice than that in leaves is shown. Note that 38 genes are commonly expressed in the four galls.

<https://doi.org/10.1371/journal.pone.0223686.g005>

At5g51060), a NADPH oxidase that is involved in ROS production at the root hair tip, is up-regulated in the four galls, suggesting the involvement of ROS during gall development, possibly regulating cell wall structure for cell expansion and/or cellular signaling [32–33].

AtMYB77 (At3g50060) is a member of the R2R3-type transcription factor family and involved in metabolism of reactive oxygen species (ROS) by direct transcriptional regulation of the *ORBITALLY MANIFESTED GENE 1 (OMG1)* [34]. These suggest that active ROS production is involved in lignification within the gall, generating a shelter-like structure.

(3) Phytohormone signaling and cell regeneration. Auxin is one of the key phytohormones in gall initiation and development. AtMYB77 is involved in lateral root formation via auxin signaling [35–36]. Since Arabidopsis cell regeneration mediates the process of lateral root development [37], the callus generation within the gall may be mediated by AtMYB77 and auxin signaling. The WRKY23 transcription factor is an auxin-response gene involved in embryogenesis and leaf venation patterning, through the regulation of PIN protein localization [38–40]. Overexpression of WRKY23 affects the localization of PIN proteins, and also the leaf venation pattern [40]. Thus, up-regulation of WRKY23 can be involved in vascular patterning in galls through regulation of auxin flux. It is also activated at the site of nematode infection in roots [41], suggesting that WRKY23 also regulates biotic responses in the galls. DOF4.6 (At4g24060) is a member of plant-specific transcription factors, and expressed in vascular cells depending on auxin flux [42], suggesting its involvement in vascular development in galls.

Table 1. Thirty-eight genes upregulated in 4 different galls.

Annotation	AGI (<i>Arabidopsis thaliana</i>)	logFC ^a				Putative molecular function	Putative biological function	References
		<i>A. montana</i>	<i>E. japonica</i>	<i>G. obovatum</i>	<i>R. javanica</i>			
ATBRCA1 breast cancer susceptibility 1	AT4G21070	8.38	4.07	1.35	7.24	DNA repair	cell cycle, DNA repair	[21–23]
FUSED Kinase family Protein kinase family protein with ARM repeat domain	AT1G50240	4.74	2.94	4.54	9.68	protein kinase	cell division, cytokinesis	[24, 25]
Integrase-type DNA-binding superfamily protein ERF115	AT5G07310	3.60	8.82	5.15	2.51	transcription factor	cell cycle regulation	[26]
DOMINO1 Protein of unknown function (DUF3223)	AT5G62440	1.16	2.95	1.52	2.70	nuclear localization	cell division, nuclear size regulation	[27]
DUT1 DUTP-PYROPHOSPHATASE-LIKE1	AT3G46940	1.60	4.50	3.83	7.44	deoxyuridine triphosphatase (dUTPase)	DNA protection	[28]
AtTLP2, TLP2 tubby-like protein 2	AT2G18280	1.01	2.89	2.22	2.68	transcription factor	cell wall, homogalacturonan biosynthesis	[29]
AtPrx25 Peroxidase superfamily protein	AT2G41480	4.94	4.85	3.56	8.87	peroxidase	lignification, ROS generation	[30, 31]
RHD2, ATRBOHC, RBOHC NADPH/respiratory burst oxidase protein D	AT5G51060	2.03	3.52	2.26	7.93	NADPH oxidase	ROS generation	[32, 33]
MYB77 myb domain protein 77	AT3G50060	7.71	5.81	2.89	1.91	transcription factor	auxin signaling, ROS metabolism	[34–36]
WRKY23, ATWRKY23 WRKYDNA-binding protein 23	AT2G47260	2.83	3.15	6.04	5.21	transcription factor	auxin flux, nematode response	[38–41]
Dof-type zinc finger DNA-binding family protein	AT4G24060	1.64	3.06	1.86	4.85	transcription factor	vascular patterning	[42]
ARR5, ATRR2, IBC6, RR5 response regulator 5	AT3G48100	3.48	2.90	3.83	5.95	histidine kinase	cytokinin signaling	[44–46]
DAG1 Dof-type zinc finger DNA-binding family protein	AT3G61850	2.42	3.33	2.18	2.57	transcription factor	phytohormone response	[47, 48]
DLO2 2-oxoglutarate(2OG) and Fe(II)-dependent oxygenase superfamily protein	AT4G10490	4.75	3.32	6.29	4.59	oxygenase	biotic stress response	[49]
Protein kinase superfamily protein, RIPK	AT2G05940	3.06	2.98	3.23	7.88	protein kinase	biotic stress response	[50]
bHLH25 Basic helix-loop-helix(bHLH) DNA-binding superfamily protein	AT4G37850	6.20	4.83	6.39	4.46	transcription factor	biotic stress response	[51]
WRKY48, ATWRKY48 WRKYDNA-binding protein 48	AT5G49520	1.32	3.39	4.16	4.46	transcription factor	biotic stress response	[52]
AtCYSTM4 CYSTEINE-RICH TRANSMEMBRANE MODULE 4	AT2G32190	8.91	2.36	3.89	3.73	transmembrane	abiotic stress response	[53]
AtMYB14 myb domain protein 14	AT2G31180	5.96	3.09	5.60	4.62	transcription factor	abiotic stress response	[54]
ATBAG7, BAG7 BCL-2-associated athanogene 7	AT5G62390	4.73	1.92	3.15	8.49	ER localization	abiotic stress response	[55–57]
HSF4, HSF1, AT-HSF1, ATHSF4 heatshock factor 4	AT4G36990	1.69	8.89	3.42	3.04	heat shock protein	abiotic- and biotic-stress responses	[58, 59]
BAM3 Leucine-richreceptor-like protein kinase family protein	AT4G20270	7.86	2.87	2.12	2.54	receptor kinase	abiotic stress response, development	[60–62]
HMG1, HMGR1, ATHMGR1 3-hydroxy-3-methylglutaryl CoA reductase1	AT1G76490	3.90	2.12	3.21	6.75	reductase	metabolic process	[63]
Galactosyltransferase family protein	AT1G77810	1.99	2.42	1.78	3.40	galactosyltransferase, Golgi apparatus localization	metabolic process	[64]
TUB1 tubulin beta-1chain	AT1G75780	6.23	4.14	2.23	2.87	tubulin	cytoskeleton	[65]

(Continued)

Table 1. (Continued)

Annotation	AGI (<i>Arabidopsis thaliana</i>)	logFC ^a				Putative molecular function	Putative biological function	References
		A. <i>montana</i>	E. <i>japonica</i>	G. <i>obovatum</i>	R. <i>javanica</i>			
ATFD3,FD3 ferredoxin 3	AT2G27510	3.13	1.83	3.32	1.91	ferredoxin	Photosystem I	[66]
ANAC100,ATNAC5,NAC100 NAC domain containing protein 100	AT5G61430	2.58	3.53	3.66	4.75	transcription factor	miR164 target	[67]
C2calcium/lipid-binding plant phosphoribosyltransferase family protein MCTP16	AT5G17980	3.23	2.55	2.10	6.17	transmembrane	unknown	[68]
APK2B protein kinase 2B	AT2G02800	1.58	2.29	7.11	8.23	Ser/Thr kinase	unknown	[69]
Adeninucleotide alphahydroxylase-like superfamily protein	AT3G17020	8.73	2.45	1.89	7.01	-	-	-
Plant invertase/pectin methylesterase inhibitor superfamily protein	AT5G62350	7.48	5.69	5.01	2.62	-	-	-
UNE1 Plant protein of unknown function (DUF641)	AT1G29300	3.50	3.15	3.05	4.89	-	-	-
GAD4 glutamate decarboxylase 4	AT2G02010	3.15	3.06	1.78	3.93	-	-	-
Protein of unknown function (DUF1635)	AT5G22930	2.64	4.18	2.64	2.87	-	-	-
RNA polymerase	AT5G56120	2.03	2.28	2.14	5.01	-	-	-
cotton fiber protein	AT3G60380	1.89	3.14	3.58	4.75	-	-	-
phosphatidylinositol 4-phosphate 5-kinase MSS4-like protein	AT1G29195	1.73	2.76	2.40	4.22	-	-	-
TIP41-like protein	AT3G54000	1.43	1.89	2.47	8.71	-	-	-

^a logFC value: the highest score among trinity contigs

<https://doi.org/10.1371/journal.pone.0223686.t001>

Cytokinin is another key phytohormone in gall development, as well as other physiological functions in plants including cell division, cell regeneration and shoot differentiation [43]. Type-A Arabidopsis response regulator 5 (ARR5, At3g48100), a cytokinin primary response gene, is up-regulated in the four galls. ARR5 expression is activated by exogenous cytokinin and negatively regulates cytokinin signaling redundantly with the other ARRs, generating a feedback regulation to decrease sensitivity to cytokinin [44–46].

Dof AFFECTING GERMINATION 1 (DAG1)/At3g61850 controls hypocotyl cell elongation by affecting the expression of auxin-, ABA- and ethylene-related genes [47], as well as seed dormancy independently of ABA [48]. DAG1 is suggested to be involved in cellular morphogenesis through the regulation of phytohormone-related genes.

Together with previous studies, our results suggest that auxin and cytokinin are common regulators for gall development, and many responsive genes to these phytohormones are activated in galls. They seem to regulate cell proliferation and vascular differentiation during gall development.

(4) Biotic and abiotic stress responses. During gall initiation and development, insects may have to suppress the plant's resistant system. Several genes involved in biotic- and abiotic-stress responses were up-regulated in galls. DLO2 (At4g10490), a homolog of DMR6 and acting redundantly with it, is upregulated in the four galls (Table 1). DLO2 is a negative regulator of plant defense and its overexpression results in reduced resistance to pathogens [49]. It is possible that insects regulate the expression of DLO2 and reducing plant defense. RIPK (At2g05940), a member of the receptor-like cytoplasmic kinase family, interacts directly with and phosphorylates RIN4, a negative regulator of immune responses against pathogen associated molecular pattern (PAMPs)-triggered immunity (PIT) [50]. RIKP overexpression lines

are more susceptible to inoculation of *Pseudomonas syringae* DC3000, suggesting that up-regulation of RIPK in galls reduces the defense system in plants. bHLH25 (At4g37850), a putative transcription factor with a basic helix-loop-helix domain, is up-regulated in developing syncytia that are generated by invasion of cyst nematode *Heterodera schachtii* [51]. The *wrky48* mutant reduces the growth of the bacterial pathogen *P. syringae*, whereas overexpression leads to enhanced growth of the pathogen [52], suggesting that up-regulation of WRKY48 in galls represses the plant's defense responses so that insects can survive.

Several abiotic-stress response genes are also up-regulated in the four galls. The expression of the cysteine-rich transmembrane module 4 (AtCYSTM4, At2g32190) is stimulated by salt, drought or oxidation stress [53]. AtMYB14 (At2g31180) is involved in cold tolerance [54]. The Bcl-2-associated athanogene (AtBAG7) is an ER-localized protein where it interacts with the molecular chaperon AtBiP2, and is involved in cold-, heat- and salinity-stress responses [55–56]. Sumoylated AtBAG7 interacts with WRKY29 in the nucleus where it is supposed to activate the molecular chaperon genes including AtBAG7 itself, leading to heat tolerance [57]. HsfB1 (At4g36690) encodes a heat shock protein that is suggested to be involved in thermotolerance response [58], as well as in salicylic acid-mediated resistance against pathogen challenge [59]. BAM3 (At4g20270) encodes a receptor-like kinase related to CLAVATA1 and functions as a receptor of CLAVATA3/EMBRYO SURROUNDING REGION (CLV3/ESR) peptides. So far, it is reported to be involved in suppression of root elongation and proto-phloem in roots as a receptor of CLE45 [60–61], and drought-stress response as a receptor of CLE25 [62]. CLE25 is up-regulated in galls of *E. japonica* and *G. obovatum* (Table 2; see below), suggesting that galls are responding to abiotic stresses, which are likely to be caused indirectly by insect infection.

In summary, up-regulation of these abiotic-response genes suggests that in the gall, both biotic and abiotic stress responses are occurring during gall development.

(5) Metabolic processes. Plants biosynthesize secondary metabolites, such as terpene, phenolic acids, and alkaloids, and use them as a defense response. In the gall, the secondary metabolites are speculated to be biosynthesized and accumulated. 3-Hydroxy-3-methylglutaryl coenzyme A reductase (HMG1/HMGR, At1g76490) is involved in isoprenoid biosynthesis through regulation of ER morphogenesis [63]. At1g77810 encodes a member of the beta-(1,3)-galactosyltransferases, located in the Golgi apparatus [64]. This enzyme is involved in modification of arabinogalactan-proteins (AGPs), playing roles in various processes such as growth and development, programmed cell death, and signaling pathways [64]. Up-regulation of this gene in the gall may contribute to the biosynthesis of AGPs.

(6) Other up-regulated genes in the four galls. There are other up-regulated genes in the four galls: β -TUBULIN gene *TUB1* (At1g75780), a component of microtubules [65]; AtFD3 (At2g27510), a ferredoxin involved in photosystem I [66]. ANAC100 (At5t61430), a target of microRNA miR164 [67]; MCTP16 (At5g17980), encoding a multiple C2 domain and transmembrane region protein expressed in vascular tissue [68]; and APK2B (At2g02800), a serine/threonine protein kinase that is expressed in roots, leaves and flowers [69]. Future work will unveil their molecular and biological functions in galls.

GO analysis suggests peptide signaling in galls

GO analysis predicts the biological and molecular functions of genes. We found that GO terms of peptide biosynthetic and peptide metabolic processes are common in four galls (S2 Table), as well as amide biosynthetic process and translation. Therefore, we extracted the CLV3/ESR-related (CLE) family genes from the gene list, and found that several genes are expressed in galls, especially *CLE44*, which is commonly up-regulated in the four galls (Table 2).

Table 2. CLE, LRR-RLK, WOX, and MADS genes expressed in galls.

Gene symbol	AGI (<i>Arabidopsis thaliana</i>)	logFC ^a			
		<i>A. montana</i>	<i>E. japonica</i>	<i>G. obovatum</i>	<i>R. javanica</i>
CLE					
CLV3	AT2G27250	2.57			
CLE6	AT2G31085	6.05		7.34	
CLE7	AT2G31082		6.76		
CLE9	AT1G26600			1.62	
CLE25	AT3G28455		2.83	11.64	
CLE26	AT1G69970	1.32			3.80
CLE44	AT4G13195	3.75	2.87	2.07 ^b	1.75
LRR-RLK					
	AT1G08590	2.84			4.15
RLK7	AT1G09970	1.69	3.11		6.07
	AT1G72180				
	AT1G75640	2.31		4.65	
CLV1	AT1G75820				2.29
	AT2G25790				7.74
ER	AT2G26330	2.64			7.94
	AT3G28040	3.40			
RLK5	AT4G28490	9.80		4.99	
	AT4G36180	5.65	3.03		
BRI1	AT4G39400			1.98	
	AT5G10020		2.42		2.75
FLS2	AT5G46330			5.00	9.80
	AT5G56040			3.07	
BAM1	AT5G65700	1.08	3.88		2.37
WOX					
WOX1	AT3G18010		7.02	4.75	
WOX2	AT5G59340				3.14
WOX4	AT1G46480	2.73	3.64		1.83
WOX13/HB-4	AT4G35550	1.40	2.66		
MADS					
API/AGL7	AT1G69120	12.13		8.85	5.83
AP3	AT3G54340			8.18	
PI	AT5G20240	2.49			
AG	AT4G18960	10.93		10.03	11.55
SEP1/AGL2	AT5G15800				12.39
SEP2/AGL4	AT3G02310	11.52			13.54
SEP3/AGL9	AT1G24260	7.29			11.41
SEP4/AGL3	AT2G03710	6.50			
SHP2/AGL5	AT2G42830			2.04	
SVP/AGL22	AT2G22540	3.65	3.69	9.23	
AGL62	AT5G60440		3.59		
TT16	AT5G23260				8.27
PHE	AT1G65330				7.23

^a logFC value: the highest score among trinity contigs.

^b *CLE44* in *G. obovatum* is up-regulated only in mature galls but not in young galls.

<https://doi.org/10.1371/journal.pone.0223686.t002>

CLE peptides are small ligands that bind to the leucine-rich repeat receptor kinase family (LRR-RLK) CLV1/CLV2 proteins, and is involved in cell-cell communication during development, symbiosis, parasitism, and abiotic stress responses [70]. Several CLE and LRR-RLK genes are up-regulated in the galls (Table 2). CLE44 and CLE41 encoding the tracheary element differentiation inhibitory factor (TDIF) are involved in suppression of xylem cell differentiation in vascular stem cells [71]. Recent findings have shown that TDIF-like peptide from cyst nematodes can mimic the CLE function *in planta*, promoting vascular cell proliferation at the feeding site by activating the CLE and LRR-RLK pathway [72]. WOX4 is involved in promotion of vascular procambial and cambial stem cells depending on the CLE41/44 [73]. The WOX4 gene as well as the other WOX family genes is up-regulated in several galls (Table 2), suggesting that CLE44 and WOX4 regulate the vascular generation in galls.

In many galls the vasculature is generated to connect to the source of host plant tissue, and this process is suggested to be regulated by CLE and LRR-RLK genes, together with the other factors such as the auxin-dependent process shown above. A previous study with grapevine gall has shown that CLE44 and WOX4 are up-regulated in galls [13], supporting our hypothesis that these factors are commonly involved in vascular development in galls.

Genes involved in floral organ development

Shape and color of some galls show similarity to flowers and fruits. From the grapevine gall research, it is suggested that genes involved in reproductive organ development are up-regulated in developing galls [13]. Floral organ identity is determined by combined actions of the floral MADS genes [74–75]. We focused on MADS genes to find out if they are up-regulated in galls (Table 2). Interestingly many floral MADS genes were up-regulated in three plant galls, whereas they were not in the gall of *E. japonica*. This may be due to the different structure of galls: the gall of *E. japonica* is thinner than the other galls (Fig 1), suggesting less proliferation and differentiation of gall cells. This indicates that each gall mobilizes a distinct set of genes to generate each unique structure.

Conclusions

Our results have provided a landscape of transcripts up- and down-regulated in four different galls, suggesting that galls are forced to mobilize the genes that are originally involved in other multiple biological processes to develop specific structure. The 38 commonly up-regulated genes may be involved in development of other leaf galls. Further transcriptome analyses of other plant species are required to validate this hypothesis. This work is based on the transcriptome of galls on plants and in order to understand the gall developmental mechanisms, we need to investigate the gall insects. To date, not many reports have been published except for that on the Hessian fly genome, transcriptome, and proteome (reviewed in [6]), and on *Schlechtendalia chinensis* [11]. Gall-causing insects, as well as the other galls on host plants, should be analyzed to understand the molecular mechanism of insect-plant interaction and gall development.

Supporting information

S1 Fig. Gene ontology (GO) analysis (biological process) of mature gall and leaf from *G. obovatum*. Colored dots indicate similar biological GO: blue, developmental process; red, phytohormone; and green, photosynthesis.
(TIF)

S1 Table. RNA-sequencing analysis.

(XLSX)

S2 Table. GO analysis of genes up-regulated in galls.

(XLSX)

Acknowledgments

We thank Ms. Kaori Kaminoyama (Kyoto Sangyo University) for technical help for library construction and RNA-sequencing.

Author Contributions

Conceptualization: Seiji Takeda.

Data curation: Seiji Takeda, Issei Ohshima, Masa H. Sato, Tomoaki Sakamoto.

Formal analysis: Seiji Takeda, Tomoaki Sakamoto, Seisuke Kimura.

Funding acquisition: Issei Ohshima, Masa H. Sato, Seisuke Kimura.

Investigation: Seiji Takeda, Makiko Yoza, Taisuke Amano, Issei Ohshima, Tomoko Hirano.

Methodology: Seiji Takeda, Makiko Yoza, Taisuke Amano, Issei Ohshima, Tomoko Hirano, Tomoaki Sakamoto, Seisuke Kimura.

Project administration: Seiji Takeda.

Resources: Seiji Takeda, Issei Ohshima, Seisuke Kimura.

Software: Tomoaki Sakamoto.

Supervision: Seiji Takeda, Issei Ohshima.

Validation: Masa H. Sato, Seisuke Kimura.

Writing – original draft: Seiji Takeda.

Writing – review & editing: Seiji Takeda.

References

1. Stone GN, Schönrogge K. The adaptive significance of insect gall morphology. *Trends Ecol Evol* 2003; 18: 512–522. [https://doi.org/10.1016/s0169-5347\(03\)00247-7](https://doi.org/10.1016/s0169-5347(03)00247-7)
2. Espírito-Santo MM, Fernandes GW. How many species of gall-inducing insects are there on earth, and where are they? *Ann Entomol Soc Am.* 2007; 100: 95–99. [https://doi.org/10.1603/0013-8746\(2007\)100\[95:HMSOGI:2.0.CO;2](https://doi.org/10.1603/0013-8746(2007)100[95:HMSOGI:2.0.CO;2)
3. Yamaguchi H, Tanaka H, Hasegawa M, Tokuda M, Asami T, Suzuki Y. Phytohormones and willow gall induction by a gall-inducing sawfly. *New Phytol.* 2012; 196: 586–595. <https://doi.org/10.1111/j.1469-8137.2012.04264.x> PMID: 22913630
4. Tanaka Y, Okada K, Asami T, Suzuki Y. Phytohormones in Japanese mugwort gall induction by a gall-inducing gall midge. *Biosci Biotechnol Biochem.* 2013; 77: 1942–1948. <https://doi.org/10.1271/bbb.130406> PMID: 24018692
5. Bartlett L, Connor EF. Exogenous phytohormones and the induction of plant galls by insects. *Arthropod-Plant Interact.* 2014; 8: 339–348. <https://doi.org/10.1007/s11829-011-9309-0>
6. Giron D, Huguet E, Stone GN, Body M. Insect-induced effects on plants and possible effectors used by galling and leaf-mining insects to manipulate their host-plant. *J Insect Physiol.* 2016; 84: 70–89. <https://doi.org/10.1016/j.jinsphys.2015.12.009> PMID: 26723843
7. Kaiser W, Huguet E, Casas J, Commin C, Giron D. Plant green-island phenotype induced by leaf-miners is mediated by bacterial symbionts. *Proc R Soc B.* 2010; 277: 2311–2319. <https://doi.org/10.1098/rspb.2010.0214> PMID: 20356892

8. Body M, Kaiser W, Dubreuil G, Casas J, Giron D. Leaf-miners co-opt microorganisms to enhance their nutritional environment. *J Chem Ecol* 2013; 39: 969–977. <https://doi.org/10.1007/s10886-013-0307-y> PMID: 23807431
9. Barnewall EC, De Clerck-Floate RA. A preliminary histological investigation of gall induction in an unconventional galling system. *Arthropod-Plant Interact*. 2012; 6: 449–459. <https://doi.org/10.1007/s11829-012-9193-4>
10. Bailey S, Percy DM, Hefer CA, Cronk QCB. The transcriptional landscape of insect galls: psyllid (Hemiptera) gall formation in Hawaiian *Metrosideros polymorpha* (Myrtaceae). *BMC Genomics*. 2015; 16: 943. <https://doi.org/10.1186/s12864-015-2109-9> PMID: 26572921
11. Liu P, Yang ZX, Chen XM, Yang P. RNA-seq-based transcriptome and the reproduction-related genes for the aphid *Schlechtendalia chinensis* (Hemiptera, Aphididae). *Genet Mol Res*. 2017; 16: gmr16019448. <https://doi.org/10.4238/gmr16019448> PMID: 28340266
12. Chen H, Liu J, Cui K, Lu Q, Wang C, Wu H, et al. Molecular mechanisms of tannin accumulation in *Rhus* galls and genes involved in plant-insect interactions. *Sci Rep*. 2018; 8: 9841. <https://doi.org/10.1038/s41598-018-28153-y> PMID: 29959354
13. Schultz JC, Edger PP, Body MJA, Appel HM. A galling insect activates plant reproductive programs during gall development. *Sci Rep*. 2019; 9: 1833. <https://doi.org/10.1038/s41598-018-38475-6> PMID: 30755671
14. Guiguet A, Ohshima I, Takeda S, Laurans F, Lopez-Vaamonde C, Giron D. Origin of gall-inducing from leaf-mining in *Caloptilia* micromoths (Lepidoptera, Gracillariidae). *Sci Rep*. 2019; 9: 6794. <https://doi.org/10.1038/s41598-019-43213-7> PMID: 31043653
15. Guiguet A, Hamatani A, Amano T, Takeda S, Lopez-Vaamonde C, Giron D, et al. Inside the horn of plenty: leaf-mining micromoth manipulates its host plant to obtain unending food provisioning. *PLoS ONE*. 2018; 13: e0209485. <https://doi.org/10.1371/journal.pone.0209485> PMID: 30576396
16. Brunner AM, Yakovlev IA, Strauss SH. Validating internal controls for quantitative plant gene expression studies. *BMC Plant Biol*. 2004; 4: 1–7. <https://doi.org/10.1186/1471-2229-4-1>
17. Grabherr MG, Haas BJ, Yassour M, Levin JZ, Thompson DA, Amit I, et al. Full-length transcriptome assembly from RNA-seq data without a reference genome. *Nat Biotechnol*. 2011; 29: 644–652. <https://doi.org/10.1038/nbt.1883> PMID: 21572440
18. Li H, Durbin R. Fast and accurate short read alignment with Burrows-Wheeler transform. *Bioinformatics* 2009; 25: 1754–1760. <https://doi.org/10.1093/bioinformatics/btp324> PMID: 19451168
19. Robinson MD, McCarthy DJ, Smyth GK. EdgeR: a bioconductor package for differential expression analysis of digital gene expression data. *Bioinformatics*. 2010; 26: 139–140. <https://doi.org/10.1093/bioinformatics/btp616> PMID: 19910308
20. Mi H, Muruganujan A, Ebert D, Huang X, Thomas PD. PANTHER version 14: more genomes, a new PANTHER GO-slim and improvements in enrichment analysis tools. *Nucleic Acids Res*. 2018; 47: D419–D426. <https://doi.org/10.1093/nar/gky1038> PMID: 30407594
21. Lafarge S, Montané MH. Characterization of *Arabidopsis thaliana* ortholog of the human breast cancer susceptibility gene 1: AtBRCA1, strongly induced by gamma rays. *Nucleic Acids Res*. 2003; 31: 1148–1155. <https://doi.org/10.1093/nar/gkg202> PMID: 12582233
22. Sjogren CA, Bolaris SC, Larsen PB. Aluminum-dependent terminal differentiation of the *Arabidopsis* root tip is mediated through an ATR-, ALT2-, and SOG1-regulated transcriptional response. *Plant Cell*. 2015; 27: 2501–2515. <https://doi.org/10.1105/tpc.15.00172> PMID: 26320227
23. Ogita N, Okushima Y, Tokizawa M, Yamamoto YY, Tanaka M, Seki M, et al. Identifying the target genes of SUPPRESSOR OF GAMMA RESPONSE 1, a master transcription factor controlling DNA damage response in *Arabidopsis*. *Plant J*. 2018; 94: 439–453. <https://doi.org/10.1111/tpj.13866> PMID: 29430765
24. Oh SA, Johnson A, Smertenko A, Rahman D, Park SK, Hussey PJ, et al. A divergent cellular role for the FUSED kinase family in the plant-specific cytokinetic phragmoplast. *Curr Biol*. 2005; 15: 2107–2111. <https://doi.org/10.1016/j.cub.2005.10.044> PMID: 16332535
25. Oh SA, Allen T, Kim GJ, Sidorova A, Borg M, Park SK, et al. *Arabidopsis* Fused kinase and the Kinesin-12 subfamily constitute a signaling module required for phragmoplast expansion. *Plant J*. 2012; 72: 308–319. <https://doi.org/10.1111/j.1365-313X.2012.05077.x> PMID: 22709276
26. Heyman J, Cools T, Vandenbussche F, Heyndrickx KS, Leene JV, Vercauteren I, et al. ERF115 controls root quiescent center cell division and stem cell replenishment. *Science* 2013; 342: 860–863. <https://doi.org/10.1126/science.1240667> PMID: 24158907
27. Lahmy S, Guillemot J, Cheng CM, Bechtold N, Albert S, Pelletier G, et al. DOMINO1, a member of a small plant-specific gene family, encodes a protein essential for nuclear and nucleolar functions. *Plant J*. 2004; 39: 809–820. <https://doi.org/10.1111/j.1365-313X.2004.02166.x> PMID: 15341625

28. Dubois E, Córdoba-Cañero D, Massot S, Siaud N, Gakière B, Domenichini S, et al. Homologous recombination is stimulated by a decrease in dUTPase in Arabidopsis. *PLoS ONE*. 2011; 6: e18658. <https://doi.org/10.1371/journal.pone.0018658> PMID: 21541310
29. Wang M, Xu Z, Ahmed RI, Wang Y, Hu R, Zhou G, et al. Tubby-like Protein 2 regulates homogalacturonan biosynthesis in Arabidopsis seed coat mucilage. *Plant Mol Biol*. 2019; 99: 421–436. <https://doi.org/10.1007/s11103-019-00827-9> PMID: 30707395
30. Shigeto J, Nagano M, Fujita K, Tsutsumi Y. Catalytic profile of Arabidopsis peroxidases, AtPrx–2, 25 and 71, contributing to stem lignification. *PLoS ONE*. 2014; 9: e105332. <https://doi.org/10.1371/journal.pone.0105332> PMID: 25137070
31. Shigeto J, Kiyonaga Y, Fujita K, Kondo R, Tsutsumi Y. Putative cationic cell-wall-bound peroxidase homologues in Arabidopsis, AtPrx2, AtPrx25, and AtPrx71, are involved in lignification. *J Agri Food Chem*. 2013; 1: 3781–3788. <https://doi.org/10.1021/jf400426g> PMID: 23551275
32. Foreman J, Demidchik V, Bothwell JHF, Mylona P, Miedema H, Torres MA, et al. Reactive oxygen species produced by NADPH oxidase regulate plant cell growth. *Nature* 2003; 22: 42–446. <https://doi.org/10.1038/nature01485> PMID: 12660786
33. Takeda S, Gapper C, Kaya H, Bell E, Kuchitsu K, Dolan L. Local positive feedback regulation determines cell shape in root hair cells. *Science* 2008; 19: 1241–1244. <https://doi.org/10.1126/science.1152505> PMID: 18309082
34. Sng NJ, Kolaczowski B, Ferl RJ, Paul AL. A member of the CONSTANS-like protein family is a putative regulator of reactive oxygen species homeostasis and spaceflight physiological adaptation. *AoB Plants*. 2018; 11: ply075. <https://doi.org/10.1093/aobpla/ply075> PMID: 30705745
35. Shin R, Burch AY, Huppert KA, Tiwari SB, Murphy AS, Guilfoyle TJ, et al. The Arabidopsis transcription factor MYB77 modulates auxin signal transduction. *Plant Cell*. 2007; 19: 2440–2453. <https://doi.org/10.1105/tpc.107.050963> PMID: 17675404
36. Zhao Y, Xing L, Wang X, Hou YJ, Gao J, Wang P, et al. The ABA receptor PYL8 promotes lateral root growth by enhancing MYB77-dependent transcription of auxin-responsive genes. *Sci Signal*. 2015; 7: ra53. <https://doi.org/10.1126/scisignal.2005051> PMID: 24894996
37. Sugimoto K, Jiao Y, Meyerowitz EM. Arabidopsis regeneration from multiple tissues occurs via a root development pathway. *Dev Cell*. 2010; 18: 463–471. <https://doi.org/10.1016/j.devcel.2010.02.004> PMID: 20230752
38. Grunewald W, Smet ID, Lewis DR, Löffke C, Jansen L, Goeminne G, et al. Transcription factor WRKY23 assists auxin distribution patterns during Arabidopsis root development through local control on flavonol biosynthesis. *Proc Natl Acad Sci USA*. 2012; 109: 155–1559. <https://doi.org/10.1073/pnas.1110541108>
39. Grunewald W, Smet ID, Rybel BD, Robert HS, van de Cotte B, Willemsen V, et al. Tightly controlled WRKY23 expression mediates Arabidopsis embryo development. *EMBO Rep*. 2013; 14: 1136–1142. <https://doi.org/10.1038/embor.2013.169> PMID: 24157946
40. Prát T, Hajný J, Grunewald W, Vasileva M, Molnár G, Tejos R, et al. WRKY23 is a component of the transcriptional network mediating auxin feedback on PIN polarity. *PLoS Genet*. 2018; 14: e1007177. <https://doi.org/10.1371/journal.pgen.1007177> PMID: 29377885
41. Grunewald W, Karimi M, Wiczorek K, de Cappelle EV, Wischnitzki E, Grundler F, et al. A role for AtWRKY23 in feeding site establishment of plant-parasitic nematodes. *Plant Physiol*. 2008; 148: 358–368. <https://doi.org/10.1104/pp.108.119131> PMID: 18599655
42. Gardiner J, Sherr I, Scarpella E. Expression of DOF genes identifies early stages of vascular development in Arabidopsis leaves. *Int J Dev Biol* 2010; 54: 1389–1396. <https://doi.org/10.1387/ijdb.093006jg> PMID: 20563990
43. Werner T, Schmülling T. Cytokinin action in plant development. *Curr Opin Plant Biol*. 2009; 12: 527–538. <https://doi.org/10.1016/j.pbi.2009.07.002> PMID: 19740698
44. D'Agostino IB, Deruère J, Kieber JJ. Characterization of the response of the Arabidopsis response regulator gene family to cytokinin. *Plant Physiol*. 2000; 124: 1706–1717. <https://doi.org/10.1104/pp.124.4.1706> PMID: 11115887
45. Rashotte AM, Carson SDB, To JPC, Kieber JJ. Expression profiling of cytokinin action in Arabidopsis. *Plant Physiol*. 2003; 132: 1998–2011. <https://doi.org/10.1104/pp.103.021436> PMID: 12913156
46. To JPC, Haberer G, Ferreira FJ, Druère J, Mason MG, Schaller GE, et al. Type-A Arabidopsis response regulators are partially redundant negative regulators of cytokinin signaling. *Plant Cell* 2004; 16: 658–671. <https://doi.org/10.1105/tpc.018978> PMID: 14973166
47. Lorrai R, Gandolfi F, Boccaccini A, Ruta V, Possenti M, Tramontano A, et al. Genome-wide RNA-seq analysis indicates that the DAG1 transcription factor promotes hypocotyl elongation acting on ABA, ethylene and auxin signaling. *Sci Rep*. 2018; 8: 15895. <https://doi.org/10.1038/s41598-018-34256-3> PMID: 30367178

48. Papi M, Sabatini S, Bouchez D, Camilleri C, Costantino P, Vttoriosio P. Identification and disruption of an Arabidopsis zinc finger gene controlling seed germination. *Genes Dev.* 2000; 14: 28–33. PMID: [10640273](https://pubmed.ncbi.nlm.nih.gov/10640273/)
49. Zeilmaker T, Ludwig NR, Elberse J, Seidl MF, Berke L, Doorn AV, et al. DOWNY MILDEW RESISTANT 6 and DMR6–LIKE OXYGENASE 1 are partially redundant but distinct suppressors of immunity in Arabidopsis. *Plant J.* 2015; 81: 210–222. <https://doi.org/10.1111/tpj.12719> PMID: [25376907](https://pubmed.ncbi.nlm.nih.gov/25376907/)
50. Liu J, Elmore JM, Lin ZJD, Coaker G. A receptor–like cytoplasmic kinase phosphorylates the host target RIN4, leading to the activation of a plant innate immune receptor. *Cell Host Microbe.* 2011; 9: 137–146. <https://doi.org/10.1016/j.chom.2011.01.010> PMID: [21320696](https://pubmed.ncbi.nlm.nih.gov/21320696/)
51. Jin J, Hewezi T, Baum TJ. The Arabidopsis bHLH25 and bHLH27 transcription factors contribute to susceptibility to the cyst nematode *Heterodera schachtii*. *Plant J.* 2011; 65: 319–328. <https://doi.org/10.1111/j.1365-313X.2010.04424.x> PMID: [21223395](https://pubmed.ncbi.nlm.nih.gov/21223395/)
52. Xing DH, Lai ZB, Zheng ZY, Vinod KM, Fan BF, Chen ZX. Stress–and pathogen–induced Arabidopsis WRKY48 is a transcriptional activator that represses plant basal defense. *Mol Plant* 2008; 1: 459–470. <https://doi.org/10.1093/mp/ssn020> PMID: [19825553](https://pubmed.ncbi.nlm.nih.gov/19825553/)
53. Xu Y, Yu Z, Zhang D, Huang J, Wu C, Yang G, et al. CYSTM, a novel non–secreted cysteine–rich peptide family, involved in environmental stresses in *Arabidopsis thaliana*. *Plant Cell Physiol.* 2018; 59: 423–438. <https://doi.org/10.1093/pcp/pcx202> PMID: [29272523](https://pubmed.ncbi.nlm.nih.gov/29272523/)
54. Chen Y, Chen Z, Kang J, Kang D, Gu H, Qin G. AtMYB14 regulates cold tolerance in Arabidopsis. *Plant Mol Biol Rep.* 2013; 31: 87–97. <https://doi.org/10.1007/s11105-012-0481-z> PMID: [24415840](https://pubmed.ncbi.nlm.nih.gov/24415840/)
55. Williams B, Kabbage M, Britt R, Dickman MB. AtBAG7, an Arabidopsis Bcl–2–associated athanogene, resides in the endoplasmic reticulum and is involved in the unfolded protein response. *Proc Natl Acad Sci USA.* 2010; 107: 3088–6093. <https://doi.org/10.1073/pnas.0912670107> PMID: [20231441](https://pubmed.ncbi.nlm.nih.gov/20231441/)
56. Pan YJ, Liu L, Lin YC, Zu YG, Li LP, Tang ZH. Ethylene antagonizes salt–induced growth retardation and cell death process via transcriptional controlling of ethylene–, BAG–and senescence–associated genes in Arabidopsis. *Frontiers Plant Sci.* 2016; 7: 696. <https://doi.org/10.3389/fpls.2016.00696> PMID: [27242886](https://pubmed.ncbi.nlm.nih.gov/27242886/)
57. Li Y, Williams B, Dickman M. Arabidopsis B–cell lymphoma2 (Bcl–2)–associated athanogene 7 (BAG7)–mediated heat tolerance requires translocation, sumoylation and binding to WRKY29. *New Phytol.* 2017; 214: 695–705. <https://doi.org/10.1111/nph.14388> PMID: [28032645](https://pubmed.ncbi.nlm.nih.gov/28032645/)
58. Ikeda M, Mitsuda N, Ohme–Takagi M. Arabidopsis HsfB1 and HsfB2b act as repressors of the expression of heat–inducible Hsfs but positively regulate the acquired thermotolerance. *Plant Physiol.* 2011; 157: 1243–1254. <https://doi.org/10.1104/pp.111.179036> PMID: [21908690](https://pubmed.ncbi.nlm.nih.gov/21908690/)
59. Pick T, Jaskiewicz M, Peterhansel C, Conrath U. Heat shock factor HsfB1 primes gene transcription and systemic acquired resistance in Arabidopsis. *Plant Physiol.* 2012; 159: 52–55. <https://doi.org/10.1104/pp.111.191841> PMID: [22427343](https://pubmed.ncbi.nlm.nih.gov/22427343/)
60. Depuydt S, Rodriguez–Villalon A, Santuari L, Wyser–Rmili C, Ragni L, Hardtke CS. Suppression of Arabidopsis protophloem differentiation and root meristem growth by CLE45 requires the receptor–like kinase BAM3. *Proc Natl Acad Sci USA.* 2013; 110: 7074–7079. <https://doi.org/10.1073/pnas.1222314110> PMID: [23569225](https://pubmed.ncbi.nlm.nih.gov/23569225/)
61. Hazak O, Brandt B, Cattaneo P, Santiago J, Rodriguez–Villalon A, Hothorn M, et al. Perception of root–active CLE peptide requires CORYNE function in the phloem vasculature. *EMBO Rep.* 2017; 18: 1367–1381. <https://doi.org/10.15252/embr.201643535> PMID: [28607033](https://pubmed.ncbi.nlm.nih.gov/28607033/)
62. Takahashi F, Suzuki T, Osakabe Y, Betsuyaku S, Kondo Y, Dohmae N, et al. A small peptide modulates stomatal control via abscisic acid in long–distance signaling. *Nature* 2018; 556: 235–238. <https://doi.org/10.1038/s41586-018-0009-2> PMID: [29618812](https://pubmed.ncbi.nlm.nih.gov/29618812/)
63. Ferrero S, Grados–Torrez RE, Leivar P, Antolın–Llovera M, Lopez–Iglesias C, Cortadellas N. et al. Proliferation and morphogenesis of the endoplasmic reticulum driven by the membrane domain of 3–hydroxy–3–methylglutaryl coenzyme A reductase in plant cells. *Plant Physiol.* 2015; 168: 899–914. <https://doi.org/10.1104/pp.15.00597> PMID: [26015445](https://pubmed.ncbi.nlm.nih.gov/26015445/)
64. Qu Y, Egelund J, Gilson PR, Houghton F, Gleeson PA, Shultz CJ, et al. Identification of a novel group of putative *Arabidopsis thaliana* β –(1,3)–galactosyltransferases. *Plant Mol Biol.* 2008; 68: 43–59. <https://doi.org/10.1007/s11103-008-9351-3> PMID: [18548197](https://pubmed.ncbi.nlm.nih.gov/18548197/)
65. Chu B, Wilson TJ, McCune–Zierath C, Snustad DP, Carter JV. Two β –tubulin genes, TUB1 and TUB8, of Arabidopsis exhibit largely nonoverlapping patterns of expression. *Plant Mol Biol.* 1998; 37: 785–790. <https://doi.org/10.1023/a:1006047129410> PMID: [9678573](https://pubmed.ncbi.nlm.nih.gov/9678573/)
66. Voss I, Goss T, Murozuka E, Altmann B, McLean KJ, Rigby SEJ, et al. FdC1, a novel ferredoxin protein capable of alternative electron partitioning, increases in conditions of acceptor limitation at photosystem I *J Biol Chem.* 2011; 286: 50–59. <https://doi.org/10.1074/jbc.M110.161562> PMID: [20966083](https://pubmed.ncbi.nlm.nih.gov/20966083/)

67. Sieber P, Wellmer F, Gheyselinck J, Riechmann JL, Meyerowitz EM. Redundancy and specialization among plant microRNAs: role of the MIR164 family in developmental robustness. *Development*. 2007; 134: 1051–1060. <https://doi.org/10.1242/dev.02817> PMID: 17287247
68. Liu L, Li C, Liang Z, Yu H. Characterization of multiple C2 domain and transmembrane region proteins in Arabidopsis. *Plant Physiol*. 2018; 176: 2119–2132. <https://doi.org/10.1104/pp.17.01144> PMID: 29259105
69. Ito T, Takahashi N, Shimura Y, Okada K. A serine/threonine protein kinase gene isolated by an *in vivo* binding procedure using the Arabidopsis floral homeotic gene product, AGAMOUS. *Plant Cell Physiol*. 1997; 38: 248–258. <https://doi.org/10.1093/oxfordjournals.pcp.a029160> PMID: 9150601
70. Yamaguchi YL, Ishida T, Sawa S. CLE peptides and their signaling pathways in plant development. *J Exp Bot*. 2016; 67: 4813–4826. <https://doi.org/10.1093/jxb/erw208> PMID: 27229733
71. Hirakawa Y, Shinohara H, Kondo Y, Inoue A, Nakanomyo I, Ogawa M, et al. Non-cell-autonomous control of vascular stem cell fate by a CLE peptide/receptor system. *Proc Natl Acad Sci USA*. 2008; 105: 15208–15213. <https://doi.org/10.1073/pnas.0808444105> PMID: 18812507
72. Guo X, Wang J, Gardner M, Fukuda H, Kondo Y, Etchells JP, et al. Identification of cyst nematode B-type peptides and modulation of the vascular stem cell pathway for feeding cell formation. *PLoS Pathog*. 2017; 13: e1006142. <https://doi.org/10.1371/journal.ppat.1006142> PMID: 28158306
73. Hirakawa Y, Kondo Y, Fukuda H. TDIF peptide signaling regulates vascular stem cell proliferation via the WOX4 homeobox gene in Arabidopsis. *Plant Cell*. 2010; 22: 2618–2629. <https://doi.org/10.1105/tpc.110.076083> PMID: 20729381
74. Theissen G, Saedler H. Floral quartets. *Nature*. 2001; 409: 469–471. <https://doi.org/10.1038/35054172> PMID: 11206529
75. Krizek BA, Fletcher JC. Molecular mechanisms of flower development: an armchair guide. *Nat Rev*. 2005; 6: 688–698. <https://doi.org/10.1038/nrg1675> PMID: 16151374

SCIENTIFIC REPORTS

OPEN

Comparative transcriptomics with self-organizing map reveals cryptic photosynthetic differences between two accessions of North American Lake cress

Hokuto Nakayama^{1,2}, Tomoaki Sakamoto^{3,9}, Yuki Okegawa², Kaori Kaminoyama², Manabu Fujie⁴, Yasunori Ichihashi^{5,6}, Tetsuya Kurata^{3,10}, Ken Motohashi⁷, Ihsan Al-Shehbaz⁸, Neelima Sinha¹ & Seisuke Kimura^{2,7}

Because natural variation in wild species is likely the result of local adaptation, it provides a valuable resource for understanding plant-environmental interactions. *Rorippa aquatica* (Brassicaceae) is a semi-aquatic North American plant with morphological differences between several accessions, but little information available on any physiological differences. Here, we surveyed the transcriptomes of two *R. aquatica* accessions and identified cryptic physiological differences between them. We first reconstructed a *Rorippa* phylogeny to confirm relationships between the accessions. We performed large-scale RNA-seq and *de novo* assembly; the resulting 87,754 unigenes were then annotated via comparisons to different databases. Between-accession physiological variation was identified with transcriptomes from both accessions. Transcriptome data were analyzed with principal component analysis and self-organizing map. Results of analyses suggested that photosynthetic capability differs between the accessions. Indeed, physiological experiments revealed between-accession variation in electron transport rate and the redox state of the plastoquinone pool. These results indicated that one accession may have adapted to differences in temperature or length of the growing season.

Recent studies involving non-model plant species have provided knowledge unobtainable from using only model plants¹. Many of these studies have described molecular mechanisms underlying interspecific differences in morphology, physiology, and ecology^{2–4}. In addition to interspecific differences, natural genetic variation within a population of a single species is garnering increasing attention from researchers^{5,6}. For instance, accessions of *Arabidopsis thaliana* (L.) Heynh. (hereafter “*Arabidopsis*”) vary in traits such as leaf morphology, flowering time, and drought response⁶, suggesting the effect of local adaptation. Several studies have addressed the evolutionary processes underlying this variation through identifying genes or miRNAs responsible for between-accession differences, prompting increased attention on accessions as experimental material⁶. Accessions are particularly powerful for studying non-model species that do not have the genetic resources (e.g., mutants) seen in model organisms. Additionally,

¹Department of Plant Biology, University of California Davis, One Shields Avenue, Davis, CA, 95616, USA.

²Department of Bioresource and Environmental Sciences, Kyoto Sangyo University, Kamigamo-Motoyama, Kita-Ku, Kyoto, 603–8555, Japan. ³Plant Global Education Project, Graduate School of Biological Sciences, Nara Institute of Science and Technology, Nara, 630–0192, Japan. ⁴Okinawa Institute of Science and Technology, 1919–1 Tancha, Onna-son, Okinawa, 904–0412, Japan. ⁵RIKEN Center for Sustainable Resource Science, 1–7–22, Suehiro, Tsurumi, Yokohama, 230–0045, Japan. ⁶JST, PRESTO, 4–1–8 Honcho, Kawaguchi, Saitama, 332–0012, Japan. ⁷Center for Ecological Evolutionary Developmental Biology, Kyoto Sangyo University, Kamigamo-Motoyama, Kita-Ku, Kyoto, 603–8555, Japan. ⁸Missouri Botanical Garden, P.O. Box 299, St. Louis, MO, 63166–0299, USA. ⁹Present address: Faculty of Life Sciences, Kyoto Sangyo University, Motoyama, Kamigamo, Kita-Ku, Kyoto, 603–8555, Japan.

¹⁰Present address: Graduate School of Life Sciences, Tohoku University, 6–3 Aoba, Aramaki, Aoba-ku, Sendai, 980–8578, Japan. Hokuto Nakayama and Tomoaki Sakamoto contributed equally to this work. Correspondence and requests for materials should be addressed to S.K. (email: seisuke@cc.kyoto-su.ac.jp)

accessions are useful for understanding how local adaptation processes may have sculpted morphological and physiological differences among populations.

Rorippa Scop. (Brassicaceae or Cruciferae) comprises 86 species⁷ distributed on all continents except Antarctica⁸. The within-genus diversity has resulted in considerable attention, with *R. aquatica* (Eaton) E.J. Palmer & Steyermark, *R. amphibia* (L.) Besser, and *R. sylvestris* (L.) Besser being particularly well studied⁹. *Rorippa aquatica*, also known as lake cress, is a semi-aquatic North American plant distributed east of the 95th meridian from eastern Wisconsin into Quebec and southern Vermont into Florida^{10,11}. This species is well adapted to the aquatic environment and exhibits heterophylly¹², which is leaf-form variation on a single plant in response to surrounding environmental cues. In nature, deeply dissected leaves develop when plants grow in submerged conditions, whereas simple leaves with entire or toothed margins develop when grown on land¹². Previously, we showed that *R. aquatica* leaf shape changes dramatically in response to varying ambient temperatures and submergence underwater¹³; an ambient temperature of 25 °C induced leaves with simpler forms compared with 20 °C. Additionally, we found that environmental variation (e.g., in ambient temperature and water levels) altered the expression levels of *KNOTTED1-LIKE HOMEBOX* (*KNOX1*) orthologs; moreover, gibberellin accumulation, thought to be regulated by *KNOX1* genes, also changed in leaf primordia.

Rorippa aquatica accessions¹⁴ from northern and southern United States clearly differed in leaf forms (Fig. 1a,b) under the same conditions. For instance, the northern sample (hereafter “accession N”) develops leaves with more complex forms than the southern sample (hereafter “accession S”). In addition to the morphological difference, accession N flowers later than accession S (Fig. 1c)¹⁵. In *Populus angustifolia*, it is known that northern and southern populations differ in photosynthetic physiology corresponding to latitude across the North American continent¹⁶. Therefore, there is a possibility that *Rorippa* accessions have a difference in photosynthetic activity. However, little is known about physiological differences between these accessions except for flowering time. Depending on environmental conditions, gene expression would be expected to vary across accessions, and these cryptic physiological differences can be uncovered with comparative transcriptome analysis using RNA-seq technology¹⁷.

In this study, we aimed to understand how local adaptation processes may have sculpted physiological differences between *R. aquatica* accessions. We performed large-scale RNA-seq, *de novo* assembly, and transcriptome annotation in addition to phylogeny reconstruction in *Rorippa*. Moreover, we variance-scaled transcriptome data separately by two accessions and compared them using principal component analysis (PCA) and self-organizing map (SOM) analysis. These methods provide more details on difference in expression pattern between accessions among different conditions than simple analyses of differential gene expression levels, because the scaling procedure allows focus on genes that exhibit between-accession variation in expression patterns. Then, based on SOM clustering results, we focused on genes with differential expression patterns between accessions. This comparative transcriptome analysis revealed cryptic differences between accessions, specifically in photosynthetic activity (e.g., electron transport rate) and the redox state of the plastoquinone pool.

Results

Accessions are closely related. Despite the attention paid to various *Rorippa* species, relatively little is known about their phylogenetic relationships. In particular, there was no report on phylogenetic relationship among *Rorippa* accessions. Sequences of cpDNA were determined from 46 samples of *Rorippa* species distributed worldwide and two samples from outgroups *Nasturtium officinale* W.T. Aiton and *Cardamine africana* L. (Fig. 1d; Table 1). In the NJ phylogenetic tree generated, all *Rorippa* samples (including *R. aquatica* accessions N and S) formed a monophyletic group, with the two accessions being the most closely related (Fig. 1e). These relationships were also confirmed in the ML phylogenetic tree (see Supplementary Fig. S1). The NJ phylogeny also suggested that *R. aquatica* is close to the European *R. pyrenaica* (L.) Reichenb., but the latter is not heterophyllous¹⁸. However, heterophylly is well documented in *R. amphibia*, a widespread Eurasian species naturalized in North America¹⁹. The latter species is placed in an entirely different clade from *R. aquatica* within *Rorippa* (Fig. 1e). Therefore, it seems to likely that heterophylly evolved independently at least twice within the genus.

Transcriptome sequencing, *de novo* assembly, and defining differentially expressed genes.

Rorippa aquatica plants (two accessions, N and S) were planted in soil and grown at three temperatures (20 °C, 25 °C, 30 °C) in a growth chamber under continuous illumination, with a light intensity of 60 or 120 $\mu\text{mol photons m}^{-2} \text{s}^{-1}$. Total RNA was extracted from the shoot apical meristem with subtending P1–P3 leaf primordia.

For *de novo* assembly, single-end sequencing of libraries with GAIx (Illumina) resulted in 935,152,744 reads, and sequencing of longer reads was obtained through RNA-seq with MiSeq (Illumina) to yield 68,782,820 paired-end reads (Table 2). All reads from N and S were used for *de novo* assembly, because Trinity tries to generate a consensus transcript even if there is allelic variation. *De novo* assembly using all reads from N and S resulted in 132,566 transcript contigs, with N_{50} and average lengths of 1,031.06 nt and 1,903 nt, respectively (Table 2). Based on the N_{50} length, which is an indicator for assembly quality, we confirmed that the *de novo* assembly has enough quality. Approximately half of the transcripts were ≤ 500 nt (Fig. 2a; Table 2). Assembled sequences were annotated against the GO database. This procedure allows us to perform GO enrichment analysis, later. After annotation, the most predominant GO terms under the “biological process” category were as follows: cellular (GO: 0009987), metabolic (GO: 0008152), and single-organism (GO: 0044699), followed by response to stimulus (GO: 0050896) and developmental processes (GO: 0032502). Under “molecular function,” binding (GO: 0005488) and catalytic activity (GO: 0003824) were the most enriched terms. Under the “cellular component” category, cell (GO: 0005623), cell part (GO: 0044464), and organelle (GO: 0043226) were the most prominent (Fig. 2b). Reported RNA-seq data are available in the DDBJ Sequenced Read Archive under accession number DRA005242.

For defining differentially expressed genes (DEGs) between accessions, we used only RNA-seq data from plants grown at 60 $\mu\text{mol photons m}^{-2} \text{s}^{-1}$. Because, decreasing the number of environmental factors that similarly affect

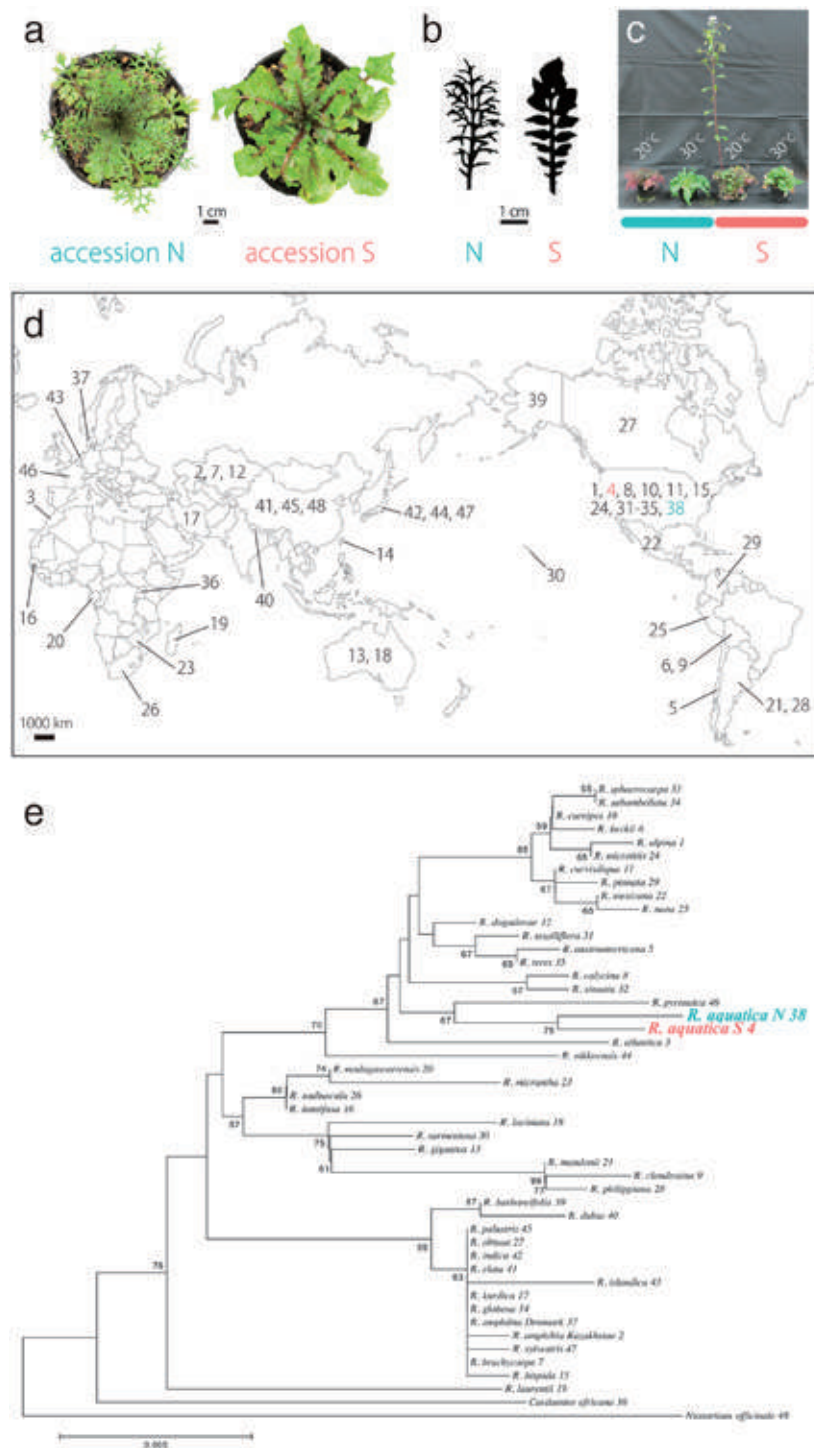


Figure 1. Comparison of leaf morphology in *Rorippa aquatica* accessions and Phylogenetic trees constructed using cpDNA sequences. **(a)** Top view of shoots in accession N (left) and S (right). Plants were cultivated in a growth chamber for a month at 20°C and under continuous illumination (light intensity of 60 μmol photons m⁻² s⁻¹). **(b)** Comparison of morphology in accession N (left) and S (right). Plants were grown under the same conditions described in (a). **(c)** Comparison of flowering time between accessions. Side view of shoots in accession N and S. These plants were grown for three months under each listed condition (light intensity of 60 μmol photons m⁻² s⁻¹). **(d)** Global distribution of *Rorippa* species. Numbers within each country correspond to the species used in the phylogenetic analysis. The map was generated by using Illustrator CS4 (Adobe Systems). **(e)** Evolutionary history was inferred using the neighbor-joining method. The bootstrap values are indicated on branches (only those > 50% are indicated on the tree). The tree is drawn to scale, with branch lengths in the same units as the evolutionary distances used to infer the phylogeny.

ID #	Species	Locality	Voucher	trnL intron	trnG-trnM	psbC-trnS	Sampling
1	<i>R. alpina</i>	USA, Nevada	A. Tiehm, (MO)	LC194527	LC194528	LC194529	This study
2	<i>R. amphibia</i>	Kazakhstan	V. V. Byalt, (MO)	LC194530	LC194531	LC194532	This study
3	<i>R. atlantica</i>	Morocco	J. Gattefosse, (MO)	LC194533	LC194534	LC194535	This study
4	<i>R. aquatica</i> (S)	USA	Kyoto Sangyo Univ., (cult.)	LC194536	LC194537	LC194538	This study
5	<i>R. austroamericana</i>	Chile, Valparaíso	O. Zöllner (MO)	LC194539	LC194540	LC194541	This study
6	<i>R. beckii</i>	Bolivia	D. Collot, (MO)	LC194542	LC194543	LC194544	This study
7	<i>R. brachycarpa</i>	Kazakhstan	I. Al-Shehbaz, N. Aralbaev & S. Nesterova, (MO)	LC194545	LC194546	LC194547	This study
8	<i>R. calycina</i>	USA, Wyoming	R. Dorn, (MO)	LC194548	LC194549	LC194550	This study
9	<i>R. clandestina</i>	Bolivia, Santa Cruz	J. Abbott, (MO)	LC194551	LC194552	LC194553	This study
10	<i>R. curvipes</i>	USA, Utah	A. Kelsey and A. J. Moore, (MO)	LC194554	LC194555	LC194556	This study
11	<i>R. curvisiliqua</i>	USA, California	G. K. Helmkamp and E. A. Helmkamp, (MO)	LC194557	LC194558	LC194559	This study
12	<i>R. dogadovae</i>	Kazakhstan	A. Dogadova and N. Tzvelev, (MO)	LC194560	LC194561	LC194562	This study
13	<i>R. gigantea</i>	Australia, Queensland	W. J. McDonald, (MO)	LC194563	LC194564	LC194565	This study
14	<i>R. globosa</i>	China, Taiwan	C. M. Wang, (MO)	LC194566	LC194567	LC194568	This study
15	<i>R. hispida</i>	USA, Missouri	J. A. Steyermark, (MO)	LC194569	LC194570	LC194571	This study
16	<i>R. humifusa</i>	Senegal, Tambacounda	J. E. Madsen (MO)	LC194572	LC194573	LC194574	This study
17	<i>R. kurdica</i>	Iran	M. L. Grant, (MO)	LC194575	LC194576	LC194577	This study
18	<i>R. laciniata</i>	Australia, New South Wales	R. G. Coveny, (MO)	LC194578	LC194579	LC194580	This study
19	<i>R. laurentii</i>	Madagascar	H. Humbert, (MO)	LC194581	LC194582	LC194583	This study
20	<i>R. madagascariensis</i>	Gabon, Ogooué-Maritime	H. P. Bourobou <i>et al.</i> , (MO)	LC194584	LC194585	LC194586	This study
21	<i>R. mandonii</i>	Argentina, Tucuman	M. Beilstein, (MO)	LC194587	LC194588	LC194589	This study
22	<i>R. mexicana</i>	Mexico, Durango	A. C. Sanders <i>et al.</i> , (MO)	LC194590	LC194591	LC194592	This study
23	<i>R. micrantha</i>	Zimbabwe	J. F. Ngoni, (MO)	LC194593	LC194594	LC194595	This study
24	<i>R. microtittis</i>	USA, Arizona	J. Ricketson and V. Walter, (MO)	LC194596	LC194597	LC194598	This study
25	<i>R. nana</i>	Peru, Arequipa	W. Galiano, (MO)	LC194599	LC194600	LC194601	This study
26	<i>R. nudiuscula</i>	South Africa, Eastern Cape	V. R. Clark and S. Ramdhani, (MO)	LC194602	LC194603	LC194604	This study
27	<i>R. obtusa</i>	Canada, Ontario	C. F. Red, (MO)	LC194605	LC194606	LC194607	This study
28	<i>R. philippiana</i>	Argentina, San Juan	J. Chiappella and E. Vitek, (MO)	LC194608	LC194609	LC194610	This study
29	<i>R. pinnata</i>	Colombia, Cundinamarca	C. Parra-O. and J. L. Fernandez-A., (MO)	LC194611	LC194612	LC194613	This study
30	<i>R. sarmentosa</i>	USA, Hawaii	G. Staples, (MO)	LC194614	LC194615	LC194616	This study
31	<i>R. sessiliflora</i>	USA, Missouri	T. E. Smith <i>et al.</i> , (MO)	LC194617	LC194618	LC194619	This study
32	<i>R. sinuata</i>	USA, Missouri	B. Summers <i>et al.</i> , (MO)	LC194620	LC194621	LC194622	This study
33	<i>R. sphaerocarpa</i>	USA, Arizona	J. S. Miller, (MO)	LC194623	LC194624	LC194625	This study
34	<i>R. subumbellata</i>	USA, California	G. L. Smith, (MO)	LC194626	LC194627	LC194628	This study
35	<i>R. teres</i>	USA, Florida	J. R. Abbott, (MO)	LC194629	LC194630	LC194631	This study
36	<i>C. africana</i>	Uganda	ATBP, (MO)	LC194632	LC194633	LC194634	This study
37	<i>R. amphibia</i>	Denmark, Jylland	A. Hansen, 198169, (TNS)	AB871924	AB871925	AB871926	Nakayama <i>et al.</i> , 2014
38	<i>R. aquatica</i> (N)	USA	Kyoto Sangyo Univ., (cult.)	AB871891	AB871892	AB871893	Nakayama <i>et al.</i> , 2014
39	<i>R. barbareaifolia</i>	USA, Alaska	W. J. Cody & T. J. M. Webster, 5902, (TI)	AB871906	AB871907	AB871908	Nakayama <i>et al.</i> , 2014
40	<i>R. dubia</i>	Nepal, Kathmandu	G. Murata <i>et al.</i> , 6303314, (TI)	AB871912	AB871913	AB871914	Nakayama <i>et al.</i> , 2014
41	<i>R. elata</i>	China, Baiyu Xian	D. E. Boufford <i>et al.</i> , 37265, (TI)	AB871918	AB871919	AB871920	Nakayama <i>et al.</i> , 2014
42	<i>R. indica</i>	Japan, Kyoto	Kyoto Sangyo Univ., (cult.)	AB871933	AB871934	AB871935	Nakayama <i>et al.</i> , 2014
43	<i>R. islandica</i>	Netherlands, Sleeuwijk	A. C. de Roon, (TI)	AB871909	AB871910	AB871911	Nakayama <i>et al.</i> , 2014
44	<i>R. nikkoensis</i>	Japan, Tochigi	J. Haginiwa, (TNS)	AB871927	AB871928	AB871929	Nakayama <i>et al.</i> , 2014
45	<i>R. palustris</i>	China, Rangtang	D. E. Boufford <i>et al.</i> , 39061, (TI)	AB871915	AB871916	AB871917	Nakayama <i>et al.</i> , 2014
46	<i>R. pyrenaica</i>	France, Loire	F. Schltz, (TI)	AB871903	AB871904	AB871905	Nakayama <i>et al.</i> , 2014
47	<i>R. sylvestris</i>	Japan, Fukui	S. Watanabe, 682661, (TNS)	AB871930	AB871931	AB871932	Nakayama <i>et al.</i> , 2014
48	<i>N. officinale</i>	China, Derong Xian	D. E. Boufford <i>et al.</i> , 30988, (TI)	AB871936	AB871937	AB871938	Nakayama <i>et al.</i> , 2014

Table 1. List of species, voucher numbers, and accession numbers of plant materials. Herbarium acronyms follow Index Herbariorum Part I.

leaf form¹³, leaving only ambient temperature to vary. This reduced data complexity and facilitated further analysis. EdgeR was used to define 8,809 DEGs between the accessions (FDR < 0.01) based on a generalized linear model (GLM) at the gene level using temperature and accession as factors.

number/length	
Number of reads from GA IIx (32 bp; SE)	93,51,52,774
Number of reads from Miseq (2x300 bp; PE)	6,87,82,820
Total gene number	87,754
Total mRNA number	1,32,566
Ave. length of mRNA	1,031
Median	527
N ₅₀	1,903

Table 2. Transcriptome sequencing and summary statistics of *de novo* assembly.

Principal components analysis reveals differences in transcriptome profile between accessions.

To compare expression profiles between accessions, we performed PCA. Major sources of variance in the transcriptome were investigated with a PCA that considered all DEGs between accessions. The eigenvalues of two components were greater than 1 (Fig. 3a). The first component (PC1) explained 72.3% of the variation and discriminated clearly between accessions. The second component (PC2) explained 16.8% of the variation and discriminated between temperatures (Fig. 3a,b). Thus, the PCA results indicated that accessions differ in transcriptome profiles even under identical conditions. Indeed, a heatmap using all DEGs confirmed the PCA, showing clear differences in the expression patterns between accessions (Fig. 3c).

Visualization and assessment of SOM clustering. We performed SOM for further understanding the difference in the expression patterns. SOM allows us to identify a subset of genes with similar expression profiles. We constructed a SOM to extract genes linked to between-accession physiological differences from DEGs between the accessions. We then used PCA to partition the resulting 20 SOM clusters following previous study²⁰ (5 × 4, rectangular; Supplementary Fig. S2). The genes in each cluster exhibited distinct expression patterns along each condition, suggesting successful clustering (Supplementary Figs S2 and S3).

Expression patterns between accessions were similar in all clusters, differing mainly in degree even under the same conditions (Supplementary Figs S2 and S3). For instance, expression levels in cluster 10 decreased across both accessions as temperature increased, although the accessions differed in expression amount under identical temperatures. Therefore, it appears that each cluster contains genes showing different expression level and similar expression pattern between accessions. For further characterization of each cluster, we performed a GO enrichment analysis with the 20 clustered gene sets. “Response to stress” and “response to abiotic stress” GO terms were enriched in many clusters ($q < 0.05$), with the former being the top term in cluster 1 (see Supplementary Table S1). The strong representation of this term is likely a reflection of plant response to changes in ambient temperature, as expression levels of cluster 1 genes from both accessions increased with increasing temperature (Supplementary Figs S2 and S3). Moreover, the GO terms “post-embryonic development,” “multicellular organismal development,” “cell differentiation,” “anatomical structure morphogenesis,” and “cell growth” were enriched in cluster 10 ($q < 0.05$; see Supplementary Table S1). In this cluster, genes from accessions N and S decreased as temperature increased (Supplementary Figs S2 and S3), possibly reflecting a known relationship between temperature and leaf complexity¹³. These GO terms may be responsible for leaf-form differences across accessions, which exist even under the same environmental conditions (Fig. 1a,b). Furthermore, the “flower development” term was enriched in some clusters ($q < 0.05$), corresponding to between-accession differences in flowering time (Fig. 1c).

Overall, these results suggest that SOM clustering successfully identified distinct transcriptome differences between accessions. However, the large number of enriched GO terms prevented us from determining which gene types played a more critical role in influencing between-accession physiological differences.

The use of SOM clustering on accession-scaled transcriptome data is sufficient for investigating cryptic differences between accessions.

We next performed PCA and SOM clustering (3 × 3, rectangular) on count data of DEGs scaled separately by accession. Gene expression values from the accessions were mean-centered and variance-scaled separately to measure differences caused by changes in accession-specific expression patterns, allowing the focus to fall on differences in expression pattern instead of expression magnitude. Using such data allows separate treatment of genes from each accession and uncovers genes that cluster differently between accessions. As a result, genes from each accession were assigned to clusters irrespective of the accessions. Nine clusters were successfully obtained (Fig. 4a,b), based on box and line plots showing genes in each cluster with distinct, non-redundant expression patterns (Fig. 4c).

Next, we focused on genes with different between-accession expression patterns based on SOM clustering results (Fig. 5a). Such displaced gene sets between accessions among clusters exhibited certain tendencies (Fig. 5b; all directions from accession N to S). Pre- and post-displacement differences in expression pattern occurred primarily at 25 °C (Fig. 5c). GO enrichment analysis with these displaced gene sets between accessions among clusters showed that the GO term “photosynthesis” was significantly enriched in the displacements 3 → 6 (q value: 0.0346), 6 → 3 (0.0149), and 9 → 6 (0.000005), as were other photosynthesis-related GO terms, such as “thylakoid” (Table 3). Among the enriched genes were putative Arabidopsis orthologs of photosystem I subunit H-1 (AT3G16140), photosystem II subunit Q-2 (AT4G05180), *CURVATURE THYLAKOID 1 C* (AT1G52220), and NAD(P)H-quinone oxidoreductase subunit 2 A (ATCG00890) (see Supplementary Table S2). We confirmed that expression levels varied between accessions (see Supplementary Fig. S4). These results suggest that *R. aquatica* accessions differ physiologically in photosynthetic activity.

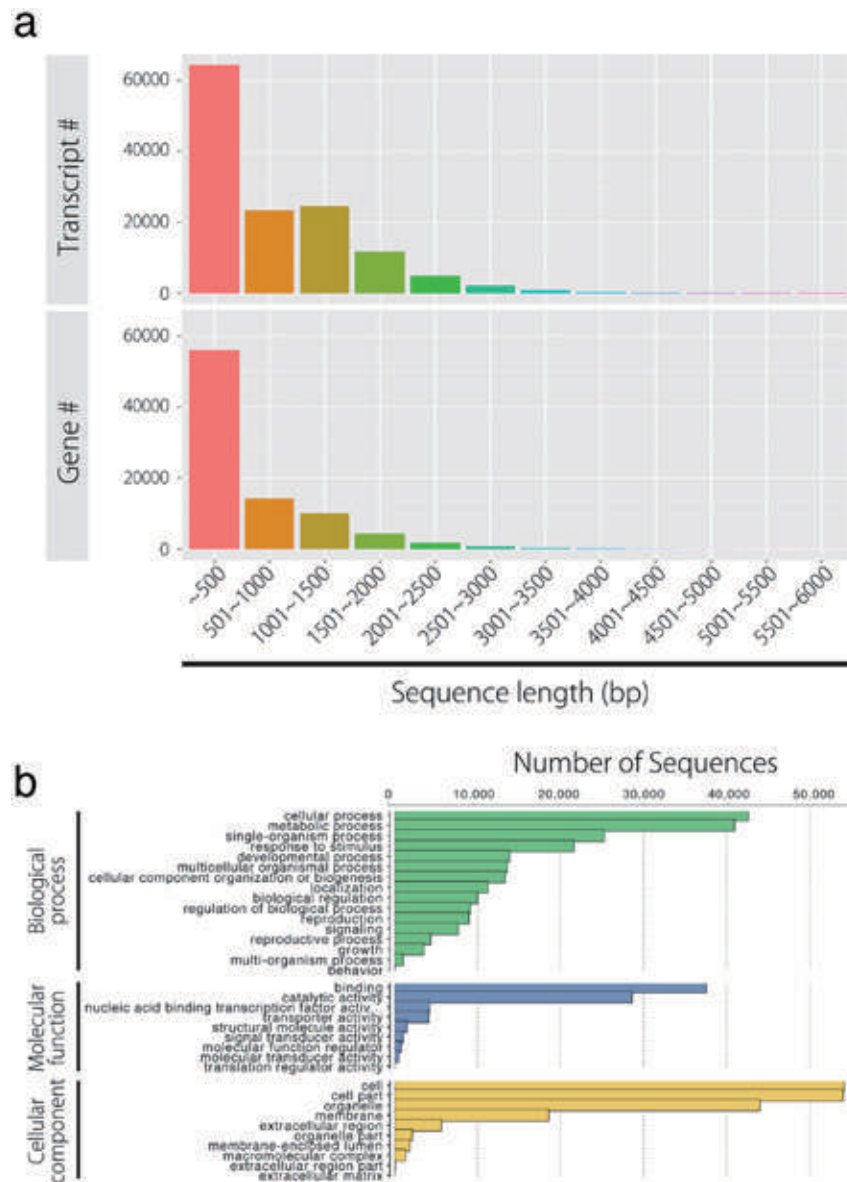


Figure 2. Transcripts, gene lengths, and gene ontology (GO) assignments for the *Rorippa aquatica* transcriptome. **(a)** Transcript and gene length distributions defined through *de novo* assembly in Trinity. **(b)** GO assignments predicting gene involvement. Top (green): biological processes; middle (blue): molecular function; bottom (yellow) cellular component. These assignments were generated in Blast2GO.

As the *q* value of “photosynthesis” was the lowest in 9 → 6 compared with other displacements such as 3 → 6 and 6 → 3 (Table 3), we then constructed an enrichment map focused on GO terms in 9 → 6. The results showed that communities 1, 2, and 3 were represented by “Biological process,” “Cellular component,” and “Molecular function,” respectively (Fig. 6a). Community 2 comprised the enrichment of terms such as “thylakoid” and “cytoplasm.” In community 3, “nucleotide binding” was enriched (see Supplementary Fig. S5). In contrast, “photosynthesis” was significantly enriched under the “metabolic process” and “cellular process” GO terms in community 1 (Fig. 6b). Therefore, we investigated photosynthetic activity to verify the presence of between-accession differences.

Electron transport rate (ETR) and redox state of the plastoquinone (PQ) pool are different between accessions. Chlorophyll fluorescence parameters were analyzed to evaluate photosynthetic activity. In accessions N and S grown at 20 °C and 25 °C, PSII activity was high, with a maximum quantum yield (Fv/Fm) greater than 0.8 (Fig. 7a), indicating that photoinhibition was not observed. Under all light intensities, both accessions grown at 20 °C showed similar ETR (Fig. 7b), an indicator of the relative electron flow rate through PSII during steady-state photosynthesis. In contrast, accession N’s ETR values were lower than accession S at 25 °C and were saturated at a lower light intensity (Fig. 7b). To analyze electron transport in more detail, the 1-qL parameter, which reflects the redox state of the PQ pool, was measured. When grown at 25 °C, accession N had higher 1-qL than

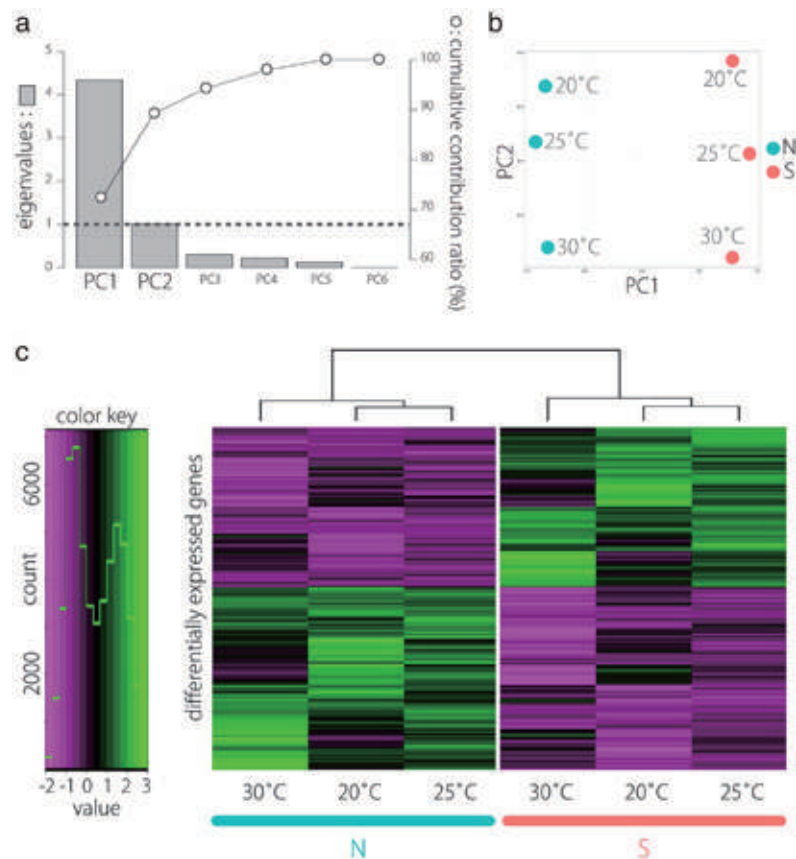


Figure 3. Principal component analysis (PCA) of gene expression. (a) Eigenvalues and cumulative contribution ratio (%) in PCA. Bars and open circles represent eigenvalues and cumulative contribution ratio, respectively. (b) The global expression profile of each transcript is represented as PC1 and PC2. Note distinct dissimilarities between the two accessions in PC1. (c) Expression profiles of genes that are differentially expressed between accessions.

accession S, indicating a more electron-reduced PQ pool in the former (Fig. 7c). These results indicated that accession S had higher photosynthetic activity than accession N at 25°C, but not at 20°C. This is unsurprising because pre- and post-displacement differences in expression pattern occurred primarily at 25°C (Fig. 5C). Additionally, we measured NPQ and observed no difference in NPQ induction between accessions (Fig. 7d).

Together, our data showed that between-accession differences in the expression of photosynthesis-related genes might contribute to the more active photosynthetic electron transfer system in accession S at warmer temperatures.

Discussion

To investigate physiological differences between two *R. aquatica* accessions, we used phylogenetic, transcriptomic, bioinformatic, and physiological approaches. First, we reconstructed a phylogeny of *Rorippa* to confirm the relationship between two accessions with different habitats. Next, we performed large-scale RNA-seq, *de novo* assembly, and transcriptome annotation of the two accessions. We then compared these transcriptomes using PCA and SOM construction. We focused especially on genes with different between-accession expression patterns, based on comparisons of results from SOM clustering (Supplementary Fig. S6). The results suggested that photosynthetic capability, as measured by ETR and 1-qL, differs between the accessions. This difference may be an adaptive response to variation in growing season length or temperature. Overall, this study demonstrated that combining RNA-seq and clustering methods can reveal cryptic physiological differences between closely related accessions.

Previous studies showed that clustering methods combining PCA and SOM are effective in extracting gene subsets associated with phenotypes of interest from large-scale transcriptome data between species²⁰. Although the use of PCA and SOM on transcriptome data identified numerous enriched GO terms related to between-accession physiological differences (including in photosynthesis), the sheer number of terms hampered our ability to focus on the most likely candidates. The high-dimensional data obtained from large-scale RNA-seq often requires simplification and conversion to become more interpretable²¹. Therefore, we reduced data dimensionality via scaling data separately by accessions before performing another PCA and SOM clustering. This fine-tuning let us uncover enrichment of photosynthesis-related genes (GO: 0015979; Q q value: 0.000005) in gene sets displaced between accessions among clusters. Indeed, our investigation of chlorophyll

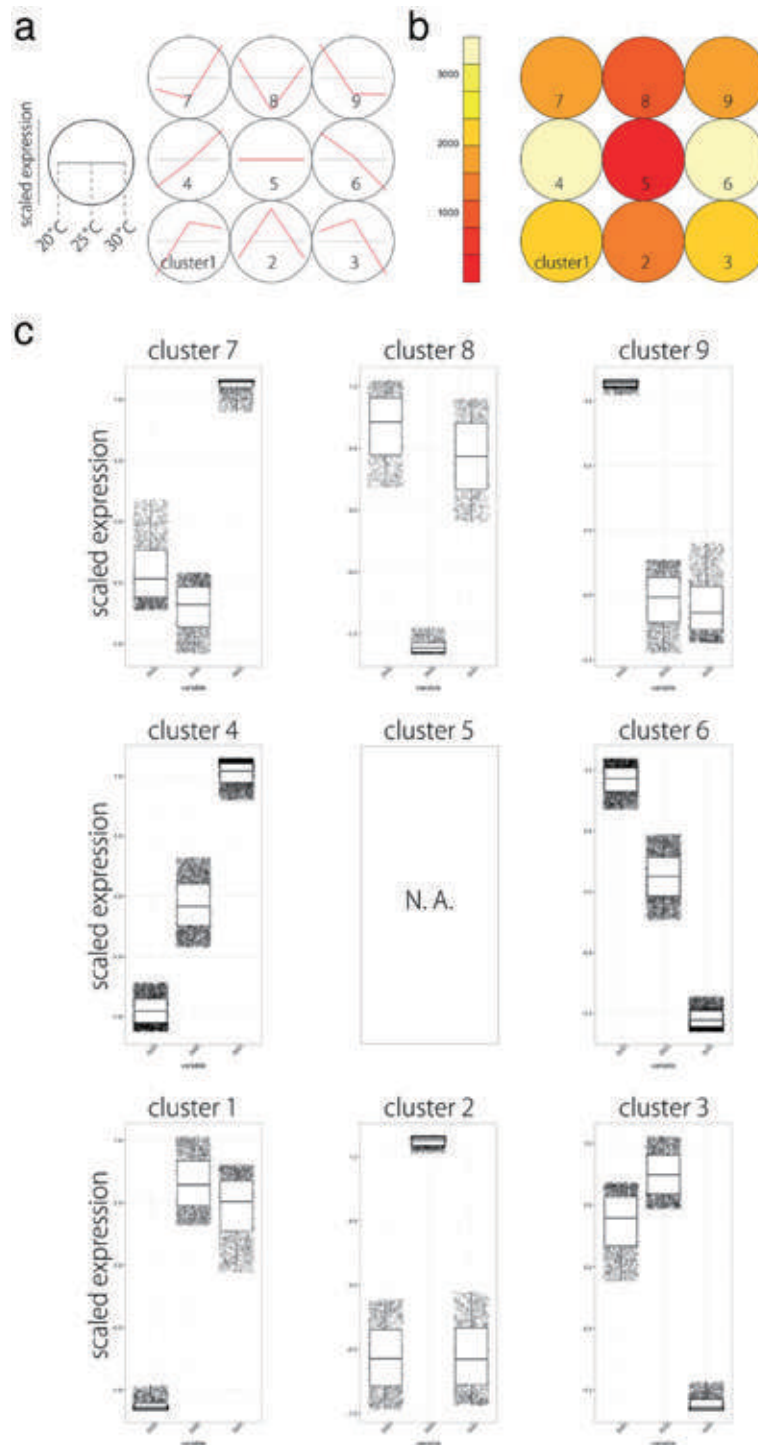


Figure 4. SOM clustering of gene expression in differentially expressed genes (DEGs) and their expression profiles. (a) Results of SOM clustering. Line plots indicate representative expression patterns at 20 °C, 25 °C, and 30 °C in each cluster. For SOM and diagrams, the 3×3 rectangular topology is shown. (b) Number of genes assigned to each SOM cluster. Red and white indicate low and high counts, respectively. (c) Scaled expression between accessions plotted under 20 °C, 25 °C, and 30 °C are shown. Box plot explanation: upper horizontal line of box, 75th percentile; lower horizontal line of box, 25th percentile; horizontal bar within box, median; upper horizontal bar outside box, 90th percentile; lower horizontal bar outside box, 10th percentile.

fluorescence parameters demonstrated between-accession differences in ETR and 1-qL, supporting results from the GO enrichment analysis. These results indicate that RNA-seq combined with SOM is remarkably effective for investigating cryptic differences between accessions, as long as data dimensionality is reduced first.

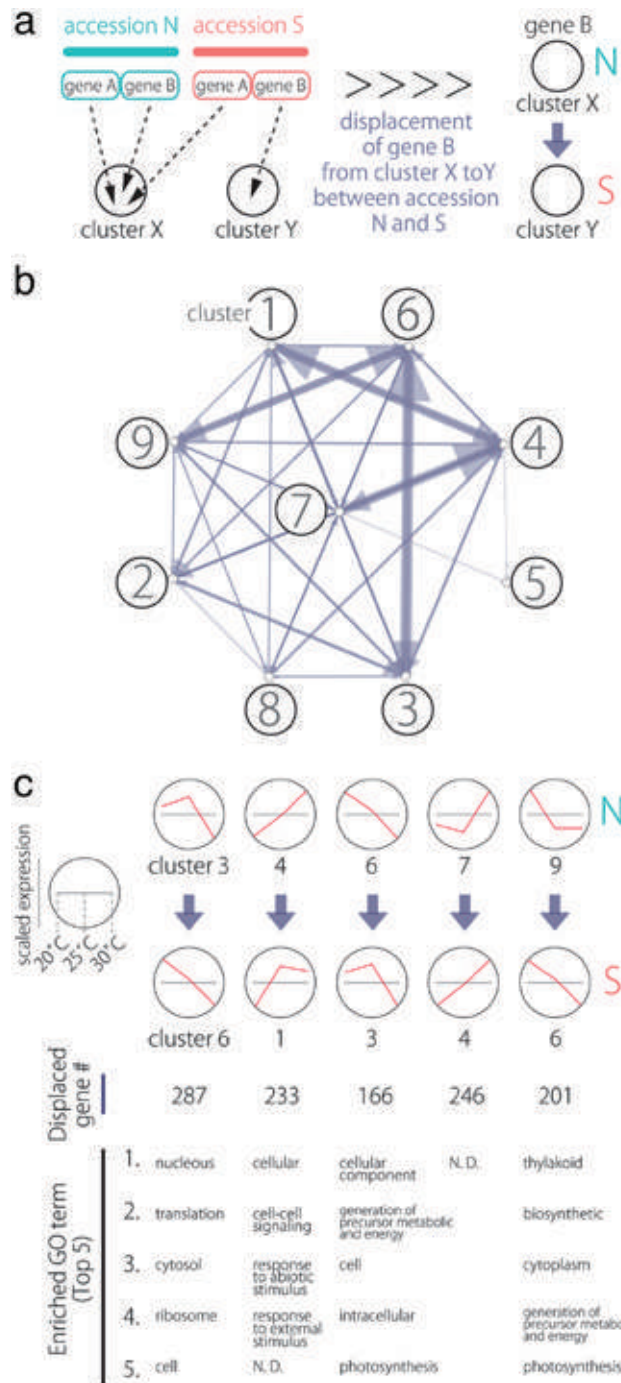


Figure 5. Displacement of orthologs to different clusters under the SOM clustering scheme. **(a)** A diagram demonstrating SOM clustering. N and S orthologs can be assigned to different clusters. **(b)** A network representation of ortholog assignment to different SOM clusters. Arrows represent displacement from accession N to S. Arrow sizes are proportional to the number of displaced orthologs. **(c)** Major displacement directions after SOM clustering of data that were scaled separately by accessions. Line plots indicate representative expression patterns in each cluster.

Physiological experiments revealed that accession S has higher ETR and lower 1-qL than accession N when both were grown at 25°C, indicating that photosynthetic activity may be higher in accession S. When grown at 20°C, however, accessions did not differ in their chlorophyll fluorescence parameters. Therefore, accession S may have a higher carbon fixation rate than accession N at 25°C. Thus, these data suggest that accession S may be better adapted to 25°C or higher temperatures.

The greater photosynthetic activity in accession S compared with accession N, particularly at higher temperatures, is useful for understanding the history of these two populations. The habitats of accessions S and N are

cluster	GO term	adjusted P value by BH (q value)
3 → 6	nucleolus	6.42E-16
	translation	6.10E-14
	cytosol	1.32E-13
	ribosome	2.05E-12
	cell	2.04E-11
	structural molecule activity	2.04E-11
	cellular_component	2.63E-11
	protein metabolic process	1.80E-10
	intracellular	5.17E-09
	plastid	1.67E-07
	external encapsulating structure	1.69E-07
	cell wall	2.94E-07
	vacuole	5.25E-07
	cytoplasm	2.34E-06
	membrane	2.46E-05
	cellular component organization	8.04E-05
	cellular process	9.28E-05
	biosynthetic process	1.38E-04
	nucleus	3.05E-04
	nucleobase, nucleoside, nucleotide and nucleic acid metabolic process	2.52E-03
	generation of precursor metabolites and energy	3.06E-03
	plasma membrane	4.22E-03
	metabolic process	1.18E-02
	protein modification process	1.22E-02
	Golgi apparatus	1.34E-02
	biological_process	2.99E-02
	photosynthesis	3.46E-02
4 → 1	cellular_component	1.03E-02
	cell-cell signaling	4.40E-02
	response to abiotic stimulus	4.40E-02
	response to external stimulus	4.40E-02
6 → 3	cellular_component	6.82E-04
	generation of precursor metabolites and energy	1.27E-03
	cell	5.96E-03
	intracellular	1.46E-02
	photosynthesis	1.49E-02
	thylakoid	1.55E-02
	cellular component organization	3.18E-02
9 → 6	thylakoid	4.12E-07
	biosynthetic process	5.05E-06
	cytoplasm	5.05E-06
	generation of precursor metabolites and energy	5.05E-06
	photosynthesis	5.05E-06
	plastid	1.61E-05
	metabolic process	2.86E-05
	intracellular	5.23E-05
	cytosol	6.85E-05
	cell	8.55E-05
	carbohydrate metabolic process	1.06E-04
	cellular process	1.02E-03
	biological_process	1.04E-03
	membrane	1.64E-03
	cellular_component	2.14E-03
	catabolic process	5.18E-03
	cellular component organization	1.78E-02
Continued		

cluster	GO term	adjusted P value by BH (q value)
	nucleobase, nucleoside, nucleotide and nucleic acid metabolic process	1.82E-02
	mitochondrion	2.59E-02
	secondary metabolic process	4.18E-02
	protein metabolic process	4.21E-02
	nucleotide binding	4.63E-02
	endosome	4.63E-02

Table 3. Result of GO enrichment analysis using displacement of orthologs to different clusters under SOM clustering scheme.

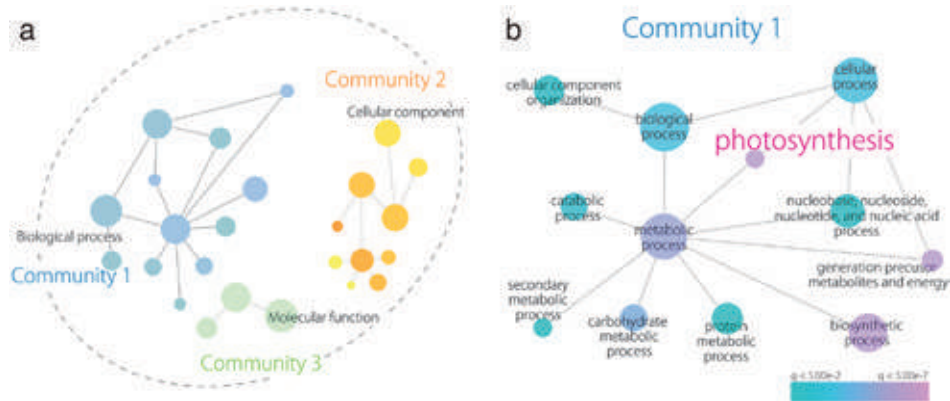


Figure 6. GO enrichment map with differentially expressed genes (DEGs) displaced from cluster 9 to cluster 6. (a) Three distinct communities (generated by Cytoscape) are on the map. (b) GO enrichment map of community 1 from (a). The red to blue scale indicates high to low q values, or P values adjusted with Benjamini-Hochberg.

thought to be respectively southern (e.g., Florida) and northern (e.g., Ohio and New England) United States¹⁵, spanning a wide range of temperatures and day lengths. These considerable environmental gradients can lead to local adaptation. It seems that our physiological experiment on photosynthetic activity provided evidence that accession S was better adapted to 25 °C than accession N. Indeed, the annual average temperature is 22 °C–26 °C in Florida and lower in Ohio (<http://www.cpc.ncep.noaa.gov>: National Weather Service Climate Prediction Center). Similarly, northern and southern *Populus angustifolia* populations differ in photosynthetic physiology corresponding to latitude across the North American continent; this variation may be an adaptive response to differences in growth season length, temperature, and insulation¹⁶. This relationship between photosynthetic physiology and latitude has also been reported in other North American plant species²². Thus, observed patterns in photosynthetic activity among *R. aquatica* accessions may be explained by similar adaptive measures.

Our method of combining RNA-seq and SOM was successful in detecting cryptic physiological differences between *R. aquatica* accessions. By using this method, further work could considerably clarify the molecular mechanisms underlying heterophyly in this species. Beyond *R. aquatica* research, this comparative technique has broad applications that can be improved further with recent advances in software, packages, and methods for fine-tuned transcriptome analysis^{23–25}. Some of these analyses include predicting co-expression networks and defining participating modules, as well as investigating differential co-expression across disparate datasets. Indeed, this comparative transcriptome method has resulted in a gene network module regulating interspecific diversity in the genus *Solanum*²⁶. Thus, comparative transcriptomics will contribute largely to uncovering key regulatory mechanisms affecting variation between and within species. The knowledge obtained from comparative transcriptomics will provide fundamental insight into evolutionary and ecological developmental biology, especially on the concept of rewiring network interactions during evolution, a process that can lead to speciation and local adaptation.

Methods

Plant materials. *Rorippa aquatica* plants (two accessions, N and S) were planted in soil and grown at three temperatures (20 °C, 25 °C, 30 °C) in a growth chamber under continuous illumination, with a light intensity of 60 or 120 $\mu\text{mol photons m}^{-2} \text{s}^{-1}$. Seedlings were watered every two days. According to previous reports, N and S accessions are thought to have representative phenotypes from northern and southern populations^{10,11,15}. All plants were cultivated in each condition for a month except those used for the physiological experiment, which were cultivated for two months. The shoot apical meristem subtending P1–P3 leaf primordia were frozen in liquid nitrogen just after sampling, and then stored at –80 °C until needed for DNA and RNA extraction.

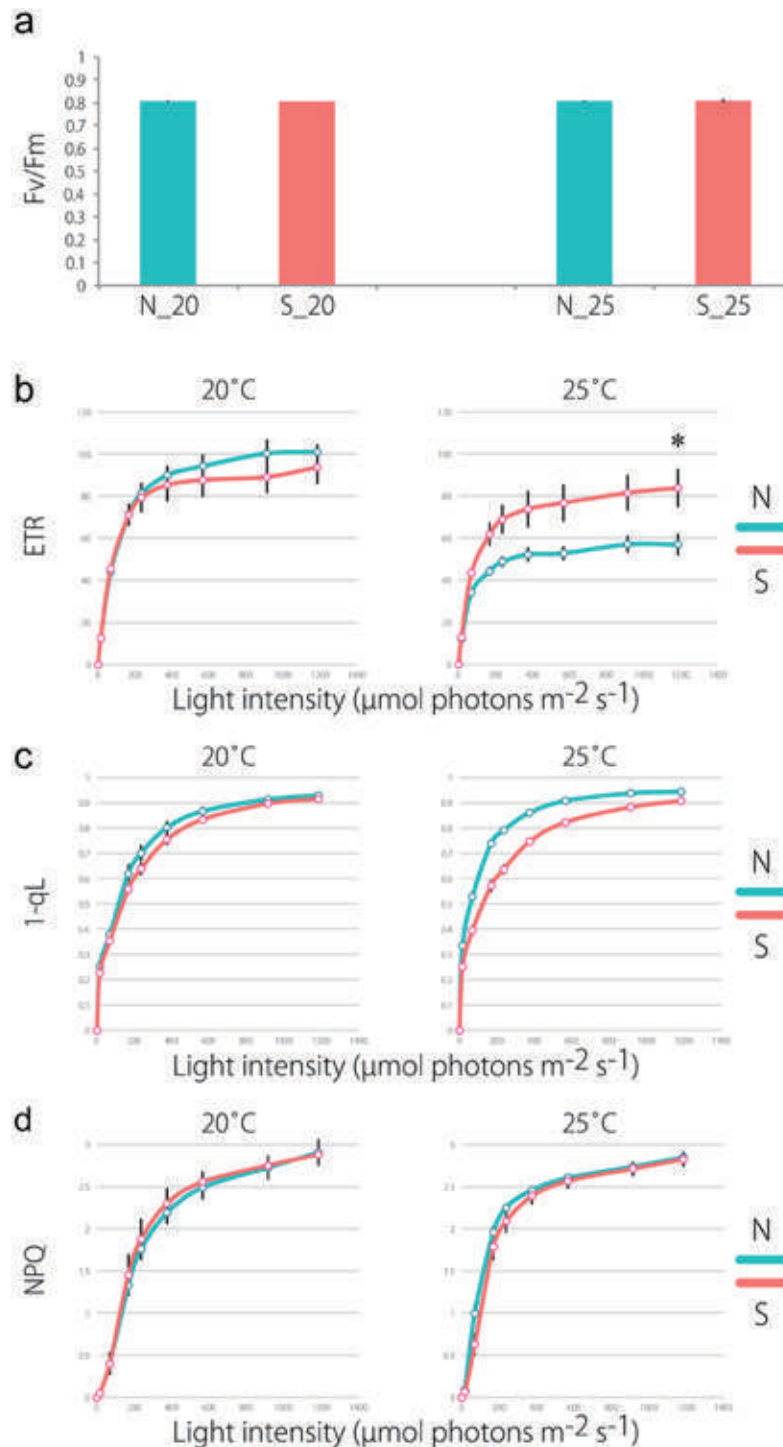


Figure 7. Measurements of photosynthetic parameters in two accessions. (a) Maximum quantum efficiency of photosystem II (Fv/Fm). (b) Light-intensity dependence of the electron transport rate (ETR). The ETR was calculated as $\Phi_{\text{PSII}} \times \text{light intensity}$ ($\mu\text{mol photons m}^{-2} \text{s}^{-1}$). (c) Light-intensity dependence of the redox state of plastoquinone (1-qL). (d) Light-intensity dependence of the non-photochemical quenching (NPQ) of chlorophyll fluorescence. All data are the means of five replicates; vertical bars represent SE. * $p < 0.05$ based on Welch's t-tests.

Phylogenetic analyses. Phylogenetic trees were reconstructed in MEGA6²⁷ with the neighbor-joining (NJ) and maximum-likelihood (ML) methods^{28,29}. Bootstrap values were derived from 1000 replicate runs.

Sequences of the non-coding regions in the *trnL* intron, *trnG* (GCC)-*trnM* (CAU), and *psbC-trnS* (UGA) were determined from 46 samples of *Rorippa* species distributed worldwide and two samples from outgroups

Nasturtium officinale W.T.Aiton and *Cardamine africana* L. (Table 1). All sequence data were deposited in the DNA Data Bank of Japan (DDBJ) (Table 1). Their lengths were 517–527 bp for *trnL* intron, 224–228 bp for *trnG-trnM*, and 205–222 bp for *psbC-trnS*.

The optimal NJ phylogenetic tree is shown in Fig. 1e (sum of branch lengths = 0.14081464), along with relationships between the clades and localities of individuals (see also Table 1). A bootstrap test of 1000 replicates³⁰ was used to calculate the percentage of replicate trees in which the associated taxa clustered together.

Evolutionary distances (number of base substitutions per site) were computed using maximum composite likelihood (MCL). The analysis involved 48 nucleotide sequences. Included codon positions were 1st + 2nd + 3rd + Noncoding, while all positions containing gaps and missing data were eliminated, resulting in a final dataset of 910 positions.

The ML phylogenetic tree with the highest log likelihood (-2191.1860) is shown in Supplemental Fig. S1. Initial tree(s) for the heuristic search were obtained automatically: Neighbor-Join and BioNJ algorithms were applied to a matrix of pairwise distances estimated with MCL, and then the topology with a superior log likelihood value was selected. The tree is drawn to scale, with branch lengths measured in the number of substitutions per site. The analysis involved 48 nucleotide sequences. Codon positions included were 1st + 2nd + 3rd + Noncoding. All positions containing gaps and missing data were eliminated to result in a final dataset of 910 positions.

RNA-seq and *de novo* assembly. Total RNA was extracted from the shoot apical meristem with subtending P1–P3 leaf primordia and shoot with an RNeasy Plant Mini Kit (QIAGEN), for multiplex sequencing in the Illumina Genome Analyzer IIx (Illumina). RNA-seq libraries were prepared using a NEBNext mRNA Library Prep Reagent Set for Illumina (NEB). To find differentially expressed genes (DEGs), 48 libraries (two accessions, three temperatures, two light intensities, and four biological replicates) were prepared. *De novo* assembly was generated with RNA from several controlled growth conditions (see “Plant materials”), because changes in ambient temperature and light intensity affect leaf morphology¹³, and because certain transcripts may only be expressed in specific environments.

Longer reads for *de novo* assembly were obtained through RNA-seq with MiSeq (Illumina). Total RNA was extracted from the shoot apex subtending the leaf primordia. Libraries for MiSeq were prepared with a TruSeq Stranded Total RNA Sample Prep Guide (Illumina), and sequenced with a MiSeq Reagent Kit v3, both following manufacturer protocols.

Short single-end and long paired-end reads were assembled into transcriptome contigs using Trinity³¹, with default assembling settings. The minimum assembled contig length in our study is 200 bp. BlastX searches of obtained contigs against non-redundant protein sequences from GenPept, SwissProt, PIR, PDE, PDB, and NCBI RefSeq (nr) databases were conducted to find similar known protein sequences. Gene ontology (GO) information was mapped to each contig based on Blastx results with Blast2GO³².

Gene expression profiling with RNA-seq data. Single-end reads were separated by indices, then trimmed and quality-filtered. Raw reads were then mapped with BWA³³ (<http://bio-bwa.sourceforge.net>). Contigs from *de novo* assembly were used as reference sequences for mapping. Transcript expression profiles and DEGs were defined with EdgeR GLMs³⁴. After quality filtering, 93.4% (80,304,302) of the single-end reads were mapped to the reference *de novo* assembly data using BWA version 0.7.5 (parameters “-n 2 -e 2”). For further analysis in R (version 3.2.1), lowly expressed genes were filtered based on a minimum sum of 10 counts over all samples (genes below this threshold were considered not expressed). Libraries were subjected to trimmed mean of *M*-values (TMM) normalization in EdgeR. Multi-dimensional scaling was performed via calculating log-fold changes between accessions and using DEGs to compute distances in EdgeR with the “plotMDS” function. Differential expression was calculated via fitting a generalized linear model (GLM) at the gene level using temperature and accession as factors. The threshold for DEGs was a false discovery rate (FDR) of < 0.01; this yielded 8,809 genes. Bioinformatics and statistical analyses were performed on the iPLANT Atmosphere cloud server (<http://www.iplantcollaborative.org>).

Principal components analysis with SOM clustering and GO analysis. We applied a gene-expression clustering method²⁰ on all 8,809 DEGs defined with EdgeR. Scaled expression values were used for multilevel 5 × 4 and 3 × 3 rectangular SOM clusters (Supplementary Fig. S6)^{35,36}. One hundred training interactions were used during clustering, and gene clusters were based on the final assignment of genes to winning units. To focus only on gene-expression patterns instead of expression magnitude, expression values were mean-centered and variance-scaled separately between accessions in a 3 × 3 rectangular SOM. Using such data allows separate treatment of genes from each accession and uncovers orthologs that cluster differently based on their existing groups (e.g., accessions or species²⁰). This procedure makes it possible to focus on genes that vary in expression patterns between accessions.

The outcome was then visualized in a PCA, with PC values calculated from gene expression across samples (R stats package, *prcomp* function). For 3 × 3 rectangular SOM clusters, network graphics in Gephi³⁷ were used to visualize—as a directed network—the assignment of genes from different accessions to separate clusters. Arrow direction indicates gene assignment to clusters, from accession N to accession S, with arrow size proportional to gene number represented. Clustered and displaced gene sets among clusters were then subjected to GO analysis using Cytoscape and visualized with the BinGO³⁸ (<http://apps.cytoscape.org/apps/bin-go>). Resultant P values were adjusted with the Benjamini-Hochberg method to yield q values. Blast2GO results were used as annotation data.

Chlorophyll fluorescence analysis. Chlorophyll fluorescence was measured with a Mini-PAM (pulse-amplitude modulation) portable chlorophyll fluorometer (Walz). For this analysis, all plants were grown

under each environmental condition for two months. Minimum fluorescence (F_0) was obtained with open Photosystem II (PSII) centers in the dark-adapted state through a low-intensity measuring light (wavelength 650 nm, $0.05\text{--}0.1\ \mu\text{mol photons m}^{-2}\ \text{s}^{-1}$). A saturating pulse of white light was applied to determine the maximum fluorescence with closed PSII centers in the dark-adapted state (F_m) and during actinic light (AL) illumination (F_m'). The steady-state fluorescence level (F_s) was recorded during AL illumination ($17\text{--}1184\ \mu\text{mol photons m}^{-2}\ \text{s}^{-1}$). The quantum yield of PSII (Φ_{PSII}) was calculated as $(F_m' - F_s)/F_m^{39}$. The relative rate of electron transport through PSII (ETR) was calculated as $\Phi_{\text{PSII}} \times$ light intensity ($\mu\text{mol photons m}^{-2}\ \text{s}^{-1}$). The fraction of the open PSII center (qL) was calculated as $[\Phi_{\text{PSII}}/(1 - \Phi_{\text{PSII}})] \times [(1 - F_v/F_m)/(F_v/F_m)] \times (\text{NPQ} + 1)^{40}$. Non-photochemical quenching (NPQ) was calculated as $(F_m - F_m')/F_m'$; this parameter is roughly indicative of excess absorbed light dissipation as heat to minimize oxygen radical formation in angiosperms. To analyze light-intensity dependence of fluorescence parameters, AL intensity was increased in a step-wise manner every two minutes after applying a saturating pulse.

References

1. Tsukaya, H. Comparative leaf development in angiosperms. *Curr Opin Plant Biol* **17**, 103–109, <https://doi.org/10.1016/j.pbi.2013.11.012> (2014).
2. Iida, S. *et al.* Molecular adaptation of rbcL in the heterophyllous aquatic plant Potamogeton. *PLoS One* **4**, e4633, <https://doi.org/10.1371/journal.pone.0004633> (2009).
3. Nakayama, H., Yamaguchi, T. & Tsukaya, H. Acquisition and diversification of cladodes: leaf-like organs in the genus Asparagus. *Plant Cell* **24**, 929–940, <https://doi.org/10.1105/tpc.111.092924> (2012).
4. Vlad, D. *et al.* Leaf shape evolution through duplication, regulatory diversification, and loss of a homeobox gene. *Science* **343**, 780–783, <https://doi.org/10.1126/science.1248384> (2014).
5. Alonso-Blanco, C. & Koornneef, M. Naturally occurring variation in Arabidopsis: an underexploited resource for plant genetics. *Trends Plant Sci* **5**, 22–29 (2000).
6. Weigel, D. Natural variation in Arabidopsis: from molecular genetics to ecological genomics. *Plant Physiol* **158**, 2–22, <https://doi.org/10.1104/pp.111.189845> (2012).
7. Al-Shehbaz, I. A. A generic and tribal synopsis of the Brassicaceae (Cruciferae). *Taxon* **61**, 931–954 (2012).
8. Appel, O. & Al-Shehbaz, A. In *The Families and Genera of Vascular Plants* (ed. Kubitzki, K.) 75–174 (Springer Verlag, 2003).
9. Stift, M., Luttikhuisen, P. C., Visser, E. J. & van Tienderen, P. H. Different flooding responses in *Rorippa amphibia* and *Rorippa sylvestris*, and their modes of expression in F1 hybrids. *The New phytologist* **180**, 229–239, <https://doi.org/10.1111/j.1469-8137.2008.02547.x> (2008).
10. La Rue, C. Regeneration in *Radicula aquatica*. *Michigan Academician* **28**, 51–56 (1943).
11. Al-Shehbaz, I. A. & Bates, V. *Armoracia lacustris* (Brassicaceae), the correct name for the North American lake Cress. *Journal of the Arnold Arboretum* **68**, 357–359 (1987).
12. Fassett, N. C. *A Manual of Aquatic Plants*. (University of Wisconsin Press, 1930).
13. Nakayama, H. *et al.* Regulation of the KNOX-GA gene module induces heterophyllic alteration in North American lake cress. *Plant Cell* **26**, 4733–4748, <https://doi.org/10.1105/tpc.114.130229> (2014).
14. Nakayama, N., Nakayama, N., Nakamasu, A., Sinha, N. & Kimura, S. Toward elucidating the mechanisms that regulate heterophylly. *Plant Morphology* **24**, 57–63 (2012).
15. Gabel, J. D. & Les, D. H. *Neobeckia aquatica* Eaton (Greene) North American Lake Cress. (New England Wild Flower Society, Framingham, MA., 2000).
16. Kaluthota, S. *et al.* Higher photosynthetic capacity from higher latitude: foliar characteristics and gas exchange of southern, central and northern populations of *Populus angustifolia*. *Tree physiology* **35**, 936–948, <https://doi.org/10.1093/treephys/tpv069> (2015).
17. Bushman, B. S., Amundsen, K. L., Warnke, S. E., Robins, J. G. & Johnson, P. G. Transcriptome profiling of Kentucky bluegrass (*Poa pratensis* L.) accessions in response to salt stress. *BMC Genomics* **17**, 48, <https://doi.org/10.1186/s12864-016-2379-x> (2016).
18. Anchev, M. E. & Tomsovic, P. The *Rorippa pyrenaica* group (Brassicaceae) in the Balkan peninsula. *Folia Geobotanica* **34**, 261–276 (1999).
19. Jonsell, B. In *Flora Helenica* (eds Strid, A. & Tan, K.) (Gartner Verlag, 2002).
20. Chitwood, D. H., Maloof, J. N. & Sinha, N. R. Dynamic Transcriptomic Profiles between Tomato and a Wild Relative Reflect Distinct Developmental Architectures. *Plant Physiology* **162**, 537–552, <https://doi.org/10.1104/pp.112.213546> (2013).
21. Sinha, N. R., Rowland, S. D. & Ichihashi, Y. Using gene networks in EvoDevo analyses. *Curr Opin Plant Biol* **33**, 133–139, <https://doi.org/10.1016/j.pbi.2016.06.016> (2016).
22. McKown, A. D. *et al.* Geographical and environmental gradients shape phenotypic trait variation and genetic structure in *Populus trichocarpa*. *The New phytologist* **201**, 1263–1276, <https://doi.org/10.1111/nph.12601> (2014).
23. Fukushima, A. *et al.* Exploring tomato gene functions based on coexpression modules using graph clustering and differential coexpression approaches. *Plant Physiol* **158**, 1487–1502, <https://doi.org/10.1104/pp.111.188367> (2012).
24. Fukushima, A. DiffCorr: an R package to analyze and visualize differential correlations in biological networks. *Gene* **518**, 209–214, <https://doi.org/10.1016/j.gene.2012.11.028> (2013).
25. Mohamed, A., Hancock, T., Nguyen, C. H. & Mamitsuka, H. NetPathMiner: R/Bioconductor package for network path mining through gene expression. *Bioinformatics (Oxford, England)* **30**, 3139–3141, <https://doi.org/10.1093/bioinformatics/btu501> (2014).
26. Ichihashi, Y. *et al.* Evolutionary developmental transcriptomics reveals a gene network module regulating interspecific diversity in plant leaf shape. *Proceedings of the National Academy of Sciences of the United States of America* **111**, E2616–E2621, <https://doi.org/10.1073/pnas.1402835111> (2014).
27. Tamura, K., Stecher, G., Peterson, D., Filipiński, A. & Kumar, S. MEGA6: Molecular Evolutionary Genetics Analysis version 6.0. *Mol Biol Evol* **30**, 2725–2729, <https://doi.org/10.1093/molbev/mst197> (2013).
28. Saitou, N. & Nei, M. The neighbor-joining method: a new method for reconstructing phylogenetic trees. *Mol Biol Evol* **4**, 406–425 (1987).
29. Tamura, K. & Nei, M. Estimation of the number of nucleotide substitutions in the control region of mitochondrial DNA in humans and chimpanzees. *Mol Biol Evol* **10**, 512–526 (1993).
30. Felsenstein, J. Phylogenies and the Comparative Method. *The American Naturalist* **125**, 1–15 (1985).
31. Grabherr, M. G. *et al.* Full-length transcriptome assembly from RNA-Seq data without a reference genome. *Nature biotechnology* **29**, 644–652, <https://doi.org/10.1038/nbt.1883> (2011).
32. Götz, S. *et al.* High-throughput functional annotation and data mining with the Blast2GO suite. *Nucleic Acids Res* **36**, 3420–3435, <https://doi.org/10.1093/nar/gkn176> (2008).
33. Li, H. & Durbin, R. Fast and accurate short read alignment with Burrows-Wheeler transform. *Bioinformatics* **25**, 1754–1760 (2009).
34. Robinson, M. D., McCarthy, D. J. & Smyth, G. K. edgeR: a Bioconductor package for differential expression analysis of digital gene expression data. *Bioinformatics (Oxford, England)* **26**, 139–140, <https://doi.org/10.1093/bioinformatics/btp616> (2010).
35. Kohonen, T. Self-Organized Formation of Topologically Correct Feature Maps. *Biol Cybern* **43**, 59–69, <https://doi.org/10.1007/Bf00337288> (1982).

36. Wehrens, R. & Buydens, L. M. C. Self- and super-organizing maps in R: The kohonen package. *J Stat Softw* **21**, 1–19 (2007).
37. Bastian, M., Heymann, S. & Jacomy, M. Gephi: an open source software for exploring and manipulating networks. In Proceedings of the Third International Conference on Weblogs and Social Media. AAAI Press, Menlo Park, CA, 361–362 (2009).
38. Maere, S., Heymans, K. & Kuiper, M. BiNGO: a Cytoscape plugin to assess overrepresentation of gene ontology categories in biological networks. *Bioinformatics* **21**, 3448–3349 (2005).
39. Genty, B., Briantais, J. M. & Baker, N. R. The Relationship between the Quantum Yield of Photosynthetic Electron-Transport and Quenching of Chlorophyll Fluorescence. *Biochim Biophys Acta* **990**, 87–92 (1989).
40. Miyake, C., Amako, K., Shiraiishi, N. & Sugimoto, T. Acclimation of tobacco leaves to high light intensity drives the plastoquinone oxidation system–relationship among the fraction of open PSII centers, non-photochemical quenching of Chl fluorescence and the maximum quantum yield of PSII in the dark. *Plant Cell Physiol* **50**, 730–743, <https://doi.org/10.1093/pcp/pcp032> (2009).

Acknowledgements

We thank Dr. Kaoru O. Yoshiyama for helpful discussions throughout our study. This research was partially supported by a Grant-in-Aid for Scientific Research on Innovative Areas (JP16H01472), JSPS KAKENHI (JP16K07408), and the MEXT-Supported Program for the Strategic Research Foundation at Private Universities (S1511023) to S.K., as well as by a Research Fellowship from JSPS (13J00161) to H.N. H.N. and N.S. were supported by a National Science Foundation grant (1558990). This work used computational resources and cyberinfrastructure provided by the iPlant Collaborative (<http://www.iplantcollaborative.org>), which is funded by NSF Grant DBI-0735191.

Author Contributions

H.N. and S.K. conceived and designed the research. H.N., T.S., Y.O., K.K., M.F., Y.I., T.K., and S.K. performed the experiments. H.N., T.S., Y.O., Y.I., K.M., I.A., N.S., and S.K. wrote the article.

Additional Information

Supplementary information accompanies this paper at <https://doi.org/10.1038/s41598-018-21646-w>.

Competing Interests: The authors declare no competing interests.

Publisher's note: Springer Nature remains neutral with regard to jurisdictional claims in published maps and institutional affiliations.



Open Access This article is licensed under a Creative Commons Attribution 4.0 International License, which permits use, sharing, adaptation, distribution and reproduction in any medium or format, as long as you give appropriate credit to the original author(s) and the source, provide a link to the Creative Commons license, and indicate if changes were made. The images or other third party material in this article are included in the article's Creative Commons license, unless indicated otherwise in a credit line to the material. If material is not included in the article's Creative Commons license and your intended use is not permitted by statutory regulation or exceeds the permitted use, you will need to obtain permission directly from the copyright holder. To view a copy of this license, visit <http://creativecommons.org/licenses/by/4.0/>.

© The Author(s) 2018

RESEARCH ARTICLE

Developmental analyses of divarications in leaves of an aquatic fern *Microsorium pteropus* and its varieties

Saori Miyoshi¹, Seisuke Kimura^{1,2}, Ryo Ootsuki^{3,4}, Takumi Higaki⁵, Akiko Nakamasu^{1,5,6*}

1 Department of Bioresource and Environmental Sciences, Faculty of Life Sciences, Kyoto Sangyo University, Kyoto, Japan, **2** Center for Ecological Evolutionary Developmental Biology, Kyoto Sangyo University, Kyoto, Japan, **3** Department of Natural Sciences, Faculty of Arts and Sciences, Komazawa University, Tokyo, Japan, **4** Faculty of Chemical and Biological Sciences, Japan Women's University, Tokyo, Japan, **5** International Research Organization for Advanced Science and Technology, Kumamoto University, Kumamoto, Japan, **6** Meiji Institute for Advanced Study of Mathematical Sciences, Meiji University, Tokyo, Japan

* nakamasu@kumamoto-u.ac.jp



OPEN ACCESS

Citation: Miyoshi S, Kimura S, Ootsuki R, Higaki T, Nakamasu A (2019) Developmental analyses of divarications in leaves of an aquatic fern *Microsorium pteropus* and its varieties. PLoS ONE 14(1): e0210141. <https://doi.org/10.1371/journal.pone.0210141>

Editor: Zhong-Hua Chen, University of Western Sydney, AUSTRALIA

Received: September 20, 2017

Accepted: December 18, 2018

Published: January 25, 2019

Copyright: © 2019 Miyoshi et al. This is an open access article distributed under the terms of the [Creative Commons Attribution License](https://creativecommons.org/licenses/by/4.0/), which permits unrestricted use, distribution, and reproduction in any medium, provided the original author and source are credited.

Data Availability Statement: All relevant data are within the paper.

Funding: The Japan Society for the Promotion of Science provided grants to AK (12J10320), SK (JP16H01472 and JP16K07408), and RO (26650146). MEXT Supported Program for the Strategic Research Foundation at Private Universities from the Ministry of Education, Culture, Sports, Science & Technology of Japan provided support to SK (S1511023). The funders had no role in study design, data collection and

Abstract

Plant leaves occur in diverse shapes. Divarication patterns that develop during early growths are one of key factors that determine leaf shapes. We utilized leaves of *Microsorium pteropus*, a semi-aquatic fern, and closely related varieties to analyze a variation in the divarication patterns. The leaves exhibited three major types of divarication: no lobes, bifurcation, and trifurcation (i.e., monopodial branching). Our investigation of their developmental processes, using time-lapse imaging, revealed localized growths and dissections of blades near each leaf apex. Restricted cell divisions responsible for the apical growths were confirmed using a pulse-chase strategy for EdU labeling assays.

Introduction

Plants are mainly consisted of stems, roots, and leaves. The leaves are critical for photosynthesis and vary widely in size and shape, although they all develop similarly from a small group of cells, called leaf primordia, which locate on shoot apical meristems. Mathematical models have been used to understand complex natures of leaf-shape formation [1], [2], [3], [4]. Developmental patterns in leaf primordia that determine leaf shapes are highly diverse among species [5]. Particularly, a diversity of cell-division sites in leaf primordia can be observed in developmental stages of different plant species with simple or compound leaves [6], [7], [8]. There are four major types of polarity in the growth patterns along longitudinal axes in simple leaves [9]: acropetal, basipetal, bidirectional (divergent), and diffuse growths (with no apparent allometry). The difference may determine initiation positions of leaf appendage in more complex leaves as mentioned in [10]. Then it could be result in formations of characteristic leaf shape.

Divarication pattern (two-dimensional branching) is one of key factors that determine leaf shapes. A variation in leaf divarications can be classified into three major types: no lobes,

analysis, decision to publish, or preparation of the manuscript.

Competing interests: The authors have declared that no competing interests exist.

bifurcation (or fused leaf) and monopodial trifurcation, the last is common among plants with compound or dissected leaves. Leaf bifurcations are rarely observed among Tracheophyta and they are limited to some plants, such as ferns, and lamina of some seaweeds [11]. Mechanisms that cause the leaf-blade bifurcations may be common among such plants. Almost all fern leaves have coiled axes (crosiers) in their early developmental stages, as a consequence of abaxial–adaxial disparities in their growth patterns [12], which make it difficult to study the developmental processes of fern leaves.

Microsorum pteropus [13], [14], a semi-aquatic, epiphytic fern, has leaves that do not tightly coil in any stages of their developments. In addition, the fern has many varieties, which exhibit the different types of leaf divarication. To examine a variation in their distal growth patterns, we used time-lapse images to analyze the growth processes in the leaves. We used a replica method to observe small-and-simple shapes of epidermal cell at each distal end of the glowing leaves in the *Microsorum* cultivars. We subsequently confirmed cell divisions only at the distal part(s) of the leaves, using pulse-chase experiments for assays using EdU of thymidine analog assays.

Materials and methods

Plant cultivation

M. pteropus wild type and its six varieties were used in the present study. The plants were grown in a room with a continuous light condition at 22°C. The plants were grown on wet soil in a plastic dish from times of differentiation of adventitious bud to nurse plant stages. Subsequently the ferns were replanted in soil in Magenta box culture boxes.

Molecular phylogenetic analysis

Genomic DNAs were extracted from leaves of the *M. pteropus* cultivars using a DNeasy plant mini kit (Quiagen, Dutch). The diluted DNAs (20 µL) were amplified with 30 to 40 PCR cycles (94°C for 1.5 min, 55°C for 30 s, and 7°C for 2 min) using a homemade Taq polymerase. We used three chloroplast genome regions (except *rps4-trnS* IGS), as described in a study by Kreier *et al.* (2008) [15]. The regions include a non-coding region (*TrnL-F*) and the following two coding regions: (1) a large subunit of a ribulose-bisphosphate carboxylase (*rbcL*) and (2) a region similar to a ribosomal protein small subunit 4 (*rps4*). The primer arrays are presented in Table 1. Obtained PCR products were purified using a Gel Extraction Kit (Quiagen, Dutch) or an Illustra ExoProStar (GE Healthcare UK Ltd.). The constructs were subsequently sequenced by FASMAC Co. Ltd. (Kanagawa).

The obtained sequences were analyzed using GENETYX-MAC version 18 (GENETYX, Tokyo). The DNA sequences of each plant were combined in the following order: *trnL-F*, *rbcL*, and *rps4* [15], [16], and then aligned. Non-identical regions within each population were removed. Phylogenetic trees were constructed using the neighbor-joining method with a bootstrap test of 5000 replicates using MEGA software version 4 (www.megasoftware.net). Sequences of reference for *M. pteropus* and other ferns were obtained from GenBank (Table 2). The sequences obtained from our analysis were deposited in GenBank (Table 3).

Time-lapse imaging

Nurse plants were placed on wet soil, pushed against the wall of a Magenta box, and they were covered with a piece of wet paper (without trapping air bubbles) and maintained at 22°C within a bio-multi incubator (LH-80WLED-6CT, Nippon Medical & Chemical Instruments Co., LTD, Osaka). Images (x20 magnification) were taken every six hours for two months

Table 1. Sequences of primer utilized in a phylogenetic analysis.

rbcL univ aF	ATGTCACCACAAACAGAGACTAAAGC
rbcL univ cR	GCAGCAGCTAGTTCGGGGCTCCA
trnL-F B49873	GGTCAAGTCCCTCTATCCC
trnL-F B49873	ATTTGAACTGGTGACACGAG
rps4 fpr micF	AAAATACCCAATTGGGAGAA
rps4 fpr micR	TGATTTAGATTCTGTTCCAAAC

Three arrays were used for a molecular phylogeny analysis: *rbcL*, *trnL-F*, and *rps4*.

<https://doi.org/10.1371/journal.pone.0210141.t001>

using a USB digital microscope (Dino Lite Pro LWD, AnMo Electronics Corporation, Taiwan). This equipment was placed on a silicon sheet to eliminate vibrations.

Observation of epidermal cells

Epidermal cells were observed using a replica method, as follows. Each cut leaf was wiped with a paper towel and mixed dental paste was applied to both sides of the leaf. After solidifying, the pastes were removed from the leaf, creating negative molds. After clear nail polish that was put on the mold form or directly applied to the leaf was dried, it was taken off, put on a glass slide, and then flattened with a glass slide cover. Pictures of the positive (or negative) molds were taken using an upright microscope. From the pictures, sizes of epidermal cell were measured using ImageJ software (<https://imagej.nih.gov/ij/>).

Detection of cell divisions

EdU-labeling assays were performed using a pulse-chase methods [9], [17], [18] to avoid signals obtained by endoreduplications, wherein cell cycles skip the mitotic phases [19]. We removed trichomes to enhance visualization of cell proliferation. Numerous trichomes (on both sides of leaf surface) were rubbed off with a glass capillary chilled in liquid nitrogen. The leaves (with trichomes removed) were immersed in a 10 μM EdU solution (Click-iT EdU Microplate Assay kit, Invitrogen, Japan) and allowed to grow for 1–2 days. The leaves were subsequently transferred to a normal water and allowed to grow for 8–16 hours until cell divisions became evident. Trichomes were removed again, and the leaves were immersed in a 90% ice-cold acetone for 10 minutes. They were washed with a phosphate buffered salts (PBS) and subsequently fixed with a formalin-acetic acid-alcohol (FAA), as outlined by Nakayama *et al.* 2015 [20]. The samples were washed two times for 5 min with 0.5% TritonX in PBSs, washed twice again with PBSs, and then, immersed for 1 hour (or 1.5 hours) under a dark condition in a reaction cocktail (Click-iT EdU Microplate Assay kit) prepared at the time of use. Subsequently, the leaves were rinsed two times for 20 minutes with PBSs. The samples were mounted on a glass slide, the abaxial side up, and observed under a fluorescent microscope (Nikon ECLIPSE 80i or OLYMPUS BX53F). Pictures were taken through the microscope’s lens.

Results

Leaf morphology and a molecular phylogenetic analysis of *Microsorum pteropus* and its varieties

Microsorum pteropus possesses many varieties, which exhibit a variety of leaf shapes (Fig 1). Although the leaves displayed indefinite-and-varying shapes even within same varieties, these mature leaves could be classified into three basic types based on their modes of divarication

Table 2. Accession numbers of plant species utilized in a phylogenetic analysis.

Species	<i>rbcl</i>	<i>rps4</i>	<i>trnL-F</i>
<i>Belvisia annamensis</i> (C. Chr.) S.H. Fu	EU482931	EU482976	EU483025
<i>Belvisia mucronata</i> (Fée) Copel.	AY362562	AY362629	DQ642232
<i>Belvisia platyrhynchos</i> (Kunze) Copel.	DQ642152	DQ642190	DQ642233
<i>Drymotaenium miyoshianum</i> (Makino) Makino	AY362563	AY362630	DQ179640
<i>Goniophlebium argutum</i> (Wall. ex Hook.) J. Sm. ex Hook.	DQ164442	DQ164473	DQ164505
<i>Goniophlebium formosanum</i> (Baker) Rödl-Linder	AB043100	AY096224	DQ642235
<i>Goniophlebium mehibitense</i> (C. Chr.) Parris	EU482932	EU482977	EU483026
<i>Goniophlebium niponicum</i> (Mett.) Bedd.	ABO43098	AY362626	EU483027
<i>Goniophlebium persicifolium</i> (Desv.) Bedd.	EU482933	AY096225	EU483028
<i>Goniophlebium pseudocommutatum</i> (Copel.) Copel.	EU482934	EU482978	EU483029
<i>Goniophlebium subauriculatum</i> (Blume) C.Presl	AF470342	DQ168812	AY083645
<i>Lecanopteris balgoyii</i> Hennipman	AF470328	EU482980	AY083631
<i>Lecanopteris carnosa</i> Blume	AF470322	AY096227	AY083625
<i>Lecanopteris celebica</i> Hennipman	AF470323	EU482981	AY083626
<i>Lecanopteris crustcea</i> Copel.	AF470329	EU482982	AY083632
<i>Lecanopteris luzonensis</i> Hennipman	AF470325	EU482983	AY083628
Species	<i>rbcl</i>	<i>rps4</i>	<i>trnL-F</i>
<i>Lecanopteris mirabilis</i> (C. Chr.) Copel.	AF470330	EU482984	AY083633
<i>Lecanopteris sarcopus</i> (Teijsm. & Binn.) Copel.	EU482935	EU482985	EU483030
<i>Lecanopteris sinuosa</i> (Hook.) Copel.	AF470321	AY362634	AY083624
<i>Lemmaphyllum accedens</i> (Blume) Donk ex. Holttum	EU482936	EU482986	EU483031
<i>Lemmaphyllum carnosum</i> (J. Sm. ex Hook.) C. Presl	AF470332	AY362631	AY083635
<i>Lemmaphyllum diversum</i> (Rosenst.) Tagawa	EU482937	EU482987	EU483032
<i>Lemmaphyllum microphyllum</i> C. Presl ▲	EU482938	EU482988	EU483033
<i>Lepidogrammitis diversa</i> (Rosenst.) Ching	EU482939	EU482989	EU483034
<i>Lepisorus clathratus</i> (C.B. Clarke) Ching	DQ642154	DQ642192	DQ642236
<i>Lepisorus excavatus</i> (Willd.) Ching	DQ642155	DQ642193	DQ642237
<i>Lepisorus kawakamii</i> (Hayata) Tagawa	EU482940	EU482990	EU483035
<i>Lepisorus longifolius</i> (Bl.) Holtt.	DQ642157	DQ642195	DQ642239
<i>Lepisorus macrosphaerus</i> (Baker) Ching	EU482941	EU482991	EU483036
<i>Lepisorus megasorus</i> (C.Ch.) Ching	DQ642158	DQ642196	DQ642240
<i>Lepisorus monilisorus</i> (Hayata) Tagawa	EU482942	EU482992	EU483037
<i>Lepisorus pseudo-ussuriensis</i> Tagawa	EU482943	EU482993	EU483038
<i>Lepisorus thunbergianus</i> (Kaulf.) Ching	U05629	AY096226	DQ642241
<i>Lepisorus waltonii</i> (Ching) S.L. Yu	EU482944	EU482994	EU483039
<i>Leptochilus cantoniensis</i> (Baker) Ching	EU482945	EU482995	EU483041
<i>Leptochilus decurens</i> Blume	AY096203	AY096228	DQ179640
<i>Leptochilus cantoniensis</i> (Baker) Ching	EU482945	EU482995	EU483041
<i>Leptochilus decurrens</i> Blume ▲	AY096203	AY096228	DQ179640
<i>Leptochilus digitatus</i> (Baker) Noot.	EU482948	EU482998	EU483044
<i>Leptochilus elliptica</i> (Thunb.) Ching	EU482949	EU482999	EU483045
<i>Leptochilus hemionitideus</i> (Wall. ex C. Presl) Noot.	U05612	EU503044	EU503045
<i>Leptochilus hemitoma</i> (Hance) Ching	EU482951	EU483001	EU483047
<i>Leptochilus henryi</i> (Baker) Ching	EU482952	EU483002	EU483048
<i>Leptochilus simplifrons</i> (H. Christ) Tagawa	EU482953	EU483003	EU483049
<i>Leptochilus macrophyllum</i> (Blume) Noot. var. <i>wrightii</i> (Hook. & Baker) Noot.	EU482954	EU483004	EU483050
<i>Microsorium commutatum</i> (Bl.) Copel. ▲	AY362571	EU483005	EU483051

(Continued)

Table 2. (Continued)

<i>Microsorium cuspidatum</i> (D. Don) Tagawa	AF470335	AY096230	AY983638
<i>Microsorium grossum</i> (Langsd. & Fisch.) S.B. Andrews ▲	EU482956	EU483007	EU483053
<i>Phymatosorus hainanensis</i> (Noot.) S.G.Lu	EU482960	EU483011	EU483059
<i>Microsorium insigne</i> (Blume) Copel.	EU482957	EU483008	EU483054
<i>Microsorium lastii</i> (Baker) Tardieu	EU482961	EU483012	EU483058
<i>Microsorium linguiforme</i> (Mett.) Copel.	AF470334	AY362635	AY083637
<i>Microsorium membranaceum</i> (D.Don) Ching	EU482962	EU483013	EU483059
<i>Microsorium membranifolium</i> (R.Br.) Ching	DQ642161	DQ642200	DQ642245
<i>Microsorium musifolium</i> (Blume) Copel.	AF470335	AY362636	AY083636
<i>Microsorium novo-zealandiae</i> (Baker) Copel.	DQ401116	DQ401126	DQ401121
<i>Microsorium papuanum</i> (Baker) Parris	DQ642162	EU483015	DQ642246
<i>Microsorium pteropus</i> (Blume) Copel.	EU482965	EU483016	EU483061
<i>Microsorium punctuatum</i> (L.) Copel.	DQ164444	DQ164475	DQ164508
Species	<i>rbcl</i>	<i>rps4</i>	<i>trnL-F</i>
<i>Microsorium pustulatum</i> (G. Forst.) Copel. ▲	DQ401117	DQ401127	DQ401122
<i>Microsorium scandens</i> (G. Forst.) Tindale	DQ401118	DQ401128	DQ401123
<i>Microsorium scolopendrium</i> (Burm.f.) Copel. ▲	DQ642163	DQ642201	DQ642247
<i>Microsorium spectrum</i> (Kaulf.) Copel. ▲	EU482967	EU483018	EU483064
<i>Microsorium thailandicum</i> T. Booknerd & Noot.	EU482969	EU483020	EU483066
<i>Microsorium varians</i> (Mett.) Hennisman & Hett. ▲	AY362566	AY362638	DQ179643
<i>Microsorium viellardii</i> (Mett.) Copel.	DQ179635	DQ179638	DQ179645
<i>Microsorium whiteheadii</i> A.R. Sm. & Hoshiz.	EU482970	EU483021	EU483067
<i>Microsorium zippelii</i> (Blume) Ching	AB23241	DQ642203	DQ642249
<i>Microsorium superficiale</i> (Blume) Bosman	EU482971	EU483022	EU483062
<i>Neocheiropteris palmatopedata</i> (Baker) H.Christ	AY362567	AY362640	DQ212059
<i>Neolepisorus phyllomanes</i> (H. Christ) Ching	EU482973	EU483024	EU483069
<i>Thylacopteris papillosa</i> (Blume) Krause ex J.Sm.	AY459174	AY459188	AY459183
<i>Pyrrosia polydactyla</i>	KY064512	DQ164502	DQ164530
<i>Platycterium stemaria</i>	EF463257	DQ164489	DQ164522

▲ symbols indicate representative fern species selected to generate second phylogenetic tree.

<https://doi.org/10.1371/journal.pone.0210141.t002>

(Fig 1). Wild-type leaves were not lobed (Fig 1A), but some varieties were bifurcated or trifurcated (or rather, had monopodial branching). For example, *M. pteropus* var. *windelov* (Fig 1B) and ‘*Gigantea*’ (Fig 1C) had bifurcated leaves, while leaves of ‘*Tropica*’ (Fig 1D), ‘*Thunder leaf*’ (Fig 1E), ‘*Fork leaf*’ (Fig 1F), and ‘*Trident*’ (Fig 1G) were monopodial. We investigated the genetic relationships among the varieties using a molecular phylogenetic analysis, based on a work of Kreier *et al.* (2008) [15]. Two species, *Platycterium stemaria* and *Pyrrosia polydactyla*,

Table 3. Accession numbers of plant species obtained in this paper.

Species	<i>rbcl</i>	<i>rps4</i>	<i>trnL-F</i>
<i>Microsorium pteropus</i> var. <i>windelov</i>	LC322102	LC325240	LC325246
<i>Microsorium pteropus</i> ‘ <i>Giagantia</i> ’	LC322103	LC325241	LC325247
<i>Microsorium pteropus</i> ‘ <i>Tropica</i> ’	LC322104	LC325242	LC325248
<i>Microsorium</i> sp. ‘ <i>Thunder leaf</i> ’	LC322105	LC325243	LC325249
<i>Microsorium</i> sp. ‘ <i>Fork leaf</i> ’	LC322106	LC325244	LC325250
<i>Microsorium</i> sp. ‘ <i>tridentleaf</i> ’,	LC322107	LC325245	LC325251

<https://doi.org/10.1371/journal.pone.0210141.t003>

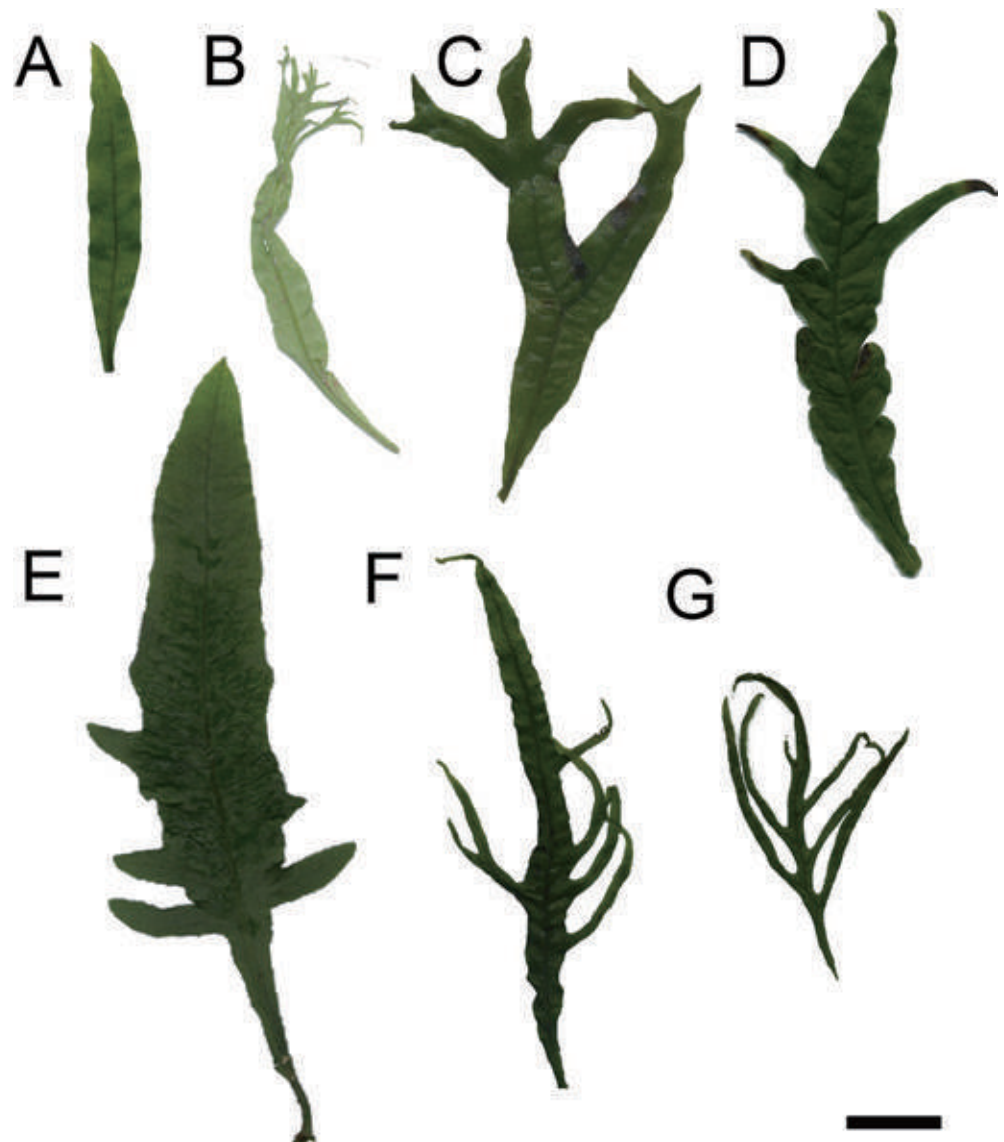


Fig 1. Leaf divarications observed in *M. pteropus* and its varieties. (A) Wild type (wt) of *M. pteropus*, varieties with bifurcated leaves; (B) *M. pteropus* var. *windelov* and (C) *M. pteropus* ‘*Gigantea*’, and varieties with monopodial leaves; (D) *M. pteropus* ‘*Tropica*’, (E) *Microsorium* sp. ‘*Thunder leaf*’, (F) *Microsorium* sp. ‘*Fork leaf*’, and (G) *Microsorium* sp. ‘*tridentleaf*’. A scale bar represents 2 cm.

<https://doi.org/10.1371/journal.pone.0210141.g001>

were used as outgroups for constructing a phylogenetic tree, which included the *M. pteropus* wt, the six varieties, and other species of *Polypodiaceae* (Fig 2A and Table 2). The accession numbers of three genes (*rbcl*, *trnL-F*, and *rps4*) are shown in Table 2. Consequently, the wt and the six varieties were classified into one group. In this analysis, some relationships within or among each clade were unsupported; however, all the clades other than *Microsorium* included all species, as previously recognized. As strongly supported by Kreier *et al.* (2008) [15], the node including *Leptochilus* plus *M. pteropus* was demonstrated to be more distantly related to the nodes of *Microsorium* radical (asterisks in Fig 2A). Our analysis also revealed that the all seven varieties investigated, were included in the *M. pteropus* branch. We further examined the representative species marked with triangles in Fig 2A or Table 2, and fitted them into

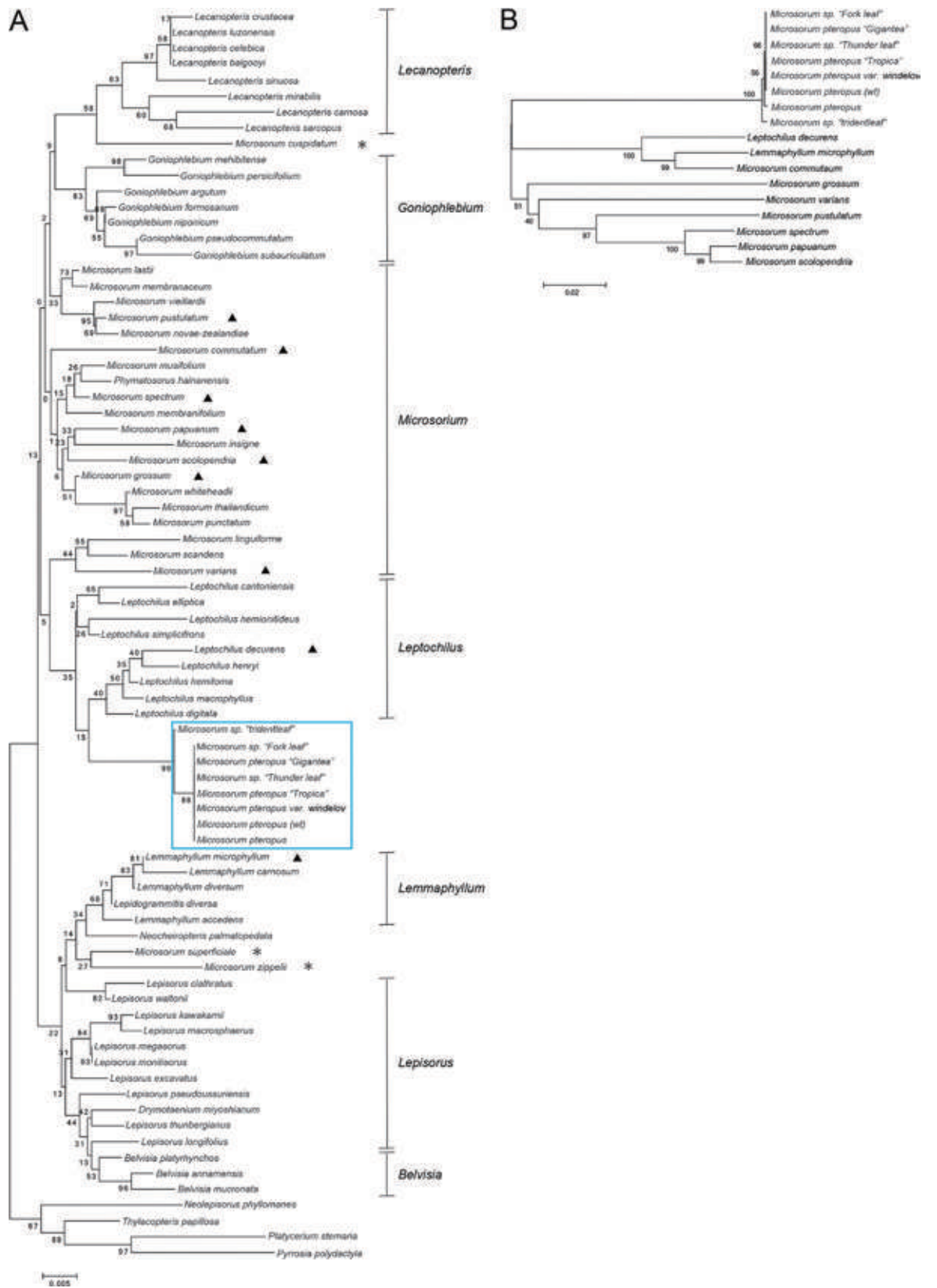


Fig 2. Phylogenetic relationships among the *M. pteropus* cultivars and other fern species. Phylogenetic tree constructions of (A) *M. pteropus*, its varieties and other fern species, and (B) the *M. pteropus* cultivars and representative fern species selected from (A) or Table 2 (denoted with triangles). The examined varieties classified into one group, are framed in a rectangle, then *Microsorum* radicals are indicated by asterisks in (A).

<https://doi.org/10.1371/journal.pone.0210141.g002>

a phylogenetic tree (Fig 2B). When the wt and the six varieties were found to be more closely related to one another than the other species (Fig 2B). Therefore, we could assume that these plants were indeed closely related.

Growths and divarications at each distal end of the leaves indicated in time-laps images

Most leaves of ferns have coiled axes, or crosiers, during their early developments [12]. This attribute makes it difficult to observe the developments in the leaves before their expansions (i.e., later mature stages of the developmental sequence). The all leaves in the *M. pteropus* cultivars that we examined only had a small, coiled crosier (i.e., hook) for the short period before the expansion, and the leaves continued to develop and divaricate even after the expansions. Therefore, we could observe the leaf growths and the formations of characteristic leaf shape using a digital microscope (Fig 3). We acquired time-lapse images (200x magnification, four images per day for two months) from post-leaf expansions to cessations of the growths in the leaves of representative species with the three types of divarication. Weekly silhouettes of the images were stacked against each other using different shades of gray coloration (Fig 3A–3C). In the leaves of *M. pteropus* cultivars, growth terminations were irregular, and dissections of the blades occurred incidentally. The above attribute could be responsible for the indefinite shapes of leaf; however, each cultivar shared certain similarities. The leaf outlines did not change in the, time-laps images, except for the apices. When trichomes and leaf venations were overlapped at the base, they provided clear pictures of how the leaves grew from their apices. In both bifurcated and monopodial leaves, the blades diverged at each distal, growing part of the apices (Fig 3B, 3C 3E and 3F). A bifurcation of the leaf vein seemed to frequently precede a corresponding bifurcation of the blade. However, some bifurcations of the leaf vein did not accompany bifurcations of blade (Fig 3E). This phenomenon was often observed in *windelov* variants. Then a bifurcation of the blade without a bifurcation of the leaf vein could be observed (Fig 3G). In Fig 3G, a freshly bifurcated blades (arrowheads) had the leaf veins bifurcated at different times.

Small epidermal cells and EdU labeled pairs of cells at each distal end of leaves

In almost all leaves, cell expansion phases initiate after cell proliferation phases; then, differences in cell sizes and shapes can often be observed along the longitudinal axes [21], [22]. When we observed epidermal cells of developing leaves in *M. pteropus* and its varieties (using a replica method), we observed that simpler and smaller cells existed at each distal end. In contrast, larger pavement cells (having jigsaw-puzzle shapes) were located in more basal regions (Fig 4A–4L and S1 Fig). However, distances from the apices to regions of the smaller cells at the distal ends usually differed among the various types of *Microsorum* that we investigated. When we measured sizes of epidermal cell, the cells at distal end were always significantly smaller than the cells in more basal regions (Fig 4M–4O). From these results, we concluded that the all types of the investigated *Microsorum* leaves grew at each distal end, and cell enlargements follows via cell proliferations.

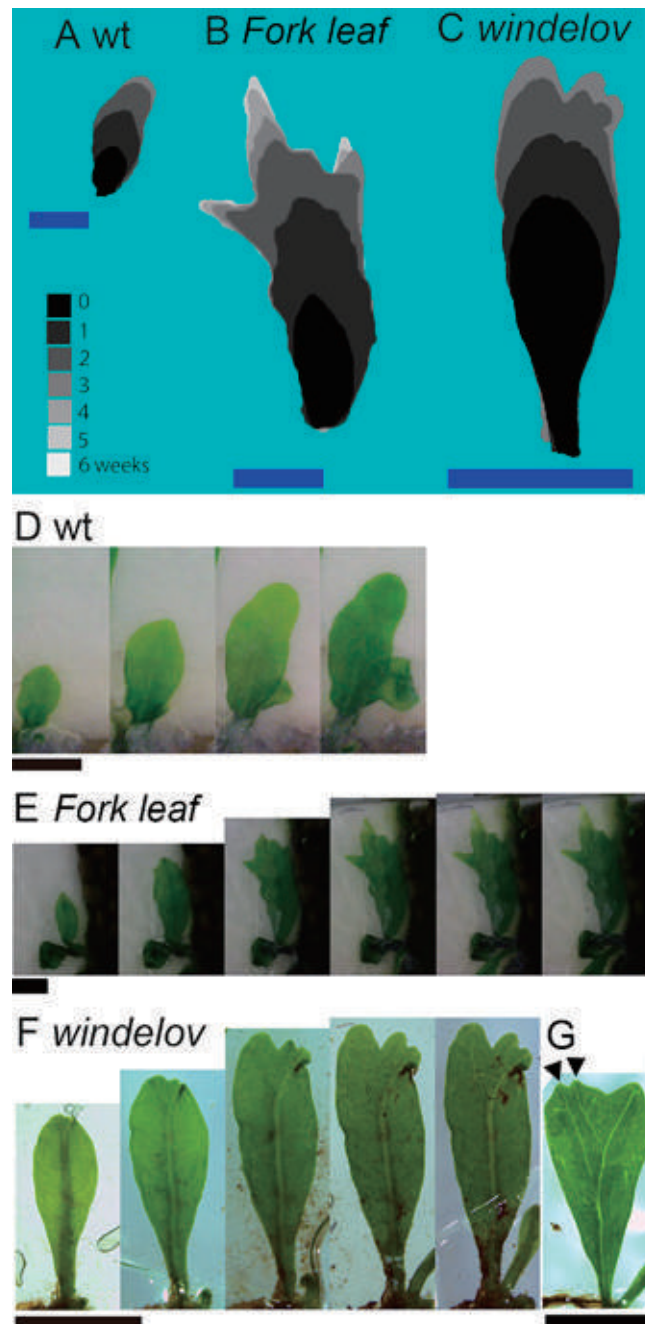


Fig 3. Time-lapse analyses of the different types of leaf divarication in *M. pteropus* and its varieties. Stacked silhouettes of representative types of growing leaves observed in *M. pteropus* cultivars (A–C). Obtained time-lapse images were stacked with silhouettes, with one-week-apart intervals (brightness of the gray scale images are assigned lighter hues over time). The color versions of each image are arranged from left to right in a time series (D–F): (A, D) *M. pteropus* wt, (B, E) *Microsorium* sp. ‘Fork leaf’, and (C, F) *M. pteropus* var. *windelov*. All the three types of leaves did not change in outline, positions of their trichomes, and leaf venation patterns, other than at each distal end. A blade bifurcation without a leaf vein bifurcation (G). Arrowheads indicate a recent blade bifurcation. All scale bars represent 5 mm.

<https://doi.org/10.1371/journal.pone.0210141.g003>

Cell divisions in leaves of *M. pteropus* varieties were labeled using EdU, an analog of nucleoside. EdU labeling assays include signals obtained by endoreduplications, wherein cell cycles skip the mitotic phases [19]. The skipping seems to be typical for leaves in seed plants [23],

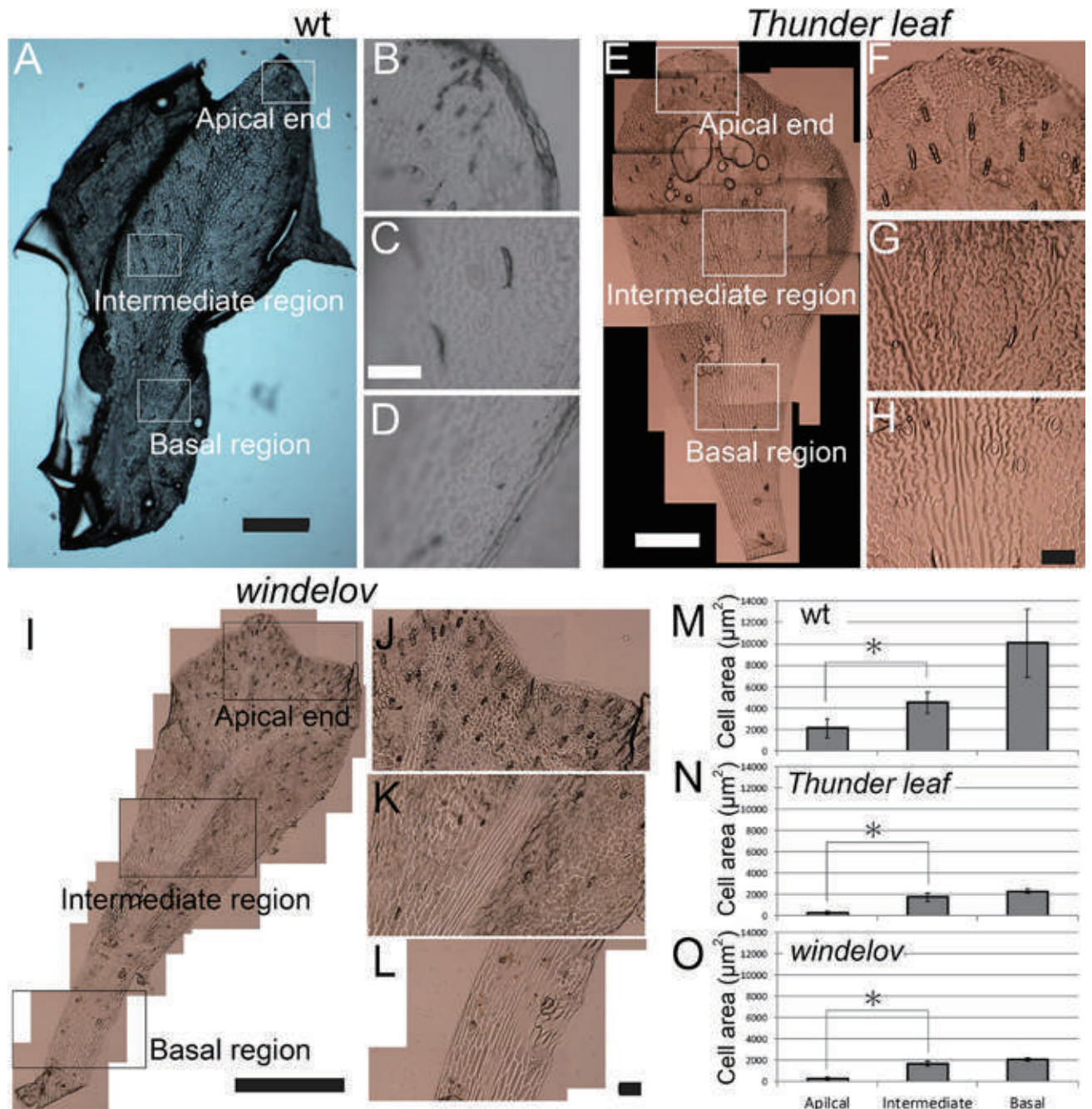


Fig 4. Sizes of epidermal cell on growing leaves in *Microsorium* varieties. (A–L) Microscopic images of epidermal cells on growing leaves of *M. pteropus* wt (A–D), *Microsorium* sp. ‘*Thunder leaf*’ (E–H), and *M. pteropus* var. *windelov* (I–L); (B–D, F–H, J–L) magnifications of each rectangular region in the left images. Images: (A, E, I) entire leaves, (B, F, J) apical ends, (C, G, K) intermediate regions, and (D, H, L) basal regions. (M–O) Cell sizes in the different regions of the leaves. (M) *M. pteropus* wt, (N) *Microsorium* sp. ‘*Thunder leaf*’, and (O) *M. pteropus* var. *windelov*. * significant difference ($p < 0.05$) by Student’s t-tests. Scale bars represent 1 mm (A, E, I) and 100 µm (B–D, F–H, J–L).

<https://doi.org/10.1371/journal.pone.0210141.g004>

[24]; however, there are few descriptions of endoreduplication in fern leaves [25]. To avoid signals obtained from endoreduplications, we used a pulse-chase strategy [9], [17], [18]. Consequently, almost all the labeled cells existed in each distal region of the leaf primordia in all investigated species, including all the three types and their branched versions (Fig 5 and S2

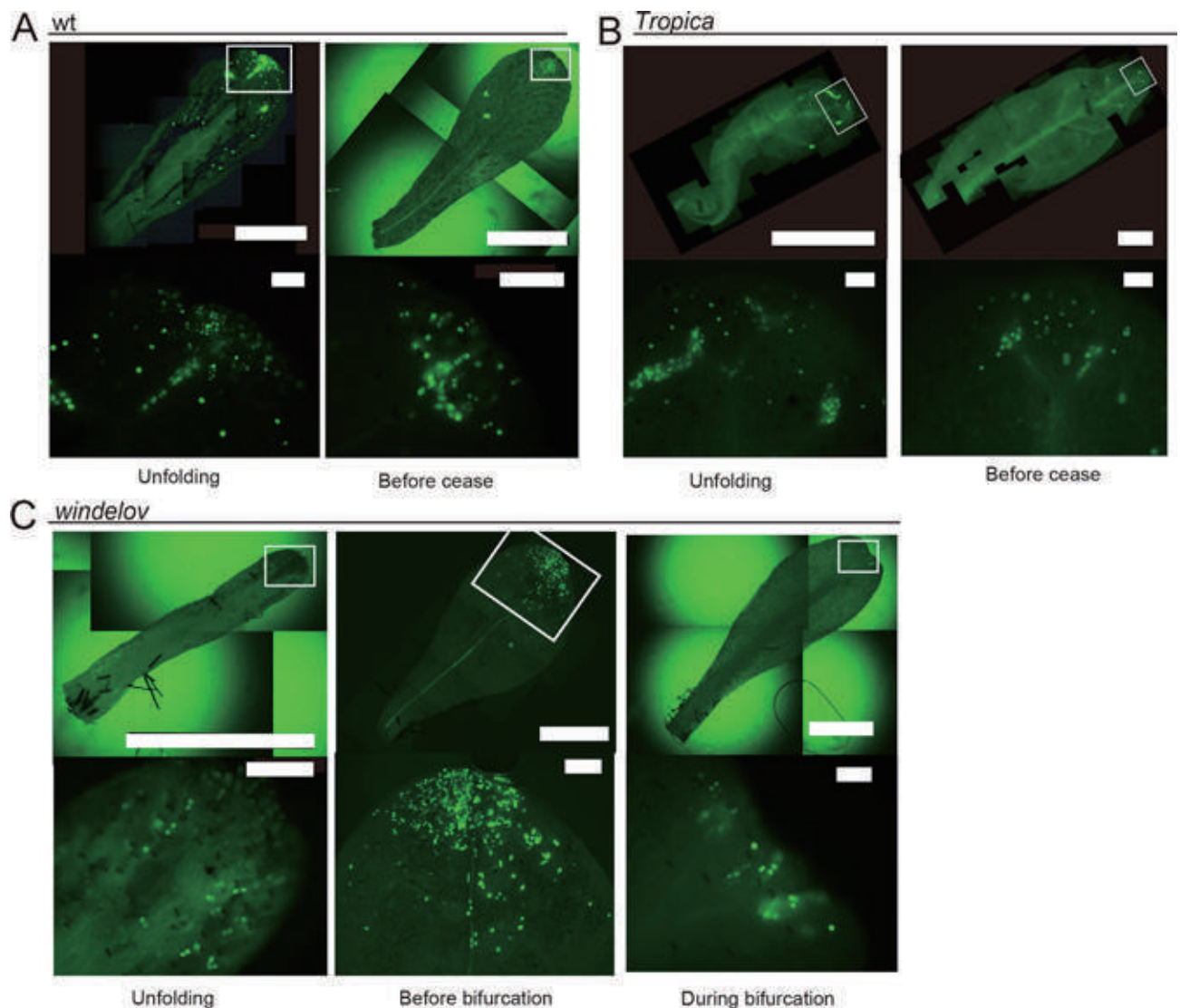


Fig 5. Pulse-chase analyses with EdU indicating the shifts of cell division sites according to leaf growth. Distributions of divided cells in leaves of (A) *M. pteropus* wt, (B) *M. pteropus* ‘*Tropica*’, and (C) *M. pteropus* var. *windelov* at two or three growth stages as visualized with EdU. The stages are indicated under the figures. In all sampled leaves, the signals were limited to each distal region (A–C). Lower panels indicate magnifications of each rectangular region in the upper images. The pair of green signals indicates divided daughter cells. Cell division sites were shifted to the distal end(s) based on growth-and-bifurcation patterns of the leaves. Scale bars represent 1 mm (upper panels) and 100 μ m (lower panels).

<https://doi.org/10.1371/journal.pone.0210141.g005>

Fig). When the blades were branching, the labelled cells became included in each tip of the growing branches (Fig 5C and S2 Fig). We recognized that some of the labeled cells were divided, indicating presences of daughter-cell pair, at the tips of leaf blade and vein (Fig 5A–5C, lower panels). Apparently, the pattern of cell division shifted to more distal parts of the leaf based on the growth-and-divarication patterns of the leaves examined (Fig 5A–5C).

Discussion

The investigated *M. pteropus* and its varieties were combined into one group based on a phylogenetic analysis (Fig 2). They exhibited a variety of leaf shapes, particularly in types of

divarication, even among the closely related plants (Figs 1 and 2). In the time-lapse images that were taken, apical growths of the leaves were prominent (Fig 3). The smallest and simplest epidermal cells were observed in each distal part of the leaves (Fig 4 and S1 Fig). In the pulse-chase experiments (using EdU), fluorescently labeled pairs of daughter cells (i.e., indications of cell division) were detected only at the distal end(s) of the leaves (Fig 5 and S2 Fig). The cells were dividing in the limited regions, in where the apical growths leaf occurred. The data indicate that cells proliferate only at the distal part(s) of the fern leaves, which are updated continuously, then the cells expand on the site. Such apical growths would generate the bifurcated shapes characteristic in the fern species. Similar bifurcations in other plants could also be explained by such distal growths.

A bifurcation arises by an even splitting of a growth point at each distal end of a leaf, for example, during some long, continued apical-growth phases in ferns [12]. Conversely, two other types of divarication, which are common in plant species other than fern, would be also explained by other developmental patterns, such as basipetal, bidirectional, and diffuse growths. The monopodial branching occurs when new growth points are added to the lateral sides of a leaf.

A bifurcation of leaf veins seemed to frequently preceded a corresponding bifurcation of blade. However, our experiments revealed that some bifurcations of *Microsorium* leaf blade were not accompanied by the bifurcation of the leaf vein (Fig 3G). This phenomenon may further indicate that a splitting of marginal growth point precedes leaf vein bifurcation. The peripheral growth pattern in a leaf can be detected by accumulations of a phytohormone (i.e., auxin maxima) [1], [26], which induce leaf protrusions (e.g., lobes and serrations) and vein formations. From previous theoretical analyses, importance of such peripheral patterns in leaf morphogenesis has been proposed, however, major sites of cell divisions were in blades. Consequently, more detailed investigations are required to understand the interaction between the peripheral patterns and blade, and how variations in leaf shapes are produced. It has been demonstrated that directions of cell division plane are critical in shaping a leaf [21]. The relationship between the peripheral events of blade dissections and the cell division planes would also be interesting.

Branching patterns are not limited to plant leaves. Many other organisms display various branching patterns. For example, in three dimensional branches of mammalian lung morphogenesis, two primary forms of branching, a side branching and a tip bifurcation, were observed [27], [28]. Theoretical approaches for explanations of the difference between the branch patterns have been proposed [2], [29], [30]. The peripheral architectures of leaf have also been explored using mathematical models, with deformations of leaf margin based on a peripheral iterative pattern [1], [2]. All the various types of leaf divarication described in the present study can be obtained (Nakamasu unpublished 2019) using a same framework of the previously reported models [1], [2].

Supporting information

S1 Fig. Sizes of epidermal cell on a growing leaf in *M. pteropus* “Tropica”. (A–D) Microscopic images of epidermal cells on a growing leaf in *M. pteropus* “Tropica”. (B) Apical end, (C) intermediate region, (D) basal region. Scale bars represent 500 μm (A) and 100 μm (B–D). (TIF)

S2 Fig. Pulse-chase analysis with EdU indicating cell division sites in a branch of *Microsorium* sp. “Thunder leaf” leaf. (A) Distributions of divided cells in a *Microsorium* sp. “Thunder leaf” leaf with a branch at the tip. (B) The magnification of the rectangular region in the left

image. Scale bars represent 500 μm (A) and 100 μm (B).
(TIF)

Acknowledgments

We thank Okamoto Y.K. and Nakayama H. for helpful discussions.

Author Contributions

Conceptualization: Saori Miyoshi, Seisuke Kimura, Ryo Ootsuki, Akiko Nakamasu.

Data curation: Saori Miyoshi, Seisuke Kimura, Akiko Nakamasu.

Formal analysis: Saori Miyoshi, Akiko Nakamasu.

Funding acquisition: Seisuke Kimura, Ryo Ootsuki, Akiko Nakamasu.

Investigation: Saori Miyoshi, Akiko Nakamasu.

Methodology: Saori Miyoshi, Seisuke Kimura, Ryo Ootsuki, Akiko Nakamasu.

Project administration: Saori Miyoshi, Akiko Nakamasu.

Resources: Seisuke Kimura, Takumi Higaki, Akiko Nakamasu.

Supervision: Seisuke Kimura, Akiko Nakamasu.

Validation: Saori Miyoshi, Seisuke Kimura, Ryo Ootsuki, Akiko Nakamasu.

Writing – original draft: Saori Miyoshi, Akiko Nakamasu.

Writing – review & editing: Saori Miyoshi, Seisuke Kimura, Ryo Ootsuki, Akiko Nakamasu.

References

1. Billsborough GD, Runions A, Barkoulas M, Jenkins HW, Hasson A, Galinha C, et al. Model for the regulation of *Arabidopsis thaliana* leaf margin development. *Proc Natl Acad Sci U S A*. 2011; 108: 3424–3429. <https://doi.org/10.1073/pnas.1015162108> PMID: 21300866
2. Nakamasu A, Nakayama H, Nakayama N, Suematsu NJ, Kimura S. A developmental model for branching morphogenesis of lake cress compound leaf. *PLOS ONE*. 2014; e111615. <https://doi.org/10.1371/journal.pone.0111615>
3. Runions A, Tsiantis M, Prusinkiewicz P. A common developmental programme can produce diverse leaf shapes. *New Phytol*. 2017; 216: 401–418. <https://doi.org/10.1111/nph.14449> PMID: 28248421
4. Nakamasu A, Suematsu NJ, Kimura S. Asymmetries in leaf branch are associated with differential speeds along growth axes: a theoretical prediction. *Dev Dyn*. 2017; 246: 981–991. <https://doi.org/10.1002/dvdy.24587> PMID: 28865166
5. Tsukaya H. Comparative leaf development in angiosperms. *Curr Opin Plant Biol*. Elsevier Ltd; 2014; 17: 103–109. <https://doi.org/10.1016/j.pbi.2013.11.012> PMID: 24507501
6. Donnelly PM, Bonetta D, Tsukaya H, Dengler RE, Dengler NG. Cell cycling and cell enlargement in developing leaves of *Arabidopsis*. *Dev Biol*. 1999; 215: 407–419. <https://doi.org/10.1006/dbio.1999.9443> PMID: 10545247
7. Nath U, Crawford BCW, Carpenter R, Coen E. Genetic Control of Surface Curvature. *Science*. 2003; 299: 1404–1407. <https://doi.org/10.1126/science.1079354> PMID: 12610308
8. Nakayama H, Nakayama N, Seiki S, Kojima M, Sakakibara H, Sinha N, et al. Regulation of the KNOX-GA gene module induces heterophyllic alteration in North American lake cress. *Plant Cell*. 2014; 26: 4733–4748. <https://doi.org/10.1105/tpc.114.130229> PMID: 25516600
9. Das Gupta M, Nath U. Divergence in patterns of leaf growth polarity is associated with the expression divergence of miR396. *Plant Cell*. 2015; 27: 2785–2799. <https://doi.org/10.1105/tpc.15.00196> PMID: 26410303

10. Ikeuchi M, Tatematsu K, Yamaguchi T, Okada K, Tsukaya H. Precocious progression of tissue maturation instructs basipetal initiation of leaflets in *Chelidonium majus* subsp. *asiaticum* (Papaveraceae). *Am J Bot*. 2013; 100: 1116–1126. <https://doi.org/10.3732/ajb.1200560> PMID: 23711907
11. Chitwood DH, Sinha NR. Evolutionary and Environmental Forces Sculpting Leaf Development. *Curr Biol*. Elsevier Ltd; 2016; 26: R297–R306. <https://doi.org/10.1016/j.cub.2016.02.033> PMID: 27046820
12. Steeves TA, Sussex IM. Patterns in plant development. Cambridge University Press; 1990.
13. Blume KL. *Enumeratio plantarum Javae et insularum adjacentium: minus cognitarum vel novarum ex herbariis Reinwardtii, Kuhlilii, Hasseltii et Blumii curavit Carol. Lugduni Batavorum*; 1828. pp.125.
14. Copeland EB. *The oriental Genera of Polypodiaceae*. University of California Press; 1929. pp. 111–113.
15. Kreier HP, Zhang XC, Muth H, Schneider H. The microsporoid ferns: Inferring the relationships of a highly diverse lineage of Paleotropical epiphytic ferns (Polypodiaceae, Polypodiopsida). *Mol Phylogenet Evol*. 2008; 48: 1155–1167. <https://doi.org/10.1016/j.ympev.2008.05.001> PMID: 18562215
16. Hasebe M, Omori T, Nakazawa M, Sano T, Kato M, Iwatsuki K. rbcL gene sequences provide evidence for the evolutionary lineages of leptosporangiate ferns. *Proc Natl Acad Sci U S A*. 1994; 91: 5730–5734. <https://doi.org/10.1073/pnas.91.12.5730> PMID: 8202555
17. Kotogány E, Dudits D, Horváth GV, Ayaydin F. A rapid and robust assay for detection of S-phase cell cycle progression in plant cells and tissues by using ethynyl deoxyuridine. *Plant Methods*. 2010; 6: 5. <https://doi.org/10.1186/1746-4811-6-5> PMID: 20181034
18. Yin X, Tsukaya H. A pulse-chase strategy for EdU labelling assay is able to rapidly quantify cell division orientation. *New Phytol*. 2016; 211: 1462–1469. <https://doi.org/10.1111/nph.13980> PMID: 27121010
19. Veylder L De, Beeckman T, Inzé D, De Veylder L. The ins and outs of the plant cell cycle. *Nat Rev Mol Cell Biol*. 2007; 8: 655–65. <https://doi.org/10.1038/nrm2227> PMID: 17643126
20. Nakayama H, Kawade K, Tsukaya H, Kimura S. Detection of the cell proliferation zone in leaves by using EdU, Bio-protocol 2015; 5: e1600 | <http://www.bio-protocol.org/e1600>
21. Green PB. (1976). Growth and cell pattern formation on an axis: critique of concepts, terminology, and modes of study. *Bot. Gaz*. 1976; 137: 187–202
22. Andriankaja M, Dhondt S, DeBodt S, Vanhaeren H, Coppens F, DeMilde L, et al. Exit from Proliferation during Leaf Development in *Arabidopsis thaliana*: a not-so-gradual process. *Dev Cell*. 2012; 22: 64–78. <https://doi.org/10.1016/j.devcel.2011.11.011> PMID: 22227310
23. Melaragno JE, Mehrotra B, Coleman AW. Relationship between endopolyploidy and cell size in epidermal tissue of *Arabidopsis*. *Plant Cell*. 1993; 5: 1661–1668. <https://doi.org/10.1105/tpc.5.11.1661> PMID: 12271050
24. Barow M, Meister A. Endopolyploidy in seed plants is differently correlated to systematics, organ, life strategy and genome size. *Plant, Cell Environ*. 2003; 26: 571–584. <https://doi.org/10.1046/j.1365-3040.2003.00988.x>
25. Bainard JD, Henry TA, Bainard LD, Newmaster SG. DNA content variation in monilophytes and lycophytes: Large genomes that are not endopolyploid. *Chromosom Res*. 2011; 19: 763–775. <https://doi.org/10.1007/s10577-011-9228-1> PMID: 21847691
26. Kawamura E, Horiguchi G, Tsukaya H. Mechanisms of leaf tooth formation in *Arabidopsis*. *Plant J*. 2010; 62: 429–441. <https://doi.org/10.1111/j.1365-313X.2010.04156.x> PMID: 20128880
27. Metzger RJ, Klein OD, Martin GR, Krasnow MA. The branching programme of mouse lung development. *Nature*. 2008; 453: 745–750. <https://doi.org/10.1038/nature07005> PMID: 18463632
28. Warburton D. Order in the lung. *Nature*. 2008; 453: 733–735. <https://doi.org/10.1038/453733a> PMID: 18528385
29. Guo Y, Chen T-H, Zeng X, Warburton D, Boström KI, Ho C-M, et al. Branching patterns emerge in a mathematical model of the dynamics of lung development. *J Physiol*. 2014; 592: 313–324. <https://doi.org/10.1113/jphysiol.2013.261099> PMID: 24247979
30. Xu H, Sun M, Zhao X. Turing mechanism underlying a branching model for lung morphogenesis. *PLoS One*. 2017; 12: 1–20. <https://doi.org/10.1371/journal.pone.0174946> PMID: 28376090

RESEARCH ARTICLE

Development of highly sensitive and low-cost DNA agarose gel electrophoresis detection systems, and evaluation of non-mutagenic and loading dye-type DNA-staining reagents

Ken Motohashi ^{1,2*}

1 Department of Frontier Life Sciences, Faculty of Life Sciences, Kyoto Sangyo University, Kamigamo Motoyama, Kita-ku, Kyoto, Japan, **2** Center for Ecological Evolutionary Developmental Biology, Kyoto Sangyo University, Kamigamo Motoyama, Kita-Ku, Kyoto, Japan

* motohas@cc.kyoto-su.ac.jp

Abstract

Highly sensitive and low-cost DNA agarose gel detection systems were developed using non-mutagenic and loading dye-type DNA-staining reagents. The DNA detection system that used Midori Green Direct and Safelook Load-Green, both with an optimum excitation wavelength at ~490 nm, could detect DNA-fragments at the same sensitivity to that of the UV (312 nm)-transilluminator system combined with ethidium bromide, after it was excited by a combination of cyan LED light and a shortpass filter (510 nm). The cyan LED system can be also applied to SYBR Safe that is widely used as a non-toxic dye for post-DNA-staining. Another DNA-detection system excited by black light was also developed. Black light used in this system had a peak emission at 360 nm and caused less damage to DNA due to lower energy of UV rays with longer wavelength when compared to those of short UV rays. Moreover, hardware costs of the black light system were ~\$100, less than 1/10 of the commercially available UV (365 nm) transilluminator (>\$1,000). EZ-Vision and Safelook Load-White can be used as non-mutagenic and loading dye-type DNA-staining reagents in this system. The black light system had a greater detection sensitivity for DNA fragments stained by EZ-Vision and Safelook Load-White compared with the commercially available imaging system using UV (365 nm) transilluminator.

 OPEN ACCESS

Citation: Motohashi K (2019) Development of highly sensitive and low-cost DNA agarose gel electrophoresis detection systems, and evaluation of non-mutagenic and loading dye-type DNA-staining reagents. PLoS ONE 14(9): e0222209. <https://doi.org/10.1371/journal.pone.0222209>

Editor: Ruslan Kalendar, University of Helsinki, FINLAND

Received: July 10, 2019

Accepted: August 23, 2019

Published: September 9, 2019

Peer Review History: PLOS recognizes the benefits of transparency in the peer review process; therefore, we enable the publication of all of the content of peer review and author responses alongside final, published articles. The editorial history of this article is available here: <https://doi.org/10.1371/journal.pone.0222209>

Copyright: © 2019 Ken Motohashi. This is an open access article distributed under the terms of the [Creative Commons Attribution License](https://creativecommons.org/licenses/by/4.0/), which permits unrestricted use, distribution, and reproduction in any medium, provided the original author and source are credited.

Data Availability Statement: All relevant data are within the manuscript and its Supporting Information files.

Introduction

DNA separation and detection by agarose gel electrophoresis is one of the most frequently used techniques in life sciences [1–3]. Traditionally, DNA fragments loaded on agarose gels have been stained with ethidium bromide and detected by ultraviolet (UV)-transilluminator system [1, 4–7]. This system is a highly sensitive and low-running-cost method that has been used by many molecular biology researchers to visualize DNA in agarose gel after electrophoresis [8–11]. However, ethidium bromide and UV-light system require careful handling of the staining solution and short wavelength UV (312 nm)-transilluminator because of the

Funding: This work was supported by JSPS KAKENHI Grant Numbers 16K07409 (to K.M.), the MEXT-Supported Program for the Strategic Research Foundation at Private Universities Grant Number S1511023 (to K.M.), and the Institute for Fermentation (Osaka) Grant Number G-2019-2-067 (to K.M.). The funders had no role in study design, data collection and analysis, decision to publish, or preparation of the manuscript.

Competing interests: The author has declared that no competing interests exist.

mutagenic effects of ethidium bromide and high energy of short-wavelength UV light that are harmful to users [12, 13]. Moreover, DNA strands are damaged by high-energy short-wave UV rays [14]. Non-mutagenic alternative DNA-staining reagents, such as SYBR-Green and SYBR-Gold, have been developed to eliminate the disadvantages of DNA staining with ethidium bromide [15–20].

Recently, non-mutagenic and loading dye-type DNA-staining reagents that are simply mixed with sample DNA solutions have been developed and made available by several suppliers, such as EZ-vision (VWR Life Science, Radnor, PA, USA), Midori Green Direct (Nippon Genetics, Tokyo, Japan), Novel Juice (Bio-Helix, Keelung City, Taiwan) and Safelook-series (Fujifilm Wako Pure Chemical Corporation, Osaka, Japan). These DNA-staining reagents are used in small amounts, thereby bearing low cost when compared with other post-staining types or precast-gel type reagents such as SYBR series, and, owing to their low toxicity, they can be used safely to detect DNA fragments on agarose gels after electrophoresis [21–26]. However, the use of these novel non-mutagenic DNA-staining reagents requires an additional excitation light and optical filter system to acquire high detection sensitivity for DNA fragments; these reagents are excited by wavelengths that are longer than the short wavelengths of the UV light used with ethidium bromide DNA staining. Moreover, detection sensitivity of these non-mutagenic DNA-staining reagents is lower than that of ethidium bromide-UV transilluminator system, and excitation by longer UV wavelengths employed with those novel reagents causes less damage to DNA strands [18]. Here, two novel, simple, and low-cost DNA detection systems, using non-mutagenic and loading dye-type of DNA-staining reagents, to detect DNA fragments by agarose gel electrophoresis were developed. In addition, sensitivities of loading dye-type DNA-staining reagents were evaluated in optimized DNA-detection systems using the excitation-light systems.

Materials and methods

Materials

Midori Green Direct (Nippon Genetics), Novel Juice (Bio-Helix), Safelook Load-Green (Fujifilm Wako Pure Chemical Corporation), EZ-Vision One (VWR Life Science), and Safelook Load-White (Fujifilm Wako Pure Chemical Corporation) were used as loading dye-type of DNA-staining reagents. Midori Green Direct was supplied as 10× loading dye. Novel Juice, Safelook Load-Green, EZ-Vision One, and Safelook Load-White were supplied as 6× loading dye. SYBR Safe (Thermo Fisher Scientific, Carlsbad, CA) was used as a major nontoxic post-DNA-staining reagent. A 1Kb DNA Ladder RTU (Bio-Helix, 100 ng/μL) was used as DNA ladder marker (10, 8.0, 6.0, 5.0, 4.0, 3.0, 2.5, 2.0, 1.5, 1.0, 0.75, 0.50, 0.25 kbp). Agarose S (Nippon Gene, Tokyo, Japan) was used for DNA gel electrophoresis.

DNA agarose gel electrophoresis

DNA agarose gel electrophoresis was performed for 25 min at 150 V with 0.8% agarose gel in a buffer containing 89 mM Tris, 89 mM borate, and 2 mM EDTA (TBE) [1, 7].

Excitation light and filter system

Compact LED viewer (https://www.sanplatec.co.jp/product_pages.asp?arg_product_id=SAN26955, Sanplatec, Osaka, Japan) as blue LED light (470 nm) and cyan LED stand light (<https://item.rakuten.co.jp/holkin-shop/hlk-12led-490nm-495nm/>, hlk-12led-490nm-495nm; Holkin, Gifu, Japan) as cyan LED light (490–495 nm) were used to excite Midori Green Direct, Novel Juice, and Safelook Load-Green. Compact black light blue lamp 27 W (<https://item>.

rakuten.co.jp/denzaido/4992712060051/, 360 nm, FPL27BLB; Sankyo Denki, Tokyo, Japan) was used as black light to excite EZ-Vision and Safelook Load-White. A shortpass filter (<https://www.asahi-spectra.co.jp/asp/syousaik.asp?key1=f41&key2=SV0510>, 50 × 50 mm, SV0510; Asahi Spectra, Tokyo, Japan) was used as an excitation light filter for the cyan LED system.

Emission filters

The common filters for photography, SC-42 (420 nm), SC-46 (460 nm), SC-48 (480 nm), SC-52 (520 nm), SC-54 (540 nm), and SC-56 (560 nm) (75 × 75 mm; Fujifilm, Tokyo, Japan) were used as longpass filters for emission systems.

Commercially available imaging systems for DNA agarose gel electrophoresis

STAGE-One (AMZ System Science, Osaka, Japan) was used to visualize DNA ladder markers with ethidium bromide by UV-transilluminator system (312 nm excitation). STAGE-2000 (AMZ System Science) was used to visualize DNA ladder markers with EZ-vision and Safelook Load-White by UV-transilluminator system (365 nm excitation) as a control of commercially available UV-transilluminator system for EZ-vision and Safelook Load-White. Blue-LED transilluminator Blook™ (Bio-Helix) was used to visualize DNA ladder markers with Midori Green Direct as a control of commercially available blue-LED transilluminator system for Midori Green Direct.

Photograph system

Images of DNA agarose gels after electrophoresis were recorded with a digital camera Power-Shot G12 (Canon, Tokyo, Japan) mounted on a photo stand shaded by blackout curtain. None of the images were cropped, and altered by image processing methods such as contrasting and enhancement.

Determination of detection sensitivities by successive dilutions of DNA markers on agarose gels

Fluorescent intensity of successive dilutions of DNA markers on agarose gels was analyzed for each sample by “Plot Profile” of Image-J [27]. Detected sensitivity was defined by the dilution when all the peaks of 13 DNA marker fragments were detected. The detection limit at standard volume, 1/3–1/6 volume, and <1/10 volume of DNA markers was defined as moderate, moderate-high, and high, respectively. When a part of the 13 peaks could not be detected with standard volume (5 μ L), the sensitivity was defined as low.

Results and discussion

Excitation and emission of non-mutagenic and loading dye-type DNA-staining reagents

Non-mutagenic and loading dye-type DNA-staining reagents used in this study were classified according to their excitation wavelength required for detection of DNA fragments in agarose gel after electrophoresis (Table 1). Midori Green Direct, Novel Juice, and Safelook Load-Green were excited by blue (470 nm) or cyan (490–495 nm) light and showed green fluorescence. EZ-Vision and Safelook Load-White were excited by ultraviolet-A (~365 nm) and they release blue fluorescence. In contrast, ethidium bromide was well-excited by short-wave UV rays (312

Table 1. Excitation and emission wavelengths of non-mutagenic and loading dye-type DNA-staining reagents.

Excitation light	DNA-staining reagent ^{*1}	Excitation wavelength (nm) ^{*2}	Emission wavelength (nm) ^{*2}
blue or	Midori Green Direct	490	530
cyan LED	Novel Juice	495	537
	Safelook Load-Green	490	525
UV-A	SYBR Safe ^{*3}	502	530
	EZ-Vision	364	454
	Safelook Load-White	370	470

^{*1}Midori Green Direct was supplied as 10× loading dye. Novel Juice, Safelook Load-Green, EZ-Vision, and Safelook Load-White were supplied as 6× loading dye.

^{*2}Optimum excitation and emission wavelengths for DNA-staining reagents were described in each instruction manual.

^{*3}SYBR Safe is listed because the reagent is widely used as a non-mutagenic DNA-staining reagent, although the reagent is of a post-staining type or precast-gel type.

<https://doi.org/10.1371/journal.pone.0222209.t001>

nm) with high energy. Detection limit of the ethidium bromide staining was evaluated by successive dilutions of DNA markers (standard volume to 1/30 volume) (Fig 1A). The detection limit of staining reagents was defined by the dilution when all peaks of 13 DNA marker fragments were detected, as described in materials and methods (Fig 1 and S1 Fig). DNA markers stained with ethidium bromide could be detected by using 1/10 of standard DNA marker volume (500 ng, 5 μL). This result indicated high sensitivity of ethidium bromide DNA staining. In this study, two DNA detection systems for agarose gel electrophoresis were built by combining a common, commercially available LED or black light (S2 Fig) and optical filters for photography, using loading dye-type DNA-staining reagents. Schematic diagram of these DNA detection systems and photographs of the systems are shown in Fig 2 and S3 Fig, respectively.

High-sensitivity detection system of DNA fragments by blue or cyan LED light-excited DNA-staining reagents

Midori Green Direct, Novel Juice, and Safelook Load-Green are generally excited by blue LED light system. Actually, commercially available Blook system that is equipped by blue LED (470 nm) could detect Midori Green Direct-stained DNA markers (Fig 1A). The sensitivity of Midori Green Direct-stained DNA markers was evaluated by low-cost blue LED light (Compact LED viewer [470 nm], Sanplatec) whose price was ~\$180 (Fig 1B and S4A Fig). Midori Green Direct-stained DNA markers were also detected by the low-cost blue LED viewer when 1/3 volume of DNA markers was loaded on an agarose gel, although the sensitivity was slightly less than that of the Blook system, which could detect 1/6 volume of DNA markers (Fig 1A and 1B). Next, to develop a low-cost DNA detection system with higher sensitivity using non-mutagenic DNA-staining reagents, Cyan LED (490–495 nm, Holkin), which emitted the optimum wavelength to excite Midori Green Direct-stained DNA markers (Table 1), was applied to the DNA detection system for Midori Green Direct. The light emitted by cyan LED (490–495 nm) could not be eliminated in the reflected extra light by longpass emission filters alone (SC-52, SC-54, and SC-56) (S4B Fig, cyan LED) because the wavelength of cyan LED was near the emission wavelength. To eliminate longer wavelength region in reflected light of cyan LED, a shortpass excitation filter (510 nm) was added to the excitation cyan LED light (S4B and S4C Fig, cyan LED and cyan LED + Excitation filter, 510 nm). However, longer wavelength components in cyan-LED could not be eliminated even by a combination of a shortpass excitation filter (510 nm) and a longpass emission filter (520 nm) because cyan LED also contains longer wavelength components in the range of 490–495 nm (S4C Fig). The background noise could be effectively reduced by using a longpass emission filter (540 nm) (S4C Fig). The combination of cyan LED, shortpass excitation filter (510 nm), and longpass emission filter

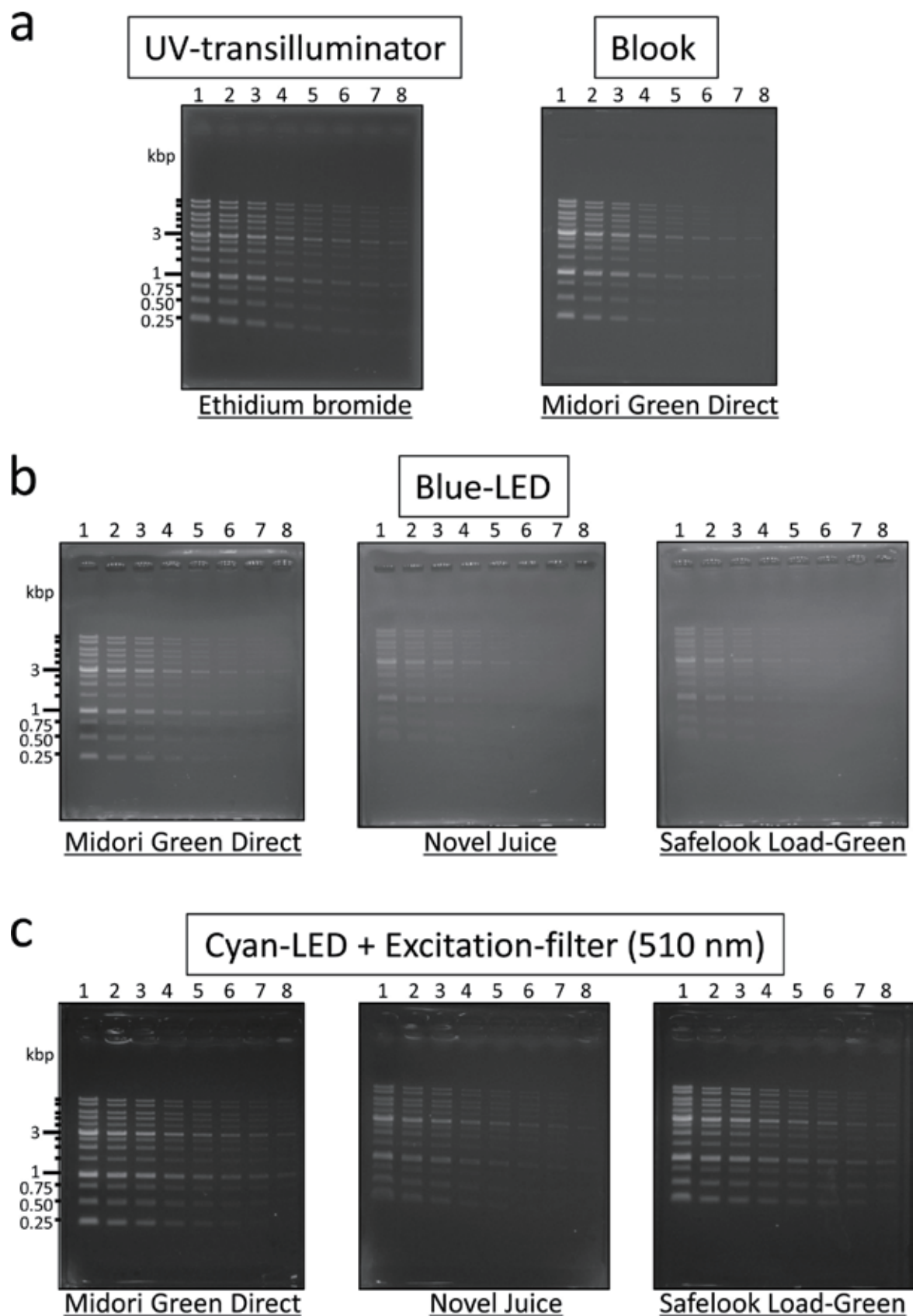


Fig 1. Detection of DNA ladder markers stained with loading dye-type DNA-staining reagents for excitation by blue or cyan-LED light. (a) Detection by UV (312 nm)-transilluminator system (STAGE-One, AMZ System Science) and Blook™ (470 nm, Bio-Helix); (b) Detection by blue-LED light (470 nm) excitation. SC-54 filter was used as longpass emission filter; (c) Detection by combination of cyan LED light (490–495 nm) excitation and a shortpass filter (510 nm). SC-54 filter was used as longpass emission filter. Each DNA-staining reagent was represented by underlined letters. DNA ladder markers were loaded by successive dilution. Lane 1, standard volume (5 μ L (500 ng), 1 volume); lane 2, 1/2 volume; lane 3, 1/3 volume; lane 4, 1/6 volume; lane 5, 1/10 volume; lane 6, 1/15 volume; lane 7, 1/20 volume; lane 8, 1/30 volume.

<https://doi.org/10.1371/journal.pone.0222209.g001>

(540 nm) reduced background noise and greatly improved the detection sensitivity of Midori Green Direct-stained DNA markers (Fig 1B and 1C). The detection limit of the improved cyan LED and shortpass excitation filter system was 1/10 volume of DNA markers and in the same range as that of the ethidium bromide-UV transilluminator system (Fig 1A and 1C). The combination system of cyan LED and the shortpass excitation filter could be also applied to other DNA-staining reagents, such as Novel Juice and Safelook Load-Green. The combination system could detect 1/10 volume of DNA markers using Safelook Load-Green, but only 1/3 volume of DNA markers using Novel Juice (Fig 1C). These results showed that Midori Green Direct and Safelook Load-Green detected DNA markers with higher sensitivity compared with Novel Juice. The hardware cost of the excitation system built by combining cyan LED and a shortpass filter was ~\$280, lower than the cost of the commercially available Blook system (~\$730). SC-54, as a longpass emission filter, effectively reduced background noise in both the blue LED (S4A Fig) and cyan LED systems combined with the excitation filter (510 nm) (S4C Fig).

Low-cost detection system of DNA-fragments based on UV-A-excited DNA-staining reagents

The optimum excitation wavelengths for EZ-Vision and Safelook Load-White were the longer waves of UV-A (360–370 nm) (Table 1). Black light has a peak emission spectrum at 360 nm

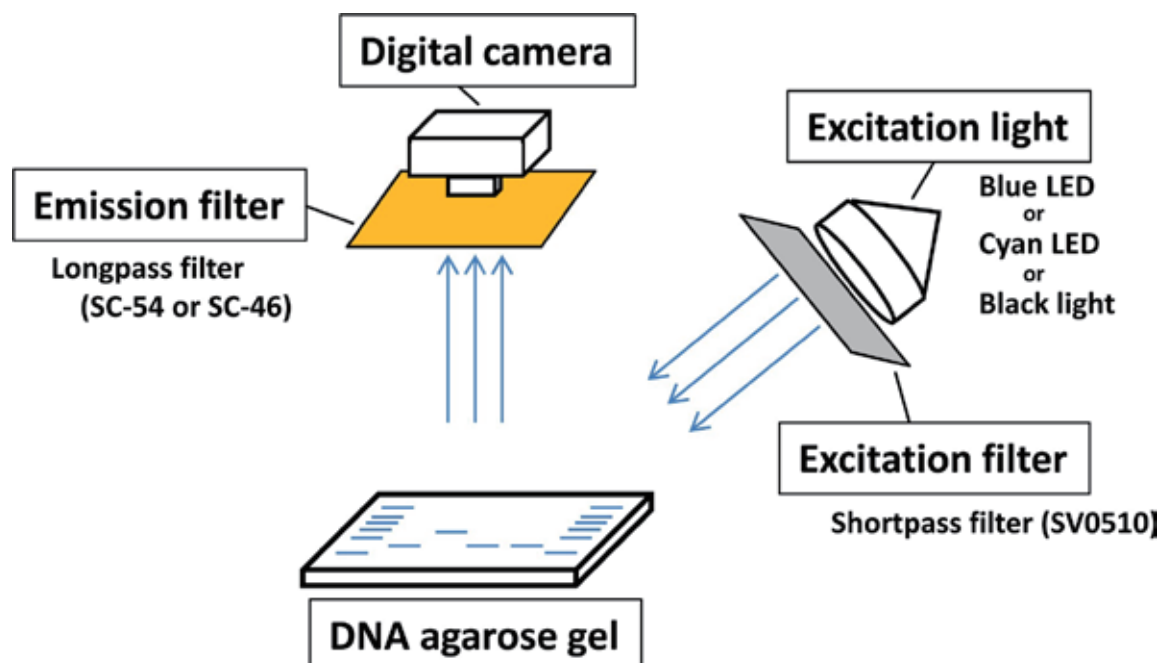


Fig 2. Schematic diagram of DNA detection system for agarose gel electrophoresis using vertical illumination system. Shortpass excitation filter, SV0510, was used for cyan-LED light. Longpass SC-46 emission filter was used for black light system, and longpass SC-54 emission filter was used for blue- or cyan-LED light.

<https://doi.org/10.1371/journal.pone.0222209.g002>

and can excite DNA markers stained with EZ-Vision and Safelook Load-White. DNA markers stained with EZ-Vision and Safelook Load-White could be detected by black light, producing the 13 peaks with standard volume of DNA markers (Fig 3), whereas the commercially available DNA imaging system with UV transilluminator at 365 nm detected the DNA markers

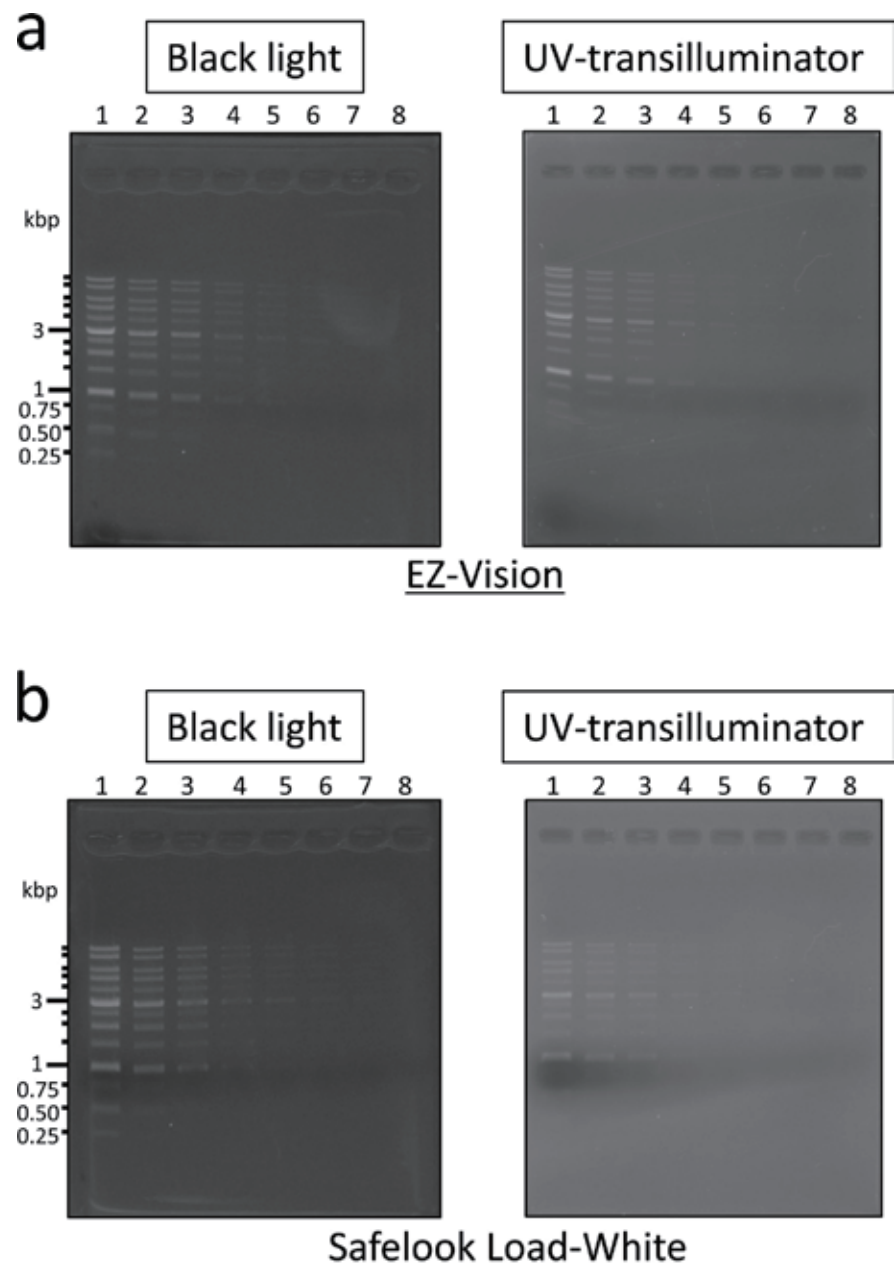


Fig 3. Detection of DNA ladder markers stained with loading dye-type DNA-staining reagents by excitation with UV-A light. (a) Detection of DNA fragments stained by EZ-Vision; (b) Detection of DNA fragments stained with Safelook Load-White. EZ-Vision and Safelook Load-White were excited by black light (~360 nm) or UV (365 nm) transilluminator system (STAGE-2000, AMZ System Science). Each excitation system is represented with boxed letters. SC-46 was used as longpass emission-filter for black light system, and the accessory filter of STAGE-2000 was used as an emission filter for UV (365 nm)-transilluminator system (STAGE-2000). DNA ladder markers were loaded by successive dilution. Lane 1, standard volume (5 μ L (500 ng), 1 volume); lane 2, 1/2 volume; lane 3, 1/3 volume; lane 4, 1/6 volume; lane 5, 1/10 volume; lane 6, 1/15 volume; lane 7, 1/20 volume; lane 8, 1/30 volume.

<https://doi.org/10.1371/journal.pone.0222209.g003>

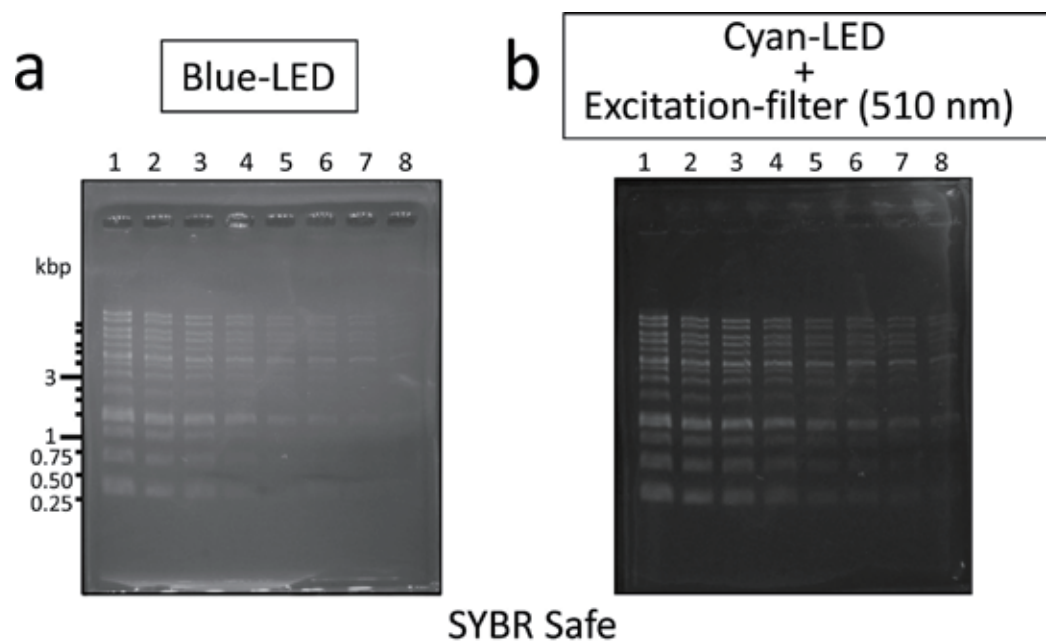


Fig 4. Detection of DNA ladder markers stained with SYBR Safe for excitation by blue or cyan-LED light. (a) Detection by blue-LED light (470 nm) excitation. SC-54 filter was used as longpass emission filter; (b) Detection by combination of cyan LED light (490–495 nm) excitation and a shortpass filter (510 nm). SC-54 filter was used as longpass emission filter. DNA ladder markers were loaded by successive dilution. Lane 1, standard volume (5 μ L (500 ng), 1 volume); lane 2, 1/2 volume; lane 3, 1/3 volume; lane 4, 1/6 volume; lane 5, 1/10 volume; lane 6, 1/15 volume; lane 7, 1/20 volume; lane 8, 1/30 volume.

<https://doi.org/10.1371/journal.pone.0222209.g004>

stained by EZ-Vision and Safelook Load-White with lower sensitivity. Black light is a very low-cost lamp that can be used to emit UV rays (~\$40), in contrast to the expensive hardware of UV-transilluminator (>\$1,000). SC-46, as a low-cost (~\$16) longpass emission-filter, was effective in reducing background noise for the black light system (S5 Fig).

Versatility of two DNA detection systems developed in this study

Both cyan-LED (or blue-LED) system and black light system can be applied to DNA gel extraction from agarose gel because agarose gel fits in the open space of both systems (Fig 2 and S3 Fig). During the cutting of the agarose gel to extract DNA fragments, DNA bands on the agarose gel excited by specific light can be visualized by orange or yellow spectacles, as an alternative to emission filters (SC-54 and SC-46). Orange spectacles (UVP, UVC-310 and Optocode, OG-HC) can be used as an alternative to SC-54 (orange filter) (S6A Fig), and yellow spectacles (TRUSCO, TSG-814Y) as an alternative to SC-46 (yellow filter) (S6B Fig).

SYBR Safe, which is widely used as a post-staining type or precast-gel type reagent, is also a non-toxic DNA-staining reagent, although its feature is different from that of the loading dye-type DNA-staining reagents used in this study. Excitation and emission wavelengths of SYBR Safe show similar features to those of Midori Green Direct, Novel Juice, and Safelook Load-Green (Table 1). To extend the versatility of the DNA detection system developed in this study, DNA agarose gel was stained with SYBR Safe (Fig 4). Consequently, DNA agarose gel stained with SYBR Safe was clearly detected by both the blue-LED and cyan-LED + Excitation filter systems. Similar to Midori Green Direct, Novel Juice, and Safelook Load-Green, SYBR Safe provided higher detection sensitivity of DNA on agarose gel by cyan-LED + Excitation

Table 2. Sensitivities and costs of systems implemented in the detection of DNA fragments on agarose gel after electrophoresis.

DNA-staining reagent	Excitation system ^{*1}	Emission filter ^{*2}	Sensitivity ^{*3}	Hardware cost ^{*4}	Running cost ^{*5}
Ethidium bromide	UV (312 nm) transilluminator	600FS80 ^{*6}	High	****	0.05
Midori Green Direct	Blue LED (Blook TM)	Blue LED (Blook TM)	Moderate-High	***	2.0
	Blue LED	SC-54	Moderate-High	**	2.0
Novel Juice	Cyan LED + Ex-filter (510 nm)	SC-54	High	**	2.0
	Cyan LED + Ex-filter (510 nm)	SC-54	Moderate-High	**	1.9
Safelook Load-Green	Cyan LED + Ex-filter (510 nm)	SC-54	High	**	3.3
SYBR Safe ^{*7}	Blue LED	SC-54	Moderate-High	**	12 or 21 ^{*8}
	Cyan LED + Ex-filter (510 nm)	SC-54	High	**	12 or 21 ^{*8}
EZ-Vision	Black light	SC-46	Moderate	*	1.0
	UV (365 nm) transilluminator	BP-5465 ^{*6}	Low	****	1.0
Safelook Load-White	Black light	SC-46	Moderate	*	2.0
	UV (365 nm) transilluminator	BP-5465 ^{*6}	Low	****	2.0

^{*1} Excitation systems are described in detail in materials and methods. A shortpass filter (50 × 50 mm, SV0510; Asahi Spectra, Tokyo, Japan) was used as excitation filter (Ex-filter, 510 nm). Commercially available UV (312 nm)-transilluminator system (STAGE-One; AMZ System Science) was used for detection of ethidium bromide-stained DNA. Commercially available BlookTM (Bio-Helix) was used for detection of Midori Green Direct-stained DNA. Commercially available UV (365 nm)-transilluminator system (STAGE-2000; AMZ System Science) was used for detection of EZ-Vision- and Safelook Load-White-stained DNA.

^{*2} Longpass filters SC-46 and SC-54 (Fujifilm) were used as emission filters.

^{*3} Sensitivities are represented by four-grade evaluation such as low, moderate, moderate-high, and high. Detected sensitivity was defined in materials and methods.

^{*4} Hardware costs containing excitation systems and emission filters are represented by * <\$100, ** \$100–300, *** \$300–1,000, **** >\$1,000.

^{*5} Running costs of DNA-staining reagents are represented as the ratio to the cost of EZ-Vision, which is assumed 1.0.

^{*6} These filters are accessories of UV-transilluminator systems.

^{*7} SYBR Safe is widely used as a nontoxic staining reagent for DNA agarose gel staining. Although SYBR Safe is a DNA-staining reagent for post-staining or precast gel staining, it was added in Table 2 to extend the versatility of the LED-illumination system developed in this study.

^{*8} Running cost of SYBR Safe was estimated as 21 for post-staining, or 12 for precast gel staining.

<https://doi.org/10.1371/journal.pone.0222209.t002>

filter system than by blue-LED alone (Fig 4 and S7 Fig). The detection sensitivities were the same as those of Midori Green Direct and Safelook Load-Green (Figs 1 and 4).

Conclusion

Sensitivities and costs of the DNA detection system using non-mutagenic and loading dye-type DNA-staining reagents are summarized in Table 2. Midori Green Direct and Safelook Load-Green can be used for highly sensitive DNA-detection systems on DNA agarose gel in combination with cyan LED (490–495 nm) and shortpass excitation filter (510 nm) (Fig 1C); although the running cost of Safelook Load-Green is 1.7-fold that of Midori Green Direct. SYBR Safe, a post-staining reagent, can be also applied to the LED systems (Fig 4), but its running cost is higher than that of loading dye-type DNA-staining reagents because SYBR Safe is used as a staining reagent for post-staining or precast gel staining (Table 2). The sensitivities of the DNA detection system with cyan-LED developed in this study were comparable to a commercially available ethidium bromide-UV (312 nm) transilluminator system (Fig 1A and 1C). The comparison of the initial costs for laboratory set up revealed that hardware cost of the system that combined cyan LED (490–495 nm) and shortpass excitation filter (510 nm), including emission filter, was ~\$300 and thus cheaper than the cost of Blook (~\$730) and UV transilluminator (>\$1,000).

Another DNA-detection system was developed that was excited by black light (~360 nm). This system caused less damage compared with damage caused by short-wave UV rays (312 nm). EZ-Vision-stained and Safelook Load-White-stained DNA gels could be observed with a black light system. Running cost of EZ-Vision was half the cost of Midori Green Direct, and therefore EZ-Vision DNA staining was cost effective, although its sensitivity was less than that of Midori Green Direct. The hardware costs of EZ-Vision were <\$100, and therefore the black light system is a cost-effective excitation system for DNA agarose gel electrophoresis.

Midori Green Direct should be used when high detection sensitivity is required, such as to detect small amounts of DNA fragments, whereas EZ-Vision can be implemented when DNA fragments are detected as part of the routine DNA work because EZ-Vision is the cheapest among non-mutagenic and loading dye-type DNA-staining reagents (Table 2).

Supporting information

S1 Fig. Detection limits by successive dilutions of DNA markers. Profiles of the detection limit under each condition were analyzed by “Plot Profile” of Image-J. Each excitation system is represented with boxed letters, and each DNA-staining reagent is represented by underlined letters. Blue arrows indicate detectable DNA bands. (a) Fig 1A left, lane 5; (b) Fig 1A right, lane 4; (c) Fig 1B left, lane 3; (d) Fig 1C left, lane 5; (e) Fig 1V middle, lane 3; (f) Fig 1V right, lane 5; (g) Fig 3A left, lane 1; (h) Fig 3A right, lane 1; (i) Fig 3B left, lane 1; (j) Fig 3B right, lane 1.

(PPTX)

S2 Fig. Parts of the excitation system used in this study. (a) Blue-LED (Compact LED viewer, Sanplatec); (b) Left, cyan-LED (hkl-12led-490nm-495nm, Holkin), right, cyan-LED with excitation filter (SV0510; Asahi Spectra); (c) left, compact black light blue lamp 27 W (360 nm, FPL27BLB; Sankyo Denki), right, black light to be mounted on a fluorescent lamp stand.

(PPTX)

S3 Fig. A photograph of DNA agarose gel electrophoresis detection systems developed in this study. Gel images were recorded with a digital camera PowerShot G12 (Canon) in a dark place shaded by blackout curtain. (a) Blue-LED system; (b) Cyan-LED + Excitation filter system; (c) Black light system.

(PPTX)

S4 Fig. Evaluation of emission filters for detection of DNA markers stained with Midori Green Direct. (a) Excitation by blue-LED light (470 nm); (b) Excitation by cyan-LED light (490–495 nm); (c) Excitation by combination of cyan LED (490–495 nm) and a shortpass filter (510 nm). SC-52, SC-54, and SC-56 filters were evaluated as longpass emission-filters. DNA ladder markers were loaded by successive dilution. Lane 1, standard volume (5 μ L (500 ng), 1 volume); lane 2, 1/2 volume; lane 3, 1/3 volume; lane 4, 1/6 volume; lane 5, 1/10 volume; lane 6, 1/15 volume; lane 7, 1/20 volume; lane 8, 1/30 volume.

(PPTX)

S5 Fig. Evaluation of emission filters for detection of DNA markers stained with DNA-staining reagents excited by black light system. (a) Detection of DNA markers stained with EZ-Vision; (b) Detection of DNA markers stained with Safelook Load-White. Black light (~360 nm) was used to excite EZ-Vision and Safelook Load-White. SC-42, SC-46, and SC-48 filters were evaluated as longpass emission filters. DNA ladder markers were loaded by successive dilution. Lane 1, standard volume (5 μ L (500 ng), 1 volume); lane 2, 1/2 volume; lane 3, 1/

3 volume; lane 4, 1/6 volume; lane 5, 1/10 volume; lane 6, 1/15 volume; lane 7, 1/20 volume; lane 8, 1/30 volume.

(PPTX)

S6 Fig. Orange and yellow spectacles used to visualize DNA while cutting it out from the agarose gel. (a) Orange spectacles (UVP, UVC-310) can be used as an alternative to SC-54, which is an orange filter. (b) Yellow spectacles (TRUSCO, TSG-814Y) can be used as an alternative to SC-46, which is a yellow filter.

(PPTX)

S7 Fig. Detection limits by successive dilutions of DNA markers. Profiles of detection limit under each condition were analyzed by “Plot Profile” of Image-J. Each excitation system is represented with boxed letters, and DNA-staining reagent is represented by underlined letters. Blue arrows indicate detectable DNA bands. (a) [Fig 4A](#), lane 3; (b) [Fig 4B](#), lane 5.

(PPTX)

Acknowledgments

I thank Dr. Akira Kawabe (Kyoto Sangyo University) for allowing us to use STAGE-One UV-transilluminator system (312 nm excitation). I also thank Dr. Seisuke Kimura (Kyoto Sangyo University) for allowing us to use STAGE-2000 UV-transilluminator system (365 nm excitation).

Author Contributions

Conceptualization: Ken Motohashi.

Formal analysis: Ken Motohashi.

Funding acquisition: Ken Motohashi.

Investigation: Ken Motohashi.

Methodology: Ken Motohashi.

Validation: Ken Motohashi.

Writing – original draft: Ken Motohashi.

Writing – review & editing: Ken Motohashi.

References

1. Voytas D. Agarose gel electrophoresis. *Curr Protoc Mol Biol.* 2001;Chapter 2:Unit2 5A. <https://doi.org/10.1002/0471142727.mb0205as51> PMID: 18265185.
2. Lee PY, Costumbrado J, Hsu CY, Kim YH. Agarose gel electrophoresis for the separation of DNA fragments. *J Vis Exp.* 2012;(62). <https://doi.org/10.3791/3923> PubMed Central PMCID: PMC4846332. PMID: 22546956
3. Green MR, Sambrook J. Analysis of DNA by Agarose Gel Electrophoresis. *Cold Spring Harb Protoc.* 2019;2019(1):pdb top100388. <https://doi.org/10.1101/pdb.top100388> PMID: 30602561.
4. Aaij C, Borst P. The gel electrophoresis of DNA. *Biochim Biophys Acta.* 1972; 269(2):192–200. [https://doi.org/10.1016/0005-2787\(72\)90426-1](https://doi.org/10.1016/0005-2787(72)90426-1) PMID: 5063906.
5. Sharp PA, Sugden B, Sambrook J. Detection of two restriction endonuclease activities in *Haemophilus parainfluenzae* using analytical agarose—ethidium bromide electrophoresis. *Biochemistry.* 1973; 12(16):3055–63. <https://doi.org/10.1021/bi00740a018> PMID: 4354250.
6. Borst P. Ethidium DNA agarose gel electrophoresis: how it started. *IUBMB Life.* 2005; 57(11):745–7. <https://doi.org/10.1080/15216540500380855> PMID: 16511967.

7. Green MR, Sambrook J. *Molecular Cloning: A Laboratory Manual*. Fourth Edition ed. Cold Spring Harbor, NY: Cold Spring Harbor Laboratory Press; 2012.
8. Motohashi K, Shibata S, Ozaki Y, Yatomi Y, Igarashi Y. Identification of lysophospholipid receptors in human platelets: the relation of two agonists, lysophosphatidic acid and sphingosine 1-phosphate. *FEBS Lett.* 2000; 468(2–3):189–93. Epub 2000/02/29. S0014-5793(00)01222-9 [pii]. [https://doi.org/10.1016/s0014-5793\(00\)01222-9](https://doi.org/10.1016/s0014-5793(00)01222-9) PMID: 10692584.
9. Wakita M, Masuda S, Motohashi K, Hisabori T, Ohta H, Takamiya K. The significance of type II and PrxQ peroxiredoxins for antioxidative stress response in the purple bacterium *Rhodobacter sphaeroides*. *J Biol Chem.* 2007; 282(38):27792–801. <https://doi.org/10.1074/jbc.M702855200> PMID: 17644813.
10. Hishiya S, Hatakeyama W, Mizota Y, Hosoya-Matsuda N, Motohashi K, Ikeuchi M, et al. Binary reducing equivalent pathways using NADPH-thioredoxin reductase and ferredoxin-thioredoxin reductase in the cyanobacterium *Synechocystis* sp. strain PCC 6803. *Plant Cell Physiol.* 2008; 49(1):11–8. <https://doi.org/10.1093/pcp/pcm158> PMID: 18003670.
11. Kobayashi K, Mochizuki N, Yoshimura N, Motohashi K, Hisabori T, Masuda T. Functional analysis of *Arabidopsis thaliana* isoforms of the Mg-chelatase CHL1 subunit. *Photochem Photobiol Sci.* 2008; 7(10):1188–95. <https://doi.org/10.1039/b802604c> PMID: 18846282.
12. Lunn G, Sansone EB. Ethidium bromide: destruction and decontamination of solutions. *Anal Biochem.* 1987; 162(2):453–8. [https://doi.org/10.1016/0003-2697\(87\)90419-2](https://doi.org/10.1016/0003-2697(87)90419-2) PMID: 3605608.
13. Ohta T, Tokishita S, Yamagata H. Ethidium bromide and SYBR Green I enhance the genotoxicity of UV-irradiation and chemical mutagens in *E. coli*. *Mutat Res.* 2001; 492(1–2):91–7. [https://doi.org/10.1016/s1383-5718\(01\)00155-3](https://doi.org/10.1016/s1383-5718(01)00155-3) PMID: 11377248.
14. Rastogi RP, Richa, Kumar A, Tyagi MB, Sinha RP. Molecular mechanisms of ultraviolet radiation-induced DNA damage and repair. *J Nucleic Acids.* 2010; 2010:592980. <https://doi.org/10.4061/2010/592980> PMID: 21209706; PubMed Central PMCID: PMC3010660.
15. Singer VL, Lawlor TE, Yue S. Comparison of SYBR Green I nucleic acid gel stain mutagenicity and ethidium bromide mutagenicity in the *Salmonella*/mammalian microsome reverse mutation assay (Ames test). *Mutat Res.* 1999; 439(1):37–47. [https://doi.org/10.1016/s1383-5718\(98\)00172-7](https://doi.org/10.1016/s1383-5718(98)00172-7) PMID: 10029672.
16. Tuma RS, Beaudet MP, Jin X, Jones LJ, Cheung CY, Yue S, et al. Characterization of SYBR Gold nucleic acid gel stain: a dye optimized for use with 300-nm ultraviolet transilluminators. *Anal Biochem.* 1999; 268(2):278–88. <https://doi.org/10.1006/abio.1998.3067> PMID: 10075818.
17. Williams LR. Staining nucleic acids and proteins in electrophoresis gels. *Biotech Histochem.* 2001; 76(3):127–32. PMID: 11475315.
18. Huang Q, Fu WL. Comparative analysis of the DNA staining efficiencies of different fluorescent dyes in preparative agarose gel electrophoresis. *Clin Chem Lab Med.* 2005; 43(8):841–2. <https://doi.org/10.1515/CCLM.2005.141> PMID: 16201894.
19. Kirsanov KI, Lesovaya EA, Yakubovskaya MG, Belitsky GA. SYBR Gold and SYBR Green II are not mutagenic in the Ames test. *Mutat Res.* 2010; 699(1–2):1–4. <https://doi.org/10.1016/j.mrgentox.2010.04.014> PMID: 20403457.
20. Haines AM, Tobe SS, Kobus HJ, Linacre A. Properties of nucleic acid staining dyes used in gel electrophoresis. *Electrophoresis.* 2015; 36(6):941–4. <https://doi.org/10.1002/elps.201400496> PMID: 25546455.
21. Okegawa Y, Motohashi K. Chloroplastic thioredoxin m functions as a major regulator of Calvin cycle enzymes during photosynthesis in vivo. *Plant J.* 2015; 84(5):900–13. Epub 2015/10/16. <https://doi.org/10.1111/tbj.13049> PMID: 26468055.
22. Motohashi K. A simple and efficient seamless DNA cloning method using SLiCE from *Escherichia coli* laboratory strains and its application to SLiP site-directed mutagenesis. *BMC Biotechnol.* 2015; 15(1):47. <https://doi.org/10.1186/s12896-015-0162-8> 10.1186/s12896-015-0162-8 [pii]. PMID: 26037246.
23. Okegawa Y, Motohashi K. A simple and ultra-low cost homemade seamless ligation cloning extract (SLiCE) as an alternative to a commercially available seamless DNA cloning kit. *Biochem Biophys Rep.* 2015; 4:148–51. <https://doi.org/10.1016/j.bbrep.2015.09.005> PMID: 29124198
24. Motohashi K. Evaluation of the efficiency and utility of recombinant enzyme-free seamless DNA cloning methods. *Biochem Biophys Rep.* 2017; 9:310–5. <https://doi.org/10.1016/j.bbrep.2017.01.010> PMID: 28956018
25. Okegawa Y, Motohashi K. Evaluation of seamless ligation cloning extract preparation methods from an *Escherichia coli* laboratory strain. *Anal Biochem.* 2015; 486:51–3. Epub 2015/07/03. S0003-2697(15)00324-3 [pii] <https://doi.org/10.1016/j.ab.2015.06.031> PMID: 26133399.

26. Motohashi K. A novel series of high-efficiency vectors for TA cloning and blunt-end cloning of PCR products. *Sci Rep.* 2019; 9(1):6417. <https://doi.org/10.1038/s41598-019-42868-6> PMID: 31015513; PubMed Central PMCID: PMC6478821.
27. Schneider CA, Rasband WS, Eliceiri KW. NIH Image to ImageJ: 25 years of image analysis. *Nat Methods.* 2012; 9(7):671–5. <https://doi.org/10.1038/nmeth.2089> PMID: 22930834; PubMed Central PMCID: PMC5554542.

SCIENTIFIC REPORTS

OPEN

Genome defense against integrated organellar DNA fragments from plastids into plant nuclear genomes through DNA methylation

Takanori Yoshida¹, Hazuka Y. Furihata¹, Taiko Kim To², Tetsuji Kakutani^{2,3,4} & Akira Kawabe¹ 

Nuclear genomes are always faced with the modification of themselves by insertions and integrations of foreign DNAs and intrinsic parasites such as transposable elements. There is also substantial number of integrations from symbiotic organellar genomes to their host nuclear genomes. Such integration might have acted as a beneficial mutation during the evolution of symbiosis, while most of them have more or less deleterious effects on the stability of current genomes. Here we report the pattern of DNA substitution and methylation on organellar DNA fragments integrated from plastid into plant nuclear genomes. The genome analyses of 17 plants show homology-dependent DNA substitution bias. A certain number of these sequences are DNA methylated in the nuclear genome. The intensity of DNA methylation also decays according to the increase of relative evolutionary times after being integrated into nuclear genomes. The methylome data of epigenetic mutants shows that the DNA methylation of organellar DNA fragments in nuclear genomes are mainly dependent on the methylation maintenance machinery, while other mechanisms may also affect on the DNA methylation level. The DNA methylation on organellar DNA fragments may contribute to maintaining the genome stability and evolutionary dynamics of symbiotic organellar and their host's genomes.

Recently, it is recognized that epigenetic mechanisms are important for regulation of foreign DNAs that are integrated into host genomes and disrupt genome stability. For example, regulation of transposable elements (TEs) is important in maintaining genome stability. In general, the mobility of TEs in plants is highly repressed by multiple factors. One of the important mechanisms involved in genome stability and repression of endogenous TEs and foreign DNA fragments is RNA interference (RNAi). RNAi participates in various nuclear processes such as repression of TEs, heterochromatin formation, and gene expression regulation^{1,2}. Such phenomena are caused by post-transcriptional gene silencing (PTGS) and epigenetic modifications such as DNA methylation by RNA-directed DNA methylation (RdDM) and histone modification. In addition to RdDM, DNA methylation is maintained by methylation maintenance machinery with DNA methyltransferase that propagate CpG methylation on newly synthesized DNA and non-CpG DNA and histone methyltransferases involved in the crosstalk of DNA and histone methylation³⁻⁹. In plant, the existence of another pathway that leads to *de novo* DNA methylation without small RNA is also suggested by analyses of mutants of the *DDM1* (*DECREASE IN DNA METHYLATION 1*) gene in the model plant *Arabidopsis thaliana*¹⁰. Since the discovery of mobile elements in maize^{11,12}, TEs were mainly considered as 'selfish DNA' that has little functional or beneficial effects to host genomes¹³. In recent years, this classical view has been challenged by a new hypothesis that TEs contribute to the expansion of genome complexity in eukaryotes¹⁴⁻¹⁶. Epigenetic modifications such as histone modification and DNA methylation on endogenous TEs and exogenous invading DNAs can be thus important not only for the repression of such sequences, but also for gene regulations, expression networks and genome evolvability.

Organellar genomes also affect the complexity of plant nuclear genomes. Plastid and mitochondrion are important plant organelles that have their own genomes. During the evolution of plastid and mitochondrion,

¹Faculty of Life Science, Kyoto Sangyo University, Kyoto, Kyoto, Japan. ²Faculty of Science, The University of Tokyo, Bunkyo-ku, Tokyo, Japan. ³Department of Integrated Genetics, National Institute of Genetics, Mishima, Shizuoka, Japan. ⁴Department of Genetics, School of Life Science, The Graduate University for Advanced Studies (SOKENDAI), Mishima, Shizuoka, Japan. Correspondence and requests for materials should be addressed to A.K. (email: akiraka@cc.kyoto-su.ac.jp)

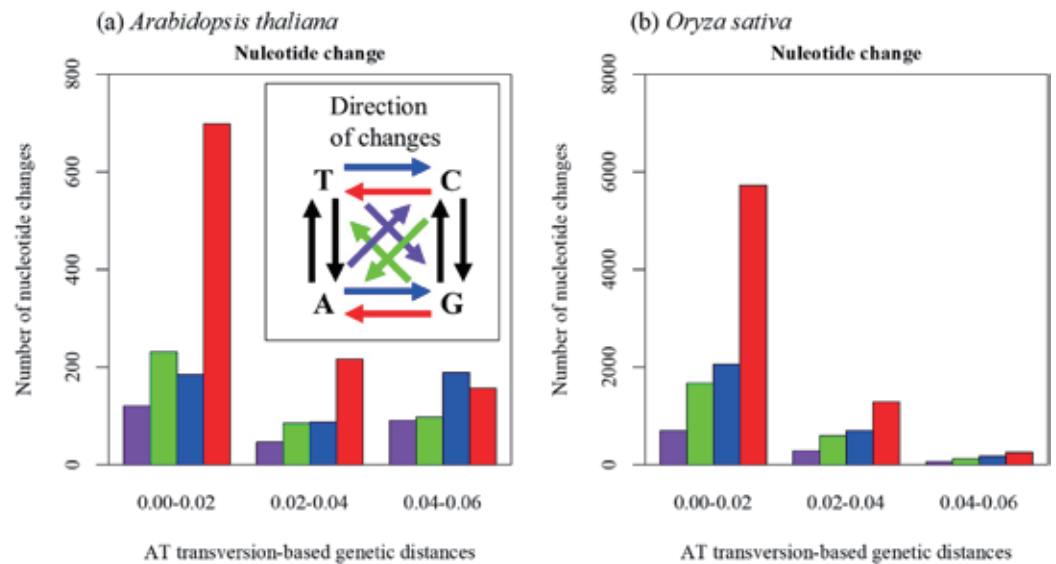


Figure 1. Difference of nucleotide change by integration time. Nucleotide change between NUPTs and corresponding plastid sequences were counted. NUPTs were grouped by AT transversion-based genetic distance that represents timing of integration. Arrows in box represents direction of nucleotide change: red bar; C to T and G to A, blue bar; T to C and A to G, green bar; C to A and G to T, and purple bar; A to C and T to G.

substantial gene transfers from organelle to host nuclear genomes had occurred¹⁷. The plant genome projects revealed that organellar genomes integration to host nuclear genomes is not limited during the establishment of symbiosis: the organelle DNA fragments from both plastid and mitochondrial genomes are still actively integrated into nuclear genomes and are so-called nuclear plastid DNA (NUPT) and nuclear mitochondrial DNA (NUMT)^{18,19}. In *A. thaliana*, almost whole mitochondrial genome is integrated into chromosome 2 in relatively recent era^{20,21}. In *Oryza sativa*, the extensive study of NUPTs organization suggested recurrent integrations from plastid genomes to nuclear genome, and rapid fragmentation and elimination of NUPTs after integration²². NUPTs are also retained in several plant nuclear genomes^{23–25}. During the process of integration and elimination of organelle DNA fragments, DNA methylation might play an important role to regulate NUPTs. NUPTs were shown to have excessed substitutions from cytosine (C) to thymine (T) and guanine (G) to adenine (A)^{26,27}. These biased substitutions might be induced by hypermethylation of integrated DNAs and subsequent deamination of 5-methylcytosine¹⁷, suggesting the importance of epigenetic regulation of integrated DNAs. Because the amount of NUPTs (lower than 1% of plant nuclear genomes)²⁵ is smaller than that of TEs and the evolutionary change since integrating in nuclear genomes can be estimated by comparing with organellar genomes, the integration and subsequent nucleotide change can be detected easier than those of TEs. Thus, the NUPTs are good materials to investigate the epigenetic mechanism regulating foreign DNA fragments in plant nuclear genomes.

In this study, we investigated the nucleotide changes and DNA methylation status of NUPTs. There are strong biased nucleotide changes correlate with time of integration. By the biased mutation, guanine and cytosine residues compositions changed along with biased substitutions. A certain number of NUPTs are DNA methylated in the nuclear genome. We also detected decay of CpG and non-CpG methylation through time after integration in nuclear genomes. The results in this study suggested that the DNA methylation on NUPTs was mainly dependent on the methylation maintenance machinery, while some NUPTs were more affected by RdDM machinery. Some observations might imply another mechanism of homology-dependent DNA methylation. The mechanism might have roles to defend plant nuclear genomes from deleterious integrations of foreign sequences.

Results

Biased mutation in NUPTs. Genome sequence data of 17 plants (13 Eudicots: *A. thaliana*, *Carica papaya*, *Vitis vinifera*, *Lotus japonicus*, *Medicago truncatula*, *Glycine max*, *Manihot esculenta*, *Ricinus communis*, *Populus trichocarpa*, *Cucumis sativus*, *Fragaria vesca*, *Solanum tuberosum*, *Solanum lycopersicum*, 4 Monocots: *Brachypodium distachyon*, *O. sativa*, *Sorghum bicolor*, *Zea mays*) were obtained from databases (Table S1). Integrated NUPTs within each nuclear genome were estimated by BLAST search and subsequent filtering steps. Nucleotide changes between plastid genomes and NUPTs were then identified for each species. To estimate the relative time of integration, the genetic distances (based on AT transversion) between plastid genomes and NUPTs were calculated. NUPTs were grouped by genetic distances (young aged NUPTs; 0.00 to 0.02, middle aged NUPTs; 0.02 to 0.04, old aged NUPTs; 0.04 to 0.06) to characterizing them as a function of integration time.

For all species analyzed, strong biased mutations from C/G to T/A were observed as previously suggested^{26,27}. These biases were mainly due to the excess of C to T and G to A transitions. The excess of C/G to T/A transition mutations implied that such bias occurred in association with DNA methylation of cytosine residues. The degree of such bias changed by the genetic distance between plastid genome sequences and NUPTs (Fig. 1). In *A. thaliana*, the ratio of T/A → C/G transitions to C/G → T/A transitions (i.e., $\frac{N_{T \rightarrow C} + N_{A \rightarrow G}}{N_{C \rightarrow T} + N_{G \rightarrow A}}$, N ; the number of transi-

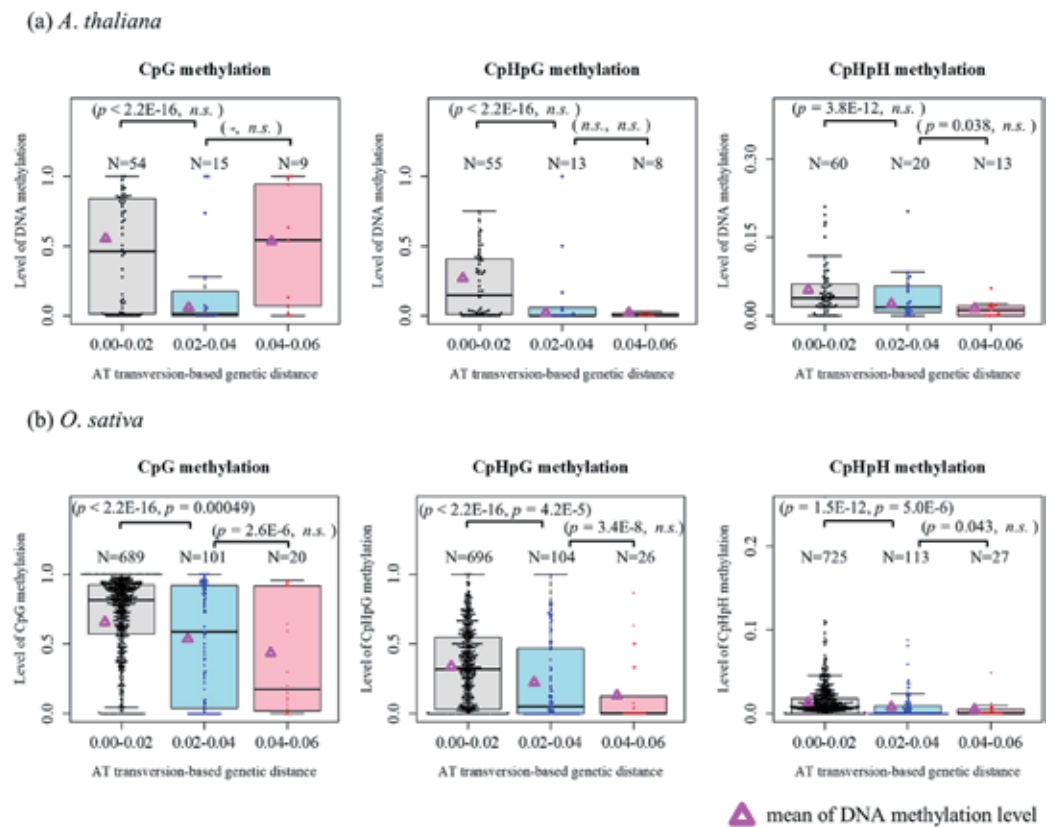


Figure 2. Comparison of DNA methylation level by integration time. Levels of DNA methylation at NUPTs were calculated for CpG, CpHpG and CpHpH sites and were plotted as dots and boxplots. The level of DNA methylation in NUPTs grouped by AT transversion-based genetic distance were plotted: black box/gray dots; small genetic distance (0.01 to 0.02), light blue box/blue dots; medium genetic (0.02 to 0.04), and pink box/red dots; (0.04 to 0.06). The mean of DNA methylation level was plotted by magenta triangles. The significance of statistical tests were shown in parentheses (X^2 test for methylated read counts, Wilcoxon rank sum test for distribution). *n.s.*; not significant. N is the number of NUPTs in each CpG/CpHpG/CpHpH dataset. NUPTs with no cytosine site of CpG/CpHpG/CpHpH context in each dataset were excluded from their plotting.

tion) was 0.26 at young aged NUPTs. In contrast, the ratio was nearly equal to 1 (1.21) at old NUPTs, suggesting a weakening of biased mutations depending on time after integration. Almost all species analyzed showed a similar pattern of alteration in substitution biases (Fig. S1, Table S2), suggesting a mechanism broadly common in higher plant species.

Nucleotide composition and patterns of integrated regions of NUPTs. The GC content of NUPTs was decreased in middle aged NUPTs (0.02 to 0.04, Table S2). The decrease of GC contents is consistent with the highly biased transitions at smaller genetic distances (shown in Fig. S1). The differences of GC contents between plastid genomes and NUPTs could be due to reduced G/C residues in majority of DNA fragments (Fig. S2). Compared with younger NUPTs, older NUPTs showed stronger correlation of GC-contents between NUPTs and its flanking regions in *A. thaliana* (Fig. S3). It may suggest that at least in *A. thaliana*, younger NUPTs are distinguishable from its flanking region by GC-content or sequence pattern of integrated DNA. Although *O. sativa* also showed correlation of GC-contents between NUPTs and its flanking regions, the relationship was weaker than that of *A. thaliana*. The gene abundance in flanking region of NUPTs (the number of genes in 50 Kb 5' and 3' flanking regions) was also surveyed (Fig. S4A). In *A. thaliana*, the gene abundance around young NUPTs (median: 18 genes/flanking region) was lower than that of older NUPTs. The density was then shifted towards average value of whole genome gene density (23 genes). There was no significant difference between gene abundance of young and older NUPTs. In *O. sativa*, medians of each integration time had no significant change and these values were similar to whole genome gene density (12 genes). Distances from nearest-neighbor gene showed no significant change among groups in both species (Fig. S4A). These results indicated that integrated NUPTs are eliminated somewhat regardless of gene density of its surrounding region.

Levels of CpG and non-CpG methylation in NUPTs. The levels of both CpG and non-CpG methylations for NUPTs were shown in Fig. 2. Interestingly, the levels of DNA methylation showed significant changes through their genetic distances. The levels of cytosine methylation in *O. sativa* were time-dependently decreased in both CpG and non-CpG motifs. In *A. thaliana*, DNA methylation of non-CpG methylation showed similar

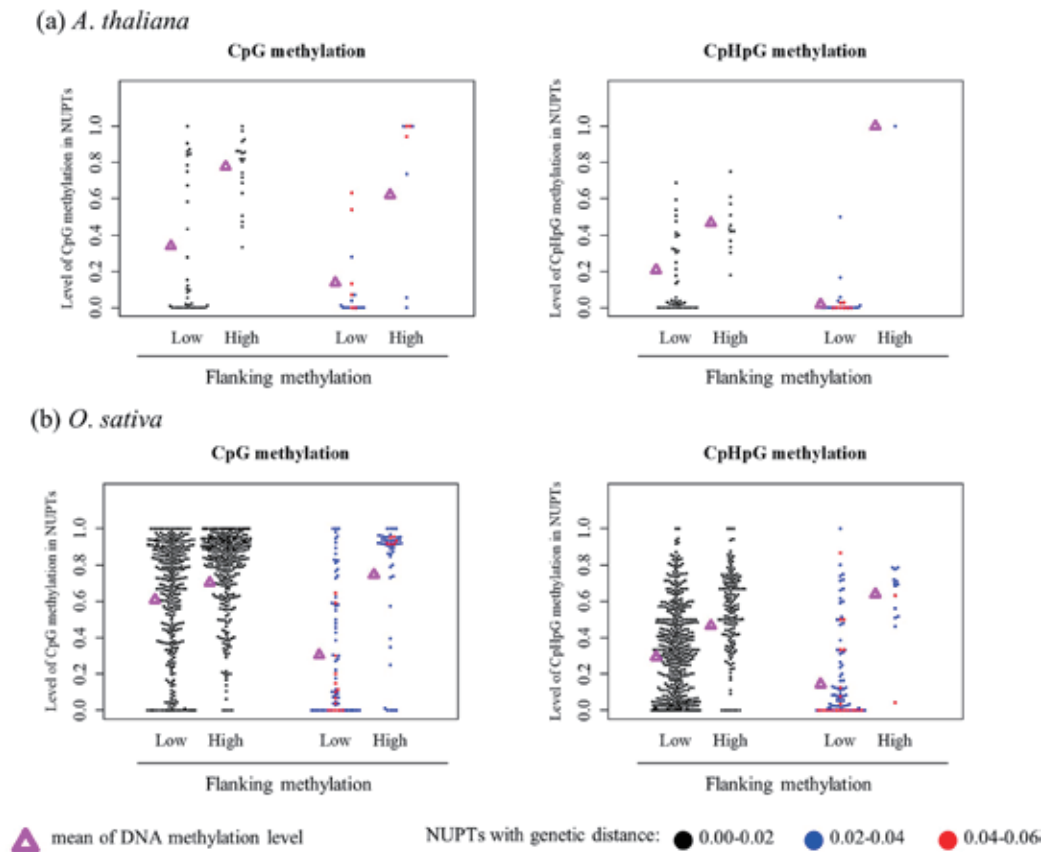


Figure 3. Possible effect of DNA methylation in flanking regions on NUPTs methylation. Adjacent sequences (1 Kb each) from both 5' and 3' flanking region of NUPTs were analyzed. Horizontal line represents a level of DNA methylation in flanking region: Low; DNA methylation level <0.5, High; DNA methylation level \geq 0.5. Vertical line represents a level of DNA methylation in NUPTs. The mean of DNA methylation level was plotted by magenta triangles.

pattern of reduction. The methylation level of CpG sites at old aged NUPTs was, however, increased compared with middle aged NUPTs. Because the number of older NUPTs was small ($N=9$), this increase of average CpG methylation was predominantly due to the presence of outliers that were strongly methylated (Fig. S5).

The highly methylated fragments with large genetic distances were also observed in *O. sativa* (Fig. S5). Most of such NUPTs were located on nearby the coding regions or within the intron of a gene (Table S3), suggesting effects of adjacent regions on the level of CpG methylation of NUPTs. Some older NUPTs would have remained hypermethylated because they are integrated too close to functional genes and hypermethylation of these NUPTs might be necessary for stable expression of adjacent genes.

The levels of DNA methylation at NUPTs were positively correlated with those at flanking sequences, especially in non-CpG methylations (Figs 3 and S6).

The DNA methylation level of NUPTs with larger genetic distance (middle and old aged NUPTs) was strongly associated with that of 5' and 3' flanking regions. In contrast, there were highly methylated NUPTs in the group of young aged NUPTs, regardless of low methylation level in flanking regions. The result indicates that the methylation status of older NUPTs depend on the same factor that decides the methylation status of their flanking regions. In contrast, the methylation status of young aged NUPTs is somewhat independent of that of their flanking regions and would be influenced by different factor(s). By these reasons, the methylation status of NUPTs would become similar to that of flanking regions according to integration time.

The observed pattern of DNA methylation levels (Fig. 2) indicates the sequence homology-dependent DNA methylation between NUPTs and their original plastid genome sequences, especially for younger NUPTs (Figs 3 and S6). Alternatively, the correlation between DNA methylation and the genetic distances may simply reflect the elimination of the highly methylated NUPTs; after new integrations, highly methylated NUPTs are predominantly eliminated from nuclear genomes. If it was true, newly integrated NUPTs would be hypermethylated not because of its homology to original plastid genome sequences, but because of its integrated location, GC-content, etc.

DNA methylation in mutant lines. The DNA methylation in NUPTs could have a similar role as that in defense against foreign DNAs and endogenous TEs. In *A. thaliana*, DNA methylation is established and maintained by several methyltransferases: *DNA Methyltransferase 1 (MET1)*, *Chromomethylase 3 & 2 (CMT3, CMT2)*, and *Domains Rearranged Methyltransferase 2 (DRM2)*^{28,29}. *DRM2* and other factors such as *Argonaute 4 (AGO4)*

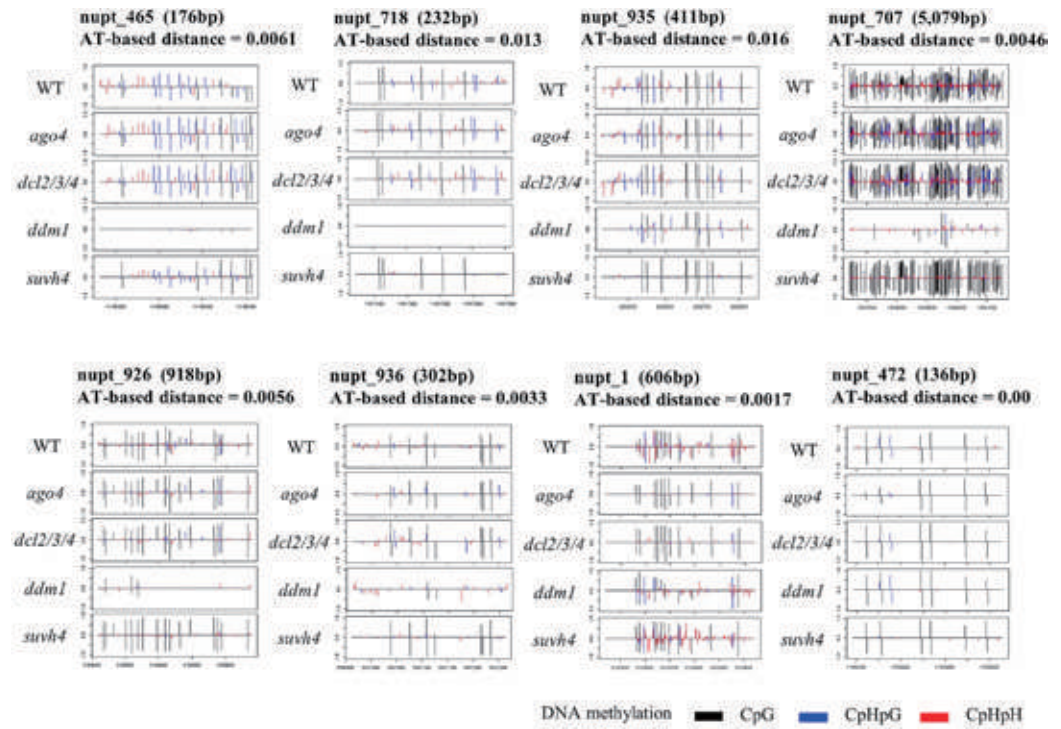


Figure 4. Status of DNA methylation in epigenetic mutant lines. Methylation status by whole genome methylome data. Proportion of CpHpG methylation in 8 representative NUPTs were shown. The sequence length and AT transversion-based genetic distance were also shown for each NUPT. DNA methylation level were shown by colored bars at each site: black; CpG methylation, blue; CpHpG methylation, red; CpHpH methylation.

and *Dicer-like 2/3/4* (*DCL2/3/4*) are involved in the RdDM machinery to repress TEs activity³⁰. In addition, there is a positive feedback between histone H3K9 methylation by *SU(VAR)3-9 HOMOLOG 4/KRYPTONITE* (*SUVH4/KYP*) and CpHpG and CpHpH methylation by *CMT3* and *CMT2*⁹. In *A. thaliana* genome wide methylome data from mutant lines of epigenetic regulation genes are available³¹ that allows us to determine possible mechanisms determining methylation status of NUPTs. In mutant lines of *AGO4* and *DCL2/3/4*, which might relate to RdDM machinery, many integrated NUPTs except 2 fragments showed no decrease of methylated CpG and non-CpG sites. In contrast, most NUPTs showed hypomethylated cytosines in *ddm1* mutant line (Figs 4 and S7). The results suggest that chromatin remodeling is associated with the maintenance of DNA methylation in NUPTs. Hypomethylations were also shown in both *suvh4/kyp*, *cmt3*, and *cmt2* mutants. The exceptional 2 NUPTs (nupt_1, nupt_472) showed loss of methylation in *ago4* and *dcl2/3/4* suggesting relation to RdDM-dependent methylation in these NUPTs. There are some TEs close to the 2 exceptional NUPTs (Table S4) that could affect the methylation pattern of adjacent NUPTs.

In *O. sativa*, *Osddm1a/1b* and *Osdrm2* whole-genome bisulfite-seq data^{32,33} were analyzed to verify the tendency observed in *A. thaliana*. Compared to *Osdrm2*, *Osddm1a/1b* showed more DNA hypomethylation of NUPTs especially for CpG and CpHpG contexts (Fig. 5). In all contexts, there were significant decreases of DNA methylation in *Osddm1a/1b* compared to DNA methylation in WT (Fig. 6), indicating that the DNA methylation of *O. sativa* NUPTs is also associated with chromatin remodeling factor as observed in *A. thaliana*. There were also significant decreases of CpHpH methylation in *Osdrm2*. In contrast, there was no significant difference between WT and *Osdrm2* CpG and CpHpG methylation (Fig. 6).

TE abundance in flanking regions of NUPTs. The difference of DNA methylation observed within NUPTs could be affected by the TE contents nearby NUPTs. To test the relationship between TEs contents and methylation level, we examined the TE abundance of 5 Kb 5' and 3' flanking regions (in total 10 Kb) for *A. thaliana* and *O. sativa* (Fig. 7). In *A. thaliana*, there was positive relationship between number of TEs and CpG/CpHpG methylation level (Pearson's $\rho = 0.2312$, $p = 0.032$ for CpG, $\rho = 0.3055$, $p = 0.0050$ for CpHpG, Fig. 7a), while there was no significant correlation with CpHpH methylation level ($\rho = 0.1627$, $p = 0.10$). In *O. sativa*, there was significant correlation between the TE number and CpHpG/CpHpH methylation level though the correlation coefficients were small ($\rho = 0.06560$, $p = 0.032$ for CpHpG, $\rho = 0.09323$, $p = 0.0019$ for CpHpH, Fig. 7b). The correlation of the TE number with CpG methylation level was not significant ($\rho = 0.02522$, $p = 0.42$). Although the result suggests positive correlation between TE contents in flanking regions and DNA methylation of NUPTs to some extent, the correlation coefficients are relatively small in both species.

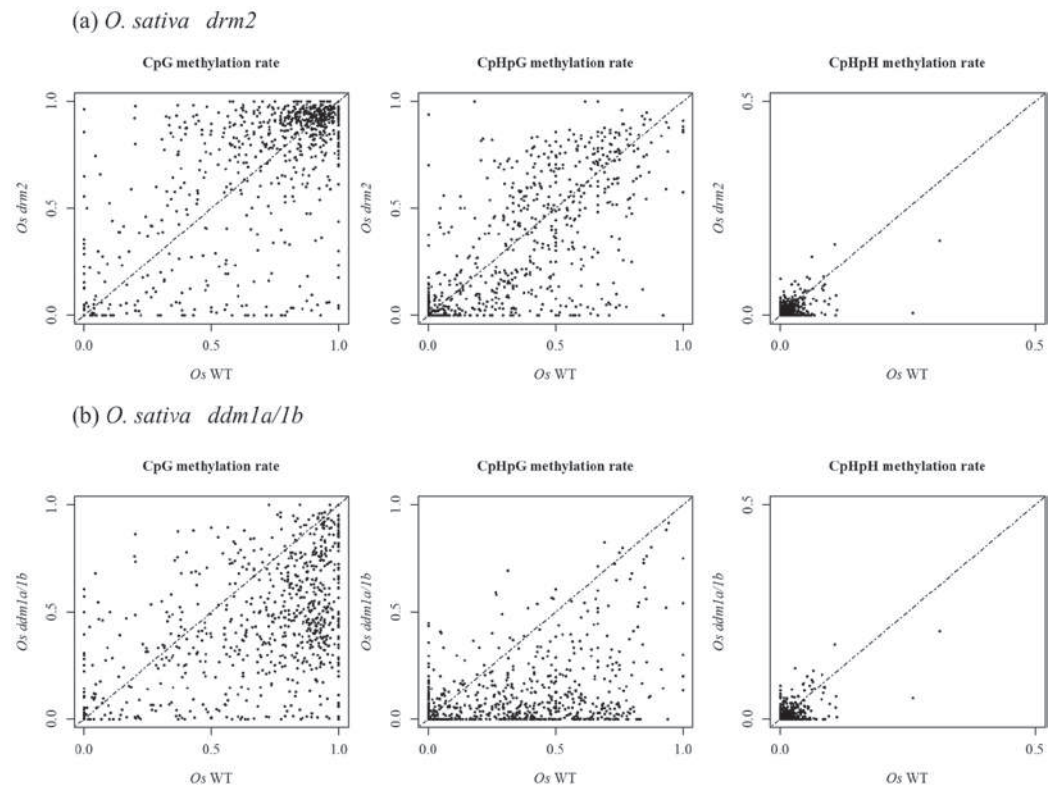


Figure 5. DNA methylation of *O. sativa* *drm2* and *ddm1a/1b* mutants. DNA methylation levels were plotted for *Osdrm2* (a) and *Osddm1a/1b* (b). Horizontal line represents the level of DNA methylation in WT. Vertical line represents the DNA methylation level of mutant line.

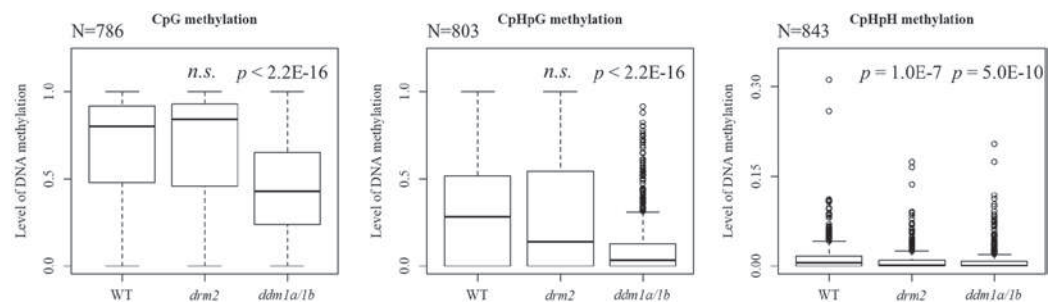


Figure 6. Comparison of DNA methylation level between *O. sativa* WT and mutants. Vertical line represents levels of DNA methylation in CpG, CpHpG and CpHpH contexts. Bold line represents medians. Upper and lower lines of boxes represent the first and third quartiles. Circle represents outliers. Wilcoxon rank sum test was conducted. *n.s.*; not significant.

Screening of mutant lines showing hypomethylated organellar DNA-like fragments. The methylome data analyses of *A. thaliana* epigenetic regulation gene mutants revealed genetic regulation on the methylation pattern of NUPTs. To elucidate the regulation pathways, over 5 thousand of EMS mutagenized lines were screened for the loss of NUPT DNA methylation by methylation-dependent endonuclease associated PCR (McrBC-PCR).

From the screening, 6 lines showed decrease of DNA methylation on organellar DNA-like fragments. Known genes involved in DNA methylation were checked for mutation within coding region by Sanger sequencing. All of 6 mutant lines had point mutations within coding regions of *DDM1*. In the analysis of mutant methylome data, *ddm1* single mutant shows significant decrease of DNA methylation in NUPTs (Figs 4 and S7), suggesting the strong effect of *ddm1* mutant on NUPTs' methylation. Although our screening method could successfully detect a single mutant with strong effect, i.e. *ddm1*, the screening did not reveal the novel factor involved in DNA methylation of NUPTs. It may suggest the complexity of the regulation mechanism of NUPTs' DNA methylation (e.g.,

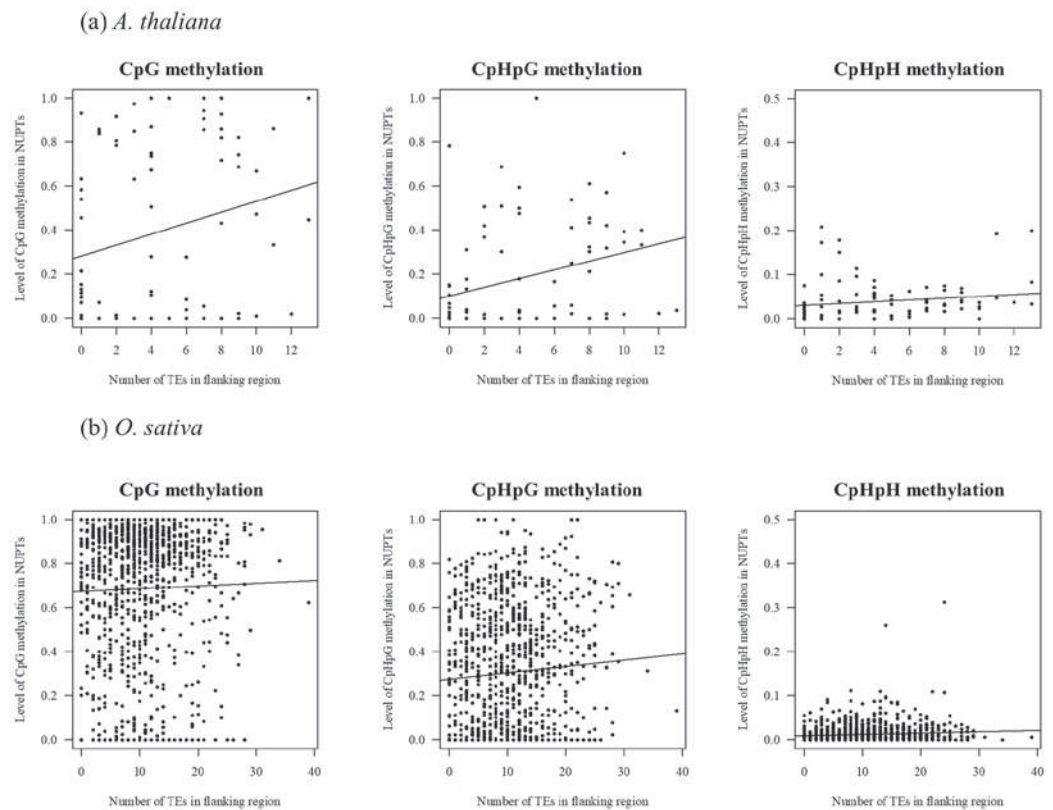


Figure 7. Relationship between levels of NUPT DNA methylation and TE contents in flanking regions. Horizontal line represents the number of TEs in 5 Kb each 5' and 3' flanking region. Vertical line represents level of DNA methylation. Solid line represents regression line for CpG, CpHpG, and CpHpH contexts.

the multiple factors and/or lethality of mutants in genes involved), rather than the presence of single responsible gene, and our screening method thus could not detect these potentially complex factors.

Discussion

After integration, NUPTs are unstable and are eliminated from host nuclear genome³⁴. The observation suggests that most *de novo* NUPTs and NUMTs are to some extent selectively deleterious^{25,35}. Our results suggest the epigenetic modification by DNA methylation against integrated NUPTs. DNA methylation observed in NUPTs may act as a genome defense for foreign DNA. This hypothetical genome defense against NUPTs by hypermethylation of NUPTs after integration may be partly sequence homology-dependent DNA methylation mechanism (Figs 2 and S5). The genome defense depending on sequence similarity is consistent with our previous results; most new integrations are deleterious and rapidly eliminated, while long-existing older NUPTs are less deleterious and have acquired mutations to become less homology²⁵.

We observed decreased GC content of middle aged NUPT compared to young aged NUPTs in all 17 species (Fig. S2). In *A. thaliana*, the increase of GC content in old aged NUPTs was also observed (Table S2). This pattern is similar to the change of GC content in TEs over time observed in *A. thaliana* genome³⁶. This observation could be explained by two mutation bias. While the younger TEs are under C→T mutational force by DNA methylation and succeeding deamination, sufficiently older TEs become out of the target of the DNA methylation machinery and are under influence of the basal mutation bias³⁶. Interestingly, while some species showed similar pattern of GC content change (*G. max*, *F. vesca*, *S. tuberosum*), the other species did not show the increase of GC content in old aged NUPTs (Table S2), implying the difference of the basal mutation bias or targeting mechanism for DNA methylation among species.

The results in this study revealed that *DDM1*, *CMT3*, *CMT2*, and *SUVH4/KYP* (Figs 4–6 and S7) affect the status of methylation in NUPTs. If most NUPTs cause deleterious effects on genome stability, they should be silenced and tightly-controlled like endogenous TEs. A major factor involved in repressing TEs in plants is DNA methylation. DNA methylation can be *de novo* induced by small interfering RNA². In addition, the DNA methylation can be maintained by DNA methyltransferases *MET1*, and the positive feedback of *CMT3/2* and *SUVH4*. For silencing of inserted DNAs in plant genomes, the feature of insertion sites such as genes and TEs abundance in those regions are important. The position effect and different mechanisms silencing the TEs are well documented for plant genome in which different mechanisms act on TEs inserted in different locations on the genome such as near genes, within genes, pericentromere, and centromeric regions³⁷. RdDM machinery is an important mechanism establishing DNA methylation to make the boundary of TEs in genic regions, while *CMT3/2* and *SUVH4*

act on maintaining such DNA methylation^{5,29,31}. In TE-rich regions such as pericentromeric region and heterochromatic knobs, chromatin remodeler *DDMI* is involved in keeping TEs silenced²⁹. The integrated NUPTs could be recognized and become the target of repression by such silencing mechanisms in different regions of nuclear genomes. Alternatively, the NUPTs are methylated by the effect of adjacent TEs in flanking regions in different manner of each region of the genome. The observation that the level of DNA methylation in NUPTs is related to the level of their flanking regions especially for older NUPTs indicates the effect of flanking regions on DNA methylation level (Fig. 3). There were weak but significant correlation between methylation level and TE contents in flanking regions (Fig. 7), suggesting the effect of TE silencing may be also elongated to the NUPTs. The methylome data showed significant decreases of CpHpH methylation in *ago4* and *Osdrm2* mutants (Figs 6 and S7), suggesting that a certain number of NUPTs in addition to 2 examples in Fig. 4 are affected by RdDM machinery in both *A. thaliana* and *O. sativa*. In previous study of TEs, it is suggested that the DNA methylation of TEs by RdDM machinery can remain active over extended periods of time³⁶, suggesting that middle/old aged NUPTs could be also affected by RdDM, as well as young aged NUPTs.

Some observations in this study might have difficulties being explained by the position effect solely. The level of DNA methylation and the rate of C/G to T/A nucleotide changes were decreased according to the genetic distance to the plastid genome sequence (Figs 1, 2 and S1, Table S2). Compared to older NUPTs, young NUPTs are prone to be methylated regardless of the methylation level of flanking regions (Fig. 3). The gene contents and distance from nearest gene were unchanged when comparing among NUPTs with different genetic distances (Fig. S4). Furthermore, there were weak correlation between the DNA methylation level of NUPTs and TE abundance in their flanking regions (Fig. 7). In *A. thaliana*, the DNA methylation could be *de novo* induced without accumulation of siRNA, possibly associated with the enrichment of histone methylation^{10,38}. In *A. thaliana*, the young TEs also showed higher level of DNA methylation compared to that of older TEs. Such homology-dependency was observed in both TEs with and without 24-nt small RNAs³⁶. A homology-dependent DNA methylation machinery could also act on NUPTs in addition to the maintenance methylation and RdDM.

In this study, we revealed a strong mutation bias of C/G to T/A transition in NUPTs of 17 species analyzed, possibly caused by DNA methylation and subsequent deamination of cytosine residues. The bias was associated with the genetic distances between plastid genome sequences and plastid DNA fragments in nuclear genomes. The results suggested that the transferred plastid DNA fragments are DNA methylated in nuclear genomes by common mechanisms for all species analyzed here. The non-CpG DNA methylation on genes probably transferred recently from organellar to nuclear genomic sequences were also observed in the study of wide range of angiosperms³⁹. The DNA methylation on NUPTs is thought to be mainly dependent on the methylation maintenance machinery, while some NUPTs are more affected by RdDM machinery. Some observations may imply another mechanism of homology-dependent DNA methylation against NUPTs, though the detail is obscure in this study. The DNA methylation on NUPTs may maintain the stability of plant nuclear genomes against the integration of organellar DNA fragments and contribute to the symbiosis of nuclear and organelle genomes. In the future, the mechanism that recognize and methylate the integrated NUPTs and their influence on the plant gene and genome evolution during the symbiosis of plastids should be investigated to reveal the whole figure of the regulation of organellar DNA-like sequences and evolutionary dynamics of the plant genomes.

Methods

Identification of plastid DNA in plant genomes. For analyses of molecular evolution, genome sequence data of 17 plants from publicly available database (NCBI: <http://www.ncbi.nlm.nih.gov/genome>, Phytozome: <http://www.phytozome.net>, and other genome consortium's databases) were used in this study (Table S1). To find homologous regions between nuclear and plastid genome sequences, program *blastn* implemented in BLAST ver.2.6.0 (<https://blast.ncbi.nlm.nih.gov/>) were used with default condition. Whole plastid genome sequences were used as queries for BLASTN search. BLAST hits with 100 bp or longer in length were collected as NUPT candidates. BLAST hits were manually inspected to remove completely identical/overlapped sequences. BLAST hits highly diverged from plastid sequences could be false positive of NUPTs. As we described later, we calculated AT transversion-based genetic distance as an indicator of homology between plastid and nuclear genomes. BLAST hits with the genetic distance larger than 0.06 were removed from NUPT candidates. Because some regions of plastid genomes have similarity to mitochondrial genomes, the origin of BLAST hits similar to such regions remains ambiguous. For 10 species with both plastid and mitochondrial genome sequences, plastid genome sequences similar to mitochondrial genomes were identified by BLASTN search between two organellar genomes. NUPT candidates homologous to such sequences were regarded as ambiguous sequences and were filtered out from the data set. The amount of ambiguous BLAST hits removed from the NUPT candidates were shown in Table S2. Finally, the remaining NUPT candidates were considered as NUPTs in this study. Because the key results of the following analysis were unchanged for all 10 species by the filtering of ambiguous sequences (Table S2, Fig. S1), the unfiltered data were used for the analysis of nucleotide changes in the remaining 7 species.

Molecular Evolutionary analyses. Nucleotide changes between plastid genomes and NUPTs were identified. Because plant organellar genomes have low mutation rate compared with nuclear genomes^{40–42}, we assumed majority of nucleotide substitutions had occurred in NUPTs. Based on this assumption, each substitution was classified into four categories: A/T to C/G transversions, C/G to A/T transversions, T/A to C/G transitions, and C/G to T/A transitions. Nucleotide substitutions were identified from the aligned sequences of BLAST search. Compositions of GC contents were also calculated for plastid DNAs and NUPTs. Alignment gaps and ambiguous nucleotides were removed from the aligned sequences and were not counted.

Genetic distances between plastid sequences and NUPTs were calculated to estimate relative integration time of NUPTs. Our results suggested biased direction of nucleotide substitutions from C/G to T/A transitions putatively caused by cytosine DNA methylation and subsequent deamination. Thus, we used transversions between

adenine (A) and thymine (T) that could have low effect by biased mutation to estimate genetic distances instead of p-distances calculated by all substitutions. This AT transversion-based genetic distance was calculated by following formula:

$$d_{AT} = \frac{(N_{A \rightarrow T} + N_{T \rightarrow A})}{L_{align}}$$

in which N_{AT} and N_{TA} represent A to T and T to A nucleotide change between plastid and nuclear sequences, L_{align} represents alignment sequence length without alignment gaps.

Levels of DNA methylation. We analyzed intensively sequenced DNA methylation data of 2 plants, *Arabidopsis thaliana*⁴³ and *Oryza sativa*⁴⁴ for analyses of CpG and non-CpG methylation within NUPTs. The mapped data of both species in previous study⁴⁵, were used in this study. In brief, the reference genomes (*A. thaliana*; Release 10 of the Arabidopsis Information Resources, *O. sativa*; Release 7 of the MSU Rice Genome Annotation Project) were processed to convert C/G to T/A for mapping of methylome data. The sequence data of both species (*A. thaliana*; GSE10966, *O. sativa*; GSE22591) were downloaded from Gene Expression Omnibus (GEO, available in: <https://www.ncbi.nlm.nih.gov/geo/>) and were mapped to the converted reference genomes by program Bowtie⁴⁶ under conditions described⁴⁷. Mapped reads were extracted and counted for each NUPT. For each NUPT, weighted methylation level⁴⁸ was calculated by following formula:

$$M_{weighted} = \frac{\sum_{i=1}^n C_i}{\sum_{i=1}^n (C_i + T_i)}$$

in which C_i and T_i represent methylated (C_i) and unmethylated (T_i) cytosine counts of the i_{th} cytosine site. NUPTs with no methylome data were excluded from the following analyses. Age distributions of CpG and non-CpG methylations were analyzed based on the genetic distance between plastid sequences and NUPTs. To analyze the effect of the status of adjacent regions on NUPTs, the level of cytosine methylations within flanking sequences was analyzed and correlations with methylation status of NUPTs were examined. Whole genome profiling of cytosine methylations reported in 86 *A. thaliana* mutant lines³¹ were used to survey the methylation status of NUPTs and to detect the factors involved in DNA methylation of these sequences. Single base-pair methylation data (GSE39901) were downloaded from GEO and were used for the analysis. To estimate the methylation pattern of *O. sativa ddm1a/1b, drm2* mutants^{32,33}, whole genome bisulfite-seq data (GSE108527, GSE81436) were downloaded from GEO. Sequence data were trimmed by Trimmomatic ver.0.36⁴⁹ and trimmed reads were mapped to reference genome by program *bismark* in Bismark suite ver. 0.14.4⁵⁰ using default parameters. Mapped reads were counted by program *bismark_methylation_extractor* implemented in Bismark suite.

TE and gene abundance in flanking regions of NUPTs. The relationship between feature of inserted site and NUPTs methylation level was analyzed using TAIR10 annotation information for *A. thaliana* and annotation information in Release 7 of the MSU Rice Genome Annotation Project for *O. sativa*. The number of genes in 50 Kb of each flanking region (in total 100 Kb region for each NUPT) and distance from nearest gene to NUPTs 5' or 3' end position were surveyed. The number of TEs in 5 Kb of each flanking region (in total 10 Kb region) was counted and correlation with DNA methylation level was tested.

Survey of genes responsible for DNA methylation of NUPTs. To find the candidate genes responsible for DNA methylation of NUPTs, the screen of *A. thaliana* mutant lines treated by ethyl methanesulfonate (EMS)^{45,51} was conducted. For screening, PCR primers for four organellar DNA-like fragments were designed. gDNA extracted from EMS mutant lines were digested by endonuclease McrBC which cleaves DNAs containing methylcytosine. If organellar DNA-like fragments are hypomethylated, PCRs with McrBC-digested gDNAs will amplify these hypomethylated DNAs. Multiplex PCR of 4 target regions were conducted.

References

- Castel, S. & Martienssen, R. RNA interference in the nucleus: roles for small RNAs in transcription, epigenetics and beyond. *Nat Rev Genet* **14**, 100–112 (2013).
- Martienssen, R. & Moazed, D. RNAi and heterochromatin assembly. *Cold Spring Harb Perspect Biol* **7**, a019323 (2015).
- Finnegan, J. E., Peacock, J. W. & Dennis, E. S. Reduced DNA methylation in *Arabidopsis thaliana* results in abnormal plant development. *Proc Natl Acad Sci USA* **93**, 8449–8454 (1996).
- Lindroth, A. *et al.* Requirement of CHROMOMETHYLASE3 for Maintenance of CpXpG Methylation. *Science* **292**, 2077–2080 (2001).
- Stroud, H. *et al.* Non-CG methylation patterns shape the epigenetic landscape in *Arabidopsis*. *Nat Struct Mol Biol* **21**, 64–72 (2014).
- Jackson, J. P., Lindroth, A. M., Cao, X. & Jacobsen, S. E. Control of CpNpG DNA methylation by the KRYPTONITE histone H3 methyltransferase. *Nature* **416**, 556–560 (2002).
- Johnson, L. M. *et al.* The SRA methyl-cytosine-binding domain links DNA and histone methylation. *Curr Biol* **17**, 379–384 (2007).
- Inagaki, S. *et al.* Autocatalytic differentiation of epigenetic modifications within the Arabidopsis genome. *EMBO J* **29**, 3496–3506 (2010).
- Du, J., Johnson, L. M., Jacobsen, S. E. & Patel, D. J. DNA methylation pathways and their crosstalk with histone methylation. *Nat Rev Mol Cell Biol* **16**, 519–532 (2015).
- Sasaki, T., Kobayashi, A., Saze, H. & Kakutani, T. RNAi-independent de novo DNA methylation revealed in *Arabidopsis* mutants of chromatin remodeling gene. *DDM1*. *Plant J* **70**, 750–758 (2012).
- McClintock, B. The origin and behavior of mutable loci in maize. *Proc Natl Acad Sci USA* **36**, 344–355 (1950).
- McClintock, B. The significance of responses of the genome to challenge. *Science* **226**, 792–801 (1984).
- Orgel, L. E. & Crick, F. H. C. Selfish DNA: the ultimate parasite. *Nature* **284**, 604–607 (1980).
- Bucher, E., Reinders, J. & Mirouze, M. Epigenetic control of transposon transcription and mobility in *Arabidopsis*. *Curr Opin Plant Biol* **15**, 503–510 (2012).

15. Oliver, K., McComb, J. & Greene, W. Transposable Elements: Powerful Contributors to Angiosperm Evolution and Diversity. *Genome Biol Evol* **5**, 1886–1901 (2013).
16. Hirsch, C. & Springer, N. Transposable element influences on gene expression in plants. *Biochimica Et Biophysica Acta* **1860**, 157–165 (2017).
17. Kleine, T., Maier, U. & Leister, D. DNA transfer from organelles to the nucleus: the idiosyncratic genetics of endosymbiosis. *Annu Rev Plant Biol* **60**, 115–138 (2009).
18. Timmis, J., Ayliffe, M., Huang, C. & Martin, W. Endosymbiotic gene transfer: organelle genomes forge eukaryotic chromosomes. *Nat Rev Genet* **5**, 123–135 (2004).
19. Leister, D. Origin, evolution and genetic effects of nuclear insertions of organelle DNA. *Trends Genet* **21**, 655–663 (2005).
20. Lin, X. *et al.* Sequence and analysis of chromosome 2 of the plant *Arabidopsis thaliana*. *Nature* **402**, 761–768 (1999).
21. Stupar, R. *et al.* Complex mtDNA constitutes an approximate 620-kb insertion on *Arabidopsis thaliana* chromosome 2: implication of potential sequencing errors caused by large-unit repeats. *Proc Natl Acad Sci USA* **98**, 5099–5103 (2001).
22. Matsuo, M., Ito, Y., Yamauchi, R. & Obokata, J. The rice nuclear genome continuously integrates, shuffles, and eliminates the chloroplast genome to cause chloroplast–nuclear DNA flux. *The Plant Cell* **17**, 665–675 (2005).
23. Smith, D., Crosby, K. & Lee, R. Correlation between nuclear plastid DNA abundance and plastid number supports the limited transfer window hypothesis. *Genome Biol Evol* **3**, 365–371 (2011).
24. Michalovova, M., Vyskot, B. & Kejnovsky, E. Analysis of plastid and mitochondrial DNA insertions in the nucleus (NUPTs and NUMTs) of six plant species: size, relative age and chromosomal localization. *Heredity* **111**, 314–320 (2013).
25. Yoshida, T., Furihata, H. Y. & Kawabe, A. Patterns of genomic integration of nuclear chloroplast DNA fragments in plant species. *DNA Res* **21**, 127–140 (2014).
26. Huang, C., Grünheit, N., Ahmadinejad, N., Timmis, J. & Martin, W. Mutational decay and age of chloroplast and mitochondrial genomes transferred recently to angiosperm nuclear chromosomes. *Plant Physiol* **138**, 1723–1733 (2005).
27. Noutsos, C., Richly, E. & Leister, D. Generation and evolutionary fate of insertions of organelle DNA in the nuclear genomes of flowering plants. *Genome Res* **15**, 616–628 (2005).
28. Law, J. & Jacobsen, S. Establishing, maintaining and modifying DNA methylation patterns in plants and animals. *Nat Rev Genet* **11**, 204–220 (2010).
29. Zemach, A. *et al.* The *Arabidopsis* nucleosome remodeler DDM1 allows DNA methyltransferases to access H1-containing heterochromatin. *Cell* **153**, 193–205 (2013).
30. Matzke, M. & Mosher, R. RNA-directed DNA methylation: an epigenetic pathway of increasing complexity. *Nat Rev Genet* **15**, 394–408 (2014).
31. Stroud, H., Greenberg, M., Feng, S., Bernatavichute, Y. & Jacobsen, S. Comprehensive analysis of silencing mutants reveals complex regulation of the *Arabidopsis* methylome. *Cell* **152**, 352–364 (2013).
32. Tan, F. *et al.* Analysis of Chromatin Regulators Reveals Specific Features of Rice DNA Methylation Pathways. *Plant Physiol* **171**, 2041–2054 (2016).
33. Tan, F. *et al.* DDM1 Represses Noncoding RNA Expression and RNA-Directed DNA Methylation in Heterochromatin. *Plant Physiol* **177**, 1187–1197 (2018).
34. Sheppard, A. & Timmis, J. Instability of Plastid DNA in the Nuclear Genome. *PLoS Genet* **5**, e1000323 (2009).
35. Yoshida, T., Furihata, H. Y. & Kawabe, A. Analysis of nuclear mitochondrial DNAs and factors affecting patterns of integration in plant species. *Genes Genet Syst* **92**, 27–33 (2017).
36. Maumus, F. & Quesneville, H. Ancestral repeats have shaped epigenome and genome composition for millions of years in *Arabidopsis thaliana*. *Nature Communications* **5**, 4104 (2014).
37. Sigman, M. & Slotkin, K. The First Rule of Plant Transposable Element Silencing: Location, Location, Location. *The Plant Cell* **28**, 304–313 (2016).
38. Rigal, M. *et al.* Epigenome confrontation triggers immediate reprogramming of DNA methylation and transposon silencing in *Arabidopsis thaliana* F1 epihybrids. *Proc Natl Acad Sci USA* **113**, E2083–E2092 (2016).
39. Niederhuth, C. E. *et al.* Widespread natural variation of DNA methylation within angiosperms. *Genome Biol* **17**, 194 (2016).
40. Wolfe, K. H., Li, W. H. & Sharp, P. M. Rates of nucleotide substitution vary greatly among plant mitochondrial, chloroplast, and nuclear DNAs. *Proc Natl Acad Sci USA* **84**, 9054–9058 (1987).
41. Gaut, B., Morton, B., McCaig, B. & Clegg, M. Substitution rate comparisons between grasses and palms: synonymous rate differences at the nuclear gene *Adh* parallel rate differences at the plastid gene *rbcl*. *Proc Natl Acad Sci USA* **93**, 10274–9 (1996).
42. Lynch, M., Koskella, B. & Schaack, S. Mutation pressure and the evolution of organelle genomic architecture. *Sci New York N Y* **311**, 1727–1730 (2006).
43. Lister, R. *et al.* Highly integrated single-base resolution maps of the epigenome in *Arabidopsis*. *Cell* **133**, 523–536 (2008).
44. Zemach, A., McDaniel, I., Silva, P. & Zilberman, D. Genome-Wide Evolutionary Analysis of Eukaryotic DNA Methylation. *Science* **328**, 916–919 (2010).
45. Saze, H. *et al.* Mechanism for full-length RNA processing of *Arabidopsis* genes containing intragenic heterochromatin. *Nat Commun* **4**, 2301 (2013).
46. Langmead, B., Trapnell, C., Pop, M. & Salzberg, S. L. Ultrafast and memory-efficient alignment of short DNA sequences to the human genome. *Genome Biol.* **10**, R25 (2009).
47. Chen, P. Y. Y., Cokus, S. J. & Pellegrini, M. BS Seeker: precise mapping for bisulfite sequencing. *BMC Bioinformatics* **11**, 203 (2010).
48. Schultz, M. D., Schmitz, R. J. & Ecker, J. R. ‘Leveling’ the playing field for analyses of single-base resolution DNA methylomes. *Trends Genet* **28**, 583–585 (2012).
49. Bolger, A. M., Lohse, M., & Usadel, B. Trimmomatic: A flexible trimmer for Illumina Sequence Data. *Bioinformatics* **btu170** (2014).
50. Krueger, F. & Andrews, S. Bismark: a flexible aligner and methylation caller for Bisulfite-Seq applications. *Bioinformatics* **27**, 1571–1572 (2011).
51. Saze, H., Shiraishi, A., Miura, A. & Kakutani, T. Control of genic DNA methylation by a jmjC domain-containing protein in *Arabidopsis thaliana*. *Science* **319**, 462–465 (2008).

Acknowledgements

We thank Prof. Toshiyuki Takano for the comment on the evolutionary analyses. We also thank two anonymous reviewers for their helpful comments and suggestions. This work was supported by MEXT Supported Program for the Strategic Research Foundation at Private Universities (S1511023 to AK), NIG-JOINT (2015B-3 to AK), Research Fellow of Japan Society for the promotion of Science (201508708 to TY), and JSPS Grant-in-aid for Early-Career Scientists (18K14758 to TY).

Author Contributions

T.Y. and A.K. wrote the manuscript text. T.Y. and H.Y.F. worked on genomic data analyses. A.K. and T.K. conceived experimental and analyses strategies. T.Y. and T.K.T. analyzed EMS mutant lines of *A. thaliana*. All authors read and approved the manuscript.

Additional Information

Supplementary information accompanies this paper at <https://doi.org/10.1038/s41598-019-38607-6>.

Competing Interests: The authors declare no competing interests.

Publisher's note: Springer Nature remains neutral with regard to jurisdictional claims in published maps and institutional affiliations.



Open Access This article is licensed under a Creative Commons Attribution 4.0 International License, which permits use, sharing, adaptation, distribution and reproduction in any medium or format, as long as you give appropriate credit to the original author(s) and the source, provide a link to the Creative Commons license, and indicate if changes were made. The images or other third party material in this article are included in the article's Creative Commons license, unless indicated otherwise in a credit line to the material. If material is not included in the article's Creative Commons license and your intended use is not permitted by statutory regulation or exceeds the permitted use, you will need to obtain permission directly from the copyright holder. To view a copy of this license, visit <http://creativecommons.org/licenses/by/4.0/>.

© The Author(s) 2019



Ser-Gln sites of SOG1 are rapidly hyperphosphorylated in response to DNA double-strand breaks

K. O. Yoshiyama & S. Kimura

To cite this article: K. O. Yoshiyama & S. Kimura (2018): Ser-Gln sites of SOG1 are rapidly hyperphosphorylated in response to DNA double-strand breaks, *Plant Signaling & Behavior*, DOI: [10.1080/15592324.2018.1477904](https://doi.org/10.1080/15592324.2018.1477904)

To link to this article: <https://doi.org/10.1080/15592324.2018.1477904>



Published online: 25 Jun 2018.



Submit your article to this journal [↗](#)



View related articles [↗](#)



View Crossmark data [↗](#)

SHORT COMMUNICATION



Ser-Gln sites of SOG1 are rapidly hyperphosphorylated in response to DNA double-strand breaks

K. O. Yoshiyama ^{a,c} and S. Kimura ^{a,b}

^aDepartment of Bioresource and Environmental Sciences, Kyoto Sangyo University, Kyoto, Japan; ^bCenter for Ecological Evolutionary Developmental Biology, Kyoto Sangyo University, Kyoto, Japan; ^cDepartment of Molecular and Chemical Life Sciences, Tohoku University, Sendai, Japan

ABSTRACT

The DNA damage response system (DDR) is crucial in addressing DNA double-strand breaks (DSBs), which pose a severe threat to genomic integrity. The SOG1 transcription factor is a master regulator of the *Arabidopsis thaliana* DDR. We previously showed that hyperphosphorylation of five Ser-Gln sites of SOG1 is the molecular switch to activate the DDR. In this study, we determined that SOG1 is hyperphosphorylated within 20 minutes following DSB-inducing treatment, followed by activation of several SOG1 target genes. Using SOG1 phosphorylation mutants, we demonstrated that although the hyperphosphorylation sites remain unchanged over time, the amount of hyperphosphorylation gradually increases. These observations suggest that rapid SOG1 hyperphosphorylation is limited by the amount of active kinases.

Abbreviations: SOG1, suppressor of gamma response; ATM, Ataxia telangiectasia mutated; ATR, ATM and Rad3-related

ARTICLE HISTORY

Received 22 February 2018
Accepted 13 May 2018

KEYWORDS

DNA damage response;
hyperphosphorylation;
SOG1; *A. thaliana*

Introduction

A sophisticated network of DNA damage response (DDR) systems has evolved to address the fundamental problem of genomic erosion.¹ The DDR of *Arabidopsis thaliana* involves DNA repair, cell-cycle arrest, endoreduplication, and programmed cell death.²⁴ Ataxia telangiectasia mutated (ATM) and ATM and Rad3-related (ATR) kinases are the central regulators of this network.⁵⁷ ATM and ATR are activated by DNA double-strand breaks (DSBs) and DNA replication stress, respectively, resulting in the phosphorylation of hundreds of target proteins. These phosphorylation events are crucial for activating downstream pathways.

The SOG1 transcription factor is also critical for regulating an appropriate DDR.² This transcription factor was originally isolated as a suppressor mutant of IR-induced cell cycle arrest of *A. thaliana xpf-2* mutants, which lack functional XPF repair endonuclease.⁸ SOG1 is one of the NAC (NAM, ATAF1/2, and CUC2) proteins, which constitute one of the largest families of plant-specific transcription factors.² SOG1 is the first identified plant-specific transcription factor involved in the DDR pathway. SOG1 protein is observed in meristematic tissues, such as the shoot and root apical meristem, lateral root primordium, root stele and young flowers.^{9,10} This observation is consistent with the fact that the DDR is important in actively dividing cells.

DNA damage in *A. thaliana* induces rapid and robust change in the transcriptional regulation of numerous genes.^{2,7} These changes in gene expression activate DNA repair, cell-cycle arrest, endoreduplication, and programmed cell death. Mutation of SOG1 causes various defects in the activation of these responses, indicating that SOG1 is a master regulator of the DDR. DSB-inducing treatment promotes hyperphosphorylation of SOG1, which is required to activate the DDR.

SOG1 contains three domains: the N-terminal extension, the central NAC domain, and the C-terminal transcription regulatory domain (Figure 1A). The C-terminus of SOG1 has five SQ (serine-glutamine) sites (350SQ, 356SQ, 372SQ, 430SQ, 436SQ), which are known as preferred sites for phosphorylation by ATM and ATR (Figure 1A). We previously showed that these five SQ sites are hyperphosphorylated in response to DSBs.⁹ Hyperphosphorylation of SOG1 induced by DSBs appears to be dependent on ATM, as it does not occur in ATM mutants.⁹ This suggests that SOG1 functions downstream of ATM and that ATM-dependent hyperphosphorylation of SQ motifs is essential for SOG1 functions.

We recently demonstrated that increased phosphorylation of SQ sites strengthens the DDR, as shown through mutation of SQ motifs (SQ to AQ) and study of SOG1 mutant lines with differing numbers of SQ phosphorylation sites.¹¹ Our data also suggest that there is no relationship between the amount of DNA damage and the number of SOG1 hyperphosphorylation sites.¹¹

CONTACT S. Kimura  seisuke@cc.kyoto-su.ac.jp  Department of Bioresource and Environmental Sciences, Kyoto Sangyo University, Kamigamo Motoyama Kitaku, Kyoto 603-8555, Japan; Center for Ecological Evolutionary Developmental Biology, Kyoto Sangyo University, Kamigamo Motoyama Kitaku, Kyoto 603-8555, Japan

Color versions of one or more of the figures in the article can be found online at www.tandfonline.com/kpsb.

© 2018 Taylor & Francis Group, LLC

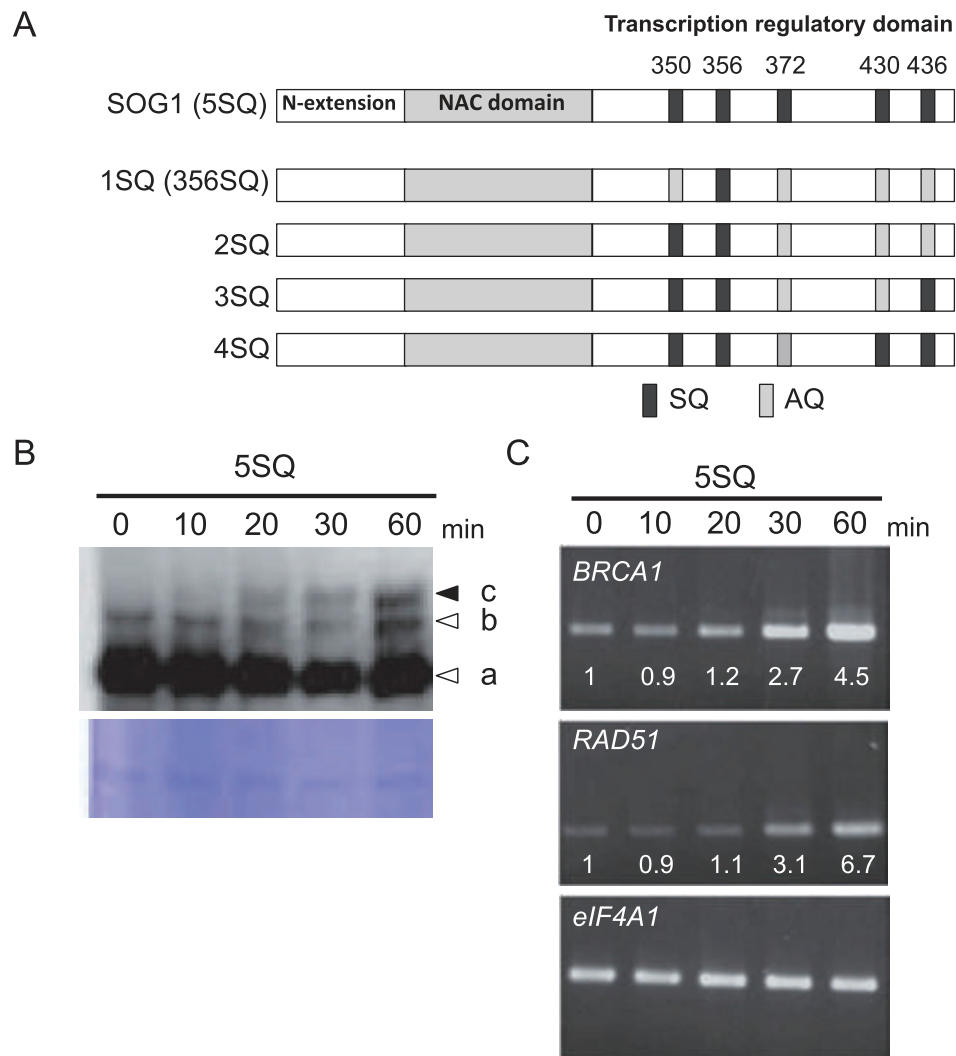


Figure 1. Time-dependent phosphorylation pattern of SOG1 and the activation of downstream genes.

Results

The function of SOG1 as a master regulator of DDR suggests that rapid SOG1 activation should occur in response to DNA damage. To examine this possibility, immunoblotting was used to observe SOG1 hyperphosphorylation over time after treatment with zeocin, a DSBs-inducing agent. We used *A. thaliana sog1-1* transgenic plants expressing *ProSOG1:SOG1(5SQ)-Myc* (5SQ line), in which the promoter and coding regions of SOG1 are fused in-frame to a 10 × Myc tag. As we previously reported, independently of DNA damage, an anti-Myc antibody detected a band for nonphosphorylated SOG1-Myc (band a) and a slower migrating band for phosphorylated SOG1-Myc (band b), with both bands consistently observed (Figure 1B). We found that hyperphosphorylated SOG1-Myc (band c), which is DNA damage dependent, was visible at 20 min after zeocin treatment in SOG1-5SQ, with band intensity incrementally increasing in a time-dependent manner (20 min–60 min) (Figure 1B). This observation indicates that SOG1 hyperphosphorylation occurs rapidly and that the phosphorylation level is incrementally induced over time. This rapid phosphorylation is consistent with the function of SOG1, as an upstream regulator of DDR.

We then investigated whether downstream target genes of SOG1 are also rapidly activated following DNA damage. Therefore, we evaluated the expression of *BRCA1* and *RAD51*, which are DNA repair genes and direct targets of SOG1¹². 5SQ seedlings were treated with 1 mM zeocin, and total RNA was extracted from root tips at several time points (0, 10, 20, 30, and 60 min). *BRCA1* and *RAD51* were faintly expressed at 0 min, the induction of both genes was observed at 30 min, and the induction became more pronounced at 60 min (Figure 1C). There was a time lag between SOG1 hyperphosphorylation and the activation of downstream genes. These results indicate that following DSB induction, SOG1 is hyperphosphorylated within 20 minutes and SOG1 target genes are induced within 30 minutes.

We next examined whether the number of SOG1 hyperphosphorylation sites changes over time following DNA damage exposure. We hypothesized that few SQ sites would be phosphorylated, immediately following DNA damage, with the number of phosphorylated SQ sites gradually increasing over time. The hyperphosphorylation patterns of various mutant strains [*ProSOG1:SOG1(1SQ-4SQ)-Myc*] (1SQ: 356SQ, 2SQ: 350SQ,

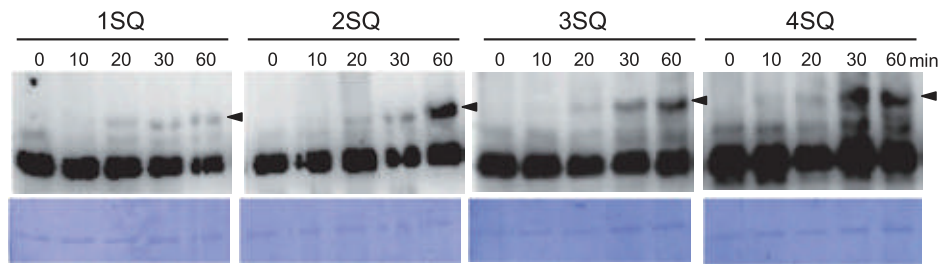


Figure 2. Time-dependent phosphorylation pattern of SOG1 phosphorylation mutants.

356SQ, 3SQ: 350AQ, 356AQ, 436AQ, 4SQ: 350SQ, 356SQ, 430SQ, 436SQ) were evaluated at different time points (Figure 2). Although hyperphosphorylation levels gradually increased over time for all mutant strains, there was no difference in the band pattern among phosphorylation mutants (Figure 2). These data suggest that there is no relationship between the time that has elapsed following DNA damage exposure and the number of SOG1 hyperphosphorylation sites.

Discussion

The integrity of plant chromosomes is under constant assault from a variety of DNA damaging factors. DSBs are one of the most cytotoxic types of DNA damage, and prompt repair is essential. In this study, we demonstrated that SOG1 hyperphosphorylation is induced within 20 minutes following zeocin treatment, indicating that DDR mediated by SOG1 is rapidly activated by DSBs. Furthermore, we showed that there is a time lag of approximately 10 min after phosphorylation before the induction of several SOG1 target genes can be observed.

Our prior data show that SOG1 hyperphosphorylation (band c) increases with the amount of DNA damage⁹; here, we demonstrated that the intensity of hyperphosphorylated bands for SOG1 mutants gradually increases over time. Furthermore, it was shown that SQ sites seem to be equally phosphorylated, as the change in phosphorylation pattern is similar among mutants. These results indicate that hyperphosphorylation at SQ sites is not dependent on the amount of DNA damage or the time since this damage occurred; however, the hyperphosphorylation frequency at SQ sites seems to be dependent on these two factors. We previously showed that the phosphorylation of all five SQ sites is required for the full activation of SOG1¹¹. 356SQ is the first phosphorylation sites, and this phosphorylation triggers the phosphorylation of other SQ sites¹¹. However, we were not able to identify a phosphorylation order in this study, perhaps because the phosphorylation events occur quite rapidly.

In mammalian cells, ATM has been shown to exist as inactive dimers in undamaged cells that rapidly undergo autophosphorylation after exposure to DNA damage-inducing agents and dissociate into active monomers.¹³ Because SQ motifs are target amino acids of ATM, active ATM may equally phosphorylate each SQ motif of SOG1. Therefore, the amount of hyperphosphorylation of SOG1 may be limited by the amount of active ATM, which is regulated by the amount of DNA damage and time. Further research is needed

to determine how the 356SQ site undergoes phosphorylation first. As protein phosphorylation can directly affect distinct aspects of transcription factor function by regulating protein-protein interactions and DNA binding,¹⁴ it will be important to determine whether SOG1 hyperphosphorylation modifies target DNA directly or affects interacting factors. Future studies are needed to fully comprehend the role of SOG1 hyperphosphorylation in the DNA damage response.

Materials and methods

Plant materials and growth conditions

The *Arabidopsis thaliana* plants used in this study were grown on MS media [1 × MS salts including vitamins, 2% (w/v) sucrose, pH 6.0, 0.8% (w/v) gellan gum agar for solid medium] under continuous light conditions at 22°C. The accession Columbia (Col-0) was used as the wild-type strain, the *sog1-1* line and transgenic SOG1 phosphorylation mutant lines have been described previously^{2,11}.

Immunoblotting

Five-day-old seedlings were transferred to MS liquid medium containing 0 or 1 mM zeocin. After a 1 h incubation, a pool of root tips (approximately 100 seedlings) was excised and ground in the following buffer: 10 mM Tris (pH 7.6), 150 mM NaCl, 2 mM EDTA, 0.5% (v/v) Nonidet P-40 (Nacalai Tesque), 1 mM DTT, a protease inhibitor cocktail (Sigma-Aldrich), and a phosphatase inhibitor cocktail (0.1 mM Na₃VO₄, 1 mM NaF, 60 mM β-glycerophosphatase, and 20 mM p-nitrophenylphosphate). The slurry was centrifuged twice to remove debris, and the supernatant was recovered and used for subsequent analysis. Proteins (1 μg) were separated using an 8% SDS-PAGE gel containing 30 μM Phos-tag and 30 μM MnCl₂. The Phos-tag reagent (NARD Institute) was used for identification of phosphorylated SOG1 protein. Phosphorylated SOG1 is visualized as bands that migrate slower than those of non-phosphorylated proteins. After electrophoresis, the proteins were electroblotted to a polyvinylidene difluoride (PVDF) membrane (Merck Millipore) in the following buffer: 6.3 mM NaHCO₃, 4.3 mM Na₂CO₃, (pH 9.5), and 20% methanol. Because SOG1-Myc can be detected using an anti-Myc antibody, the membrane was incubated for 2 h at room temperature in the anti-Myc primary antibody A-14 (1:2000 dilution, Santa Cruz Biotechnology), rinsed 3 times with 1 × TBST, and incubated with an anti-rabbit immunoglobulin horseradish peroxidase-conjugated secondary antibody (1:4000, Promega) to detect SOG1-Myc. Next the

membrane was washed 3 times with $1 \times$ TBST and processed with a LAS-4000 luminescent image analyzer (Fujifilm) after incubation with the ECL Prime enhanced chemiluminescence kit (GE Healthcare).

Semi-quantitative RT-PCR analysis

Five-day-old seedlings were transferred to MS liquid medium containing 0 or 1000 μ M zeocin. After 0, 10, 20, 30, and 60 min incubation, total RNA was extracted from a pool of root tips containing approximately 100 seedlings using an RNeasy Plant Mini Kit (Qiagen) following to the manufacturer's instructions. All samples were treated with DNase I on a column using the Qiagen RNase-Free DNase Set (Qiagen) and quantified. To produce cDNA for qRT-PCR, 0.3 μ g of total RNA was reverse-transcribed, using Prime Script RT reagent kit (TAKARA), according to the manufacturer's protocol. The expression level relative to that measured at 0 min was calculated using the value of the relative RNA levels normalized to the internal control *ELF4A-1* (eukaryotic translation initiation factor 4A-1, At3g13920). The following primer sets were used: *ELF4A1* control primers (*elf4A1* and *elf4A5*); *BRCA1* primers (*brca1F2* and *brca1RtR2*); and *RAD51* primers (*rad51AF1* and *rad51ArtR1*), which are found in Supplemental Table 1.

- (A) Structural features of SOG1 and phosphorylated mutant SOG1. The N-terminal extension, NAC domain, and transcription regulatory domain are shown. The five Ser-Gln (SQ) motifs are represented by dark gray boxes, and the mutated motifs (Ala-Gln) are represented by light gray boxes. (B) Detection of the phosphorylated form of SOG1. *sog1-1* lines harboring *ProSOG1:SOG1 [5SQ]-Myc* were used. Five-day-old seedlings grown on MS plates were transferred to liquid medium containing 1 mM zeocin, and total protein from root tips was extracted 0, 10, 20, 30, and 60 min later. Phosphorylated forms of SOG1 were detected using an SDS-PAGE gel containing Phos-tag. Coomassie blue staining is shown below. Nonphosphorylated and phosphorylated SOG1-Myc (bands a and b) are indicated by white arrow heads, and hyperphosphorylated SOG1-Myc (bands c) is indicated by black arrowheads. (C) Semiquantitative RT-PCR analysis of *BRCA1* and *RAD51*. *sog1-1* lines harboring *ProSOG1:SOG1 [5SQ]-Myc* were used. Five-day-old seedlings grown on MS plates were transferred to liquid medium containing 1 mM zeocin, and total RNA was extracted from root tips 0, 10, 20, 30, and 60 min later. Using the total RNA, cDNA was prepared and RT-PCR was performed. The RT-PCR product of *elf4A* (eukaryotic initiation factor) was employed as a standard for RT-PCR amplification. The number below each band denotes its relative expression level (first normalized to *elf4A*) compared to the sample at 0 min. Average from two biological replicates was shown.

sog1-1 lines harboring *ProSOG1:SOG1 [1SQ (356SQ), 2SQ, 3SQ, and 4SQ]-Myc* were used. Hyperphosphorylated SOG1-

Myc (bands c) is indicated by black arrowheads. Coomassie blue staining is shown below. This experiment was conducted similarly to the ones shown in Figure 1B.

Disclosure of Potential Conflicts of Interest

No potential conflicts of interest were disclosed.

Funding

This work was supported by JSPS KAKENHI (13J40017 and 17K07455 to K.O.Y., 16H01472, 16K07408, 18H04787 and 18H04844 to S. K.) and by the MEXT Supported Program for the Strategic Research Foundation at Private Universities from the Ministry of Education, Culture, Sports, Science & Technology of Japan, Grant Number S1511023 to S.K.

ORCID

K. O. Yoshiyama  <http://orcid.org/0000-0002-8115-4778>
S. Kimura  <http://orcid.org/0000-0002-6796-3675>

References

- Ciccia A, Elledge SJ. The DNA damage response: making it safe to play with knives. *Mol Cell*. 2010;40:179–204.
- Yoshiyama K, Conklin PA, Huefner ND, Britt AB. Suppressor of gamma response 1 (SOG1) encodes a putative transcription factor governing multiple responses to DNA damage. *Proc Natl Acad Sci U S A*. 2009;106:12843–12848.
- Adachi S, Minamisawa K, Okushima Y, Inagaki S, Yoshiyama K, Kondou Y. Programmed induction of endoreduplication by DNA double-strand breaks in Arabidopsis. *Proc Natl Acad Sci U S A*. 2011;108:10004–10009.
- Furukawa T, Curtis MJ, Tominey CM, Duong YH, Wilcox BW, Aggoune D, Hays JB, Britt AB. A shared DNA-damage-response pathway for induction of stem-cell death by UVB and by gamma irradiation. *DNA Repair (Amst)*. 2010;9:940–948.
- Culligan K, Tissier A, Britt A. ATR regulates a G2-phase cell-cycle checkpoint in Arabidopsis thaliana. *Plant Cell*. 2004;16:1091–104.
- Garcia V, Bruchet H, Comesca D, Granier F, Bouchez D, Tissier A. AtATM is essential for meiosis and the somatic response to DNA damage in plants. *Plant Cell*. 2003;15:119–132.
- Culligan KM, Robertson CE, Foreman J, Doerner P, Britt AB. ATR and ATM play both distinct and additive roles in response to ionizing radiation. *Plant J*. 2006;48:947–961.
- Preuss SB, Britt AB. A DNA-damage-induced cell cycle checkpoint in Arabidopsis. *Genetics*. 2003;164:323–334.
- Yoshiyama KO, Kobayashi J, Ogita N, Ueda M, Kimura S, Maki H, Umeda M. ATM-mediated phosphorylation of SOG1 is essential for the DNA damage response in Arabidopsis. *EMBO Rep*. 2013;14:817–822.
- Yoshiyama KO. SOG1: a master regulator of the DNA damage response in plants. *Genes Genet Syst*. 2016;90:209–216.
- Yoshiyama KO, Kaminoyama K, Sakamoto T, Kimura S. Increased phosphorylation of Ser-Gln sites on SUPPRESSOR OF GAMMA RESPONSE1 strengthens the DNA damage response in Arabidopsis thaliana. *Plant Cell*. 2017;29:3255–3268.
- Ogita N, Okushima Y, Tokizawa M, Yamamoto YY, Tanaka M, Seki M, Makita Y, Matsui M, Okamoto-Yoshiyama K, Sakamoto T, et al. Identifying the target genes of SUPPRESSOR OF GAMMA RESPONSE 1, a master transcription factor controlling DNA damage response in Arabidopsis. *Plant J*. 2018;94:439–453.
- Bakkenist CJ, Kastan MB. DNA damage activates ATM through intermolecular autophosphorylation and dimer dissociation. *Nature*. 2003;421:499–506.
- Hill CS, Treisman R. Transcriptional regulation by extracellular signals: mechanisms and specificity. *Cell*. 1995;80:199–211.

Review

Plant Temperature Sensors

Tomoaki Sakamoto ^{1,2}  and Seisuke Kimura ^{1,2,*} 

¹ Department of Bioresource and Environmental Sciences, Kyoto Sangyo University, Kamigamo Motoyama Kitaku, Kyoto 603-8555, Japan; k5774@cc.kyoto-su.ac.jp

² Center for Ecological Evolutionary Developmental Biology, Kyoto Sangyo University, Kamigamo Motoyama Kitaku, Kyoto 603-8555, Japan

* Correspondence: seisuke@cc.kyoto-su.ac.jp

Received: 29 October 2018; Accepted: 6 December 2018; Published: 10 December 2018



Abstract: Temperature is one of the most important environmental signals for plants. High and low temperatures have a variety of effects that affect plant growth and development profoundly. Further, temperature is an indication of seasonal change. Plants must survive under severe conditions in winter and prepare to resume growth and reach their reproductive stage in the following spring. Recent studies have focused on plant mechanisms responsible for sensing temperature and the molecular systems underlying plant reactions in response to this signal. In this review, we describe how plants sense ambient temperature to adapt to ambient-temperature changes.

Keywords: temperature sensor; phytochrome; heat shock transcription factor A1s

1. Temperature and Living Organisms

Living organisms can be found in widespread regions of the world. Each habitat consists of a certain set of environmental factors, among which one of the most important for any organism is ambient temperature. In some habitats, temperatures may be higher than 40 °C or lower than freezing point. Temperatures outside the narrow range within which a given living organism finds itself comfortable are not suitable for successful growth and reproduction and, indeed, might be harmful and even limiting to survival. Temperature affects different biological phenomena in living organisms, for example, enzyme activity is markedly temperature dependent, and molecular processes working inside organisms are regulated by enzymes that show optimal temperature ranges for best performance. Homeotherms, such as mammals, keep body temperature within a narrow optimal range through the production of heat inside their body, and by a set of thermoregulation mechanisms. Other animals move away in an attempt to escape severe environmental temperature changes. As this is impossible for plants, they do their best to adapt to temperature change by modulating their physiological function in response to temperature changes. Temperature also acts as a seasonal signal for plants. In temperate zones, temperature and other environmental factors change seasonally. Because some seasonal conditions are not favorable for plants, they stop growing and do not reproduce for prolonged periods while severe conditions prevail, and adjust so as to grow in the preferred condition. Some systems of plant adaptation use regular, periodical change in ambient temperature as a cue for sensing seasonal change.

The study of the plant response systems to temperature change has revealed the underlying molecular mechanisms. Here, we review the plant temperature response systems and the core mechanisms of temperature sensors.

2. Effects of Temperature on Growth and Development

Plants have systems that regulate their internal physiological reactions according to ambient temperature. As a result, plants sometimes show modulation of growth and morphological changes in response to temperature changes.

2.1. Tissue Elongation under High Temperature

Light condition affects tissue size. In the dark, seedlings grow long hypocotyls and etiolated cotyledons, like soybean sprouts. High temperature also causes tissue elongation. For example, the hypocotyl of *Arabidopsis thaliana* elongated at high temperature even in the presence of light [1]. Leaf petiole elongation and leaf hyponasty responses were also studied in *A. thaliana* under high temperature [2]. The hyponastic response consists of an upward bending of the petiole by increased cell elongation on their lower longitudinal side. At low temperature leaves grew horizontally, while at high temperature the angle of leaf turned upright.

2.2. Leaf Shape Modification

Leaf shape is another aspect of plant development affected by temperature. Some plants show a change in leaf shape induced by an environmental cue; this phenomenon is called heterophylly. *Rorippa aquatica*, a semi-aquatic plant that lives both on land and in water, grows leaves with different shapes under different growing conditions. When submerged, the leaves become narrow and highly dissected, compared to those grown on land. Furthermore, under high temperature the plant developed round simple leaves, while low temperature induced dissected compound leaves [3]. Leaves of red maple trees (*Acer rubrum*) grown under cooler temperatures tended to have more teeth on the leaf edge and to be more highly dissected [4].

A similar phenomenon was studied in the pitcher plant, *Cephalotus follicularis* [5]. In addition to normal flat leaves, this carnivorous plant is provided with pitcher leaves to capture insects. The ratio of pitcher to flat leaves varied depending on temperature. Most leaves were flat at 15 °C, while about 90% of them developed into pitcher leaves at 25 °C.

2.3. Thermotolerance

For any given plant species, temperatures above physiological range eventually cause cellular metabolic imbalance, thereby interfering with growth and reproductive development, and eventually lead to death. Thermotolerance is the resistance to high temperature. Plants have evolved both an inherent resistance to high temperature (basal thermotolerance) and an ability to activate tolerance in response to heat stress (acquired thermotolerance). Acquired thermotolerance was induced by either exposure to a short period of high temperature [6,7] or a gradual temperature increase [6]. These results showed that plants positively prepare for prolonged heat conditions by activating the heat-shock response pathway.

3. Temperature as a Seasonal Cue

Day length and temperature vary annually, especially in temperate zones. Extreme low temperature in winter is severe for plant growth and reproduction. Plants use temperature as a seasonal cue. The accumulation of the temperature signal acts as a seasonal signal that determines the timing of crucial physiological events.

3.1. Flowering Time

In some plant species, the timing of flowering is regulated by temperature. Based on several research data sets, Jagadish et al. [8] reported a trend for earlier flowering in many plant species in response to increased temperature under natural conditions, beginning with observations made as early as the 19th century. Effects of temperature on flowering have been examined under experimental

conditions. In *Arabidopsis*, wild-type strain Landsberg erecta (Ler) flowered when the total leaf number reached about 40 under short day conditions at 23 °C; on the other hand, it flowered when the leaf number reached 15 at 27 °C [9]. Similarly, rice plants grown at 23 °C bloomed later than at 27 °C [10]. In these plant species, high temperature accelerated flowering. However, this does not apply to all plant species. For example, high temperature delayed flowering of *Chrysanthemum morifolium* and *C. seticuspe* [11].

3.2. Vernalization

Vernalization is one of the long-term seasonal effects of temperature. It is the phenomenon whereby flowering is induced by exposure to a relatively long period of cold. Subsequently, flowering initiates upon exposure to favorable conditions in the following growing season. Vernalization was first reported as a treatment of winter wheat planted in autumn to ensure abundant flowering the following spring. Vernalization is a widespread trait in plants of temperate zones. The pathway has been studied in several plant species and was recently reviewed [12]. The following steps have been elucidated: A suppression of flowering before winter and achievement of competence to flower by cold via the suppression of a floral repressor (e.g., *Arabidopsis*) or the activation of a floral promoter (e.g., Pooideae).

4. The Mechanisms Sensing Temperature

As described above, temperature is an important environmental factor for plants. To respond to temperature changes, plant tissues must have the way to sense it. The sensory systems have been studied since these temperature dependent responses were first observed. Recent studies have focused on identifying the elements comprising such sensory systems. However, only a part of the temperature sensory systems was identified, and unknown temperature sensors might still exist. In this section, we note the identified mechanism whereby plants sense temperature and its primary signal transduction.

4.1. Phytochrome B

One of the temperature sensors best established and analyzed is phytochrome B (phyB). Phytochrome B is the gene that encodes a light-sensing protein present in two alternative forms, depending on intensity and quality of light [13,14] (Figure 1). The inactive form of phyB, which is called Pr, absorbs maximally at the red wavelength of the electromagnetic spectrum. When phyB Pr is exposed to red light, it changes to the active Pfr form. Active phyB Pfr shows maximum absorbance in the far-red region of the spectrum. Far-red radiation accelerates the rate at which Pfr converts to Pr. The phyB Pfr spontaneously relaxed into Pr independent of light. This phenomenon is called dark or thermal reversion. Under natural conditions, sunlight activates phyB to the Pfr form and phyB becomes inactive at night.

Some temperature-mediated responses (elongation of hypocotyl and petiole, and leaf hyponasty) are similar to shade-avoidance responses, which occur under shade to escape from the shade of a tree canopy. This similarity suggested that responses to high temperature and light–dark transitions likely share the same molecular pathway. Under shade, light quality differs from direct sunlight. The ratio of red to far-red (R/FR) decreases since plants absorb red and blue light. Phytochrome B is the main photoreceptor controlling tissue elongation under shade conditions [15]. In a recent study, it was identified that phyB acts as temperature sensor through temperature-dependent reversion of phyB. The measurement of the half-life of active state phyB (Pfr) in vitro [16] and in vivo [17] showed that reversion from Pfr to Pr proceeded faster at higher temperature. This indicated that phyB became more inactive at a higher temperature if the light condition was the same. Thus, phyB acts as a temperature sensor through the interconversion between active and inactive states in response to temperature.

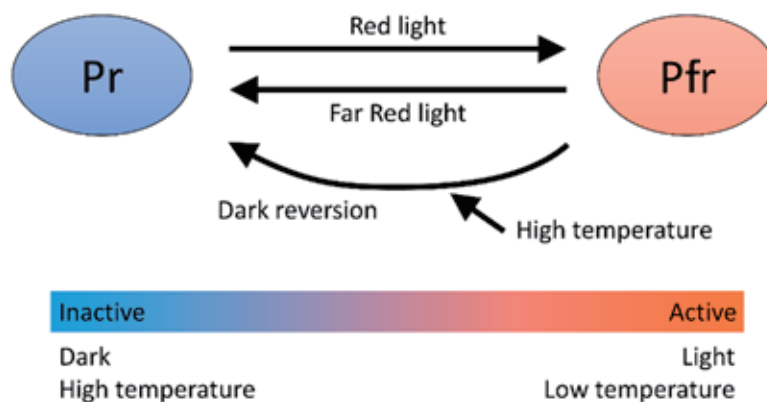


Figure 1. Light and temperature regulation of phyB activity. Phytochrome B state changes in response to light and temperature. It is activated by light, while it is inactivated in the dark and by high temperature through acceleration of dark reversion.

Phytochrome B might work as a temperature sensor by the conversion of its states. It must output the temperature signal to regulate various physiological responses. Phytochromes can interact with other proteins called Phytochrome Interacting Factors (PIFs) [18,19]. These are the genes encoding transcriptional factor proteins which have the basic helix–loop–helix (bHLH) DNA binding domain. Transcriptional factor proteins enter the cell nucleus and bind to a specific region of genomic DNA and regulate the transcription of target genes. In *Arabidopsis*, *PIF1* (also named *PIF3-LIKE 5* or *PIL5*), *PIF3*, *PIF4*, *PIF5* (*PIL6*) and *PIF7* belong to the *PIF* gene family. In this family, *PIF4* might be most essential for temperature-dependent responses. Loss of function mutant of *PIF4* did not show hypocotyl elongation under high temperature, while other tested mutants of *PIF3* and *PIF5* showed hypocotyl elongation similar to the wild type [2]. The mechanism whereby phyB regulates *PIF4* activity has been elucidated by the study of light-dependent responses. It consists of two different strategies: Degradation and sequestration (Figure 2).

An experiment using a transformant in which *PIF4* was constitutively expressed showed that *PIF4* protein was degraded in response to red light and re-accumulated under dark conditions [20]. A similar phenomenon was reported for the temperature response. The *PIF4* protein was more stable at 25 °C than at 15 °C [21]. In the experiment using *PIF4* conjugated-green-fluorescent protein, *PIF4* abundance increased more at 28 °C than at 22 °C, especially in nuclei [22]. These results suggest that the system positively degraded *PIF4* under red light and low temperature. The mechanisms of degradation consist of ubiquitination of the *PIF4* protein and subsequent degradation by 26S proteasomes. Ubiquitination serves to label proteins for degradation. Ubiquitinated proteins are transferred to 26S proteasomes, which are sites of protein degradation. In a very recent study, it was revealed how *PIF4* was ubiquitinated [23]. Ubiquitination of PIFs is executed by the CUL3-based E3 ligase complexes composed of a CUL3 backbone, an E2-Ub-docking RING Box1 (RBX1) protein and a member from BTB-domain containing protein family. A BTB-domain containing protein acts as a target-substrate recognition component [24]. The kind of BTB-domain containing protein in complex decides which protein is ubiquitinated. For degradation of *PIF4*, two BLADE ON PETIOLE proteins (*BOP1* and *BOP2*) in the BTB-ankyrin protein family are related to reorganization of *PIF4*. The ubiquitination and degradation of *PIF4* are reduced in the *bop1 bop2* mutant background, compared with the wild type not only under red light but also under elevated temperature. It is suggested that CUL3-based E3 ligase complexes containing *BOP* proteins control *PIF4* protein abundance under red light as well as under elevated temperature.

Phytochrome B also controls *PIF4* activity by sequestration. The site where *PIF4* acts to regulate gene expression is the cell nucleus. The *PIF4* binds expression-regulatory regions of target genes in genomic DNA through its bHLH domain. Localization of *PIF4* in nuclei is an essential condition for their activity. The phyB Pfr binds to PIFs through an Active phyB-Binding (APB) domain. After binding to PIFs in

the nucleus, this complex is removed from the binding site on genomic sequence. In an experiment using a phyB mutant without degradation activity, the expression of genes promoted by PIFs were reduced under red light conditions [25]. This result indicated that active phyB can repress PIF activity by sequestration without degradation.

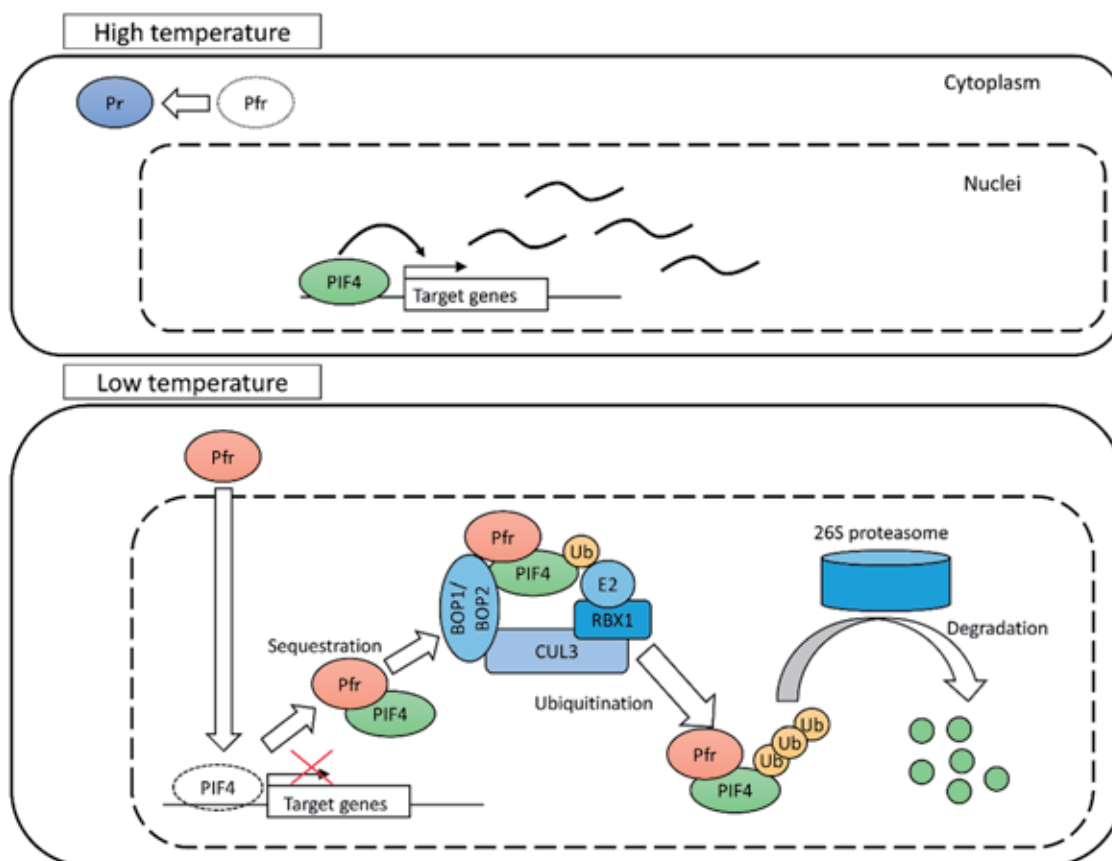


Figure 2. The mechanism of the temperature sensing system based on phyB and PIF4. At high temperature, phyB gets converted to the inactive Pr state and is located in the cytoplasm. The PIF4 binds to the regulatory region of target genes and regulates their expression. At low temperature, phyB is in an active state and enters the cell nucleus. The PIF4 is sequestered from target genes by binding to phyB. The PIF4 is degraded by 26 proteasomes through ubiquitination. The activity of PIF4 is suppressed at low temperature.

The repression of PIF activity was confirmed as an exclusive response to light that might vary depending on temperature. Eventually temperature signal in this pathway is output through the change of transcriptional regulation activity of PIF4. The PIF4 up-regulates expression of the genes related to biosynthesis of auxin, which is a kind of phytohormone and control growth and development [26,27].

4.2. Temperature Sensing for Heat Shock Response

Heat shock transcription factorA1s (HSFA1s) belongs to a cluster of critical factors in the heat shock response. Knockdown or multiple knockout mutations of HSFA1 genes in tomato and *Arabidopsis* cause the reduction of thermotolerance [28,29]. HSFA1s encodes a master transcriptional regulator of downstream heat-shock responsive genes. The regulation of their activities in response to heat stress is central to the mechanisms underlying heat shock responses. Phosphorylation/dephosphorylation and protein–protein interactions control HSFA1s activity. The HSFA1s protein is phosphorylated by calmodulin-binding protein kinase 3 (CBK3) [30] and dephosphorylated by protein phosphatase 7 (PP7) [31]. The fact that cbk3 and pp7 mutants show less thermotolerance led us to conclude that

the modulation of the phosphorylation status of HSFA1s by these genes has an important role in heat-stress response through HSFA1s. However, phosphorylation/dephosphorylation sites and the mechanisms that regulate phosphorylation activity in response to high temperature are not clear.

Another mechanism for the regulation of HSFA1s involves protein–protein interactions, for example, Heat Shock Protein 70 (HSP70) and HSP90. They are up-regulated by heat stress, although they exist under normal conditions, in which they bind to HSFA1s to repress its nuclear localization and subsequent transcriptional activation [32,33]; when plants are subjected to heat stress, HSFA1s protein is released by HSP70 and HSP90, thereby becoming active in triggering the heat responsive cascade [34].

4.3. Other Temperature Sensing Systems

The mechanism of vernalization was analyzed using *Arabidopsis*, in which a floral repressor *FLOWERING LOCUS C (FLC)* represses differentiation into floral stage by suppression of *FLOWERING LOCUS T (FT)*, which is a component of florigen, the flowering inducing factor [35,36] (Figure 3). This suppression was overcome by *COLD AIR*, which is a long noncoding RNA transcribed from the first intron of *FLC* [37]. *COLD AIR* started to express after transition to cold temperature and its expression peaked 20 days later, decreasing thereafter even under prolonged cold conditions. *COLD AIR* RNA formed secondary structures and bound to Polycomb Repressive Complex 2 (PRC2). This is one of the chromatin-remodeling complexes that regulate transcriptional activity by modulating chromatin state of target genes in the genome [38,39]. *COLD AIR*-PRC2 complex bound to *FLC* region and suppressed *FLC* expression through conversion of chromatin into the inactive state through histone methylation [40]. As a result of the suppression of *FLC*, the expression of *FT* and other flowering-regulating genes were able to activate in a subsequent warm period, thereby initiating flowering-associated differentiation. Although the pathway that promotes flowering by the cold signal was identified, the regulation of *COLD AIR* expression and chromatin modification in response to low temperature is not clear. Temperature sensing components that are not yet known might be involved in this pathway.

Another component of thermo-sensory responses is H2A.Z, a variant of H2A, which is a kind of histone and a component of the nucleosome. An *ARP6* mutant involved in the activity of H2A.Z histone substitution in place of H2A revealed various traits responding to temperature: Hypocotyl elongation, petiole elongation and acceleration of flowering. Increased occupancy by H2A.Z near the transcription start-site prevents expression of that gene. Temperature dependent variation of H2A.Z occupancy regulated the expression of temperature responsive genes [41]. In further analysis, Kumar et al. [42] showed that H2A.Z-nucleosomes were present at the *FT* promoter at 17 °C and the levels of H2A.Z-nucleosomes at the *FT* promoter decrease under higher temperature (27 °C). In a recent study, it was found that H2A.Z-nucleosomes occupancy and the depletion of them in response to high temperature are enriched at temperature responsive genes regulated by HSFA1 [43]. These results suggest that H2A.Z is important for various temperature mediated responses. However, how to convert H2A.Z level in response to temperature is still unknown.

Involvements of other photoreceptors in temperature responses were shown in a recent study. Although high temperature induces elongation of hypocotyl as described above, radiation of blue light inhibits the high temperature mediated hypocotyl elongation and blue-light receptors Cryptochrome 1 (CRY1) is essential for this inhibition [44]. A similar phenomenon was found in relation to ultraviolet-B light (UV-B). Ultraviolet-B light also represses high temperature mediated elongation of hypocotyl and petiole. Ultraviolet-B light photoreceptor UV RESISTANCE LOCUS 8 (UVR8) is relevant to this inhibition [45]. These photosensors might be involved in temperature response through PIF4 by regulation of E3 ubiquitin ligase activity of COP1 (CONSTITUTIVE PHOTOMORPHOGENIC 1) [44,45]. In another case of involvement of photoreceptor, blue light photoreceptor phototropin might act as temperature sensor. Chloroplasts change their intracellular position in response to light and temperature conditions. Phototropin has an important role in sensing blue light and temperature for

this response. The temperature-sensing mechanism of phototropin might be similar to that of phyB. The lifetime of activated phototropin by blue light became longer at low temperature [46].

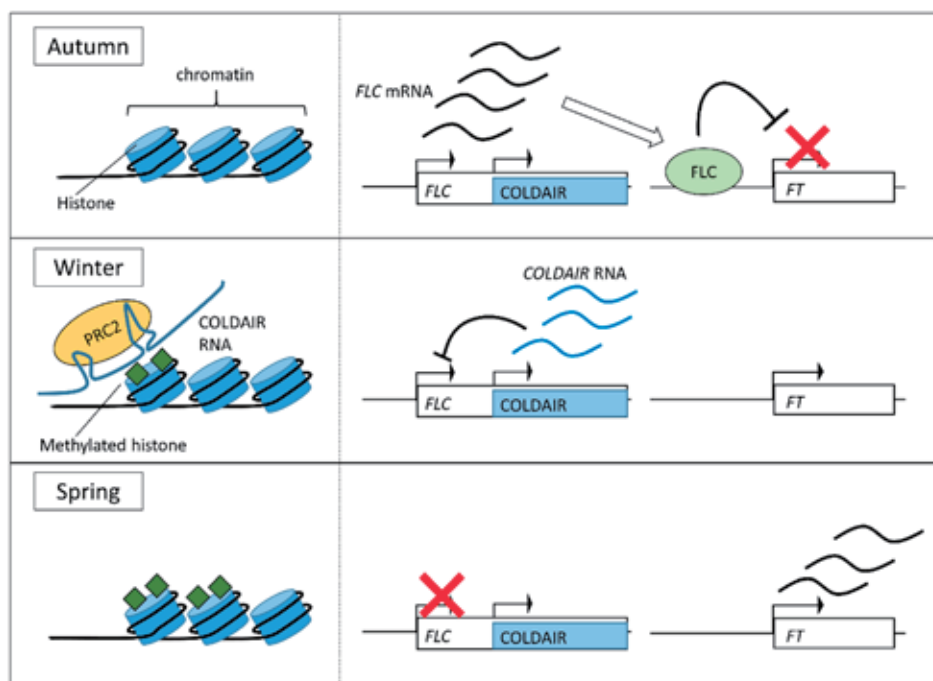


Figure 3. The mechanism of the vernalization system. The diagram shows chromatin state near the *FLOWERING LOCUS C* (*FLC*) gene (left), *FLC* and *COLDAIR* regions and their expression (center) and *FT* region (right). In autumn or under conditions which did not include a prolonged cold period, the *FLC* gene is expressed and the *FLC* protein suppresses the expression of *FLOWERING LOCUS T* (*FT*). Conversely, in winter, *COLDAIR* noncoding RNA is transcribed from the 1st intron of *FLC*. *COLDAIR* RNA binds to Polycomb Repressive Complex 2 (*PRC2*) and guides it to the *FLC* region in the chromosome. Polycomb Repressive Complex 2 starts methylation of histones in the *FLC* region and this methylation deactivates the expression of *FLC*. In the following spring, expression of *COLDAIR* stops, but *FLC* still remains suppressed. The *FT* is activated and then differentiation into flowering begins.

5. Conclusions

Evidence shows that plants possess various types of temperature-sensing systems, some of which have been identified and, at least partially, characterized in terms of composition and operation. In this review, we have discussed only the core aspect of temperature sensing and the response systems involved. As a whole, all of these systems, including related pathways and downstream reactions, are highly complex and have not been thoroughly elucidated.

Plants have multiple temperature sensors to adapt to various aspects of temperature effect. Although both phyB/PIF4 pathway and heat shock response are able to respond to short-term temperature change, the responsiveness of each one is different. Small temperature elevation causes morphological change in phyB/PIF4 pathway. On the other hand, it acts as a cue for following heat stress in heat shock response [43].

Although temperature is an important environmental signal, it is not independent from other environmental factors under natural conditions; indeed, it is tightly linked to other factors. Light, in particular, is closely related to temperature. A decrease in light irradiation causes temperature to drop in winter, whereas an increase causes temperature to rise in spring. In plants, sensing systems for each environmental factor might actively crosstalk to each other. The activity of phyB is regulated by both light and temperature, and other photosensors are also related in temperature-mediated responses. The heat shock response pathway enhances the resistance to drought, as well as heat stress [47]. The response system for each environmental factor might also share downstream pathways.

Plant growth and development are controlled by phytohormones (auxins, gibberellins and others), and several response systems are based on regulation of these phytohormones. Even in more upstream hormone regulation, temperature response systems are affected by other pathways. PhyB shares the transcriptional regulation pathway of PIF4 with Cry1 and UVR8. The phyB signal pathway and circadian clock signal are integrated through regulation of PIF4. A component of circadian clock, Evening Complex (EC) bound to PIF4 promoter and repressed its expression [48,49]. High temperature reduced the binding of EC to PIF4 promoter and thereby the repression of PIF4 was released [49]. These results suggested that PIF4 was also regulated on a transcriptional level dependent on temperature through circadian clock signal pathway. The relationship between EC and phyB was studied. Evening Complex and phyB showed protein–protein interaction [50] and co-binding to transcriptional regulatory region of target genes [49]. Multiple environmental signals were integrated and output through these signal pathways. The expression of HSP70 is controlled by both heat shock response pathway and light-induced chloroplast signaling. The gating by light-induced chloroplast signaling limits heat shock gene expression to the daytime [51]. Although temperature sensors consist of simple components, whole pathways for responding to temperature are complex.

Further, temperature-response systems show downstream feedback-regulation. The phyB-PIF4 pathway for control of phytohormones provides a clear illustration. A kind of phytohormones, brassinosteroid was up-regulated by PIF4, whereby the brassinosteroid responsive gene enhanced the expression of PIF4 [52]. They formed a positive feedback loop. In the heat-stress pathway, the amounts of HSP70 and HSP90 increased in response to high temperature [33]. This increase might have affected the interaction between HSPs and HSFA1s. This relation suggested that the sensory system was affected by feedback from downstream through these HSPs.

The study of various temperature-response systems has resulted in the identification of some of the temperature sensors involved in each case. However, the details of the molecular mechanisms that sense temperature in plants are still unknown. Further studies are necessary to fully elucidate the complete pathway of temperature sensing and temperature-signal-transduction leading to temperature responses in plants.

Funding: This work was supported by JSPS KAKENHI (JP16H01472, JP16K07408, 18H04787 and 18H04844 to S.K.) and by the MEXT Supported Program for the Strategic Research Foundation at Private Universities from the Ministry of Education, Culture, Sports, Science and Technology of Japan, Grant Number S1511023 to S.K.

Conflicts of Interest: The authors declare no conflict of interest.

References

1. Gray, W.M.; Ostin, A.; Sandberg, G.; Romano, C.P.; Estelle, M. High temperature promotes auxin-mediated hypocotyl elongation in *Arabidopsis*. *Proc. Natl. Acad. Sci. USA* **1998**, *95*, 7197–7202. [[CrossRef](#)] [[PubMed](#)]
2. Koini, M.A.; Alvey, L.; Allen, T.; Tilley, C.A.; Harberd, N.P.; Whitlam, G.C.; Franklin, K.A. High temperature-mediated adaptations in plant architecture require the bHLH transcription factor PIF4. *Curr. Biol.* **2009**, *19*, 408–413. [[CrossRef](#)] [[PubMed](#)]
3. Nakayama, H.; Nakayama, N.; Seiki, S.; Kojima, M.; Sakakibara, H.; Sinha, N.; Kimura, S. Regulation of the KNOX-GA gene module induces heterophyllic alteration in North American lake cress. *Plant Cell* **2014**, *26*, 4733–4748. [[CrossRef](#)] [[PubMed](#)]
4. Royer, D.L. Leaf shape responds to temperature but not CO₂ in *Acer rubrum*. *PLoS ONE* **2012**, *7*, e49559. [[CrossRef](#)] [[PubMed](#)]
5. Fukushima, K.; Fang, X.; Alvarez-Ponce, D.; Cai, H.; Carretero-Paulet, L.; Chen, C.; Chang, T.; Farr, K.; Fujita, T.; Hiwataishi, Y.; et al. Genome of the pitcher plant *Cephalotus* reveals genetic changes associated with carnivory. *Nat. Ecol. Evol.* **2017**, *1*, 59. [[CrossRef](#)]
6. Larkindale, J.; Vierling, E. Core genome responses involved in acclimation to high temperature. *Plant Physiol.* **2008**, *146*, 748–761. [[CrossRef](#)]
7. Hong, S.W.; Vierling, E. Mutants of *Arabidopsis thaliana* defective in the acquisition of tolerance to high temperature stress. *Proc. Natl. Acad. Sci. USA* **2000**, *97*, 4392–4397. [[CrossRef](#)]

8. Jagadish, S.V.K.; Bahuguna, R.N.; Djanaguiraman, M.; Gamuyao, R.; Prasad, P.V.V.; Craufurd, P.Q. Implications of High Temperature and Elevated CO₂ on Flowering Time in Plants. *Front. Plant Sci.* **2016**, *7*, 913. [[CrossRef](#)]
9. Balasubramanian, S.; Sureshkumar, S.; Lempe, J.; Weigel, D. Potent induction of *Arabidopsis thaliana* flowering by elevated growth temperature. *PLoS Genet.* **2006**, *2*, e106. [[CrossRef](#)]
10. Luan, W.; Chen, H.; Fu, Y.; Si, H.; Peng, W.; Song, S.; Liu, W.; Hu, G.; Sun, Z.; Xie, D.; et al. The effect of the crosstalk between photoperiod and temperature on the heading-date in rice. *PLoS ONE* **2009**, *4*, e5891. [[CrossRef](#)]
11. Nakano, Y.; Higuchi, Y.; Sumitomo, K.; Hisamatsu, T. Flowering retardation by high temperature in *chrysanthemums*: Involvement of *FLOWERING LOCUS T-like 3* gene repression. *J. Exp. Bot.* **2013**, *64*, 909–920. [[CrossRef](#)] [[PubMed](#)]
12. Bouche, F.; Woods, D.P.; Amasino, R.M. Winter Memory throughout the Plant Kingdom: Different Paths to Flowering. *Plant Physiol.* **2017**, *173*, 27–35. [[CrossRef](#)] [[PubMed](#)]
13. Rockwell, N.C.; Su, Y.; Lagarias, J.C. Phytochrome structure and signaling mechanisms. *Annu. Rev. Plant Biol.* **2006**, *57*, 837–858. [[CrossRef](#)]
14. Burgie, E.S.; Bussell, A.N.; Walker, J.M.; Dubiel, K.; Vierstra, R.D. Crystal structure of the photosensing module from a red/far-red light-absorbing plant phytochrome. *Proc. Natl. Acad. Sci. USA* **2014**, *111*, 10179–10184. [[CrossRef](#)]
15. Franklin, K.A.; Davis, S.J.; Stoddart, W.M.; Vierstra, R.D.; Whitelam, G.C. Mutant analyses define multiple roles for Phytochrome C in *Arabidopsis* photomorphogenesis. *Plant Cell* **2003**, *15*, 1981–1989. [[CrossRef](#)] [[PubMed](#)]
16. Legris, M.; Klose, C.; Burgie, E.S.; Rojas, C.C.R.; Neme, M.; Hiltbrunner, A.; Wigge, P.A.; Schafer, E.; Vierstra, R.D.; Casal, J.J. Phytochrome B integrates light and temperature signals in *Arabidopsis*. *Science* **2016**, *354*, 897–900. [[CrossRef](#)]
17. Jung, J.; Domijan, M.; Klose, C.; Biswas, S.; Ezer, D.; Gao, M.; Khattak, A.K.; Box, M.; Charoensawan, V.; Cortijo, S.; et al. Phytochromes function as thermosensors in *Arabidopsis*. *Science* **2016**, *354*, 886–889. [[CrossRef](#)]
18. Ni, M.; Tepperman, J.M.; Quail, P.H. Binding of phytochrome B to its nuclear signalling partner PIF3 is reversibly induced by light. *Nature* **1999**, *400*, 781–784. [[CrossRef](#)]
19. Shimizu-Sato, S.; Huq, E.; Tepperman, J.M.; Quail, P.H. A light-switchable gene promoter system. *Nat. Biotechnol.* **2002**, *20*, 1041–1044. [[CrossRef](#)] [[PubMed](#)]
20. Lorrain, S.; Allen, T.; Duek, P.D.; Whitelam, G.C.; Fankhauser, C. Phytochrome-mediated inhibition of shade avoidance involves degradation of growth-promoting bHLH transcription factors. *Plant J.* **2008**, *53*, 312–323. [[CrossRef](#)] [[PubMed](#)]
21. Foreman, J.; Johansson, H.; Hornitschek, P.; Josse, E.; Fankhauser, C.; Halliday, K.J. Light receptor action is critical for maintaining plant biomass at warm ambient temperatures. *Plant J.* **2011**, *65*, 441–452. [[CrossRef](#)] [[PubMed](#)]
22. Legris, M.; Nieto, C.; Sellaro, R.; Prat, S.; Casal, J.J. Perception and signalling of light and temperature cues in plants. *Plant J.* **2017**, *90*, 683–697. [[CrossRef](#)] [[PubMed](#)]
23. Zhang, B.; Holmlund, M.; Lorrain, S.; Norberg, M.; Bako, L.; Fankhauser, C.; Nilsson, O. BLADE-ON-PETIOLE proteins act in an E3 ubiquitin ligase complex to regulate PHYTOCHROME INTERACTING FACTOR 4 abundance. *eLife* **2017**, *6*, e26759. [[CrossRef](#)] [[PubMed](#)]
24. Genschik, P.; Sumara, I.; Lechner, E. The emerging family of CULLIN3-RING ubiquitin ligases (CRL3s): Cellular functions and disease implications. *EMBO J.* **2013**, *32*, 2307–2320. [[CrossRef](#)] [[PubMed](#)]
25. Park, E.; Kim, Y.; Choi, G. Phytochrome B Requires PIF Degradation and Sequestration to Induce Light Responses across a Wide Range of Light Conditions. *Plant Cell* **2018**, *30*, 1277–1292. [[CrossRef](#)] [[PubMed](#)]
26. Franklin, K.A.; Lee, S.H.; Patel, D.; Kumar, S.V.; Spartz, A.K.; Gu, C.; Ye, S.; Yu, P.; Breen, G.; Cohen, J.D.; et al. Phytochrome-interacting factor 4 (PIF4) regulates auxin biosynthesis at high temperature. *Proc. Natl. Acad. Sci. USA* **2011**, *108*, 20231–20235. [[CrossRef](#)] [[PubMed](#)]
27. Sun, J.; Qi, L.; Li, Y.; Chu, J.; Li, C. PIF4-mediated activation of *YUCCA8* expression integrates temperature into the auxin pathway in regulating *Arabidopsis* hypocotyl growth. *PLoS Genet.* **2012**, *8*, e1002594. [[CrossRef](#)] [[PubMed](#)]

28. Mishra, S.K.; Tripp, J.; Winkelhaus, S.; Tschiersch, B.; Theres, K.; Nover, L.; Scharf, K.-D. In the complex family of heat stress transcription factors, HsfA1 has a unique role as master regulator of thermotolerance in tomato. *Genes Dev.* **2002**, *16*, 1555–1567. [[CrossRef](#)]
29. Liu, H.-C.; Liao, H.-T.; Charng, Y.-Y. The role of class A1 heat shock factors (HSFA1s) in response to heat and other stresses in *Arabidopsis*. *Plant Cell Environ.* **2011**, *34*, 738–751. [[CrossRef](#)]
30. Liu, H.-T.; Gao, F.; Li, G.-L.; Han, J.-L.; Liu, D.-L.; Sun, D.-Y.; Zhou, R.-G. The calmodulin-binding protein kinase 3 is part of heat-shock signal transduction in *Arabidopsis thaliana*. *Plant J.* **2008**, *55*, 760–773. [[CrossRef](#)]
31. Liu, H.-T.; Li, G.-L.; Chang, H.; Sun, D.-Y.; Zhou, R.-G.; Li, B. Calmodulin-binding protein phosphatase PP7 is involved in thermotolerance in *Arabidopsis*. *Plant Cell Environ.* **2007**, *30*, 156–164. [[CrossRef](#)] [[PubMed](#)]
32. Hahn, A.; Bublak, D.; Schleiff, E.; Scharf, K. Crosstalk between Hsp90 and Hsp70 chaperones and heat stress transcription factors in tomato. *Plant Cell* **2011**, *23*, 741–755. [[CrossRef](#)] [[PubMed](#)]
33. Yamada, K.; Fukao, Y.; Hayashi, M.; Fukazawa, M.; Suzuki, I.; Nishimura, M. Cytosolic HSP90 regulates the heat shock response that is responsible for heat acclimation in *Arabidopsis thaliana*. *J. Biol. Chem.* **2007**, *282*, 37794–37804. [[CrossRef](#)] [[PubMed](#)]
34. Ohama, N.; Kusakabe, K.; Mizoi, J.; Zhao, H.; Kidokoro, S.; Koizumi, S.; Takahashi, F.; Ishida, T.; Yanagisawa, S.; Shinozaki, K.; et al. The Transcriptional Cascade in the Heat Stress Response of *Arabidopsis* Is Strictly Regulated at the Level of Transcription Factor Expression. *Plant Cell* **2016**, *28*, 181–201. [[CrossRef](#)] [[PubMed](#)]
35. Michaels, S.D.; Amasino, R.M. *FLOWERING LOCUS C* encodes a novel MADS domain protein that acts as a repressor of flowering. *Plant Cell* **1999**, *11*, 949–956. [[CrossRef](#)] [[PubMed](#)]
36. Sheldon, C.C.; Burn, J.E.; Perez, P.P.; Metzger, J.; Edwards, J.A.; Peacock, W.J.; Dennis, E.S. The *FLF* MADS box gene: A repressor of flowering in *Arabidopsis* regulated by vernalization and methylation. *Plant Cell* **1999**, *11*, 445–458. [[CrossRef](#)] [[PubMed](#)]
37. Heo, J.B.; Sung, S. Vernalization-mediated epigenetic silencing by a long intronic noncoding RNA. *Science* **2011**, *331*, 76–79. [[CrossRef](#)] [[PubMed](#)]
38. Sung, S.; Amasino, R.M. Vernalization in *Arabidopsis thaliana* is mediated by the PHD finger protein VIN3. *Nature* **2004**, *427*, 159–164. [[CrossRef](#)] [[PubMed](#)]
39. De Lucia, F.; Crevillen, P.; Jones, A.M.E.; Greb, T.; Dean, C. A PHD-polycomb repressive complex 2 triggers the epigenetic silencing of *FLC* during vernalization. *Proc. Natl. Acad. Sci. USA* **2008**, *105*, 16831–16836. [[CrossRef](#)] [[PubMed](#)]
40. Kim, D.; Xi, Y.; Sung, S. Modular function of long noncoding RNA, COLDAIR, in the vernalization response. *PLoS Genet.* **2017**, *13*, e1006939. [[CrossRef](#)]
41. Kumar, S.V.; Wigge, P.A. H2A.Z-containing nucleosomes mediate the thermosensory response in *Arabidopsis*. *Cell* **2010**, *140*, 136–147. [[CrossRef](#)] [[PubMed](#)]
42. Kumar, S.V.; Lucyshyn, D.; Jaeger, K.E.; Alos, E.; Alvey, E.; Harberd, N.P.; Wigge, P.A. Transcription factor PIF4 controls the thermosensory activation of flowering. *Nature* **2012**, *484*, 242–245. [[CrossRef](#)] [[PubMed](#)]
43. Cortijo, S.; Charoensawan, V.; Brestovitsky, A.; Buning, R.; Ravarani, C.; Rhodes, D.; van Noort, J.; Jaeger, K.E.; Wigge, P.A. Transcriptional Regulation of the Ambient Temperature Response by H2A.Z Nucleosomes and HSF1 Transcription Factors in *Arabidopsis*. *Mol. Plant* **2017**, *10*, 1258–1273. [[CrossRef](#)] [[PubMed](#)]
44. Ma, D.; Li, X.; Guo, Y.; Chu, J.; Fang, S.; Yan, C.; Noel, J.P.; Liu, H. Cryptochrome 1 interacts with PIF4 to regulate high temperature-mediated hypocotyl elongation in response to blue light. *Proc. Natl. Acad. Sci. USA* **2016**, *113*, 224–229. [[CrossRef](#)] [[PubMed](#)]
45. Hayes, S.; Sharma, A.; Fraser, D.P.; Trevisan, M.; Cragg-Barber, C.K.; Tavridou, E.; Fankhauser, C.; Jenkins, G.I.; Franklin, K.A. UV-B Perceived by the UVR8 Photoreceptor Inhibits Plant Thermomorphogenesis. *Curr. Biol.* **2017**, *27*, 120–127. [[CrossRef](#)] [[PubMed](#)]
46. Fujii, Y.; Tanaka, H.; Konno, N.; Ogasawara, Y.; Hamashima, N.; Tamura, S.; Hasegawa, S.; Hayasaki, Y.; Okajima, K.; Kodama, Y. Phototropin perceives temperature based on the lifetime of its photoactivated state. *Proc. Natl. Acad. Sci. USA* **2017**, *114*, 9206–9211. [[CrossRef](#)] [[PubMed](#)]
47. Bechtold, U.; Albihlal, W.S.; Lawson, T.; Fryer, M.J.; Sparrow, P.A.C.; Richard, F.; Persad, R.; Bowden, L.; Hickman, R.; Martin, C.; et al. *Arabidopsis* *HEAT SHOCK TRANSCRIPTION FACTOR1b* overexpression enhances water productivity, resistance to drought, and infection. *J. Exp. Bot.* **2013**, *64*, 3467–3481. [[CrossRef](#)] [[PubMed](#)]

48. Box, M.S.; Huang, B.E.; Domijan, M.; Jaeger, K.E.; Khattak, A.K.; Yoo, S.J.; Sedivy, E.L.; Jones, D.M.; Hearn, T.J.; Webb, A.A.R.; et al. *ELF3* controls thermoresponsive growth in *Arabidopsis*. *Curr. Biol.* **2015**, *25*, 194–199. [[CrossRef](#)] [[PubMed](#)]
49. Ezer, D.; Jung, J.H.; Lan, H.; Biswas, S.; Gregoire, L.; Box, M.S.; Charoensawan, V.; Cortijo, S.; Lai, X.; Stockle, D.; et al. The evening complex coordinates environmental and endogenous signals in *Arabidopsis*. *Nat. Plants* **2017**, *3*, 17087. [[CrossRef](#)] [[PubMed](#)]
50. Huang, H.; Alvarez, S.; Bindbeutel, R.; Shen, Z.; Naldrett, M.J.; Evans, B.S.; Briggs, S.P.; Hicks, L.M.; Kay, S.A.; Nusinow, D.A. Identification of Evening Complex Associated Proteins in *Arabidopsis* by Affinity Purification and Mass Spectrometry. *Mol. Cell. Proteom.* **2016**, *15*, 201–217. [[CrossRef](#)] [[PubMed](#)]
51. Dickinson, P.J.; Kumar, M.; Martinho, C.; Yoo, S.J.; Lan, H.; Artavanis, G.; Charoensawan, V.; Schottler, M.A.; Bock, R.; Jaeger, K.E.; et al. Chloroplast Signaling Gates Thermotolerance in *Arabidopsis*. *Cell Rep.* **2018**, *22*, 1657–1665. [[CrossRef](#)] [[PubMed](#)]
52. Ibanez, C.; Delker, C.; Martinez, C.; Burstenbinder, K.; Janitza, P.; Lippmann, R.; Ludwig, W.; Sun, H.; James, G.V.; Klecker, M.; et al. Brassinosteroids Dominate Hormonal Regulation of Plant Thermomorphogenesis via BZR1. *Curr. Biol.* **2018**, *28*, 303–310. [[CrossRef](#)] [[PubMed](#)]



© 2018 by the authors. Licensee MDPI, Basel, Switzerland. This article is an open access article distributed under the terms and conditions of the Creative Commons Attribution (CC BY) license (<http://creativecommons.org/licenses/by/4.0/>).



How Do Plants and Phytohormones Accomplish Heterophylly, Leaf Phenotypic Plasticity, in Response to Environmental Cues

Hokuto Nakayama¹, Neelima R. Sinha¹ and Seisuke Kimura^{2,3*}

¹ Department of Plant Biology, University of California, Davis, Davis, CA, United States, ² Department of Bioresource and Environmental Sciences, Kyoto Sangyo University, Kyoto, Japan, ³ Center for Ecological Evolutionary Developmental Biology, Kyoto Sangyo University, Kyoto, Japan

OPEN ACCESS

Edited by:

Elena M. Kramer,
Harvard University, United States

Reviewed by:

Natalia Pabón-Mora,
University of Antioquia, Colombia
Lachezar A. Nikolov,
Max Planck Institute for Plant
Breeding Research (MPG), Germany

*Correspondence:

Seisuke Kimura
seisuke@cc.kyoto-su.ac.jp

Specialty section:

This article was submitted to
Plant Evolution and Development,
a section of the journal
Frontiers in Plant Science

Received: 24 July 2017

Accepted: 20 September 2017

Published: 04 October 2017

Citation:

Nakayama H, Sinha NR and
Kimura S (2017) How Do Plants
and Phytohormones Accomplish
Heterophylly, Leaf Phenotypic
Plasticity, in Response
to Environmental Cues.
Front. Plant Sci. 8:1717.
doi: 10.3389/fpls.2017.01717

Plant species are known to respond to variations in environmental conditions. Many plant species have the ability to alter their leaf morphology in response to such changes. This phenomenon is termed heterophylly and is widespread among land plants. In some cases, heterophylly is thought to be an adaptive mechanism that allows plants to optimally respond to environmental heterogeneity. Recently, many research studies have investigated the occurrence of heterophylly in a wide variety of plants. Several studies have suggested that heterophylly in plants is regulated by phytohormones. Herein, we reviewed the existing knowledge on the relationship and role of phytohormones, especially abscisic acid, ethylene, gibberellins, and auxins (IAA), in regulating heterophylly and attempted to elucidate the mechanisms that regulate heterophylly.

Keywords: phenotypic plasticity, heterophylly, phytohormones, *Potamogeton nodosus*, *Rorippa aquatica*, *Ludwigia arcuata*

INTRODUCTION; WHAT IS HETEROPHYLLY?

Plants have the ability to alter their morphology in response to environmental conditions. This phenomenon is known as phenotypic plasticity (Alpert and Simms, 2002; Zotz et al., 2011). Phenotypic plasticity exhibited as leaf form alteration in response to environmental conditions such as light intensity and quality, ambient temperature, and water availability is called heterophylly (Figures 1A,B). The original definition of heterophylly was not strictly linked to the environmental control. However, recently, it has been often the case that heterophylly refers to leaf form alteration in response to environmental cues (Anderson, 1978; Goliber and Feldman, 1990; Kuwabara et al., 2003; Wanke, 2011; Sicard et al., 2014). This phenomenon differs from heteroblasty, which refers to conspicuous morphological changes in leaves throughout the lifecycle of plants (Zotz et al., 2011). Additionally, heterophylly differs from anisophylly, which is a special case of dorsiventral shoot symmetry in which leaves inserted on the dorsal and ventral sides of the stem differ in size and shape. Anisophylly is normally coupled with leaf and stem asymmetry and modified phyllotaxis (Dengler, 1999). Therefore, heteroblasty and anisophylly do not include morphological changes induced by environmental stimuli, whereas heterophylly is expressed as the environmentally induced switch between two or more leaf morphologies in the same plant (Zotz et al., 2011).

Heterophylly is exhibited by various land plants including terrestrial and aquatic species (Wanke, 2011; Nakayama et al., 2012). Among angiosperms, heterophylly occurs in diverse taxa. Several studies (Goliber and Feldman, 1990; Kuwabara et al., 2003; Iida et al., 2016) on heterophylly have indicated that this trait has evolved multiple times during plant evolution among various unrelated taxa. In some cases, heterophylly is perceived to be an adaptive mechanism that allows plants to optimally respond to environmental heterogeneity (Palacio-Lopez et al., 2015). Adaptive plasticity hypothesis predicts that plants capable of exhibiting heterophylly in leaf architecture in response to heterogeneous environment are expected to have better fitness compared to other plants. However, there is limited information on the adaptive significance of heterophylly. Moreover, theoretical studies indicate that the acquisition of heterophylly may be constrained by the genetic costs and limits of plasticity (Ernande and Dieckmann, 2004). Hence, it is debatable whether all heterophylly evolved as an adaptive response (Palacio-Lopez et al., 2015).

Heterophylly is the focus of many studies due to its uniqueness (Fassett, 1930). Studies on the molecular mechanisms underlying heterophylly have been published recently (Kuwabara et al., 2003; Nakayama et al., 2014; Sicard et al., 2014). Interestingly, many studies have suggested that various phytohormones are involved in the regulation of heterophylly. Therefore, we considered it worthwhile to review the existing knowledge on the relationships and interactions between heterophylly and phytohormones to gain valuable insight into this phenomenon.

HOW DOES ABA REGULATE HETEROPHYLLY?

Potamogeton nodosus (Potamogetonaceae), an aquatic plant native to Eurasia and North America, exhibits heterophylly in the form of two distinct types of leaves: long narrow submerged leaves and oblong elliptical floating leaves (Anderson, 1978). A report published in 1978 showed that a low concentration of exogenous abscisic acid (ABA) induced floating leaves in *P. nodosus* (Figure 2) (Anderson, 1978).

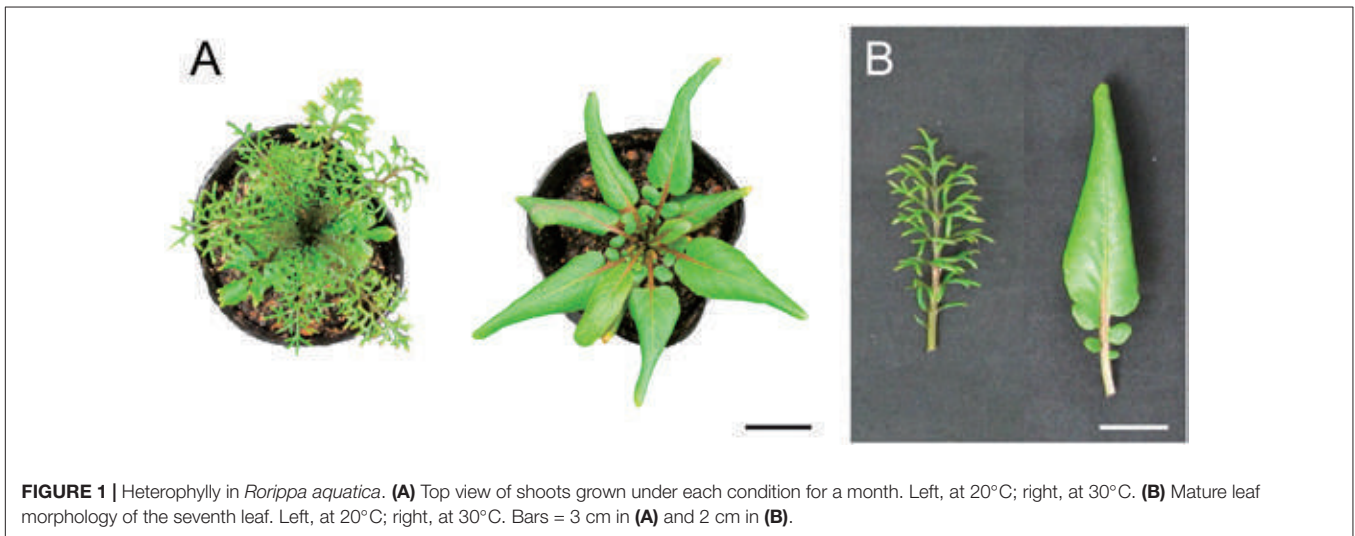
Abscisic acid, a tiny molecule classified as a sesquiterpene, is one of the well-known hormones regulating abiotic stress responses in plants (Vishwakarma et al., 2017). ABA is thought to be synthesized in the vasculature and in the guard cells of the vegetative part of the plant (Boursiac et al., 2013). Interestingly, ABA as a signaling molecule has been reported in a phylogenetically wide range of organisms from cyanobacteria to human (Maršálek et al., 1992; Bruzzone et al., 2007). Some studies have suggested that the ABA pathway is conserved in the green plant lineage (Takezawa et al., 2011). However, little is known about why various kinds of organisms utilize and respond to ABA (Lievens et al., 2017). ABA is involved in controlling growth and development of plants such as leaf abscission, inhibition of fruit ripening, and drought stress response.

Ludwigia arcuata (Onagraceae) is one of the well-characterized aquatic plants exhibiting heterophylly. This plant forms narrow leaves under submergence, and round leaves

under aerial growth conditions (Figure 2) (Kuwabara et al., 2003). Analytical studies of the different developmental stages of *L. arcuata* demonstrated that ABA plays an important role during the change in leaf morphology between submergence and aerial conditions as is also reported in *P. nodosus* (Anderson, 1978). In *L. arcuata*, application of exogenous ABA to submerged shoots resulted in aerial leaf form even under submerged condition (Kuwabara et al., 2003). As described above, a notable feature of ABA synthesis is for drought stress response. Several studies on a variety of plant species have suggested that osmotic stress conditions induce the production of ABA, which acts as a controller in stress response and tolerance of plants (Yamaguchi-Shinozaki and Shinozaki, 2006; Nakashima and Yamaguchi-Shinozaki, 2013) and the accumulated ABA in vegetative tissues induces ABA-responsive gene expression (Goda et al., 2008). These studies substantiate the role of ABA in the regulation of heterophylly, especially in aquatic plants that can sense changes in the surrounding environment, in particular, water level and/or availability, via ABA. Indeed, in addition to functioning as a short-distance signaling molecule, it has been suggested that ABA is a long-distance signaling molecule that is transported from mature leaves to developing leaves to optimize some phenotypes such as stomatal development in response to environmental changes (Chater et al., 2014). Hence, when submerged *L. arcuata* leaves were brought in contact with air, the endogenous levels of ABA increased and this is presumed to initiate and induce heterophylly in *L. arcuata* (Kuwabara et al., 2003). Interestingly, ABA application was sufficient for the formation of the terrestrial leaf form in other heterophyllous aquatic plants also (Kane and Albert, 1987; Goliber and Feldman, 1989; Hsu et al., 2001). Regulation of heterophylly by ABA in many plants is not surprising, since the origin of ABA signaling pathway is thought to be ancient and is conserved in the green plant lineage (Takezawa et al., 2011). Thus, these facts indicate that the ABA signaling pathway can be considered a hotspot in plant evolution to acquire heterophylly, even though this trait is suggested to have evolved multiple times in distant plant species.

HOW DOES ETHYLENE REGULATE HETEROPHYLLY?

Ethylene has a long history as a gaseous phytohormone since its discovery from studies initiated in the late 1800s (Fahnestock, 1858). Subsequently, researchers identified ethylene as the active component of the illuminating gas that affects plant growth and ethylene synthesis by plants was reported in the early 1900s (Neljubow, 1901). Ethylene (C₂H₄) regulates many aspects of plant developmental and physiological processes, including seed germination, root initiation, flower and leaf senescence, abscission, fruit ripening, wound response, and defense against diseases (Schaller, 2012). Some studies have shown the relationship between ethylene and heterophylly. In *L. arcuata*, ethylene as well as ABA are known to be the key factors regulating heterophylly; ethylene treatment induced the formation of submerged leaves in this plant (Kuwabara et al., 2003; Figure 2). Additionally, endogenous concentration of



Species (Family)	Aerial-type leaves	Submerged-type leaves	Related hormones	Mechanism of heterophylly
<i>Potamogeton nodosus</i> (Potamogetonaceae)			ABA <chem>CC1=C(C(=O)O)C(=O)C(C)C1O</chem>	Unknown
<i>Ludwigia arcuata</i> (Onagraceae)			ABA <chem>CC1=C(C(=O)O)C(=O)C(C)C1O</chem> Ethylene <chem>C=CC=C</chem>	Change in cell division and elongation pattern
<i>Rorippa aquatica</i> (Brassicaceae)			GA <chem>CC1=C(C(=O)O)C(=O)C(C)C1O</chem>	Change in organogenetic activity through regulation of differentiation

FIGURE 2 | Comparison of heterophylly seen in *Potamogeton nodosus*, *Ludwigia arcuata*, and *Rorippa aquatica*.

ethylene was higher in these plants under submergence compared to those under terrestrial conditions (Kuwabara et al., 2003). Developmental and anatomical studies have suggested that the changes in cell division patterns induced by ethylene resulted in leaf form alteration in *L. arcuata* (Kuwabara and Nagata, 2006). Several studies have indicated that ethylene not only regulates cell size, often restricting cell elongation, but also regulates cell division (Iqbal et al., 2017). Ethylene is thought to be synthesized in almost all plant tissues and accumulates in the plant tissues under submergence because solubility of ethylene in water is low (Davis and McKetta, 1960) and it cannot evaporate easily from the submerged plant parts. The increased

concentration of ethylene accumulated in the submerged parts of *L. arcuata* is assumed to induce changes in cell elongation and cell division and regulate leaf morphology. Moreover, it is known that ethylene not only acts on ABA metabolism to reduce ABA levels, but also negatively regulates ABA signaling during germination in *Arabidopsis thaliana* (L.) Heynh. (*Arabidopsis* hereafter) (Gazzarrini and McCourt, 2001). Indeed, ethylene treatment reduced endogenous level of ABA in *L. arcuata* (Kuwabara et al., 2003), suggesting that ethylene regulates heterophylly through suppression of ABA and regulating cell division and elongation. In addition to heterophylly, ethylene is also reported to be involved in submergence responses in deepwater rice

(Hattori et al., 2009). The increase in concentration of ethylene in the submerged parts of deepwater rice triggers remarkable elongation of internodes, which have a hollow structure to allow gas exchange with the atmosphere. Moreover, ethylene is known to be involved in development of aerenchyma, which is an intercellular space that acts as a mediator of internal gas exchange and maintains physical strength of tissues (Dengler, 1999). These phenomena are also a type of phenotypic plasticity. These studies indicate that utilization of the ethylene signaling pathway under submergence by plants has evolved multiple times for the regulation of phenotypic plasticity, including heterophylly. Thus, it is likely that the ethylene-related pathway may be a well-used machinery of phenotypic plasticity in aquatic plants, as is the case with ABA.

HOW DO GIBBERELLINS REGULATE HETEROPHYLLY?

Gibberellins (GAs or GA) were first identified in response to the pathogenic fungus *Gibberella fujikuroi*, which causes excessive elongation of the stem in *Oryza sativa* (rice) (Yabuta and Sumiki, 1938). To date, more than 130 GAs have been identified from fungi, bacteria, and plants (Yamaguchi, 2008). GA is indispensable for various kinds of plant processes such as seed germination, stem elongation, expansion of leaf lamina, pollen maturation, and flowering (Sun, 2010). GA is also involved in the regulation of heterophylly. In the North American semi-aquatic plant *Rorippa aquatica*, GA is thought to be a key factor for the regulation of heterophylly (Nakayama et al., 2014); this plant produces deeply dissected leaves under water and simple leaves with smooth margins under terrestrial conditions (**Figure 2**). Leaf complexity of *R. aquatica* is similarly affected by changes in the ambient temperature; deeply dissected leaves develop when plants grow at 20°C, whereas simple leaves with entire margins develop when plants are grown at 25°C (**Figures 1A,B**). A previous study showed that in *R. aquatica*, the expression level of *KNOTTED1 LIKE HOMEBOX (KNOX1)* ortholog changes in response to changes in the ambient temperature. KNOX1 protein is known to regulate GA levels in leaf primordia (Sakamoto et al., 2001). GA concentration in leaf primordia changes in response to the ambient temperature, and exogenous GA application alters the leaf complexity in *R. aquatica*. Similarly, in *Solanum lycopersicum* (tomato), GA promotes differentiation of leaf primordia, and disables transient organogenetic activity in the leaf margins, from which marginal serrations and leaflets arise; thus, GA reduces leaf complexity in *S. lycopersicum* (Yanai et al., 2011). Therefore, heterophylly in *R. aquatica* is thought to be regulated by the alteration of GA concentrations in leaf primordia via the *KNOX1* gene. Developmental studies in *R. aquatica* have indicated that proximal leaflet initiation in leaf primordia is an important factor in determining final leaf form. These studies suggest that the local GA concentration in leaf primordia is important for the regulation of heterophylly in *R. aquatica*. In addition to heterophylly, Arabidopsis mutants, which are insensitive to the GA and defective in its biosynthesis show

a delayed appearance of the first adult leaf compared to WT (Chien and Sussex, 1996), suggesting that GA is involved in the heteroblasty. Therefore, GA may be utilized both of heterophylly and heteroblasty. Interestingly, a previous study showed that a single leaf can sense and transmit changes in ambient temperature to newly developed leaves in *R. aquatica* (Nakayama and Kimura, 2015), suggesting that a long distance signal may be generated at a certain developmental stage of leaves. Transmembrane transport of GA in Arabidopsis is reported to be regulated by AtSWEET13, AtSWEET14, and AtNPF2.10/GTR proteins (Kanno et al., 2016). *R. aquatica* belongs to the same family as Arabidopsis and hence the expression pattern and function of many genes are expected to be similar in both the plant species. Similar orthologs may also be responsible for cellular GA uptake in leaf primordia of *R. aquatica*. Although GA can be transported through the phloem (Hoad and Bowen, 1968), the detailed molecular mechanism of the long distance GA transport remains unclear. A better understanding on the long distance GA transport may reveal its role in regulating heterophylly.

HOW DO AUXINS REGULATE HETEROPHYLLY?

Auxins play a key role in an extraordinarily wide variety of biological processes in terrestrial plants. For example, auxins are involved in plant growth and development such as abscission, apical dominance, cell division and differentiation, flowering, senescence, and tropic responses (Sauer et al., 2013). Auxin biosynthesis is intricate and multiple pathways have been postulated to explain auxin biosynthesis (Chandler, 2009; Normanly, 2010; Zhao, 2010). Additionally, auxin biosynthetic pathways are differentially regulated in response to environmental stimuli (Tao et al., 2008; Le et al., 2010). In Arabidopsis, auxin is thought to be synthesized throughout the shoot apical meristem (Cheng et al., 2006; Stepanova et al., 2008) and transported with transporter proteins such as PIN1 (Galweiler et al., 1998). Several papers and reviews detail their mechanism of auxin transport (Adamowski and Friml, 2015). The polarization of auxins is indispensable for the initiation of leaf primordia and leaf lamina outgrowth during leaf development (Byrne, 2012; Townsley and Sinha, 2012). First, auxin maxima develop at the tip of the leaf primordia, and are thought to lead to distal growth. The auxin is then transported from the leaf margins and distributed on either side of the midvein; this facilitates leaf lamina outgrowth as a downstream target of the adaxial-abaxial polarity pathway (Scarpella et al., 2010). Additionally, auxins are also involved in vascular patterning in leaves (Scarpella et al., 2010), which is known to affect leaf morphology. Several studies have demonstrated that auxins affect leaf morphology and development (Barkoulas et al., 2008; Koenig et al., 2009). Therefore, auxins may also be related to heterophylly as a downstream target of some upstream regulators including other phytohormones. Although there is substantial evidence on the importance of auxins in leaf development, the relationship between auxin and heterophylly

remains unclear. Recently some studies have demonstrated that a basic helix-loop-helix transcription factor, *PHYTOCHROME-INTERACTING FACTOR 4* (*PIF4*), regulates levels of auxin and expression of genes involved in auxin biosynthesis in response to change in ambient temperature (Franklin et al., 2011). Changes in ambient temperature are known to affect leaf morphology in *R. aquatica* (Nakayama et al., 2014). A blue light receptor protein, Cryptochrome 1 (*CRY1*), is reported to interact with the transcription factor *PIF4* to regulate hypocotyl elongation in response to blue light (Ma et al., 2016). Blue light is one of the key environmental cues for plants under submerged conditions and is known to induce the development of submerged leaves on plants grown under the submergence (Kao and Lin, 2010). These results suggest that auxin may be one regulator of heterophylly via the transcription factors *PIF4* and receptor protein *CRY1*, in addition to its role as a candidate for downstream target gene expression regulation.

WHAT IS THE SCOPE FOR FUTURE STUDIES ON HETEROPHYLLY?

Research in the past few decades has elucidated the transport processes and receptor mechanisms of various phytohormones as well as their role in various developmental processes using model plant species. These studies have demonstrated that phytohormones mutually regulate signaling and metabolic networks (Verma et al., 2016). Recent studies have identified new hormones related to the regulation of plant architecture and/or morphology (Waters et al., 2017). An interesting observation in a recent study emphasized the role of defensin-like secretory epidermal patterning factor (*EPF*) peptide hormones in regulating stomatal development in plants (Hara et al., 2009; Sugano et al., 2010). In many heterophyllous plants, it is known that stomatal density is altered in response to changes in the surrounding environment. Therefore, it is likely that *EPF* peptide hormones are also involved in the regulation of stomatal density in heterophyllous plants. These facts indicate that there is scope to study the relationships between heterophylly and the new phytohormones and their interactions with classic phytohormones for a better understanding of the phenomenon of heterophylly. Such studies will elucidate the mechanisms of acquired phenotypic plasticity, including heterophylly, through the modification of existing networks. Sequencing methods that reveal transcriptomic and epigenetic changes in response to surrounding environments have been developed during the past decade (Buenrostro et al., 2013). Additionally, a high-throughput system to measure endogenous concentration of

multiple hormones, including various derivative species, has also been developed (Kojima et al., 2009). Modeling methods to integrate different levels of large-scale data and explore cause-effect relationships from the integrated data have been developed (Granier and Vile, 2014). Combination of these techniques can help to explore and understand the intricate interaction of hormones and their interactions with mechanisms of heterophylly.

Heterophylly has evolved multiple times independently during plant evolution. As expected, the mechanism of heterophylly in each plant seems to be different. For instance, heterophylly in *R. aquatica* is expressed via the *KNOX-GA* gene module, which regulates organogenetic activity, whereas the ethylene related pathway, which regulates cell division and elongation pattern, is reported to regulate heterophylly in *L. arcuata* (Kuwabara et al., 2003; Nakayama et al., 2014). In *P. nodosus*, the *ABA*-related pathway is thought to induce heterophylly (Anderson, 1978). Hence, heterophylly is an interesting model to study the convergent evolution of plant species. Although debatable, the major biological question provoked by previous studies is the implication that phenotypic plasticity can promote divergence among populations and occasionally lead to speciation (Pfennig et al., 2010). These facts signify the urgent need to study heterophylly to explore the evolution of plants as well as to understand the underlying ecological and physiological interactions.

Thus, the answer to the question “What is the scope for future studies on heterophylly?” would be to understand the relationship between heterophylly and the new hormones and the relationship between heterophylly and speciation. These studies will yield novel insights into not only the molecular mechanisms of phenotypic plasticity in plants but the evolution of plants.

AUTHOR CONTRIBUTIONS

All authors listed have made a substantial, direct and intellectual contribution to the work, and approved it for publication.

FUNDING

This research was supported by a Grant-in-Aid for Scientific Research on Innovative Areas (JP16H01472), JSPS KAKENHI (JP16K07408) and the MEXT-Supported Program for the Strategic Research Foundation at Private Universities (S1511023) to SK, as well as by a Research Fellowship from JSPS to HN. HN and NS were supported by a NSF grant (1558900).

REFERENCES

- Adamowski, M., and Friml, J. (2015). PIN-dependent auxin transport: action, regulation, and evolution. *Plant Cell* 27, 20–32. doi: 10.1105/tpc.114.134874
- Alpert, P., and Simms, E. L. (2002). The relative advantages of plasticity and fixity in different environments: when is it good for a plant to adjust? *Evol. Ecol.* 16, 285–297. doi: 10.1023/A:1019684612767
- Anderson, L. W. (1978). Abscisic acid induces formation of floating leaves in the heterophyllous aquatic angiosperm *Potamogeton nodosus*. *Science* 201, 1135–1138. doi: 10.1126/science.201.4361.1135
- Barkoulas, M., Hay, A., Kougioumoutzi, E., and Tsiantis, M. (2008). A developmental framework for dissected leaf formation in the Arabidopsis relative *Cardamine hirsuta*. *Nat. Genet.* 40, 1136–1141. doi: 10.1038/ng.189

- Boursiac, Y., Leran, S., Corratge-Faillie, C., Gojon, A., Krouk, G., and Lacombe, B. (2013). ABA transport and transporters. *Trends Plant Sci.* 18, 325–333. doi: 10.1016/j.tplants.2013.01.007
- Bruzzone, S., Moreschi, I., Usai, C., Guida, L., Damonte, G., Salis, A., et al. (2007). Abscisic acid is an endogenous cytokine in human granulocytes with cyclic ADP-ribose as second messenger. *Proc. Natl. Acad. Sci. U.S.A.* 104, 5759–5764. doi: 10.1073/pnas.0609379104
- Buenrostro, J. D., Giresi, P. G., Zaba, L. C., Chang, H. Y., and Greenleaf, W. J. (2013). Transposition of native chromatin for fast and sensitive epigenomic profiling of open chromatin, DNA-binding proteins and nucleosome position. *Nat. Methods* 10, 1213–1218. doi: 10.1038/nmeth.2688
- Byrne, M. E. (2012). Making leaves. *Curr. Opin. Plant Biol.* 15, 24–30. doi: 10.1016/j.pbi.2011.10.009
- Chandler, J. W. (2009). Local auxin production: a small contribution to a big field. *Bioessays* 31, 60–70. doi: 10.1002/bies.080146
- Chater, C. C., Oliver, J., Casson, S., and Gray, J. E. (2014). Putting the brakes on: abscisic acid as a central environmental regulator of stomatal development. *New Phytol.* 202, 376–391. doi: 10.1111/nph.12713
- Cheng, Y., Dai, X., and Zhao, Y. (2006). Auxin biosynthesis by the YUCCA flavin monooxygenases controls the formation of floral organs and vascular tissues in *Arabidopsis*. *Genes Dev.* 20, 1790–1799. doi: 10.1101/gad.1415106
- Chien, J. C., and Sussex, I. M. (1996). Differential regulation of trichome formation on the adaxial and abaxial leaf surfaces by gibberellins and photoperiod in *Arabidopsis thaliana* (L.) Heynh. *Plant Physiol.* 111, 1321–1328. doi: 10.1104/pp.111.4.1321
- Davis, J. E., and McKetta, J. J. (1960). Solubility of ethylene in water. *J. Chem. Eng. Data* 5, 374–375. doi: 10.1021/je60007a039
- Dengler, N. G. (1999). Anisophylly and dorsiventral shoot symmetry. *Int. J. Plant Sci.* 160, S67–S80. doi: 10.1086/314218
- Ernande, B., and Dieckmann, U. (2004). The evolution of phenotypic plasticity in spatially structured environments: implications of intraspecific competition, plasticity costs and environmental characteristics. *J. Evol. Biol.* 17, 613–628. doi: 10.1111/j.1420-9101.2004.00691.x
- Fahnestock, G. W. (1858). Memoranda of the effects of carburetted hydrogen gas upon a collection of exotic plants. *Proc. Acad. Nat. Sci. Phila.* 1, 118–134.
- Fassett, N. C. (1930). *A Manual of Aquatic Plants*. Madison, WI: University of Wisconsin press.
- Franklin, K. A., Lee, S. H., Patel, D., Kumar, S. V., Spartz, A. K., Gu, C., et al. (2011). Phytochrome-interacting factor 4 (PIF4) regulates auxin biosynthesis at high temperature. *Proc. Natl. Acad. Sci. U.S.A.* 108, 20231–20235. doi: 10.1073/pnas.1110682108
- Galweiler, L., Guan, C., Muller, A., Wisman, E., Mendgen, K., Yephremov, A., et al. (1998). Regulation of polar auxin transport by AtPIN1 in *Arabidopsis* vascular tissue. *Science* 282, 2226–2230. doi: 10.1126/science.282.5397.2226
- Gazzarrini, S., and McCourt, P. (2001). Genetic interactions between ABA, ethylene and sugar signaling pathways. *Curr. Opin. Plant Biol.* 4, 387–391. doi: 10.1016/S1369-5266(00)00190-4
- Goda, H., Sasaki, E., Akiyama, K., Maruyama-Nakashita, A., Nakabayashi, K., Li, W., et al. (2008). The AtGenExpress hormone and chemical treatment data set: experimental design, data evaluation, model data analysis and data access. *Plant J.* 55, 526–542. doi: 10.1111/j.0960-7412.2008.03510.x
- Goliber, T. E., and Feldman, L. J. (1989). Osmotic stress, endogenous abscisic acid and the control of leaf morphology in *Hippuris vulgaris* L. *Plant Cell Environ.* 12, 163–171. doi: 10.1111/j.1365-3040.1989.tb01929.x
- Goliber, T. E., and Feldman, L. J. (1990). Developmental analysis of leaf plasticity in the heterophyllous aquatic plant *Hippuris vulgaris*. *Am. J. Bot.* 77, 399–412. doi: 10.2307/2444726
- Granier, C., and Vile, D. (2014). Phenotyping and beyond: modelling the relationships between traits. *Curr. Opin. Plant Biol.* 18, 96–102. doi: 10.1016/j.pbi.2014.02.009
- Hara, K., Yokoo, T., Kajita, R., Onishi, T., Yahata, S., Peterson, K. M., et al. (2009). Epidermal cell density is autoregulated via a secretory peptide, EPIDERMAL PATTERNING FACTOR 2 in *Arabidopsis* leaves. *Plant Cell Physiol.* 50, 1019–1031. doi: 10.1093/pcp/pcp068
- Hattori, Y., Nagai, K., Furukawa, S., Song, X. J., Kawano, R., Sakakibara, H., et al. (2009). The ethylene response factors SNORKEL1 and SNORKEL2 allow rice to adapt to deep water. *Nature* 460, 1026–1030. doi: 10.1038/nature08258
- Hoad, G. V., and Bowen, M. R. (1968). Evidence for gibberellin-like substances in phloem exudate of higher plants. *Planta* 82, 22–32. doi: 10.1007/bf00384695
- Hsu, T. C., Liu, H. C., Wang, J. S., Chen, R. W., Wang, Y. C., and Lin, B. L. (2001). Early genes responsive to abscisic acid during heterophyllous induction in *Marsilea quadrifolia*. *Plant Mol. Biol.* 47, 703–715. doi: 10.1023/A:1013612331583
- Iida, S., Ikeda, M., Amano, M., Sakayama, H., Kadono, Y., and Kosuge, K. (2016). Loss of heterophylly in aquatic plants: not ABA-mediated stress but exogenous ABA treatment induces stomatal leaves in *Potamogeton perfoliatus*. *J. Plant Res.* 129, 853–862. doi: 10.1007/s10265-016-0844-x
- Iqbal, N., Khan, N. A., Ferrante, A., Trivellini, A., Francini, A., and Khan, M. I. R. (2017). Ethylene role in plant growth, development and senescence: interaction with other phytohormones. *Front. Plant Sci.* 8:475. doi: 10.3389/fpls.2017.00475
- Kane, M. E., and Albert, L. S. (1987). Abscisic acid induces aerial leaf morphology and vasculature in submerged *Hippuris vulgaris* L. *Aquat. Bot.* 28, 81–88. doi: 10.1016/0304-3770(87)90057-X
- Kanno, Y., Oikawa, T., Chiba, Y., Ishimaru, Y., Shimizu, T., Sano, N., et al. (2016). AtSWEET13 and AtSWEET14 regulate gibberellin-mediated physiological processes. *Nat. Commun.* 7:13245. doi: 10.1038/ncomms13245
- Kao, W. Y., and Lin, B. L. (2010). Phototropic leaf movements and photosynthetic performance in an amphibious fern, *Marsilea quadrifolia*. *J. Plant Res.* 123, 645–653. doi: 10.1007/s10265-009-0300-2
- Koenig, D., Bayer, E., Kang, J., Kuhlemeier, C., and Sinha, N. (2009). Auxin patterns *Solanum lycopersicum* leaf morphogenesis. *Development* 136, 2997–3006. doi: 10.1242/dev.033811
- Kojima, M., Kamada-Nobusada, T., Komatsu, H., Takei, K., Kuroha, T., Mizutani, M., et al. (2009). Highly sensitive and high-throughput analysis of plant hormones using MS-probe modification and liquid chromatography-tandem mass spectrometry: an application for hormone profiling in *Oryza sativa*. *Plant Cell Physiol.* 50, 1201–1214. doi: 10.1093/pcp/pcp057
- Kuwabara, A., Ikegami, K., Koshihara, T., and Nagata, T. (2003). Effects of ethylene and abscisic acid upon heterophylly in *Ludwigia arcuata* (Onagraceae). *Planta* 217, 880–887. doi: 10.1007/s00425-003-1062-z
- Kuwabara, A., and Nagata, T. (2006). Cellular basis of developmental plasticity observed in heterophyllous leaf formation of *Ludwigia arcuata* (Onagraceae). *Planta* 224, 761–770. doi: 10.1007/s00425-006-0258-4
- Le, C. S., Schmelz, E. A., and Chourey, P. S. (2010). Sugar levels regulate tryptophan-dependent auxin biosynthesis in developing maize kernels. *Plant Physiol.* 153, 306–318. doi: 10.1104/pp.110.155226
- Lievens, L., Pollier, J., Goossens, A., Beyaert, R., and Staal, J. (2017). Abscisic acid as pathogen effector and immune regulator. *Front. Plant Sci.* 8:587. doi: 10.3389/fpls.2017.00587
- Ma, D., Li, X., Guo, Y., Chu, J., Fang, S., Yan, C., et al. (2016). Cryptochrome 1 interacts with PIF4 to regulate high temperature-mediated hypocotyl elongation in response to blue light. *Proc. Natl. Acad. Sci. U.S.A.* 113, 224–229. doi: 10.1073/pnas.1511437113
- Maršálek, B., Zahradníčková, H., and Hronková, M. (1992). Extracellular abscisic acid produced by cyanobacteria under salt stress. *J. Plant Physiol.* 139, 506–508. doi: 10.1016/S0176-1617(11)80503-1
- Nakashima, K., and Yamaguchi-Shinozaki, K. (2013). ABA signaling in stress-response and seed development. *Plant Cell Rep.* 32, 959–970. doi: 10.1007/s00299-013-1418-1
- Nakayama, H., and Kimura, S. (2015). Leaves may function as temperature sensors in the heterophylly of *Rorippa aquatica* (Brassicaceae). *Plant Signal. Behav.* 10, e1091909. doi: 10.1080/15592324.2015.1091909
- Nakayama, H., Nakayama, N., Seiki, S., Kojima, M., Sakakibara, H., Sinha, N., et al. (2014). Regulation of the KNOX-GA gene module induces heterophyllic alteration in North American lake cress. *Plant Cell* 26, 4733–4748. doi: 10.1105/tpc.114.130229
- Nakayama, N., Nakayama, N., Nakamasu, A., Sinha, N., and Kimura, S. (2012). Toward elucidating the mechanisms that regulate heterophylly. *Plant Morphol.* 24, 57–63. doi: 10.5685/plmorphol.24.57
- Neljubow, D. (1901). Über die horizontale nutation der stengel von *Pisum sativum* und einiger anderen pflanzen. *Beih. Bot. Zentralb.* 10, 128–139.
- Normanly, J. (2010). Approaching cellular and molecular resolution of auxin biosynthesis and metabolism. *Cold Spring Harb. Perspect. Biol.* 2:a001594. doi: 10.1101/cshperspect.a001594

- Palacio-Lopez, K., Beckage, B., Scheiner, S., and Molofsky, J. (2015). The ubiquity of phenotypic plasticity in plants: a synthesis. *Ecol. Evol.* 5, 3389–3400. doi: 10.1002/ece3.1603
- Pfennig, D. W., Wund, M. A., Snell-Rood, E. C., Cruickshank, T., Schlichting, C. D., and Moczek, A. P. (2010). Phenotypic plasticity's impacts on diversification and speciation. *Trends Ecol. Evol.* 25, 459–467. doi: 10.1016/j.tree.2010.05.006
- Sakamoto, T., Kamiya, N., Ueguchi-Tanaka, M., Iwahori, S., and Matsuoka, M. (2001). KNOX homeodomain protein directly suppresses the expression of a gibberellin biosynthetic gene in the tobacco shoot apical meristem. *Genes Dev.* 15, 581–590. doi: 10.1101/gad.867901
- Sauer, M., Robert, S., and Kleine-Vehn, J. (2013). Auxin: simply complicated. *J. Exp. Bot.* 64, 2565–2577. doi: 10.1093/jxb/ert139
- Scarpella, E., Barkoulas, M., and Tsiantis, M. (2010). Control of leaf and vein development by auxin. *Cold Spring Harb. Perspect. Biol.* 2:a001511. doi: 10.1101/cshperspect.a001511
- Schaller, G. E. (2012). Ethylene and the regulation of plant development. *BMC Biol.* 10:9. doi: 10.1186/1741-7007-10-9
- Sicard, A., Thamm, A., Marona, C., Lee, Y. W., Wahl, V., Stinchcombe, J. R., et al. (2014). Repeated evolutionary changes of leaf morphology caused by mutations to a homeobox gene. *Curr. Biol.* 24, 1880–1886. doi: 10.1016/j.cub.2014.06.061
- Stepanova, A. N., Robertson-Hoyt, J., Yun, J., Benavente, L. M., Xie, D. Y., Dolezal, K., et al. (2008). TAA1-mediated auxin biosynthesis is essential for hormone crosstalk and plant development. *Cell* 133, 177–191. doi: 10.1016/j.cell.2008.01.047
- Sugano, S. S., Shimada, T., Imai, Y., Okawa, K., Tamai, A., Mori, M., et al. (2010). Stomagen positively regulates stomatal density in Arabidopsis. *Nature* 463, 241–244. doi: 10.1038/nature08682
- Sun, T. P. (2010). Gibberellin-GID1-DELLA: a pivotal regulatory module for plant growth and development. *Plant Physiol.* 154, 567–570. doi: 10.1104/pp.110.161554
- Takezawa, D., Komatsu, K., and Sakata, Y. (2011). ABA in bryophytes: how a universal growth regulator in life became a plant hormone? *J. Plant Res.* 124, 437–453. doi: 10.1007/s10265-011-0410-5
- Tao, Y., Ferrer, J. L., Ljung, K., Pojer, F., Hong, F., Long, J. A., et al. (2008). Rapid synthesis of auxin via a new tryptophan-dependent pathway is required for shade avoidance in plants. *Cell* 133, 164–176. doi: 10.1016/j.cell.2008.01.049
- Townsley, B. T., and Sinha, N. R. (2012). A new development: evolving concepts in leaf ontogeny. *Annu. Rev. Plant Biol.* 63, 535–562. doi: 10.1146/annurev-arplant-042811-105524
- Verma, V., Ravindran, P., and Kumar, P. P. (2016). Plant hormone-mediated regulation of stress responses. *BMC Plant Biol.* 16:86. doi: 10.1186/s12870-016-0771-y
- Vishwakarma, K., Upadhyay, N., Kumar, N., Yadav, G., Singh, J., Mishra, R. K., et al. (2017). Abscisic acid signaling and abiotic stress tolerance in plants: a review on current knowledge and future prospects. *Front. Plant Sci.* 8:161. doi: 10.3389/fpls.2017.00161
- Wanke, D. (2011). The ABA-mediated switch between submersed and emerged lifestyles in aquatic macrophytes. *J. Plant Res.* 124, 467–475. doi: 10.1007/s10265-011-0434-x
- Waters, M. T., Gutjahr, C., Bennett, T., and Nelson, D. C. (2017). Strigolactone signaling and evolution. *Annu. Rev. Plant Biol.* 68, 291–322. doi: 10.1146/annurev-arplant-042916-040925
- Yabuta, T., and Sumiki, Y. (1938). On the crystal of gibberellin, a substance to promote plant growth. *J. Agric. Chem. Soc. Japan* 14:1526. doi: 10.1271/nogeikagaku1924.14.12_1526
- Yamaguchi, S. (2008). Gibberellin metabolism and its regulation. *Annu. Rev. Plant Biol.* 59, 225–251. doi: 10.1146/annurev-arplant.59.032607.092804
- Yamaguchi-Shinozaki, K., and Shinozaki, K. (2006). Transcriptional regulatory networks in cellular responses and tolerance to dehydration and cold stresses. *Annu. Rev. Plant Biol.* 57, 781–803. doi: 10.1146/annurev-arplant.57.032905.105444
- Yanai, O., Shani, E., Russ, D., and Ori, N. (2011). Gibberellin partly mediates LANCEOLATE activity in tomato. *Plant J.* 68, 571–582. doi: 10.1111/j.1365-3113.2011.04716.x
- Zhao, Y. (2010). Auxin biosynthesis and its role in plant development. *Annu. Rev. Plant Biol.* 61, 49–64. doi: 10.1146/annurev-arplant-042809-112308
- Zotz, G., Wilhelm, K., and Becker, A. (2011). Heteroblasty—a review. *Bot. Rev.* 77, 109–151. doi: 10.1007/s12229-010-9062-8

Conflict of Interest Statement: The authors declare that the research was conducted in the absence of any commercial or financial relationships that could be construed as a potential conflict of interest.

Copyright © 2017 Nakayama, Sinha and Kimura. This is an open-access article distributed under the terms of the Creative Commons Attribution License (CC BY). The use, distribution or reproduction in other forums is permitted, provided the original author(s) or licensor are credited and that the original publication in this journal is cited, in accordance with accepted academic practice. No use, distribution or reproduction is permitted which does not comply with these terms.

SCIENTIFIC REPORTS

OPEN

A novel series of high-efficiency vectors for TA cloning and blunt-end cloning of PCR products

Ken Motohashi ^{1,2}

An efficient PCR cloning method is indispensable in modern molecular biology, as it can greatly improve the efficiency of DNA cloning processes. Here, I describe the development of three vectors for TA cloning and blunt-end cloning. Specifically, pCRT and pCRZeroT were designed to improve the efficiency of TA cloning. pCRZeroT can also be used with pCRZero to facilitate blunt-end cloning using the *ccdB* gene. Using pCRZero and pCRZeroT and applying the Golden Gate reaction, I developed a direct PCR cloning protocol with non-digested circular vectors and PCR products. This direct PCR cloning protocol yielded colony-formation rates and cloning efficiencies that are comparable with those obtained by conventional PCR cloning with pre-digested vectors and PCR products. The three plasmids I designed are available from Addgene (<https://www.addgene.org/>).

Polymerase chain reaction (PCR) is an indispensable tool for amplification of genomic DNA and transcripts to analyze their functions¹. Improvements to the basic technique to facilitate highly efficient molecular cloning of PCR products into a vector are required to promote research projects. Various types of thermostable DNA polymerases are commercially available for PCR amplification. Of these, Taq DNA polymerase is the most widely used; this enzyme attaches a deoxyadenosine triphosphate (dA) to the 3'-end of amplified DNA². In contrast, various high-fidelity thermostable DNA polymerases that possess 3' to 5' exonuclease activity for proofreading, such as Pfu DNA polymerase³, KOD DNA polymerase⁴ and Phusion DNA polymerase⁵, produce the blunt-end DNA fragments. Due to the diverse types of PCR product that are generated, choice of cloning vector is a critical step that can ultimately determine cloning efficiency⁶.

Vectors that have a T-overhang at the 3'-end were developed as so-called 'T-vectors' for cloning of dA-tailed PCR products amplified by Taq DNA polymerase^{7,8}. To prepare the T-overhang vector from general cloning vectors, dideoxythymidine triphosphate (ddT) is incorporated at the 3'-terminus of a linearized blunt end vector by using terminal deoxynucleotidyl-transferase⁷. Unfortunately, this strategy is not widely adopted by researchers, as the reagents are not frequently used. The availability of commercially available ready-to-use T-vectors has obviated the need for very specific and complicated procedures; however, while the vectors are generally very convenient, they are expensive. Another T-vector preparation-method uses XcmI (a well-known type IIS restriction enzyme that recognizes an asymmetric nucleotide sequence) to digest outside of this recognition sequence and generate a T-overhang for TA cloning⁸. To use these T-vectors, the two XcmI sites that are designed to produce the 3'-end T-overhang are introduced into a specific vector⁹⁻¹¹. Preparation of T-vectors by XcmI cleavage is a relatively easy way to produce T-overhangs, because XcmI is a commonly used restriction enzyme. However, XcmI-dependent T-vector preparation is hampered by a high background colony rate; this is attributable to re-ligation of small excised DNA fragments into the digested empty vector^{9,10}.

In contrast to TA cloning using a single nucleotide T-overhang, blunt-end cloning of PCR products is less efficient because the terminal ends of the DNA fragment are not sticky^{12,13}. To overcome the low efficiency, ZERO-background-cloning using the *ccdB* gene, an active cytotoxic factor in *Escherichia coli*, was developed as a positive-selection system¹⁴. *ccdB*-sensitive *E. coli* cells carrying empty vectors cannot survive in this system because the expression of CcdB protein is lethal¹⁵.

Based on their needs, researchers should therefore choose either a T-overhang vector or a blunt-end vector including the *ccdB* gene^{14,16,17}. Ideally, a complete vector system that covers both choices should be available. However, such a vector has been realized only partially. pPCV can be used for both TA-cloning and blunt-end

¹Department of Frontier Life Sciences, Faculty of Life Sciences, Kyoto Sangyo University, Kamigamo Motoyama, Kita-ku, Kyoto, 603-8555, Japan. ²Center for Ecological Evolutionary Developmental Biology, Kyoto Sangyo University, Kamigamo Motoyama, Kita-Ku, Kyoto, 603-8555, Japan. Correspondence and requests for materials should be addressed to K.M. (email: motohas@cc.kyoto-su.ac.jp)

cloning, but is not applicable to positive screening because the plasmid does not contain the *E. coli*-lethal *ccdB* gene¹³. pBS2nnd and pBS3nnd are also utilized as bifunctional vectors for TA-cloning and blunt-end cloning, but screening of the vectors requires blue/white selection using the *lacZ* α gene¹⁸. pCAMBIA1300¹⁹ and modified pGreen vectors²⁰, which contain the *ccdB* gene, can be applied to the ZERO-background screening system of TA-cloning for plant functional genomics, but not to blunt-end cloning. Attempts have also been made to develop bifunctional pKILPCR vectors using the ZERO-background screening system for both TA-cloning and blunt-end cloning²¹. However, the linearization of T-overhang of pKILPCRs by type IIS restriction enzyme AspEI (Eam1105, AhdI) lacked adequate reproducibility and the vector showed low cloning efficiency owing to the contaminant exonuclease activity in the AspEI, which led to the blunting of DNA fragments.

In this study, I developed a series of three types of PCR cloning vectors to meet the need for a vector suitable for both TA and blunt-end cloning. Further, I demonstrate here the utility of this vector series using a direct PCR cloning protocol. This protocol inserts PCR products into non-digested circular vectors via the Golden Gate reaction that can simultaneously digest, ligate, and assemble several DNA-fragments into a vector^{22,23}. All three PCR cloning vectors (pCRT, pCRZero, and pCRZeroT) are available to researchers via the Addgene repository (<https://www.addgene.org/>).

Results and Discussion

Design of plasmid vectors for PCR cloning. I constructed three plasmid vectors for PCR cloning in this study (Fig. 1). In pCRT (2,728 bp) for TA cloning, T-overhang vector for cloning of dA-tailed PCR products amplified by Taq DNA polymerase can be prepared with one step digestion by a type IIS restriction enzyme, XcmI (Fig. 1a). An NheI site was also introduced into the pCRT vector to reduce background colony formations due to empty vector. In pCRZero (3,272 bp) that is used for blunt-end cloning, positive colonies are selected when the *lacZ* α -*ccdB* fusion gene in the vector is disrupted due to insertion of PCR products at an EcoRV site in the vector (Fig. 1b). The inserted PCR fragments can be excised from pCRZero with twelve restriction enzymes (Fig. 1b). The pCRZeroT (2,975 bp) vector is compatible with both TA cloning and blunt-end cloning (Fig. 1c). The SmaI site on the *ccdB* gene in pCRZeroT was introduced as the cloning site for positive selection of blunt-end cloning. pCRZeroT can be also prepared as a T-vector for TA cloning by performing a one-step digestion with XcmI. pCRZeroT has an additional SmaI/XmaI restriction site between two XcmI restriction sites; this reduces background colony-formation due to empty vectors that persist after TA cloning. The introduced SmaI site (CCC|GGG) in pCRZeroT can also be used as an XmaI site (C|CCGGG) to reduce background colony formation (Fig. 1c). The DNA sequence and the plasmid text map of three plasmids are attached in Supplementary Dataset S1. Primers listed in Table S3 can be used for DNA sequencing of cloned PCR-fragments (Table S3).

Lethality of the CcdB protein in *E. coli* cells carrying *ccdB*-encoding plasmids. Expression of the *ccdB* gene is lethal in *E. coli ccdB*-sensitive strains, such as DH5 α ^{15,24}. PCR cloning using the pCRZero and pCRZeroT plasmids, which encode the *ccdB* gene, reduce empty vector-dependent background because *E. coli ccdB*-sensitive strains carrying empty vectors cannot form colonies following plating. *E. coli* lethality caused by expression of the *ccdB* gene was checked by transformation of the *ccdB*-sensitive strain, DH5 α , with pCRZero and pCRZeroT (Fig. 2). The *E. coli* strain XL10-Gold (a *ccdB*-resistant strain) carrying pCRT, pCRZero and pCRZeroT efficiently formed colonies at the expected frequency (Fig. 2, XL10-Gold). In contrast, no colonies were formed by DH5 α (the *ccdB*-sensitive strain) carrying pCRZero and pCRZeroT (Fig. 2, DH5 α). On the other hand, DH5 α carrying pCRT formed approximately the same number of colonies as XL10-Gold carrying pCRT. These results indicate that pCRZero can reduce empty vector-dependent background during blunt-end cloning, and that pCRZeroT can also reduce the background during both TA cloning and blunt-end cloning.

Evaluation of cloning efficiencies for TA cloning and blunt-end cloning with the novel vector series. The cloning efficiencies of pCRT and pCRZeroT during PCR cloning were evaluated by TA cloning of dA-tailed PCR products. Both pCRT and pCRZeroT vectors could be screened using the blue/white selection system based on *lacZ* α complementation (Table 1)²⁵. A pair of T-overhangs can be prepared with single digestion at XcmI restriction sites in pCRT and pCRZeroT (Fig. 1a,c). However, excised fragments from the vector region can be re-ligated to XcmI sites in pCRT or pCRZeroT. In fact, pCRT and pCRZeroT prepared by digestion with a single restriction enzyme, XcmI, exhibited a ratio of white colonies to total colonies of $38.0 \pm 2.4\%$ (for pCRT (XcmI digestion)) and $96.3 \pm 6.5\%$ (for pCRZeroT (XcmI digestion)) (Table 1). To avoid the possibility that excised fragments were re-ligated to the vectors, NheI or XmaI sites were introduced into pCRT or pCRZeroT, respectively (Fig. 1a,c). In double digestion (XcmI/NheI for pCRT and XcmI/XmaI for pCRZeroT), white colony formation ratios were improved to $57.0 \pm 6.8\%$ (for pCRT) and $100.0 \pm 0.0\%$ (for pCRZeroT) when compared to single digestion by XcmI (Table 1). In contrast, the PCR cloning efficiencies were similar in the context of both single and double digestions. As a control for commercially available T-vector, pGEM-T Easy was used for TA-cloning (Table 1). Ratio of white colonies using pGEM-T Easy was $11.9 \pm 0.5\%$ and lower than the ratio of white colonies using pCRT and pCRZeroT, although the cloning efficiency was higher than that of pCRT and pCRZeroT. These results showed that the T-vectors developed in this study had higher cloning efficiency than the commercially available pGEM-T Easy.

The PCR cloning efficiencies of pCRZero and pCRZeroT were evaluated by blunt-end cloning of PCR products amplified with Tks Glex DNA polymerase. Both pCRZero and pCRZeroT vectors could be screened by a ZERO-background cloning system using the *ccdB* gene (Table 2). In fact, both blunt-end ligations of pCRZero (EcoRV) and pCRZeroT (SmaI) yielded high cloning efficiencies in blunt-end PCR cloning of PrxIIE (0.6 kbp) and G6PDH1 (1.6 kbp) (Table 2).

The three-types of vectors developed in this study worked well in both dA-tailed and blunt-end PCR cloning; the features of the three vectors are summarized in Fig. 3. The pCRT and pCRZeroT vectors are useful for TA

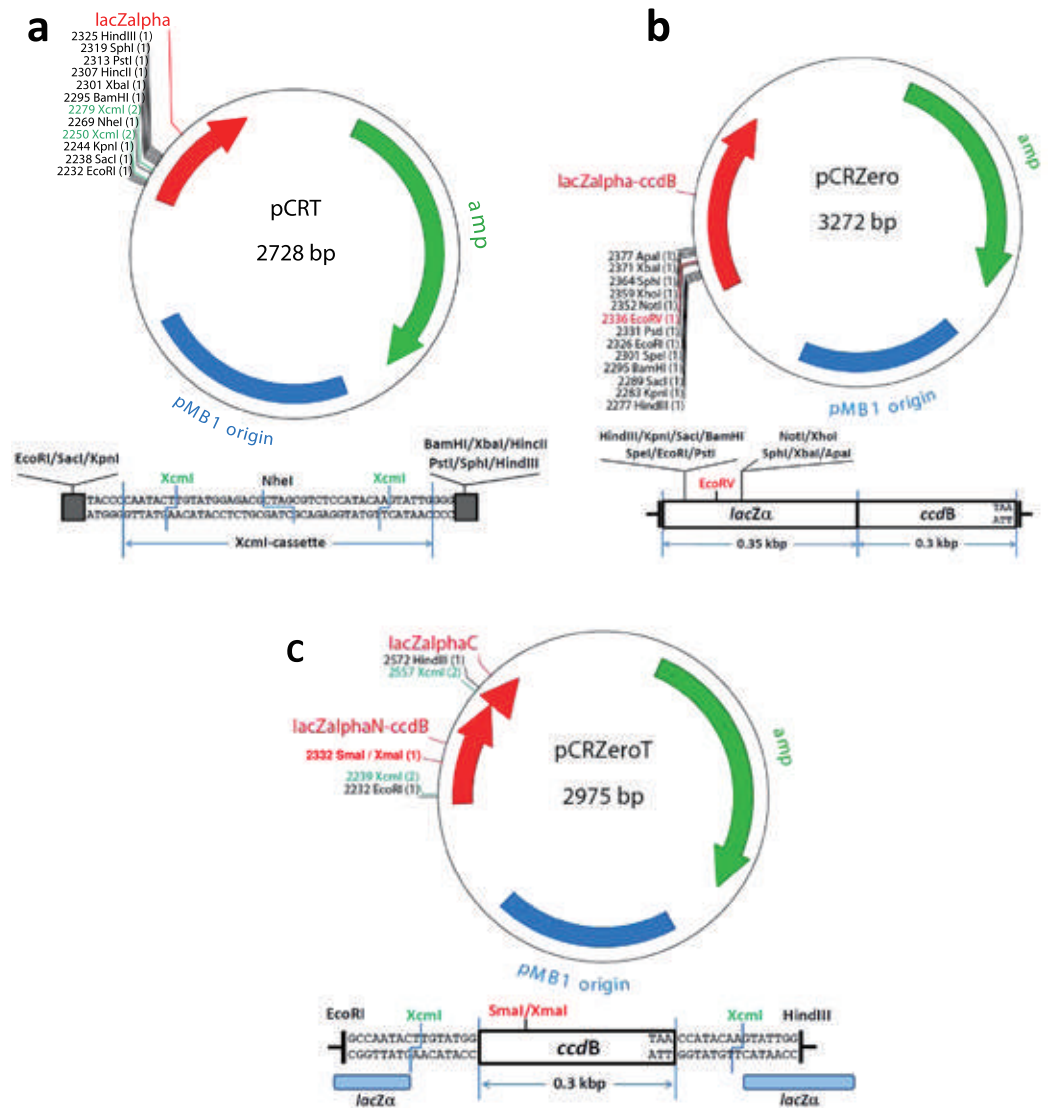


Figure 1. Graphical maps and cloning site regions of pCRT, pCRZero and pCRZeroT plasmids. The restriction sites for TA cloning are indicated with green letters, and the restriction sites for blunt-end cloning are indicated with red letters. The maps were drawn by ApE v2.0.55 software. (a) Graphical map and cloning site regions of pCRT. The pCRT was digested by XcmI for TA cloning. (b) Graphical map and cloning site region of pCRZero. The pCRZero was digested by EcoRV for blunt-end cloning. (c) Graphical map and cloning site region of pCRZeroT. pCRZeroT was digested by XcmI for TA cloning, or by SmaI for blunt-end cloning. A SmaI site in the *ccdB* gene of pCRZeroT was introduced without altering the CcdB amino acid sequence using the SLiP method³⁵; this site was used as the cloning site for blunt-end PCR products.

cloning using XcmI digestion. Double digestion with XcmI/NheI (for pCRT) or XcmI/XmaI (for pCRZeroT) reduced the formation of background colonies due to empty vectors, and improved the rate of white colony formation. The pCRZero and pCRZeroT vectors are useful for blunt-end cloning using single digestion with EcoRV (for pCRZero) or SmaI (for pCRZeroT). This system does not require any additional reagents, such as IPTG/X-gal, and the procedure used with system is simple to follow.

Commercially available T-vectors and blunt-end vectors are generally expensive compared with in-house prepared vectors. For example, the cost of commercially available T-vectors from Promega, Novagen, and Thermo Fisher Scientific were in the range of \$8.1 to \$14.9 per reaction and that of commercially available blunt-end vectors with the *E. coli*-lethal *ccdB* gene from Thermo Fisher Scientific was ~\$18 per reaction. In contrast, the preparation costs of T-vectors from pCRT and pCRZeroT and blunt-end vectors from pCRZero and pCRZeroT were ~\$0.06 per reaction, including the cost of the medium required to proliferate the plasmid-carrying *E. coli* cells, the plasmid midi-kit for preparation of plasmids, restriction enzymes for linearization of vectors, and the DNA-purification kit for purification of linearized vectors.

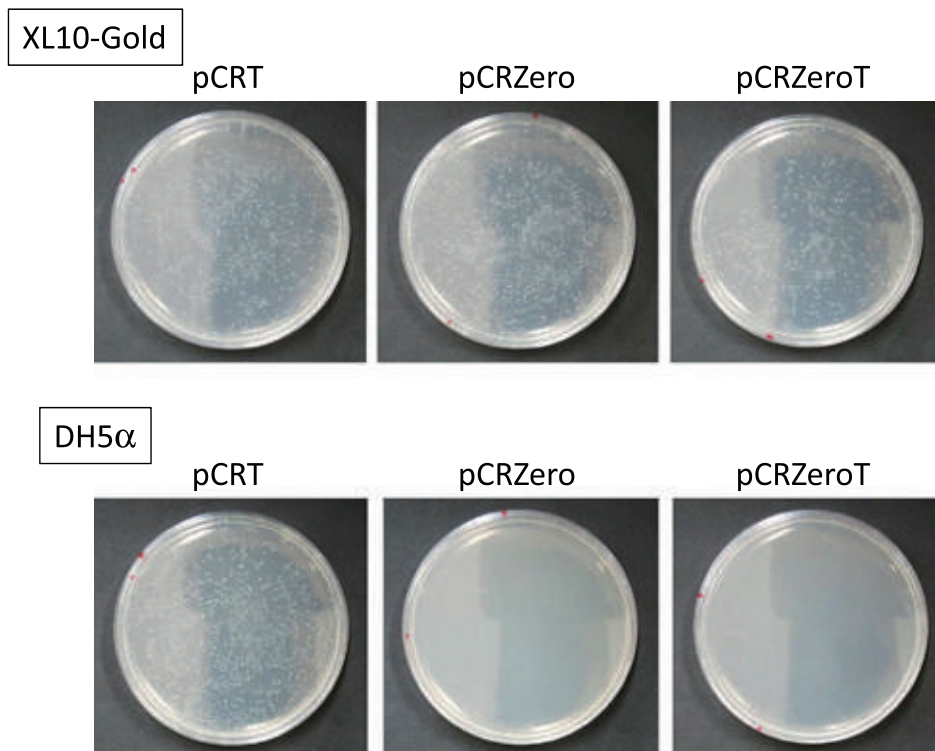


Figure 2. Lethality of the plasmids carrying the *ccdB* gene in the *ccdB*-sensitive *E. coli* strain. *E. coli* XL10-Gold (the *ccdB*-resistant strain) and DH5 α (the *ccdB*-sensitive strain) were transformed with pCRT, pCRZero and pCRZeroT plasmids (0.1 ng). The transformation efficiency of the *E. coli* chemically competent cells (XL10-Gold and DH5 α) was $\sim 1 \times 10^7$ CFUs/ μ g of pUC19 DNA.

Vector (Restriction enzymes for linearization)	White colonies (%) ^a	Cloning efficiencies ^b
pCRT (XcmI)	38.0 \pm 2.4	8/16
pCRT (XcmI/NheI)	57.0 \pm 6.8	8/16
pCRZeroT (XcmI)	96.3 \pm 6.5	7/16
pCRZeroT (XcmI/XmaI)	100.0 \pm 0.0	6/16
pGEM-T Easy	11.9 \pm 0.5	15/16

Table 1. Efficiencies with which dA-tailed PCR products were cloned into the T-vectors. T-overhangs were generated in pCRT and pCRZeroT with the indicated restriction enzymes before the ligation reaction. The T-vectors and dA-tailed PCR products (G6PDH1; 1.6 kbp) were purified using a Gel/PCR Extraction Kit. The T-vectors (50 ng) and the dA-tailed PCR products (G6PDH1, 130 ng) were ligated using the ligation convenience kit (Nippon Gene). Half the volume of the ligation mixture was used to transform 50 μ L of ECOS Competent *E. coli* DH5 α chemically competent cells. Commercially available T-vector pGEM-T Easy was used as a control. ^aThe fraction of white colonies as a percentage of total colonies was calculated and expressed as mean percentage \pm standard deviation of three independent experiments. ^bThe cloning efficiencies are represented as “the number of clones with the confirmed correct length of insert DNA by colony PCR/number of white colonies subjected to colony PCR”.

Direct PCR cloning into non-digested vectors using the Golden Gate reaction. To develop a method that exploits the features of *ccdB*-dependent lethality, I attempted ligation with PCR products and non-digested vectors, applying the Golden Gate reaction that simultaneously digests and ligates vectors and PCR products (Fig. 4a,b)^{22,23}. At the first step, pCRZero and pCRZeroT are digested by each restriction enzyme, and PCR products are inserted into each cloning site of the vectors. At the next step, vectors that contain ligated PCR-products are not digested, as the restriction site is destroyed during the ligation; in contrast, empty vectors remain susceptible to digestion (Fig. 4b). By repeating the Golden Gate reaction, the PCR cloning efficiencies increase, because *E. coli* DH5 α carrying empty pCRZero and pCRZeroT vectors are unable to form colonies (Fig. 2 and Table 3). The dA-tailed PCR products of G6PDH1 (1.6 kbp) were cloned into T-overhangs of pCRZeroT with high efficiencies (>87%). The blunt-end PCR-products of G6PDH1 (1.6 kbp) and Prx IIE (0.6 kbp) were also cloned into a blunt-end site in pCRZero or pCRZeroT (Table 3) with efficiencies >95%. These

Vector (Restriction enzyme for linearization)	Insert	Cloning efficiencies ^a
pCRZero (EcoRV)	Prx IIE	21/24
pCRZero (EcoRV)	G6PDH1	22/24
pCRZeroT (SmaI)	G6PDH1	23/24

Table 2. Efficiencies with which blunt-end PCR products were cloned into the blunt-end vectors carrying the *E. coli*-lethal *ccdB* gene. The pCRZero and pCRZeroT were digested with indicated restriction enzymes. The digested blunt-end vectors and, blunt-end PCR products (Prx IIE (0.6 kbp) or G6PDH1 (1.6 kbp) were purified by a Gel/PCR Extraction Kit. The blunt-end vectors (50 ng) and the blunt-end PCR products (Prx IIE 50 ng, G6PDH1 130 ng) were ligated with Quick ligase. Half the volume of ligation mixture was used to transform 50 μ L of ECOS Competent *E. coli* DH5 α chemically competent cells. ^aThe cloning efficiencies are represented as “the number of clones with the confirmed correct length of insert DNA by colony-PCR/number of colonies subjected to colony PCR”.

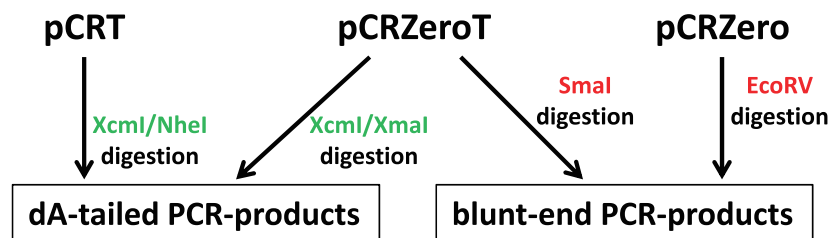


Figure 3. Selection of pCRT, pCRZero and pCRZeroT vectors for PCR cloning. pCRT and pCRZeroT can be used for TA cloning, whereas pCRZero and pCRZeroT can be used for blunt-end cloning. The pCRZeroT vector is compatible for both TA cloning and blunt-end cloning of PCR products. When blunt-end PCR products are directly cloned into non-digested vectors, SmaI (for pCRZeroT) or EcoRV (for pCRZero) can be selected, depending on the restriction sites present in the PCR product. Restriction enzymes to produce T-overhang for T-vectors are indicated by green letters. Restriction enzymes to produce blunt-end of vectors are indicated by red letters.

high cloning efficiencies were comparable to those of a commercially available vector, pZerO2.1 (Thermo Fisher Scientific) containing the *E. coli*-lethal *ccdB* gene. Furthermore, colony formation rates were similar for both pre-digested vectors and non-digested vectors when using Golden Gate reaction (Fig. S1). However, this system requires that the PCR fragments do not contain the restriction enzyme site that is exploited for digestion of the vector. The end user can therefore choose between pCRZero and pCRZeroT based on a survey of restriction enzyme sites in their PCR products.

Evaluation of a rapid protocol without purification steps in PCR cloning. Standard PCR cloning protocols generally use purified PCR products. Indeed, the three vectors developed in this study exhibited high cloning efficiencies using purified PCR fragments. To determine whether the procedure could be simplified even further, I determined whether colony-formation rate and cloning efficiencies were also acceptable when unpurified PCR products were used for both TA cloning and blunt-end cloning (Fig. 5). Strikingly, colony-formation rate and cloning efficiencies were almost identical for unpurified and purified PCR fragments when pCRZeroT was used for TA cloning and blunt-end cloning (Table 4). Therefore, purification of PCR products is not required in this ZERO-background cloning system. Moreover, the ratio of white colonies obtained using pCRZeroT as a T-vector was 100%, whereas that using pGEM-T Easy, a commercially available T-vector, was $10.8 \pm 2.4\%$ (– Purification) and $17.7 \pm 1.8\%$ (+Purification). When pCRZeroT was used as a T-vector, blue/white selection by IPTG/X-gal was not required.

Blunting and blunt-end cloning of the dA-tailed DNA fragments in blunt-end positive-selection system using the *ccdB* gene. Although TA cloning is a standard cloning method for dA-tailed PCR-products, it requires blue/white selection using IPTG and X-gal in order to maximize cloning efficiency. The selection procedure is long, since time is required for expression of lacZ α protein; furthermore, the system is prone to false positives as a result of insufficient lacZ α expression. Hi-fidelity thermostable DNA polymerases such as KOD DNA polymerase, have 3' to 5' exonuclease activity for proofreading, and can delete the dA added at the 3' terminus of the dA-tailed PCR-fragments⁴. To estimate blunting activities of the dA-tailed PCR-products polished by KOD DNA polymerase, PCR fragments amplified by KAPATaq EXtra DNA polymerase were directly treated with KOD DNA polymerase in order to blunt the dA-tailed PCR-fragments (Fig. 6). The 3'-exonuclease activity of DNA polymerase polishes the ends of the PCR fragments in the presence of dNTPs²⁵. When the dA-tailed PCR-products were ligated to pCRZeroT (SmaI), no positive clones were obtained (Table 5). By contrast, colony formation rates increased in a blunting reaction-dependent manner, and cloning efficiencies were 58.3% and 66.7% after 2 and 30 min treatment with high-fidelity KOD DNA polymerase, respectively.

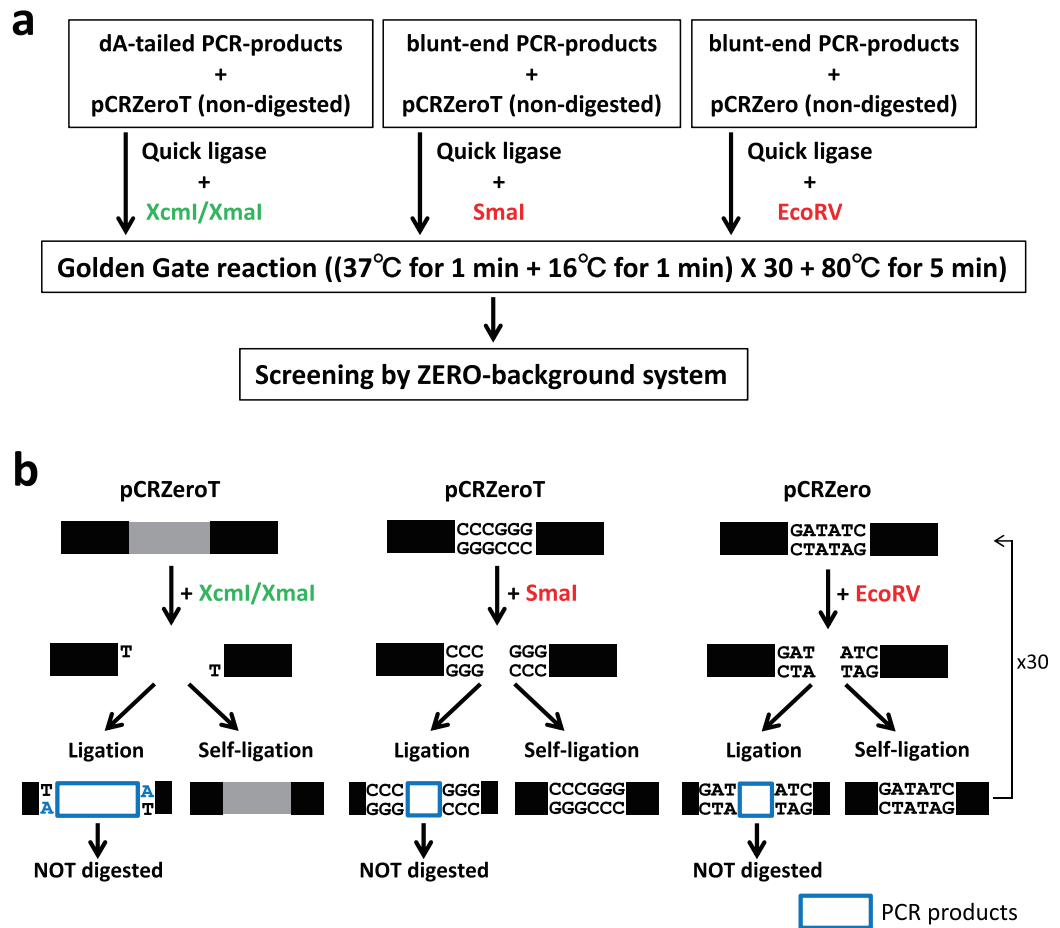


Figure 4. Overview of PCR cloning into non-digested circular vectors using the Golden Gate reaction. (a) Outline of PCR cloning into non-digested vectors. (b) Reaction cycle of Golden Gate reaction. Non-digested vector and PCR products were ligated in the presence of both ligase and indicated restriction enzymes and used in the following Golden Gate reaction cycle: (37 °C for 1 min + 16 °C for 1 min) × 30 cycles, then 80 °C for 5 min. Restriction enzymes to produce T-overhang for T-vectors are indicated by green letters. Restriction enzymes to produce blunt-end of vectors are indicated by red letters.

vector	Restriction enzyme (Buffer)	Insert	White colonies (%) ^a	Cloning efficiencies ^b
pCRZeroT	XcmI/XmaI (CutSmart)	G6PDH1	100.0 ± 0.0	21/24
pCRZeroT	SmaI (CutSmart)	G6PDH1	—	24/24
pCRZero	EcoRV (CutSmart)	Prx IIE	—	23/24
pZErO2.1	EcoRV (CutSmart)	Prx IIE	—	24/24

Table 3. Direct PCR cloning into non-digested vectors using the Golden Gate reaction. The PCR products (G6PDH1; 1.6 kbp or Prx IIE; 0.6 kbp) were purified by a Gel/PCR Extraction Kit. The pCRZeroT, pCRZero, or pZErO2.1 (Non-digested, 50 ng) and the purified blunt-end PCR products (G6PDH1 130 ng or Prx IIE 50 ng) were ligated with Quick ligase and each restriction enzyme in the Golden Gate reaction. Half of the ligation mixture volume was used to transform 50 μL of ECOS Competent *E. coli* DH5α chemically competent cells. Plasmid pZErO2.1 was used as a control for commercially available vectors, and positive clones in pZErO2.1 were screened on an LB agar plate containing kanamycin (50 μg/mL). ^aThe fraction of white colonies as a percentage of total colonies was calculated and expressed as mean percentage ± standard deviation of three independent experiments. ^bThe cloning efficiencies are represented as “the number of clones with the confirmed correct length of insert DNA by colony PCR/number of colonies subjected to colony PCR”.

Conclusion

Three types of PCR cloning vectors were developed in this study. The pCRT and pCRZeroT vectors can be used for TA cloning, and are far less susceptible to false positives due to the empty vector digestion strategy using additional restriction enzymes I developed. The pCRZero and pCRZeroT can be used for blunt-end cloning by

Vector (Restriction enzymes for linearization)	Purification	White colonies (%) ^a	Number of colonies ^b	Cloning efficiencies ^c
pCRZeroT (XcmI/XmaI)	–	100.0 ± 0.0	8.0 ± 5.6	15/24
pCRZeroT (XcmI/XmaI)	+	100.0 ± 0.0	31.7 ± 7.4	17/24
pCRZeroT (SmaI)	–	–	483.7 ± 43.6	22/24
pCRZeroT (SmaI)	+	–	673.7 ± 55.5	23/24
pGEM-T Easy	–	10.8 ± 2.4	30.0 ± 10.5	17/24
pGEM-T Easy	+	17.7 ± 1.8	112.7 ± 12.1	21/24

Table 4. Evaluation of a simple protocol without purification of PCR products in PCR cloning. The G6PDH1 (1.6 kbp) gene was amplified by KAPATaq EXtra DNA polymerase (for pCRZeroT (XcmI/XmaI)) or Tks Gflex DNA polymerase (for pCRZeroT (SmaI)) in a 50- μ L reaction. pCRZeroT was linearized by digestion with the indicated restriction enzymes, and purified by a Gel/PCR Extraction Kit. The linearized pCRZeroT (50 ng) and each of the PCR products (\pm purification, 1/20 volume) were then ligated. Two and a half microliters of the 50- μ L PCR reaction (Purification (–)) or 1 μ L of 20 μ L purified PCR-products (Purification (+)) was used for ligation. Three tenths of the ligation reaction volume was used to transform 30 μ L of ECOS Competent *E. coli* DH5 α chemically competent cells. Commercially available T-vector pGEM-T Easy was used as a control. ^aThe fraction of white colonies as a percentage of total colonies was calculated and expressed as mean percentage \pm standard deviation of three independent experiments. ^bThe number of colonies is the mean \pm standard deviation of three independent experiments. When pCRZeroT (XcmI/XmaI) and pGEM-T Easy were used as T-vectors, the number of colonies was represented as the number of white colonies. ^cThe cloning efficiencies are represented as “the number of clones with the confirmed correct length of insert DNA by colony PCR/number of white colonies subjected to colony PCR”.

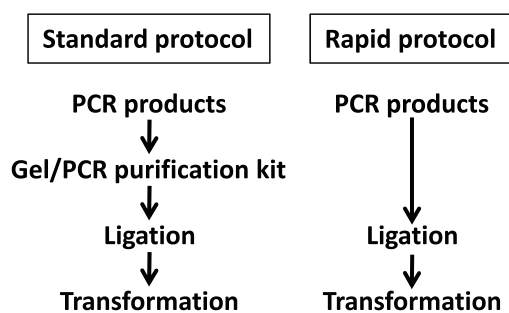


Figure 5. Outline of the PCR cloning processes of standard and rapid protocols.

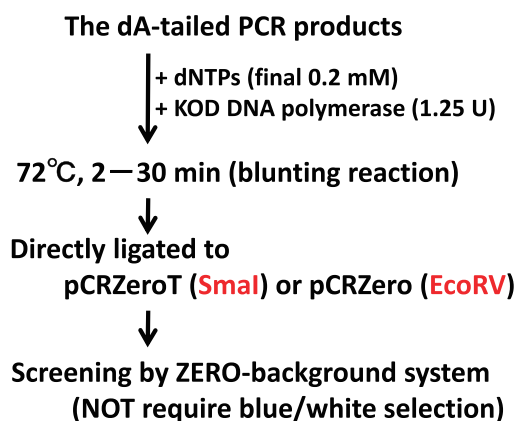


Figure 6. Description of the blunting reaction and blunt-end cloning process for dA-tailed PCR-products. Restriction enzymes to produce blunt-ends within vectors are indicated by red letters.

exploiting *ccdB*-dependent lethality. As an application of the ZERO-background system, I developed a direct PCR cloning method with the PCR products and non-digested vectors using a Golden Gate reaction. This system does not require pre-digestion of cloning vectors, and can therefore be used when the amount of vector is limiting, since purification is not required. In addition, researchers can select either pCRZero and pCRZeroT based on the restriction sites that are present in their PCR products. Furthermore, the PCR cloning procedure

Vector (Restriction enzyme for linearization)	Blunting reaction	Number of colonies ^a	Cloning efficiencies ^b
pCRZeroT (SmaI)	None	11.3 ± 3.1	0/24
pCRZeroT (SmaI)	KOD DNA pol. 2 min	59.7 ± 22.0	14/24
pCRZeroT (SmaI)	KOD DNA pol. 30 min	84.7 ± 7.1	16/24

Table 5. Blunting and blunt-end cloning of the dA-tailed DNA fragments in the blunt-end positive-selection system using the *ccdB* gene. The pCRZeroT was linearized by blunt-end digestion with SmaI, and purified by a Gel/PCR Extraction Kit. The G6PDH1 (1.6 kbp) gene was amplified by KAPATaq EXtra DNA polymerase in a 50 μ L reaction volume. The dNTPs (final 0.2 mM) and KOD DNA polymerase (1.25 U) were directly added to 50 μ L of unpurified dA-tailed PCR-products. Blunting reactions were performed for 2 or 30 min at 72 °C. pCRZeroT (SmaI) (50 ng) and 2.5 μ L of the 50 μ L PCR reaction were then ligated. Three tenths of the ligation mixture were used to transform 30 μ L of ECOS Competent *E. coli* DH5 α chemically competent cells. ^aThe number of colonies is the mean \pm standard deviation of three independent experiments. ^bThe cloning efficiencies are represented as “the number of clones with the confirmed correct length of insert DNA by colony PCR/number of colonies subjected to colony PCR”.

is simplified by elimination of purification steps and blunting of the dA-tailed PCR products. Blue/white selection with IPTG/X-gal can be omitted by using the blunt-end cloning strategy of the ZERO-background system. The plasmids, along with maps and sequences, can be accessed via Addgene (<https://www.addgene.org/>) as IDs 120274 (pCRT), 120275 (pCRZero) and 120276 (for pCRZeroT).

Methods

Materials. Plasmid pUC18 (Takara-Bio, Otsu, Japan) was used to construct pCRT, pCRZero and pCRZeroT vectors. Plasmid pZerO2.1 (Thermo Fisher Scientific, Carlsbad, CA) served as the *ccdB* gene donor vector. Plasmid pZerO2.1 was also used as a control vector for blunt-end cloning using the lethal *ccdB* gene. T-vector pGEM-T Easy (Promega, Madison, WI) was used as a control for commercially available T-vectors. *E. coli* JM109²⁶, XL10-Gold (Agilent Technologies, Santa Clara, CA) or NEB Turbo (NEB, Ipswich, MA) that contain the F-plasmid, were used to prepare pCRZero and pCRZeroT plasmids expressing the *ccdB* gene^{14,27}. *E. coli* DH5 α (a *ccdB*-sensitive strain)²⁸ was used for positive selection during PCR cloning with either pCRZero and pCRZeroT, which express the *ccdB* gene in the absence of ligated PCR products. The *Arabidopsis* type II peroxiredoxin E (Prx IIE, 0.6 kbp, AT3G52960)^{29,30} and chloroplast glucose-6-phosphate dehydrogenase 1 (G6PDH1, 1.6 kbp, AT5G35790)³¹ genes were used as sources for PCR amplification.

In silico cloning. Serial Cloner 2.6 (http://serialbasics.free.fr/Serial_Cloner.html) was used to analyze sequence data, design primers, and design cloning strategies. ApE v2.0.55 (<http://jorgensen.biology.utah.edu/wayned/ape/>) was used to generate the plasmid maps shown in the figures. Additionally, PlasMapper (<http://wis-hart.biology.ualberta.ca/PlasMapper/>)³² was used to generate the plasmid text maps in Supplementary Dataset S1.

Construction of pCRT, pCRZero, and pCRZeroT vectors. In pCRT, two complementary single strand DNA oligonucleotides containing an XcmI cassette (42-mer) were inserted in order to generate the T-overhang of the T-vector (Table S1) for seamless ligation cloning extract (SLiCE)-cloning^{33,34}. Two single strand oligonucleotides, pUC18TXcmIcassette42merSLiCE-F (10 μ M) and pUC18TXcmIcassette42merSLiCE-R (10 μ M) in 100 μ L solution containing 10 mM Tris-HCl (pH 8.0) and 0.1 mM EDTA in a 1.5 mL microtube, were denatured at 85 °C in a 500-mL glass beaker filled with water, and the sample was left for 150 min until it reached room temperature. Annealed XcmI-cassette oligonucleotides for SLiCE-cloning (0.3 μ L) were inserted into a XmaI site (C|CCGGG) in pUC18 (25 ng), using the SLiCE from a laboratory *E. coli* strain, JM109³⁵. In pCRZero, the *ccdB* gene was amplified by KOD DNA polymerase (Toyobo, Osaka, Japan)⁴ with pUC18Zero-F and pUC18Zero-R primers (Table S1), using pZerO2.1 plasmid as the template. Amplified DNA fragments were inserted into EcoRI and HindIII sites in pUC18, by seamless ligation of the SLiCE from a laboratory *E. coli* strain, JM109^{34,36}. In pCRZeroT, *ccdB* was amplified as two fragments by KOD DNA polymerase using two pairs of primers (pUCR18ZeroT-Xcm-CcdB-NF/pUC18ZeroT-CcdB-NR_{sma} and pUC18ZeroT-CcdB-CF_{sma}/pUC18ZeroT-Xcm-CcdB-CR2); this introduced a SmaI site (CCC|GGG) for blunt-end cloning into the *ccdB* gene (Table S1). The mutation that substituted CC \overline{C} GGG to CC \overline{C} GGG allowed the introduction of a SmaI site without changing the amino acid sequence of CcdB. Two amplified DNA fragments were simultaneously inserted into EcoRI and HindIII sites in pUC18 using the SLiP-method^{33,35}. These plasmids were used to transform the *ccdB*-resistant strains XL10-Gold and NEB Turbo prior to screening by colony PCR (Table S1)^{37–39}. The DNA sequence of all plasmids was confirmed by sequencing⁴⁰.

Preparation of linearized pCRT, pCRZero, and pCRZeroT vectors for PCR cloning. The pCRZero and pCRZeroT plasmids were amplified in *ccdB*-gene resistant strains carrying the F-plasmid, such as JM109, XL10-Gold and NEB Turbo^{14,27}. pCRT was digested by XcmI for TA cloning. As an additional restriction enzyme, NheI was also added to reduce background colony formation due to empty vector. pCRZero was digested by EcoRV in order to generate blunt ends for cloning. pCRZeroT was digested by XcmI for use in TA cloning. As an additional restriction enzyme, XmaI was also added to reduce background colony formation. pCRZeroT for use in blunt-end cloning was digested by SmaI. All linearized vectors were purified by a FastGene Gel/PCR Extraction Kit (Nippon Genetics, Tokyo, Japan); this procedure did not require separation by agarose gel electrophoresis.

Amplification of dA-tailed or blunt-end PCR-products by thermostable DNA polymerase. Prx IIE (0.6 kbp, AT3G52960) and G6PDH1 (1.6 kbp, AT5G35790) genes were amplified with specific primers (Table S2)³³. The dA-tailed PCR-products were amplified by KAPATaq EXtra DNA polymerase (KAPA Biosystems, Wilmington, MA), and the blunt-end PCR-products were amplified by Tks Gflex DNA polymerase (Takara-Bio, Otsu, Japan). When purification was required for PCR cloning, both PCR products were purified using a FastGene Gel/PCR Extraction Kit without prior separation via agarose gel-electrophoresis.

Evaluation of cloning efficiency by pCRT and pCRZeroT for TA cloning of PCR products. Cloning efficiencies with the pCRT and pCRZeroT vectors (in which a T-overhang was produced by XcmI digestion) were evaluated using dA-tailed PCR-products. Linearized pCRT or pCRZeroT (50 ng), and purified dA-tailed PCR products (G6PDH1, 130 ng) were mixed with a vector:insert molar ratio of 1:5, and then ligated for 30 min at 16 °C using ligation convenient kit (Nippon Gene, Tokyo, Japan) or Quick Ligation Kit (NEB; used throughout unless stated otherwise). After the reaction the ligation mixtures were used directly to transform ECOS Competent *E. coli* DH5 α chemically competent cells (100 μ L, $\sim 1 \times 10^7$ CFUs/ μ g of pUC19 DNA) as described in the Figure and Table Legends. The percentage of white colonies was determined by blue/white selection using α -complementation mediated by the *lacZ* gene. The cloning efficiency of PCR products was estimated by colony PCR, using the primers described in Table S3. For this and all subsequent sections, the number of colonies was represented as colony number on an LB agar plate containing ampicillin (final 100 μ g/mL). Similarly, cloning efficiencies for the insert DNA were given as the ratio of colonies with an insert of the confirmed correct length as estimated by colony PCR.

Evaluation of cloning efficiency by pCRZero and pCRZeroT for blunt-end cloning of PCR products. Cloning efficiency of pCRZero and pCRZeroT vectors linearized to blunt-ends with EcoRV (for pCRZero) or SmaI (for pCRZeroT), were evaluated using blunt-end PCR-products amplified by Tks Gflex DNA polymerase (Takara-Bio, Otsu, Japan). Linearized pCRZero or pCRZeroT (50 ng), and blunt-end PCR products (50 ng (Prx IIE) or 130 ng (G6PDH1)) were mixed with a vector:insert molar ratio of 1:5, and then ligated for 30 min at 16 °C. After the reaction, ligation mixtures were used to transform ECOS Competent *E. coli* DH5 α cells as described in the Figure and Table Legends. The cloning efficiency of PCR products was estimated by colony PCR, using primers described in Table S3.

Direct PCR cloning into non-digested vectors carrying the *ccdB* gene using the Golden Gate reaction. Prx IIE (0.6 kbp) and G6PDH1 (1.6 kbp) genes were templates for PCR cloning (Table S2). The dA-tailed DNA fragments were amplified by KAPATaq EXtra DNA polymerase for pCRZeroT (XcmI/XmaI), and the blunt-end DNA fragments were amplified by Tks Gflex DNA polymerase for pCRZero (EcoRV) and pCRZeroT (SmaI). All PCR-amplified DNA fragments were purified by a FastGene Gel/PCR Extraction Kit without separation of agarose gel-electrophoresis. Non-digested vectors (50 ng) and, PCR products (50 ng (Prx IIE) or 130 ng (G6PDH1)) were ligated. Ligation for non-digested vectors using the Golden Gate reaction was performed as following: 1 min at 37 °C followed by 1 min at 16 °C, both repeated 30 times followed by 5 min at 80 °C, in a total volume of 10 μ L containing CutSmart Buffer (2 \times), 1 mM ATP and restriction enzymes (XcmI 10 U, XmaI 5 U, SmaI 10 U or EcoRV 15 U). As a control experiment, pre-digested vectors (50 ng) and PCR products (50 ng (Prx IIE) or 130 ng (G6PDH1)) were ligated. Ligation of pre-digested vectors and the PCR products was performed for 30 min at 16 °C in a total volume of 10 μ L containing CutSmart Buffer (2 \times), 1 mM ATP. Then, one and a half microliters of the ligation mix was used to transform 20 μ L of ECOS Competent *E. coli* DH5 α cells. The cloning efficiency of PCR products was estimated by colony PCR using the primers listed in Table S3.

PCR cloning into the pCRZeroT vector of unpurified or purified insert DNA fragments. G6PDH1 (1.6 kbp) gene was amplified in a 50- μ L PCR mixture by KAPATaq EXtra DNA polymerase (for pCRZeroT (XcmI/XmaI)) or Tks Gflex DNA polymerase (for pCRZeroT (SmaI)). Two and a half microliters (1/20 volume) of the 50- μ L PCR mixture and linearized vector (50 ng) were directly ligated in a 10- μ L ligation solution, without purification of PCR products. When purification was required, PCR mixtures (50 μ L) were processed with a FastGene Gel/PCR Extraction Kit, and eluted in 20 μ L elution buffer. One microliter (1/20 volume) of purified PCR products and linearized vector (50 ng) were ligated in 10- μ L ligation solutions. After the reaction, ligation mixtures were used to transform ECOS Competent *E. coli* DH5 α cells as described in the Figure and Table Legends.

Blunting reaction of the dA-tailed PCR fragments and blunt-end cloning at a SmaI site in pCRZeroT. dNTPs (final 0.2 mM) and KOD DNA polymerase (1.25 U; this enzyme has 3' to 5' exonuclease activity) were directly added to the reaction mixture (50 μ L) after PCR reaction, for blunting of the dA-tailed PCR fragments (G6PDH1; 1.6 kbp) amplified by KAPATaq EXtra DNA polymerase. The mixtures were incubated at 72 °C for 2 min or 30 min, and used directly to transform ECOS Competent *E. coli* DH5 α cells without any purification step. Two and a half microliters (1/20 volume) of the 50- μ L PCR mixture and linearized vector (50 ng) were then ligated for 30 min at 16 °C in a total volume of 10 μ L containing CutSmart Buffer (2 \times) and 1 mM ATP. Three microliters of the 10 μ L ligation mixtures was used to transform 30 μ L of ECOS Competent *E. coli* DH5 α cells.

References

- Hui, E. K., Wang, P. C. & Lo, S. J. PCR-based strategies to clone unknown DNA regions from known foreign integrants. An overview. *Methods Mol Biol* **192**, 249–274, <https://doi.org/10.1385/1-59259-177-9:249> (2002).
- Clark, J. M. Novel non-templated nucleotide addition reactions catalyzed by procaryotic and eucaryotic DNA polymerases. *Nucleic Acids Res* **16**, 9677–9686 (1988).

3. Lundberg, K. S. *et al.* High-fidelity amplification using a thermostable DNA polymerase isolated from *Pyrococcus furiosus*. *Gene* **108**, 1–6 (1991).
4. Takagi, M. *et al.* Characterization of DNA polymerase from *Pyrococcus* sp. strain KOD1 and its application to PCR. *Appl Environ Microbiol* **63**, 4504–4510 (1997).
5. Wang, Y. *et al.* A novel strategy to engineer DNA polymerases for enhanced processivity and improved performance *in vitro*. *Nucleic Acids Res* **32**, 1197–1207, <https://doi.org/10.1093/nar/gkh271> (2004).
6. Guo, B. & Bi, Y. Cloning PCR products. *An overview. Methods Mol Biol* **192**, 111–119, <https://doi.org/10.1385/1-59259-177-9:111> (2002).
7. Holton, T. A. & Graham, M. W. A simple and efficient method for direct cloning of PCR products using ddT-tailed vectors. *Nucleic Acids Res* **19**, 1156 (1991).
8. Kovalic, D., Kwak, J. H. & Weisblum, B. General method for direct cloning of DNA fragments generated by the polymerase chain reaction. *Nucleic Acids Res* **19**, 4560 (1991).
9. Schutte, B. C., Ranade, K., Pruessner, J. & Dracopoli, N. Optimized conditions for cloning PCR products into an XcmI T-vector. *Biotechniques* **22**, 40–44 (1997).
10. Borovkov, A. Y. & Rivkin, M. I. XcmI-containing vector for direct cloning of PCR products. *Biotechniques* **22**, 812–814 (1997).
11. Jo, C. & Jo, S. A. A simple method to construct T-vectors using XcmI cassettes amplified by nonspecific PCR. *Plasmid* **45**, 37–40, <https://doi.org/10.1006/plas.2000.1500> (2001).
12. Liu, Z. G. & Schwartz, L. M. An efficient method for blunt-end ligation of PCR products. *Biotechniques* **12**(28), 30 (1992).
13. Janner, C. R., Brito, A. L., Moraes, L. M., Reis, V. C. & Torres, F. A. pPCV, a versatile vector for cloning PCR products. *Springerplus* **2**, 441, <https://doi.org/10.1186/2193-1801-2-441> (2013).
14. Bernard, P. Positive selection of recombinant DNA by CcdB. *Biotechniques* **21**, 320–323 (1996).
15. Hu, L. L., Zhang, S. S., Li, X. X. & Wang, B. L. The use of the ccdB lethal gene for constructing a zero background vector in order to clone blunt-end PCR products. *Mol Biol (Mosk)* **44**, 161–164 (2010).
16. Trower, M. K. & Elgar, G. S. Cloning PCR products using T-vectors. *Methods Mol Biol* **58**, 313–324, <https://doi.org/10.1385/0-89603-402-X:313> (1996).
17. Nichols, W. A. Cloning PCR products with T-vectors. *Methods Mol Biol* **235**, 141–152, <https://doi.org/10.1385/1-59259-409-3:141> (2003).
18. Rotchanapreeda, T., Ngonsawan, W., Klomtun, M. & Somana, J. The plasmid vectors, pBS2nnd and pBS3nnd, for versatile cloning with low background in *Escherichia coli*. *World J Microbiol Biotechnol* **34**, 85, <https://doi.org/10.1007/s11274-018-2466-z> (2018).
19. Chen, S., Songkumarn, P., Liu, J. & Wang, G. L. A versatile zero background T-vector system for gene cloning and functional genomics. *Plant Physiol* **150**, 1111–1121, <https://doi.org/10.1104/pp.109.137125> (2009).
20. Wang, C. *et al.* A series of TA-based and zero-background vectors for plant functional genomics. *PLoS One* **8**, e59576, <https://doi.org/10.1371/journal.pone.0059576> (2013).
21. Gabant, P., Dreze, P. L., Van Reeth, T., Szpirer, J. & Szpirer, C. Bifunctional lacZ alpha-ccdB genes for selective cloning of PCR products. *Biotechniques* **23**, 938–941, <https://doi.org/10.2144/97235pf01> (1997).
22. Engler, C. & Marillonnet, S. Generation of families of construct variants using golden gate shuffling. *Methods Mol Biol* **729**, 167–181, https://doi.org/10.1007/978-1-61779-065-2_11 (2011).
23. Engler, C. & Marillonnet, S. Golden Gate cloning. *Methods Mol Biol* **1116**, 119–131, https://doi.org/10.1007/978-1-62703-764-8_9 (2014).
24. Bernard, P. & Couturier, M. Cell killing by the F plasmid CcdB protein involves poisoning of DNA-topoisomerase II complexes. *J Mol Biol* **226**, 735–745 (1992).
25. Green, M. R. & Sambrook, J. *Molecular Cloning: A Laboratory Manual*. Fourth Edition edn, (Cold Spring Harbor Laboratory Press, 2012).
26. Yanisch-Perron, C., Vieira, J. & Messing, J. Improved M13 phage cloning vectors and host strains: nucleotide sequences of the M13mp18 and pUC19 vectors. *Gene* **33**, 103–119 (1985).
27. Bernard, P., Gabant, P., Bahassi, E. M. & Couturier, M. Positive-selection vectors using the F plasmid ccdB killer gene. *Gene* **148**, 71–74 (1994).
28. Bethesda Research Laboratories. BRL pUC host: *E. coli* DH5 α TM competent cells. *Focus* **8**, 9–12 (1986).
29. Dietz, K. J., Horling, F., König, J. & Baier, M. The function of the chloroplast 2-cysteine peroxiredoxin in peroxide detoxification and its regulation. *J Exp Bot* **53**, 1321–1329 (2002).
30. Brehelin, C., Meyer, E. H., de Souris, J. P., Bonnard, G. & Meyer, Y. Resemblance and dissemblance of Arabidopsis type II peroxiredoxins: similar sequences for divergent gene expression, protein localization, and activity. *Plant Physiol* **132**, 2045–2057 (2003).
31. Wakao, S. & Benning, C. Genome-wide analysis of glucose-6-phosphate dehydrogenases in Arabidopsis. *Plant J* **41**, 243–256, <https://doi.org/10.1111/j.1365-3113X.2004.02293.x> (2005).
32. Dong, X., Stothard, P., Forsythe, I. J. & Wishart, D. S. PlasMapper: a web server for drawing and auto-annotating plasmid maps. *Nucleic Acids Res* **32**, W660–664, <https://doi.org/10.1093/nar/gkh410> (2004).
33. Motohashi, K. A simple and efficient seamless DNA cloning method using SLiCE from *Escherichia coli* laboratory strains and its application to SLiP site-directed mutagenesis. *BMC Biotechnol* **15**, 47, <https://doi.org/10.1186/s12896-015-0162-8> (2015).
34. Okegawa, Y. & Motohashi, K. Evaluation of seamless ligation cloning extract preparation methods from an *Escherichia coli* laboratory strain. *Anal Biochem* **486**, 51–53, <https://doi.org/10.1016/j.ab.2015.06.031> (2015).
35. Motohashi, K. Seamless Ligation Cloning Extract (SLiCE) Method Using Cell Lysates from Laboratory *Escherichia coli* Strains and its Application to SLiP Site-Directed Mutagenesis. *Methods Mol Biol* **1498**, 349–357, https://doi.org/10.1007/978-1-4939-6472-7_23 (2017).
36. Okegawa, Y. & Motohashi, K. A simple and ultra-low cost homemade seamless ligation cloning extract (SLiCE) as an alternative to a commercially available seamless DNA cloning kit. *Biochem Biophys Rep* **4**, 148–151, <https://doi.org/10.1016/j.bbrep.2015.09.005> (2015).
37. Okegawa, Y., Koshino, M., Okushima, T. & Motohashi, K. Application of preparative disk gel electrophoresis for antigen purification from inclusion bodies. *Protein Expr Purif* **118**, 77–82, <https://doi.org/10.1016/j.pep.2015.10.008> (2016).
38. Okegawa, Y. & Motohashi, K. Expression of spinach ferredoxin-thioredoxin reductase using tandem T7 promoters and application of the purified protein for *in vitro* light-dependent thioredoxin-reduction system. *Protein Expr Purif* **121**, 46–51, <https://doi.org/10.1016/j.pep.2016.01.005> (2016).
39. Motohashi, K. Evaluation of the efficiency and utility of recombinant enzyme-free seamless DNA cloning methods. *Biochem Biophys Rep* **9**, 310–315, <https://doi.org/10.1016/j.bbrep.2017.01.010> (2017).
40. Sanger, F., Nicklen, S. & Coulson, A. R. DNA sequencing with chain-terminating inhibitors. *Proc Natl Acad Sci USA* **74**, 5463–5467 (1977).

Acknowledgements

This work was supported by JSPS KAKENHI Grant Numbers 16K07409 (to K.M.), the MEXT-Supported Program for the Strategic Research Foundation at Private Universities Grant Number S1511023 (to K.M.), and the Institute for Fermentation (Osaka) Grant Number G-2019-2-067 (to K.M.).

Author Contributions

K.M. designed and performed the experiments, analyzed the data, and wrote the manuscript. The author read and approved the final manuscript.

Additional Information

Supplementary information accompanies this paper at <https://doi.org/10.1038/s41598-019-42868-6>.

Competing Interests: The author declares no competing interests.

Publisher's note: Springer Nature remains neutral with regard to jurisdictional claims in published maps and institutional affiliations.



Open Access This article is licensed under a Creative Commons Attribution 4.0 International License, which permits use, sharing, adaptation, distribution and reproduction in any medium or format, as long as you give appropriate credit to the original author(s) and the source, provide a link to the Creative Commons license, and indicate if changes were made. The images or other third party material in this article are included in the article's Creative Commons license, unless indicated otherwise in a credit line to the material. If material is not included in the article's Creative Commons license and your intended use is not permitted by statutory regulation or exceeds the permitted use, you will need to obtain permission directly from the copyright holder. To view a copy of this license, visit <http://creativecommons.org/licenses/by/4.0/>.

© The Author(s) 2019



Evaluation of the efficiency and utility of recombinant enzyme-free seamless DNA cloning methods



Ken Motohashi^{a,b,*}

^a Department of Bioresource and Environmental Sciences, Faculty of Life Sciences, Kyoto Sangyo University, Kamigamo Motoyama, Kita-ku, Kyoto 603-8555, Japan

^b Center for Ecological Evolutionary Developmental Biology, Kyoto Sangyo University, Kamigamo Motoyama, Kita-Ku, Kyoto 603-8555, Japan

ARTICLE INFO

Keywords:

Homologous recombination
in vivo *Escherichia coli* cloning
Seamless DNA cloning
SLiCE

ABSTRACT

Simple and low-cost recombinant enzyme-free seamless DNA cloning methods have recently become available. *In vivo* *Escherichia coli* cloning (iVEC) can directly transform a mixture of insert and vector DNA fragments into *E. coli*, which are ligated by endogenous homologous recombination activity in the cells. Seamless ligation cloning extract (SLiCE) cloning uses the endogenous recombination activity of *E. coli* cellular extracts *in vitro* to ligate insert and vector DNA fragments. An evaluation of the efficiency and utility of these methods is important in deciding the adoption of a seamless cloning method as a useful tool. In this study, both seamless cloning methods incorporated inserting DNA fragments into linearized DNA vectors through short (15–39 bp) end homology regions. However, colony formation was 30–60-fold higher with SLiCE cloning in end homology regions between 15 and 29 bp than with the iVEC method using DH5 α competent cells. *E. coli* AQ3625 strains, which harbor a *sbcA* gene mutation that activates the RecE homologous recombination pathway, can be used to efficiently ligate insert and vector DNA fragments with short-end homology regions *in vivo*. Using AQ3625 competent cells in the iVEC method improved the rate of colony formation, but the efficiency and accuracy of SLiCE cloning were still higher. In addition, the efficiency of seamless cloning methods depends on the intrinsic competency of *E. coli* cells. The competency of chemically competent AQ3625 cells was lower than that of competent DH5 α cells, in all cases of chemically competent cell preparations using the three different methods. Moreover, SLiCE cloning permits the use of both homemade and commercially available competent cells because it can use general *E. coli* *recA*⁻ strains such as DH5 α as host cells for transformation. Therefore, between the two methods, SLiCE cloning provides both higher efficiency and better utility than the iVEC method for seamless DNA plasmid engineering.

1. Introduction

Seamless DNA cloning methods are useful for plasmid engineering because DNA fragments can be ligated in a restriction enzyme site-independent manner. In the past decade, several purified-enzyme-dependent seamless DNA cloning methods have been developed [1–3]. Seamless cloning methods generally rely on short (~15 bp) end homology regions for ligation of insert and vector DNA fragments. These methods are available through commercial kits, which are widely used [4–14]; however, seamless cloning kits are cost-prohibitive. Recently, several simple and recombinant enzyme-free seamless DNA cloning methods have been described [15–18], which utilize the endogenous homologous recombination activity of laboratory

Escherichia coli strains.

The most simple method is the *in vivo* *E. coli* cloning (iVEC) system [16–18]. This method directly introduces only DNA fragments containing insert and vector DNA molecules into *E. coli* competent cells. The introduced DNA molecules can be combined through short (30–50 bp) end homology regions using the endogenous *in vivo* homologous recombination activity of *E. coli* [18]. The iVEC system was originally reported by two groups more than 20 years ago [19,20], but longer end homology regions were required for efficient cloning. Jacobus et al. and Kostylev et al. recently reported that several DNA fragments can be simultaneously incorporated into a common linearized vector using the iVEC method with *E. coli* DH5 α [17,18]. More recently, the National BioResource Project (NIG, Japan) has characterized and distributed a

Abbreviations: CFU, colony-forming units; G6PDH1, glucose-6-phosphate dehydrogenase 1; iVEC, *in vivo* *Escherichia coli* cloning; PCR, polymerase chain reaction; Prx IIE, type II peroxiredoxin E; SLiCE, seamless ligation cloning extract; TSS, transformation and storage solution.

* Correspondence address: Department of Bioresource and Environmental Sciences, Faculty of Life Sciences, Kyoto Sangyo University, Kamigamo Motoyama, Kita-ku, Kyoto 603-8555, Japan.

E-mail address: motohas@cc.kyoto-su.ac.jp.

<http://dx.doi.org/10.1016/j.bbrep.2017.01.010>

Received 23 July 2016; Received in revised form 7 November 2016; Accepted 25 January 2017

Available online 26 January 2017

2405-5808/ © 2017 The Author(s). Published by Elsevier B.V.

This is an open access article under the CC BY-NC-ND license (<http://creativecommons.org/licenses/by-nc-nd/4.0/>).

specific *E. coli* strain, AQ3625 (same as JC8679), for efficient iVEC [21]. Oliner *et al.* reported that the efficiency of *in vivo* cloning was higher with AQ3625 than with DH5 α , likely because AQ3625 harbors a mutation in *sbcA23*, which activates the RecE homologous recombination pathway [20].

Seamless ligation cloning extract (SLiCE) cloning uses the endogenous homologous recombination activity of cellular extracts from laboratory *E. coli* strains, to ligate DNA fragments *in vitro* [15,22,23]. The homologous recombination activity of *E. coli* cellular extracts is preserved by using specific detergent buffers during lysis [15,22,24]. PCR-amplified fragments with short (15–19 bp) end homology regions can be efficiently ligated into a vector *in vitro* using SLiCE cloning with cellular extracts of various laboratory *E. coli* strains including JM109, DH5 α , DH10B, and XL10-Gold [15,23]. SLiCE prepared from *E. coli* JM109 can be used in place of a commercial kit [22], such as the In-Fusion HD Cloning Kit from Clontech Laboratories. Moreover, SLiCE cloning can be used to simultaneously ligate two unpurified PCR fragments into a common vector [15,25], and to assemble various DNA fragments of small (90 bp) to large (13.5 kbp) size [26].

These two recombinant enzyme-free seamless DNA cloning methods are simple and greatly reduce the cost of seamless DNA cloning. However, the efficiency and accuracy of these seamless DNA cloning methods have not been directly compared to date. Therefore, in the present study, the efficiency, accuracy, and utility of iVEC and SLiCE cloning were evaluated using DNA fragments with short-end homology lengths (15–39 bp) that were suitable for standard seamless DNA cloning.

2. Materials and methods

2.1. *Escherichia coli* strains

E. coli DH5 α [27] and AQ3625 (same as JC8679) [28] were used for transformations. *E. coli* AQ3625 (ME No. ME9276) was provided by the National BioResource Project (NIG, Japan): *E. coli*. *E. coli* JM109 [29] was used to prepare cellular extracts for *in vitro* SLiCE cloning. Genotypes of these strains are listed in Table S1.

2.2. Preparation of competent *E. coli* cells

Chemically competent *E. coli* cells were prepared using the modified transformation and storage solution (TSS) method [30]. Glycerol (10% (v/v), final concentration) was added to the original TSS solution [31]. The competency of chemically competent DH5 α and AQ3625 cells prepared using the modified TSS method was 1.5×10^6 colony forming units (CFU)/ μ g pUC19 DNA and 0.78×10^6 CFU/ μ g pUC19 DNA, respectively. To compare the competency of chemically competent cells between DH5 α and AQ3625, Inoue's method [32] and calcium chloride method [33] were also used.

2.3. Preparation of vector and insert DNA

DNA sequences encoding *Arabidopsis* type II peroxiredoxin E (*PrxIIIE*, 0.5 kbp, AT3G52960) [34,35] and chloroplast glucose-6-phosphate dehydrogenase 1 (*G6PDH1*, 1.6 kbp, AT5G35790) [36] were used as insert DNAs. Two genes were cloned from an *Arabidopsis* cDNA library [37,38]. Insert DNA fragments and linearized pET23a vector DNA were amplified by PCR using Tks Gflex DNA polymerase (Takara-Bio, Otsu, Japan) and the primers listed in Table S2.

2.4. Preparation of SLiCE from *E. coli* JM109

The SLiCE from *E. coli* JM109 was prepared as described previously [23]. Briefly, *E. coli* JM109 cells pre-cultured in LB Miller medium (1 mL) at 37 °C were transferred to 2 \times YT medium (50 mL) in a 100-mL round-bottom, long-neck Sakaguchi shake flask. The cells

were grown at 37 °C in a reciprocal shaker (160 rpm with 25 mm stroke) until the OD₆₀₀ reached a value of 2.0 (late log phase). The cultures were incubated for 5.0 h. The cells were harvested by centrifugation at 5000 \times g for 10 min at 4 °C. The cells were then washed with 50 mL of sterilized water (ice-cold), and centrifuged at 5000 \times g for 5 min at 4 °C. The wet cells were recovered with a yield of 0.37g, and gently resuspended in 1.2 mL of CelLytic B Cell Lysis Reagent (Sigma, B7435), which was a commercially available bacterial cell lysis buffer containing 40 mM Tris-HCl (pH 8.0) and zwitterionic detergents. The resuspended cell mixture was left to stand for 10 min at room temperature to allow the lysis reaction to proceed. The cell lysates were then centrifuged at 20,000 \times g for 2 min at 4 °C. All subsequent procedures were performed on ice. The supernatants were carefully transferred into 1.5-mL microtubes to remove the insoluble materials, and an equal volume of ice-cold 80% (v/v) glycerol was added and mixed gently. Each SLiCE extract (40 μ L) was aliquoted into a 0.2-mL 8-strip PCR tube. The SLiCE extracts were snap-frozen in a bath of liquid nitrogen and stored at –80 °C in 40% (v/v, final concentration) glycerol.

2.5. SLiCE cloning of PCR fragments

SLiCE buffer (10 \times , 500 mM Tris-HCl, pH 7.5, 100 mM MgCl₂, 10 mM ATP and 10 mM dithiothreitol) was prepared as described previously [15,23]. The standard SLiCE reaction was performed as described previously [23]. Briefly, one microliter of SLiCE and one microliter of SLiCE buffer (10 \times) were added into the mixture of insert (4–67 ng) and vector (10–50 ng) DNA fragments, and then filled up to total 10 μ L with sterilized distilled water, and then SLiCE reactions (10 μ L total) were performed at 37 °C for 15 min. Reaction conditions including the quantities of insert and vector DNA fragments are described in detail in the figure and table legends. The mixtures after the SLiCE reaction were transformed into chemically competent DH5 α cells using the standard heat-shock procedure [23].

2.6. iVEC cloning of PCR fragments

The same amount of insert and vector DNA fragments used in SLiCE cloning were mixed in a total of 10 μ L and directly transformed into chemically competent DH5 α or AQ3625 cells, using the standard heat-shock procedure [23]. Quantities of insert and vector DNA fragments in the mixture are described in detail in the figure and table legends.

2.7. Evaluation of cloning efficiency

The number of colonies formed on agar plates after transformation was counted in each experiment. Cloning efficiency was defined as the fraction of total colonies in which a PCR product of the correct length was amplified by colony PCR amplification. In particular, cloning efficiencies were represented as "the number of colonies with the correct length of insert DNA confirmed by colony-PCR/the number of colonies subjected to colony-PCR" [15]. Cloning accuracy was expressed as the fraction of correctly cloned expression vectors in colony-PCR-positive clones. In particular, cloning accuracies were represented as "the number of correct clones confirmed by DNA sequencing/the number of colony-PCR positive clones". DNA sequences were determined by Sanger DNA sequencing [39].

2.8. Insert-check by colony-PCR in transformed *E. coli*

Colony PCR amplification was performed as described previously [25,38]. Briefly, each colony was picked with a sterile toothpick, and put into the bottom of a 0.2-mL 8-strip PCR tube or a 96-well PCR plate. After the toothpicks were removed from the PCR-tube, 10 μ L of KAPATaq Extra DNA polymerase (KAPA Biosystems, Wilmington, MA)

PCR mix was added to each sample; this mixture included the T7P and T7T primers corresponding to the T7 promoter and T7 terminator sequences of the pET vectors, respectively (Table S2, and [15]). PCR reactions were performed following the KAPATaq Extra standard protocol. For target DNAs > 1.5 kbp, Tks Gflex DNA polymerase was used in place of KAPATaq Extra DNA polymerase.

3. Results and Discussion

3.1. Evaluation of the cloning efficiency of iVEC (DH5 α) and SLiCE using purified PCR fragments

The iVEC method using *E. coli* DH5 α (iVEC-DH5 α) [17,18] and the SLiCE method using cellular extracts prepared from the *E. coli* JM109 strain [15,22–24] are recombinant enzyme-free seamless cloning methods, and these methods do not require any purified recombinant enzymes or special *E. coli* strains. To determine which of the two recombinant enzyme-free seamless DNA cloning methods provided a potential advantage, the cloning ability of both methods was compared by measuring the rate of colony formation (*i.e.*, number of colonies formed after transformation) and cloning efficiency (*i.e.*, the fraction of colonies in which a PCR product of the correct size could be amplified by colony PCR amplification) (Fig. 1). These two indices are important for evaluating cloning methods in general [15]. The colony formation rate was 30–60-fold higher for purified PCR fragments with short (15–29 bp) end homology regions using the SLiCE method compared to that using the iVEC-DH5 α method (Fig. 2). Even when purified PCR fragments with longer (39 bp) end homology regions were used, which is an optimal length for the iVEC-DH5 α method [17,18], the colony formation rate was still 5-fold higher using the SLiCE method than the iVEC-DH5 α method (Fig. 2). The cloning efficiency of the SLiCE method using purified PCR fragments with short (15, 19, or 29 bp) end homology regions was also higher than that of the iVEC-DH5 α method, although the cloning accuracy was the same between the two methods (Table 1). These results clearly indicate that the SLiCE method had more efficient cloning ability than the iVEC-DH5 α method, with short (15, 19, or 29 bp) end homology regions. Using purified PCR fragments with longer (39 bp) end homology regions, the

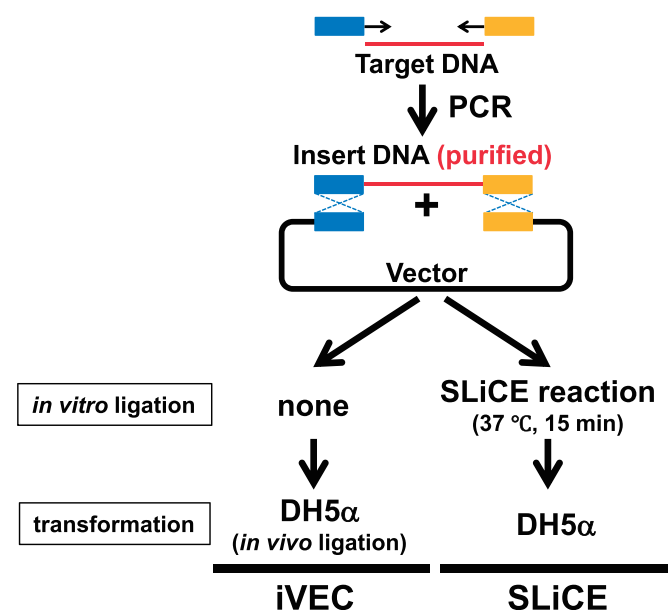


Fig. 1. Workflow of iVEC-DH5 α and SLiCE cloning with purified PCR fragments. Insert DNA fragments were PCR-amplified, purified, and mixed with linearized vector DNA. The mixture of insert and vector DNAs was directly transformed into DH5 α cells in the iVEC method (*in vivo* ligation). The mixture ligated using SLiCE (*in vitro* ligation) was transformed into DH5 α cells in the SLiCE method. Chemically competent DH5 α cells were prepared by the modified TSS method (DH5 α , 1.5×10^6 CFU/ μ g pUC19 DNA)).

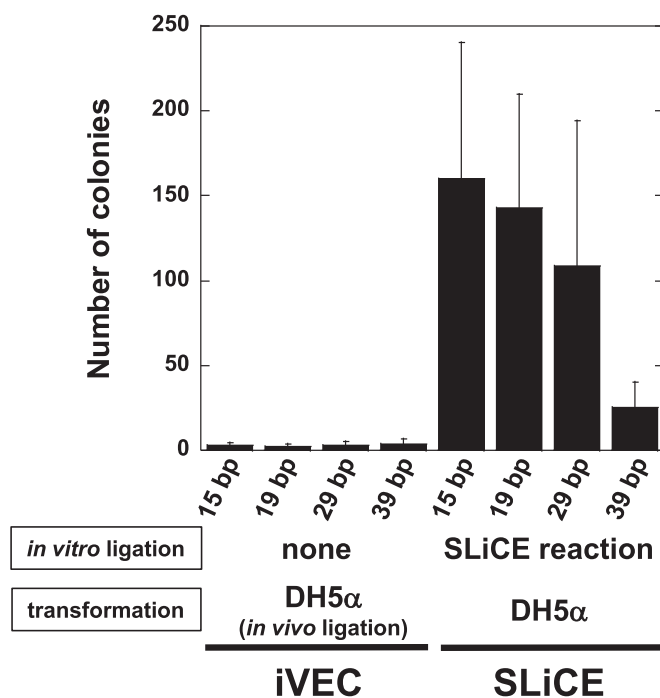


Fig. 2. Cloning efficiency of iVEC-DH5 α and SLiCE using purified PCR fragments. The number of colonies formed (*i.e.*, colony formation rate) with purified PCR fragments of variable end homology region lengths (15, 19, 29, or 39 bp) using the iVEC-DH5 α method [17,18] or the SLiCE method [15,23]. Number of colonies indicates the number of colonies that formed when 3 ng of vector DNA was transformed. Purified insert DNA fragments of *PrxIII*E (4 ng) and linearized pET23a vector (10 ng) were mixed in 10 μ L. iVEC was directly transformed to DH5 α competent cells using 3 μ L in 10 μ L. The SLiCE sample was reacted in a total volume of 10 μ L, and then 3 μ L of the 10 μ L was used for transformation to DH5 α . Each value for the number of colonies is the mean \pm standard deviation of three independent experiments. DH5 α chemically competent cells for both the iVEC-DH5 α method and the SLiCE method were prepared with a competency of 1.5×10^6 (CFU/ μ g pUC19 DNA) by the modified TSS method.

Table 1

Cloning efficiency and cloning accuracy of iVEC-DH5 α and SLiCE cloning methods using purified PCR fragments (*PrxIII*E).

Method ^a	Homology length (bp)	Cloning efficiency ^b	Cloning accuracy ^c
iVEC (DH5 α)	15	6/11 (54.5%)	4/6 (66.7%)
	19	2/7 (28.6%)	2/2 (100%)
	29	7/11 (63.6%)	6/7 (85.7%)
	39	10/14 (71.4%)	10/10 (100%)
SLiCE	15	10/16 (62.5%)	9/10 (90.0%)
	19	15/16 (93.8%)	12/15 (80.0%)
	29	15/16 (93.8%)	13/15 (86.7%)
	39	11/16 (68.8%)	10/11 (90.9%)

^a Insert DNA fragments of the *PrxIII*E gene (0.5 kbp) and linearized pET23a vector DNA were amplified by PCR, and purified by agarose gel electrophoresis and a Gel/PCR Extraction Kit (FastGene). Purified insert DNA fragments (4 ng) and linearized pET23a vector DNA (10 ng) were used at an insert:vector molar ratio of 3:1. Part (3 μ L) of the total 10 μ L solution was used to transform DH5 α competent cells (1.5×10^6 CFU/ μ g pUC19 DNA) prepared by the modified TSS method [30].

^b Cloning efficiency is defined as the fraction of total colonies in which a PCR product of the correct expected size was amplified by colony PCR amplification.

^c Cloning accuracy is defined as the fraction of clones correctly confirmed by DNA sequencing among colony-PCR positive clones.

cloning efficiency of the iVEC-DH5 α method was the same as that of the SLiCE method. This result is consistent with the conclusion that longer end homology regions (30–50 bp) are optimal for the iVEC-DH5 α method [18]. In contrast, the cloning efficiency of SLiCE was high at 63–94% (Table 1, cloning efficiency), irrespective of the length of the end homology regions (15, 19, 29, or 39 bp). These results indicate that SLiCE cloning has higher flexibility and robustness as a seamless DNA cloning method than the iVEC-DH5 α method.

3.2. Evaluation of the cloning efficiency of iVEC (AQ3625) and SLiCE cloning using unpurified PCR fragments

Seamless DNA cloning methods can also successfully ligate unpurified PCR-amplified fragments into vectors because of their high cloning efficiency. Gel-band purification of PCR-amplified DNA fragments is a time consuming step for DNA cloning, as it takes approximately one hour. Recently, it has become possible to skip DNA purification by agarose gel electrophoresis because high-fidelity thermostable DNA polymerases can specifically amplify the target DNA fragments without amplification of nonspecific DNA fragments. However, DNA cloning of unpurified PCR products requires high efficiency. In the present study, the cloning efficiencies of unpurified PCR fragments into vectors by iVEC and SLiCE were evaluated next. The colony formation rate was low with the iVEC-DH5 α method using purified PCR fragments of the *PrxIIE* gene, compared that of SLiCE cloning using the same DNA (Fig. 2). As a result, colony formation was not expected with the iVEC-DH5 α method using unpurified PCR fragments because of the 1/10–1/100 colony formation rate for seamless cloning of unpurified PCR fragments [15]. Therefore, *E. coli* AQ3625 was used as a host strain to ligate unpurified PCR fragments with the iVEC method (Fig. 3). *E. coli* AQ3625 harbors a mutation in the *sbcA23* gene, which activates the RecE homologous recombination pathway. The efficiency of the iVEC method with AQ3625 was higher than that with DH5 α [20]. The National BioResource Project (NIG, Japan) started to distribute a specific *E. coli* AQ3625 strain for efficient iVEC in April 2016 [21]. Use of *E. coli* AQ3625 in the present study improved the rate of colony formation of the iVEC method (Table 2). In fact, the number of colonies that formed with unpurified PCR fragments was higher with the iVEC-AQ3625 method than with the SLiCE method using DH5 α cells (Table 2). In addition to the rate of colony formation, both cloning efficiency and cloning accuracy are important indices of the utility of DNA cloning methods [15]. In the present study, with unpurified PCR fragments of *G6PDH1* gene, it was not possible to obtain any correct clones by 16-colony screening, and only one correct clone was obtained with that of *PrxIIE* gene (Table 2,

Table 2

Colony formation rate, cloning efficiency, and cloning accuracy of iVEC-AQ3625 and SLiCE cloning methods using unpurified PCR fragments (*PrxIIE* and *G6PDH1*).

Method ^a	Insert DNA	Number of colonies ^b	Cloning efficiency ^c	Cloning accuracy ^d
iVEC(AQ3625)	<i>PrxIIE</i>	58 \pm 8	3/16 (18.8%)	1/3 (33.3%)
	<i>G6PDH1</i>	43 \pm 23	0/16 (0.00%)	–
SLiCE	<i>PrxIIE</i>	27 \pm 11	15/16 (93.8%)	13/15 (86.7%)
	<i>G6PDH1</i>	25 \pm 11	10/16 (62.5%)	9/10 (90.0%)

^a Insert DNA fragments of *PrxIIE* (0.5 kbp) and *G6PDH1* (1.6 kbp) genes, which have short (19 bp) end homology regions, were amplified by PCR, and treated by *DpnI*. Unpurified insert DNA fragments of *PrxIIE* (21 ng) or *G6PDH1* (67 ng), and linearized pET23a vector DNA (purified, 50 ng) were used at an insert:vector molar ratio of 3:1. Part (3 μ L) of the total 10 μ L solution was used to transform chemically competent cells prepared by the modified TSS method [30]: AQ3625 (0.78×10^6 CFU/ μ g pUC19 DNA) or DH5 α (1.5×10^6 CFU/ μ g pUC19 DNA).

^b Number of colonies indicates the number of colonies that formed when 15 ng of vector DNA was transformed. Each value for the number of colonies is the mean \pm standard deviation of three independent experiments.

^c Cloning efficiency is defined as the fraction of total colonies in which a PCR product of the correct expected size was amplified by colony PCR amplification.

^d Cloning accuracy is defined as the fraction of clones correctly confirmed by DNA sequencing among colony-PCR positive clones.

iVEC (AQ3625)). In contrast, the cloning efficiency of the SLiCE method was 15/16 clones (for *PrxIIE*) and 10/16 clones (for *G6PDH1*), and the cloning accuracy of the SLiCE method was > 85% (Table 2, SLiCE). These results show that the SLiCE method is a more efficient recombinant enzyme-free seamless DNA cloning method than iVEC-AQ3625, even though the competency of the AQ3625 and DH5 α strains is the same. The higher cloning efficiency and cloning accuracy of SLiCE (*in vitro* cloning) when compared to iVEC-AQ3625 (*in vivo* cloning) might be explained by a difference in transformation efficiency between circular DNA and linear DNA. As another possible explanation, the cell lysis buffer might specifically extract the homologous recombination activity required for seamless cloning, but not nuclease activity in *E. coli* cells.

3.3. Utility of iVEC and SLiCE seamless DNA cloning

In this study, I evaluated the efficiency of two simple seamless DNA cloning methods under the same conditions. For the purpose, competent cells prepared by modified TSS method [30] were used because these competent cells of the DH5 α and AQ3625 strains have similar competency ($\sim 10^6$ CFU/ μ g pUC19 DNA) (Table 3). However, as a practical consideration, the intrinsic competency of competent *E. coli* cells is an important determinant of the efficiency of DNA cloning methods. To determine the effect of cell competency on the efficiency of each cloning method, chemically competent cells of both DH5 α and AQ3625 strains were prepared by three different methods: the modified TSS method [30], Inoue's method [32], and the CaCl₂ method [33]. In all cases, AQ3625 cells were less competent than the corresponding DH5 α cells (Table 3), which might be due to the lower

Table 3

Competency of *E. coli* DH5 α and AQ3625 chemically competent cells.

methods	strain	competency (CFU / μ g pUC19 DNA)
Modified TSS method ^a	DH5 α	1.5×10^6
	AQ3625	7.8×10^5
Inoue's method ^b	DH5 α	1.8×10^7
	AQ3625	0.5×10^5
Calcium chloride method ^c	DH5 α	1.2×10^5
	AQ3625	0.1×10^5

^a DH5 α and AQ3625 were harvested at OD₆₀₀=0.55 and 0.41, respectively.

^b DH5 α and AQ3625 were harvested at OD₆₀₀=0.16 and 0.27, respectively.

^c DH5 α and AQ3625 were harvested at OD₆₀₀=0.46 and 0.56, respectively.

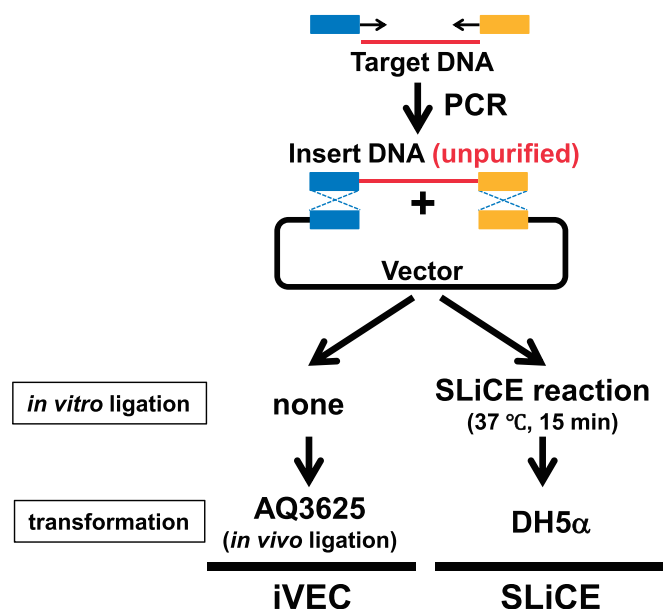


Fig. 3. Workflow of iVEC-AQ3625 and SLiCE cloning with unpurified DNA fragments. Insert DNA fragments were PCR-amplified and mixed with linearized vector DNA, without purification. The mixture of insert and vector DNAs was directly transformed into AQ3625 cells in the iVEC method (*in vivo* ligation). The mixture ligated using SLiCE (*in vitro* ligation) was transformed into DH5 α cells in the SLiCE method. Chemically competent DH5 α (1.5×10^6 CFU/ μ g pUC19 DNA) and AQ3625 (0.78×10^6 CFU/ μ g pUC19 DNA) cells were prepared by the modified TSS method [30]. Short (19 bp) end homology regions between insert and vector DNAs were used.

competency of *RecA*⁺ strains including *E. coli* AQ3625 and BL21 (DE3). Chemically competent cells of DH5 α and other *recA*⁻ strains prepared by Inoue's method are generally highly competent [32], and are referred as ultracompetent cells ($\sim 10^8$ CFU/ μ g plasmid DNA) [40]. In fact, competent DH5 α cells prepared by Inoue's method were also highly competent in this study (1.8×10^7 CFU/ μ g pUC19 DNA) (Table 3). Transformation of purified PCR fragments ligated *in vitro* with the SLiCE method into competent DH5 α cells prepared by Inoue's method [32] resulted in significantly increased colony formation (> 2000 colonies) (Table S3, SLiCE), compared to that (25–160 colonies) of the same reactions but with transformation into DH5 α cells prepared by the modified TSS method (Fig. 2). Use of unpurified PCR fragments also provided similar results (Table 2 and Table S4). In contrast, few colonies were observed with the iVEC method using *E. coli* AQ3625 competent cells prepared by Inoue's method (Table S3). More efficient AQ3625 competent cells (> 10^7 (CFU/ μ g pUC19 DNA)) could not be prepared by Inoue's method, although 7.8×10^5 (CFU/ μ g pUC19 DNA) AQ3625 competent cells were prepared by the modified TSS method (Table 3). Preparation of AQ3625 competent cells might require a specific method. Thus, the competency of *E. coli* cells is also a significant determinant of the efficiency and utility of seamless DNA cloning.

4. Conclusion

Both iVEC and SLiCE cloning offer simple and low-cost recombinant enzyme-free seamless DNA cloning. Here, the efficiency and utility of each method were evaluated in terms of cloning efficiency and accuracy. The colony formation rate, cloning efficiency, and cloning accuracy of the SLiCE method were high for a wide range of end homology region lengths (Fig. 2 and Table 1), and increasing the intrinsic competency of the host cells greatly improved the colony formation rate of SLiCE cloning (Fig. 2 and Table S3). The colony formation rate and cloning efficiency were lower with the iVEC-DH5 α method than with the SLiCE method at short end homology regions (15, 19, or 29 bp), although the colony formation rate of the iVEC method was improved by using the AQ3625 strain. Furthermore, the SLiCE method had higher cloning efficiency and cloning accuracy than iVEC-AQ3625, even when DH5 α and AQ3625 cells having similar competency were used (Table 2). In addition, AQ3625 cells were less competent than DH5 α cells in all three different preparation methods for chemically competent cells. In future work, the cloning efficiency of AQ3625 cells and the competency of cells in the AQ3625 strain should be further improved. Both improvements will contribute to the development of efficient recombinant enzyme-free seamless DNA cloning.

Acknowledgements

I thank to the National BioResource Project (NBRP): *E. coli* (<https://shigen.nig.ac.jp/ecoli/strain/>) for providing an *E. coli* strain (AQ3625, ME No. ME9276). I also thank Yuki Okegawa for critically reading the manuscript. This work was supported by JSPS KAKENHI Grant Numbers 16K07409 (to K.M.), and the MEXT-Supported Program for the Strategic Research Foundation at Private Universities (to K.M.).

Appendix A. Transparency document

Transparency document associated with this article can be found in the online version at <http://dx.doi.org/10.1016/j.bbrep.2017.01.010>.

Appendix B. Supporting information

Supplementary data associated with this article can be found in the online version at <http://dx.doi.org/10.1016/j.bbrep.2017.01.010>.

References

- [1] B. Zhu, G. Cai, E.O. Hall, G.J. Freeman, In-fusion assembly: seamless engineering of multidomain fusion proteins, modular vectors, and mutations, *Biotechniques* 43 (2007) 354–359.
- [2] M.Z. Li, S.J. Elledge, Harnessing homologous recombination *in vitro* to generate recombinant DNA via SLiC, *Nat. Methods* 4 (2007) 251–256.
- [3] D.G. Gibson, L. Young, R.Y. Chuang, J.C. Venter, C.A. Hutchison 3rd, H.O. Smith, Enzymatic assembly of DNA molecules up to several hundred kilobases, *Nat. Methods* 6 (2009) 343–345.
- [4] C.H. Baek, J. Chesnut, F. Katzen, Positive selection improves the efficiency of DNA assembly, *Anal. Biochem.* 476 (2015) 1–4.
- [5] T. Lanyon-Hogg, N. Masumoto, G. Bodakh, A.D. Konitsiotis, E. Thion, U.R. Rodgers, R.J. Owens, A.I. Magee, E.W. Tate, Click chemistry armed enzyme-linked immunosorbent assay to measure palmitoylation by hedgehog acyltransferase, *Anal. Biochem.* 490 (2015) 66–72.
- [6] T.B. Jacobs, P.R. LaFayette, R.J. Schmitz, W.A. Parrott, Targeted genome modifications in soybean with CRISPR/Cas9, *BMC Biotechnol.* 15 (2015) 16.
- [7] Y. Nakagawa, T. Sakuma, T. Sakamoto, M. Ohmuraya, N. Nakagata, T. Yamamoto, Production of knockout mice by DNA microinjection of various CRISPR/Cas9 vectors into freeze-thawed fertilized oocytes, *BMC Biotechnol.* 15 (2015) 33.
- [8] J. Haustant, A. Sil, C. Maillo-Rius, A. Hocquellet, P. Costaglioli, B. Garbay, W. Dieryck, Use of the human hepcidin gene to build a positive-selection vector for periplasmic expression in *Escherichia coli*, *Anal. Biochem.* 500 (2016) 35–37.
- [9] D. Dovala, W.S. Sawyer, C.M. Rath, L.E. Metzger, Rapid analysis of protein expression and solubility with the SpyTag-SpyCatcher system, *Protein Expr. Purif.* 117 (2016) 44–51.
- [10] P. Pakarian, P.D. Pawelek, A novel set of vectors for Fur-controlled protein expression under iron deprivation in *Escherichia coli*, *BMC Biotechnol.* 16 (2016) 68.
- [11] L. Bataille, W. Dieryck, A. Hocquellet, C. Cabanne, K. Bathany, S. Lecommandoux, B. Garbay, E. Garanger, Recombinant production and purification of short hydrophobic Elastin-like polypeptides with low transition temperatures, *Protein Expr. Purif.* 121 (2016) 81–87.
- [12] H.P. Dulal, M. Nagae, A. Ikeda, K. Morita-Matsumoto, Y. Adachi, N. Ohno, Y. Yamaguchi, Enhancement of solubility and yield of a beta-glucan receptor Dectin-1C-type lectin-like domain in *Escherichia coli* with a solubility-enhancement tag, *Protein Expr. Purif.* 123 (2016) 97–104.
- [13] S. Wang, Z. Xiang, Y. Wang, H. Xu, D. Zhang, X. Wang, J. Sheng, Expression and purification of human MHC class I-related chain molecule B-alpha1 domain, *Protein Expr. Purif.* 123 (2016) 83–89.
- [14] Y. Zheng, J. Xie, X. Huang, J. Dong, M.S. Park, W.K. Chan, Binding studies using *Pichia pastoris* expressed human aryl hydrocarbon receptor and aryl hydrocarbon receptor nuclear translocator proteins, *Protein Expr. Purif.* 122 (2016) 72–81.
- [15] K. Motohashi, A simple and efficient seamless DNA cloning method using SLiCE from *Escherichia coli* laboratory strains and its application to SLiP site-directed mutagenesis, *BMC Biotechnol.* 15 (2015) 47.
- [16] C. Li, A. Wen, B. Shen, J. Lu, Y. Huang, Y. Chang, FastCloning: a highly simplified, purification-free, sequence- and ligation-independent PCR cloning method, *BMC Biotechnol.* 11 (2011) 92.
- [17] A.P. Jacobus, J. Gross, Optimal cloning of PCR fragments by homologous recombination in *Escherichia coli*, *PLoS ONE* 10 (2015) e0119221.
- [18] M. Kostylev, A.E. Otwell, R.E. Richardson, Y. Suzuki, Cloning should be simple: *Escherichia coli* DH5alpha-mediated assembly of multiple DNA fragments with short end homologies, *PLoS ONE* 10 (2015) e0137466.
- [19] P. Bubeck, M. Winkler, W. Bautsch, Rapid cloning by homologous recombination *in vivo*, *Nucleic Acids Res.* 21 (1993) 3601–3602.
- [20] J.D. Oliner, K.W. Kinzler, B. Vogelstein, *In vivo* cloning of PCR products in *E. coli*, *Nucleic Acids Res.* 21 (1993) 5192–5197.
- [21] National Institute of Genetics, National BioResource Project *E. coli* Strain, Mishima, Japan [updated April 18, 2016; cited 2016 June 3, 2016]. Available from: (<https://shigen.nig.ac.jp/ecoli/strain/>), 2016.
- [22] Y. Okegawa, K. Motohashi, A simple and ultra-low cost homemade seamless ligation cloning extract (SLiCE) as an alternative to a commercially available seamless DNA cloning kit, *Biochem. Biophys. Rep.* 4 (2015) 148–151.
- [23] K. Motohashi, Seamless Ligation Cloning Extract (SLiCE) method using cell lysates from laboratory *Escherichia coli* strains and its application to slip site-directed mutagenesis, *Methods Mol. Biol.* 1498 (2017) 349–357.
- [24] Y. Okegawa, K. Motohashi, Evaluation of seamless ligation cloning extract preparation methods from an *Escherichia coli* laboratory strain, *Anal. Biochem.* 486 (2015) 51–53.
- [25] Y. Okegawa, K. Motohashi, Expression of spinach ferredoxin-thioredoxin reductase using tandem T7 promoters and application of the purified protein for *in vitro* light-dependent thioredoxin-reduction system, *Protein Expr. Purif.* 121 (2016) 46–51.
- [26] K. Messerschmidt, L. Hochrein, D. Dehm, K. Schulz, B. Mueller-Roeber, Characterizing seamless ligation cloning extract for synthetic biological applications, *Anal. Biochem.* 509 (2016) 24–32.
- [27] Bethesda Research Laboratories, BRL pUC host: *E. coli* DH5cTM competent cells, *Focus*, 8 (1986) 9–12.
- [28] T. Asai, S. Sommer, A. Bailone, T. Kogoma, Homologous recombination-dependent initiation of DNA replication from DNA damage-inducible origins in *Escherichia coli*, *EMBO J.* 12 (1993) 3287–3295.
- [29] C. Yanisch-Perron, J. Vieira, J. Messing, Improved M13 phage cloning vectors and host strains: nucleotide sequences of the M13mp18 and pUC19 vectors, *Gene* 33 (1985) 103–119.

- [30] A.J. Walhout, G.F. Temple, M.A. Brasch, J.L. Hartley, M.A. Lorson, S. van den Heuvel, M. Vidal, GATEWAY recombinational cloning: application to the cloning of large numbers of open reading frames or ORFeomes, *Methods Enzym.* 328 (2000) 575–592.
- [31] C.T. Chung, S.L. Niemela, R.H. Miller, One-step preparation of competent *Escherichia coli*: transformation and storage of bacterial cells in the same solution, *Proc. Natl. Acad. Sci. USA* 86 (1989) 2172–2175.
- [32] H. Inoue, H. Nojima, H. Okayama, High efficiency transformation of *Escherichia coli* with plasmids, *Gene* 96 (1990) 23–28.
- [33] M. Mandel, A. Higa, Calcium-dependent bacteriophage DNA infection, *J. Mol. Biol.* 53 (1970) 159–162.
- [34] K.J. Dietz, F. Horling, J. König, M. Baier, The function of the chloroplast 2-cysteine peroxiredoxin in peroxide detoxification and its regulation, *J. Exp. Bot.* 53 (2002) 1321–1329.
- [35] C. Brehelin, E.H. Meyer, J.P. de Souris, G. Bonnard, Y. Meyer, Resemblance and dissemblance of Arabidopsis type II peroxiredoxins: similar sequences for divergent gene expression, protein localization, and activity, *Plant Physiol.* 132 (2003) 2045–2057.
- [36] S. Wakao, C. Benning, Genome-wide analysis of glucose-6-phosphate dehydrogenases in *Arabidopsis*, *Plant J.* 41 (2005) 243–256.
- [37] K. Motohashi, Y. Okegawa, Method for enhancement of plant redox-related protein expression and its application for in vitro reduction of chloroplastic thioredoxins, *Protein Expr. Purif.* 101 (2014) 152–156.
- [38] Y. Okegawa, M. Koshino, T. Okushima, K. Motohashi, Application of preparative disk gel electrophoresis for antigen purification from inclusion bodies, *Protein Expr. Purif.* 118 (2016) 77–82.
- [39] F. Sanger, S. Nicklen, A.R. Coulson, DNA sequencing with chain-terminating inhibitors, *Proc. Natl. Acad. Sci. USA* 74 (1977) 5463–5467.
- [40] M.R. Green, J. Sambrook, *Molecular Cloning: A Laboratory Manual*, Fourth edition, Cold Spring Harbor Laboratory Press, Cold Spring Harbor, NY, 2012.

ARTICLE

DOI: 10.1038/s41467-017-02150-7

OPEN

Evolution of sequence-specific anti-silencing systems in *Arabidopsis*

Aoi Hosaka^{1,2}, Raku Saito^{1,2}, Kazuya Takashima¹, Taku Sasaki^{1,3}, Yu Fu^{1,2}, Akira Kawabe⁴, Tasuku Ito^{1,3}, Atsushi Toyoda⁵, Asao Fujiyama⁵, Yoshiaki Tarutani^{1,2} & Tetsuji Kakutani^{1,2,3}

The arms race between parasitic sequences and their hosts is a major driving force for evolution of gene control systems. Since transposable elements (TEs) are potentially deleterious, eukaryotes silence them by epigenetic mechanisms such as DNA methylation. Little is known about how TEs counteract silencing to propagate during evolution. Here, we report behavior of sequence-specific anti-silencing proteins used by *Arabidopsis* TEs and evolution of those proteins and their target sequences. We show that VANC, a TE-encoded anti-silencing protein, induces extensive DNA methylation loss throughout TEs. Related VANC proteins have evolved to hypomethylate TEs of completely different spectra. Targets for VANC proteins often form tandem repeats, which vary considerably between related TEs. We propose that evolution of VANC proteins and their targets allow propagation of TEs while causing minimal host damage. Our findings provide insight into the evolutionary dynamics of these apparently “selfish” sequences. They also provide potential tools to edit epigenomes in a sequence-specific manner.

¹Department of Integrated Genetics, National Institute of Genetics, Yata 1111, Shizuoka 411-8540, Japan. ²Department of Genetics, School of Life Science, SOKENDAI (The Graduate University for Advanced Studies), Yata 1111, Shizuoka 411-8540, Japan. ³Department of Biological Sciences, Graduate School of Science, The University of Tokyo, Hongo, Bunkyo-ku, Tokyo 113-0033, Japan. ⁴Department of Bioresource and Environmental Sciences, Faculty of Life Sciences, Kyoto Sangyo University, Motoyama Kamigamo, Kyoto 606-8555, Japan. ⁵Center for Information Biology, National Institute of Genetics, Yata 1111, Shizuoka 411-8540, Japan. Aoi Hosaka and Raku Saito contributed equally to this work. Correspondence and requests for materials should be addressed to A.H. (email: ahosaka@nig.ac.jp) or to T.K. (email: tkakutan@nig.ac.jp)

The arms race between parasitic sequences and hosts is a major driving force for evolution of gene control systems. As a defense against parasitic sequences such as viruses and transposable elements (TEs), hosts employ mechanisms such as RNAi, chromatin modifications, and DNA methylation^{1–11}. Viruses in turn often deploy anti-defense mechanisms^{12–15}. Anti-defense mechanisms are widespread in pathogens but the target specificity of these mechanisms is generally low and non-specific anti-defense strategies often reduce host fitness severely. Non-specific anti-defense is less common in TEs, likely reflecting their life cycle in which they generally remain in the same host and depend on host survival. Although horizontal transfer of TEs is known^{16,17}, this apparently occurs rarely compared to horizontal transfer of viruses, and it is generally thought to be important for TEs to proliferate while avoiding damage to their host. Despite a major impact of TEs on genome evolution, little is known about strategies of TEs to counteract silencing and propagate.

Arabidopsis serves as an ideal model organism to investigate control of TEs, with precise TE sequences throughout the genome and *trans*-acting mutations affecting TE activity^{6,8}. We have previously reported that an *Arabidopsis* TE, named *Hiun* (*Hi*), is normally silenced by DNA methylation but has an activity to counteract this silencing^{9,18}. Expression of VANC, one of the proteins encoded in *Hi*, induces transcriptional derepression of *Hi*-encoded genes and mobilization of *Hi*. In addition, when full-length *Hi* is transformed into wild-type *Arabidopsis* plants, the transgene induces loss of DNA methylation in the entire *Hi*. DNA methylation in other TEs is unaffected. A very enigmatic feature of this demethylation activity is how the specificity can be determined for such long target sequences.

Another intriguing feature of anti-silencing is its evolution. *Hi* belongs to a TE family called *VANDAL21*, which is one of multiple *VANDAL* TE families found in the *Arabidopsis* genome^{18–20}. Although *Hi* transgenes induce DNA methylation loss in *VANDAL21* copies, other *VANDAL* copies are unaffected. Still, many other *VANDAL* family members encode proteins related to VANC.

Here, we report behavior and evolution of the anti-silencing proteins VANC and their target sequences. After showing that VANC is sufficient for inducing sequence-specific loss of DNA methylation in the entire length of target TEs, we show that VANC proteins have evolved to induce loss of DNA methylation in TEs of completely different spectra. The most enigmatic features of VANC function are how one protein can recognize the long targets in a very sequence-specific manner and yet could have evolved to change targets. We show that tandem repeat formation is central to the specificity of related VANC proteins. VANC binds a short DNA motif *in vivo* and *in vitro*. This motif appears to have accumulated and evolved together by tandem repeat formation. We propose that through coevolution of VANC proteins and target DNA motifs, these *VANDAL* TEs escaped epigenetic silencing to propagate while causing minimal host damage.

Results

VANC protein evolves to affect different target TEs. We have previously reported that a full-length transgene of *Hi* induces DNA methylation loss at endogenous *VANDAL21* copies¹⁸. Strikingly, entire TEs of several kilobases in length are extensively hypomethylated in the *Hi* transgenic lines¹⁸. This raises the question how such long sequences can be hypomethylated in a sequence-specific manner. One possibility is that the sequence specificity is defined directly by the nucleotide sequence of the transgene, rather than by the encoded protein. In order to see if regions other than VANC are involved in sequence specificity, we

examined the hypomethylation effect of a transgene that lacked the other open reading frames (ORFs) of *Hi* (*VANA21* and *VANB21*) (ΔAB ; Fig. 1a). Whole-genome bisulfite sequencing (WGBS) revealed that ΔAB induced sequence-specific loss of methylation very similar to that of the full-length *Hi* (Fig. 1b–d; Supplementary Fig. 1; Supplementary Data 1), suggesting that VANC expression is sufficient for inducing a loss of DNA methylation at the endogenous *VANDAL21* elements. In order to test if the VANC protein, rather than the transcribed RNA, is responsible for the induced anti-silencing effect, we examined the effect of a VANC transgene with nonsense mutations within the coding sequences (Fig. 1a). For both of two transgenes with nonsense mutations in the VANC ORF, the anti-silencing effects were abolished; they did not induce transcriptional derepression or mobilization of the endogenous *Hi* (Supplementary Fig. 2). These observations suggest that VANC (hereafter referred to as VANC21) protein function is responsible for the loss of DNA methylation.

Although VANC21 induced hypomethylation in *VANDAL21* members specifically, proteins related to VANC21 are encoded in many other *VANDAL* family members¹⁸. In order to detect the effects of these VANC21-related proteins, we introduced one of them, a VANC21-like gene in *VANDAL6* (AT4G09370, hereafter referred to as VANC6), into wild-type plants by transformation (Fig. 1a, bottom). WGBS of the VANC6 transgenic lines revealed that *VANDAL6* copies and related *VANDAL* family members, such as *VANDAL8* copies, were hypomethylated in them (Fig. 1e, f; Supplementary Fig. 3). Again, the hypomethylation was sequence-specific. Importantly, the spectra of hypomethylated TEs were completely different between VANC21 and VANC6 transgenic lines (Fig. 1g). In addition to the hypomethylation of *VANDAL6* and related copies, VANC6 induced transcriptional derepression in these hypomethylated loci (Supplementary Fig. 4). These results show that these VANC genes have evolved to induce anti-silencing that is specific for the TE sequences similar to that of the copy encoding the VANC. It is mysterious how the sequence specificity is defined for such long targets that share high sequence similarity. The separation of the *VANDAL* families during evolution was relatively recent¹⁸, and therefore the anti-silencing mechanism must differentiate efficiently among closely related sequences.

VANC21 is localized in non-coding regions in *VANDAL21*. To examine how VANC proteins function, we determined VANC21 localization within the genome using chromatin immunoprecipitation followed by sequencing (ChIP-seq). Chromatin from transgenic plants expressing FLAG-tagged VANC21 was immunoprecipitated with anti-FLAG antibody and associated DNA was sequenced. The ChIP signal was highly enriched at *VANDAL21* loci (Fig. 2a; Supplementary Fig. 5). *VANDAL21*-specific localization was also confirmed by ChIP-seq using an antibody against the intact VANC21 protein (Supplementary Fig. 5d). Interestingly, the accumulation of VANC21 was not uniform; stronger signals were found in non-coding regions within *VANDAL21* copies (Fig. 2b; Supplementary Fig. 6), such as in introns, intergenic regions, and terminal non-coding regions.

VANC21 localization matched well with its effect on DNA methylation. The hypomethylation effect of VANC21 is generally stronger in non-CG sites compared to CG sites (Figs. 1b, 2b). Although the entire *VANDAL21* sequence tends to lose DNA methylation in non-CG sites, the hypomethylation effect on CG sites tends to be local (Figs. 1b, 2b). This local hypomethylation effect corresponds closely to the localization of VANC21 protein (Fig. 2b, c). The localization also corresponds to hypomethylation of non-CG sites, but the effect is broader than that observed at

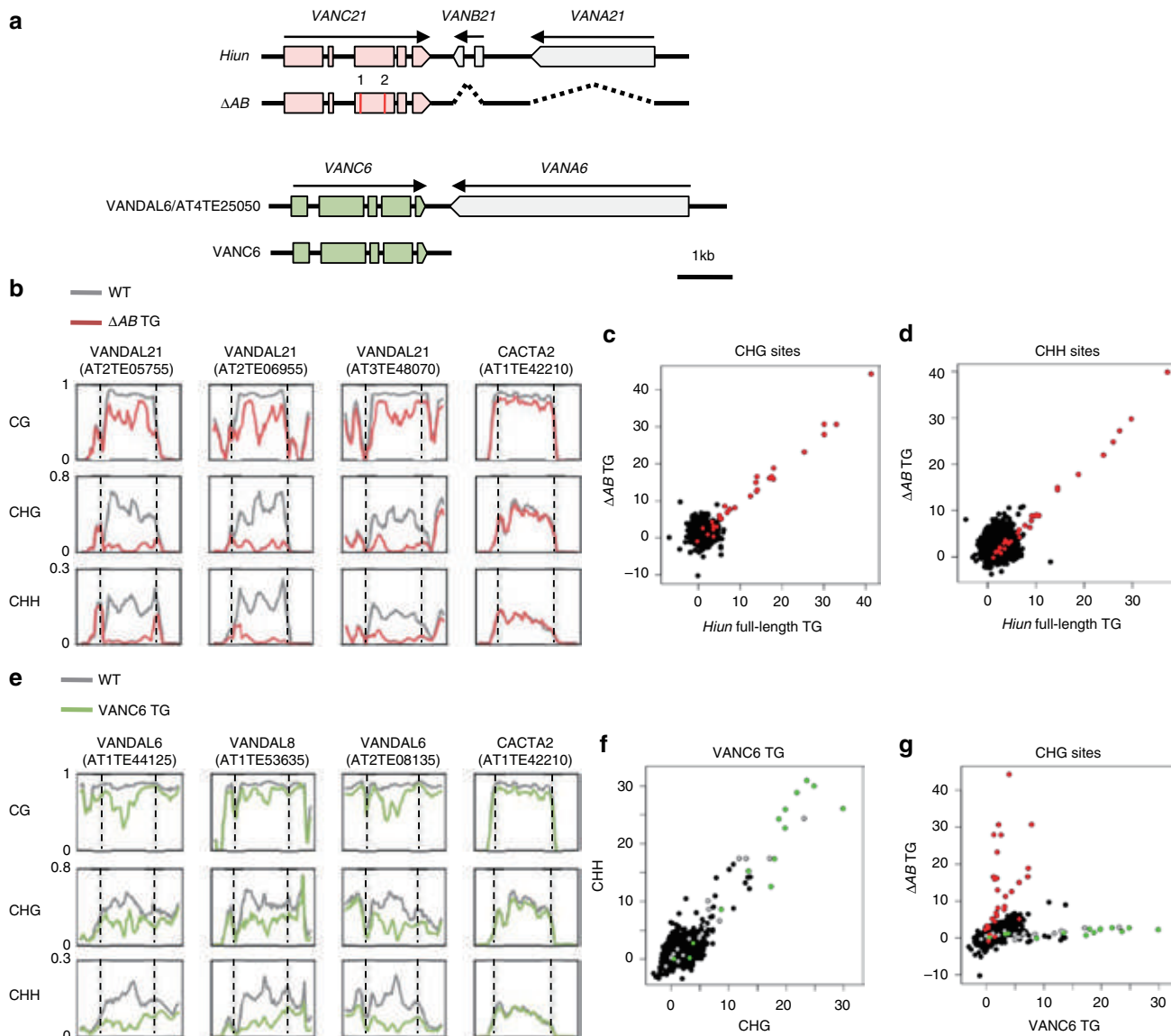


Fig. 1 Sequence-specific hypomethylation by VANC proteins. **a** Schematic diagram of structures of VANDAL transposons and the modified transgenes used. Boxes indicate exons. Vertical red lines show the positions of two nonsense mutations in VANC21 (Supplementary Fig. 2). **b** DNA methylation levels of VANDAL21 copies in ΔAB transgenic plants and parental wild-type plants (WT). Broken lines show TE ends. Each point represents proportion of methylated cytosine for a sliding window with seven fractions after separating each TE for 100 fractions. Right and left flanking regions are also analyzed by the same conditions. **c, d** Comparison of DNA hypomethylation between full-length *Hi* and ΔAB transgenic plants for CHG (**c**) and CHH sites (**d**). VANDAL21 copies are colored red. **e, f** Hypomethylation effects of VANC6 transgene. In **e**, conditions are as in **b**. In **f**, DNA hypomethylation is shown for each TE at CHG sites and CHH sites. VANDAL6 copies and VANDAL8 copies are colored green and gray, respectively. **g** Comparison of DNA hypomethylation between ΔAB and VANC6 transgenic plants at CHG sites. Results at CHH sites are shown in Supplementary Fig. 1f–h. In the panels **c, d, f**, and **g**, TEs more than 1 kb long are plotted ($N = 5866$). The significance of decrease in DNA methylation was assessed by the value $(Mn/Cn - Mt/Ct) / (1/\sqrt{Cn} + 1/\sqrt{Ct})$, where $Mn, Cn, Mt,$ and Ct are methylated cytosine (M) and total cytosine (C) counts mapped for each TE in the non-transgenic (n) and transgenic (t) plants, respectively¹⁸. This value shows the significance by weighing the change in the methylation ratio with root of the count number. Effects of ΔAB and VANC6 transgenes on DNA methylation status of TEs longer than 1 kb are also shown in Supplementary Data 1

CG sites (Fig. 2d, e), reflecting a spread of hypomethylation to surrounding regions extending to entire TEs (Figs. 1b, 2b).

VANC21 is bound to specific motifs in vivo and in vitro. To understand how VANC21 determines its targets, we searched for sequences statistically overrepresented in regions where VANC21 localized. A nine-base motif, “YAGTATTAY (Y = T or C)” was the most overrepresented candidate motif (Fig. 3a; Supplementary Table 1). Next, we examined the ability of VANC21 to bind DNA containing this motif in vitro by electrophoretic mobility

shift assay (EMSA). Consistent with the prediction from ChIP-seq, VANC21 induced a mobility shift for double-stranded DNA with sequences of five non-coding regions with this motif within VANDAL21 (probes 1, 2, 3, 6, and 7 in Fig. 3b, c, and Supplementary Fig. 7). In all of these 40-bp probes, single-base substitutions within the YAGTATTAY motif resulted in drastic reductions of the protein-binding efficiency, suggesting that this motif is indeed important for efficient binding of VANC21. The binding was much less efficient for sequences in coding regions within VANDAL21 (probes 4 and 5 in Fig. 3b, c), which do not have the YAGTATTAY motif. Taken together, these results

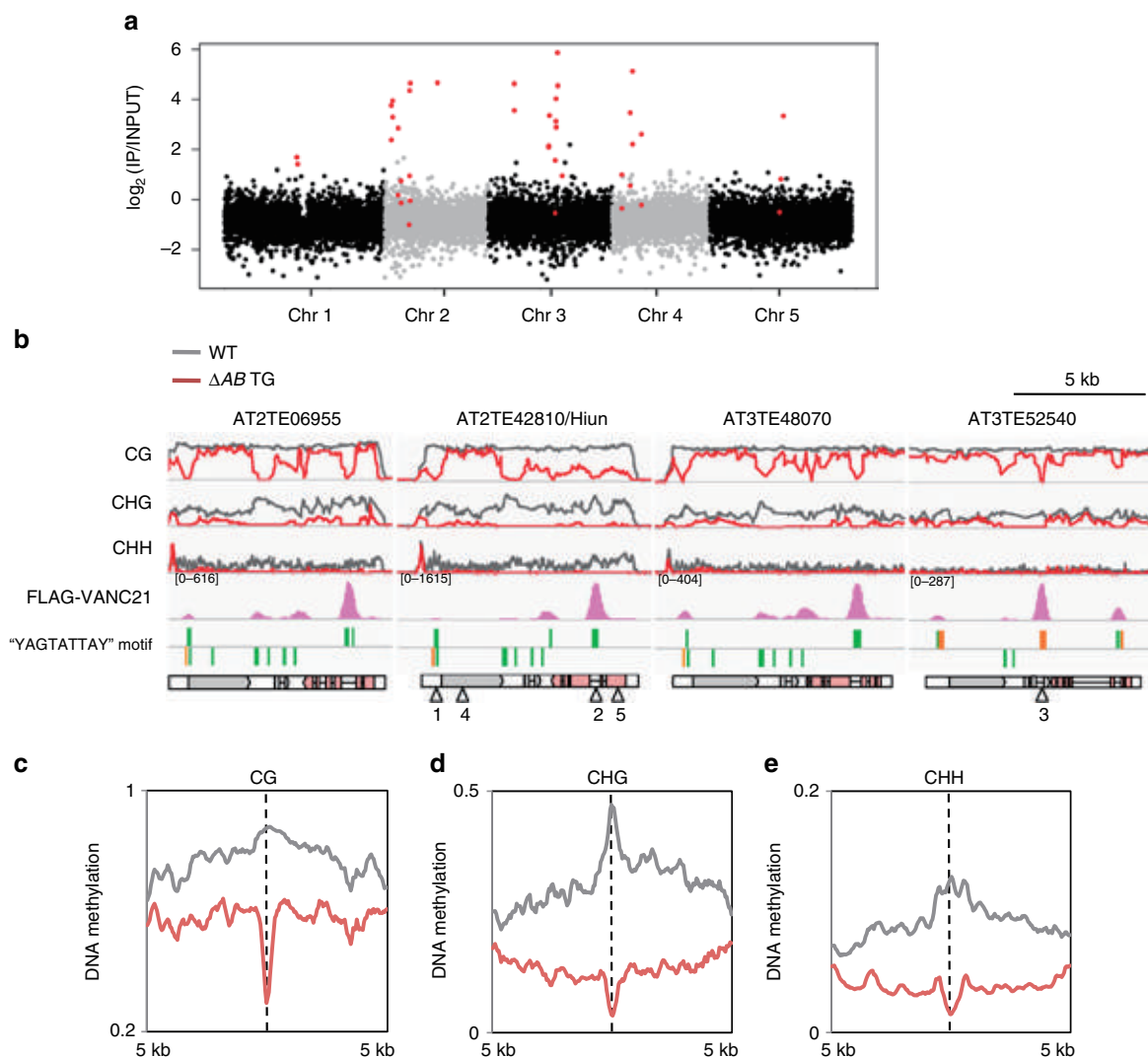


Fig. 2 Genomic localization of the VANC21 protein. **a** A genome-wide view showing the enrichment of FLAG-VANC21 signal. Each dot represents signal in a 10 kb region. Red dots indicate the regions with *VANDAL21* copies more than 1 kb long. **b** Genome browser views showing the FLAG-VANC21 signals with normalized coverages (per million mapped reads) and DNA methylation profiles (0–100%) of WT and ΔAB transgenic plants at *VANDAL21* copies. Each point represents proportion of methylated cytosine counted within five successive cytosine residues. *VANC21* exons are colored red. Arrowheads indicate probe sites used in EMSA (Fig. 3). **c–e** Three contexts of DNA methylation level around *VANC21* binding loci. Around the summits of *VANC21*-binding loci within *VANDAL21* ($N = 89$), 500 bp-binned averages of DNA methylation profiles were plotted for WT and ΔAB transgenic plants with steps of 50 bp

suggest that VANC21 was directed to these non-coding regions of *VANDAL21* copies through recognition of specific DNA sequences.

Within the *Arabidopsis thaliana* genome, this motif, YAGTATTAY, was highly enriched in *VANDAL21* copies, but it is rarely found in other TEs, including other *VANDAL* family members (Fig. 3d; Supplementary Fig. 8a). The motif was mainly found in non-coding regions of *VANDAL21* copies, which is consistent with the VANC21-binding pattern (Fig. 2b; Supplementary Fig. 6). As the YAGTATTAY sequence is short, this motif is also found sporadically outside of *VANDAL21* loci within the genome. A specific feature in the regions with VANC21 localization is that multiple motifs are arrayed in the same orientation at high density (Fig. 2b; Supplementary Fig. 6). The high density of the YAGTATTAY motif was unique to the *VANDAL21* loci (Supplementary Fig. 8b), and a low density of the YAGTATTAY motif outside *VANDAL21* was not associated with VANC21 localization. These results suggest that VANC21 recognizes “YAGTATTAY” motifs and that motif density is important for the specific chromosomal localization of VANC21.

VANC targets evolve through tandem repeat formation. The *VANDAL21* family can be classified into two subgroups based on sequence similarity (Fig. 3d; Supplementary Fig. 8c). They are shown as *VANDAL21_1* and *VANDAL21_2* in Fig. 3d. *VANDAL21_1* is the group with the autonomously-mobile copy *Hi*. We noticed that while “YAGTATTAC” motifs (hereafter called C-type) were found in both subfamilies, “YAGTATTAT” motifs (hereafter called T-type) accumulated only in *VANDAL21_2*. Although *VANDAL21_2* copies exist in *A. lyrata*, these copies do not possess the T-type motif (Fig. 3d; *A. lyrata*-specific lineages are shown by red). These results suggest that gain or loss of multiple motifs occurred relatively recently and occurred even within *VANDAL21* members.

We then wondered how the multiple motifs have accumulated so rapidly. Separation between *A. thaliana* and *A. lyrata* has been estimated to be 5–10 million years^{21,22}, and average base substitution rate between these two species for neutral sites has been estimated to be 0.13²³. It is hard to account for the accumulation of multiple motifs by simple base substitutions.

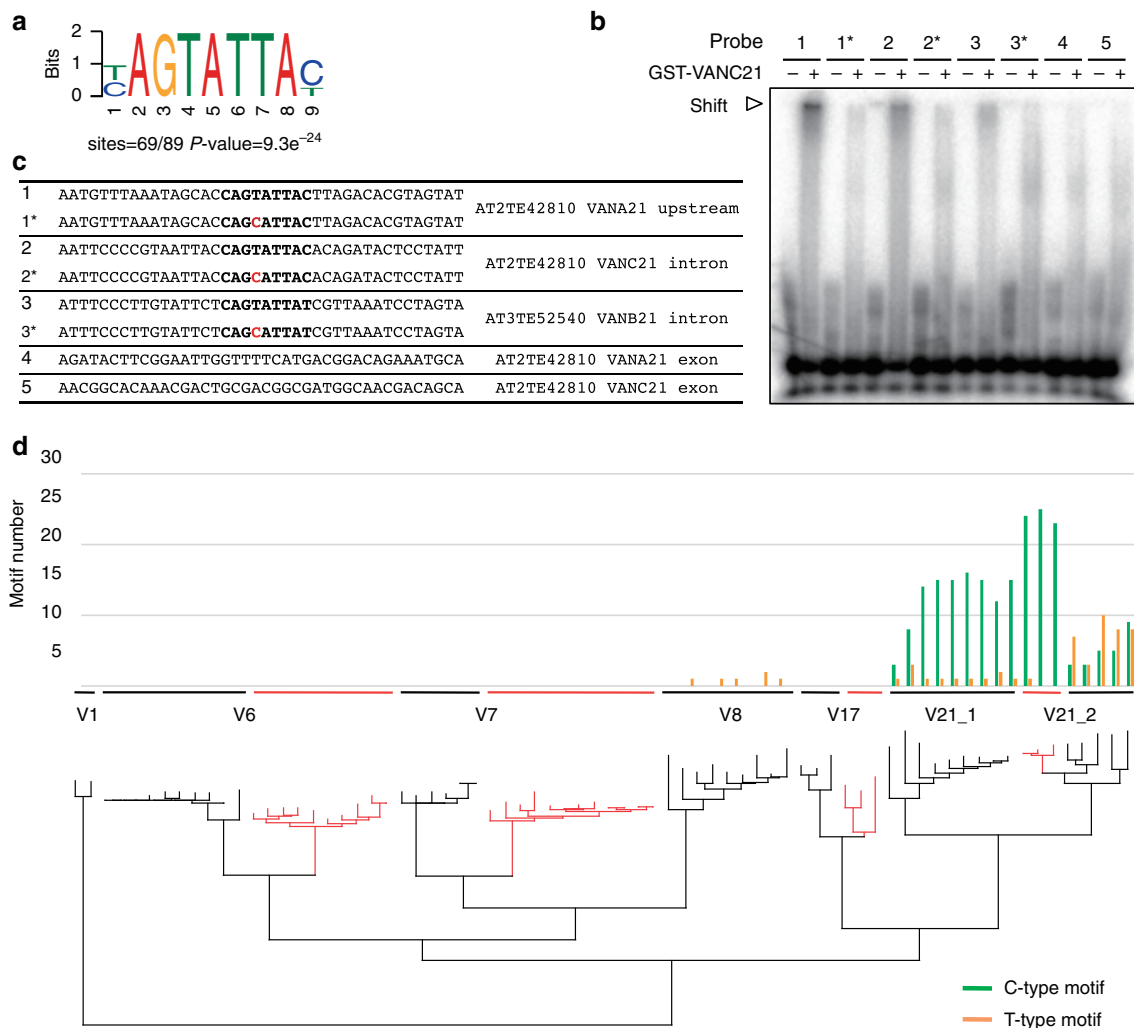


Fig. 3 VANC21-binding motifs and their distribution among VANDAL families. **a** DNA sequence motif most commonly found at FLAG-VANC21-binding sites in VANDAL21 TEs. Localizations of the motif are shown in Fig. 2b and Supplementary Fig. 6, with green and orange bars indicating positions of the C-type (“YAGTATTAC”) and T-type (“YAGTATTAT”) motifs, respectively. **b** Electrophoretic mobility shift assay (EMSA) by VANC21 protein for double-stranded DNA of the sequences shown in **c**. The probe sites are also shown by white arrowheads in Fig. 2b. 1*, 2*, and 3* have single-base substitutions within the motif relative to the original sequences. 4 and 5 are control sequences from the exons, where VANC21 localization was not detected. Results for dependence of the shift to the protein amount and a competition assay are shown in Supplementary Fig. 7. **c** Sequences of the dsDNA probe used in EMSA (**b**). **d** Numbers of C- and T-type motifs within VANDAL21 and related VANDAL family members within the genomes of *A. thaliana* and *A. lyrata*. *A. lyrata*-specific lineages are shown with red lines. IDs for these TE copies and bootstrap probabilities are shown in Supplementary Fig. 8c

Interestingly, regions with the motifs are often part of tandem repeats, and comparison of these sequences among different VANDAL21 copies revealed extensive gain and/or loss of the repeats in related copies (Fig. 4a–f; Supplementary Fig. 9). Furthermore, multiple units of sequences within a repeat often diverged together. For example, as illustrated in Fig. 4d, copy #2 has six motifs while copy #3 only has two motifs even though they both have a tandem repeat structure of similar organization. This pattern suggests that multiple copies within the repeat evolved together. These features were found in the introns of VANC21 and VANB21, as well as in upstream regions of VANA21 (Fig. 4b–f), suggesting that these tandem repeats are very dynamic.

As shown in Fig. 1, VANC proteins have also evolved to change their target specificities. Interestingly, VANC proteins have conserved domains and highly variable regions; and the variable regions often contain tandemly arrayed peptide motifs (Fig. 5a; Supplementary Fig. 10). In addition, VANC genes have diverse exon/intron organizations, which are frequently

associated with tandem repeat formation (Fig. 5b). We speculate that these tandem repeats within VANC proteins might play roles in defining target specificity, as is the case for the tandem repeats in their targets.

Sequences affected by VANC6 have different motifs. We also characterized the targets of VANC6. As VANC21 localization is associated with local loss of CG methylation (Fig. 2), we predicted targets of VANC6 by loss of CG methylation in transgenic lines expressing VANC6 (Supplementary Table 2). Motifs identified, “AGTTGTCC (CC-type)” and “AGTTGTAC (AC-type)”, are at least two nucleotides different from target motifs of VANC21 (Supplementary Fig. 11; Supplementary Table 2). These motifs are enriched in VANDAL6 and related VANDAL family members, such as VANDAL8 (Supplementary Fig. 11c), which show hypomethylation in VANC6 transgenic lines (Supplementary Fig. 3). In addition, VANC6 protein bound to a region with high density of the motifs in vitro (Supplementary Fig. 12).

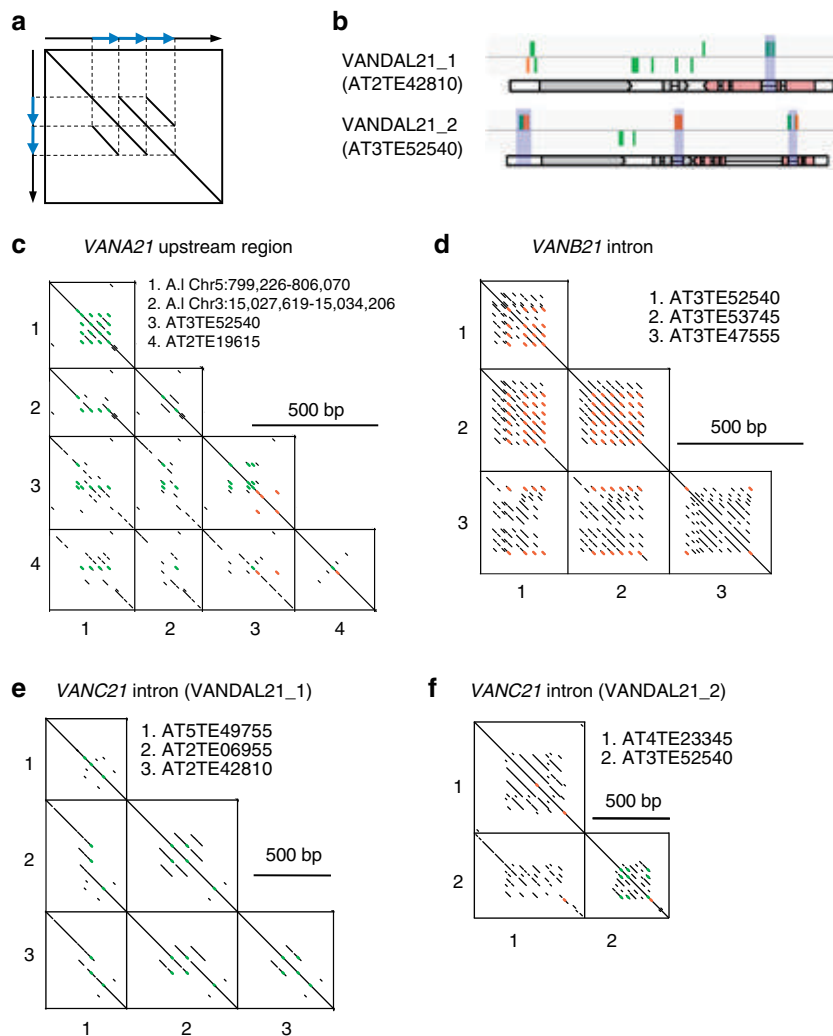


Fig. 4 Evolution of VANC21-binding regions. **a** Schematic diagram of dot plot for sequences with tandem repeat structures. Blue arrows indicate tandem repeats. Because of sequence identity, tandem repeat structure generates parallel lines. Difference in copy number can also be detected; in this case, three and two repetitions for X- and Y-axes, respectively. **b** Structures of VANDAL21 copies, with regions analyzed in **c-f** shown with shadow. Green and orange bars show C-type and T-type motifs. **c-f** Dot plots comparing the VANDAL21 sequences upstream of VANA21 (**c**), VANB21 intron (**d**), and VANC21 intron (**e**, **f**). Regions with 10 bp exact match are shown by dots. Green and orange indicate regions with C- and T-type motifs, respectively. Sequence alignments in these tandem repeat regions are shown in Supplementary Fig. 9

Interestingly, these motifs recognized by VANC6 are also found in *AT9TSD1*, which show hypomethylation in VANC6 transgenic lines (Supplementary Fig. 4; Supplementary Data 1), even though *AT9TSD1* is not related to VANDAL. In addition, some of *AT9TSD1* are transcriptionally derepressed in VANC6 transgenic lines (Supplementary Fig. 4). These results support our interpretation that each VANC protein induces loss of DNA methylation and transcriptional derepression by recognizing specific local sequences. The CC- and AC-type motifs are found as tandem repeats in non-coding regions of corresponding VANDAL copies, as is the case for motifs recognized by VANC21 (Supplementary Fig. 13). Thus, despite having a completely different spectra of target TEs (Fig. 1g; Supplementary Fig. 1f-h), VANC6 appears to function in a manner similar to that of VANC21 and their target sequences have similar evolutionary dynamics.

Discussion

In this report, we show that VANC proteins have high specificity for their target sequences and evolve together with their targets. The differentiated target regions of VANCs accumulated

recognized motifs in the form of tandem repeats (Fig. 4). Theoretically, tandem repeats can expand and contract by replication slippage and/or unequal crossing-over²⁴. The evolution of tandem repeats can occur rapidly, as is the case for centromeric tandem repeats in animals and plants^{25,26}. In the case of centromeric tandem repeats, centromeric histone H3, a protein localizing in the repeat, also evolves rapidly in its N-terminal domain, although the C-terminal core region is conserved^{27,28}. Interestingly, VANC proteins also have conserved domains and highly variable regions; and the variable regions are frequently associated with tandem repeat structures (Fig. 5). Investigation of regions within VANC proteins defining target specificity will be a focus of future studies.

Tandem repeats are often a target of epigenetic silencing. For instance, tandem repeats were formed multiple times independently during evolution of *FWA* gene promoters in the genus *Arabidopsis*²⁹. *FWA* is an imprinted gene and its promoter is a target of active DNA demethylation by DEMETER protein^{30,31}. It is tempting to speculate that anti-silencing by VANC also increases the frequency of tandem repeat formation during evolution. Tandem repeats can also be target of RNAi machinery^{32,33}. Evolution

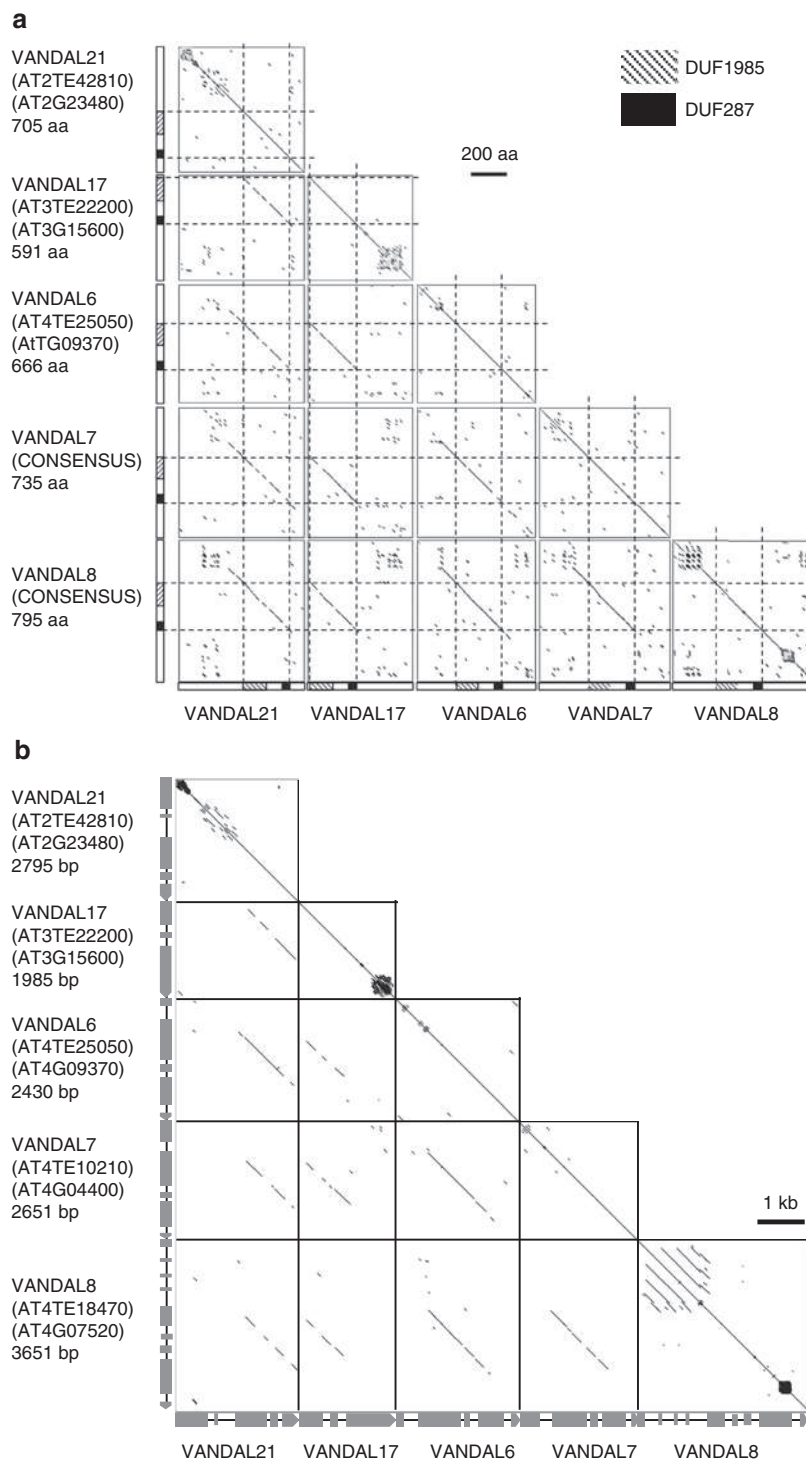


Fig. 5 Dot plot analyses of the VANC proteins. **a** Comparison of amino-acid sequences of the VANC proteins. Homologous regions were plotted with dotmatcher program (window size: 10, threshold: 23). Amino-acid sequences (N'-C') were ordered from top to bottom and left to right. Scale bar for 200 a.a. was shown in the right of plots. Two domains (DUF1985 and DUF287) are shown by shaded and filled areas, respectively. VANA (transposase), another protein encoded in these VANDAL members, is much more conserved (Supplementary Fig. 10). **b** Comparison of the nucleotide sequences of VANC genes. VANC genes were plotted with YASS program under default parameters⁵². DNA sequences are ordered from top to bottom and left to right. Gray boxes indicate exons. Divergence between these VANDAL families as well as divergence between the VANDAL copies in *A. thaliana* and *A. lyrata* is shown in Supplementary Tables 3, 4 and Supplementary Fig. 14

of motifs targeted by RNAi may offer a short-term advantage to escape from the host defense system. Such a short-term advantage may lead to a long-term advantage in allowing proliferation while causing minimal damage to the host, because differentiation of anti-silencing systems would limit the number of proliferating TEs.

An important remaining question is how the anti-silencing is achieved after the sequence-specific binding of VANCs. One possible pathway could be that VANC primarily functions as a transcription activator and that transcription induces the loss of silent marks. However, VANC21 induced hypomethylation not

only in coding regions but also in intergenic regions. In addition, hypomethylation was also found in the *VANDAL* copies without detectable transcriptional activation (Supplementary Figs. 4, 6), suggesting that the primary effect of *VANC21* is not transcriptional activation but removal of silent mark(s). We are currently trying to establish systems to genetically screen for mutants affecting *VANC*-mediated anti-silencing, in order to identify host factors involved in this process.

As our results demonstrate that a combination of short motifs and the *VANC* proteins can induce anti-silencing in diverse sequences, they could potentially be used to engineer epigenetic states at specific loci. For example, the anti-silencing may be used to ensure expression of transgenes in genetically modified crops^{34,35}. It would also be interesting to learn if some of the host machinery for the sequence-specific anti-silencing is conserved in other kingdoms.

Methods

Plant materials. *A. thaliana* strain Columbia-0 (Col-0) was used as “wild type”. Transgenic lines with full-length *Hi* and ΔAB *Hi* in pPZP2H-lac were described previously¹⁸. The *VANC6* construct was generated by two rounds of PCR from genomic DNA and cloned into pPZP2H-lac vector after digestion by *SpeI* and *XhoI*. Primer sequences for this and other constructions are available upon request. The FLAG-tagged *VANC21* construct was generated by two steps: (i) For generating FLAG-*VANC21* construct in which 3x FLAG tag was fused at C-terminus *VANC21* CDS, 3x FLAG sequence (5'-GACTACAAAGACGATGACGA-CAAGGATTATAAGGATGACGATGATAAAGACTATAAAGATGATGATGACAAA-3') and linear ΔAB *Hi* in pBluescript II SK (-) were generated by PCR and they were combined using In-Fusion HD cloning kit (Takara); (ii) The FLAG-tagged *VANC21* sequence was PCR amplified and cloned in *SmaI*-digested pPZP2H-lac vector using an In-Fusion HD cloning kit.

Whole-genome bisulfite sequencing. Mature rosette leaves were used for genomic DNA extraction. Bisulfite treatments and library preparations were performed as described previously¹⁸. Paired-end reads were qualified using Trimmomatic-0.33 software with following options “ILLUMINACLIP:TruSeq3-PE.fa:2:30:10 LEADING:3 TRAILING:3 SLIDINGWINDOW:4:15 MINLEN:36”³⁶. Qualified reads were mapped using the “bismark” command of bismark (0.14.3) software with following options “-n 1 -l 20”. PCR duplicates were removed from mapped bam files by “deduplicate_bismark” command³⁷. Base resolution of read counts of methylated and unmethylated cytosines were obtained as CX_reports files by “bismark_methylation_extractor” command with following options “-bedGraph -CX -cytosine_report”. Reads from previous study were used for the wild-type data³⁸. Differentially methylated regions at CG sites (CG-DMRs) induced by *VANC* genes were defined as previously described³⁸. Briefly, in each 100-bp window, DMRs were defined when a difference of methylation level at CG sites was 0.5 or more. Multiple DMRs were merged if they were adjacent to each other or there was only one gap of the 100-bp window. DNA sequences of CG-DMRs at *VANDAL21* TEs induced by ΔAB ($N=93$), and CG-DMRs at *VANDAL6*, 7, 8, 17, and *AT9TSD1* TEs induced by *VANC6* ($N=89$), were used for identifying statistically enriched short motifs, respectively (described below).

ChIP-seq. ChIP was performed according to the methods reported by Gendrel et al.³⁹ but with modification. Approximately 5.0 g of mature rosette leaves was fixed with 1% of formaldehyde. The fixed leaves were ground in liquid nitrogen, resuspended with 50 ml of extraction buffer 1 (0.4 M sucrose, 10 mM Tris-HCl pH 8, 5 mM β -mercaptoethanol, cOmplete, EDTA-free protease Inhibitor Cocktail (hereafter cOmplete; Sigma-Aldrich)), and the solution was filtrated with two layers of Miracloth (Millipore). The filtrated solution was centrifuged (1900 \times , 20 min) and the precipitate was washed twice with 5 ml of extraction buffer 2 (0.25 M sucrose, 10 mM Tris-HCl (pH 8.0), 10 mM MgCl₂, 1% Triton X-100, 5 mM 2-mercaptoethanol, cOmplete). The precipitate was resuspended with extraction buffer 3 (1.7 M sucrose, 10 mM Tris-HCl, 0.15% Triton X-100, 2 mM MgCl₂, cOmplete), layered on 500 μ l of extraction buffer 3, and centrifuged (15,000 \times , 40 min). The precipitate containing chromatin was resuspended with 500 μ l of nuclei lysis buffer (50 mM Tris-HCl (pH 8.0), 10 mM EDTA, 1% SDS, cOmplete). Chromatin was sheared by Branson Sonifier 250D with the conditions of Duty 17%, Pulse 60 s, 15 times. After centrifugation, 100 μ l of supernatant was diluted with ChIP Dilution buffer (1.1% Triton X-100, 1.2 mM EDTA, 16.7 mM Tris-HCl (pH 8.0), 167 mM NaCl) into 1000 μ l, and incubated with either 10 μ l of antiserum of 6xHis-*VANC21*-immunized rabbit, or 7 μ g of anti-FLAG antibody (F7425 Sigma-Aldrich) overnight. Immune complexes were captured by incubating with 100 μ l of Dynabeads Protein G (Thermo Fisher Scientific) for 1 h. Above procedures were performed at 4 °C. After rinsing the magnetic beads, immunoprecipitated DNA-protein complexes were eluted and reverse-crosslinked by incubation of the beads with 200 μ l of direct elution buffer (10 mM Tris-HCl (pH 8.0), 0.2 M

NaCl, 5 mM EDTA, 0.5% SDS) for overnight at 65 °C. Amount of DNA was quantified with the Qubit dsDNA High Sensitivity Assay Kit (Thermo Fisher Scientific). About 1.2 ng of DNA was used for library construction using a KAPA hyper prep kit (Kapa Biosystems) following manufacturer’s protocol. The libraries were amplified by 15 cycles of PCR using KAPA HiFi-PCR solution, and sequenced either by Miseq as 74 bp of paired-end reads or Hiseq 4000 as 50 bp of single-end reads. Reads were mapped by Bowtie (0.12.8)⁴⁰. For paired-end reads, “-X 1000” option was used. For single-end reads, “-n 2 -M 1 --best” option was used, because reads derived from repetitive regions were often not mapped uniquely and this option allows non-unique reads to be mapped on a region selected randomly from multiple best hits. Resulting sam files were converted into bam files and sorted by SAMtools (0.1.18)⁴¹. To identify peaks of FLAG-*VANC21*, a sorted bam file of anti-FLAG immunoprecipitated sample of FLAG-*VANC21* transgenic plants was analyzed using the MACS2 (2.1.0) “callpeak” command with the options “-g 135000000 -B -q 0.01”⁴². DNA sequences of *VANC21*-enriched regions defined by MACS2 in *VANDAL21* TEs were extracted. Short motifs that were statistically enriched at the *VANC21*-binding regions in *VANDAL21* TEs were searched by a DREME script of MEME software (4.11.0) under default parameters except maximum core width was set as 9⁴³. Same parameters were used for searching short motifs at CG-DMRs induced by *VANC* genes (Supplementary Table 2). In the plots of Fig. 2a and Supplementary Fig. 5d–g, regions with centromeric satellite repeats are excluded, because those regions show unstable signals for both IP and input samples. Reads mapped on specific regions were counted by “coverage” command of BEDtools (2.16.2)⁴⁴. These data sets were visualized on IGV genome browser⁴⁵. TAIR10 annotation was used for all sequence analyses.

Generation of anti-*VANC21* polyclonal antibody. Total RNA was isolated from *Hi* transgenic plants by the PureLink Plant RNA Reagent (Thermo Fisher Scientific). About 1 μ g of RNA was used for complimentary DNA (cDNA) synthesis with AMV ver3.0 (Takara). *VANC21* cDNA was amplified by PrimeSTAR GXL (98 °C 10 s, 60 °C 15 s, 68 °C 3 min; 30 cycles) and A-tailed by ExTaq (Takara). The cDNA was TA-cloned into pGEM T-easy vector (Promega) by Mighty Mix (Takara). Cloned full length of *VANC21* cDNA was amplified with PrimeSTAR GXL and primers with AttB1 and AttB2 sequences. The PCR fragment was cloned into pDEST17 vector by one-tube BP and LR Gateway reaction system following manufacturer’s protocol (Thermo Fisher Scientific). The pDEST17 vector containing *VANC21* cDNA was transformed into *Escherichia coli* of BL21-AI strain. Cells were pre-cultured for 8 h in 5 ml of LB liquid medium and the 0.5 ml of the culture was inoculated in 25 ml of LB liquid medium. After 3 h of incubation, expression of 6xHis-tagged *VANC21* protein (6xHis-*VANC21*) was induced for 3 h by adding up to 0.2% of l-arabinose. All culture steps were performed at 37 °C. Cells were harvested by centrifugation at 6000 \times g for 10 min. Cells were lysed, and the insoluble fraction containing 6xHis-*VANC21* was purified using Bugbuster Master Mix (Millipore) following manufacturer’s protocol. The purified insoluble fraction was solubilized in denaturing binding buffer (6 M urea, 30 mM imidazole, 1 \times PBS buffer). 6xHis-*VANC21* was captured by HisTrap Ni sepharose column (GE), and eluted with elution buffer (6 M urea, 200 mM imidazole, 1 \times PBS buffer). Purified 6xHis-*VANC21* was used for immunizing rabbits (MBL).

Western blotting. To extract nuclear proteins without fixation, 1.2 g of frozen mature leaves was ground and resuspended in 25 ml of nuclear extraction buffer 1 (0.4 M sucrose, 10 mM Tris-HCl (pH 8.0), 10 mM MgCl₂, 5 mM β -mercaptoethanol, and cOmplete). Extract was filtered through Miracloth (Millipore) and incubated on ice for 20 min. After centrifuging at 2000 \times g for 10 min, supernatant was discarded and pellet was resuspended in 1 ml of nuclear extraction buffer 2 (0.25 M sucrose, 10 mM Tris-HCl (pH 8.0), 10 mM MgCl₂, 1% Triton X-100, 5 mM β -mercaptoethanol, cOmplete). This washing step was repeated three times. Supernatant was discarded and pellet was resuspended in 350 μ l of lysis buffer (50 mM Tris-HCl (pH 8.0), 10 mM EDTA, 1% SDS, cOmplete) and sonicated three cycles of 10 s, followed by 50 s incubation on ice. After centrifuging at 12,000 rpm for 10 min, supernatant was mixed with SDS sample buffer. After heating at 95 °C for 5 min, protein was separated by SDS-PAGE (8%) and transferred to PVDF membrane (GE) by wet condition in transfer buffer (192 mM glycine, 25 mM Tris, 15% methanol). After the transfer, the membrane was immuno-hybridized with the following steps: blocking in TBS-T buffer (50 mM Tris-HCl, 150 mM NaCl, 0.05% Tween 20) containing 0.5% of skim milk (Nacalai Tesque) for 1 h, washed with TBS-T buffer three times, incubated in Can Get Signal Solution I (TOYOBO) containing 1:1000 dilution of either anti-*VANC21* antiserum or anti-FLAG antibody (F7425 Sigma-Aldrich) for 1 h, washed with TBS-T buffer three times, incubated in Can Get Signal Solution II containing 1:10,000 dilution of anti-rabbit HRP-labeled secondary antibody (074-1506 KPL) for 1 h, and washed with TBS-T buffer three times. ECL prime western blotting detection reagents (GE) was used to induce chemiluminescence. Signals were analyzed by LAS4000mini (GE).

RNA-seq. RNA was extracted from mature rosette leaves of WT or ΔAB *Hi* plants by PureLink Plant RNA Reagent (Thermo Fisher Scientific) and sent to Takara Biomedical Center (Takara) for strand-specific library preparation and sequencing. For RNA-seq, paired-end reads were mapped by tophat (2.1.0) with

the following parameters⁴⁶ “--library-type fr-firststrand --mate-inner-dist 200 --max-multihits 1”.

EMSA. VANC proteins were synthesized in *E. coli*. For VANC6, total RNA was isolated from *ddm1-1* plants by TRIzol (Thermo Fisher Scientific). About 1 µg of RNA was used for cDNA synthesis with PrimeScript RT-PCR Kit (Takara) using random 6-mer primers. VANC6 cDNA was amplified by Phusion (NEB) (98 °C 5 s, 58 °C 10 s, 72 °C 1 min; 30 cycles) and A-tailed by ExTaq (Takara). The cDNA was TA-cloned into pGEM T-easy vector (Promega). The cDNA of VANC21 and VANC6 was cloned into pDEST15 vector as described above. These vectors were then transformed into *E. coli* of BL21-AI strain. Cells were pre-cultured for 8 h in 5 ml of LB liquid medium and 1 ml of the culture was inoculated in 100 ml of LB liquid medium. After 3 h of incubation at 37 °C, the culture was incubated at 25 °C for 1 h. Expression of N-terminus-GST-tagged VANC21 protein (GST-VANC21) was induced for 24 h at 25 °C by adding up to 0.2% of L-arabinose. Cells were harvested and lysed by BugBuster Master Mix. The lysed solution was diluted with PBS buffer up to 50 ml and incubated with 0.125 g of glutathione-agarose beads (Sigma-Aldrich, equilibrated with PBS buffer to 1.4 ml) for overnight at 4 °C. The beads were washed with PBS buffer four times and the GST-VANC21 protein was eluted in buffer containing 10 mM glutathione and 50 mM Tris-HCl (pH 7.5). The protein concentration was quantified using a Nanodrop 2000 (Thermo Fisher Scientific). About 10 pmol of double-stranded DNAs (dsDNAs) was radiolabeled with 1 U of T4PNK (Takara) by incubation with 0.5 MBq of [γ -³²P] ATP for 1 h at 37 °C in 10 µl of reaction solution, and the radiolabeled dsDNAs were column purified using MicroSpin G-25 Columns (GE). About 2.5 µg of GST-VANC21 was incubated at 4 °C for 30 min in 15 µl of reaction solutions with 0.15 pmol of radiolabeled dsDNA in buffer containing 15 mM Tris-HCl (pH 7.5), 300 mM NaCl, 3 mM MgCl₂, 0.04% Triton X, 4% glycerol, 0.5 mM DTT, and 30 ng of Poly: IC. The reaction solutions were separated on 6% non-denaturing polyacrylamide gel with 1 × TBE buffer by 350 V for 15 min. Radioactivity signals were detected using a FLA-9000 (FUJI). In EMSA in Supplementary Fig. 12, VANC proteins without GST tag were used. After cloning VANC cDNAs into pDEST15 vector, PreScission Protease (GE) recognition sequence was added by inverse PCR. VANC proteins were purified with same procedures described above, except for elution with PreScission Protease (GE).

Phylogenetic analyses. Estimation of phylogeny of VANDAL families was performed as described previously¹⁸, except that sequences were aligned by MUSCLE algorithm, and ClustalX (2.0.12) was used for constructing neighbor-joining tree^{47–50}. Alignments of non-coding regions were also performed using the MUSCLE algorithm.

Dot plot analyses of VANA and VANC proteins. The CDS regions were used for the analyses. CDS regions were obtained based on the TAIR10 annotation for VANDAL17, VANDAL21, and VANDAL6. For VANDAL7 and VANDAL8 families, consensus sequences were generated and used for the analyses, because most members have become pseudogene. For VANDAL8, VANC annotations differ between loci due to several indel variations in the possible exon regions. Thus exon–intron junctions were determined based on the cDNA sequence data. Dot plots were made by using amino-acid sequences with EMBOSS dotmatcher default setting (10 window size, 23 threshold).

Estimation of genetic distance. Genetic distances between species and between families of VANDAL TEs were estimated by Poisson correction distances. Amino-acid sequences of conserved domains of VANA and VANC were used for the alignment. VANA (transposase) sequences used for calculating genetic distances were as described previously¹⁸. For VANC gene, exon–intron structure of *A. thaliana* copies was used for CDS structure in *A. lyrata* and used for between species comparisons only. Number of tandemly repeated regions was estimated by using Tandem repeat finder program⁵¹. Sequences used were retrieved from TAIR database, of which we used only copies with both VANA and VANC genes annotated in the TE and with VANC having complete structure of CDS. Full-length CDSs of VANC were then used for the analyses. When multiple patterns of repeat structure can be identified in the overlapping region, we only used that covering the longest region.

Data availability. The sequence data were deposited into DDBJ (WGBS, ChIP-seq, and RNA-seq data as DRA006000, DRA006001, and DRA006002, respectively). The authors declare that all other data supporting the findings of this study are available within the article and its Supplementary Information files, or from the corresponding authors on request.

Received: 15 April 2017 Accepted: 9 November 2017

Published online: 18 December 2017

References

- Molaro, A. & Malik, H. S. Hide and seek: how chromatin-based pathways silence retroelements in the mammalian germline. *Curr. Opin. Genet. Dev.* **37**, 51–58 (2016).
- Martienssen, R. & Moazed, D. RNAi and heterochromatin assembly. *Cold Spring Harb. Perspect. Biol.* **7**, a019323 (2015).
- Iwasaki, Y. W., Siomi, M. C. & Siomi, H. PIWI-interacting RNA: its biogenesis and functions. *Annu. Rev. Biochem.* **84**, 405–433 (2015).
- Weng, K. F., Hsieh, P. T., Huang, H. I. & Shih, S. R. Mammalian RNA virus-derived small RNA: biogenesis and functional activity. *Microbes Infect.* **17**, 557–563 (2015).
- Matzke, M. A. & Mosher, R. A. RNA-directed DNA methylation: an epigenetic pathway of increasing complexity. *Nat. Rev. Genet.* **15**, 394–408 (2014).
- Kim, M. Y. & Zilberman, D. DNA methylation as a system of plant genomic immunity. *Trends Plant. Sci.* **19**, 320–326 (2014).
- Wendte, J. M. & Pikaard, C. S. The RNAs of RNA-directed DNA methylation. *Biochim. Biophys. Acta* **1860**, 140–148 (2017).
- Ito, H. & Kakutani, T. Control of transposable elements in *Arabidopsis thaliana*. *Chromosome Res.* **22**, 217–223 (2014).
- Tsukahara, S. et al. Bursts of retrotransposition reproduced in *Arabidopsis*. *Nature* **461**, 423–426 (2009).
- Matzke, M. A. & Birchler, J. A. RNAi-mediated pathways in the nucleus. *Nat. Rev. Genet.* **6**, 24–35 (2005).
- Law, J. & Jacobsen, S. Establishing, maintaining and modifying DNA methylation patterns in plants and animals. *Nat. Rev. Genet.* **11**, 204–220 (2010).
- Zhao, J. H., Hua, C. L., Fang, Y. Y. & Guo, H. S. The dual edge of RNA silencing suppressors in the virus-host interactions. *Curr. Opin. Virol.* **17**, 39–44 (2016).
- Bivalkar-Mehla, S. et al. Viral RNA silencing suppressors (RSS): novel strategy of viruses to ablate the host RNA interference (RNAi) defense system. *Virus Res.* **155**, 1–9 (2011).
- Wang, M. B. & Metzloff, M. RNA silencing and antiviral defense in plants. *Curr. Opin. Plant Biol.* **8**, 216–222 (2005).
- Zamore, P. D. Plant RNAi: How a viral silencing suppressor inactivate siRNA. *Curr. Biol.* **14**, R198–R200 (2004).
- Peccoud, J., Loiseau, V., Cordaux, R. & Gilbert, C. Massive horizontal transfer of transposable elements in insects. *Proc. Natl Acad. Sci. USA* **114**, 4721–4726 (2017).
- El Baidouri, F. et al. Widespread and frequent horizontal transfers of transposable elements in plants. *Genome Res.* **24**, 831–838 (2014).
- Fu, Y. et al. Mobilization of a plant transposon by expression of the transposon-encoded anti-silencing factor. *EMBO J.* **32**, 2407–2417 (2013).
- Le, Q. H., Wright, S., Yu, Z. & Bureau, T. Transposon diversity in *Arabidopsis thaliana*. *Proc. Natl Acad. Sci. USA* **97**, 7376–7381 (2000).
- Yu, Z., Wright, S. I. & Bureau, T. Mutator-like elements in *Arabidopsis thaliana*. Structure, diversity and evolution. *Genetics* **156**, 2019–2031 (2000).
- Koch, M. A. & Matschinger, M. Evolution and genetic differentiation among relatives of *Arabidopsis thaliana*. *Proc. Natl Acad. Sci. USA* **104**, 6272–6277 (2007).
- Beilstein, M. A. et al. Dated molecular phylogenies indicate a Miocene origin for *Arabidopsis thaliana*. *Proc. Natl Acad. Sci. USA* **107**, 18724–18728 (2010).
- Wright, S. I., Lauga, D. & Charlesworth, D. Rates and pattern of molecular evolution in inbred and outbred *Arabidopsis*. *Mol. Biol. Evol.* **19**, 1407–1420 (2002).
- Charlesworth, B., Sniegowski, P. & Stephan, W. The evolutionary dynamics of repetitive DNA in eukaryotes. *Nature* **371**, 215–220 (1994).
- Drinnenberg, I. A., Henikoff, S. & Malik, H. S. Evolutionary turnover of kinetochore proteins: a ship of theseus? *Trends Cell Biol.* **26**, 498–510 (2015).
- Henikoff, S. & Malik, H. S. Centromeres: selfish drivers. *Nature* **417**, 227 (2002).
- Talbert, P. B., Masuelli, R., Tyagi, A. P., Comai, L. & Henikoff, S. Centromeric localization and adaptive evolution of an *Arabidopsis* histone H3 variant. *Plant Cell* **14**, 1053–1066 (2002).
- Malik, H. S., Vermaak, D. & Henikoff, S. Recurrent evolution of DNA-binding motifs in the *Drosophila* centromeric histone. *Proc. Natl Acad. Sci. USA* **99**, 1449–1454 (2002).
- Fujimoto, R. et al. Evolution and control of imprinted FWA genes in the genus *Arabidopsis*. *PLoS Genet.* **4**, e1000048 (2008).
- Gehring, M. et al. DEMETER DNA glycosylase establishes MEDEA polycomb gene self-imprinting by allele-specific demethylation. *Cell* **124**, 495–506 (2006).
- Kinoshita, T. et al. One-way control of FWA imprinting in *Arabidopsis* endosperm by DNA methylation. *Science* **303**, 521–523 (2004).
- Martienssen, R. Maintenance of heterochromatin by RNA interference of tandem repeats. *Nat. Genet.* **35**, 213–214 (2003).
- Alleman, M. et al. An RNA-dependent RNA polymerase is required for paramutation in maize. *Nature* **442**, 295–298 (2006).
- Rajeevkumar, S., Anunanthini, P. & Sathishkumar, R. Epigenetic silencing in transgenic plants. *Front. Plant Sci.* **6**, 693 (2015).

35. Kamthan, A., Chaudhuri, A., Kamthan, M. & Datta, A. Genetically modified (GM) crops: milestones and new advances in crop improvement. *Theor. Appl. Genet.* **129**, 1639–1655 (2016).
36. Bolger, A. M., Lohse, M. & Usadel, B. Trimmomatic: a flexible trimmer for Illumina sequence data. *Bioinformatics* **30**, 2114–2120 (2014).
37. Krueger, F. & Andrews, S. R. Bismark: a flexible aligner and methylation caller for bisulfite-Seq applications. *Bioinformatics* **27**, 1571–1572 (2011).
38. Ito, T. et al. Genome-wide negative feedback drives transgenerational DNA methylation dynamics in Arabidopsis. *PLoS Genet.* **11**, e1005154 (2015).
39. Gendrel, A.-V., Lippman, Z., Martienssen, R. & Colot, V. Profiling histone modification patterns in plants using genomic tiling microarrays. *Nat. Methods* **2**, 213–218 (2005).
40. Langmead, B., Trapnell, C., Pop, M. & Salzberg, S. Ultrafast and memory-efficient alignment of short DNA sequences to the human genome. *Genome Biol.* **10**, R25 (2009).
41. Li, H. et al. The sequence alignment/map format and SAMtools. *Bioinformatics* **25**, 2078–2079 (2009).
42. Zhang, Y. et al. Model-based analysis of ChIP-Seq (MACS). *Genome Biol.* **9**, R137 (2008).
43. Bailey, T. L. DREME: motif discovery in transcription factor ChIP-seq data. *Bioinformatics* **27**, 1653–1659 (2011).
44. Quinlan, A. R. & Hall, I. M. BEDTools: a flexible suite of utilities for comparing genomic features. *Bioinformatics* **26**, 841–842 (2010).
45. Robinson, J. T. et al. Integrative genomics viewer. *Nat. Biotechnol.* **29**, 24–26 (2011).
46. Kim, D. et al. TopHat2: accurate alignment of transcriptomes in the presence of insertions, deletions and gene fusions. *Genome Biol.* **14**, 1–13 (2013).
47. Edgar, R. C. MUSCLE: multiple sequence alignment with high accuracy and high throughput. *Nucleic Acids Res.* **32**, 1792–1797 (2004).
48. Thompson, J. D., Gibson, T. J. & Higgins, D. G. Multiple sequence alignment using ClustalW and ClustalX. *Curr. Protoc. Bioinformatics* **Chapter 2**, Unit2.3 (2002).
49. Larkin, M. A. et al. Clustal W and Clustal X version 2.0. *Bioinformatics* **23**, 2947–2948 (2007).
50. Saitou, N. & Nei, M. The neighbor-joining method: a new method for reconstructing phylogenetic trees. *Mol. Biol. Evol.* **4**, 406–425 (1987).
51. Benson, G. Tandem repeats finder: a program to analyze DNA sequences. *Nucleic Acids Res.* **27**, 573–580 (1999).
52. Noé, L. & Kucherov, G. YASS: enhancing the sensitivity of DNA similarity search. *Nucleic Acids Res.* **33**, W540–W543 (2005).

Acknowledgements

We thank Kae Kato and Akiko Terui for technical assistance, Hiroyuki Araki, Kenichi Nonomura, Naruya Saito, and Taiko To for technical advice, Yasushi Hiromi, Hideki

Innan, Damon Lisch, and Eric Richards for comments on the manuscript. This work used the Vincent J. Coates Genomics Sequencing Laboratory at UC Berkeley, supported by NIH S10 OD018174 Instrumentation Grant. Computations were partially performed on the NIG supercomputer at NIG, Japan. Supported by grants from Mitsubishi Foundation (to T.K.), Japanese Ministry of Education, Culture, Sports, Science and Technology (26221105 and 15H05963, to T.K.), JST CREST Grant, Japan (JPMJCR1501 to T.K.), and Systems Functional Genetics Project of the Transdisciplinary Research Integration Center, ROIS, Japan (to A.T., A.F., Y.T., and T.K.).

Author contributions

A.H., R.S., K.T., T.S., Y.F., A.T., A.F. and Y.T. contributed to the experiments. A.H., R.S., T.S., A.K. and T.I. contributed to data analyses. A.H. and T.K. contributed to writing the paper.

Additional information

Supplementary Information accompanies this paper at <https://doi.org/10.1038/s41467-017-02150-7>.

Competing interests: The authors declare no competing financial interests.

Reprints and permission information is available online at <http://npg.nature.com/reprintsandpermissions/>

Publisher's note: Springer Nature remains neutral with regard to jurisdictional claims in published maps and institutional affiliations.



Open Access This article is licensed under a Creative Commons Attribution 4.0 International License, which permits use, sharing, adaptation, distribution and reproduction in any medium or format, as long as you give appropriate credit to the original author(s) and the source, provide a link to the Creative Commons license, and indicate if changes were made. The images or other third party material in this article are included in the article's Creative Commons license, unless indicated otherwise in a credit line to the material. If material is not included in the article's Creative Commons license and your intended use is not permitted by statutory regulation or exceeds the permitted use, you will need to obtain permission directly from the copyright holder. To view a copy of this license, visit <http://creativecommons.org/licenses/by/4.0/>.

© The Author(s) 2017

RESEARCH ARTICLE

A Decrease in Ambient Temperature Induces Post-Mitotic Enlargement of Palisade Cells in North American Lake Cress

Rumi Amano¹, Hokuto Nakayama^{1,2}, Yurika Morohoshi³, Yaichi Kawakatsu¹, Ali Ferjani³, Seisuke Kimura^{1*}

1 Department of Bioresource and Environmental Sciences, Kyoto Sangyo University, Kyoto-City, Kyoto, Japan, **2** Department of Plant Biology, University of California Davis, Davis, California, United States of America, **3** Department of Biology, Tokyo Gakuji University, Koganei-City, Tokyo, Japan

☯ These authors contributed equally to this work.

* seisuke@cc.kyoto-su.ac.jp



CrossMark
click for updates

OPEN ACCESS

Citation: Amano R, Nakayama H, Morohoshi Y, Kawakatsu Y, Ferjani A, Kimura S (2015) A Decrease in Ambient Temperature Induces Post-Mitotic Enlargement of Palisade Cells in North American Lake Cress. PLoS ONE 10(11): e0141247. doi:10.1371/journal.pone.0141247

Editor: Gerrit T.S. Beemster, University of Antwerp, BELGIUM

Received: May 11, 2015

Accepted: October 5, 2015

Published: November 16, 2015

Copyright: © 2015 Amano et al. This is an open access article distributed under the terms of the [Creative Commons Attribution License](https://creativecommons.org/licenses/by/4.0/), which permits unrestricted use, distribution, and reproduction in any medium, provided the original author and source are credited.

Data Availability Statement: All relevant data are within the paper and its Supporting Information files. All sequence files are available from the DDBJ database (accession numbers: LC054303 and LC054304).

Funding: This work was partially supported by Grants-in-Aid from MEXT-Supported Program for the Strategic Research Foundation at Private Universities (2015–2019), the Japan Society for the Promotion of Science (JSPS; <http://www.jsps.go.jp/english/e-grants/index.html>) (KAKENHI Grant Numbers 22870031 and 24770047), The Science Research

Abstract

In order to maintain organs and structures at their appropriate sizes, multicellular organisms orchestrate cell proliferation and post-mitotic cell expansion during morphogenesis. Recent studies using *Arabidopsis* leaves have shown that compensation, which is defined as post-mitotic cell expansion induced by a decrease in the number of cells during lateral organ development, is one example of such orchestration. Some of the basic molecular mechanisms underlying compensation have been revealed by genetic and chimeric analyses. However, to date, compensation had been observed only in mutants, transgenics, and γ -ray-treated plants, and it was unclear whether it occurs in plants under natural conditions. Here, we illustrate that a shift in ambient temperature could induce compensation in *Rorippa aquatica* (Brassicaceae), a semi-aquatic plant found in North America. The results suggest that compensation is a universal phenomenon among angiosperms and that the mechanism underlying compensation is shared, in part, between *Arabidopsis* and *R. aquatica*.

Introduction

Multicellular organisms have a wide variety of forms. In particular, plant species display an intriguing variety of leaf shapes and sizes [1,2]. Recently, the molecular mechanisms underlying the diversification of leaf shape have been revealed in various model species [3–5]. The molecular mechanisms underlying the regulation of leaf size, which is one component of final leaf form, have mainly been studied in the model plant *Arabidopsis thaliana* (L.) Heynh. (*Arabidopsis* hereafter). These studies demonstrated that cell proliferation occurs throughout the developing leaf primordia during very early stages and that cell expansion begins after cessation of proliferation. Finally, the cell proliferation zone is restricted at the basal part of the leaf blade to a constant size [6–9]. Together, these studies suggest that the spatiotemporal coordination of cell proliferation and expansion allows leaves to attain an appropriate final size that is characteristic of each species [10]. To date, a number of genes, whose loss or gain of function is

Promotion Fund from the Promotion and Mutual Aid Corporation for Private Schools of Japan (http://www.shigaku.go.jp/g_about_pmac.htm) to S.K., by a Research Fellowship from JSPS to H.N., MEXT Grant-in-Aid for Young Scientists (B) and Grant-in-Aid for Scientific Research on Innovative Areas to A.F.

Competing Interests: The authors have declared that no competing interests exist.

associated with changes in cell number, cell size, or both, have been isolated [7,11–14]. Of note, these studies have proposed that leaf size is not simply a function of cell number and size. Interestingly, in several mutants, defects in cell proliferation are known to induce increased post-mitotic cell enlargement. This phenomenon is called compensation [15,16].

Compensation requires regulatory mechanisms that operate post-mitotically to coordinate cell proliferation and expansion. Post-mitotic compensatory cell expansion (CCE) is thought to be unique to plants [17]. To date, this phenomenon had been observed only in plants in which the genes associated with cell proliferation were mutated or in plants that had been subjected to unusual conditions, such as high γ -ray irradiation [11,18]. Transgenic rice (*Oryza sativa*) plants that overexpress genes encoding Kip-related proteins and the petals of *Antirrhinum majus* mutants also showed compensation-like cell enlargement [19–21]. Although these studies suggest that compensation is widespread in angiosperms, it has been unclear whether compensation occurs in plants in their natural environments.

Rorippa aquatica (Eaton) EJ Palmer & Steyermark (Brassicaceae), also known as lake cress, is a semi-aquatic plant found in bays, lakes, ponds, and streams in North America [22]. *R. aquatica* shows heterophylly, defined as variable leaf form on the same or different shoots of a plant in response to environmental cues. Deeply dissected leaves develop when grown in submerged conditions, whereas simple leaves with smooth margins develop when grown in terrestrial conditions [23,24]. Previously, we showed that the leaf shape of *R. aquatica* changes dramatically in response to varying temperatures, as well as to underwater submergence [24]. High ambient temperatures induced formation of leaves with simpler forms compared to those of plants grown at lower temperatures (Fig 1). Previous studies have examined the molecular mechanism underlying heterophylly and have revealed that the regulation of gibberellin (GA) levels via *KNOTTED1-LIKE HOMEBOX (KNOX1)* genes is involved in this phenomenon [25]. In addition, studies using *Arabidopsis* and *A. majus* indicated that compensation may play a role in environmental responses and that it may be induced by changing growth conditions [20,26]. Thus, *R. aquatica* showing heterophylly is a useful model to investigate whether compensation occurs in response to environmental cues.

To examine cellular features of *R. aquatica* leaves exhibiting heterophylly, we first measured the number and size of palisade cells in the sub-epidermal layer in mature leaves of plants reared at 20°C and 30°C. We then measured the size and complexity of adaxial epidermal cells and investigated in parallel the features of inner tissue cells in mature leaves. Finally, we analyzed expression of *R. aquatica* genes whose orthologs in *Arabidopsis* have been implicated by loss- or gain-of-function mutation analysis in triggering CCE. Together, these results showed that lower temperature (20°C) induces compensation in *R. aquatica*. To our knowledge, this is the first report that confirms the occurrence of compensation in response to environmental changes under natural conditions.

Material and Methods

Plant materials and growth conditions

R. aquatica plants were grown in a growth chamber under continuous illumination with light intensity of $\sim 50 \mu\text{mol photons m}^{-2} \text{s}^{-1}$. Seedlings were planted in pots containing soil and watered every 2 days with 1/2 HYPONeX solution (HYPONeX, Japan). For histological observation, plants were cultivated at 20°C or 30°C for 50 days. For RNA extraction, plants were cultivated at 20°C or 30°C for 1 month. Leaf primordia were then frozen in liquid nitrogen immediately after sampling and stored at -80°C until RNA extraction.

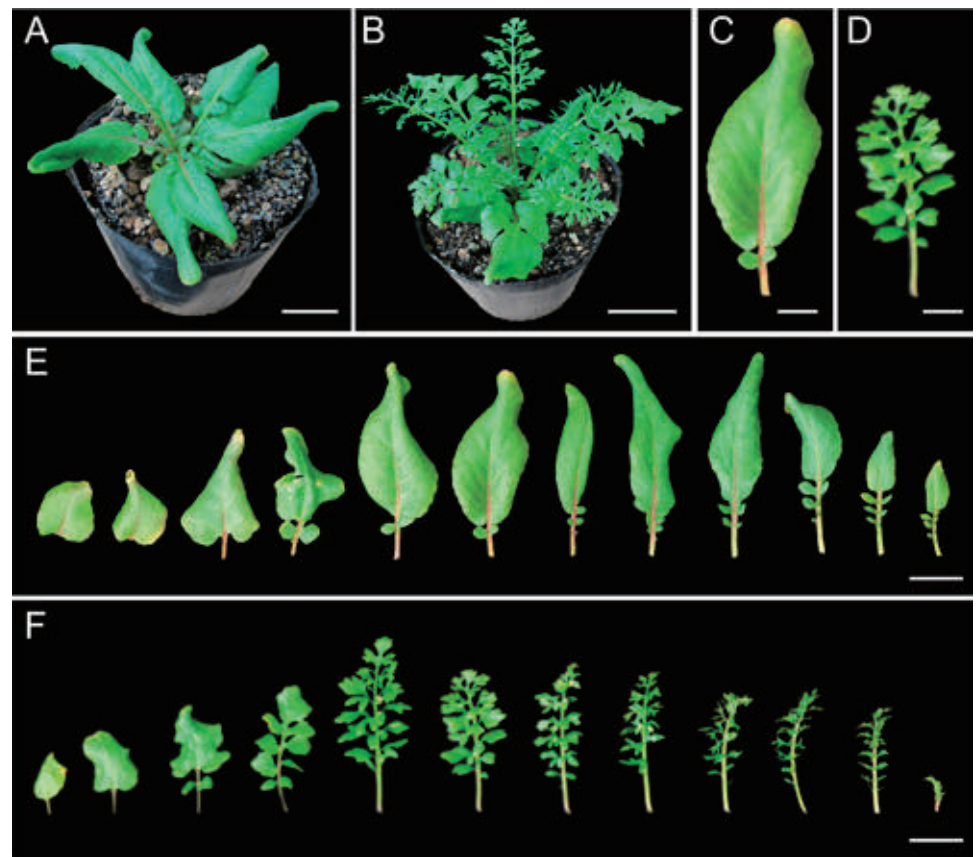


Fig 1. Gross morphology of *Rorippa aquatica* grown at different ambient temperatures. Top views of *R. aquatica* plants grown at 30°C (A) and 20°C (B) for 50 days. Leaves (LN6) of *R. aquatica* grown at 30°C (C) and 20°C (D). Comparison of leaf forms of *R. aquatica* grown at 30°C (E) and 20°C (F). The oldest leaf is depicted at the left and the youngest at the right. Scale bars = 3 cm (A) and (B); 1 cm (C) and (D); 2 cm (E) and (F).

doi:10.1371/journal.pone.0141247.g001

Histological observations

The distal portions of mature leaves (leaf number 6; hereafter LN6) were used for histological observation ($n = 6$ biological replicates) to measure leaf area, cell area, and cell number. In the case of dissected leaves, apical leaflets were used for observations (Fig 1). To measure leaf area, leaves were photographed using a digital camera (PowerShot G11; Canon, Japan). Leaves were fixed in a formalin–acetic acid–alcohol (FAA) solution and cleared using a chloral hydrate solution as described previously [27]. Palisade cells in the sub-epidermal layer were observed using a differential interference microscope (DMI6000; Leica, Germany) and were photographed using a CCD camera (DFC3600 FX; Leica, Germany). Leaf and cell areas were calculated using ImageJ release 1.47v (<http://rsb.info.nih.gov/ij/>). To calculate cell area, a total of 20 cells in each sample were analyzed (Fig 2A).

Calculation of complexity in epidermal cells

To calculate the complexity of epidermal cell forms, we used a dental paste to create a mold of the cells (Take 1 Advanced; Kerr, USA). The distal parts of mature leaves (LN6) were used to calculate complexity ($n = 6$ biological replicates). In the case of dissected leaves, apical leaflets were used. Pictures of epidermal cells were traced with Adobe Photoshop CS4 (Adobe, USA),

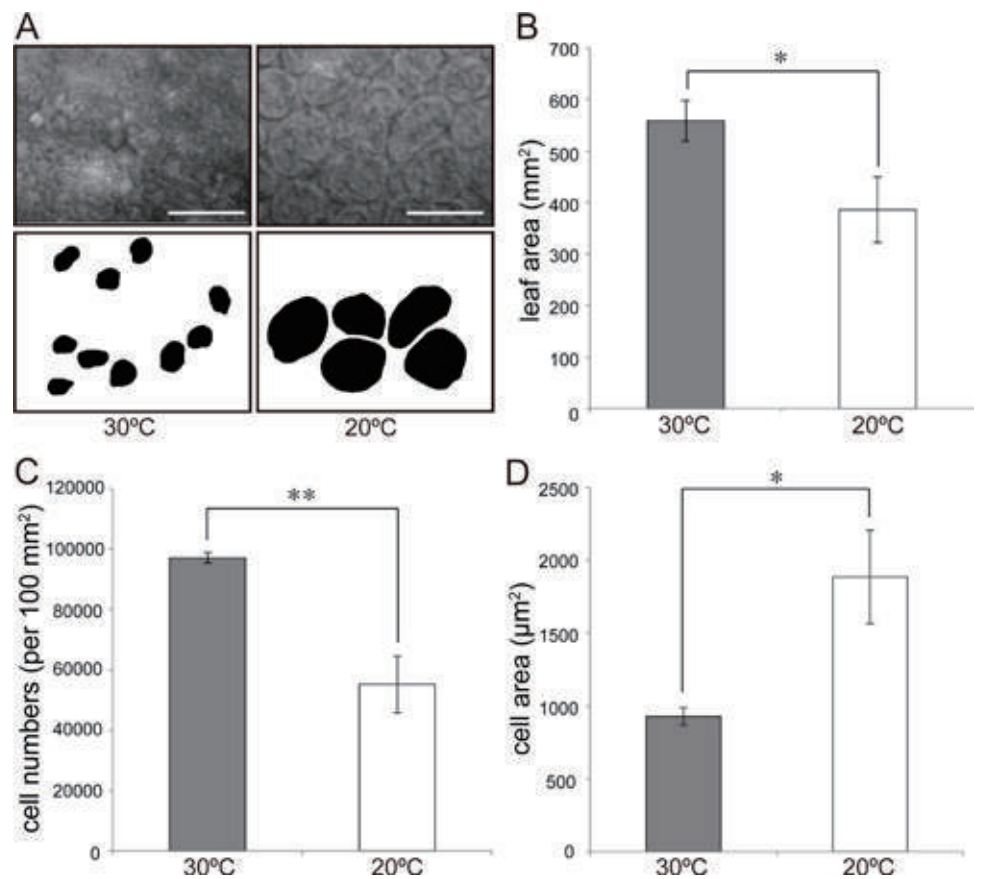


Fig 2. Cellular phenotypes of leaves from plants grown at 30°C and 20°C. (A) Palisade cells in LN6 of *Rorippa aquatica* grown at 30°C (left) and 20°C (right). The upper panels show differential interference microscopy images, and the lower panels show the silhouettes of randomly selected cells. Scale bars = 100 μm. (B–D) Leaf area, number of cells per 100 mm², and palisade cell area, respectively. Error bars represent the standard error (SE); * = $p < 0.05$; ** = $p < 0.01$ by Student's t -test ($n = 6$).

doi:10.1371/journal.pone.0141247.g002

and epidermal cell areas were subsequently calculated. Epidermal cell form complexity was estimated by the dissection index (DI), calculated as $(cell\ periphery) / \sqrt{cell\ area}$. All calculations were performed using ImageJ 1.47v (<http://rsb.info.nih.gov/ij/>). A total of 20 cells in each sample were analyzed to calculate epidermal cell DI.

Morphological observations

The central part of the LN6 leaf blade was fixed as previously described. The fixed samples were dehydrated in an ethanol series (50, 60, 70, 80, 90, 95, 99.5, and 100% v/v; 30 min per grade of alcohol) and stored overnight in 100% (v/v) ethanol at room temperature. The samples were embedded in Technovit resin (Technovit 7100; Heraeus Kulzer GmbH, Germany). Embedded samples were sectioned using a microtome (HM325; Thermo Scientific, Japan) and were subsequently stained with 0.1% toluidine blue. The stained sections were observed using an optical microscope (Wraycam G500; Nikon, Japan) and photographed with a CCD camera (Eclipse E200; Nikon, Japan; $n = 6$ biological replicates). Cell area (excluding palisade cells) and leaf thickness were measured using ImageJ 1.47v (<http://rsb.info.nih.gov/ij/>). A total of 20 cells from three independent locations in the central portion of the leaf blade were analyzed in order to calculate cell area and leaf thickness.

RNA extraction, cDNA synthesis, and molecular cloning

Total RNA from leaf primordia of plants grown for 1 month was extracted using an RNeasy Plant Mini Kit (Qiagen, USA) including DNase I treatment. cDNA was synthesized from 1 μ g of the total RNA using Transcriptor Universal cDNA Master (Roche, USA). Diluted cDNA was used for Real-time PCR. We used de novo assembly data from a previously performed mRNA-seq [25] to design primers for PCR amplification specific to the genes of interest. Accession numbers are LC054303 (Ra *AN3*), LC054304 (Ra *KRP2*), LC068567 (Ra *ERECTA*), LC068568 (Ra *FUGU2*), and LC068569 (Ra *FUGU5*).

Phylogenetic analyses

Predicted amino acid sequences of cloned genes were aligned using ClustalW and readjusted manually when necessary. Phylogenetic trees were reconstructed with MEGA5 [28] using the neighbor-joining method [29]. Bootstrap values were derived from 1000 replicate runs.

Real-time PCR analyses

Total RNA was extracted from leaf primordia of plants grown for 1 month and used to synthesize cDNA, as described above. To investigate the expression levels of *ANGUSTIFOLIA3* (*AN3*), *ERECTA*, *FASCIATA1/FUGU2* (*FUGU2*), *AVP1/FUGU5* (*FUGU5*), and *KIP-RELATED PROTEIN2* (*KRP2*) orthologs, expression analysis was conducted using the following gene-specific primer pairs: RaAN3_RT_F and RaAN3_RT_R; RaERECTA_RT_F and RaERECTA_RT_R; RaFUGU2_RT_F and RaFUGU2_RT_R; RaFUGU5_RT_F and RaFUGU5_RT_R; and RaKRP2_RT_F and RaKRP2_RT_R (S1 Table). Real-time PCR amplification was performed using the KAPA SYBR Fast qPCR kit (Kapa Biosystems, USA) in a 7500 Real-Time PCR System (Applied Biosystems, Japan). Experiments were performed in quadruplicate from independent tissue RNA extractions ($n = 4$ biological replicates) with three technical replicates. Expression was normalized to an *Ra TUB4* β control (RaTUB4_RT_F and RaAN3_RT_R; S1 Table).

Results

Microscopic observation of leaf palisade cells

To investigate whether cellular changes are induced by different temperatures, cell count and cell area of sub-epidermal palisade tissue in LN6 leaves were compared in plants grown at 30°C and 20°C (Figs 1 and 2). We found that leaf area of plants grown at 30°C was larger than that of plants grown at 20°C (Fig 2B). The number of sub-epidermal palisade cells per 100 mm² at 30°C and 20°C was approximately 97,090 and 55,180, respectively (Fig 2C), and the average cell area was approximately 930 and 1880 μ m² at 30°C and 20°C, respectively (Fig 2D). In other words, number and area of sub-epidermal palisade tissue cells in plants grown at 20°C were 49% lower and 57% higher, respectively, than those in plants grown at 30°C. Altogether, our results suggest that CCE is induced in the leaves of *R. aquatica* plants grown at 20°C. Incidentally, microscopic observation in a previous study found that palisade cell area of plants reared at 20°C and 25°C was similar [25]; however, the growing conditions differed between that study and the present study. In the previous study, LN7 leaves from plants that had been cultivated for only 30 days were used [25] and were as such younger and less expanded than those used in the present study. We believe that differences in sampling stage and in leaf position used influenced the results of sub-epidermal cell size.

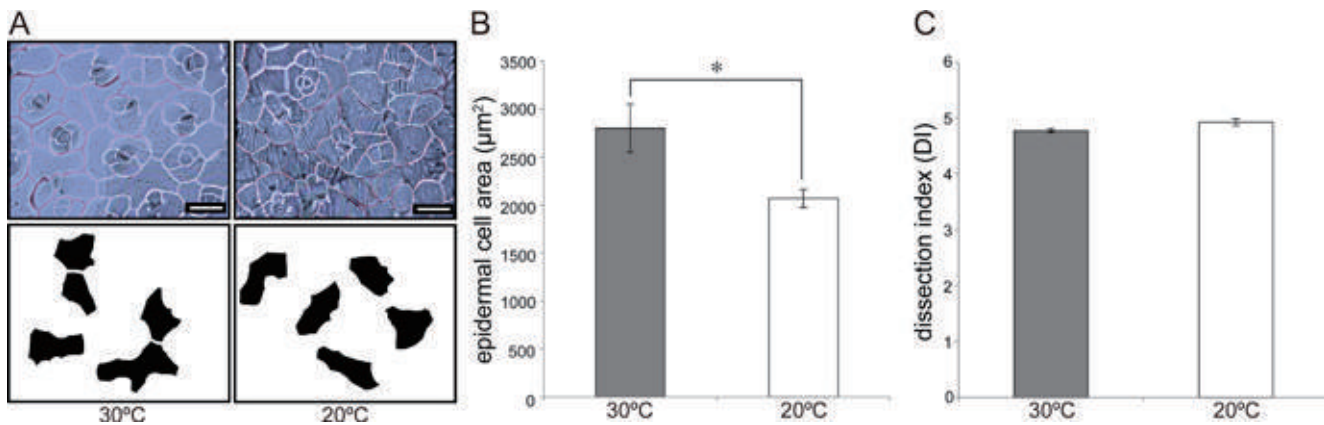


Fig 3. Observation of epidermal cells from plants grown at 30°C and 20°C. (A) Epidermal cells in LN6 of *Rorippa aquatica* grown at 30°C (left) and 20°C (right). The upper panels show images of epidermal cells, and the lower panels show the silhouettes of randomly selected cells. Scale bars = 50 µm. (B) Epidermal cell area. (C) Dissection index (DI) of epidermal cells. Error bars represent the standard error (SE); * = $p < 0.05$ by Student's *t*-test ($n = 6$).

doi:10.1371/journal.pone.0141247.g003

Observation of epidermal cells and leaf cross-sections

In addition to the cells in the sub-epidermal layer (palisade tissue), cell area and dissection index (DI) of LN6 adaxial epidermal cells of plants reared at 30°C and 20°C were also analyzed (Fig 3A). Interestingly, whereas epidermal cell area was larger after growth at 30°C than at 20°C (Fig 3B), DI did not significantly differ between plants grown at the two temperatures (Fig 3C).

We also examined cells in inner leaf tissues, excluding palisade and epidermal cells, to determine whether their form and/or size were affected by different ambient temperatures. As shown in leaf cross-sections, cell area of inner tissue was similar between leaves grown at different temperatures (Fig 4A and 4B). Leaf thicknesses between adaxial and abaxial epidermal cells were approximately 215 and 250 µm, respectively, for plants reared at both 30°C and 20°C (Fig 4C).

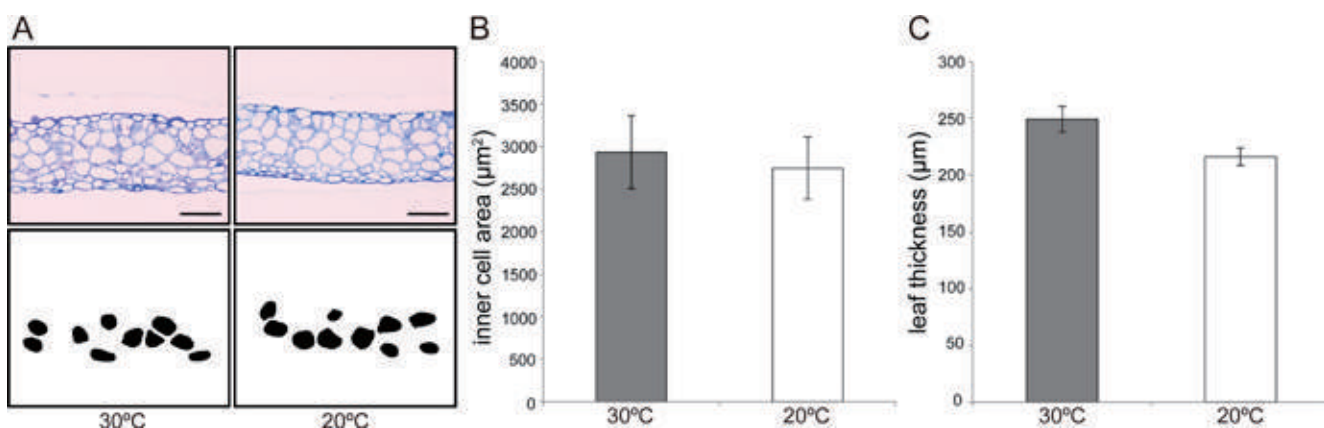


Fig 4. Observation of inner structure of leaves of *Rorippa aquatica* grown at 30°C and 20°C. (A) Inner cells in LN6 leaf blade of *R. aquatica* grown at 30°C (left) and 20°C (right). Cross-sections in the upper panels show images of inner leaf tissue cells, and the lower panels show the silhouettes of randomly selected cells. Scale bars = 100 µm. (B) Area of inner cells. (C) Thickness of leaves. Error bars represent the standard error (SE) ($n = 6$).

doi:10.1371/journal.pone.0141247.g004

Expression analysis of orthologous genes involved in compensation

To examine the molecular mechanism behind the drastic size increase of *R. aquatica* leaf palisade cells, we analyzed expression levels of orthologs of *AN3*, *ERECTA*, *FUGU2*, *FUGU5*, and *KRP2*. The misexpression of each gene is known to trigger different modes of CCE that are sub-classified into three different classes in Arabidopsis (class I: *an3*, *erecta*, and *fugu2*; class II: *fugu5*; class III: *KRP2o/x*) [7,11,19]. These orthologs in *R. aquatica* were identified by BLAST searches, which revealed that putative amino acid sequences encoded by the isolated fragments were similar to those of each target gene in Arabidopsis. In addition, multiple sequence alignments showed that each putative protein had a characteristic functional domain or domains conserved among the homologs in a diverse array of species (S1–S5 Figs). Our phylogenetic analyses consistently supported the identity of the orthologs of the targeted genes. Importantly, quantitative RT-PCR showed that although the expression levels of Ra *AN3*, Ra *ERECTA*, and Ra *FUGU5* were unaffected, that of Ra *FUGU2* was significantly reduced in leaf primordia of *R. aquatica* grown at 20°C as compared to those of plants grown at 30°C (Fig 5). Thus, the reduction in Ra *FUGU2* expression levels might be associated with the induction of CCE in *R. aquatica*. The expression level of Ra *KRP2* was also reduced in the leaf primordia of plants grown at 20°C (Fig 5). However, previous studies using a *KRP2* over-expressor showed that it is the higher expression of *KRP2* that induces CCE [7]. Therefore, the reduced expression of Ra *KRP2* observed in this study might not be related to CCE in *R. aquatica*.

Discussion

Compensation as a response to change in ambient temperature

In the present study, we demonstrated that CCE is induced in response to environmental factors such as altered ambient temperature. This is the first report that confirms the occurrence of CCE without genetic manipulation and under natural conditions. For example, in plants grown at 20°C, the number of sub-epidermal palisade cells per unit area was significantly lower than that in plants grown at 30°C, whereas sub-epidermal cell size was significantly larger than that in plants grown at 30°C. This cellular behavior seems to be similar to that observed in Arabidopsis mutants exhibiting CCE [7,11–14]. Genetic studies using the *oligocellula* (*oli*) mutant series demonstrated that there is a threshold for triggering compensation [12]. Double mutants such as *oli2-1 oli5-1* and *oli2-1 oli7-1* showed that a large decrease in cell number (e.g., 40–60%) effectively triggers CCE [12]. In *R. aquatica*, the sub-epidermal palisade cell density in plants grown at 20°C was approximately 50% lower than in plants grown at 30°C; therefore, a reduction in cell number may suffice to induce compensation. On the other hand, a previous study suggested that it is not the total number of cells in the leaf primordia, but rather the cell proliferation pattern and/or activity that is important for triggering compensation [17]. Indeed, cell proliferation pattern and activity in leaf primordia are altered by changes in ambient temperature in *R. aquatica* [25]. Therefore, compensation in *R. aquatica* may be induced by such stimuli as were indicated before. Additionally, to reveal whether epidermal and inner cells also exhibit CCE, we examined the features of leaf inner tissue cells using histological cross-sectioning in *R. aquatica*. The analysis showed that cell enlargement does not occur in leaf inner cells. Together, our findings indicate the possibility that CCE could preferentially occur in the palisade cells of the sub-epidermal layer in *R. aquatica*.

Previous studies revealed that there are three classes of CCE (class I–III) [7,17]. Studies using a *fugu2* mutant showed that the *FUGU2* gene encodes the p150 subunit of Chromatin Assembly Factor 1, and the *fugu2* mutation triggers class I CCE via cell-cycle arrest [14]. Importantly, the results of our quantitative RT-PCR analyses revealed that the expression level

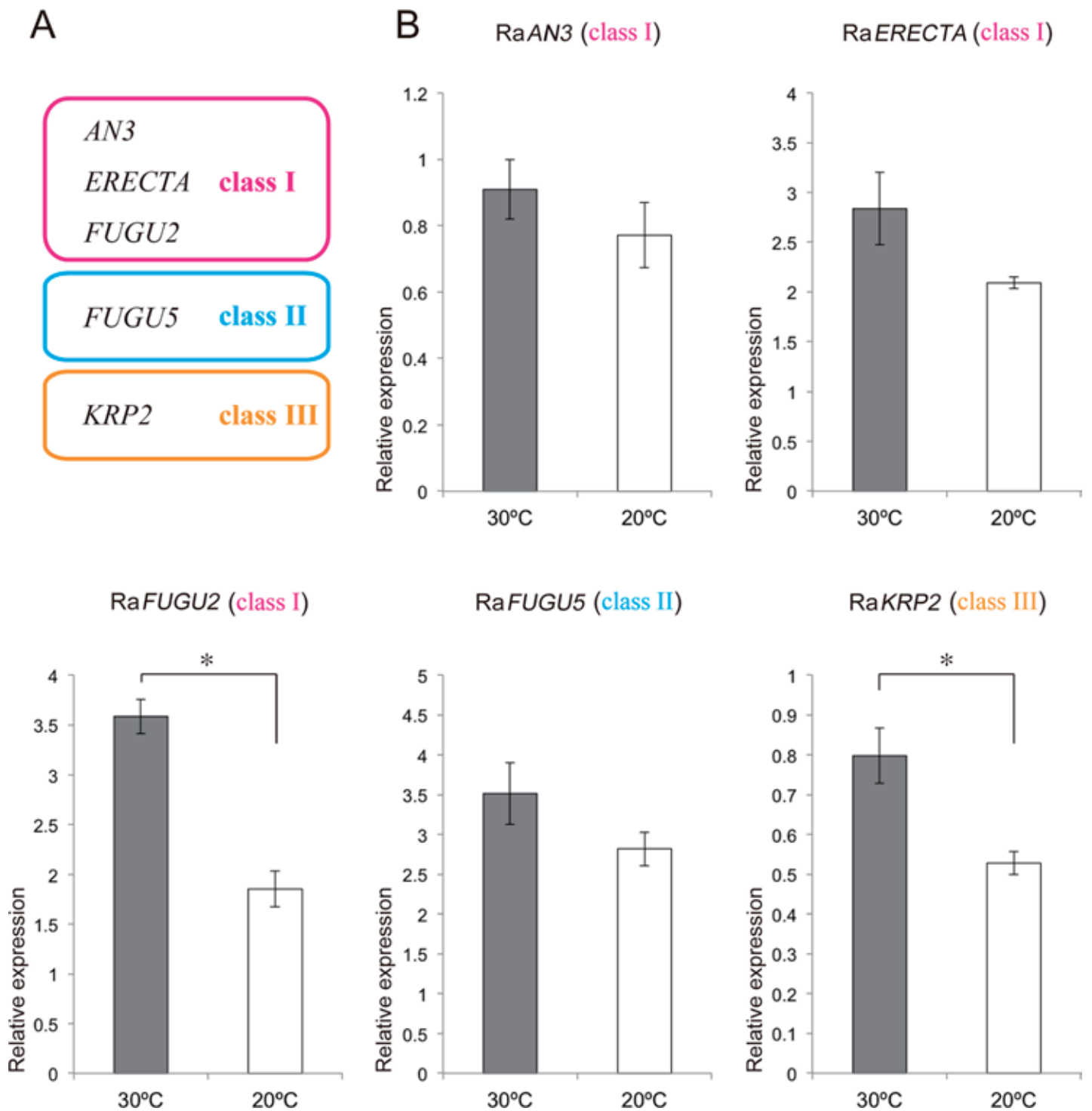


Fig 5. Expression analyses of orthologous genes related to compensation. (A) Schematic presentation of three classes of compensation. (B) Expression levels of Ra *AN3*, Ra *ERECTA*, Ra *FUGU2*, Ra *FUGU5*, and Ra *KRP2* in leaf primordia of *Rorippa aquatica* grown at 30°C and 20°C. Error bars represent the standard error (SE). * = $p < 0.05$ by Welch's *t*-test ($n = 4$).

doi:10.1371/journal.pone.0141247.g005

of a *FUGU2* ortholog (Ra *FUGU2*) significantly decreased in the leaf primordia of plants grown at 20°C, whereas the expression levels of the *AN3*, *ERECTA*, and *FUGU5* orthologs remained

unaffected. This suggests that chromatin structure differs between plants grown at 20°C and 30°C, inducing class I compensation. Moreover, the *fugu2* Arabidopsis mutant develops leaves that are more narrow and serrated than the wild type [7]. Therefore, in addition to the cellular behavior (i.e., occurrence of CCE), the deeply dissected leaves of *R. aquatica* grown at 20°C appear somewhat similar to those of *fugu2* mutants. However, further detailed analyses are required to determine whether a shared mechanism exists between morphologically close leaf forms in *R. aquatica* and Arabidopsis.

A previous study revealed that chloroplast proliferation is promoted in the enlarged cells that exhibit compensation [30]. Thus, compensation may be a mechanism to secure photosynthetic activity by increasing leaf area and/or thickness and promoting chloroplast proliferation in response to a defect in cell proliferation. If so, aspects of photosynthetic activity, such as the efficiency of CO₂ fixation per unit of leaf-area, should be investigated in plants exhibiting CCE. However, it is important to note that not only the total number of sub-epidermal cells in leaves, but also leaf morphology differed between *R. aquatica* plants grown at 20°C and 30°C. Hence, further analyses are necessary to determine the adaptive significance of compensation, as is the case with its molecular mechanisms.

Finally, our findings provide evidence that compensation is a universal phenomenon seen in nature. Moreover, in *R. aquatica* plants grown at a lower temperature, a failure to stably maintain a silent chromatin state via the reduction of *Ra FUGU2* expression (the Arabidopsis counterpart of chromatin assembly factor-1: CAF-1) might trigger a decrease in the number of palisade cells and induce CCE. Further analyses using plants other than Arabidopsis will provide insight into the mechanisms underlying the establishment of appropriate organ size in response to environmental cues.

Supporting Information

S1 Fig. A phylogenetic tree and alignments of AN3 orthologs.
(TIF)

S2 Fig. A phylogenetic tree and alignments of ERECTA orthologs.
(TIF)

S3 Fig. A phylogenetic tree and alignments of FUGU2 orthologs.
(TIF)

S4 Fig. A phylogenetic tree and alignments of FUGU5 orthologs.
(TIF)

S5 Fig. A phylogenetic tree and alignments of KRP2 orthologs.
(TIF)

S1 Table. List of oligonucleotide PCR primers used in this study.
(XLS)

Acknowledgments

We thank Drs. Naomi Nakayama, Kaoru O. Yoshiyama, and Akiko Nakamasu for helpful discussion throughout our study.

Author Contributions

Conceived and designed the experiments: RA HN AF SK. Performed the experiments: RA HN YM YK. Analyzed the data: RA HN YM YK. Wrote the paper: RA HN AF SK.

References

1. Bell AD. Plant Form: An Illustrated Guide to Flowering Plant Morphology. Portland: Timber Press; 2008.
2. Tsukaya H. Comparative leaf development in angiosperms. *Curr Opin Plant Biol.* 2014; 17: 103–109. doi: [10.1016/j.pbi.2013.11.012](https://doi.org/10.1016/j.pbi.2013.11.012) PMID: [24507501](https://pubmed.ncbi.nlm.nih.gov/24507501/)
3. Kimura S, Koenig D, Kang J, Yoong FY, Sinha N. Natural variation in leaf morphology results from mutation of novel *KNOX* gene. *Curr Biol.* 2008; 18: 672–677. doi: [10.1016/j.cub.2008.04.008](https://doi.org/10.1016/j.cub.2008.04.008) PMID: [18424140](https://pubmed.ncbi.nlm.nih.gov/18424140/)
4. Piazza P, Bailey CD, Cartolano M, Krieger J, Cao J, Ossowski S, et al. *Arabidopsis thaliana* leaf form evolved via loss of *KNOX* expression in leaves in association with a selective sweep. *Curr Biol.* 2010; 20: 2223–2228. doi: [10.1016/j.cub.2010.11.037](https://doi.org/10.1016/j.cub.2010.11.037) PMID: [21129970](https://pubmed.ncbi.nlm.nih.gov/21129970/)
5. Vlad D, Kierzkowski D, Rast MI, Vuolo F, Dello Iorio R, Galinha C, et al. Leaf shape evolution through duplication, regulatory diversification, and loss of a homeobox gene. *Science.* 2014; 343: 780–783. doi: [10.1126/science.1248384](https://doi.org/10.1126/science.1248384) PMID: [24531971](https://pubmed.ncbi.nlm.nih.gov/24531971/)
6. Donnelly PM, Bonetta D, Tsukaya H, Dengler RE, Dengler NG. Cell cycling and cell enlargement in developing leaves of *Arabidopsis*. *Dev Biol.* 1999; 215: 407–419. PMID: [10545247](https://pubmed.ncbi.nlm.nih.gov/10545247/)
7. Ferjani A, Horiguchi G, and Tsukaya H. Analysis of leaf development in *fugu* mutants of *Arabidopsis* reveals three compensation modes that modulate cell expansion in determinate organs. *Plant physiol.* 2007; 144: 988–99. PMID: [17468216](https://pubmed.ncbi.nlm.nih.gov/17468216/)
8. Kazama T, Ichihashi Y, Murata S, Tsukaya H. The mechanism of cell cycle arrest front progression explained by a *KLUH/CYP78A5*-dependent mobile growth factor in developing leaves of *Arabidopsis thaliana*. *Plant Cell Physiol.* 2010; 51: 1046–54. doi: [10.1093/pcp/pcq051](https://doi.org/10.1093/pcp/pcq051) PMID: [20395288](https://pubmed.ncbi.nlm.nih.gov/20395288/)
9. Ichihashi Y, Kawade K, Usami T, Horiguchi G, Takahashi T, Tsukaya H. Key proliferative activity in the junction between the leaf blade and leaf petiole of *Arabidopsis*. *Plant Physiol.* 2011; 157: 1151–1162. doi: [10.1104/pp.111.185066](https://doi.org/10.1104/pp.111.185066) PMID: [21880932](https://pubmed.ncbi.nlm.nih.gov/21880932/)
10. Breuninger H, Lenhard M. Control of tissue and organ growth in plants. *Curr Top Dev Biol.* 2010; 91: 185–220. doi: [10.1016/S0070-2153\(10\)91007-7](https://doi.org/10.1016/S0070-2153(10)91007-7) PMID: [20705183](https://pubmed.ncbi.nlm.nih.gov/20705183/)
11. Horiguchi G, Kim GT, Tsukaya H. The transcription factor *AtGRF5* and the transcription coactivator *AN3* regulate cell proliferation in leaf primordia of *Arabidopsis thaliana*. *Plant J.* 2005 43: 68–78. PMID: [15960617](https://pubmed.ncbi.nlm.nih.gov/15960617/)
12. Fujikura U, Horiguchi G, Ponce MR, Micol JL, Tsukaya H. Coordination of cell proliferation and cell expansion mediated by ribosome-related processes in the leaves of *Arabidopsis thaliana*. *Plant J.* 2009; 59: 499–508. doi: [10.1111/j.1365-313X.2009.03886.x](https://doi.org/10.1111/j.1365-313X.2009.03886.x) PMID: [19392710](https://pubmed.ncbi.nlm.nih.gov/19392710/)
13. Ferjani A, Segami S, Horiguchi G, Muto Y, Maeshima M, Tsukaya H. Keep an Eye on PPI: The Vacuolar-Type H⁺-Pyrophosphatase Regulates Postgerminative Development in *Arabidopsis*. *The Plant Cell* 2011; 23: 2895–2908 doi: [10.1105/tpc.111.085415](https://doi.org/10.1105/tpc.111.085415) PMID: [21862707](https://pubmed.ncbi.nlm.nih.gov/21862707/)
14. Hisanaga T, Ferjani A, Horiguchi G, Ishikawa N, Fujikura U, Kubo M, et al. The ATM-dependent DNA damage response acts as an upstream trigger for compensation in the *fas1* mutation during *Arabidopsis* leaf development. *Plant physiol.* 2013; 162: 831–841. doi: [10.1104/pp.113.216796](https://doi.org/10.1104/pp.113.216796) PMID: [23616603](https://pubmed.ncbi.nlm.nih.gov/23616603/)
15. Tsukaya H. Interpretation of mutants in leaf morphology: Genetic evidence for a compensatory system in leaf morphogenesis that provides a new link between cell and organismal theory. *Int Rev Cytol.* 2002; 217: 1–39. PMID: [12019561](https://pubmed.ncbi.nlm.nih.gov/12019561/)
16. Beemster GT, Fiorani F, Inzé D. Cell cycle: The key to plant growth control? *Trends Plant Sci.* 2003; 8: 154–158. PMID: [12711226](https://pubmed.ncbi.nlm.nih.gov/12711226/)
17. Hisanaga T, Kawade K, Tsukaya T. Compensation: a key to clarifying the organ-level regulation of lateral organ size in plants. *J Exp Bot.* 2015; 66: 1055–1063. doi: [10.1093/jxb/erv028](https://doi.org/10.1093/jxb/erv028) PMID: [25635111](https://pubmed.ncbi.nlm.nih.gov/25635111/)
18. Haber A. Nonessentiality of concurrent cell divisions for degree of polarization of leaf growth. 1. Studies with radiation-induced mitotic inhibition. *Am J Bot.* 1962; 49: 583–589
19. Barrôco RM, Peres A, Droual AM, De Veylder L, Nguyen LSL, De Wolf J, et al. The cyclin-dependent kinase inhibitor *orysa*; *KRP1* plays an important role in seed development of rice. *Plant Physiol.* 2006; 142: 1053–1064. PMID: [17012406](https://pubmed.ncbi.nlm.nih.gov/17012406/)
20. Delgado-Benarroch L, Weiss J, Egea-Cortines M. The mutants *compacta ähnlich*, *Nitida* and *grandiflora* define developmental compartments and a compensation mechanism in floral development in *Antirrhinum majus*. *J Plant Res.* 2009; 122: 559–569. doi: [10.1007/s10265-009-0236-6](https://doi.org/10.1007/s10265-009-0236-6) PMID: [19412653](https://pubmed.ncbi.nlm.nih.gov/19412653/)

21. Delgado-Benarroch L, Weiss J, Egea-Cortines M. *FORMOSA* controls cell division and expansion during floral development in *Antirrhinum majus*. *Planta* 2009; 229: 1219–1229. doi: [10.1007/s00425-009-0910-x](https://doi.org/10.1007/s00425-009-0910-x) PMID: [19271234](https://pubmed.ncbi.nlm.nih.gov/19271234/)
22. La Rue CD. Regeneration in *Radicula aquatica*. *Michigan Academician* 1943; 28: 51–61.
23. Fassett NC. *A manual of Aquatic Plants*. 1930; (Madison, Wisconsin: The University of Wisconsin Press).
24. Nakayama H, Nakayama N, Nakamasu A, Sinha N, Kimura S. Toward elucidating the mechanisms that regulate heterophylly. *Plant Morph.* 2012; 24: 57–63.
25. Nakayama H, Nakayama N, Seiki S, Kojima M, Sakakibara H, Sinha N, et al. Regulation of the KNOX-GA gene module induces heterophyllic alteration in North American lake cress. *The Plant Cell* 2014; 12: 4733–4748.
26. Horiguchi G, Tsukaya H. Organ size regulation in plants: insights from compensation. *Front Plant Sci.* 2011; doi: [10.3389/fpls.2011.00024](https://doi.org/10.3389/fpls.2011.00024) PMID: [22639585](https://pubmed.ncbi.nlm.nih.gov/22639585/)
27. Tsuge T, Tsukaya H, and Uchimiya H. Two independent and polarized processes of cell elongation regulate leaf blade expansion in *Arabidopsis thaliana* (L.) Heynh. *Development.* 1996; 122: 1589–600. PMID: [8625845](https://pubmed.ncbi.nlm.nih.gov/8625845/)
28. Tamura K, Peterson D, Peterson N, Stecher G, Nei M, Kumar S. MEGA5: Molecular evolutionary genetics analysis using maximum-likelihood, evolutionary distance, and maximum parsimony methods. *Mol. Biol. Evol.* 2011; 8: 2731–2739.
29. Saitou N, Nei M. The neighbor-joining method: a new method for reconstructing phylogenetic trees. *Mol Biol Evol.* 1987; 4: 406–425. PMID: [3447015](https://pubmed.ncbi.nlm.nih.gov/3447015/)
30. Kawade K, Horiguchi G, Ishikawa N, Hirai YM, Tsukaya H. Promotion of chloroplast proliferation upon enhanced post-mitotic cell expansion in leaves. *BMC Plant Biol.* 2013; 23: 143–150.

METHODOLOGY ARTICLE

Open Access

A simple and efficient seamless DNA cloning method using SLiCE from *Escherichia coli* laboratory strains and its application to SLiP site-directed mutagenesis

Ken Motohashi

Abstract

Background: Seamless ligation cloning extract (SLiCE) is a simple and efficient method for DNA assembly that uses cell extracts from the *Escherichia coli* PPY strain, which expresses the components of the λ prophage Red/ET recombination system. This method facilitates restriction endonuclease cleavage site-free DNA cloning by performing recombination between short stretches of homologous DNA (≥ 15 base pairs).

Results: To extend the versatility of this system, I examined whether, in addition to bacterial extracts from the PPY strain, other *E. coli* laboratory strains were suitable for the SLiCE protocol. Indeed, carefully prepared cell extracts from several strains exhibited sufficient cloning activity for seamless gene incorporation into vectors with short homology lengths (approximately 15–20 bp). Furthermore, SLiCE was applied to the polymerase chain reaction (PCR)-based site-directed mutagenesis method, in a process termed “SLiCE-mediated PCR-based site-directed mutagenesis (SLiP site-directed mutagenesis)”. SLiP site-directed mutagenesis simplifies the steps of PCR-based site-directed mutagenesis, as it exploits the capability of the SLiCE method to insert multiple fragments.

Conclusions: SLiCE can be performed in the laboratory with no requirement for a special *E. coli* strain, and the technique is easily established. This method increases the cloning efficiency, shortens the time for DNA manipulation, and greatly reduces the cost of seamless DNA cloning.

Keywords: Homologous recombination, Seamless DNA cloning, SLiCE, Site-directed mutagenesis, Plant redox-related gene

Background

The manipulation of recombinant DNA molecules is an indispensable step in current molecular biology research. Type IIP restriction endonucleases and DNA ligases were the original “workhorses” utilized to generate plasmids or other types of DNA vectors [1]. Recently, various restriction endonuclease cleavage site-independent cloning methods, which overcome the limitations associated with the lack of unique restriction enzyme sites, have been described [2–13]. These methods are based on homologous recombination, in which overlapping sequences present at the 5′ and 3′ ends of DNA fragments are combined.

Seamless Ligation Cloning Extract (SLiCE), which was initially developed as a novel bacterial cell extract-based DNA cloning method, utilizes the *in vitro* homologous recombination activity of *Escherichia coli* cell extracts. Zhang *et al.* reported that cell extracts from the *E. coli* PPY strain, which contains the λ prophage Red/ET recombination system, could efficiently assemble DNA fragments with short end overlaps of at least 15 base pairs (bp) *in vitro* [14]. SLiCE is a simple and highly cost-effective approach for vector construction because, apart from adenosine triphosphate (ATP) and commonly used buffers, only an *E. coli* lysate was required for the seamless ligation of DNA fragments into vectors. However, cell extracts from DH10B (a common *E. coli* laboratory strain) did not exhibit efficient cloning activity

Correspondence: motohas@cc.kyoto-su.ac.jp
Department of Bioresource and Environmental Sciences, Faculty of Life Sciences, Kyoto Sangyo University, Kamigamo Motoyama, Kita-ku, Kyoto 603-8555, Japan

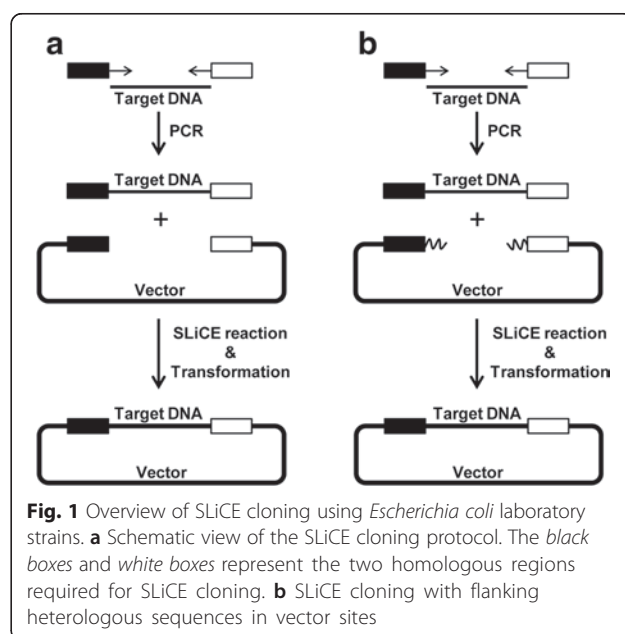
with short end homology fragments (lengths with a range of 15–20 bp) [14].

Many methods for site-directed mutagenesis have been developed, including QuickChange site-directed mutagenesis [15], the overlap extension method [16, 17], and the megaprimer method [18, 19]. QuickChange site-directed mutagenesis is widely used as a simple polymerase chain reaction (PCR)-based method that does not require the purification of PCR fragments [20–23]. However, mutations may occur in the vector at non-desired sites during PCR amplification, which can compromise the fidelity of the approach. On the other hand, because the overlap extension and megaprimer methods utilize vectors that have been digested with restriction endonucleases, introduction of mutations in the vector region is avoided [24–26]. However, vector construction by these methods requires two sequential PCR reactions, and the purification of insert DNA fragments. To simplify these multiple-step methods, SLiCE has been applied to overlap extension PCR-based site-directed mutagenesis, because it can simultaneously integrate several DNA fragments into a vector [14]. In this study, I demonstrated that SLiCE-mediated PCR-based site-directed mutagenesis (SLiP site-directed mutagenesis) could be performed using extracts of a regular laboratory *E. coli* strain. This approach can be adopted in studies that require precise generation of mutants in the absence of unwanted alterations to the vector backbone.

Results

Estimation of SLiCE from *E. coli* laboratory strains

Both the colony formation rate (number of colonies) and the ratio of correct clones (cloning efficiency) in transformation are important determinants for efficient cloning of PCR fragments. Cell lysates from *E. coli* RecA⁻ strains such as DH10B contain endogenous *in vitro* homologous recombination activity, and can be used to clone PCR fragments into vectors with homology regions. However, cloning with lysates from this strain is not efficient, particularly in the case of inserts with short homology lengths (approximately 15–20 bp), because of a lower colony formation rate [14]. An *E. coli* PPY strain that expresses an optimized λ prophage Red/ET recombination system circumvents this problem by increasing the colony formation rate during PCR fragment cloning [14]. To extend the utility of this method, I prepared SLiCE extracts from several *E. coli* laboratory strains with some modifications, and estimated the efficiency with which redox-related genes from *Arabidopsis* could then be cloned into expression vectors [27–30] (Fig. 1a). The SLiCE extracts from common RecA⁻ *E. coli* laboratory strains such as DH10B, JM109, DH5 α , XL10-Gold and Mach1 T1 supported the cloning of PCR fragments containing a 19-bp overlap region into the vectors, and were associated with a high



colony formation rate (Table 1). Additionally, SURE2, a RecA⁺, *recB recJ* strain, also facilitated the cloning of PCR fragments with almost the same efficiency. No extract that contained only insert DNA fragments and linearized vector could also clone the PCR fragments into vectors using homologous recombination activity *in vivo* in host cells (Table 1) [31]. However, the transformation efficiencies (“Number of colonies” in Table 1) were less effective with 1/40 – 1/200 of bacterial SLiCE from several *E. coli* laboratory strains. Together, these data highlight the specificity of the new method. The improved SLiCE preparation could support the cloning of the PCR fragments into vector, with an efficiency of $2 - 10 \times 10^3$ colonies/ng vector; this yield was obtained with a 19-bp overlap region and using $\sim 2 \times 10^8$ CFU/ μ g of pUC19 DNA chemically competent cells. In contrast, a previously reported SLiCE from the DH10B strain yielded a more modest efficiency of 75–80 colonies/ng vector; in this case, 15–20 bp overlap lengths and 1×10^{10} CFU/ μ g of pUC19 DNA high efficiency electrocompetent cells were used [14]. The SLiCEs from *E. coli* laboratory RecA⁻ strains used in this study were sufficiently active to achieve seamless cloning with respect to both colony formation rate (number of colonies) and the ratio of the correct clones (cloning efficiency). These results indicate that *E. coli* laboratory strains other than *E. coli* PPY can be used as the SLiCE sources. Therefore, SLiCE from the JM109 strain was used in all subsequent experiments.

Next, the effect of short homology length on cloning efficiency was evaluated using PCR fragments containing overlaps of varied lengths (Table 2). To determine whether the cloning fidelity was maintained at all overlap lengths, DNA sequencing was performed. This revealed

Table 1 The cloning efficiencies using SLiCE from different *E. coli* laboratory strains

Strain	Number of colonies ^a		Cloning efficiency ^b	
	Prx IIE (AT3G52960)	G6PDH1 (AT5G35790)	Prx IIE (AT3G52960)	G6PDH1 (AT5G35790)
no extract	47.0 ± 4.6	63.7 ± 5.5	16/18	17/18
DH10B	4,630 ± 879	3,020 ± 63.5	17/18	18/18
JM109	9,960 ± 240	5,300 ± 820	18/18	18/18
DH5α	6,130 ± 348	4,340 ± 979	18/18	18/18
XL10-Gold	6,210 ± 652	3,610 ± 287	17/18	18/18
Mach1 T1	9,530 ± 411	2,310 ± 416	18/18	18/18
SURE2	8,490 ± 896	6,040 ± 1,380	16/18	17/18

^aNumber of colonies is represented as CFU per nanogram of vector. Each value of "number of colonies" is the mean ± standard deviation of three independent experiments. ^bCloning efficiencies for the insert DNA are represented as "number of clones with the confirmed correct insert length by colony-PCR/number of colonies subjected to colony-PCR". The insert DNA fragments were amplified using 19-bp overlap primers. The linearized vector DNA was prepared by PCR. The SLiCE reaction was performed for 60 min at 37 °C with an insert:vector ratio of 1:1 and 3:1 for Prx IIE and G6PDH1, respectively

that a minimum overlap length of 15 bp was required for correct insertion of the DNA fragments into the vector. Although DNA assembly by homologous recombination with a SLiCE from the PPY strain required more than 15 bp of overlapping homology [14], I found that a 10-bp overlap was sufficient for the assembly of insert DNA into the vector. However, both the cloning efficiency and fidelity of a 10-bp overlap assembly were slightly reduced. PCR fragments with a 19-bp overlap region resulted in the maximum number of colonies upon transformation.

SLiCE can assemble insert DNA fragments into restriction enzyme-digested vectors with flanking heterologous sequences

PCR-amplified insert DNAs have often been cloned into vectors digested at restriction enzyme cleavage sites as a standard protocol [32–37]. To evaluate the cloning efficiency using such an approach, pET23 vectors were digested with restriction enzymes to yield flanking heterologous sequences (Fig. 1b). The cloning efficiency for the digested vector was determined using multiple pairwise combinations of cloning sites (Table 3). I found that inserts could be incorporated into vectors with heterologous flanking regions, although the cloning efficiency

varied according to the precise combination of restriction enzymes used (Table 3 and Additional file 1: Figure S1). The presence of the heterologous flanking region at the 5' or 3' end of the vector DNA did not inhibit the correct ligation of the insert DNA to the vector (Table 3; *NdeI*[or *NcoI*]-*Bam*HI and *Bam*HI-*Xho*I). However, the presence of heterologous flanking regions at both the 5' and 3' ends of the vector DNA markedly reduced the cloning efficiency (Table 3; *Bam*HI). The fidelity of colony-PCR positive clones was minimally affected by the presence of the heterologous flanking sequences.

Optimization of the SLiCE reaction

Next, the conditions for the SLiCE reaction were optimized for extracts from *E. coli* JM109. Time-course experiments indicated that transformation efficiencies were more than 3×10^3 colonies/ng vector over incubation periods between 5 and 60 min, and the reaction reached saturation rapidly (Fig. 2a). These transformation efficiencies were sufficient for usual DNA cloning, using conventional chemically competent cells. Incubations lasting more than 90 min reduced the colony formation rate. Longer incubation times might induce degradation of the insert and vector DNA, since the SLiCE contains

Table 2 Effect of end homology length on SLiCE cloning

Homology length (bp)	Number of colonies ^a		Cloning efficiency		Cloning accuracy (%) ^b	
	Prx IIE	G6PDH1	Prx IIE	G6PDH1	Prx IIE	G6PDH1
10	558 ± 74.5	585 ± 121	11/16	16/16	100.0	93.8
15	875 ± 43.9	777 ± 186	16/16	15/16	100.0	100.0
19	972 ± 162	1,070 ± 289	15/16	16/16	100.0	100.0
24	926 ± 28.6	519 ± 74.8	16/16	16/16	100.0	100.0
29	483 ± 34.8	520 ± 51.4	16/16	16/16	100.0	100.0
34	105 ± 37.2	150 ± 47.1	14/16	16/16	100.0	87.5

^aEach value of "number of colonies" is the mean ± standard deviation of three independent experiments. ^bCloning accuracies are given as the percentage of correctly cloned expression vectors in colony-PCR positive clones. The insert DNA fragments and linearized vector DNA were prepared by PCR. The SLiCE (JM109) reaction was performed for 10 min at 37 °C with 1:1 and 3:1 molar ratios of insert to vector for Prx IIE and G6PDH1, respectively

Table 3 The SLiCE cloning efficiencies of linearized vectors prepared by digestion with different restriction enzymes

Restriction enzymes	Flanking heterologous length (bp)	Number of colonies ^a		Cloning efficiency		Cloning accuracy (%)	
		Prx IIE	G6PDH1	Prx IIE	G6PDH1	Prx IIE	G6PDH1
<i>NdeI</i> - <i>XhoI</i>	0 + 0	9,680 ± 651	-	18/18	-	100	-
<i>NcoI</i> - <i>XhoI</i>	0 + 0	-	8,470 ± 2,180	-	17/18	-	94.1
<i>Bam</i> HI	40 + 40	926 ± 62.0	576 ± 17.6	1/18	5/18	100	100
<i>NdeI</i> - <i>Bam</i> HI	0 + 40	164 ± 20.8	-	12/18	-	75.0	-
<i>NcoI</i> - <i>Bam</i> HI	0 + 40	-	195 ± 83.3	-	4/18	-	100
<i>Bam</i> HI - <i>XhoI</i>	40 + 0	857 ± 298	960 ± 71.3	9/18	12/18	88.9	83.3

The insert DNA fragment was prepared by PCR. The linearized pET23a or pET23d vectors were prepared by digestion with restriction enzymes. The multiple cloning site of pET23a (or pET23d) are displayed in Additional file 1: Figure S1. The SLiCE (JM109) reaction was performed for 60 min at 37 °C with 1:1 and 3:1 molar ratios of insert to vector for Prx IIE and G6PDH1, respectively. ^aEach value of "number of colonies" is the mean ± standard deviation of three independent experiments

bacterial nucleases. A 1:1 to 3:1 molar ratio of insert:vector yielded highly efficient cloning, with more than 2×10^3 colonies/ng vector being formed (Fig. 2b). The enhancement of transformation efficiency in *E. coli* by modification of the SLiCE preparation protocol allows the simplification of several steps, including purification of insert and vector DNA fragments. Therefore, the influence of the DNA fragment purification steps on cloning efficiency was also evaluated (Table 4). Unpurified PCR fragments could be inserted to the vector, although with a lower transformation efficiency. By contrast, ethanol precipitation or ExoSAP-IT (Affymetrix, Santa Clara, CA) treatment of insert DNA fragments improved the transformation efficiency between 5- and 7-fold. PCR purification columns or purification via agarose gel electrophoresis improved the efficiency between 37- and 138-fold. We also observed a high cloning efficiency (at the optimal insert:vector ratio) regardless of the purification steps used.

Application of SLiCE to PCR-based site-directed mutagenesis

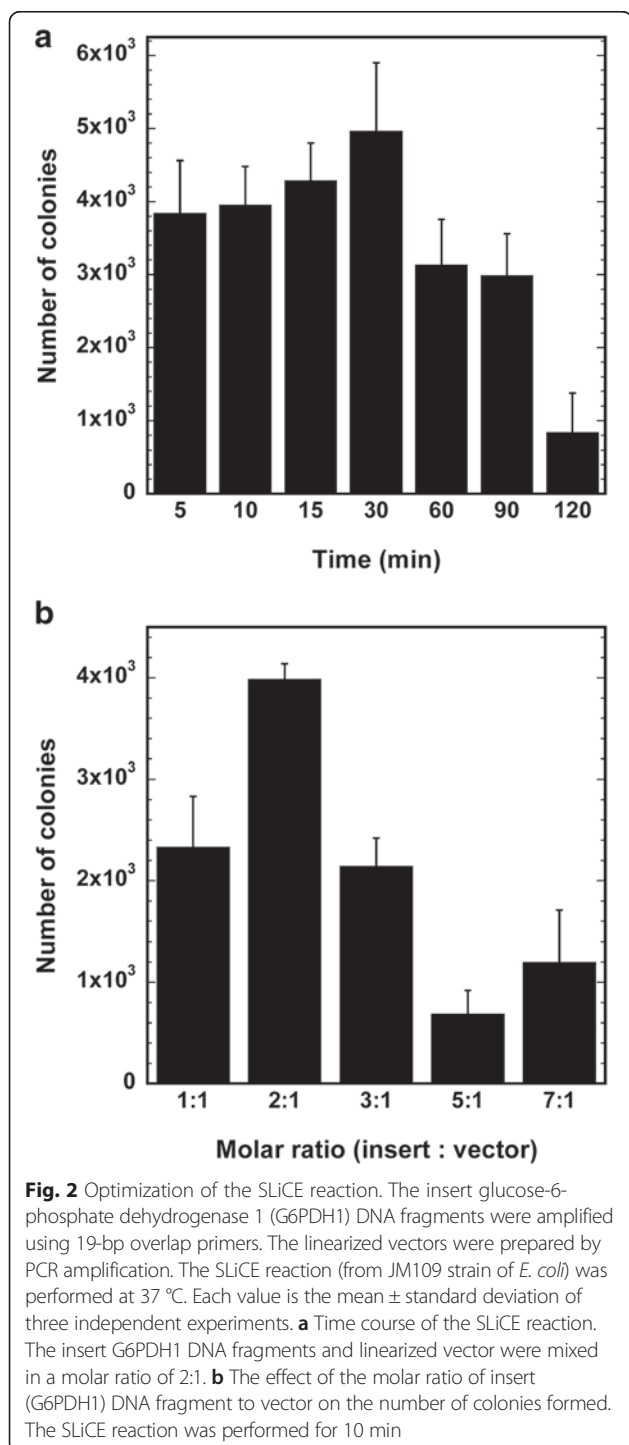
Previously, the SLiCE method, using the *in vitro* homologous recombination activity of lysates from the *E. coli* PPY strain, was employed to integrate multiple DNA fragments into vectors in a single cloning reaction [14]. The overlap extension method, which is used for PCR-based site-directed mutagenesis (Fig. 3a), has an advantage in that it can use restriction enzyme-digested vectors, which excludes the possibility of acquiring a mutation in the vector region [16, 17]. SLiCE was applied to generate cysteine-to-serine mutants at critical residues in redox-related proteins [26, 38–40]. To generate the cysteine mutants, pairs of insert DNA fragments containing a mutation site and short end homologies at both sides were amplified by PCR, and two fragments were simultaneously integrated into pET vectors using SLiCE (Fig. 3b). Both unpurified and column-purified DNA fragments could be inserted into the vector. The use of column-purified insert DNA increased the number of colonies following transformation by approximately 4- to 16-fold, although the

cloning efficiencies were not improved (Table 5). Thus, this new SLiCE-mediated PCR-based site-directed mutagenesis (SLiP site-directed mutagenesis) technique simplifies the original overlap extension method by removing several steps. Although QuickChange site-directed mutagenesis also minimizes the number of steps, SLiP site-directed mutagenesis has the added advantage that only the insert region (and not the whole plasmid) is amplified by PCR.

Discussion

In this study, I demonstrated that a wide variety of laboratory RecA⁻ strain extracts can be used to clone PCR fragments, in the absence of any special modifications to the strains. In the case of short homology lengths (approximately 15–20 bp), SLiCEs from several *E. coli* laboratory strains yielded good colony formation rates, which were at least three orders of magnitude greater than those obtained in a previous study [14]. Unexpectedly, SURE2, which is a RecA⁺, *recB recJ* strain, also retained SLiCE activity. Although the mechanisms associated with the *in vitro* homologous recombination activity of *E. coli* extracts are not fully characterized, routine cloning using several *E. coli* extracts works well even with cells that are not highly electrocompetent. The SLiCEs from *E. coli* laboratory strains in this study have such high transformation efficiencies because several steps of the original SLiCE preparation protocol [14] have been modified. Firstly, *E. coli* cells were harvested at OD₆₀₀ = 2.0–3.0 (late log phase). Secondly, extraction of *E. coli* lysates was performed under 4 °C, and ice-cold solutions were used during the preparation. These modifications might improve the transformation efficiency following the use of SLiCEs from *E. coli* laboratory strains.

In addition, the SLiCE method was simplified by optimizing the reaction conditions (Fig. 2 and Table 4). Although purification of insert DNA fragments was not essential for the assembly of fragments into the vectors, selecting a purification step improved cloning efficiency (Table 4). A 19-bp overlap sequence is recommended as



the short end homology region, since this yielded the maximum number of transformants (Table 2). However, a 15-bp overlap sequence was also sufficient to provide colonies harboring the correct clone. The SLiCE method also has the advantage that linearized vectors (generated by either PCR amplification or restriction enzyme digestion) may be used, as its efficiency and accuracy were

Table 4 Effect of PCR fragment purification method on SLiCE efficiency

Purification method	Number of colonies ^f		Cloning efficiency	
	Prx IIE	G6PDH1	Prx IIE	G6PDH1
None ^a	86.3 \pm 2.3	76.0 \pm 4.0	15/18	17/18
EtOH ppt ^b	546 \pm 102	514 \pm 68.7	18/18	17/18
ExoSAP-IT ^c	481 \pm 117	507 \pm 105	18/18	18/18
Column ^d	7,170 \pm 806	4,660 \pm 1,400	18/18	18/18
Agarose gel ^e	11,900 \pm 1,750	2,830 \pm 100	18/18	18/18

The insert DNA fragments were amplified using 19-bp overlap primers and KOD DNA polymerase [51] (for Prx IIE gene) and PrimeSTAR Max DNA polymerase (for G6PDH1). The linearized vector DNA was prepared by PCR. The PCR solutions were treated with *DpnI*. The SLiCE (JM109) reaction was performed for 10 min at 37 °C. ^aUnpurified insert DNA was directly used for the SLiCE reaction. ^bInsert DNA was precipitated by ethanol. ^cPCR solution was treated with ExoSAP-IT (Affymetrix). ^dInsert DNA was purified from the PCR solution using a Gel/PCR Extraction Kit (FastGene). ^eInsert DNA was purified by agarose gel electrophoresis and using a Gel/PCR Extraction Kit (FastGene). An equivalent volume to 1/20 of the PCR solution was used for the SLiCE reaction. ^fEach value of "number of colonies" is the mean \pm standard deviation of three independent experiments

not affected by the presence of blunt ends or 5' sequence overhangs at the ends of the vector (Table 2 and Table 3). I summarize the SLiCE protocol from *E. coli* laboratory strains in Fig. 4. For the standard protocol, various insert DNA fragments, including small amounts of PCR-products amplified as multiple bands can be cloned into vectors with high efficiency. In contrast, a rapid protocol is available for high abundance PCR-products that have been amplified as a single band.

Seamless DNA assembly kits based on *in vitro* homologous recombination activity have recently become

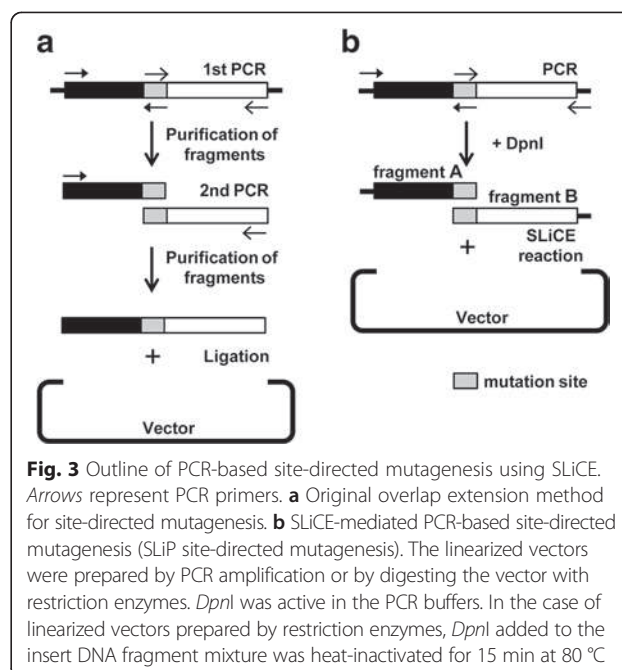


Table 5 SLiCE-mediated PCR-based site-directed mutagenesis

Mutation site	Number of colonies ^c	Cloning efficiency	Mutation(%) ^d
Prx IIE C51S ^a	22.0 ± 14.0	10/16	100
Prx IIE C76S ^a	18.0 ± 7.5	15/16	100
G6PDH1 C97S ^a	32.0 ± 4.6	9/16	93.3
G6PDH1 C105S ^a	54.0 ± 13.5	9/16	88.9
Prx IIE C51S ^b	197 ± 49.2	14/16	100
Prx IIE C76S ^b	283 ± 21.2	15/16	100
G6PDH1 C97S ^b	189 ± 39.0	6/16	100
G6PDH1 C105S ^b	220 ± 30.0	9/16	100

Target cysteine residues that are reduced by chloroplast thioredoxins were substituted with serine residues [26, 52]. The insert DNA fragments were prepared by PCR using PrimeSTAR Max DNA polymerase. pET23a and pET23d vectors were linearized using restriction enzymes *NdeI* and *XhoI* (for pET23a) and *NcoI* and *XhoI* (for pET23d). The SLiCE (JM109) reaction was performed for 60 min at 37 °C. ^aOne microliter of unpurified insert DNA fragments in 20 μL PCR solution was directly used for the SLiCE reaction. ^bPCR solution (20 μL) was purified using a Gel/PCR Extraction Kit (FastGene) and an equivalent volume to 1/20 of the PCR solution was used for the SLiCE reaction. ^cEach value of “number of colonies” is the mean ± standard deviation of three independent experiments. ^dThe ratio of mutants generated is given as the percentage of mutated clones (determined by DNA sequencing) among colony PCR-positive clones

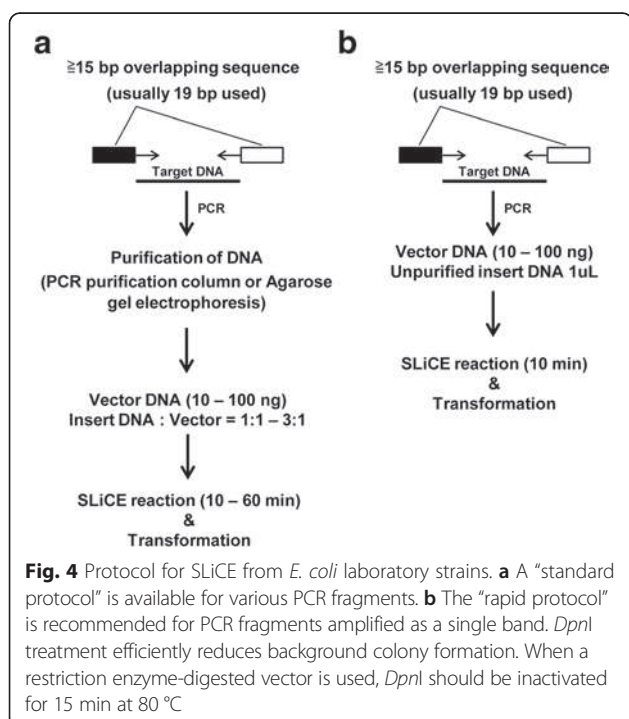
commercially available. These include the In-Fusion HD Cloning Kit [41, 42] (Clontech), GeneArt Seamless Cloning and Assembly Kit (Life Technologies), and Gibson Assembly Cloning Kit [2, 43] (New England BioLabs). However, many of the commercially available kits are associated with a high cost per reaction. The SLiCE method uses extracts from common *E. coli* laboratory strains. These extracts can be prepared easily in the laboratory and the use of this method greatly reduces the costs associated with DNA manipulation. SLiCE is highly efficient and maintains high fidelity for gene cloning. These results also allow the use of either commercial or

laboratory “homemade” chemically competent cells. As an approximate guide, our laboratory has successfully used SLiCE with chemically competent *E. coli* cells that yield $>10^7$ CFU/μg of pUC19 DNA [44].

PCR-based site-directed mutagenesis is a common technique used in molecular biology experiments. The QuickChange mutagenesis kit is frequently used for site-directed mutagenesis because it is a simple process that does not require the purification of PCR fragments. However, this method relies on PCR amplification of the entire plasmid, which is accompanied by the risk of introducing a mutation in the vector region. In contrast, in the overlap extension method only the insert DNA is amplified. Furthermore, the possibility of introducing a mutation in the vector region is excluded by the use of a restriction enzyme-digested vector. A limitation of the overlap extension method is that it follows an elaborate protocol and requires multiple steps (Fig. 3a). SLiP site-directed mutagenesis removes one PCR cycle and two DNA purification steps from the overlap extension method, and thus provides an efficient and accurate method for the generation of site-directed mutants.

Conclusions

SLiCEs prepared from a wide variety of laboratory RecA⁻ *E. coli* strains could be used to clone PCR fragments, in the absence of any special modifications to the strains. SLiP site-directed mutagenesis is a simple and efficient method that removes any possibility of mutation in the vector region. The combination of SLiCE using *E. coli* laboratory strains and SLiP site-directed mutagenesis will facilitate the generation of recombinant plasmids and mutants, and shorten the time for DNA manipulation in the laboratory. The elucidation of mechanisms that control *in vitro* homologous recombination activity in *E. coli* lysates will lead to further enhancement of SLiCE efficiency.



Methods

Reagents

CellLytic B Cell Lysis Reagent (SIGMA B7435) was used for *E. coli* cells lysis buffer. Adenosine-5'-triphosphate disodium salt hydrate from yeast (Nacalai Tesque, Inc. 01072-24) was used for ATP contained in SLiCE buffer (10×).

E. coli strains

The following *E. coli* laboratory strains were used to prepare SLiCE extracts (Additional file 1: Table S1): DH10B [45], JM109 [46], DH5α [47], XL10-Gold (Agilent Technologies, Santa Clara, CA), Mach1 T1 (Life Technologies, Carlsbad, CA) and SURE2 (Agilent Technologies, Santa Clara, CA). ECOS X Competent *E. coli* DH5α (Nippon gene, Tokyo, Japan) chemically competent cells were used to transform the recombinant DNA generated using the SLiCE method, in order to obtain the constant transformation efficiency.

Preparation of the SLiCE extract from *E. coli* laboratory strains

E. coli strains precultured in LB Miller medium (1 mL) at 37 °C were transferred to 2× YT medium (50 mL) in a 100-mL round-bottom, long-neck Sakaguchi shake flask. The cells were grown at 37 °C in a reciprocal shaker (160 rpm) until OD₆₀₀ reached a value of 2.0–3.0 (late log phase). The cultures were generally incubated for 3.5–6.5 h. The cells were harvested by centrifugation at 5,000 × *g* for 10 min at 4 °C. The cells were then washed with 50 mL sterilized water (ice-cold), and centrifuged at 5,000 × *g* for 5 min at 4 °C. The wet cells were recovered with a yield of 0.25–0.40 g, and gently resuspended in 1.2 mL CellLytic B Cell Lysis Reagent and incubated for 10 min at room temperature. The cell lysates were then centrifuged at 20,000 × *g* for 2 min at 4 °C. All subsequent procedures were performed on ice. The supernatants were carefully transferred into 1.5-mL microtubes to remove the insoluble materials, and an equal volume of ice-cold 80 % (v/v) glycerol was added and mixed gently. Forty microliters of each SLiCE extract was aliquoted into a 0.2-mL 8-strip PCR tube. The SLiCE extracts were snap-frozen in a bath of liquid nitrogen, and stored at –80 °C in 40 % (v/v, final concentration) glycerol. For short-term storage, the aliquoted SLiCE extracts could be stored at –20 °C in 40 % (v/v, final concentration) glycerol for about 3 months without significant loss of activity.

SLiCE reaction and transformation

SLiCE buffer (10×; 500 mM Tris–HCl, pH 7.5, 100 mM MgCl₂, 10 mM ATP, and 10 mM dithiothreitol) was passed through a 0.2-μm filter, and dispensed in 40-μL aliquots into 0.2-mL 8-strip PCR tubes and stored at –20 °C. The *Arabidopsis* type II peroxiredoxin E (Prx IIE, 0.6 k base pairs (kbp), AT3G52960) [48, 49] and chloroplastic

glucose-6-phosphate dehydrogenase 1 (G6PDH1, 1.6 kbp, AT5G35790) [50] genes were used as insert DNA molecules. The linearized pET23a DNA and insert DNA fragments were amplified using the primers listed in Additional file 1: Table S2 and Tks Gflex DNA polymerase (Takara-Bio, Otsu, Japan) by PCR. To compare the reaction efficiency of SLiCE with that of restriction enzyme-digested vectors, the pET23a and pET23d vectors were linearized by digestion with restriction enzyme and purified using a Gel/PCR Extraction Kit (FastGene) following agarose gel electrophoresis.

After the SLiCE reaction solution had been prepared, the SLiCE extract was thawed on ice and mixed gently. The standard SLiCE reaction solution comprised the following components: 10 ng linear vector (PCR amplified or restriction enzyme-digested), an appropriate amount of insert DNA (1:1 to 3:1 molar ratio of insert to vector), 1 μL 10× SLiCE buffer, 1 μL SLiCE extract, and sterilized distilled water to a total volume of 10 μL. The SLiCE reaction mixture was incubated at 37 °C for the indicated time (5–120 min). One microliter of the SLiCE reaction solution was chemically transformed into 20 μL ECOS X Competent *E. coli* DH5α (Nippon gene, Tokyo, Japan) according to the instruction manual. The transformation efficiency of the competent cells (20 μL) was approximately 2 × 10⁸ CFU/μg of pUC19 DNA. Transformed *E. coli* cells were plated on LB agar plates containing ampicillin and incubated at 37 °C for 12–16 h.

Evaluation of the SLiCE reaction

Various parameters were used to measure the efficiency of the SLiCE reactions under each experimental condition. Number of colonies was represented as CFU per nanogram of vector. Cloning efficiencies for the insert DNA were given as the ratio of colonies with an insert of the confirmed correct length as estimated by colony-PCR. In particular, cloning efficiencies were represented as “the number of clones with the confirmed correct length of insert DNA by colony-PCR/number of colonies subjected to colony-PCR”. The cloning accuracy was expressed as the percentage of correctly cloned expression vectors in colony-PCR positive clones. The insert cloning sites were determined by DNA sequencing.

Insert-check by colony PCR in transformed *E. coli*

Each colony was picked with a sterile toothpick and put into the bottom of a 0.2-mL 8-strip PCR tube or a 96-well PCR plate. After the toothpicks were removed from the PCR-tube, 10 μL of KAPATaq EXtra DNA polymerase (KAPA Biosystems, Wilmington, MA) PCR mix was added to each sample; this mixture included the T7P and T7T primers corresponding to the T7 promoter and T7 terminator sequences of the pET vectors, respectively (Additional file 1: Table S3). The sample solutions were

reacted according to the KAPATaq EXtra standard protocol. When the target DNA was >1.5 kbp in length, the Tks Gflex DNA polymerase (Takara-Bio, Otsu, Japan) was used instead of KAPATaq EXtra.

SLiCE-mediated PCR-based site-directed mutagenesis (SLiP site-directed mutagenesis)

Primers for site-directed mutagenesis were designed using the PrimerX program (<http://www.bioinformatics.org/primerx/>) under the following conditions: melting temperature >78 °C and primer termination with guanine (G) or cytidine (C) for QuickChange site-directed mutagenesis kit (Additional file 1: Table S3). Pairs of insert DNA fragments for a cysteine mutant of Prx IIE and G6PDH1 were amplified in a 20- μ L reaction volume using PrimeSTAR Max DNA polymerase (Takara-Bio, Otsu, Japan) along with the T7P primer/Mutant reverse primers and Mutant forward primers/T7T primer (Additional file 1: Table S3). The two PCR fragments for mutant generation were incubated with *DpnI* for 60 min at 37 °C to digest the template plasmid DNA. Subsequently, *DpnI* was inactivated by incubating the mixture at 80 °C for 15 min. For the unpurified insert DNA fragments, 1 μ L of each unpurified insert DNA fragment in a 20- μ L PCR reaction solution was mixed with the linearized pET23a vector (10 ng; digested using *NdeI* and *XhoI* [*NcoI* and *XhoI* for pET23d]), and then added to the SLiCE reaction. For the purified insert DNA fragments, an equivalent volume to 1/20 of the PCR solution was added to the SLiCE reaction.

Additional file

Additional file 1: Figure S1. The multiple cloning site of pET23a (or pET23d) vector. **Table S1.** *Escherichia coli* strains used for SLiCE preparation. **Table S2.** Oligonucleotides for PCR amplification. **Table S3.** Oligonucleotides for site-directed mutagenesis.

Abbreviations

ATP: Adenosine triphosphate; CFU: Colony-forming units; G6PDH1: Glucose-6-phosphate dehydrogenase 1; PCR: Polymerase chain reaction; Prx IIE: Type II peroxiredoxin E; SLiCE: Seamless ligation cloning extract; SLiP site-directed mutagenesis; SLiCE-mediated PCR-based site-directed mutagenesis.

Competing interests

The author declares that he has no competing interests.

Authors' contributions

KM designed and performed the experiments, analyzed the data and wrote the manuscript. The author read and approved the final manuscript.

Acknowledgements

I thank Yuki Okegawa for critically reading the manuscript. This work was supported by JSPS KAKENHI Grant Numbers 25650037 (to K.M.), and the Science Research Promotion Fund from the Promotion and Mutual Aid Corporation for Private Schools of Japan (to K.M.).

Received: 20 October 2014 Accepted: 5 May 2015

Published online: 03 June 2015

References

- Green MR, Sambrook J. *Molecular Cloning: A Laboratory Manual*, Fourth Edition edn. Cold Spring Harbor: NY Cold Spring Harbor Laboratory Press; 2012.
- Gibson DG, Young L, Chuang RY, Venter JC, Hutchison 3rd CA, Smith HO. Enzymatic assembly of DNA molecules up to several hundred kilobases. *Nat Methods*. 2009;6(5):343–5.
- Klock HE, Lesley SA. The Polymerase Incomplete Primer Extension (PIPE) method applied to high-throughput cloning and site-directed mutagenesis. *Methods Mol Biol*. 2009;498:91–103.
- Quan J, Tian J. Circular polymerase extension cloning of complex gene libraries and pathways. *PLoS One*. 2009;4(7):e6441.
- Li MZ, Elledge SJ. SLiC: a method for sequence- and ligation-independent cloning. *Methods Mol Biol*. 2012;852:51–9.
- Warren TD, Coolbaugh MJ, Wood DW. Ligation-independent cloning and self-cleaving intein as a tool for high-throughput protein purification. *Protein Expr Purif*. 2013;91(2):169–74.
- Scholz J, Besir H, Strasser C, Suppmann S. A new method to customize protein expression vectors for fast, efficient and background free parallel cloning. *BMC Biotechnol*. 2013;13:12.
- Stevenson J, Krycer JR, Phan L, Brown AJ. A practical comparison of ligation-independent cloning techniques. *PLoS One*. 2013;8(12):e83888.
- Thieme F, Marillonnet S. Quick and clean cloning. *Methods Mol Biol*. 2014;1116:37–48.
- Camilo CM, Polikarpov I. High-throughput cloning, expression and purification of glycoside hydrolases using Ligation-Independent Cloning (LIC). *Protein Expr Purif*. 2014;99:35–42.
- Chino A, Watanabe K, Moriya H. Plasmid construction using recombination activity in the fission yeast *Schizosaccharomyces pombe*. *PLoS One*. 2010;5(3):e9652.
- Matsuo Y, Kishimoto H, Horiuchi T, Tanae K, Kawamukai M. Simple and effective gap-repair cloning using short tracts of flanking homology in fission yeast. *Biosci Biotechnol Biochem*. 2010;74(3):685–9.
- Goto K, Nagano Y. Ultra-low background DNA cloning system. *PLoS One*. 2013;8(2):e56530.
- Zhang Y, Werling U, Edelmann W. SLiCE: a novel bacterial cell extract-based DNA cloning method. *Nucleic Acids Res*. 2012;40(8):e55.
- Papworth C, Bauer JC, Braman J, Wright DA. Site-directed mutagenesis in one day with >80 % efficiency. *Strategies*. 1996;9:3–4.
- Higuchi R, Krummel B, Saiki RK. A general method of *in vitro* preparation and specific mutagenesis of DNA fragments: study of protein and DNA interactions. *Nucleic Acids Res*. 1988;16(15):7351–67.
- Ho SN, Hunt HD, Horton RM, Pullen JK, Pease LR. Site-directed mutagenesis by overlap extension using the polymerase chain reaction. *Gene*. 1989;77(1):51–9.
- Sarkar G, Sommer SS. The "megaprimer" method of site-directed mutagenesis. *Biotechniques*. 1990;8(4):404–7.
- Landt O, Grunert HP, Hahn U. A general method for rapid site-directed mutagenesis using the polymerase chain reaction. *Gene*. 1990;96(1):125–8.
- Makio H, Niwa H, Motohashi K, Taguchi H, Yoshida M. Stabilization of FtsH-unfolded protein complex by binding of ATP and blocking of protease. *Biochem Biophys Res Commun*. 2002;296(1):8–12.
- Ueoka-Nakanishi H, Nakanishi Y, Konno H, Motohashi K, Bald D, Hisabori T. Inverse regulation of rotation of F1-ATPase by the mutation at the regulatory region on the gamma subunit of chloroplast ATP synthase. *J Biol Chem*. 2004;279(16):16272–7.
- Wakita M, Masuda S, Motohashi K, Hisabori T, Ohta H, Takamiya K. The significance of type II and PrxQ peroxiredoxins for antioxidative stress response in the purple bacterium *Rhodobacter sphaeroides*. *J Biol Chem*. 2007;282(38):27792–801.
- Kojima K, Motohashi K, Morota T, Oshita M, Hisabori T, Hayashi H, et al. Regulation of translation by the redox state of elongation factor G in the cyanobacterium *Synechocystis* sp. PCC 6803. *J Biol Chem*. 2009;284(28):18685–91.
- Roy I, Smith O, Clouthier CM, Keillor JW. Expression, purification and kinetic characterisation of human tissue transglutaminase. *Protein Expr Purif*. 2013;87(1):41–6.
- Plattner S, Gruber C, Altmann F, Bohlmann H. Self-processing of a barley subtilase expressed in *E. coli*. *Protein Expr Purif*. 2014;101:76–83.
- Motohashi K, Koyama F, Nakanishi Y, Ueoka-Nakanishi H, Hisabori T. Chloroplast cyclophilin is a target protein of thioredoxin. Thiol modulation

- of the peptidyl-prolyl cis-trans isomerase activity. *J Biol Chem.* 2003;278(34):31848–52.
27. Michelet L, Zaffagnini M, Morisse S, Sparla F, Perez-Perez ME, Francia F, et al. Redox regulation of the Calvin-Benson cycle: something old, something new. *Front Plant Sci.* 2013;4:470.
 28. Serrato AJ, Fernandez-Trijueque J, Barajas-Lopez JD, Chueca A, Sahrawy M. Plastid thioredoxins: a “one-for-all” redox-signaling system in plants. *Front Plant Sci.* 2013;4:463.
 29. Balsera M, Uberegui E, Schurmann P, Buchanan BB. Evolutionary development of redox regulation in chloroplasts. *Antioxid Redox Signal.* 2014;21(9):1327–55.
 30. Geigenberger P, Fernie AR. Metabolic control of redox and redox control of metabolism in plants. *Antioxid Redox Signal.* 2014;21(9):1389–421.
 31. Li C, Wen A, Shen B, Lu J, Huang Y, Chang Y. FastCloning: a highly simplified, purification-free, sequence- and ligation-independent PCR cloning method. *BMC Biotechnol.* 2011;11:92.
 32. Motohashi K, Kondoh A, Stumpp MT, Hisabori T. Comprehensive survey of proteins targeted by chloroplast thioredoxin. *Proc Natl Acad Sci U S A.* 2001;98(20):11224–9.
 33. Yamayo Y, Motohashi K, Takamiya K, Hisabori T, Ohta H. *In vitro* reconstitution of monogalactosyldiacylglycerol (MGDG) synthase regulation by thioredoxin. *FEBS Lett.* 2006;580(17):4086–90.
 34. Granger JB, Lu Z, Ferguson JB, Santa Maria PJ, Novak WR. Cloning, expression, purification and characterization of an iron-dependent regulator protein from *Thermobifida fusca*. *Protein Expr Purif.* 2013;92(2):190–4.
 35. Wang HC, Chen YC, Huang CT, Hseu RS. Cloning and characterization of a thermostable and pH-stable cellobiohydrolase from *Neocallimastix patriciarum* J11. *Protein Expr Purif.* 2013;90(2):153–9.
 36. Yang Y, Ma J, Zhang X, Wang Y, Yang L, Sun M. Yeast 3',5'-bisphosphate nucleotidase: an affinity tag for protein purification. *Protein Expr Purif.* 2014;97:81–7.
 37. Pourmejati R, Karbalaeei-Heidari HR, Budisa N. Secretion of recombinant archeal lipase mediated by SVP2 signal peptide in *Escherichia coli* and its optimization by response surface methodology. *Protein Expr Purif.* 2014;101:84–90.
 38. Motohashi K, Romano PG, Hisabori T. Identification of thioredoxin targeted proteins using thioredoxin single cysteine mutant-immobilized resin. *Methods Mol Biol.* 2009;479:117–31.
 39. Motohashi K, Hisabori T. CcdA is a thylakoid membrane protein required for the transfer of reducing equivalents from stroma to thylakoid lumen in the higher plant chloroplast. *Antioxid Redox Signal.* 2010;13(8):1169–76.
 40. Motohashi K, Okegawa Y. Method for enhancement of plant redox-related protein expression and its application for *in vitro* reduction of chloroplastic thioredoxins. *Protein Expr Purif.* 2014;101:152–6.
 41. Hamilton MD, Nuara AA, Gammon DB, Buller RM, Evans DH. Duplex strand joining reactions catalyzed by vaccinia virus DNA polymerase. *Nucleic Acids Res.* 2007;35(1):143–51.
 42. Zhu B, Cai G, Hall EO, Freeman GJ. In-fusion assembly: seamless engineering of multidomain fusion proteins, modular vectors, and mutations. *Biotechniques.* 2007;43(3):354–9.
 43. Gibson DG, Smith HO, Hutchison 3rd CA, Venter JC, Merryman C. Chemical synthesis of the mouse mitochondrial genome. *Nat Methods.* 2010;7(11):901–3.
 44. Inoue H, Nojima H, Okayama H. High efficiency transformation of *Escherichia coli* with plasmids. *Gene.* 1990;96(1):23–8.
 45. Grant SG, Jessee J, Bloom FR, Hanahan D. Differential plasmid rescue from transgenic mouse DNAs into *Escherichia coli* methylation-restriction mutants. *Proc Natl Acad Sci U S A.* 1990;87(12):4645–9.
 46. Yanisch-Perron C, Vieira J, Messing J. Improved M13 phage cloning vectors and host strains: nucleotide sequences of the M13mp18 and pUC19 vectors. *Gene.* 1985;33(1):103–19.
 47. Bethesda Research Laboratories. BRL pUC host: *E. coli* DH5 α^m competent cells. *Focus.* 1986;8:9–12.
 48. Dietz KJ, Horling F, Konig J, Baier M. The function of the chloroplast 2-cysteine peroxiredoxin in peroxide detoxification and its regulation. *J Exp Bot.* 2002;53(372):1321–9.
 49. Brehelin C, Meyer EH, de Souris JP, Bonnard G, Meyer Y. Resemblance and dissemblance of Arabidopsis type II peroxiredoxins: similar sequences for divergent gene expression, protein localization, and activity. *Plant Physiol.* 2003;132(4):2045–57.
 50. Wakao S, Benning C. Genome-wide analysis of glucose-6-phosphate dehydrogenases in Arabidopsis. *Plant J.* 2005;41(2):243–56.
 51. Takagi M, Nishioka M, Kakahara H, Kitabayashi M, Inoue H, Kawakami B, et al. Characterization of DNA polymerase from *Pyrococcus* sp. strain KOD1 and its application to PCR. *Appl Environ Microbiol.* 1997;63(11):4504–10.
 52. Motohashi K, Hisabori T. HCF164 receives reducing equivalents from stromal thioredoxin across the thylakoid membrane and mediates reduction of target proteins in the thylakoid lumen. *J Biol Chem.* 2006;281(46):35039–47.

Submit your next manuscript to BioMed Central and take full advantage of:

- Convenient online submission
- Thorough peer review
- No space constraints or color figure charges
- Immediate publication on acceptance
- Inclusion in PubMed, CAS, Scopus and Google Scholar
- Research which is freely available for redistribution

Submit your manuscript at
www.biomedcentral.com/submit



Leaves may function as temperature sensors in the heterophylly of *Rorippa aquatica* (Brassicaceae)

Hokuto Nakayama & Seisuke Kimura

To cite this article: Hokuto Nakayama & Seisuke Kimura (2015) Leaves may function as temperature sensors in the heterophylly of *Rorippa aquatica* (Brassicaceae), *Plant Signaling & Behavior*, 10:12, e1091909, DOI: [10.1080/15592324.2015.1091909](https://doi.org/10.1080/15592324.2015.1091909)

To link to this article: <http://dx.doi.org/10.1080/15592324.2015.1091909>



Accepted author version posted online: 14 Sep 2015.



Submit your article to this journal [↗](#)



Article views: 40



View related articles [↗](#)



View Crossmark data [↗](#)

Full Terms & Conditions of access and use can be found at
<http://www.tandfonline.com/action/journalInformation?journalCode=kpsb20>

Leaves may function as temperature sensors in the heterophylly of *Rorippa aquatica* (Brassicaceae)

Hokuto Nakayama^{1,2} and Seisuke Kimura^{2,*}

¹Department of Plant Biology; University of California Davis; One Shields Avenue, Davis, CA USA; ²Department of Bioresource and Environmental Sciences; Kyoto Sangyo University; Kyoto, Japan

Keywords: Brassicaceae, heterophylly, leaf morphology, leaves, phenotypic plasticity, *Rorippa aquatica*, single-leaf warming treatment

Abbreviations: DI, dissection index; GA, gibberellin; *KNOX1*, *KNOTTED1-LIKE HOMEBOX*; LN, leaf number; SLWT, single-leaf warming treatment.

Many plants show heterophylly, which is variation in leaf form within a plant owing to environmental change. The molecular mechanisms underlying heterophylly have recently been investigated in several plant species. However, little is known about how plants exhibiting heterophylly sense environmental cues. Here, we used *Rorippa aquatica* (Brassicaceae), which shows heterophylly, to investigate whether a single leaf can sense and transit changes in ambient temperature. The morphology of newly developed leaves after single-leaf warming treatment was significantly different from that of mock-treated control leaves, suggesting that leaves are sensing organs that mediate the responses to changes in ambient temperature in *R. aquatica*.

Heterophylly in *Rorippa aquatica*

Many organisms show phenotypic plasticity in response to surrounding environments; this often results in variation among individuals. Heterophylly is a type of phenotypic plasticity that results in variation in leaf form within a single plant owing to environmental variation, and many land plants including ferns show patterns of heterophylly.^{1,2} Some such leaf form alterations are thought to be adaptive responses to environmental changes.³ Several plants showing heterophylly have been described and the underlying mechanisms have been investigated.^{1,4,5} These studies have shown that various hormones, such as ethylene and abscisic acid, are involved in the alteration of leaf form.

Recently, we studied the mechanism underlying heterophylly in a semi-aquatic plant, *Rorippa aquatica* (Eaton) EJ Palmer & Steyermark (Brassicaceae).^{6,7} *R. aquatica* is found in bays, lakes, ponds, and streams in North America, and shows drastic heterophylly. In submerged conditions, deeply dissected leaves develop, whereas in terrestrial conditions, simple leaves with smooth margins develop. Additionally, *R. aquatica* is closely related to *Cardamine hirsuta* and *Arabidopsis thaliana* (hereafter, *Arabidopsis*),⁸ which are the most well-studied model plants with respect to leaf development.^{8,9,10} Hence, *R. aquatica* is an ideal model plant to determine the mechanisms of heterophylly.

Changes in ambient temperature induce heterophylly in *R. aquatica*.⁷ Under terrestrial conditions, dissected leaves

develop at 20°C, whereas simpler-formed leaves with smooth margins develop at 30°C (Fig. 1A). Previously, we showed that regulation of the gibberellin (GA) level via *KNOTTED1-LIKE HOMEBOX* (*KNOX1*) is involved in this phenomenon. Moreover, a transcriptome analysis indicated that light intensity also affects leaf form alterations. Consistent with this, we have demonstrated that light intensity induces heterophylly.⁷ Together, these results suggest that the KNOX-GA module, which is involved in the morphological diversification of leaf form among species, may also govern variation in leaf form within a species, and even within individuals, in response to environmental changes.⁷

However, the precise organs that sense environmental cues, such as ambient temperature, in *R. aquatica* and other plants that show heterophylly remain unclear. Thus, it is necessary to identify the organs that sense these cues to further understand the mechanisms underlying plant heterophylly.

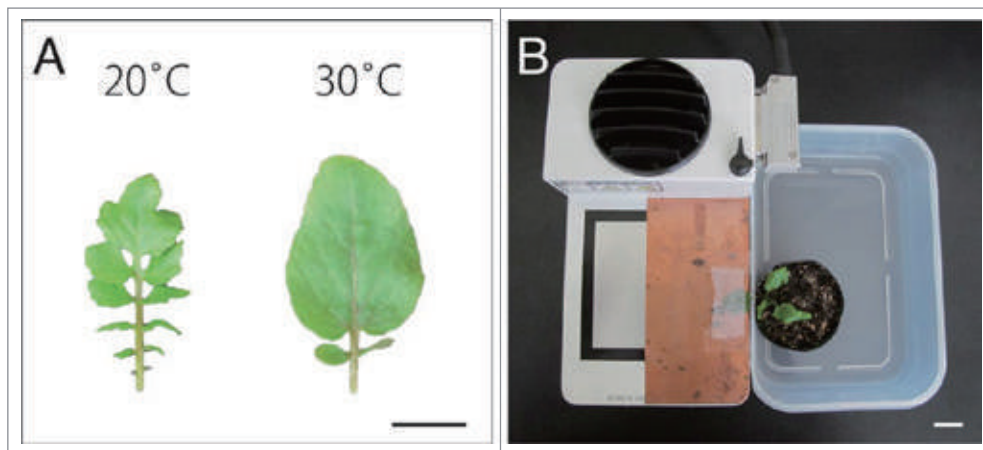
Leaves may function as temperature sensors

Previous studies have demonstrated that some developing leaf phenotypes, such as stomatal density, palisade tissue size, and leaf thickness, are independent of local light irradiance. However, in addition to a change in CO₂ concentration, irradiance to mature leaves affects the phenotypes of developing leaves.¹¹⁻¹⁴ Additionally, the effect from mature to developing leaves is conserved among eudicots and monocots,¹⁴ suggesting that the system is

*Correspondence to: Seisuke Kimura; Email: seisuke@cc.kyoto-su.ac.jp

Submitted: 06/19/2015; Revised: 09/02/2015; Accepted: 09/03/2015

<http://dx.doi.org/10.1080/15592324.2015.1091909>



changes in the surrounding environment, resulting in heterophylly of *R. aquatica*.

In this study, we investigated the morphology of newly developed leaves after warming single leaves within the same *R. aquatica* plant. To warm an individual leaf, a plate-type temperature control system (CP-085; SCINICS) was used (Fig. 1B). This single-leaf warming treatment (SLWT) has been successfully performed using *Arabidopsis* leaves.¹⁵ Leaf number 3 (LN3) was warmed at 30°C by the system for 30 days in a chamber that was maintained at 20°C. On the other hand, in mock-treated control, LN3 was cooled at 20°C for 30 days in a chamber

Figure 1. Gross morphology of *Rorippa aquatica* leaves. (A) A comparison of the morphology of leaf number 5 (LN5) for different temperatures. Left: 20°C; right: 30°C. (B) Experimental set up for single-leaf warming treatment using a plate-type temperature control system (CP-085; SCINICS). Bars = 2 cm.

relatively common in angiosperms. As indicated previously, light intensity also affects leaf morphology in *R. aquatica*.⁷ Hence, leaves are candidate organs with respect to the ability to sense

that was maintained at 20°C. All plants were cultivated at 20°C without treatment for an additional 30 days (60 days in total) to ensure full lamina expansion. To investigate the complexity in leaf morphology, the dissection index (DI), which is an index of leaf complexity, was calculated as $(\text{perimeter})/\sqrt{(\text{leaf area})}$. To measure the leaf area and perimeter, mature leaves (LN4–7) were photographed using a digital camera (PowerShot G11; Canon). Leaf areas and perimeters were calculated using ImageJ v1.48 (<http://rsb.info.nih.gov/ij/>).

As expected, the form of newly developed leaves (LN5 and 6) after the SLWT (30°C) was simpler than that of leaves in mock-treated control (Fig. 2). This result suggests that there is a long distance signal from older leaves to newly developed leaves in the heterophylly of *R. aquatica*, as has been suggested for anatomical alterations between leaves exposed to sun and shade in some plants.^{11,12} However, we did not observe a statistically significant decrease in DI for LN4. This may be due to the determinacy of LN4 primordia. A previous study showed that the form of leaf primordia appears to be determined between stages P4 and P5.⁷ When the SLWT was initiated, the form of LN4 seemed to be determined already. Hence, we might not expect to observe a significant decrease in the DI of LN4. Interestingly, although we observed a statistically significant decrease in the DI of LN5 and LN6, the DI of LN7 did not show a decrease (Fig. 2B), suggesting that not all newly developed leaves were affected by the treatment applied to LN3. These results suggest a few potential

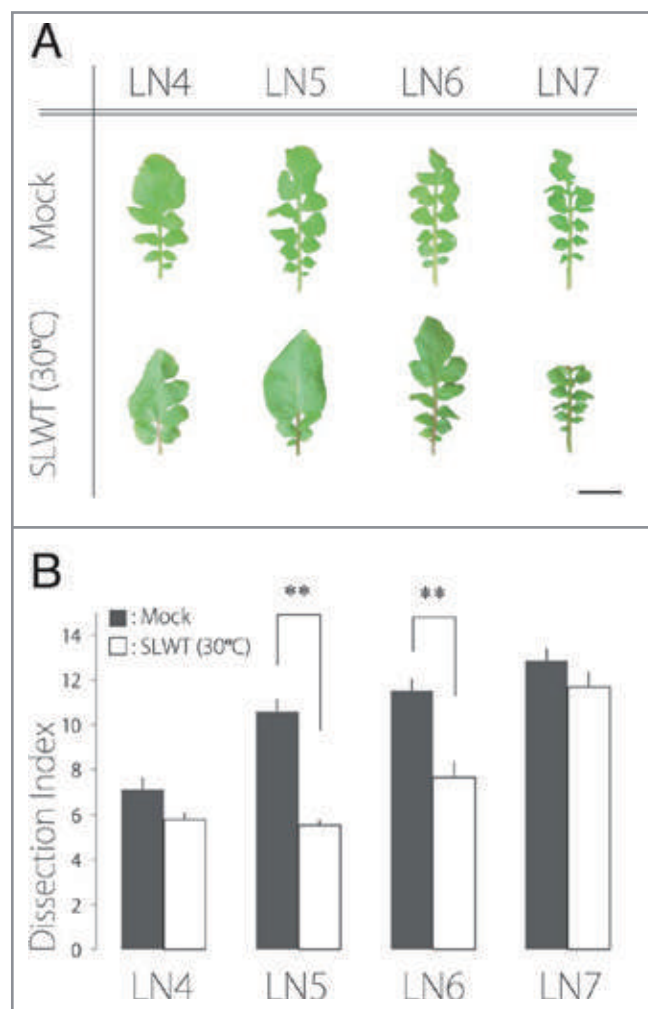


Figure 2. Leaf morphology and dissection index after single-leaf warming treatment. (A) Effects of single-leaf warming treatment (SLWT). LN3 was warmed at 30°C or cooled at 20°C using a plate-type temperature control system for 30 days in chamber maintained at 20°C. Upper: leaves from plants grown at 20°C with SLWT (20°C; mock-treated control); Lower: leaves from plants grown at 20°C with SLWT (30°C). The oldest leaf is shown on the left and the youngest on the right. Bar = 2 cm. (B) Dissection index (DI) of leaves. Error bars represent the standard error (SE); ** = $p < 0.01$ based on Welch's t -tests ($n = 4$; 2 plants were treated per single experiment).

interpretations. One possibility is that the long distance signal is only generated at a certain developmental stage of leaves. After the stage elapses, the signaling mechanism becomes less effective. Another possibility is that the signal from a leaf subjected to the warming treatment becomes weak owing to signals from other, newly developed leaves that are not treated. Indeed, the SLWT (30°C) did not totally mimic leaf form of plants maintained at 30°C (Fig. 2B). The result suggests that the signal from a leaf subjected to the treatment is not enough to mimic the leaf form of plants maintained at 30°C, and that signals from multiple leaves may be needed to fully mimic. In fact, both mechanisms may affect the form of newly developed leaves. In *R. aquatica*, GA is involved in leaf form alterations,⁷ suggesting that the relationship between GA and the long distance signal should be investigated. Although a recent study showed a gradation in the concentration of GA in maize leaves,¹⁶ little is known about their translocation and effect on other leaves. Therefore, the detailed mechanisms require further investigation.

In this study, we demonstrated that the morphology of newly developed leaves is regulated by signals from older leaves in the heterophylly of *R. aquatica*. Thus, an understanding of heterophylly will provide new insights into the relationship between

developed and developing leaves with respect to the formation of the appropriate final leaf morphology at the individual plant level.

Disclosure of Potential Conflicts of Interest

No potential conflicts of interest were disclosed.

Acknowledgments

We thank Dr. Mitsutomo Abe for helpful suggestions regarding the single-leaf treatment using a plate-type temperature control system.

Funding

This work was partially supported by Grants-in-Aid from the Japan Society for the Promotion of Science (JSPS) (KAKENHI Grant Numbers 22870031 and 24770047), the Science Research Promotion Fund from the Promotion and Mutual Aid Corporation for Private Schools of Japan to S.K., MEXT-Supported Program for the Strategic Research Foundation at Private Universities and by a Research Fellowship from JSPS to H.N.

References

1. Wanke D. The ABA-mediated switch between submersed and emerged life-styles in aquatic macrophytes. *J Plant Res* 2011; 124:467-75; PMID:21674229; <http://dx.doi.org/10.1007/s10265-011-0434-x>
2. Zotz G, Wilhelm K, Becker A. Heteroblasty—A Review. *Botanical Rev* 2011; 77:109-51; <http://dx.doi.org/10.1007/s12229-010-9062-8>
3. Cook SA, Johnson MP. Adaptation to heterogenous environments I. Variation in heterophylly in *Ranunculus flammula* L. *Evolution* 1968; 22:496-516; <http://dx.doi.org/10.2307/2406876>
4. Kuwabara A, Ikegami K, Koshihara T, Nagata T. Effects of ethylene and abscisic acid upon heterophylly in *Ludwigia arcuata* (Onagraceae). *Planta* 2003; 217:880-7; PMID:12844266; <http://dx.doi.org/10.1007/s00425-003-1062-z>
5. Iida S, Miyagi A, Aoki S, Ito M, Kadono Y, Kosuge K. Molecular adaptation of *rbcL* in the heterophyllous aquatic plant *Potamogeton*. *PLoS One* 2009; 4:e4633; PMID:19247501; <http://dx.doi.org/10.1371/journal.pone.0004633>
6. Nakamasu A, Nakayama H, Nakayama N, Suematsu NJ, Kimura S. A developmental model for branching morphogenesis of lake cress compound leaf. *PLoS One* 2014; 9:e111615; PMID:25375102; <http://dx.doi.org/10.1371/journal.pone.0111615>
7. Nakayama H, Nakayama N, Seiki S, Kojima M, Sakakibara H, Sinha N, Kimura S. Regulation of the KNOX-GA gene module induces heterophyllic alteration in North American lake cress. *Plant Cell* 2014; 26:4733-48; PMID:25516600; <http://dx.doi.org/10.1105/tpc.114.130229>
8. Koenig D, Weigel D. Beyond the thale: comparative genomics and genetics of Arabidopsis relatives. *Nat Rev Genet* 2015; 16:285-98; PMID:25854181; <http://dx.doi.org/10.1038/nrg3883>
9. Hepworth J, Lenhard M. Regulation of plant lateral-organ growth by modulating cell number and size. *Curr Opin Plant Biol* 2014; 17:36-42; PMID:24507492; <http://dx.doi.org/10.1016/j.pbi.2013.11.005>
10. Vlad D, Kierzkowski D, Rast MI, Vuolo F, Dello Ioio R, Galinha C, Gan X, Hajheidari M, Hay A, Smith RS, et al. Leaf shape evolution through duplication, regulatory diversification, and loss of a homeobox gene. *Science* 2014; 343:780-3; PMID:24531971; <http://dx.doi.org/10.1126/science.1248384>
11. Woodward F. Stomatal numbers are sensitive to increases in CO₂ from pre-industrial levels. *Nature* 1987; 327:617-8; <http://dx.doi.org/10.1038/327617a0>
12. Yano ST, I. Separate localization of light signal perception for sun or shade type chloroplast and palisade tissue differentiation in *Chenopodium album*. *Plant Cell Physiol* 2001; 42:1303-10; PMID:11773522; <http://dx.doi.org/10.1093/pcp/pce183>
13. Miyazawa S, Livingston NJ, Turpin DH. Stomatal development in new leaves is related to the stomatal conductance of mature leaves in poplar (*Populus trichocarpus* P. deltoides). *J Exp Bot* 2006; 57:373-80; PMID:16172139; <http://dx.doi.org/10.1093/jxb/eri278>
14. Jiang CD, Wang X, Gao HY, Shi L, Chow WS. Systemic regulation of leaf anatomical structure, photosynthetic performance, and high-light tolerance in sorghum. *Plant Physiol* 2011; 155:1416-24; PMID:21245193; <http://dx.doi.org/10.1104/pp.111.172213>
15. Notaguchi M, Abe M, Kimura T, Daimon Y, Kobayashi T, Yamaguchi A, Tomita Y, Dohi K, Mori M, Araki T. Long-distance, graft-transmissible action of Arabidopsis FLOWERING LOCUS T protein to promote flowering. *Plant Cell Physiol* 2008; 49:1645-58; PMID:18849573; <http://dx.doi.org/10.1093/pcp/pcn154>
16. Nelissen H, Rymen B, Jikumaru Y, Demuyneck K, Van Lijsebettens M, Kamiya Y, Inzé D, Beemster GT. A local maximum in gibberellin levels regulates maize leaf growth by spatial control of cell division. *Curr Biol* 2012; 22:1183-7; PMID:22683264; <http://dx.doi.org/10.1016/j.cub.2012.04.065>



2019.12.13 第57回植物バイテクシンポジウム
変身する生き物、変身させる生き物



環境に応じて変身する植物：
*Rorippa aquatica*の異形葉性の研究

木村成介
京都産業大学
生命科学部・生態進化発生学研究センター

1

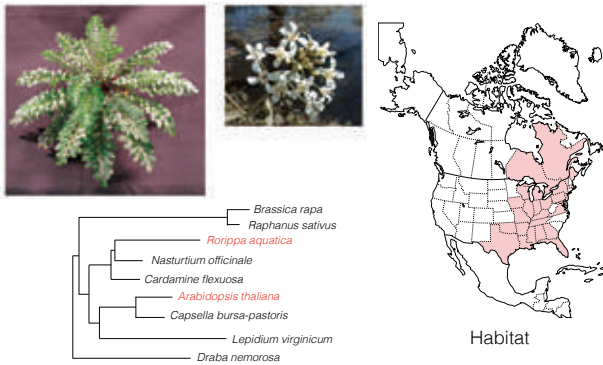
Diversity of leaf shape



One of the most diverse characters in all of biology

2

North American Lake cress, *Rorippa aquatica* (Brassicaceae)



An herbaceous perennial aquatic mustard found in marsh

3

Heterophylly of Lake cress
異形葉性（葉の形態の表現型可塑性）

Terrestrial condition

Submerged condition

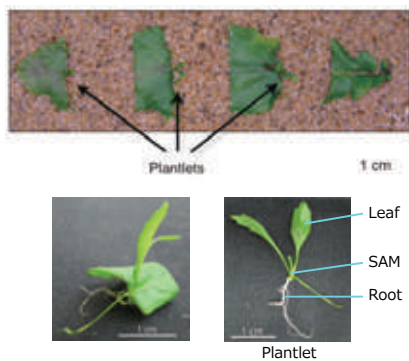


Nakayama et al. 2014

Adaptive response to marsh environments

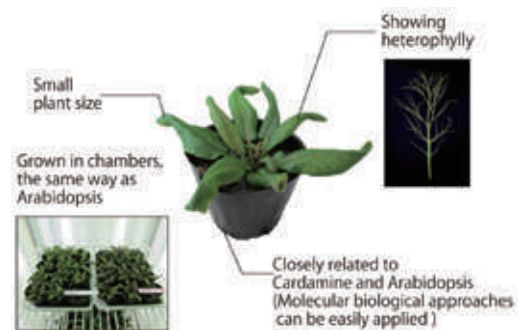
4

Rorippa aquatica: Vegetative propagation



5

Advantages as a model



Nakayama et al. 2012

Lake cress is an excellent model to study heterophylly

6

Aim of the research

Revealing the developmental processes and molecular mechanism underlying **heterophylly** and **regeneration** of *Rorippa aquatica*

- Developmental Analysis
- Genome analysis
- Transcriptome analysis

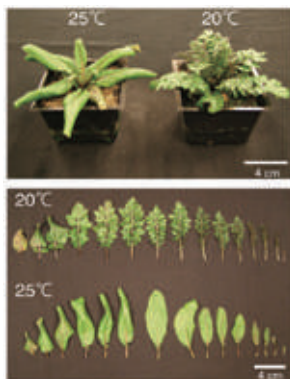
Ecological and Evolutionary Developmental Biology
(Eco-Evo-Devo/生態進化発生学)

7

Developmental Analysis

8

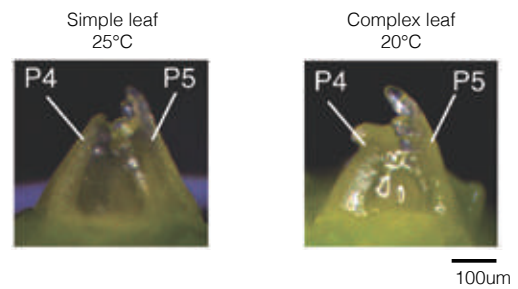
Heterophylly of Lake cress



Leaf form alternation is induced by ambient temperature

9

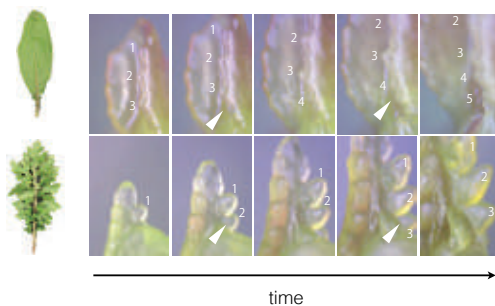
Leaf primordia of Lake cress



Leaf shape is determined in early stage of leaf development

10

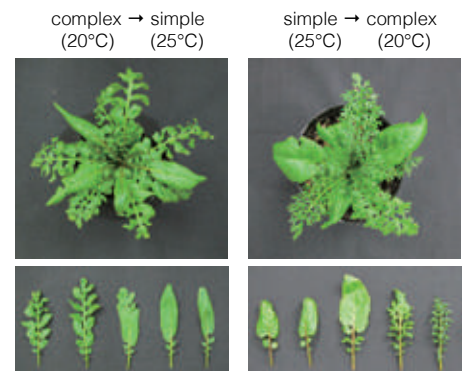
Time-lapse observations of leaf development



Basal part is important for the morphogenesis

11

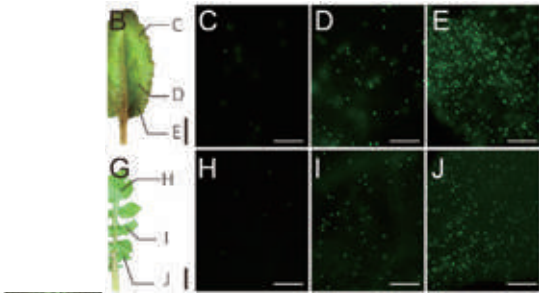
Temperature shift analysis



Basal part of LP is important for leaf shape determination

12

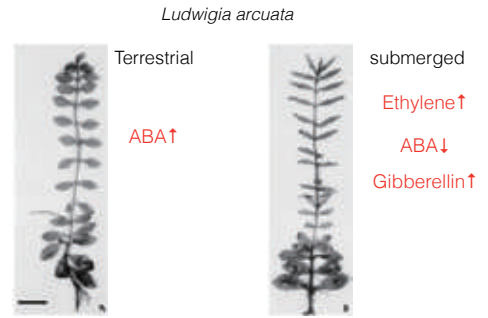
Detection of cell proliferation zone in leaves by EdU



Mitotic cells were concentrated in basal part of LP

13

Importance of phytohormones

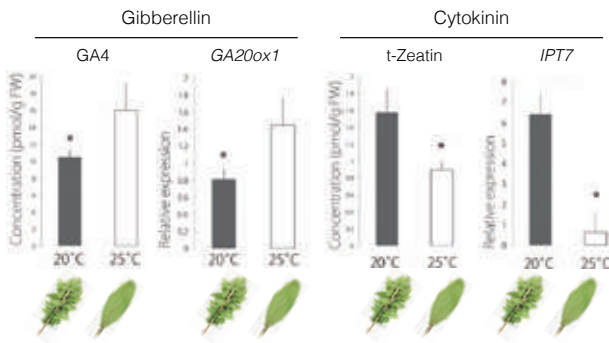


Kuwabara et al. 2003

Phytohormones is known to be involved in the heterophylly

14

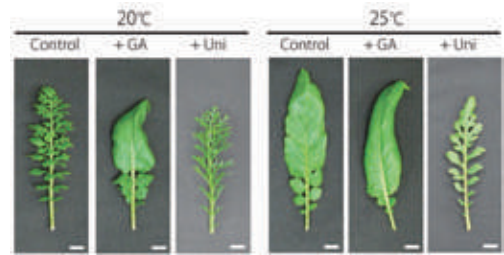
Quantification of phytohormones



GA is lower and tZeatin is higher in compound leaf condition

15

Effect of GA application



GA is sufficient for alternation of leaf form

16

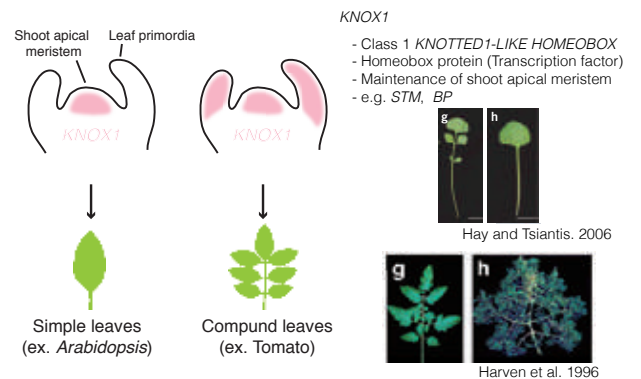
Effect of phytohormones in heterophylly



GA and CK must be key phytohormones for the heterophylly

17

KNOX1 and compound leaf development



KNOX1 is a TF that is involved in compound leaf development

18

Function of KNOX1

KNOX homeodomain protein directly suppresses the expression of a gibberellin biosynthetic gene in the tobacco shoot apical meristem

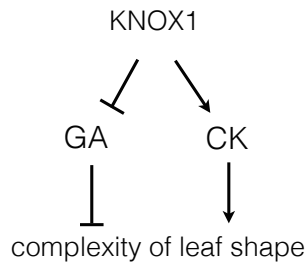
Tomomi Matsuoka, Yoshio Saito, Masaki Inagaki, Kazuo Mochida, and Masao Shimizu
Journal of Experimental Botany, Volume 51, Number 1, January 2000, pp. 117-123, doi: 10.1093/jxb/51.1.117

Published: 01-01-2000 07:10:00 AM

Cytokinin Regulates Compound Leaf Development in Tomato

Mark Stone, Nadia Ben-Hery, Sherrill Shuman-Barker, Roger Bailey, David Moore, and Robert Hill
The Journal of Heredity, Volume 93, Number 1, February 2002, pp. 40-45, doi: 10.1093/heredity/93.1.40

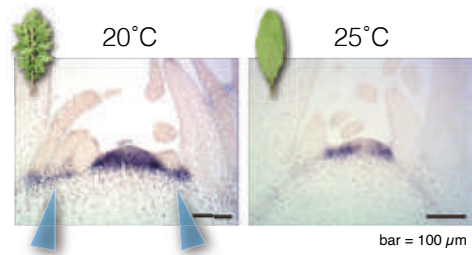
Published: 02-01-2002 07:10:00 AM



KNOX1 suppresses GA and promotes CK

19

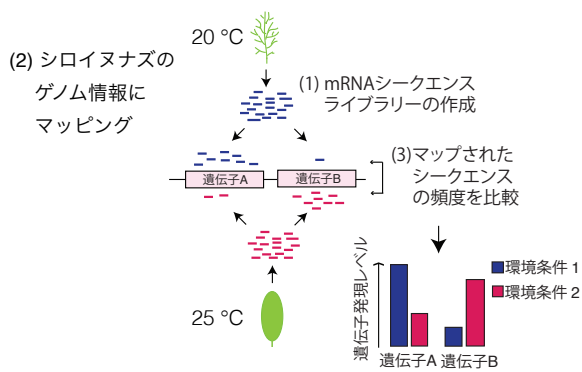
Expression pattern of a KNOX1 gene (*NaSTM*)



NaSTM expression is changed in compound leaf condition

20

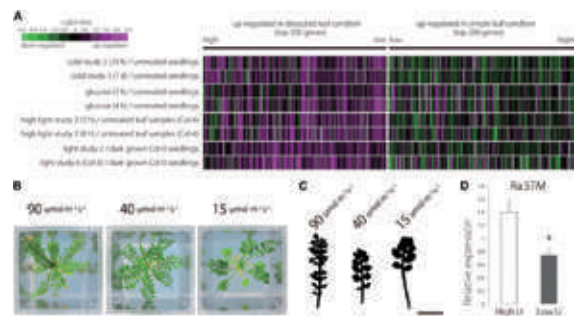
RNA-seqによる網羅的遺伝子発現解析



シロイヌナズナのゲノムを参照配列にする

21

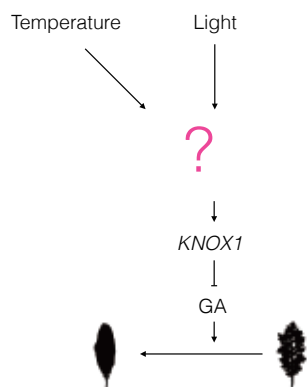
RNA-seqの結果



光も葉の形に影響することがわかった

22

Model



23

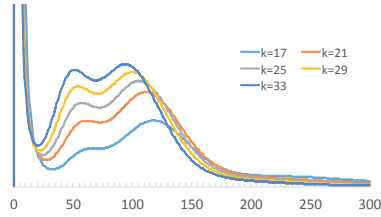
Genome Analysis

24

Genome size estimation based on K-mer distribution



2n = 30



	k=17	k=21	k=25	k=29	k=33
total number of k-mers (x10 ⁶)	49,594	47,728	45,964	44,055	42,019
peak frequency	117	111	105	100	95
estimated genome size (Mbase)	423.89	429.99	437.76	440.55	442.31

Estimated genome size is 420 - 450 Mbp

25

Genome sequencing

Illumina sequencing (200X coverage)

	read length	insert size	yield (Gbase)
Line A	150bp x 2	600	97.62
	300bp x 2	600	2.9
Line J	150bp x 2	600	109.43
	300bp x 2	600	2.8

PacBio sequencing for Line A (30X coverage)

Library	Sequenced PacBio cell number	average read number / pacbio cell	average read length	total yields (Mbase)
RaA 1st	10	90,157	2,761	2,498
RaA 2nd	5	112,309	8,102	4,549
RaA-3rd	10	80,782	10,674	8,658

We got enough sequence data

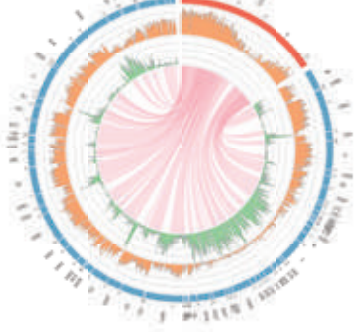
26

Genomic analysis of *R. aquatica*

illumina (200x) + PacBio (30x)

Rorripa aquatica

Cardamine hirsuta



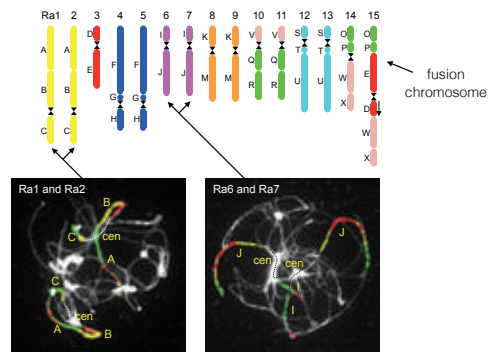
- Contigs : 1,797
- Total length : 440 Mbp
- GC : 35.26 %
- N50 : 1.35 Mbp
- Largest : 8.9 Mbp
- Genes : 49,599
- Transcripts : 117,530
- High synteny
- Genome duplication

27

Comparative cytogenetics



2n = 30

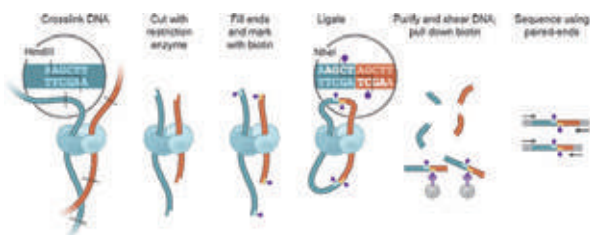


Collaboration with T. Mandakova and M.A. Lysak, CEITEC, Masaryk Univ.

2n = (16 x 2) - 2 = 30

28

Chromosome Conformation Capture Sequencing (Hi-C)



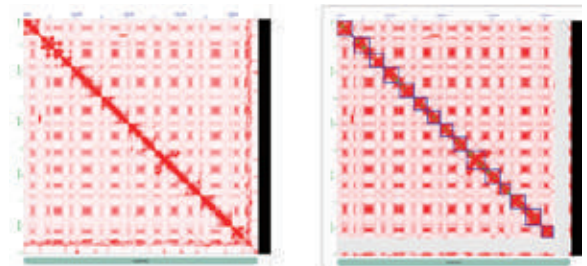
染色体の近い配列を同定できる
(応用生物・松永先生と坂本先生との共同研究)

29

Chromosome Conformation Capture Sequencing (Hi-C)

automatic

manual

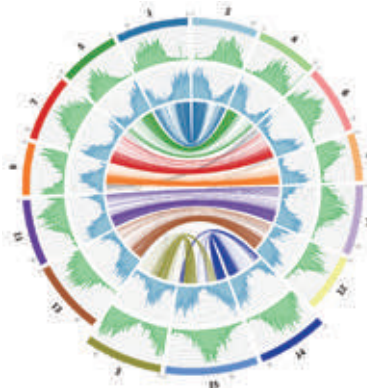


15 chromosome like sequences and 2043 scaffolds
94.4 % of core genes (1440 genes) were found on the chromosome like sequences

松永研との共同研究

30

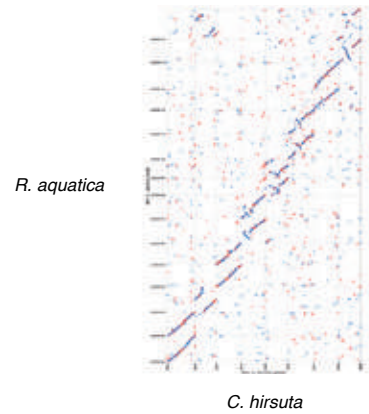
Chromosome level assembly of *R. aquatica* genome



Chr. # : 15
 Total length : 450 Mbp
 GC : 35.31 %
 N50 : 30.00 Mbp
 Largest : 35.6 Mbp
 Genes : 46,200
 Transcripts : 94,666

31

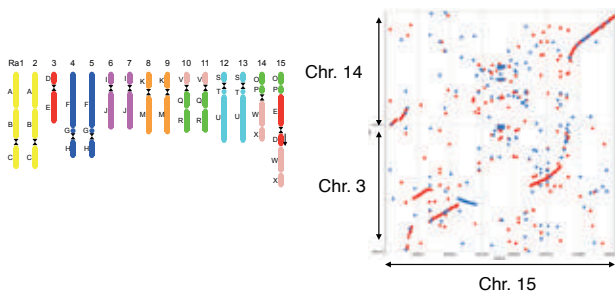
Similarity between *R. aquatica* and *C. hirsuta*



C. hirsuta

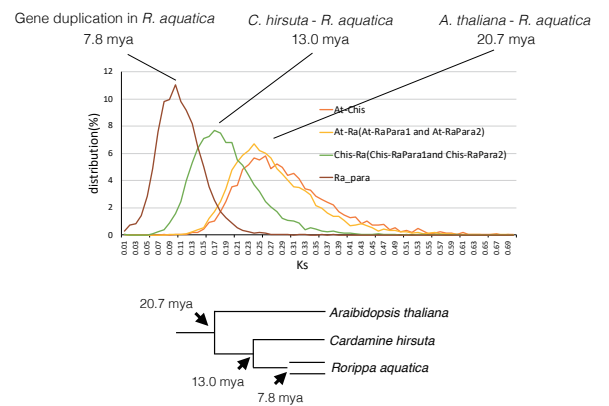
32

Fusion chromosome



33

Divergence time estimation

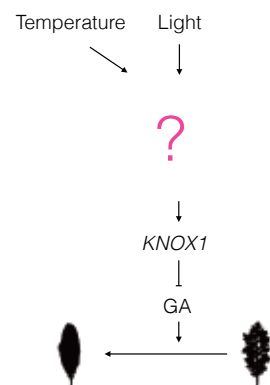


34

Transcriptome Analysis

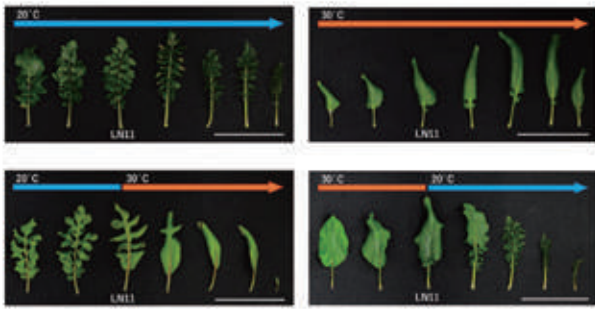
35

Model



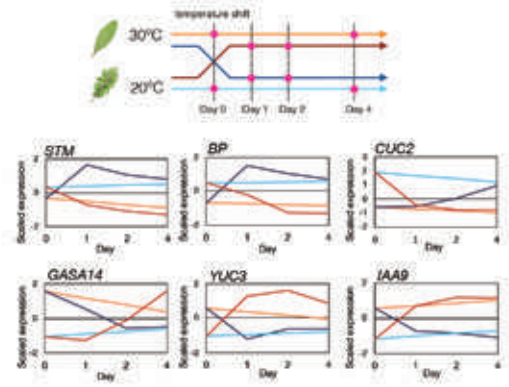
36

Temperature shift



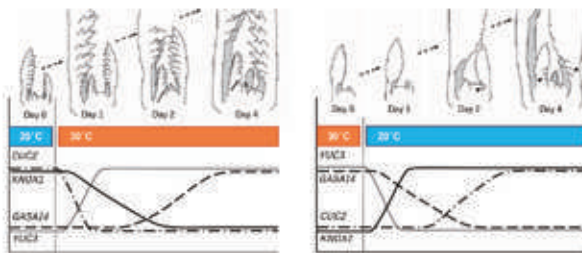
37

RNA-seq for Temperature shift



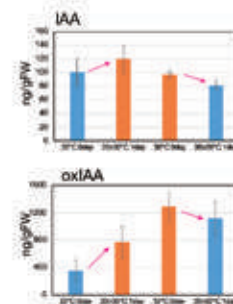
38

RNA-seq for submergence response



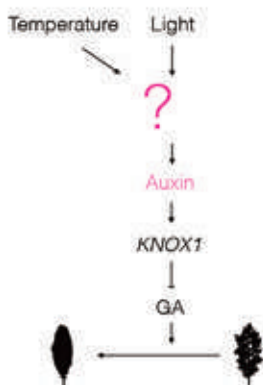
39

Quantification of auxin



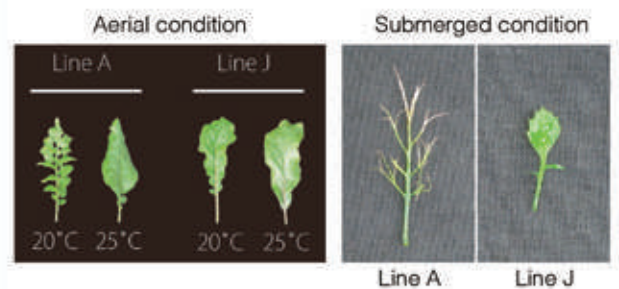
40

Model



41

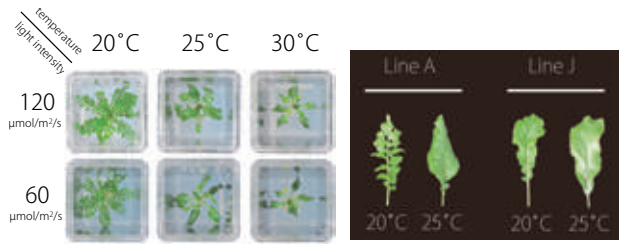
Natural variation of *R. aquatica*



Line A and J show different response

42

RNA-seq analysis

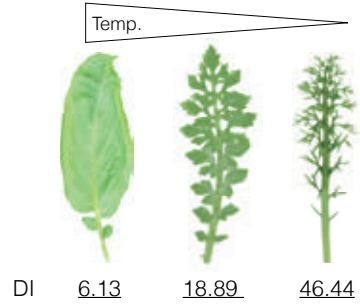


6 conditions x 2 accessions x 4 biological replicates

48 libraries are sequenced and mapped to *de novo* assembled contigs fro global expression analysis

43

Correlation analysis (gene expression vs. leaf shape)

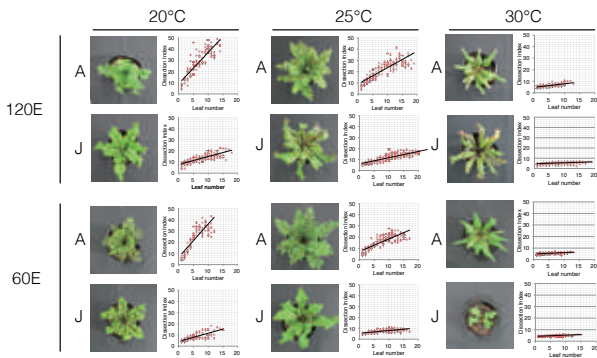


Dissection Index (DI) = (perimeter)/($\sqrt{\text{area}}$)

Complexity of leaf shape can be quantified

44

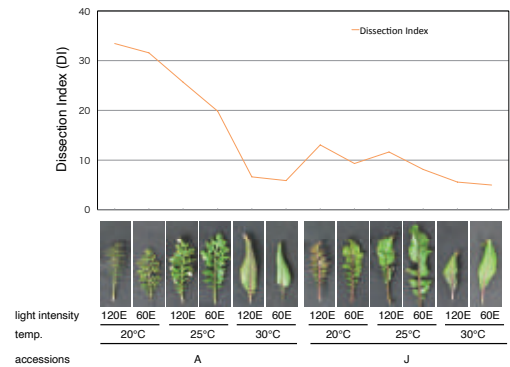
Dissection Index



Complexity of leaf shape were quantified

45

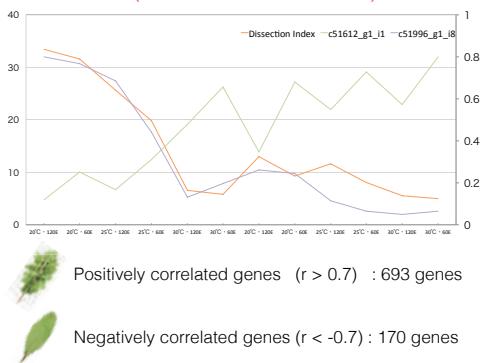
Correlation analysis (gene expression vs. leaf shape)



Complexity of leaf shape were quantified

46

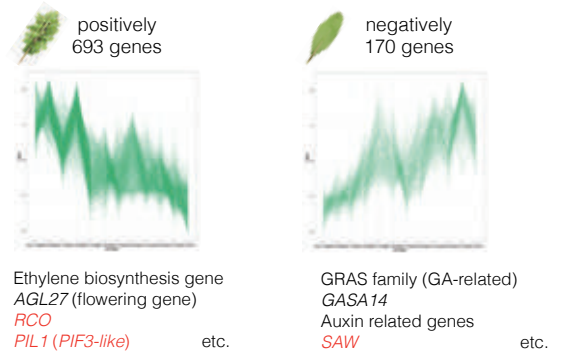
Pearson's correlation analysis (with dissection index)



Important genes might be able to be identified

47

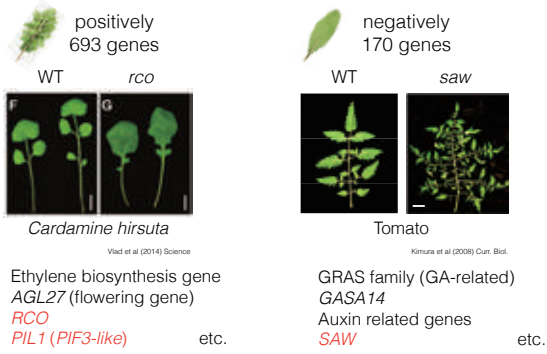
Correlated genes



Bunch of genes are identified

48

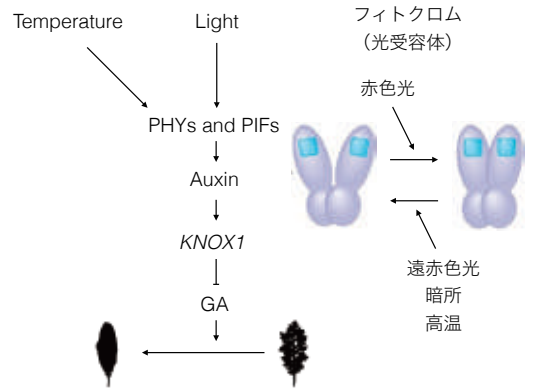
Correlated genes



Bunch of genes are identified

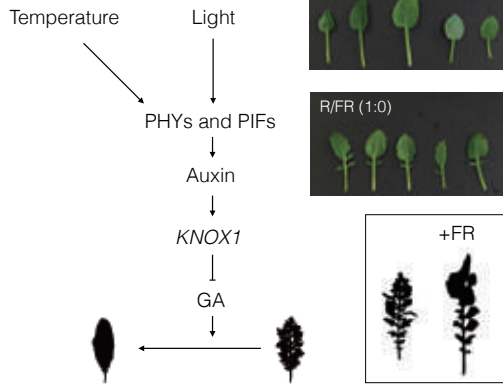
49

Model



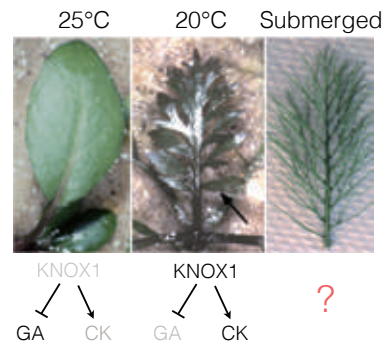
50

Model



51

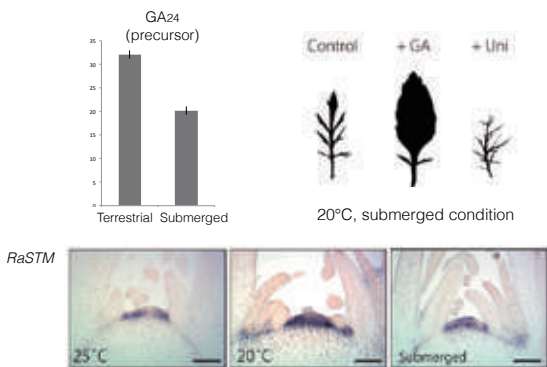
Submerged leaf shape



What is going on at submerged condition?

52

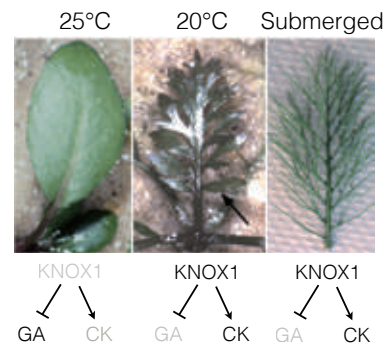
GA level and KNOX1 expression in submerged condition



KNOX-GA module is changed also in submerged condition

53

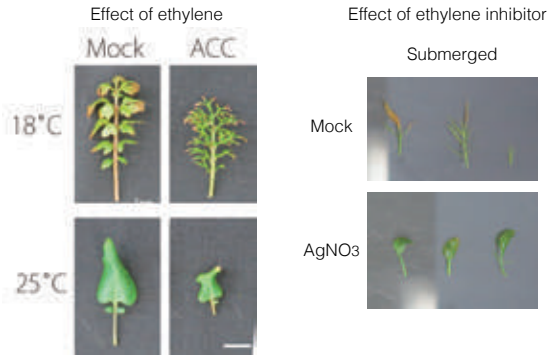
Heterophylly and phytohormones



Ethylene ?

54

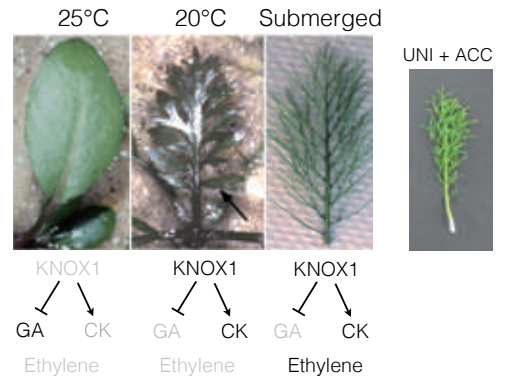
Effect of ethylene and inhibitor



Ethylene is also involved in leaf shape change

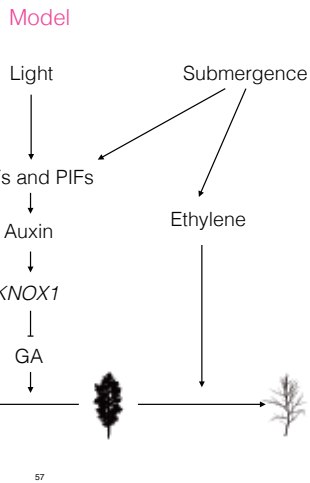
55

Heterophylly and phytohormones

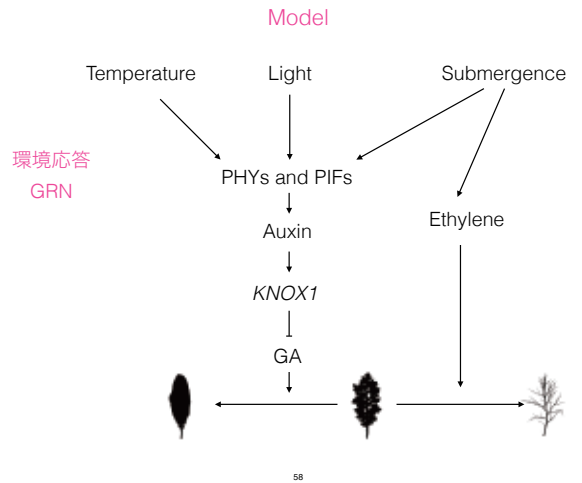


GA and Ethylene are important for the heterophylly

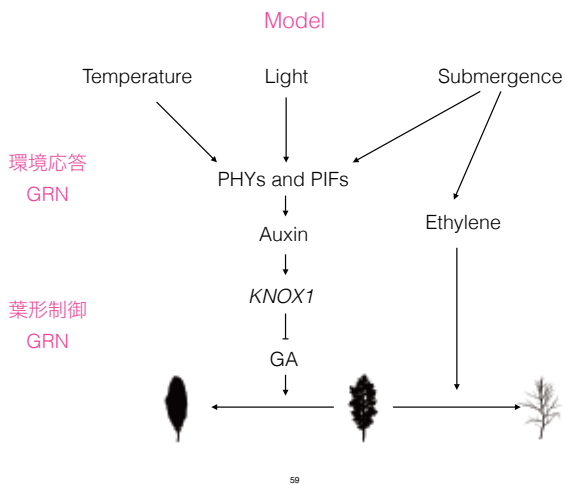
56



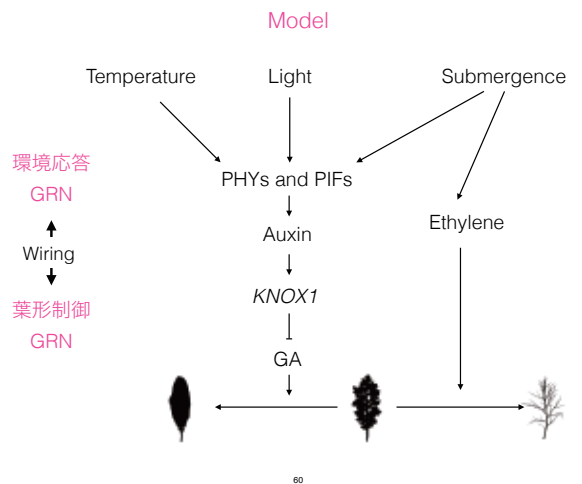
57



58



59



60

変身する植物・変身させられている植物



発生プログラム

環境

表現型可塑性

誘導

分化全能性

幹細胞



61

Acknowledgements



Kyoto Sangyo University

Dr. Tomoaki Sakamoto

Dr. Shuka Ikematsu

Kaori Kaminoyama

Rumi Amano

Risa Momoi

Shuji Yamaguchi



University of California, Davis

Dr. Neelima Sinha



University of Edinburgh

Dr. Naomi Nakayama

Masaryk Univ.



Dr. Martin A. Lysak



The University of Tokyo

Dr. Hokuto Nakayama



RIKEN

Dr. Keiko Sugimoto

Dr. Momoko Ikeuchi

Dr. Yasunori Ichihashi

Dr. Hitoshi Sakakibara

Dr. Mikiko Kojima



TAT Tokyo Univ. of Agri. and Tech.

Dr. Hiroyuki Kasahara

Tokyo Gakugei Univ.



Dr. Ali Ferjani

62



Plant regeneration in nature: Studies on natural vegetative propagation

Seisuke Kimura

Faculty of Life Sciences
Center for Ecological Evolutionary Developmental Biology
Kyoto Sangyo University

1

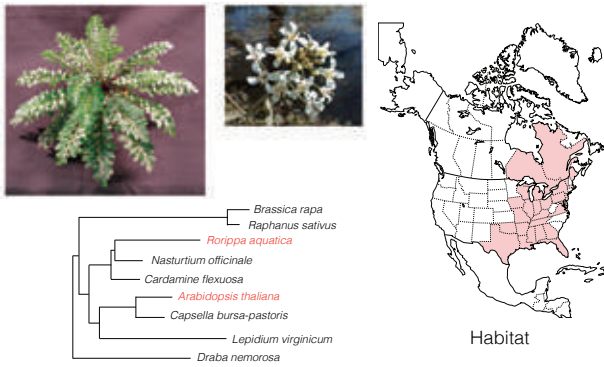
Plant regeneration in nature



The underlying mechanisms are largely unknown

2

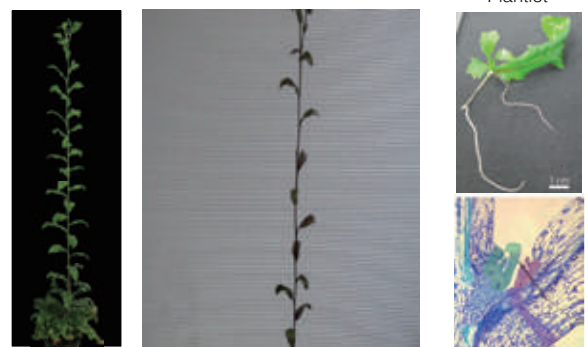
Rorippa aquatica (Brassicaceae)



Propagate by two type of vegetative propagation

3

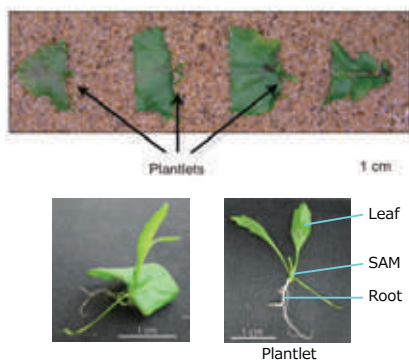
Vegetative propagation of *R. aquatica*



Specialized buds for vegetative propagation are formed

4

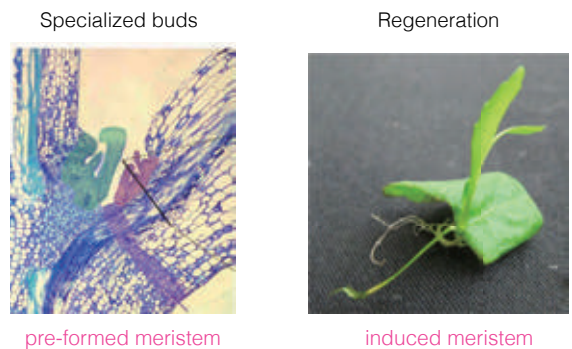
Regeneration of *R. aquatica*



De novo organogenesis without any external treatments

5

Two ways for vegetative propagation



pre-formed meristem

induced meristem

6

Aim of the research

Revealing the developmental processes and molecular basis for vegetative propagation of *Rorippa aquatica*



- Developmental analysis
- Genome analysis
- Transcriptome analysis

7

Developmental analysis

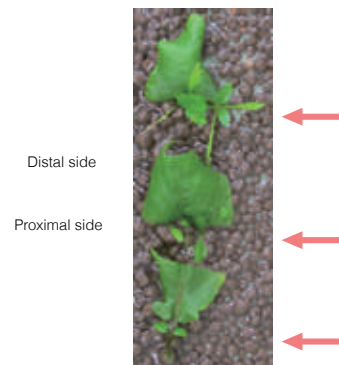
8

Regeneration of *R. aquatica*



9

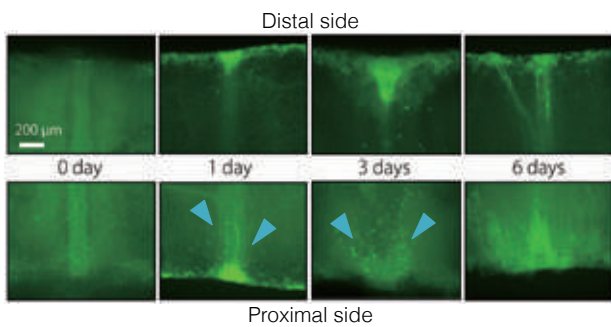
Regeneration of *R. aquatica*



Plantlet forms only at proximal side of leaf fragments

10

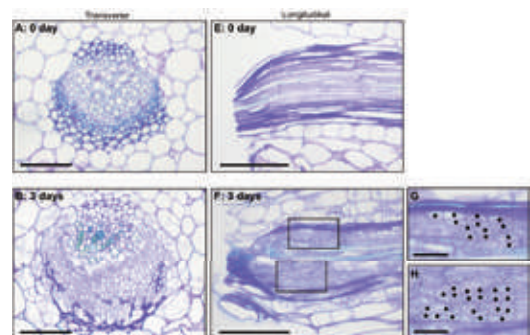
Visualization of cell proliferation by EdU



Cell proliferation is re-started after 1 day

11

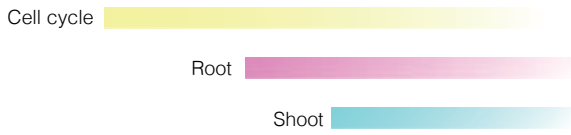
Cell division pattern



Dividing cells are found around vascular tissue

12

Regeneration process of *R. aquatica*



Molecular basis ?

Genome and transcriptome analysis

13

Genomic analysis

14

Genomic analysis of *R. aquatica*

illumina (200x) + PacBio (30x)

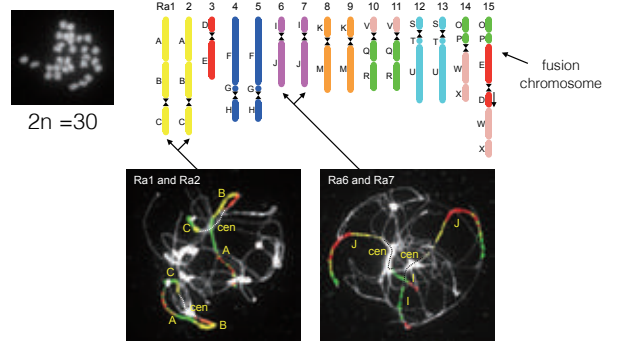


Contigs : 1,797
 Total length : 440 Mbp
 GC : 35.26 %
 N50 : 1.35 Mbp
 Largest : 8.9 Mbp
 Genes : 49,599
 Transcripts : 117,530
 High synteny
 Genome duplication

We got nice assembled genome sequence data

15

Comparative cytogenetics

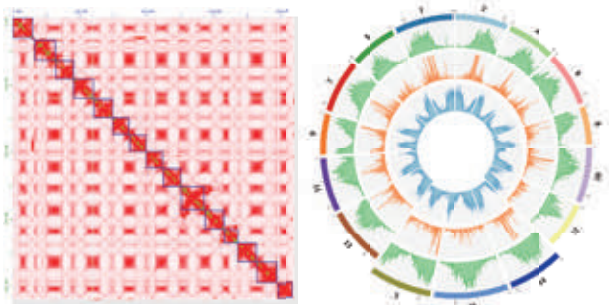


Collaboration with T. Mandakova and M.A. Lysak, CEITEC, Masaryk Univ.

$$2n = (16 \times 2) - 2 = 30$$

16

Chromosome Conformation Capture Sequencing (Hi-C)



Collaboration with Dr. Sakamoto and Dr. Matsunaga, Tokyo Univ. of Science

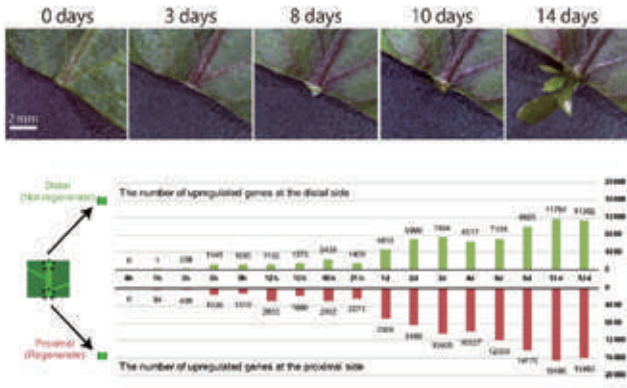
15 chromosome like sequences and 2043 scaffolds
 94.4 % of core genes (1440 genes) were found on
 the chromosome like sequences

17

Transcriptome analysis

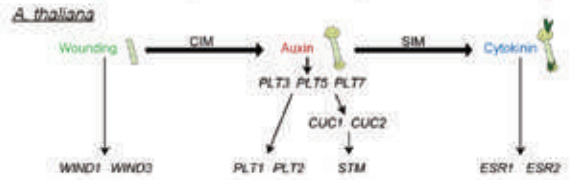
18

Time-series RNA-seq analysis



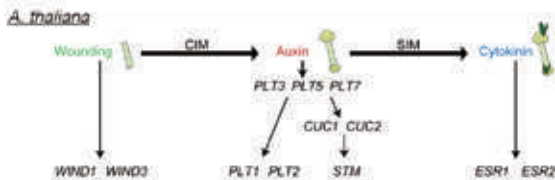
18

Gene expression profiles for the regeneration-related genes



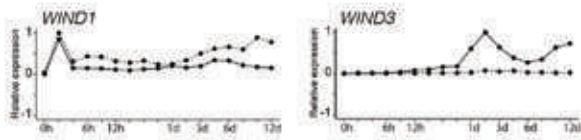
20

Gene expression profiles for the regeneration-related genes



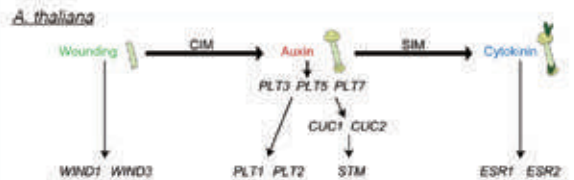
R. aquatica

Wound response



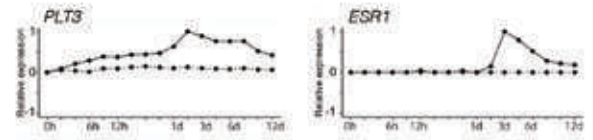
21

Gene expression profiles for the regeneration-related genes



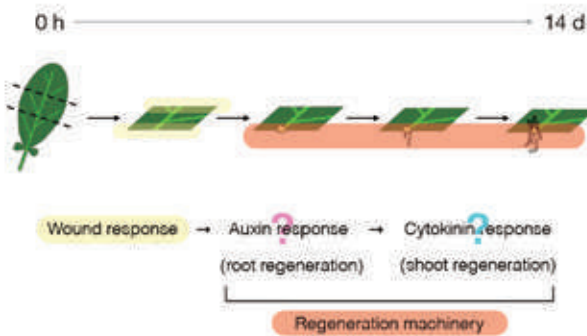
R. aquatica

regeneration



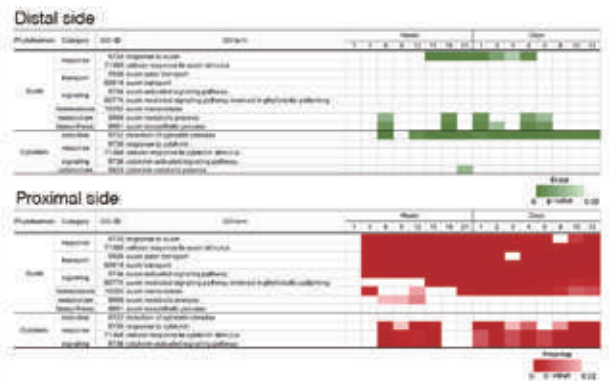
22

Regeneration of *R. aquatica*



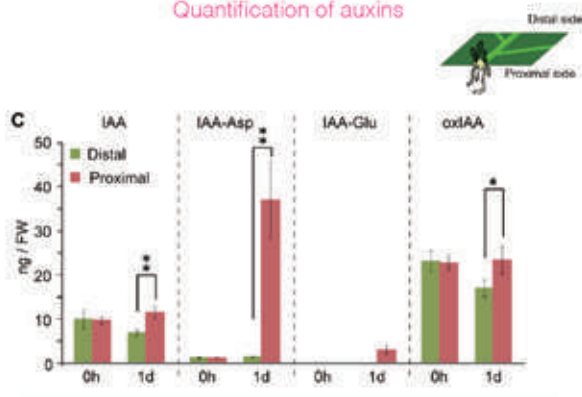
23

GO enrichment analysis for DEGs



24

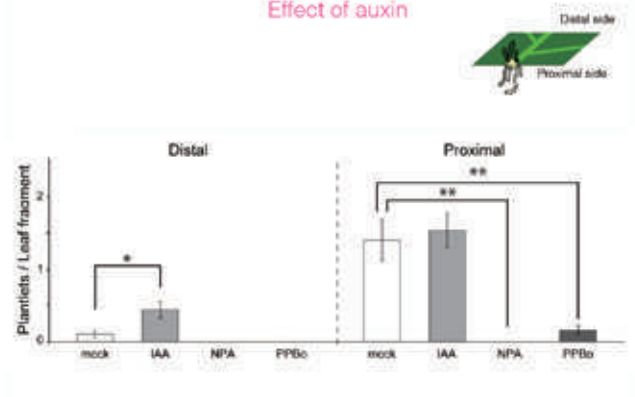
Quantification of auxins



Auxins are accumulated at proximal side

28

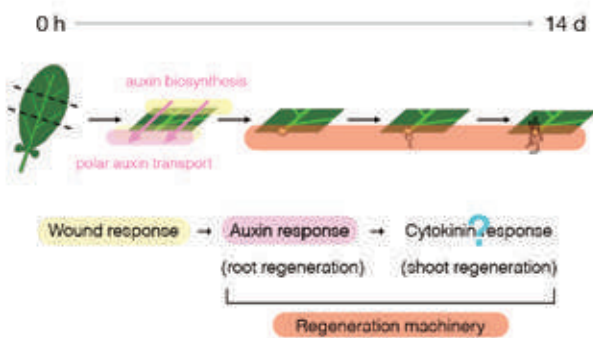
Effect of auxin



Auxin is important for regeneration

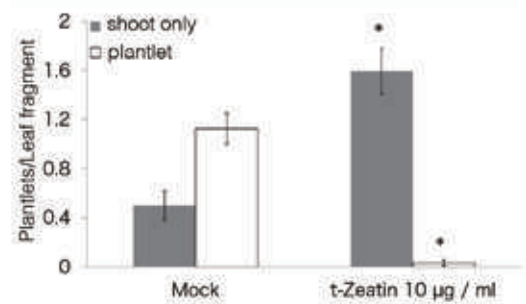
28

Regeneration of *R. aquatica*



27

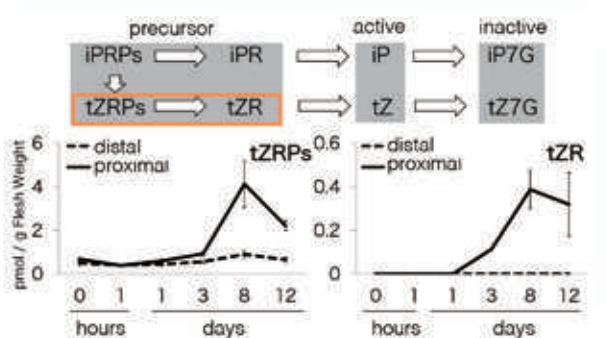
Effect of cytokinin



Cytokinin is important for shoot regeneration

28

Quantification of cytokinin

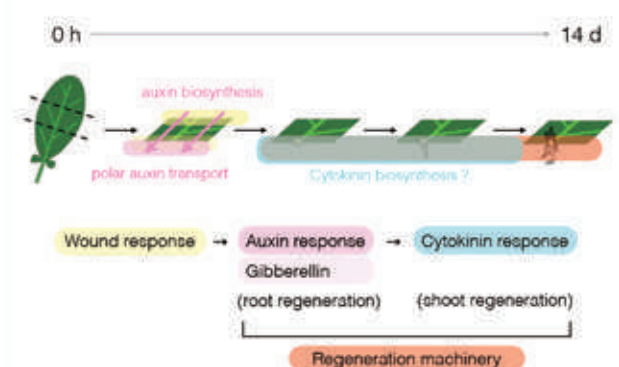


Collaboration with Dr. Sorachitani, RKEF

Cytokinin is up-regulated

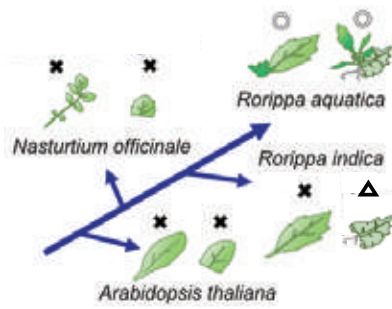
28

Summary



28

Future plan



Revealing the molecular basis and evolutionary background for natural vegetative propagation by a comparative genomics approaches

31

Acknowledgements

- | | | | |
|---|---|---|--|
|  | Kyoto Sangyo University
Rumi Amano
Risa Momoi
Dr. Tomoaki Sakamoto
Dr. Shuka Ikematsu
Kaori Kaminoyama |  | Tokyo Gakugei Univ.
Dr. Ali Ferjani |
| | |  | Tokyo Univ. of Agri. and Tech.
Dr. Hiroyuki Kasahara |
| | |  | RIKEN
Dr. Keiko Sugimoto
Dr. Momoko Ikeuchi
Dr. Hitoshi Sakakibara
Dr. Mikiko Kojima |
|  | University of California, Davis
Dr. Neelima Sinha
Dr. Hokuto Nakayama | | Warwick University
Dr. Jose Gutierrez-Marcos |
|  | University of Edinburgh
Dr. Naomi Nakayama |  | Tokyo University of Science
Dr. Sachihiro Matsunaga |
|  | Masaryk Univ.
Dr. Martin A. Lysak |  | Dr. Takuya Sakamoto |

32

「野生植物集団の遺伝的多様度と変異の維持機構」

「Genetic diversity and its maintenance mechanism in wild plant populations」

河邊昭

京都産業大学

1

これまでの（これからも）研究目標

植物野生集団がもつDNA変異の維持機構の解明

染色体構造のDNA変異に及ぼす効果の解明

- 1) 動原体領域の進化
- 2) 組換え量が種内変異量に与える影響
- 3) エピジェネティックな制御を受ける遺伝子の進化機構

2

研究の入り口

京都大学農学部 植物遺伝学研究室（遠藤隆 宮下直彦 那須田周平）

ヤマノイモ属の *PgiC* 遺伝子の分子進化 日本遺伝学会 6 9 回大会
G G S 72 : 253-262 1997

シロイヌナズナの種内多型 G G S 78 : 11-21 2003

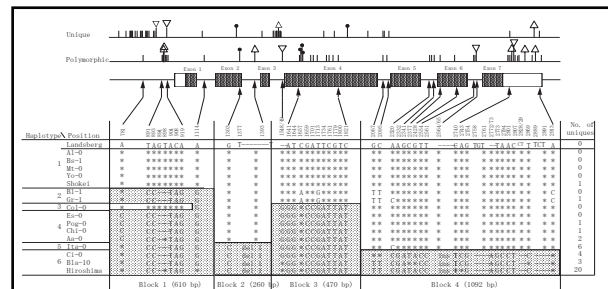
シロイヌナズナ近縁種の種内多型 G G S 77 : 159-165 2002

G G S 77 : 167-175 2002

植物のコドンバイアス G G S 78 : 343-352 2003

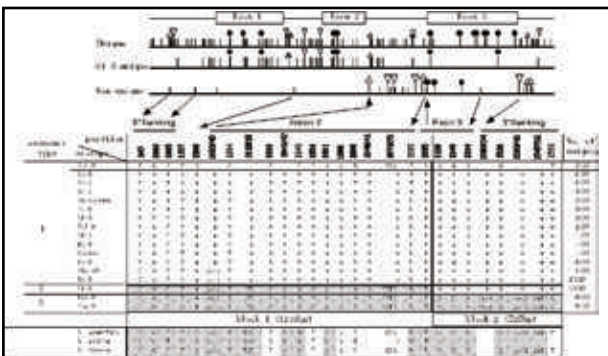
シロイヌナズナ近縁種の動原体構造 G G S 81 : 287-290 2006

3



Summary of DNA polymorphism at the *Adh* locus (Innan et al. Genetics 1996)

4



Summary of DNA polymorphism at the *ChiA* locus. (Kawabe et al. MBE 1997)

5

シロイヌナズナ *Arabidopsis thaliana*

- 2倍体 ($2n = 2x = 10$)
- 小さいゲノムサイズ (130MB)
- 短い世代時間 (2~6か月)
- 自殖性 (99.7%)

- 世界中に分布
- 比較的開けた場所に生息

ハクサンハタザオ *Arabidopsis halleri ssp. gemmifera*

- シロイヌナズナの最も近縁な種の一つ
- 2倍体 ($2n = 2x = 16$)
- 他殖性

- 日本、朝鮮半島、中国等に分布
- 林床や川沿い等の比較的暗く湿った場所に生息

6



7

ハクサンハタザオにおける種内変異の比較

領域	<i>Adh</i>	<i>ChiA</i>	<i>PgiC1</i>	<i>PgiC2</i> ϕ
全体の変異量	0.0053	0.0032	0.0033	0.0033
翻訳領域の変異量	0.0040	0.0025	0.0027	0.0044
イントロンの変異量	0.0041	0.0022	0.0033	0.0027
Singletonの割合	94%	97%	87%	91%
Tajima のテスト	有意 (負)	有意 (負)	有意 (負)	有意 (負)
非同義置換の割合	80%	69%	52%	68%
MK テスト	有意	有意	有意	有意

8

ハクサンハタザオのDNA多型

- 1) 変異量が異なる遺伝子座、領域で同程度
- 2) 過剰にsingletonが存在
- 3) 高い非同義置換の割合

ハクサンハタザオの集団構造の影響?

Kawabe and Miyashita MBE 2003

9

1) 動原体領域の進化

動原体のパラドックス：
機能的、構造的に非常に高度に保存されているにもかかわらず、DNA配列レベルでは殆ど類似性が見られない。

機能 紡錘糸の接着による染色体分離
間期の染色体の位置取り

クロマチン構造 非常に高度に凝集
ヒストンやDNAの特異的な修飾
動原体特異的たんぱく質の存在

DNA配列 縦列型反復配列 (種特異的、100-500bp)
転移因子の存在

10

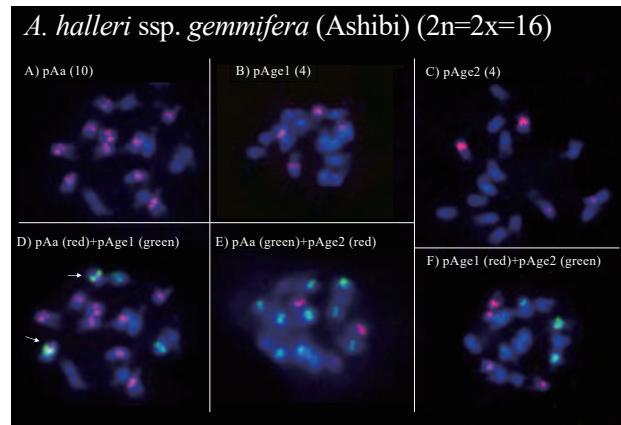
種特異的動原体反復配列

動原体の機能的部位は高度反復配列からなる。

種特異的であり、ごく近縁種でも異なる配列をもつ場合が多い。

配列は染色体が異なっても同一であり、染色体間を転移する機構が存在する。

11



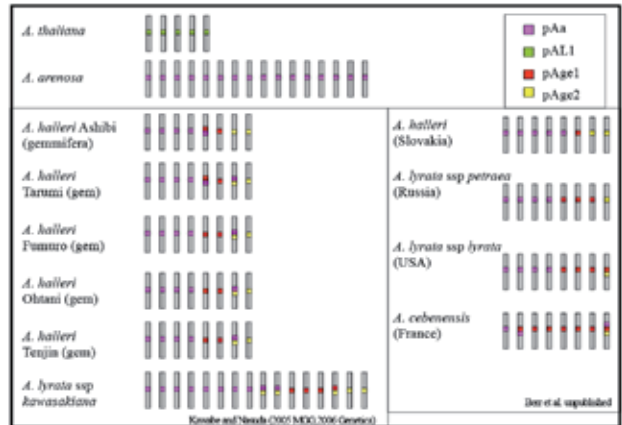
12

ハクサンハタザオおよび *Arabidopsis lyrata* における動原体特異的反復配列の進化

現象：
これらの種では3種類の異なる反復配列が存在する。
シロイヌナズナ近縁種ではこれまで1種からは1種類の反復配列が単離され、またそれぞれは種特異的であった。

疑問：
複数の動原体配列が共存する状態は平衡状態なのか移行期なのか。
それぞれの配列ファミリー間で変異のパターンは異なるのか。
どのように染色体を超えて移動するのか。

13



14

動原体特異的的反復配列が異なる種間での染色体構造の比較

4つの動原体領域はシロイヌナズナと *A. lyrata* でシンテニーが存在
これらの染色体では動原体の位置は変化していない。

それまで存在した反復配列の消失、新規配列の増加、新規配列が染色体間を越える移動は既に存在している動原体領域で起こっている。

Kanobe et al. 2009 Genetics

15

動原体領域の進化に関するまとめ

ハクサンハタザオや *A. lyrata* は3種類の動原体特異的的反復配列を持つ。

異なる種や同種でも地域集団間では染色体特異性は異なる。
反復配列は現在も染色体間を超えて転移し、また増減している。
pAge2ファミリーは高い種特異性、地域集団特異性を示す。
自然選択によりこの配列が有利になった可能性

動原体領域周辺の染色体構造は動原体配列が完全に異なる種でも保存されている。
動原体特異的的反復配列は染色体構造を変えることなく転移する。

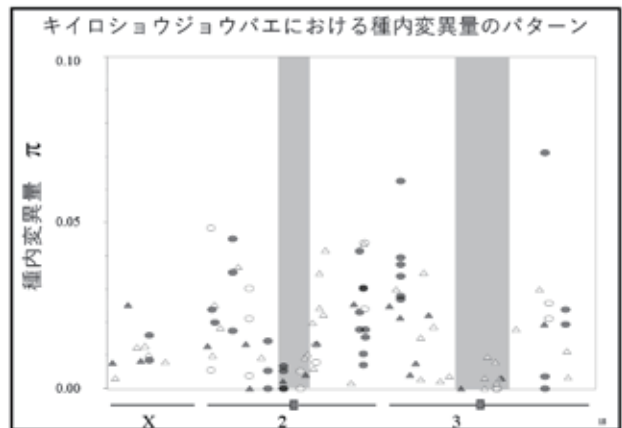
16

2) 組換え量が種内変異量に与える影響

過去の知見：組換えが低い領域では種内変異が低く抑えられている。
(種間の分化の程度は変わらない。)

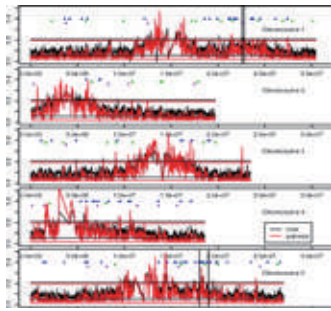
仮説：自然選択の影響が強い連鎖により広範な領域におよぶ。
Hill-Robertson effect (Hill and Robertson 1966)
Hitch-hiking effect (Maynard Smith and Haigh 1974)
Background selection (Charlesworth et al. 1993)

17



18

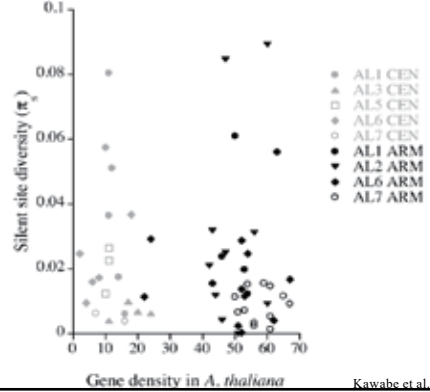
シロイヌナズナのゲノム全体での変異量のパターン



Borevitz J. O. et al. PNAS 2007;104:12057-12062

19

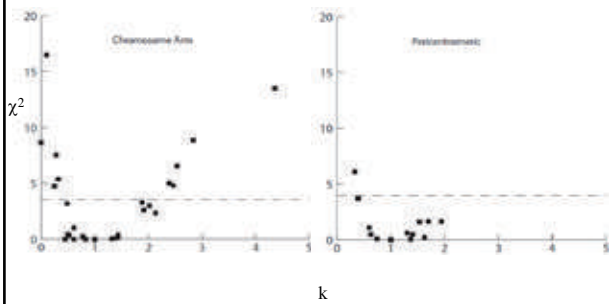
A. lyrata の種内変異量と遺伝子密度の関係



Kawabe et al. 2008 Genetics

20

自然選択の効果



Kawabe et al. 2008 Genetics

21

組換えが低い動原体近傍領域のDNA多型のまとめ

シロイヌナズナ属では、

- 1, 種内変異量は染色体腕領域の遺伝子と変わらない。
- 2, 染色体腕領域の遺伝子には自然選択の影響がみられるものが多く存在する。

低遺伝子密度、小さな有効集団サイズによる**自然選択の影響の減少**
動原体領域の低い種内変異は動原体そのものに働く自然選択の影響

22

3) エピジェネティックな制御を受ける遺伝子の進化機構

エピジェネティックな遺伝現象：
DNA配列情報によらない遺伝子発現や表現系の差異

ゲノミックインプリンティング
片親由来の対立遺伝子の非活性化（胚乳発生遺伝子の片親由来発現）

遺伝子量調節
コピー数の異なる遺伝子座の発現量調節（倍数体の遺伝子制御）

トランスポゾンの転移制御
トランスポゾンの不活化（斑入り等）

23

ゲノムインプリンティング

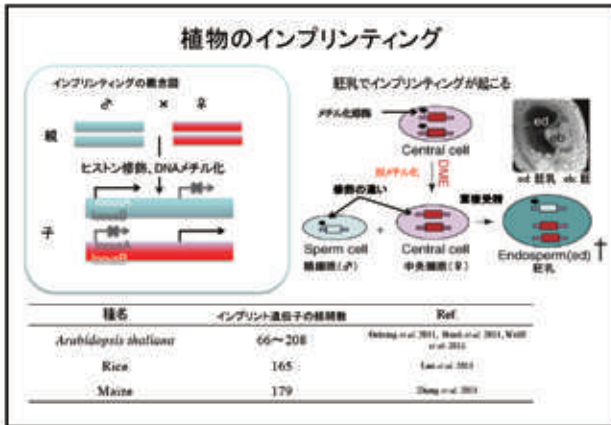
ゲノムインプリンティングは哺乳類や種子植物で見られる現象で、父親と母親の片親由来の遺伝子発現のことである。

哺乳類の胎盤や種子植物の胚乳などで観察され、オスとメスの利害の対立が原因ではないかと考えられていた。

DNAやヒストンの修飾により一方の対立遺伝子が不活化される。



24



25

インプリンティングの進化

インプリンティングは両親間や子供の間での利害の対立が原因で進化したと考えられてきた。

インプリンティングに関わる遺伝子(認識する側、認識される側どちらも)は軍拡競争によって早い進化をしているのではないかと予想される。

このような進化は自殖性の生物では見られないのでは？(生殖様式によって進化パターンに違いがある？)

26

インプリンティング制御を受けるシロイヌナズナ遺伝子

Medea: ポリコム複合体を形成するヒストンメチル基転移酵素
プロモーター領域のヒストンメチル化
母親由来対立遺伝子特異的発現
胚乳発生を抑制

Pheres: タイプI MADSタンパク質
プロモーター領域のヒストンメチル化
父親由来対立遺伝子
胚乳発生を増長

FWA: プロモーター領域に存在するSINE様配列のDNAメチル化
母親由来対立遺伝子特異的発現
花成時期の遅延

(FIS2, MDC, ...)

27

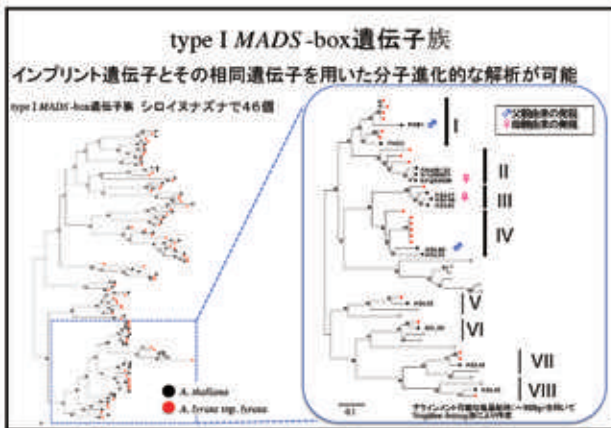
インプリンティング制御を受ける遺伝子の進化パターン

Medea: プロモーター領域における平衡選択
Kondoh et al. 2007 Current Biology

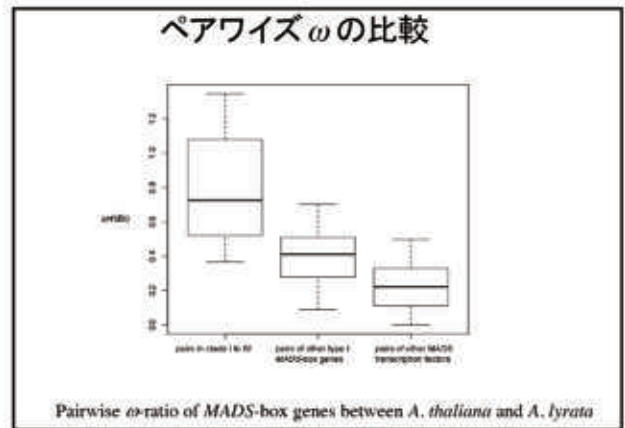
Pheres: 遺伝子重複によるコピー数の増減
プロモーター領域の遺伝子変換による均一化

FWA: プロモーター領域に存在するSINE様配列の重要性
プロモーター領域の高い変異量
(DNAメチル化による突然変異率の上昇)
プロモーター領域に対する負の自然選択
Dipardo et al. 2008 PLoS Genetics

28



29



30

Aim of the research

Revealing the developmental processes and molecular basis for vegetative propagation of *Rorippa aquatica*



- Developmental analysis
- Genome analysis
- Transcriptome analysis

7

Developmental analysis

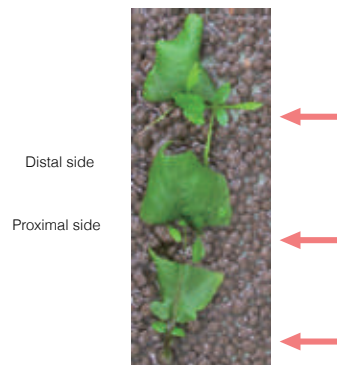
8

Regeneration of *R. aquatica*



9

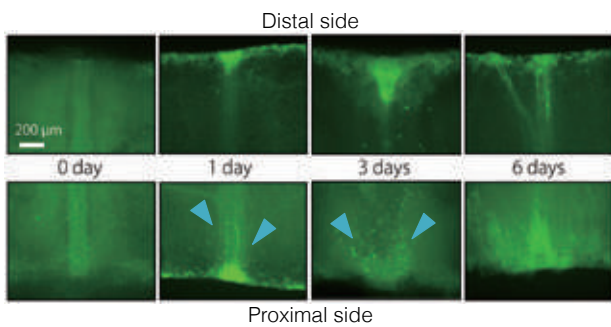
Regeneration of *R. aquatica*



Plantlet forms only at proximal side of leaf fragments

10

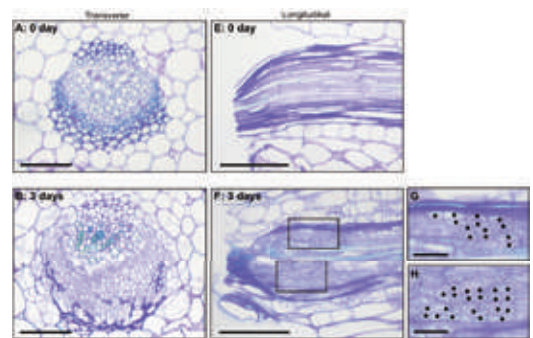
Visualization of cell proliferation by EdU



Cell proliferation is re-started after 1 day

11

Cell division pattern

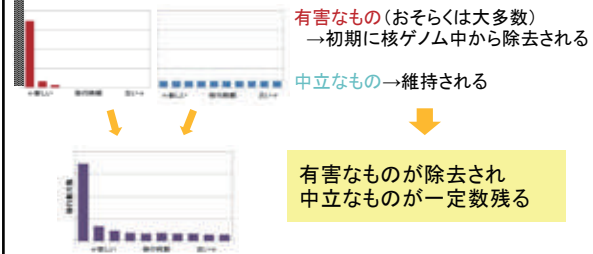


Dividing cells are found around vascular tissue

12

NUPTの維持・除去パターン

ゲノム断片の移行は頻繁に起こるが...



37

平成 27 年度～平成 31 年度私立大学戦略的研究基盤形成支援事業 研究成果報告書

「植物における生態進化発学研究拠点の形成-統合オミックス解析による展開-」

令和 2 年 5 月

発行 京都産業大学
生態進化発生物学研究センター
〒603-8555 京都市北区上賀茂本山
印刷 株式会社プレスハウス

